Institute of Condensed Matter and Nanosciences
Bio and Soft Matter division

Bio-derived polymer-based electrolytes for Lithium-metal batteries

Ashish RAJ

Supervisor : Prof. Jean-François GOHY

Jury Members:
Prof. Jean-François GOHY, Supervisor, UCLouvain
Prof. Charles-André FUSTIN, Member, UCLouvain
Prof. Alexandru VLAD, Member, UCLouvain
Prof. Evelyne Van RUYMBEKE, President, UCLouvain
Prof. Christophe DETREMBLEUR, Member, ULiège
Prof. Laurent RUBATAT, Member, Université de Pau et des Pays de l'Adour

Thesis submitted in fulfilment of
the degree of Doctor in Sciences

Louvain-la-Neuve 2024

Dedicated to my family, teachers, friends, and loved ones who impacted me directly or indirectly in the process of establishing my identity.

Acknowledgements

My peers have taught me that, a strategized smart and quantitative effort always presents a higher possibility of making a long-lasting impact and success than just smart work. My PhD journey has been interesting with little ups and downs and was fortunate to have a very friendly work environment and colleagues with cooperative team spirit. On that note, first I would like to acknowledge my Supervisor, Prof. Jean-François Gohy, who has been very supportive in all aspects of my doctoral training from the first day. He not only imparts his knowledge and experience within research problems but also guides in attaining the solutions. His practical approach to addressing the questions has been remarkable and diminished the hurdles. His faith, patience and optimism towards me taught me other skills besides just working on the thesis. Away from the lab, I appreciated his aura and energy in the team activities which has marked great memories of my PhD days. I am deeply grateful to associate, work and learn from him for these years with a positive mind even in unprecedented situations.

I would like to thank Dr. Satyannarayana Panchireddy, a former Postdoc in my Project. I owe him huge gratitude for the development of monomers, his assistance and leading the collaboration at the beginning of this thesis. His initial professional guidance supported me not only in understanding the project but also direction the future work. I would like to thank two members of my PhD committee and Jury, Prof. Charles-André Fustin and Prof. Alexandru Vlad for their time and corrections throughout the meetings. I have learned a lot from them in our interactions and while working on the same floor/building. Their suggestions/feedback not only improved the quality of the thesis but also expanded my knowledge with their experiences. Then, I would like to extend thanks to other Jury members, Prof. Evelyne Van Ruymbeke (UCLouvain) Christophe Detrembleur (University of Liège) and Prof. Laurent Rubatat, (University of Pau and des Pays de l'Adour) for their constructive questions and feedbacks. In addition, I express my gratitude to Prof. Tom Leyssens for his suggestion during my confirmation.

My collaborators and mentors of the project have been very helpful in key suggestions, and sharing their expertise and important feedback. Starting with the University of Liège, I owe Prof. Christophe Detrembleur and Dr. Bruno Grignard for supplying me with interesting material for this project as well as others. Prof. Christophe has been pivotal in correcting my manuscripts and thesis with his insightful suggestions. And I am looking forward to having more feedback from him

on our manuscript submissions. My project collaborators namely, Lieven Bekaert and Mesfin Haile Mamme at VUB-SURF deserve applause for our successful exchange over multiple projects with their theoretical expertise. A few of the industrial mentors also contributed toward this project involving Ir. Fernand Gauthy from Solvay and Dr. Elise Nanini Maury from Engie with their advice through our project meetings. I wish to convey my thanks to Fabio Lucaccioni for facilitating the lab and for all his help. I owe thanks to the instrument specialists/experts for training me to learn new techniques involving Pierre Eloy, Pascal Pascal Van Velthem, Gabriella Barozzino Consiglio, Stéphanie Wautier and Delphine Magnin.

My direct and indirect co-workers have been instrumental in this journey in and outside the lab. I would like to express my pleasure to meet them as my work colleagues and cherish good moments over various research and fun activities. I would like to express deep gratitude to my office fellows, Carla and Hamid. I enjoyed several scientific and non-scientific exchanges with them over a lovely bond. The conference trips were incomplete without Benoit, Issac and Yinghui. It has been a fun time with them which stays in a good book in addition to technical discussions. I thank my present and former colleagues, Oriane (thanks for the card), Shanshan, Ketje, Zhenni, He, Garance, Lu, Zehan, Romeo. Thanks to Danish, Raphael, Swetha, Atul, Charlene Gregary, Clement, Rowann, Lobnan, Hao, Martin, and Yoan from Prof Charles-André's research group which complete the lab. Beyond B2 lab, I was lucky to have a friendly interaction with guys from the A3 wing, I thank Deepak, Rambabu, Petru, Gulshan, Tom, Binson, Vasu, Subhodip, Geraldine, and Sepideh for their little help as well. I regret if I missed some names from the lab with whom I had a short interaction. So, thank you!

Far away from home, I consider myself fortunate to have friends and a community which made me feel like a member of their family. I cannot imagine my days at Louvain la Neuve(LLN) without wonderful people from Bharatiye in the LLN group. From good times to bad times, they have been always there to support. They made me evolve and understand the power of togetherness with such warmth. Time flew so fast with research and community activities like BBQ or celebrating festivals either Diwali, Holi or Independence Day. I express huge pleasure to be impacted by the presence of Vishank, Kaushal, Pooja, Tejasee, Danish, Swetha and a few colleagues who literally helped me in my darkest hour of accident and Surgery. I also thank Gulshan-Sonia, Saroj, Deepak, Vikash, Jagadish, Itika, and Nilanjan, for sharing quality time over meals, games and talks. I found myself lucky to meet new people in last year of PhD, I thank Vittoria, Mahesh, Sayandeep, Shreeparna, Catherine, Vishal,

Richa, Subhajit, Arka, Naveen, and Sanjay for their nice company.I am really grateful to build meaningful relationships in these years which I hope to carry forward.

I like to also express my gratitude to my Alumni school, Institute along with involved teachers and Professors for the training and skills built over the years which gave me the competence to start my PhD research. I would like to acknowledge INNOVIRIS, Brussels for funding the BRIDGE-FUSE project. With the support and faith of my supervisor, the work was carried out for this thesis and interesting academic collaboration was built. Last but not least, I want to thank my family for their endless support in all situations. I have been grateful to my brother who stayed close to my family so that I can continue to realize my ambitions without worrying about home. My two elder sisters have always showered love from my childhood and shown me the right direction. Life would not have been ever easier without my family's continuous strength and confidence in me. It would be wrong to say "If I have achieved/would achieve in life until now/in future", because it was/is/will be always, "We, not I". I am sure there are many other personalities which I have not highlighted in this small text. However, I want to mention, all your contributions are beyond words. Thank you everyone again and I am always grateful to you for both good and bad experiences in moulding myself into a better person.

Abstract

Solid-state batteries are expected to upgrade the lithium battery (LB) technology with their safety, higher energy density and superior characteristics over conventional liquid electrolyte-based LIB. Polymers based on polyethylene oxide (PEO), polycarbonate *etc*. are front runners toward this goal in realization of solid polymer electrolytes. However, most of these polymers have relatively less environmental benignity. Counting on that, bio-derived polymers synthesized through non-toxic routes excite many researchers, including us, leading to the core motivation of this thesis. We synthesized a series of polymers via facile chemistry starting from solvent-free viscous monomer carbonated soybean oil (CSBO) to poly(hydroxyurethanes) (PHU) network and their analogues. The work carried out in this thesis is classified into three categories: a) Non-opened cyclic carbonate (CC), b) ring-opened CC, PHU and c) composite polymer electrolyte. Novel non-isocyanate and catalyst-free methods were exploited for the synthesis of these PHU networks via polyaddition includind blending, plasticization and composites, respectively. We were able to achieve ionic conductivity in the range of 10^{-6} to 10^{-3} S cm^{-1} for various formulations with an electrochemical stability window as high as ESW > 4.5 V versus Li/Li^{+}. Further, lithium metal battery prototypes fabricated with Lithium ferrophosphate ($LiFePO_4$/LFP) were subjected to coin cell testing for potential limited galvanostatic charge-discharge over several cycles and current densities. The fundamental understanding of the decomposition of an electrolyte subjected to its functionalities has also been one of the key objectives of this work. The thesis covers various states of solvent-free CSBO-derived electrolytes from viscous, gel-like networks to free-standing solid membranes with and without separators targeting attempts to inspire more efforts in bio-derived battery materials with high performance.

List of abbreviations

EV: Electric vehicle

LIB: Lithium ion battery

LB: Lithium battery

LMB: Lithium metal battery

LFP: Lithium ferrophosphate

NMC: Nickel cobalt manganese oxide

CNT: Carbon nanotubes

LE: Liquid electrolyte

SE: Solid electrolyte

PC: Propylene carbonate

EC: Ethylene carbonate

DEC: Dethyl carbonate

DMC: Dimethyl carbonate

EMC : Ethyl methyl carbonate

FEC: Fluorinated ethylene carbonate

VC: Vinyl carbonate

CP: Cellulose paper

GC: Glassy fibre

LiTFSI: Lithium bis(trifluoromethane)sulfonimide

SEI: Solid electrolyte interphase

CEI: Cathode electrolyte interphase

LEDC : Lithium ethylene dicarbonate

CNT: Carbon nanotubes

LTO: Lithium titanate oxide

SEM: Scanning electron microscopy

ESW: Electrochemical stability window

XPS: X-ray photoemission spectroscopy

HR-XPS: High resolution X-ray photoemission spectroscopy

FTIR: Fourier transform Infra-red

NMR: Nuclear magnetic resonance

DSC: Differential scanning calorimetry

TGA: Thermal gravimetric analysis

PEIS: Potential electrical impedance spectroscopy

CV: Cyclic voltammetry

LSV: Linear sweep voltammetry

OCP: Open circuit potential

CA: Chronoamperometry

GCPL: Galvanostatic cycling potential limitation

AC: Alternating current

DC: Direct current

LCA: Life cycle assessment

SPE: Solid polymer electrolyte

CPE: composite polymer electrolyte

ASSB: All Solid state batteries

SSE: Solid state electrolyte

ISE: Inorganic solid electrolyte

GPE: Gel polymer electrolyte

CC: Cyclic carbonate

HOMO: Highest occupied molecular orbital

LUMO: Lowest unoccupied molecular orbital

SLIC: Single lithium conducting

PVDF: Poly(vinylidene fluoride)

PPC: Poly(propylene carbonate)

PEC: Poly(ethylene carbonate)

PAN: Polyacrylonitrile

PU: Polyurethane

NIPU : Non-isocyanate Polyurethane

PHU: Poly(hydroxyurethanes)

ESBO : Epoxidized soybean oil

CSBO: Carbonated soybean oil

PEO: Poly(ethylene oxide)

PEG: Poly(ethylene glycol)

PEGTA: Poly(ethylene glycol) terminated amine

PEGDCE: Poly(ethylene glycol) diglycidyl ether

TDD: 4,7,10-trioxa-1,13-tridecanediamine

EDEA: 2,2′-(ethylenedioxy)bis(ethylamine)

NMP: N-Methyl-2-pyrrolidone

THF: Tetrahydrofuran

DCM: Dichloromethane

TBAB: Tetrabutylammonium bromide

HFI: 1,3-bis(2-hydroxyhexafluroisopropyl) benzene

List of symbols

μ : Chemical potential

k_b : Boltzmann constant

E_α : Activation energy

Ω : Ohm

Ω : Angular frequency

∑ : Summation

Φ : Phase angle

n : number of moles

M_w : Molecular weight

F: Faraday constant

Δ : Delta (difference)

Z : Impedance

σ : Conductivity

R : Resistance

T : Temperature

V : Voltage

I: Current

C : Capacitor

t_+ : Transference number

Contents

Chapter 1 Background of the Lithium-based batteries

Abstract

Lithium battery technology has revolutionarily impacted human life and thus has been awarded the Nobel Prize in 2019. However, its invention covered an arduous path along the materials development, i.e., electrodes, electrolytes, additives and binders, *etc*. overcoming underlying complexities and hurdles. A decent background is necessary to build familiarity with innovations in these components to demonstrate mutual compatibility. Chapter 1 aims to serve the goal with discussion of those components along with a brief detailed history and timeline of technical evolution as well as milestones and mistakes. Lithium-based battery technology overshadows other rechargeable batteries due to their high energy density covering a vast range of device applications. They rely on electrodes (cathode and anode) and electrolytes with supporting materials for high performance and thrive innovations for improvement and advancement. Three main sections in this chapter start the discussions, first, from the discovery of energy storage technology to highlights on the lithium battery technology. The second section covers the generic review on the state of art battery materials, research interest, current trends and challenges to overcome underlying disadvantages. Subsequently, the last sections talk about the environmental challenges and insightful findings on the adverse effect of the battery technology.

1.1 Outlook of the clean energy

Energy conservation principle says energy cannot be created nor destroyed in nature. An exchange of energy creates every aspect of living and non-living entities. Over year and years, we find different forms of energy conversion and storage catering to the need of forthcoming generations. We have already advanced to the era of high-powered portable and wireless devices with fast-growing technological innovation and thus increasing energy consumptions.[1] Right from the agriculture sector to artificial intelligence, electrical energy is at the heart of the operation. Conventional source of electricity generation involved used of fossils fuels which emits heavy greenhouse gases into air predominantly from energy sector (> 73.2%) as shown in Figure 1.1.[2,3] The subsequent increasing energy demands led to the imbalance in the reversible self-intoxication of nature, increase in temperature and thus global warming. [2,3]

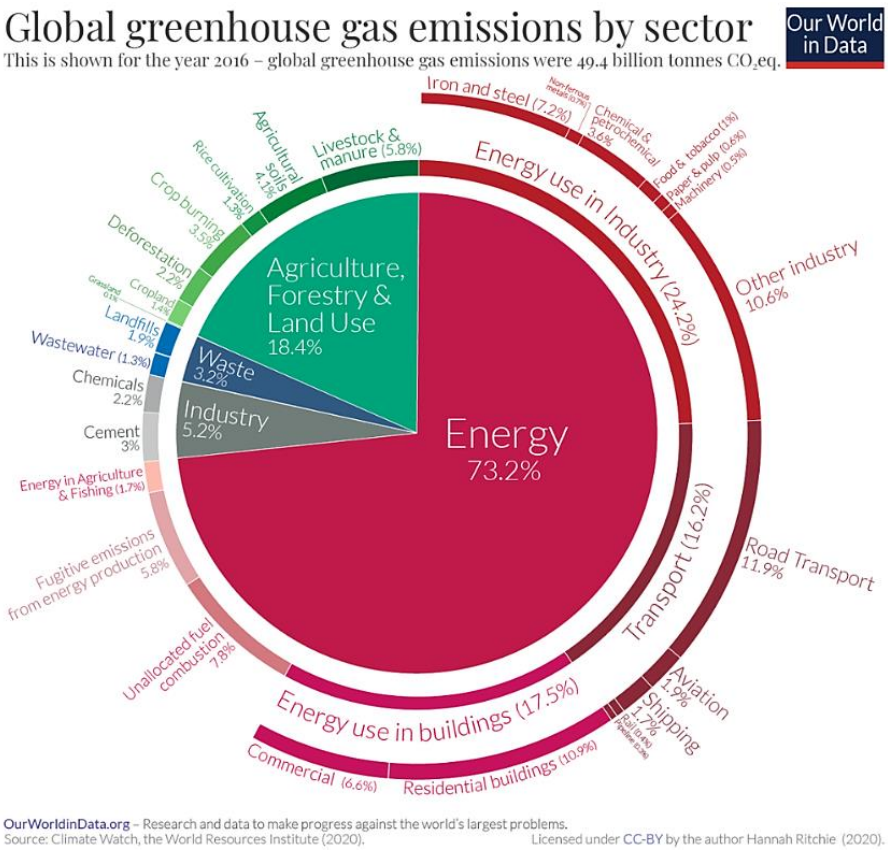

Figure 1. 1: Chart of emission of greenhouse gases. Reprinted with permission from the reference.[2]

The fact that the fossils fuels take millions of years to produce and are limited in their natural reserve raises loud alarm for the future generations. It is estimated that coal, a major source of electricity generation, would run out of its reserve in 114.00 years.[4]Nevertheless, we are already in the era when we are witnessing the melting of glaciers, drying rivers, poisoning of marine life, lowering ground water, degrading air quality and unpredictable climate in different parts of the world.[5] The catastrophic change in the climate is not restricted to one geographic landscape, rather, the entire ecosystem faces this backlash, and it will pertain if no stern actions are taken. Thanks to scientists and innovators, alternative solutions are developed targeting renewables towards sustainability. Major types of renewable energy involve thermal, hydropower, wind, tidal, nuclear, solar and small-scale sources. However, these offer the biggest drawback of their dependence on weather conditions and intermittent nature, which strikes the importance of storage technology. Energy storage devices in that context address the former concern, which has witnessed ground breaking discoveries and innovation in decades over decades, as highlighted in the next section.[6,7]

The electrochemical storage devices like fuel cells, supercapacitor, and batteries have been leading technologies as shown in the Ragone plot (Figure 1.2).[8] Supercapacitors first conceptualized as Leyden jar in 1740s offer high power density, fast charging and long cycle life (>100000).[9] Although, they fall short of energy density to batteries and fuel cells. Commercial supercapacitors deliver energy density of 5 Wh kg^{-1}

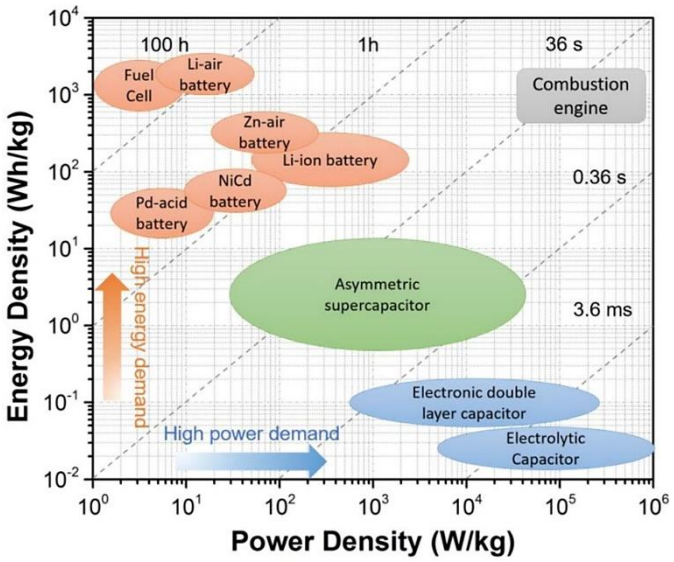

Figure 1. 2 : Ragone plot highlighting comparison of energy density and power density of various energy storage electrochemical technologies (Times shown in the plot are the discharge time which is calculated by dividing the energy density by the power density). Reprinted with permission,[8] copyright 2018, ACS.

compared to higher energy density of ≤ 200 Wh kg^{-1} and ≤ 350 Wh kg^{-1} for batteries and fuel cells, respectively.[8] Limited by energy density, the former cannot draw its market in various sectors. Among batteries and fuel cells, batteries lie somewhere in compromised state between supercapacitor and fuel cells in terms of power density. The difference between these two can also be made by defining them as open and close system, batteries as a close system and fuel cell as an open system. In batteries, active masses undergo reactions within electrode and cell while in fuel cell, it undergoes outside the cell. Batteries dominated the market because they presented relatively efficient and safe solutions to low to medium load devices for mobility and stationary devices. Fuel cells are cheaper and better alternatives in case of heavy carriage vehicles over higher range of distance >800 km.[10] Provided all these edges over other devices, batteries always strive to fresh developments to meet market needs.

With burgeoning of events, we have already entered in the era of batteries from nanoscale to macro-scale ranging in vast application from nano chips to large grid storage. In the race of high performance and affordability, long existing battery technology like metal acid, metal hydride and alkaline batteries *etc.* have not been succeeded much and faced significant shrinkage in their market capital excluding lead-acid batteries. On the other hand, the monotonic increase in the global market capital of < $ 50 bn as of 2020 to predicted < $100 bn, lithium-based batteries continue to climb the ladders in parallel to extensive research depicted in Figure 1.3.[11] The obvious reason lies in the high energy density, vast application and attempts towards carbon neutrality. This greater need of switching to renewables and clean energy was realized owing to excess global warming, addressed in 2015 Paris climate change accord as well as Glasgow in 2020. The conference envisioned the necessity to identify the effects of global warming on our planet, side-effects of technological advancement comforting human lives and the need for a sustainable way of living. Although, the 5 years goals were not achieved as published in 2020 Glasgow climate change conference organized in 2021. Most of the countries, including the top global economies, pledged to bring down their emission to net zero in a certain year by switching to clean and renewable energy policy shared cooperation.

The common goal could not be realized without a collective approach in lieu of different national policy. Therefore, renewables, as mentioned above, are crucial to be part of our routine life for future sustainability. The developed countries could lead the way, owing to their resources and cutting-edge technology, to set up the models for the underdeveloped and developing economies. Many public and private firms are encouraging their workforce to adapt to greener lifestyles by encouraging a policy of electric vehicles, public transport, organic food consumption, biodegradable consumables and recycling habits.[12] Although it's a never-ending journey, the path has already been taken. For example, Norway uses largely hydropower generated

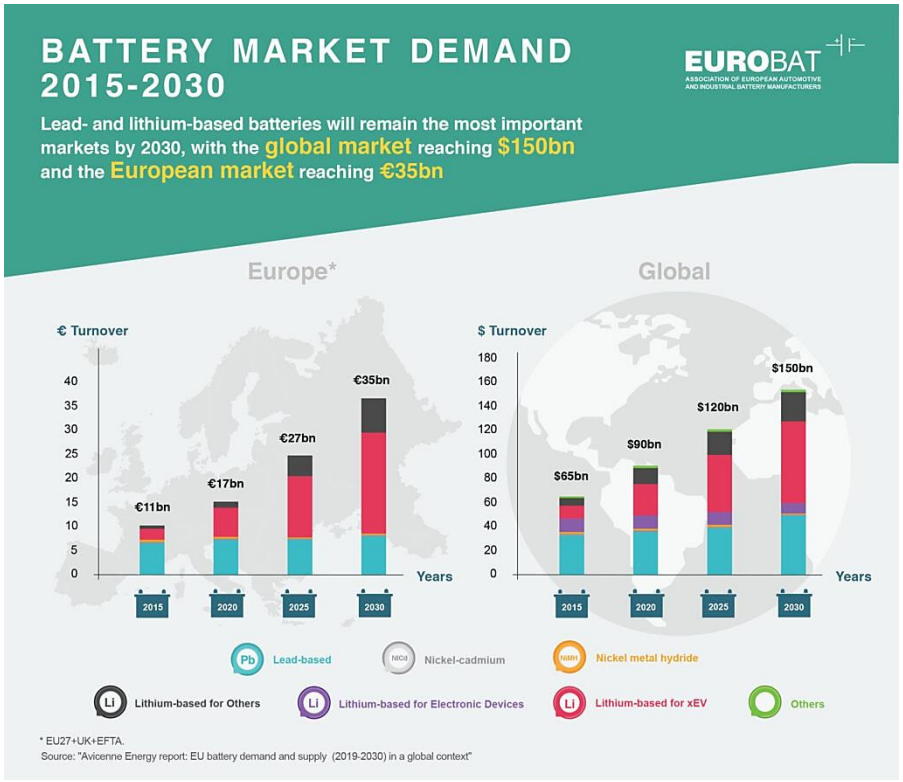

Figure 1. 3: Market share of battery technologies in Europe and globally. Reprinted with permission, copyright 2021, EUROBAT.[11]

electricity as its primary and major energy consumption.[13] Although, replicating these models to bigger geography like India and China is not a simple task and needs to be addressed in stepping milestones. Focusing precisely on the energy storage needs, the Lithium-based battery is an excellent candidate so far for both our mobile and stationary needs. Specifically, all-time booming transport industry and their large share of CO_2 release to the atmosphere are credited to the burning of fossil fuels like petrol and diesel, *etc.* Other solutions, like biofuels, hydrogen energy has been tested and working in some part of the world in small scale but does not fill the gap to turn to large-scale application accounting for the safety and logistic challenges. Electric vehicles driven via different technology continued to develop from 1830s while first few EVs based on rechargeable secondary batteries was introduced around mid-1960s by Scottish Aviation Scamp and Electrovair as demonstrated in Figure 1.4. Quite a few successful efforts were observed for EVs based on lithium-rechargeable batteries, but it was not until 2008 when Tesla Roadster became the first production EV for the market use. However, the lithium-ion batteries have their own limitations with their power and energy density. It in turns limits its deliverance and distance by 320 km in a single charge.[14] For this reason, many big automobile companies were not producing

the full EVs owing to their poor performance and unavailability of charging stations. To address this concern, the concept of hybrid electric vehicles developed by Porsche around 125 years ago, gained larger interest in the market, which combines both combustion and electric engine together.[15]

This increasing demand, on one side, contributes toward the greener footprint of the environment and, on the other side, poses a high safety risk of property and life damage. The current lithium ion battery technology is largely based on liquid electrolytes, which do not meet the targeted expectations in performance for large commercial application. In addition, they are flammable and attract packaging and leakage issues. Nevertheless, many companies are working on the improvement of the lithium ion batteries technology with liquid electrolytes via addressing packaging, higher voltage electrodes materials and so on. But storming research and development have been undergoing in solid state lithium metal batteries by various institutions and industries to boost the clean energy transition. The market capital forecast is itself clear proof of overwhelming growth in the energy economy. In particular, lithium batteries economy is bigger than ever expected, and is projected to soar in its share out of total battery market over 10 years (Figure 1.3).

Although a safe, high energy and power density, long-lasting battery pack could only be achieved with high voltage cathodes, lighter anodes and solid-state electrolytes. Huge amount of research funding and grants in billion dollars across the globe have been allocated for more than 5 years to innovate superior solutions with all solid-state batteries and their application for EV.[16] Besides mobility, high energy density stationary power grid storage is also a need of the Era due to climate dependence and intermittent nature of solar, wind and hydrothermal energy. Lithium ion battery pack again fulfils the purpose by providing large storage in small batteries over conventional batteries technology.[17] These utilities have already been well validated and operational in the market for daily need for energy in case of bad weather and non-operational renewables. Although, more and more research and development could facilitate the lower cost and higher energy and power density.

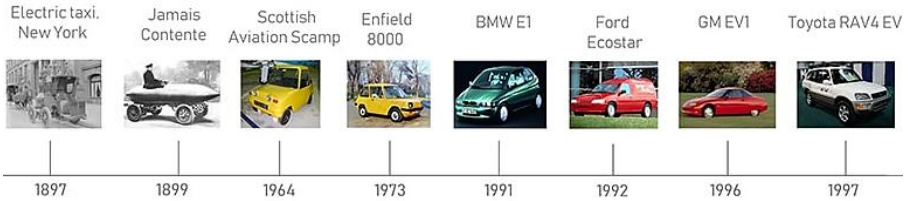

Figure 1. 4: Timeline of EV development over several decades. Reprinted with permission,[18] copyright 2019.

1.2 Early developments in the battery research

After the discovery of electricity by Benjamin Franklin in 1740, the understanding of static charge or current was yet to be flourished. The first battery was believed to be invented around 250 BCE, referred as Baghdad battery discovered by Wilhelm König, one German archaeologist.[19,20] Although the first practical battery's invention is credited to Alessandro Volta, it was not possible without the accidental contribution of Luigi Galvani's frog leg experiment. He observed the twitching in the frog's leg upon touching with two different metals. The false hypothesis of animal electricity was later explained to be caused by two dissimilar metals and humid conductor by Volta in 1791.[21] The Voltaic Pile is the actual battery developed by Volta which is also called the first wet cell battery with copper and zinc as electrode and cloth soaked in brine. Several important findings were highlighted regarding battery along with challenges like electrolyte leak, short-circuit, internal resistance *etc.*[22,23] Figure 1.5 shows the milestone with key developments in batteries over a century from Voltaic Pile to next generation lithium battery technology.[23] Around 1859, a key development led to the lead-acid batteries followed by the Daniel cells on overcoming major drawback associated with Voltaic pile in 1820. So far, all the batteries discovered were primary batteries, meaning they could not be used again once discharged.

The lead acid battery was one of the first few rechargeable secondary batteries discovered by Gaston Planté and enhanced by Camille Alphonse Faure.[21] The initial

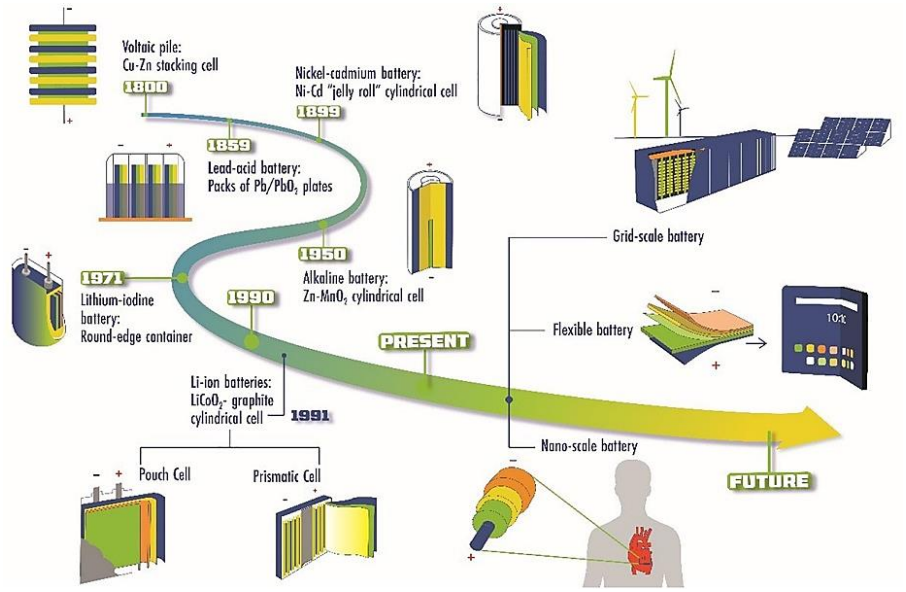

Figure 1. 5: Evolutionary timeline of invention and development of battery technology. Reprinted with permission,[24] copyright 2020, Frontiers.

model composed of two lead sheets divided by rubber strips forming spiral while the enhanced one used lead grid lattice in which the lead oxide paste was pressed in series connections. Nevertheless, it did not stop there within the same decade. French scientist Georges Leclanché came up with the first dry cell battery in 1866. It was composed of a zinc anode with a manganese dioxide cathode wrapped inside a porous material.[25] Thereafter, Nickel cadmium rechargeable battery by Swedish engineer Waldemar Jungner in 1901 and alkaline batteries came into existence with the potential nickel-cadmium metal and other electrodes separated with alkaline electrolytes. The first experimentation for so-called popular lithium batteries was conducted by Gilbert Newton Lewis in 1912. The period of post 1950s was very historical in view of high power and energy density batteries for the growing electronic, medical and military needs.[26] While regulations and improvements continued to move in the domain of lead acid battery in the mid 1970s, Sony commercialized the first secondary lithium ion battery only in 1992, two years after commercialization of Ni-metal hydride battery in 1990.

During 19th and 20th century, larger interest was not confined neither to primary nor secondary batteries, but more on fundamental aspects. With compiled effort and early discoveries right from the material innovation and working principle, physicist and chemist continued to strive towards better technology in a collaborated manner. Primary batteries, on the other hand once discharged cannot be charged again and are subjected to recycling, while secondary batteries continue to bring attention of many researchers and companies due to their potential and long durability. The understanding of electrochemical reversibility in secondary batteries coupled with high energy density was seen as a torchbearer in energy storage research. Figure 1.6 demonstrates types of popular rechargeable batteries based on distinct elements and operational chemistry.[27] Lead-acid batteries, the first rechargeable batteries of 2 V is a long-live innovation by Plante and is continued to be in market from various small to medium scale applications.[28,29,30] Although they offer really low energy density (80–90 Wh L^{-1}), they compensate the former with superior power density (180 W kg^{-1}) and inexpensive manufacturing.[31] Until 1999, lead-acid batteries already held more than 50% of the market of all batteries sales globally.[32] Year-long innovations upgraded the Pb-batteries from liquid electrolytes to gel-based cells and absorbed glass-mat batteries popularly called as VRLA (Valve-regulated lead–acid) batteries. Solely based on the lead and lead oxide electrolytes, it does pose major toxicity and environment concerns and challenges in manufacturing and recycling.[33,34] The Nickel-cadmium battery developed in 1901, believed to surpass the drawbacks of Pb-acid batteries, facilitates longer cycles and rated capacity at the higher discharge capacity with several advantages like higher energy density (50–150 Wh L^{-1} and comparable power 150 W kg^{-1} to Pb-acid).[32] With 1.2 V, they are quite often used in portable

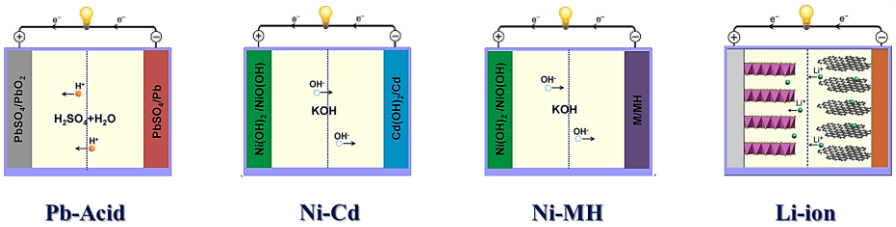

Figure 1. 6: Illustration of Secondary/ rechargeable batteries. Reproduced with permission,[27] copyright 2019, Wiley.

applications like power tools, electronic devices *etc.* due to their packaging, stability and low temperature performance. However, both nickel oxide and cadmium as positive and negative electrodes, respectively, are environmentally hazardous and toxic to living beings.[32,35] In addition to their environmental concern, they could not meet the market need of specific capacity and cost effectiveness. While further developments in NiCd led to the invention and hence commercialization of Ni-metal hydride battery replacing cadmium hydrogen-absorbing metal alloy in 1990. It catered the devices with much more energy and power density (140–300 Wh L^{-1}, 250–1000 W Kg^{-1}) than former with similar nominal voltage of 1.2 V. They have been widely used an alternative to alkaline batteries but are expensive compare to other two batteries explained above and are susceptible to higher self-discharge.[32,34] Nevertheless, all these secondary batteries suffer from trade-off, which is why the lithium battery was seen as a game changer. Lithium ion batteries outperformed all those existing technologies in terms of energy density (250–693 Wh L^{-1}), power density (250–340 W Kg^{-1}) and longer cycles. Figure 1.2 shows the comparison of lithium-based batteries with other technologies.

Undoubtedly, the lithium-based batteries market is increasing drastically with li-ion and li-metal as of predictions. However, the supply chain and natural reserve of minerals such as lithium, Ni, and Co metals are limited and would run out in a few decades if dependence increases at the current pace. Other challenges associated are energy density, cost reduction and safety.[36] Therefore, other technologies including alkali metals (Na^+ ion and K^+ ion) and multivalent metal ions (Mg^{+2}, Ca^{+2}, Al^{+3}, Zn^{+2} *etc*.) are showing promising alternatives which could relax our dependence on Li-ion. Among all these alternatives, Na-ion batteries have been the front runner crediting to the decades of research, resulting in early commercialization as well.[37] An interesting development in cathodes such as polyanion, NASICON *etc*. and hard carbon as anodes, for Na-ion batteries have marked higher energy densities up to 500 Wh Kg^{-1} with state-of-art limitations respectively.[38] K-ion battery is quite immature in the race with a major focus on polyanionic cathodes and carbon anodes. However, in both these alkali metal ions, the higher volume expansion for similar capacity poses a key issue with their large cation size associated with sluggish kinetics.[38-40]

Multivalent metal ion batteries call upon various possibilities with unique challenges. Due to multiple charges, they can facilitate a higher number of charge storage for a smaller number of working ions. They offer higher safety and higher volumetric energy density, such as Mg metal, ~3833 mAh cm^{-3} and ~2046 mAh cm^{-3} for Li metal as they are less prone to dendrites.[41] Zn batteries gained broad interest due to their remarkable ability to use aqueous electrolytes. However, it is limited by a lower voltage limit and is thus applied in large-flow battery grids. Another multivalent, Al-battery remains at its nascent stage of interest due to its challenging mobility.[42, 43] In reality, they are more than a decade behind commercialization for market uses. Nevertheless, the research is accelerating in the electrodes and electrolytes compatible with respective multivalent metal ion batteries.

1.2.2 Timescale of the lithium ion chemistry

Lithium metal was first identified by Johan August Arfwedson during 1817 in Petalite, a mineral ore. Although, its isolation was credited to William Thomas Brande and Sir Humphry Davy around 1821 by applying voltaic pile to the fused lithium carbonate and lithium oxide, respectively.[44,45] It took almost 200 years from its discovery to the battery application (Figure 1.7a). Being the lightest and among the most electropositive elements, it showed 3.3042 V versus calomel electrode. The lower weight and facile oxidation translate Li to possess a very high gravimetric capacity of 3560 mAh g^{-1} just after beryllium (5950 mAh g^{-1}). However, low density of lithium places it behind in terms of volumetric capacity with other multivalent cations such as Be^{+2}, Al^{+3}, Ca^{+2}, Zn^{+2} and Mg^{+2} (Figure 1.7b). Li dominated the race of further exploration due to their relative higher abundance, lower toxicity and cost on contrary to beryllium with potential radioactivity despite higher volumetric and gravimetric capacity.[46,47]

Even though it took years of arduous efforts for the lithium-based battery development. It presents as many complications as it can in contrast to conventional simplified batteries. It came to the spotlight due to its miniaturized applications and further was seen as a chink of light in semi-conductor and electronics industry. The dependence on mobility of ions, which are lot heavier than electrons, makes their diffusion and transport complex. The basic components, including cathode (positive electrode), anode (negative electrode) and electrolyte, involve various tortuous chemistry at the bulk and interface as well. Although, other components like separator, additives, electrode substrates and casing play less critical role in apt functioning of an electrochemical cell, plenty of research on each component has been undergoing to find sustainable yet superior alternatives, looking at need of cost effective, high performance and cleaner choices.

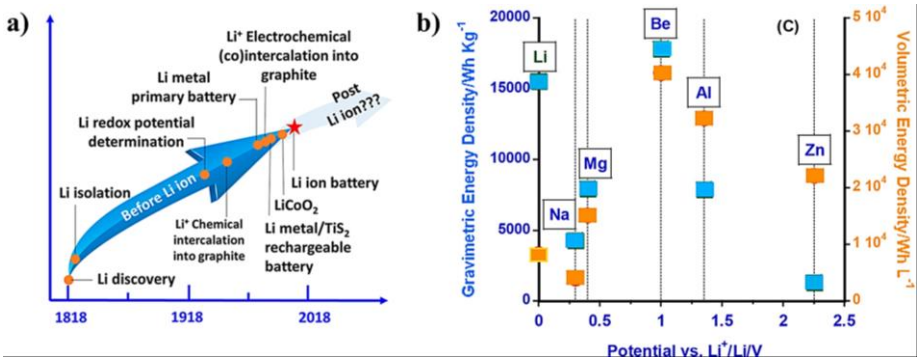

Figure 1. 7: a) Illustration of timeline from discovery of lithium to lithium ion battery, and b) Projected gravimetric and volumetric energy density of metal anodes when coupled with hypothetical 4 V cathode versus electrode potential (relative to Li/Li^+). Reproduced with permission,[47] copyright 2018, ACS.

Coming back to events that led to the discovery of a lithium metal battery, it would not be wrong to say that the series of serendipitous and strenuous effort were involved in it, as shown in the Figure 1.7.[47] The hunt to isolate and deposit lithium metal led to the realization of a congruent solvent that could be employed. It was discovered that non-aqueous electrolytes based on cyclic carbonates ester and alkylic ethers are beneficial for better solvation of cations than anions. Much later, major findings on the crucial properties of electrolytes were found and still studied, including conductivity, transference numbers, interfacial studies dealing with charge-transfer *etc*.[48,49] In correlation with solubility issues with LiF and LiCl, alternative lithium salts were also discovered including, $LiBF_4$, $LiPF_6$ *etc*..[50] In early 1960s, governmental and military fueled the development of Li-based batteries with lithium metal coupled with transition metal halide as cathode in nonaqueous electrolytes.[51, 52] Moreover, apart from performance, the cells were unsuccessful with underlying issues in every component like reactivity of lithium metal with nonaqueous electrolytes, their unstable morphology and the irreversibility of cathodes conversion-reaction-type materials MX_n (M = Ag, Cu, Fe, Co, *etc*.; X = F, Cl).[50] Instead of discrete understanding of material behavior, consolidated effort on voltages, compatibilities and underlying mismatch between electrodes and electrolyte was a much awaited area to be focused consolidated effort on voltages, compatibilities and underlying mismatch between electrodes and electrolyte was a much awaited area to be focused as depicted for certain materials in Figure 1.8.

One of the biggest mistakes which might have delayed the commercialization was the lack of understanding of lithiation chemistry of graphitic materials and need of defined interphases. It was falsely assumed that PC and EC should be essentially the same as of far as their electrochemical properties were concerned.[53,54,55,56] It took decades to notice that their difference in viscosity, melting point and dielectric constant could affect the lithiation.[50] It was during this period that the passivation

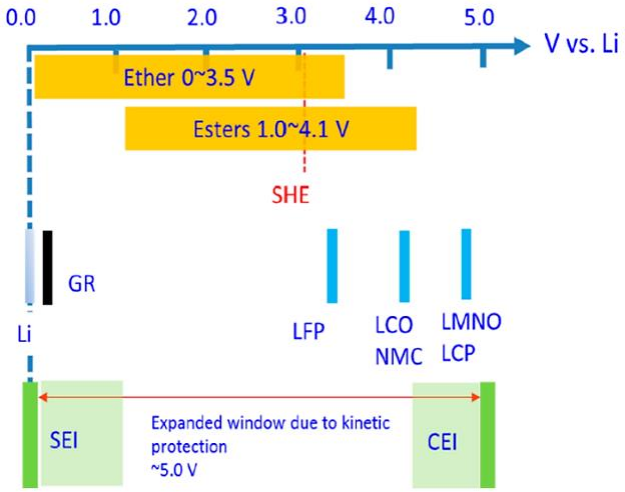

Figure 1. 8 Schematic potential diagram showing the mismatch between the electrochemical stabilities of electrolyte and the redox potentials of most anode and cathode materials used in modern LIBs (whereas, GR, LFP, LCO, NMC, LMNO, and LCP stand for graphite, lithium iron phosphate, lithium cobalt oxide, lithium nickel manganese cobalt oxide, lithium manganese nickel oxide, and lithium cobalt phosphate, respectively). Reprinted with permission,[47] copyright 2018, ACS.

layer formed at the Li-metal with the electrolyte was highlighted, later coined as solid electrolyte interphase (SEI) by Peled. Dey and Peled, in their contributions, established that SEI constitutes of solid species from reaction of Li-metal and electrolyte, which conducts lithium ions but is a poor electron conductor.[54, 57] During the 1970s, the first commercialization of primary Li batteries was realized although core issues of Li-electrolyte compatibility, unstable reactions, dendrites and safety concerns limited their progress and pushed more efforts for rechargeable Li metal batteries.

Moli energy developed the first-generation technology in 1985 of rechargeable AA cells (later named as Molicel) based on MoS_2 cathode with a rating of > 2 Wh which was also not very successful due to a number of fire accidents recorded. In parallel research, attempts to develop a solid polymer electrolyte turned successful in 1978 by the first dry SPE battery prototype by Michel Armand with lithium metal.[58] Simultaneously, another mechanism for ions host and mobility was actively looked upon for both cathode and anode via intercalation/insertion, unlike conversion. The name of the technology was called as rock-chair batteries, ion transfer cells, shuttle-cock batteries *etc*., later it was named lithium-ion batteries represented in Figure 1.9.[59] It took longer to understand anode-electrolyte compatibility than cathode-electrolyte. Most popular carbon-based anodes such as graphite and its different form as intercalation host was bet and investigated dealing with interfacial chemistry. The

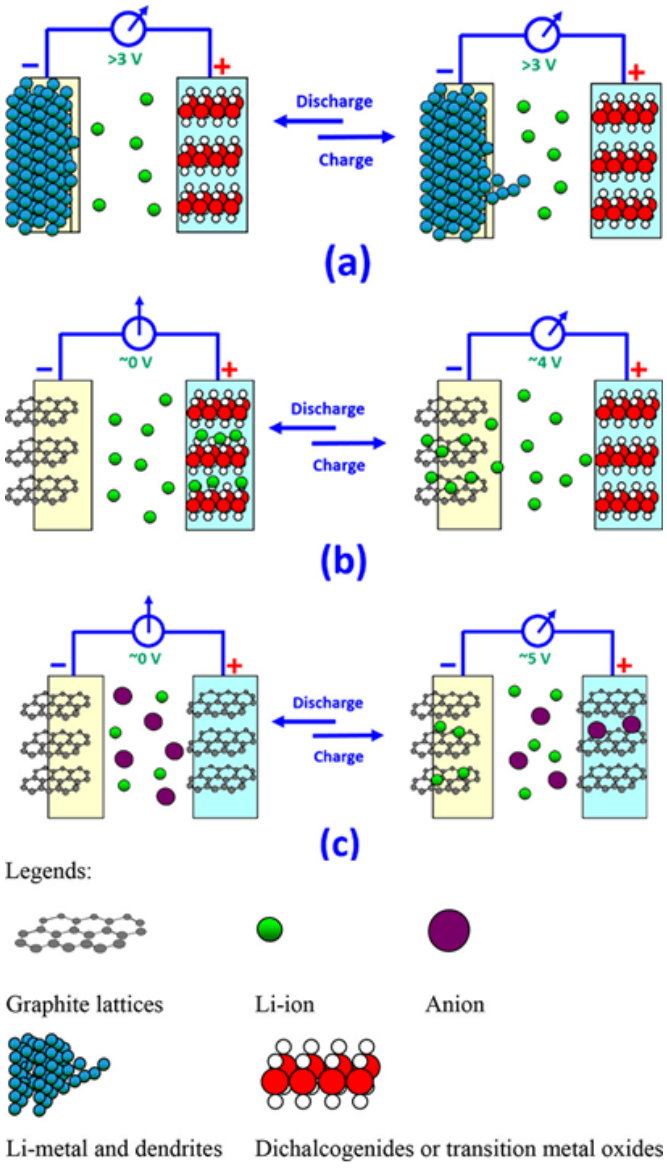

Figure 1. 9: Scheme of typical battery configurations: a) a half intercalation cell with cathode as intercalation host for Li^+ and Li metal anode, b) modern LIB cells consisting of two intercalation hosts that accommodate Li^+ at different potentials, and c) a "dualion intercalation" battery based on simultaneous cation (Li^+) and anion intercalations into graphite. Reproduced with permission,[59] copyright 2014, RSC.

intercalation host was studied for insertion to observe the associated changes, structurally and electrochemically like topotactic phase, electrode potential in correlation with reversibility.[60] Stanley Whittingham who was awarded Nobel Prize in chemistry for Lithium batteries development first demonstrated the distinction

between conversion and intercalation reaction, as minor structural changes undergo in the host lattice with cell reversibility.[61, 62]

Having learned from Hever's description of symmetric cell[63, 64] Armand established a mathematical model for two different intercalation hosts whose first demonstration was reported by Lazzari and Scrosati.[65, 66] Although slow pace in material development was still a hurdle for an appealing secondary li-ion battery which could overshadow the exciting Li-metal batteries hopes. While the intercalation materials were under development in phase, companies like Exxon mobile were also exploring the possibility of Aluminium anode following alloying chemistry which highlighted the issue of volume change.[67] It was just a few years later, Goodenough and co-workers came up with a series of transition metal oxide-based cathode materials around1980s for which he was co-awarded Nobel prize in 2019.[68, 69] The next challenge was to find a potential anode for which graphite was looked upon with huge expectations, as discussed above briefly. But it took a lot of years to come up with the answers to the inherent issues for graphite and electrolyte.[57] However, the next milestone was achieved by an industrial partner specifically a Japanese company, Asahi chemical (later collaborated with SONY) which took the task of integration of $LiCoO_2$ with a series of carbonaceous materials in real battery prototypes while overcoming hurdles posed by current collectors at anode and cathode. It was in 1990, after a long wait of safety and performance tests, that Sony commercialized and announced the 4 V LIB technology with a claim of its energy density three times as existing Ni-Cd batteries as indicated in Figure 1.10.[70,71]

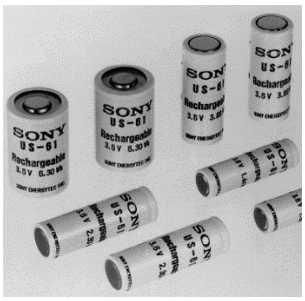

Figure 1. 10: Image of lithium-ion batteries used in some of the early Kyocera cellular phones. Reprinted with permission from Sony.[71]

1.2.3 Introduction to the present lithium-based batteries

Like traditional battery configuration, lithium-based batteries also comprise anode, cathode and electrolyte, as highlighted above. However, they also consist of current collectors, additives and binders, *etc*. Lithium batteries are superior to other storage technologies so far, not only because of high energy and power density but also huge

potential for improvement with underlying material innovations. For a few years, the urgent need for clean energy transition focuses on the high-performance lithium batteries development for electric vehicles, which could be a significant change for carbon emission free transport and mobility. In this section, we will briefly discuss state-of-the-art battery materials. The components of batteries which directly contribute toward the capacity and energy density are often termed as active materials and others as passive materials whose role cannot be ignored and often support the cell for buffering the issues related to active materials and provide robustness and reversibility.

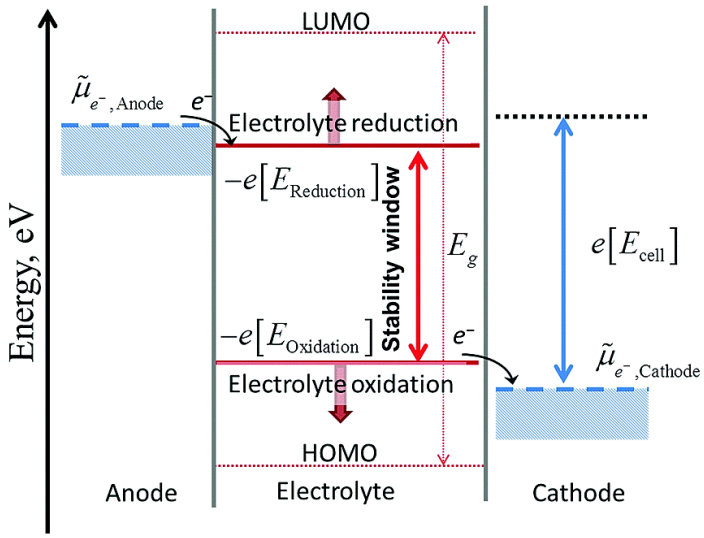

Figure 1. 11: Voltage diagram of negative and positive potential limits for the electrolyte stability with HOMO and LUMO energy levels. Reprinted with permission,[72] copyright 2018, RSC.

An energy diagram explains the operation of the cell as indicated in Figure 1.11,[72] indicating potentials of electrode and electrolytes. An anode and a cathode with chemical potentials μ_A and μ_C respectively, undergo reduction and oxidation at the electrolyte surface within its HOMO-LUMO. The operating voltage of an electrolyte is referred to as an electrochemical stability window, an indicator for the identification of suitable electrodes for avoiding parasitic decompositions. The current lithium battery market is dominated by lithium-ion batteries (based on liquid electrolytes). However, there are various materials already in mature phase to enter the market from electrodes to electrolyte with crucial parameters such as cost, performance and environment-friendly features. In a clear tabular representation (Figure 1.12), the battery materials are highlighted as some appear to possess huge potential in coming

years. Subsequent section discusses the trends in some of these materials of these materials affecting the net performance of a cell.

	2010s		2020s		2030s	
1 Cathode	LCO[1]	LMO[2] LFP[3] NMC[4]/NCA[5]	LFP[3] NMC[4]/NCA[5]	LFP[3] NMC[4]/NCA[5] LMFP[6]/LMNO[7]	NMC[4]/NCA[5] LMFP[6]/LMNO[7] Sulphur	LMFP[6]/LMNO[7] Sulphur
2 Separator/ electrolyte	Polymer/liquid	Polymer/liquid	Polymer/liquid	Polymer/liquid	Polymer/liquid Advanced liquid Semi-solid	Advanced liquid Semi-solid Solid
3 Anode	Graphite	Graphite	Graphite	Graphite Graphite and silicon	Graphite and silicon Lithium metal Silicon anode	Lithium metal Silicon anode
4 Casing	Cylindrical	Cylindrical Pouch	Prismatic Cylindrical Pouch	Prismatic Cylindrical Pouch	Cylindrical Pouch Prismatic	Cylindrical Pouch

[1]Lithium cobalt.
[2]Lithium manganese oxide.
[3]Lithium, iron, phosphate.
[4]Lithium, manganese cobalt.
[5]Lithium, nickel, cobalt, aluminum oxide.
[6]Lithium manganese iron phosphate.
[7]Lithium, manganese nickel oxide.
Source: McKinsey Battery Insights, 2022

Figure 1. 12: Timeline of present battery materials and forecast in the market for 20+ years. Reprinted with permission from,[16] copyright 2023, McKinsey & Company.

1.3 Start of the art materials: A brief review

1.3.1 Positive electrode/Cathode

Positive electrodes in batteries are referred to as cathodes, unlike in loads where the latter is called negative electrodes. Electrons move into the cathode from the external circuit in the state of discharge of batteries and out of the cathode in the state of charge. A complete cell cannot be completed without the active materials, which can reversibly react/store lithium mobile cations for cell reaction. Talking about the cathode, there are certain parameters for their selection such as, high voltage, energy density (volumetric and specific), fast and reversible electrode kinetics, good conductivity, low or no electrode dissolution, overcharge comparability, high rate capabilities, longer cycles, electrolyte compatibility, safety, cost and thermodynamically and kinetically stable *etc*.[73,74, 75] Over the years, various cathode materials have been developed and continuously undergo further improvement. The chart in Figure 1.13 summarizes the state-of-the-art investigated cathodes and anodes with their potential and capacity.[76] It clearly indicates the choice of both electrodes holds primary responsibility for delivery high energy density with durability given applied with a compatible electrolyte.[76] The specific capacity and energy for an active material is calculated by the following equation 1.1 and 1.2,

$$\text{Charge density} = \frac{nF}{3.6 * M_{w_c}} \ (\text{Ah Kg}^{-1}) \qquad 1.1$$

$$\text{Energy density} = \frac{nFE}{3.6 * M_{w_{tot}}} \ (\text{Wh Kg}^{-1}) \qquad 1.2$$

Whereas, n as number of transferred electrons, F, Faraday constant and $M_{w_c}$the molecular weight, in g mol^{-1}, of the active material), E, at a specified rate or current density and not as open-circuit voltages, $M_{w_{tot}}$, in g mol^{-1}, as the sum of molecular weights of the reaction partners (in Wh kg^{-1}). There has been extensive design and developments in cathode-materials, some of them are discussed in subsequent material section. They are classified as insertion and conversion materials based on the mechanism of lithiation. Beside they can be also categorized based on the Li-transport mechanism into four classes as non-frame (conversion), one-dimension (1D) (polyanionic cathode like olivine, tavorite, NASICON), two-dimension (2D) (Layered material, LCO, NMC), and three-dimension (3D) (disordered rock-salt, spinel type).[77]

1.3.1.1 Layered materials

The concept of intercalation in materials was not solely discovered for cathode chemistry, rather it was derived from the host-guest phenomena of supramolecular structures enabled by non-covalent bonding between guest and host. It was well verified in early investigations that the complex demonstrated different properties than parent species in addition to reversibility.[78] The discovery of layered materials such as $LiMO_2$ (M = Co, Ni, Mn, also referred as Li-rich), could be credited to the

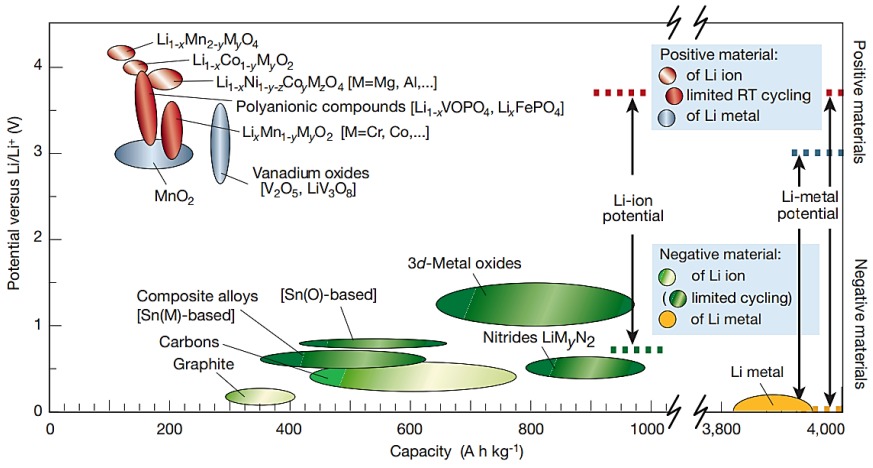

Figure 1. 13 Potential versus specific capacity for most explored and yet potential positive and negative-electrode materials for rechargeable Li-based cells (The output voltage values for Li-ion cells or Li-metal cells are represented). Reprinted with permission,[76] copyright 2001, Nature.

former idea of insertion and vice versa. They hold the crystal structure similar to α-$NaFeO_2$ in cubic closed-packed oxygen array occupying at 6c while Li and M ions at octahedral sites along 111 plane forming ABC stacking, respectively in their state of charge and discharge (Figure 1.14a).[77, 79] In 1980, $LiCoO_2$ (Lithium cobalt oxide) was created by John Goodenough which is also referred as the first generation of commercial cathode. As it appears, $LiCoO_2$ possesses layered structure which can insert and de-insert Li ions reversibly via consecutive migration between octahedral voids,[80] but when excess of Li ($x > 0.5$) is extracted then it can pose irreversible defects.[81] This was further validated by Amatucci that 95% of Li can be reinserted when complete extraction is carried with 5% of loss of Li.[82] The theoretical capacity $LiCoO_2$ is calculated to be 274 mAh g^{-1} with 1363 mAh cm^{-3} as volumetric capacity. While, practically it can deliver > 175 mAh g^{-1} with cut-off charging voltage of 4.5 V as shown in Figure 1.14b.[83, 84] While it suffered from instabilities issues which lead to voltage decay and irreversible capacity loss. The reason for capacity fading is due to change in Co-O covalence that changes with Li content relating to structural distortion.[85] However, interfacial degradation relates to the surface phase transformation layer and cathode electrolyte interphase (CEI) layer.[86]

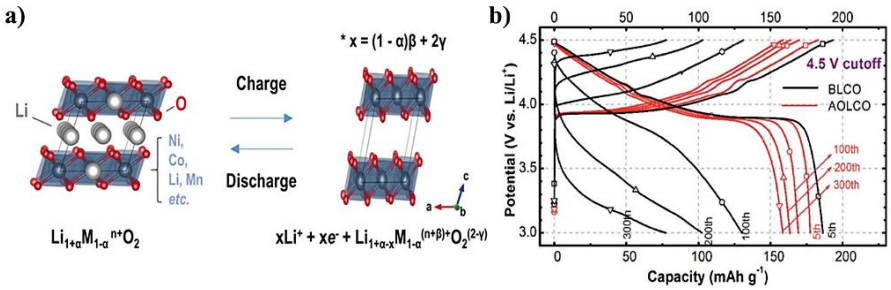

Figure 1. 14: a) Scheme for reaction mechanism of layered oxide (Li-rich) during charge-discharge. Reproduced with permission,[77] copyright 2020, Wiley. b) Charge-discharge Voltage-capacity plot of bare $LiCoO_2$ (BLCO) and Al_2O_3 coated $LiCoO_2$ (AOLCO) at the cut-off voltage of 4.5 V for 5th, 100th, 200th and 300th cycle, respectively. Reproduced with permission,[87] copyright 2017, RSC.

Nickel based $LiNiO_2$, which is less expensive and toxic than $LiCoO_2$, shows superior capacity of 240 mAh g^{-1} than former.[88] While it did not gain much popularity owing to the synthetic challenge of cation mixing and higher thermal instability at low temperature.[89,90,91] Similar kind of material owing to Manganese, $LiMnO_2$ was also bet upon due to their lower toxicity and cost than oxides of Co and Ni. Although, it was found be thermodynamically unstable as explained by Jahn-Teller effect which leads to the distortion of its structure to less symmetrical orthorhombic. The underlying issues were addressed by employing surface coating, doping, size control, and modifying synthetic routes. For instance, surface coating by Al_2O_3 (evidenced in

Figure 1.14b), ZrO_2, SiO_2, $LiWO_4$ was observed to improve the performance of the LMO_2 (M~ Ni, Co, Mn) layered materials.[87,92,93,94,95,96]

1.3.1.2 Layered Ternary metal oxides

Following the pursuit of metallic oxides with lithium, development of ternary metal oxides paved the way for researchers with aim to overcome the underlined issues with $LiMO_2$. The idea to introduce elements like Cobalt, Nickel, Manganese, Aluminium *etc*. led to the development of $LiM_xM_yO_2$ and $LiM_xM_yM_zO_2$. For example, Ni-rich, $LiNi_{1-x}M_xO_2$ with M= Ni, Co, Mn, Al are well investigated to exploit the synergy of the ternary metal structures (Figure 1.15a). Similar to the layered materials, they also fall in the category of 2D transport of Lithium with oxygen dumbbell hopping (ODH) and tetrahedral site hopping (TSH) mechanism in particular.[97] $LiNi_{0.5}Mn_{0.5}O_2$ containing less toxic metal than Co, was believed to have a capacity of ~280 mAh g^{-1} by preventing Jahn-Teller distortion due to Mn^{+4} and cation mixing of Li^+/Ni^{+2}.[98, 99] However, with $LiM_xM_yM_zO_2$, the existing issues were reduced even further including the stability, safety, capacity and cost that than $LiM_xM_yO_2$.

Among the family of $LiM_xM_yM_zO_2$, two major commercialized ternary metal oxides are $LiNi_xCo_yMn_zO_2$ (NCM) and $LiNi_xCo_yAl_zO_2$ (NCA) that can deliver as high capacity as >200 mAh g^{-1} when charged up to 4.6 V vs. Li/Li^+.[100,101] The Mn and Al ions improve the structural stability and lowers the cost while Ni allows for a high Li extraction and provides a high capacity. Co ions prevent Ni from occupying the Li sites for assuring lower irreversible capacity loss. Some formulation for NMC and NCA such as 3:3:3, 5:2:3, 6:2:2 or 8:1:1 and 0.8:0.15:0.05, respectively are depicted in Figure 1.15b. It is clearly indicative that the specific capacity and capacity retention is dependent on Ni-content for both NCA and NMC.[102]

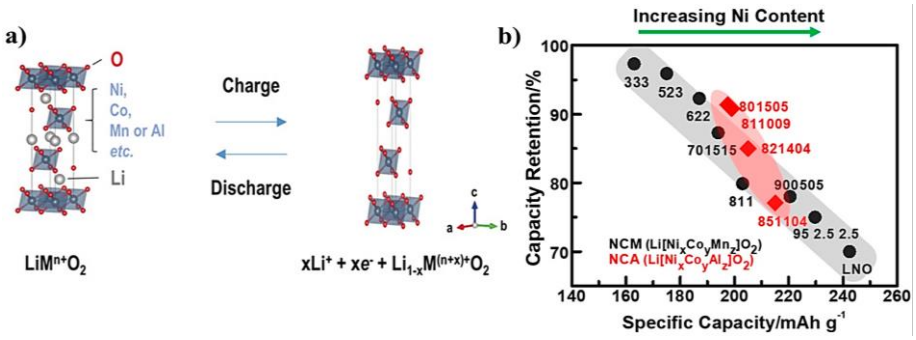

Figure 1. 15: a) Scheme for reaction mechanism of layered oxide (Ni-rich). Reproduced with permission,[77] copyright 2020, Wiley. b) Specific capacity (mAh g^{-1}) versus capacity retention over 100 cycles (%) plot of various layered NCM and NCA cathodes showing the trade-off between stability and capacity for increasing Ni content. Compounds are labelled by their composition (Ni, Co, Mn) = x:y:z. Reproduced with permission,[102] copyright 2020, MDPI.

Some of their degradation factors are high-temperature storage,[103] high voltage operation[104] and long-term cycling that result in transition-metal dissolution and surface reconstruction. The surge in the demand of E-vehicle is speculated be met significantly with layered ternary metal oxides such as NMC and NCA due to their relatively high performance with merits highlighted above.[84]

1.3.1.3 Spinel structures

Lithium manganese oxide, $LiMn_2O_4$, is another transition metal oxide, developed by Goodenough and co-workers in 1983.[69,105] It is relatively more environmentally friendly, low cost and offers higher thermal stability. The cubic spinel structure with 3D MnO_2 host and Mn vacancies facilitates transport of Li through 3D diffusion channel (Figure 1.16a and 1.16b). Thanks to its active diffusion channel, it offers good rate capability, high cycle with a theoretical capacity of ~148 mAh g^{-1} practically achievable up to 120 mAh g^{-1}. The higher cut-off voltage (> 4 V) also makes it interesting for its high-power demand application (Figure 1.16c). The common issue with it is a dissolution of Mn^{+3} also called the Jan-Teller effect, which leads to irreversible structural transformation and thus capacity loss.[84] In order to improve their properties, often dopants are introduced within a spinel framework, denoted as $LiM_{0.5-x}Mn_{1.5+x}O_4$ (M=Al, Ti, Cr, Fe, Co, Ni, Cu, and Zn *etc*.).[106, 107] Ni-dopant have successfully resulted in high capacity for ordered spinel $Li_xNi_{0.5}Mn_{1.5}O_4$ ($P4_332$) and disordered spinel $Li_xNi_{0.5}Mn_{1.5}O_{4-\delta}$ (Fd3m).[32]

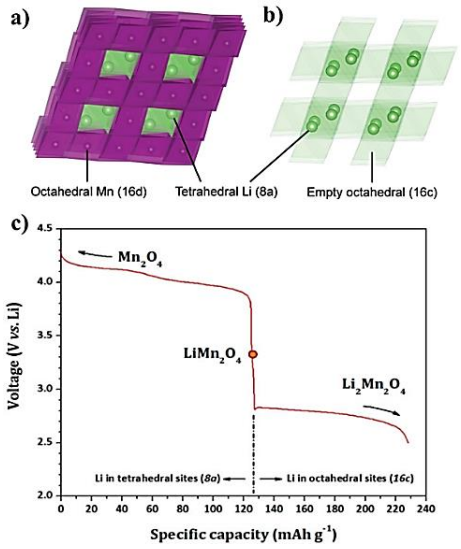

Figure 1. 16: a) Crystal structure and b) Li^+ diffusion channel of $LiMn_2O_4$. Reproduced with permission,[108] copyright 2020, Nature. c) Voltage profile of $LiMn_2O_4$ during lithiation and delithiation. Reproduced with permission,[109] copyright 2013, ACS.

The $Li_xNi_{0.5}Mn_{1.5}O_4$ shows one dominant plateau at 4.7 V instead of two plateaus between 4 and 5 V for $LiMn_2O_4$, which makes them a superior candidate.

1.3.1.4 Polyanionic cathodes

Cathodes with the tetrahedral polyanion structure unit $(XO_4)^{n-}$ and $(X_mO_{3m+1})^{n-}$ (X= P, S, As, Mo or W) covalently bonded with MO_x (M = transition metal) are referred as polyanionic cathodes. For example, NASICON, Olivine, tavorite, silicate *etc*, are well known investigated system in this category (Figure 1.17). They possess higher thermal stability than conventional layered materials because of strongly linked oxygen and gained popularity in real battery application due to their lower cost, sustainability and safety. Among various classes of polyanionic cathodes, we have discussed some commonly known ones namely, NASICON, phosphates and silicates as highlighted in recent reviews.[110-112] Phosphate-containing polyanionic cathodes shows ordered olivine structure and are often denoted as ($LiMPO_4$, with M = Fe, Mn, Co or Ni) as indicated in Figure 1.18a.[113-115]

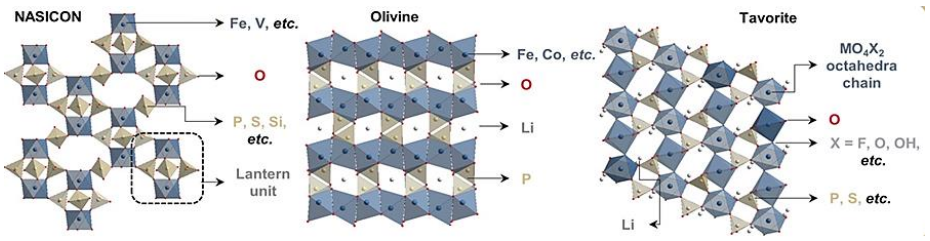

Figure 1. 17: Illustration of crystal structure of polyanion cathodes such as NASICON, Olivine and Tavorite. Reprinted with permission,[77] copyright 2020, Wiley.

Triphylite Lithium ferrophosphate is one of the popular commercial cathode materials which is based on low-cost iron. Coincidently, this is also credited to the Nobel Prize winner Goodenough's research group effort in 1997.[105] It attracts a lot of attention due to its lower toxicity, safety, high theoretical capacity (170 mAh g^{-1}) at moderate current densities, stable $Fe^{3+/}Fe^{4+}$ redox potential of 3.5 V vs. Li^+/Li, higher thermal, electrochemical and chemical stabilities and properties.[116] It is crystallized into distorted hexagonal close packed oxygen atoms with two existing phases, $LiFePO_4$ and $FePO_4$, whose interface motion is led by intercalation and de-intercalation of the Li^+. $LiFePO_4$ has been limited to low power application, which is explained by its ability to sustain applied current the moment the surface area of the interface reaches the critical surface area upon one dimensional (zigzag route) lithiation.[105] Its performance is affected by the electrochemical potential, operating temperature, and particle size, electronic and ionic conductivity.

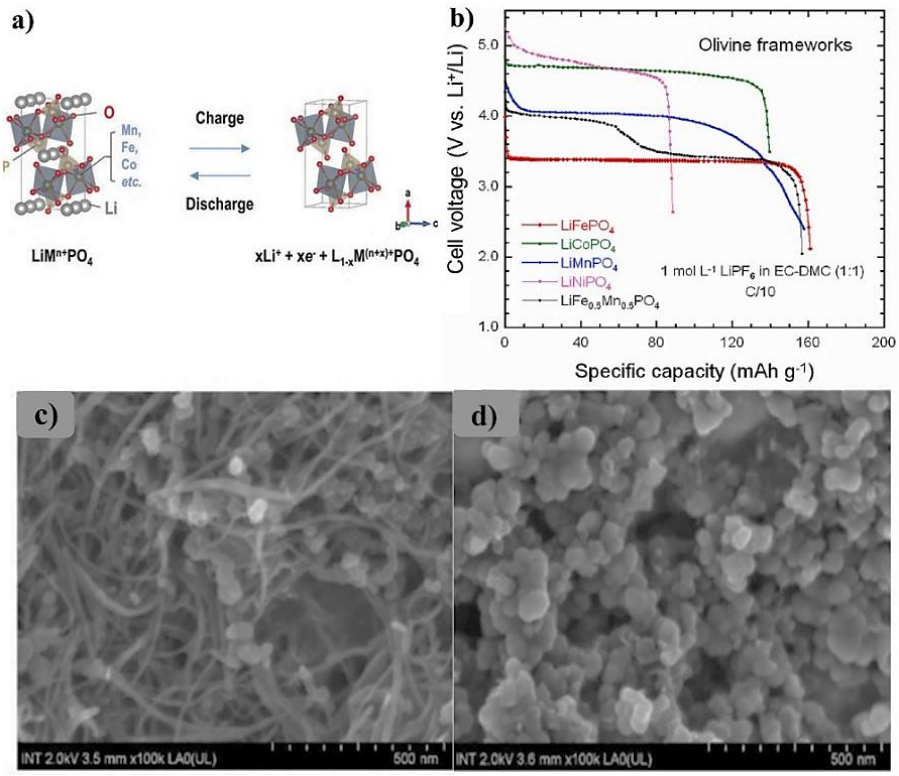

Figure 1. 18: a) Scheme for reaction mechanism of olivine cathode following charge-discharge. Reprinted with permission,[77] copyright 2020, Wile. b) Discharge profiles of $LiMPO_4$ (M = Fe, Mn, Ni, Co) olivines and $LiFe_{0.5}Mn_{0.5}PO_4$ solid solution as cathodes of Li-ion batteries (Voltages were measured in half cells versus lithium metal). Reproduced with permission, copyright 2018, MDPI. SEM images of LFP samples (c) LFP-CNTs and (d) LFP-C65. Reproduced with permission,[117] copyright 2023, Wiley.

Some reports suggest that an LFP based battery performs better at room temperature than higher temperature (higher than 55 ^oC) which was explained by the increased inter-surface layer thickness and accelerated electrolyte decomposition at higher temperature resulting in the loss of Li^+ and thus capacity fading.[118, 119] Another challenge related to the lower conductivity of LFP has also been well looked at by dopants, smaller size LFP, carbon composites like CNT, C65 (SEM images of LFP-carbon composites as in Figure 1.18c and 1.18d) or shortening the ionic and electronic diffusion.[120, 121,122, 123] Other $LiMPO_4$ like $LiMnPO_4$, $LiCoO_4$ and $LiNiPO_4$ were also seen as attractive cathodes due to their higher electrode voltage of 4.1 V, 4.8 V and 5.1 V, respectively (as compared in Figure 1.18b).[124, 125] Despite higher potential andspecific capacity (170 mAh g^{-1}), $LiMnO_4$ could not beat $LiFePO_4$ owing to its poor conductivity and distortion by the Jahn-Teller effect.[126] While $LiCoPO_4$ and $LiNiPO_4$

are potential candidates which need to be more investigated, but are limited due to lagging research in the electrolyte with higher ESW (>5.1 V). [127, 128]

Addition of a higher electronegative element, Fluorine, to the phosphate led to the discovery of fluorophosphates which were aimed to increase the cathode potential and hence energy density. $LiVPO_4F$ isostructural with $LiFePO_4.OH$[129] demonstrated 4.2 V (V^{+3}/V^{4+}) of potential, 0.3 V higher than $Li_3V_2(PO_4)_3$ with a theoretical capacity of 156 mAh g^{-1} at lower current rate.[130] Moving further, lithium rich $Li_5(VPO_4)_2F_2$ was also synthesized with improvement in the potential and capacity to 4.65 V and 170 mAh g^{-1}, respectively.[130]

Other fluorophosphates denoted as Li_xMPO_4F (x=1, 2 and M= Co, Ni, Fe) have also been looked upon actively uncovering the dissimilarity in the structures. Tavorite belonging $LiFePO_4F$ was limited to 3 V while Li_2CoPO_4F and Li_2NiPO_4F have shown excellent potential of 5.0 V and 5.3 V, respectively with theoretical capacity of 310 mAh g^{-1} via two Lithium exchange.[131, 132] While the commercial electrodes discussed above as shown in Figure 1.19 with their comparative crystal structure and voltage plateau, pave the way for next generation cathodes, it's equally important to address the drawbacks in the existing ones. Nevertheless, early findings hint towards potential improvement overdue because of doping, composites and structural modification.

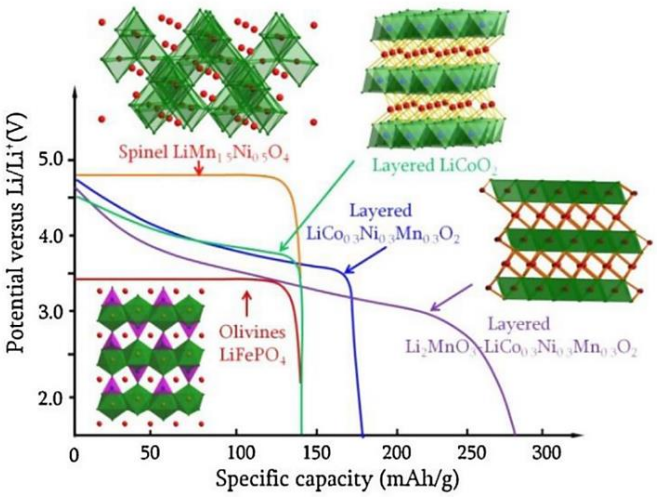

Figure 1. 19: Comparison among cathode materials of different crystal structures, showing the relationship between crystal structure and slope of the voltage plateau. Reproduced with permission,[133] copyright 2016, Elsevier.

1.3.1.5 Other inorganic cathodes

Besides phosphates, Sulphur was neither left to be explored as polyanionic cathodes. By replacing $(PO_4)^{3-}$ with $(SO_4)^{2-}$ and attaching an electronegative F^-, $LiMSO_4F$ (M= Fe, Mn, Co) was developed by Tarascon and co-workers.[134] It was demonstrated that $LiFeSO_4F$ resembles Tavorite like structure with 3.6 V and 156 mAh g^{-1} of theoretical capacity, higher ionic conductivity and similar electronic conductivity as of $LiFePO_4$. Moreover, its thermal stability is at good compromise compared to other fluorophosphates, $LiNiSO_4F$ (350 °C) < $LiCoSO_4F$ (375 °C) < $LiFeSO_4F$ (400 °C) < $LiMnSO_4F$ (600 °C).[135, 136]

Another interesting class of high voltage cathode is based on orthosilicates, Li_2MSiO_4 (M = Fe, Mn, Co, Ni) which gained popularity with an idea to increase the number of reversibly exchanged lithium ions in the cell reaction.[110] Its structural similarity points to $LiPO_4$, distorted hexagonal close packing with temperature and pressure dependent polymorphism.[137] With theoretical capacity of ~333 mAh g^{-1}, Li_2MSiO_4 based on manganese and iron are more attractive than Ni and Co when it comes to the cost, safety and stability. They possess poor intrinsic conductivity and structural instability like $LiMPO_4$, leading to capacity loss. However, second lithium redox occurs at higher potential which is limited by the narrow ESW electrolytes.[138, 139]

As far as the weight of polyanion is concerned, borate $(BO_3)^{3-}$ has been considered as an interesting choice due to its lighter weight. $LiMBO_3$ (M= Mn, Fe, Co) were investigated as cathodes with larger emphasis on $LiFeBO_3$.[140, 141] Both $LiCoBO_3$ and $LiFeBO_3$ show structural similarity with 3D distorted hexagonal closed- packed while h-$LiMnBO_3$ mimics $LiCdBO_3$. Iron-based borate, $LiFeBO_3$, was observed to deliver reversible capacity of 200 mAh g^{-1} with potential of 3 V versus Li and higher rate capability even at fast current rate.[127] The major issue accompanying borate is the surface poisoning against the ambient atmosphere.

Given all these insertion cathode materials, there has been a constant buzz for the conversion cathode materials. Unlike the former, their crystal structure continuously undergoes bond breaking and formation because of electrochemical cell reaction. The advantage in inexpensive conversion cathode lies in its ability to engage more than one lithium ion, leading to higher charge density. Most explored among them include metal chalcogenides and metal halides for their theoretical capacity as high as 1675 mA h g^{-1} and 713 mAh g^{-1} with potential upto ~ 2.3 V and ~4.0 V, respectively as highlighted in various reviews and Figure 1.20a and 1.20b.[142,143] However metal fluoride beats the metal sulphides and others due to their higher discharge potential and capacity. While there are some hurdles in its commercialization like its low conductivity, voltage hysteresis, volume change, loss of active materials,

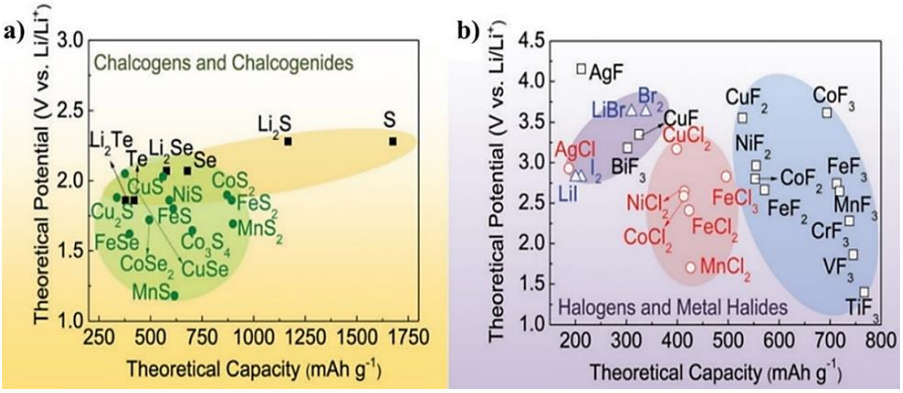

Figure 1. 20: Theoretical gravimetric and volumetric capacities with theoretical potential of selected conversion cathode materials, a) chalcogens and chalcogenides, and b) halogens and metal halides. Reproduced with permission,[142] copyright 2017, RSC.

a result of dissolution, which leads to poor reversibility, lower coulombic efficiency and huge capacity loss.[131, 132] Nevertheless, simultaneous approaches have been explored to avoid the highlighted issues via making composites, modifying particle size, developing compatible electrolytes and adapting the cell operational configuration and components.[144, 145] Globally, the challenges in understanding these materials and the path to achieve their best performance are still underway and positively predicted.

1.3.1.6 Organic and bio-based cathodes

Organic materials are always riveting owing to their environment friendly, cost, abundance, safety, structural tunability and high theoretical specific capacity. Tracing back to their concept development in 1970 with $(CF_x)_n$–Li compounds, they have been overshadowed by inorganic cathode materials for many years.[146] Based on their structural distinction, they are categorized into conductive polymers,[147] carbonyl conjugated compounds,[148] imine compounds,[149] organosulfur compounds[150] and oxynitride radical compounds (Figure 1.21).[151] Each of these suffers from certain issues. Conductive polymers (polypyrole, polyaniline) activated by dopants still perform poorly due structural instabilities. Organosulfur compounds, despite having higher specific capacity, suffer from insulation of sulfur and polysulfide dissolution, resulting in worse cycling in addition to their sluggish electrochemical processes.[140, 141]

The first nitroxyl radical polymer, poly(2,2,6,6-tetramethyl-1-piperidinyloxy-4-yl methacrylate) (PTMA) gave hope due to its fast kinetics of transfer of electrons to polymer chain and free radical to participate in highly reversible cell reactions. However, it offers less specific capacity due to high mass polymer chains and side groups.[152, 153] The imine group with its nitrogen as redox active center has been

investigated as well in the last two decades with promising high theoretical capacity (420 mAh g^{-1} for 2D triqui-noxalinylene (3Q) compound).[154] However, low conductivity and dissolution of active materials lead to poor capacity retention.

In an interesting development, covalent organic frameworks were developed supporting superior cycling with defined channels for the conduction of Li^+ ions and avoiding the dissolution.[155] Carbonyl conjugated compounds contain contain multiple functional carbonyl groups in conjugation which drive fast redox kinetics and thus higher capacity.[156-158] Most investigated systems include quinone, acid anhydride and imide derivatives like benzoquinone (BQ, 496 mAh g^{-1})[146, 159] perylene tetra-carboxylic dianhydride (PTCDA, 273 mAh g^{-1})[160] and pyromellitic diimide lithium salt (Li_2–PMDI~220 mAh g^{-1}).[161] PTCDA is a well-studied molecule whose many

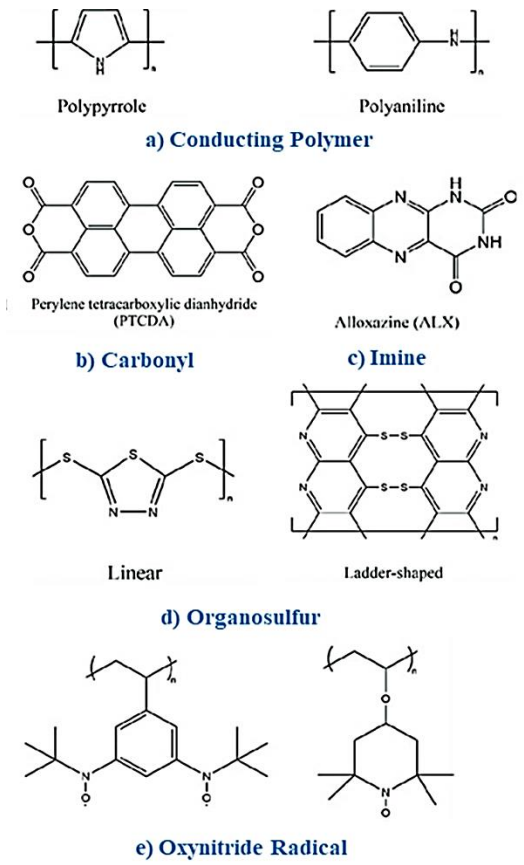

Figure 1. 21: Molecular structures of selected typical organic cathode materials for LIBs, a) conductive polymers, b) carbonyl compounds, c) imine compounds, d) organosulfur compounds, and e) free radical polymer compounds. Reproduced with permission,[162] copyright 2021, Wiley.

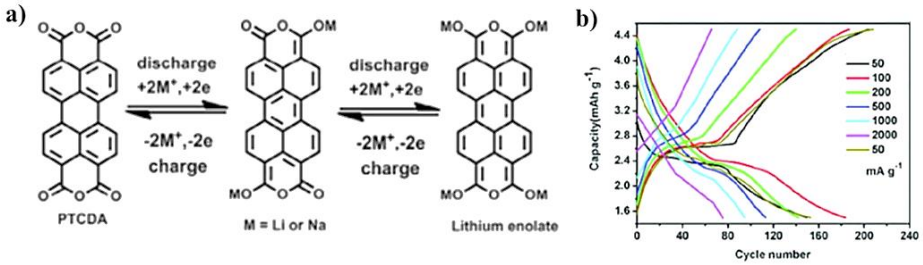

Figure 1. 22: a) Electrochemical redox reaction mechanism of perylene tetra-carboxylic dianhydride (PTCDA), and b) Galvanostatic charge–discharge curves of PGC40 (PTCDA/graphene aerogel composite) at different current densities. Reproduced with permission,[163] copyright 2018, ACS.

variants have been reported due its voltage tenability and satisfactory charge density as shown in Figures 1.22a and 1.22b. The holy grail to develop a superior organic cathode highlights on overcoming the underlying issues like low conductivity, solubility issue, lower potential than their counterpart. [156, 164, 165]

1.3.2 Negative electrode/Anode

The negative electrode of a lithium battery is also referred as anode, which is equally crucial for the overall performance of a battery. The development in the cathode materials has been fructuous and led to a series of breakthroughs, while it was not the case with anode materials. The lack of electrolyte understanding and its compatibility with anodes were a major hurdle in developing a desired material. Early studies found carbonaceous material as one of the potential candidates with capacity limited to its theoretical value around 372 mAh g^{-1}, corresponding to the stable LiC_6 phase. At that prospect, there has been a different class of materials developed so far for high-capacity batteries, as depicted in Figure 1.13. In order to commercialize an anode material, low cost, highly safe, low potential, high capacity, long cycle life and easy recyclability are key requirements. Figure 1.23 shows the classification of materials based on the lithiation-delithiation/electrochemical reaction at the anode, namely intercalation/insertion compounds, conversion compounds and alloy compounds. The volume expansion is one of the major hurdles that limits the use of many high capacity metal-based anodes. In the following section, a variety of anode material is briefly explained with their merits and challenges encountered with the possible solutions.

1.3.2.1 Insertion/Intercalation anodes

Insertion/extraction mechanism:

$$MO_x + yLi^+ + ye^- \leftrightarrow Li_yMO_x$$

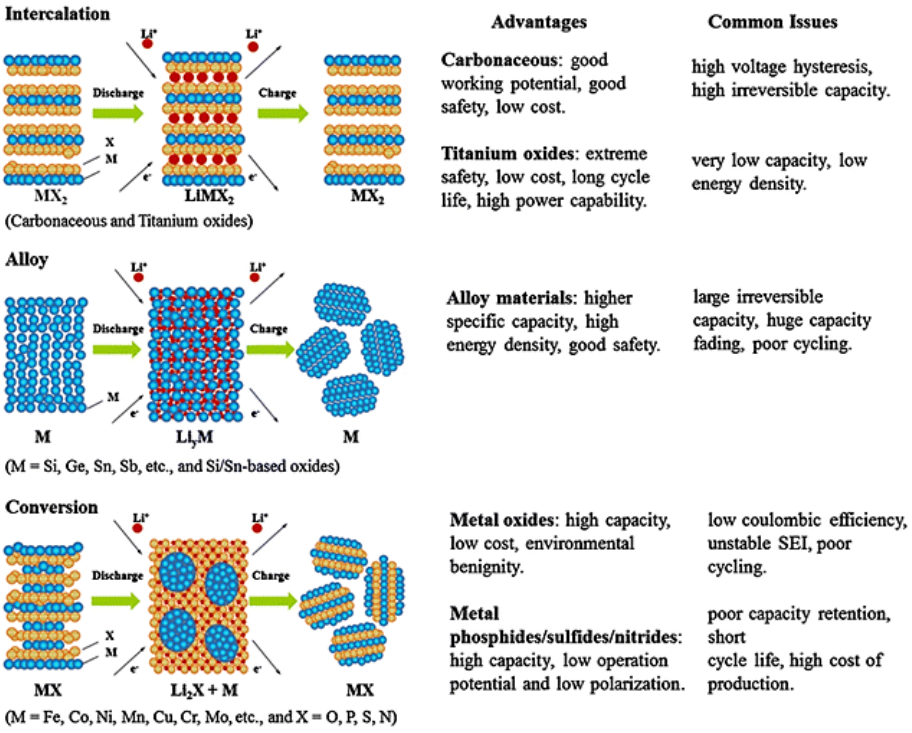

Figure 1. 23: Schematic illustration of different types of anodes based on the lithium storage mechanism with their advantages and issues encountered. Reproduced with permission,[166] copyright 2018, Springer.

Similar to layered cathode materials, here also lithium ions shuttle into the layered structure of the anode in a guest-host pattern following cell reaction above. Graphite was the first established carbon layered material, as depicted in Figure 1.24a, for the intercalation of 1-Li^+, forming LiC_6 with 0.2 V (vs. Li/Li^+), 372 mAh g^{-1} and 735 mAh cm^{-3} of theoretical and volumetric capacity, respectively.[167] It was commercialized later than coke carbon, which recorded 1.0 V vs. Li/Li^+ and < 250 mAh g^{-1} (Figure 1.24b). Carbon atoms are arranged in hexagonal rings largely within two stacks AB (hexagonal) and ABC (rhombohedral) in graphite.[168, 169] It is reported that Li-ion can easily be inserted from edge plane along with a layer spacing change i.e. from 0.3354 nm to 0.3720 nm.[170] It faces exfoliation with certain electrolytes, which leads to formation of various modified graphitic materials like inter-layered tuned graphite, element-doped graphite (boron, nitrogen, fluorine, sulphur), few layered graphite, graphene, *etc*. All these developments led to the better understanding of graphite and its failure to achieve its target capacity with modified structure and materials.[171, 172]

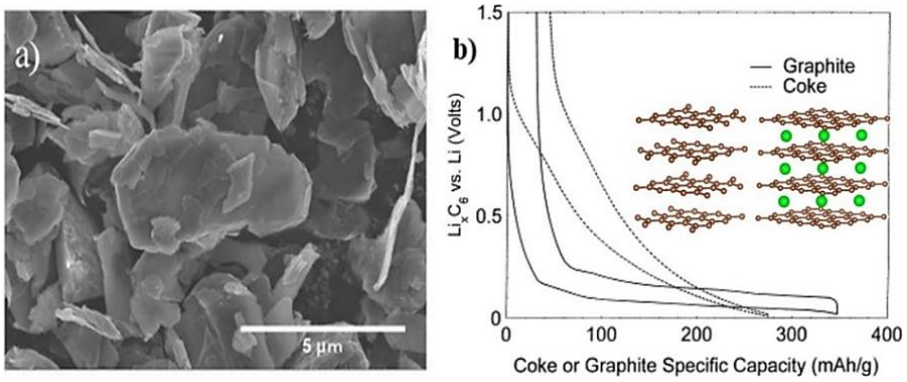

Figure 1. 24: a) SEM image of pristine graphite electrode. Reproduced with permission,[173] copyright 2017, Nature. b) Voltage profiles of graphite and coke material depicting lithium insertion voltage (Data were collected using a carbon/lithium foil half-cell with EC:DMC (2:1 w/w) and $LiPF_6$ lithium salt recorded at slow rate, Inset: Graphite with and without lithiation kinetically determined phase transition from stage II (LiC_{12}) to stage I (LiC_6) in a graphite anode for Li-Ion batteries). Reproduced with permission,[174] copyright 1998, Elsevier.

But later with the development of electrolytes, the co-intercalation was avoided and it has demonstrated to deliver reversible capacity as much as theoretical capacity. While graphite is cheap and offers good capacity, the next step remains focused toward its faster capability. Besides carbonaceous materials, inorganic layered compounds have been also a key player in anode development. Spinel resembling lithium titanate oxide, $Li_4Ti_5O_{12}$ (LTO) is one of the popular known anode materials for its higher safety, fast rate capabilities and cycle life over graphite despite offering lower capacity of ~175 mAh g^{-1}.[175, 176] Sun and coworkers synthesized micron secondary nano primary LTO/ MSNP-LTO particles as shown in SEM image, Figure 1.25a. The delithiation occurs at ~1.55 V vs. Li/Li^+ which restricts Li- plating and formation of SEI and thus no parasitic reaction at interface. The structural integrity remains almost the same without much volume change up to insertion of 3 Li^+.[84] Its spinel structural framework allows lithium to diffuse faster in charge and discharge state (Figure 1.25b).

However, LTO possesses a very low intrinsic conductivity (10^{-13} S cm^{-1}) which requires a synthesis of its carbon composite, ion doping or modification of surface.[167, 177, 178] Doping with chromium and niobium to form LiCrTiO and $TiNb_xO_{2+2.5x}$ has been actively studied which recorded remarkable structural stability, high potential (1.0–2.0 vs. Li/Li^+) and higher theoretical capacity due to multiple redox couples.[179] Nevertheless, conductivity for TNO is also low which prospected its composite development like TNO based on CNT or graphene delivering outstanding cycling even at 30C.[180] Superior to LTO, Li_3VO_4 (lithium vanadate oxide) is also an

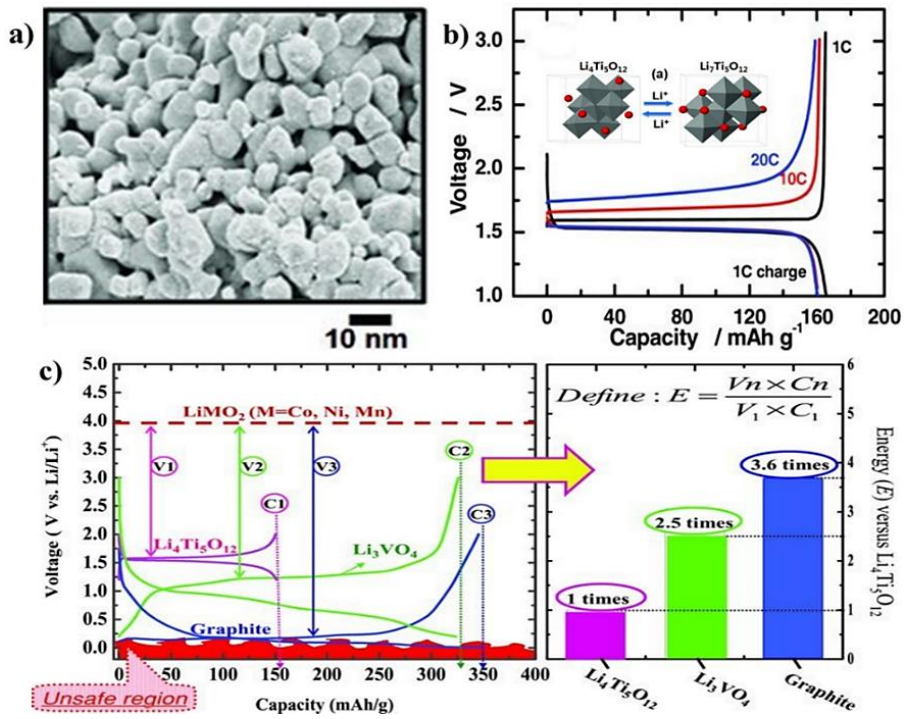

Figure 1. 25: a) SEM image of MSNP-LTO showing secondary and primary particles under high magnification, b) Voltage-capacity profile of MSNP-LTO in halfcell from 0.2-C rate to 1-C rate. Inset: Structure of $Li_4Ti_5O_{12}$ and $Li_7Ti_5O_{12}$, showing no volume change after charge and discharge. Reproduced with permission,[176] copyright 2010, Wiley. c) The comparison of Li_3VO_4 with two typical insertion anodes, $Li_4Ti_5O_{12}$ and graphite in reference to intercalation potential, specific capacity and energy density, reproduced with permission,[181] copyright 2013, Wiley.

eye-catching material with intercalation voltage between 0.5-1.0 V and high theoretical capacity of 394 mAh g^{-1} whose comparative plot is shown in Figure 1.25c with LTO and graphite.[181] It behaves as a solid ionic conductor existing in several polymorphs.[182, 183] Although it delivers double reversible capacity of LTO, certain parameters like electronic conductivity need to be addressed by smaller particle size and developing composites for lower polarization, higher cycling with less irreversible capacity loss.[181]

1.3.2.2 Alloying anodes

Given the safety, lower capacity and potential of lithium deposition in graphite, alloy anode was looked upon as an appealing choice. Alloys consisting of aluminium, antimony, magnesium, tin, silver, silicon and those belonging to IVA and VA groups find their potential reactions with lithium as anode materials.[184, 185] They possess the ability to hold 3-4.4 lithium per metal atom, marking their capacity and onset voltage

higher than conventional intercalation anodes, especially carbon-based (Figure 1.26a).

They undergo alloying reaction, as indicated below to form Li_zM ($z > 1$) which could be divided into addition and displacement reaction.Addition reaction is termed for pure metals or their composites with inert metal, while displacement reaction corresponds to an extra step of decomposition to the addition reaction. Li-alloy reaction mechanism:

$$M_xO_y + 2yLi+ 2ye^- \rightarrow xM + yLi_2O$$

$$M + zLi^+ + ze^- \leftrightarrow Li_zM$$

Silicon, which is one of the most desired elements in the semi-conductor industry, is a potential candidate due to its highest theoretical capacity of 3580 mAh g^{-1} at room temperature for $Li_{15}Si_4$.[186] As a result of intercalation and deintercalation (< 1.0 V *vs.*

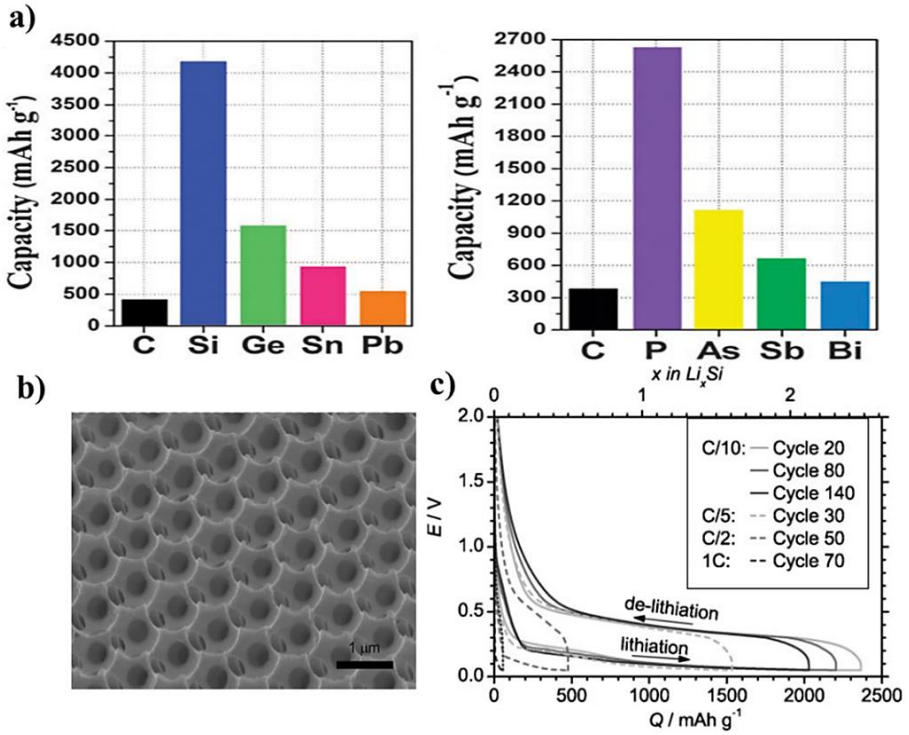

Figure 1. 26: a) Gravimetric capacities of IV group elements C (LiC_6), Si ($Li_{4.4}Si$), Ge ($Li_{4.25}Ge$), Sn ($Li_{4.25}Sn$), and Pb ($Li_{4.25}Pb$) and V group elements P (Li_3P), As (Li_3As), Sb (Li_3Sb), and Bi (Li_3Bi), respectively, reproduced with permission,[187] copyright 2010, RSC, b) SEM image of 10 µm a-Si:H film templated from 890-nm pre-sintered silica microspheres; and c) Galvanostatic cycling of 10 µm a-Si:H film, reproduced with permission,[188] copyright 2009, Wiley.

Li/Li^+), it undergoes several phase changes from amorphous $Li_{3.75}Si$ to crystalline $Li_{15}Si_4$ and back-forth. This expansion and contraction contribute to more than ~400% of volume change, resulting in cracks, aggregation of active particles, electrolyte rupture, which eventually lead to the degradation in the performance of the cells.[189-191] Various morphologies subjected to size and surface area have been attempted to buffer the high strain for undisturbed lithium diffusion in addition to its composite or binary alloy.[192, 193] In a report, researchers synthesized hydrogenated amorphous silica from 890 nm microspheres as shown in the SEM image, Figure 1.26c. The electrodes delivered a high capacity of >2500 mAh g^{-1} during the first few cycles with better capacity retention of ~70% in compared to films prepared with smaller size microspheres.[188]

Tin and antimony are well explored metals for their alloying and intermetallic compounds owing to their high theoretical capacity of 959 mAh g^{-1} for $Li_{17}Sn_4$ and 660 mAh g^{-1} for Li_3Sb at suitable working potential.[194] Like silicon, Sn also forms many alloy phases with lithium namely Li_2Sn_5, LiSn to $Li_{17}Sn_4$ *etc.*[195] Despite achieving high experimental capacity of 940 mAh g^{-1} and 500 mAh g^{-1} with tin and antimony metal nanoparticles, their volume expansion limits performance over longer cycles.[196] Although, antimony suffers relatively lower change of ~135% than ~300% in case tin-based anodes. Factors like buffer coating layer, size and dimensionality control for binary intermetallic, oxides of metals and their composites have shown remarkable improvement in both reversible capacity and capacity retention.[197-199]

Other elements have also drawn research attention like bismuth and germanium analogous to popular silicon and tin. Germanium precedes over silicon for their better conductivity and 400 times higher diffusivity of lithium than Si with the capacity of 1568 mAh g^{-1} for $Li_{17}Ge_4$ at room temperature.[200] However, bismuth which resembles graphite in its pseudo-layer structure and capacity of 386 mAh g^{-1} offering less volume expansion of 74% due to formation of Li_3Bi.[201, 202] While there are hundreds of materials in this area of research, decade long progress suggests composites could lead the race of anode materials.

1.3.2.3 Conversion alloy anodes

Conversion type anode materials (CTAMs) are known for high theoretical capacity over a vast family of compounds due to the redox reaction of Li^+ and transition metal cations.[203, 204] Starting from metal oxides, CTAMs include nitrides, fluorides, phosphides, sulfides, selenides, tellurides *etc*,[205-207] They are generally cheaper at the cost of production due to their naturally occurring raw materials like MnO_2, Fe_3O_4, *etc*. They also possess lower intercalation potential than many other types of anodes, which limits the li-dendrite growth over the long cycles. This class of anode materials follows the two-reaction mechanism in combination of conversion and alloying as

highlighted in Figure 1.27a, such as, oxides, sulfides of Sn, Sb or Zn *etc*. Although, these compounds have lower intrinsic electronic and ionic conductivity which call upon the synthesis of a composite with conductor. As a result of redox reaction, the change in volume of the active materials could be seen as high as 200% including the decomposition of electrolyte. The reaction mechanism of conversion proceeds via cell reaction, as below, which suggests that the formation of Li_nX is thermodynamically feasible. The voltage hysteresis between charge-discharge due to the structural rearrangements results in lower round trip energy density efficiency and internal heat evolution.[208] This hysteresis depends on the nature of anionic species in CTAMs in order of fluorides > oxides > sulfides > nitrides > phosphides.[203, 208]

$$M_aX_b + (b\text{-}n)Li^+ + (b\text{-}n)e^- \leftrightarrow aM + bLi_nX$$

$$M_xO_y + 2_yLi^+ + 2ye^- \leftrightarrow xM + yLi_2O$$

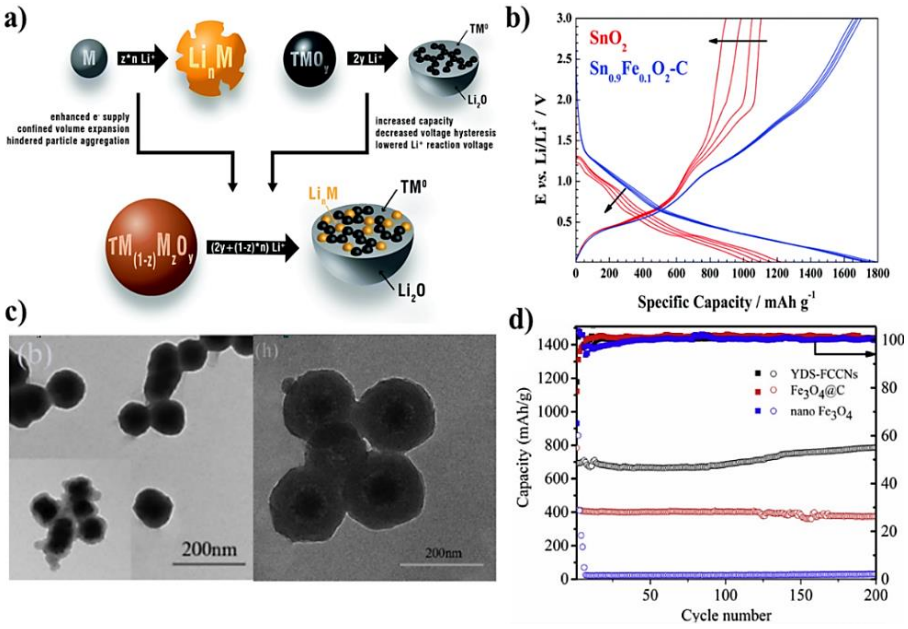

Figure 1. 27: a) Scheme for demonstrating the beneficial combination of conversion and alloying-type lithium storage in conversion/alloying materials (CAMs), reproduced with permission,[208] copyright 2016, RSC, b) Representative potential profiles (cycles 2–5) of alloying-type metal oxides (SnO_2 in red) and conversion/alloying-type binary metal oxides (carbon-coated $Sn_{0.9}Fe_{0.1}O_2$ in blue; reproduced with permission,[209] copyright 2015, Elsevier, c) TEM images of Fe_3O_4@C (left) and YDS-FCCNs (right); and d) Comparison in cycling stability of nano Fe_3O_4, Fe_3O_4@C and YDS-FCCNs at current density of 0.5 A g^{-1}, reproduced with permission,[210] copyright 2020, Elsevier.

There are some interesting approaches including nanostructures and porosity for reduced diffusion length, introducing multi-dimensional channels, coating/composites and other techniques, proving to be successful in mitigating the conductivity and volume expansion issues.[211-213] For example, combining iron oxide carbon composite to the tin oxide is a smart choice to curb the volume expansion and improve the capacity retention as demonstrated by Stefano *et al*.[209] in comparison of SnO_2 to carbon-coated $Sn_{0.9}Fe_{0.1}O_2$.

Among CTAMs, metal oxides are quite explored due to their non-toxic, low cost, high theoretical capacity and power density with cell reaction mentioned above. For instance, Fe_3O_4 gained quite an attention due to iron and it possesses higher theoretical capacity of ~926 mAh g^{-1}. However, it is gifted with intrinsic issues of conductivity and pulverization, which lead to rapid capacity fade. Carbon-based nanosphere of Fe_3O_4 was reported to deliver reversible capacity of 780 mAh g^{-1} at 0.5 A g^{-1} after 500 cycles.[214] Another carbon composite, named yolk-double shell Fe_3O_4@C@C nanosphere (YDS-FCCNs), was synthesized and compared with Fe_3O_4@C and nano Fe_3O_4@C for the cycling performance. The TEM image in Figure 1.27c. shows YDS-FCCNs with a diameter of 200 nm. On galvanostatic cycling at 0.5 A g^{-1} in 200 cycles, YDS-FCCNs delivered capacity > 700 mAh g^{-1} compared to <400 mAh g^{-1} and < 50 mAh g^{-1} after 200 cycles, respectively for Fe_3O_4@C@ and nano Fe_3O_4@C. Other popular layered materials which found their way are MoS_2, carbides, MXenes due to their higher reversible capacity and coulombic efficiency.

Metal phosphide has been exploited as well, such as Sn_4P_3, MnP, Cu_3P, FeP and amorphous phosphorous with carbon composites.[215,216, 217] They show working potential of ~1.2 V vs. Li/Li^+ and one of the report with amorphous phosphorous shows a carbon composite anode delivering 1950–2200 mAh g^{-1} for 100 cycles at 1000 mA g^{-1}.[218, 219]

Li-metal

One of the most explored anodes which has been looked with high hopes for more than 5 decades is pure Li-metal. Li metal offers super high theoretical capacity of 3860 mAh g^{-1} and a low potential (-3.04 V *vs.* standard hydrogen electrode/SHE). Based on the type of cathodes, lithium metal batteries can be divided into three categories: Lithium/lithium intercalation compounds, lithium/O_2, and lithium/sulfur batteries as represented in Figure 1.28.[220] The clean energy transition for mobility depends on a large supply of E-vehicles which has been betting on improving the performance of current LIB or lithium metal based solid state battery technology. With this, the energy density is expected to be more than double, 600 Wh kg^{-1} credited from their lightweight and high capacity. Although lithium metal limits its widespread market

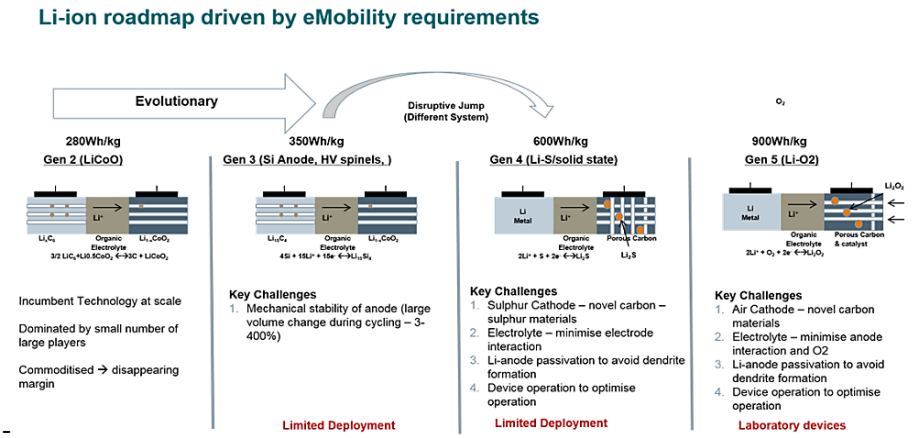

Figure 1. 28: A roadmap for lithium-based batteries for mobility applications highlighting drastic elevation on the use of Li-metal anode. Reprinted with permission from Siemens.[220]

application due to its high reactivity, dendrite growth, flammability and safety with state of art electrolytes.[221]

It undergoes infinite volume expansion with high decomposition of active lithium metal surface via electrolyte. The reduction of products at anode leads to the formation of SEI, an important component whose understanding came to existence quite later unfortunately (explained in subsequent section).[221, 222] One of the major issues, dendrite growth, challenges its safe operation with conventional liquid electrolytes. Various investigations uncovered the factors affecting dendrite growth, the nature of dendrite and methods to prevent them. It was revealed that, with larger overpotential, dendrites follow whiskers growth while surface growth is observed for lower potential as shown in Figure 1.29a.[223]

As recorded in ex-situ SEM (Figure 1.29c), Li-growth looks like islands due to larger nucleation sites at very low current densities while smaller nucleation sites and close packing in the dendrites were observed with an increase in current densities.[224] In absence of robust separator, dendrites are reaching the cathode and short-circuit the cells with possibility of other phenomena such aggravated adverse reactions and dead lithium, highlighted in Figure 1.29b.[221] Thermodynamically, it cannot be stopped and rather need to be prevented employing various techniques like introduction of additives, artificial coating and SEI, solid electrolyte, and 3D anode hosts, *etc*. which can also result in suppressing volume expansion.

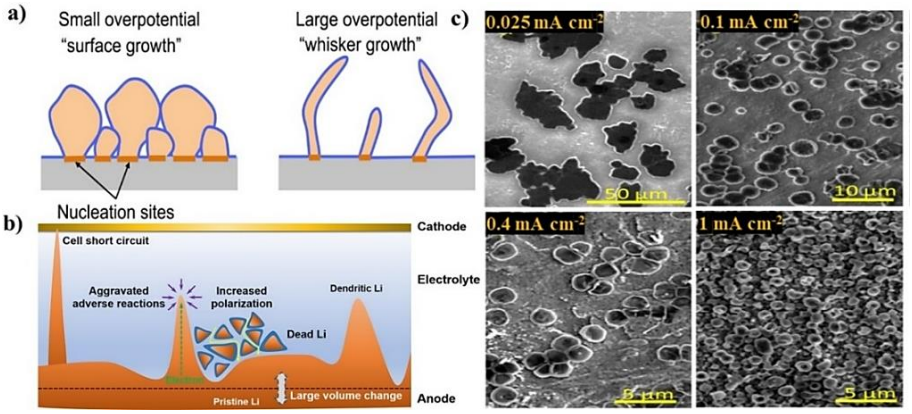

Figure 1. 29: a) Scheme of dendrite growth with overpotential. Reproduced with permission,[223] copyright 2017, Elsevier. b) Illustration of possible phenomena at the surface highlighting the dilemma for Li metal anode in rechargeable batteries. Reproduced with permission,[221] copyright 2017, ACS. c) SEM image of Li nuclei deposited at different current densities from 0.025 mA cm^{-2} on Cu electrode for an equivalent amount of total areal capacity of 0.1 mAh cm^{-2}. Reproduced with permission,[224] copyright 2017, ACS.

1.3.3 Electrolyte and its components

Transport channels for ions conduction and electrons insulation refer to the electrolyte which separates and integrates two electrodes at different potential. Electrolyte has always been underestimated since the beginning of the battery research, which resulted in a huge lag in understanding the challenges at the interface of an electrode-electrolyte. An electrolyte is the combination of salt and salt-containing host which change from one system to another, say liquid, gel or solid. Here, we are discussing the liquid electrolyte which has popularly been based on lithium salt and organic solvents such as carbonates, esters and ethers from early studies. Figure 1.30a shows a typical scheme of LIB shows typical scheme of LIB with an emphasis of electrolyte and its component.[225] For compatibility with other cell components, an electrolyte should comply with certain parameters/properties like, high ionic conductivity and dielectric constant, large electrochemical stability window, higher melting and vapor point, stable interface, lower flammability and chemical and electrochemical inertness to other cells constituents.[226] Nevertheless, these parameters don't guarantee an electrolyte to be an ideal candidate for batteries. Further, they need to show a higher transference number and diffusion coefficient, form stable interfaces, and show lower thermal degradation. Given the development in the cathode and electrodes, an electrolyte has been always subjected to scrutiny. For an instance, some high voltage cathodes (> 5 V) could not be exploited to their full potential due to the lack of high oxidative potential electrolyte. In this particular section, we will briefly discuss essential components of electrolytes and possible components which can overcome the underlying issues with electrolyte or originating from an electrode-electrolyte

interface. They particularly include solvents (organic and some inorganic element containing solvents), salts, additives and alternative ionic liquids.

1.3.3.1 Organic and other solvents

Solvent solvates the salt via weak coordination or covalent bonds facilitating ion-mobility and diffusion. An organic solvent is expected to have the following properties: 1.) safe and environment friendly 2.) high solvation of lithium salts which is directly related to the dielectric constant. 3.) low melting and high boiling point with good thermal stability, 4.) inertness to the cell components like electrodes, current collector, 5.) low viscosity for facile mobility of ions, 6.) broader ESW covering the range of cell components, 7.) good wettability and interface with ability

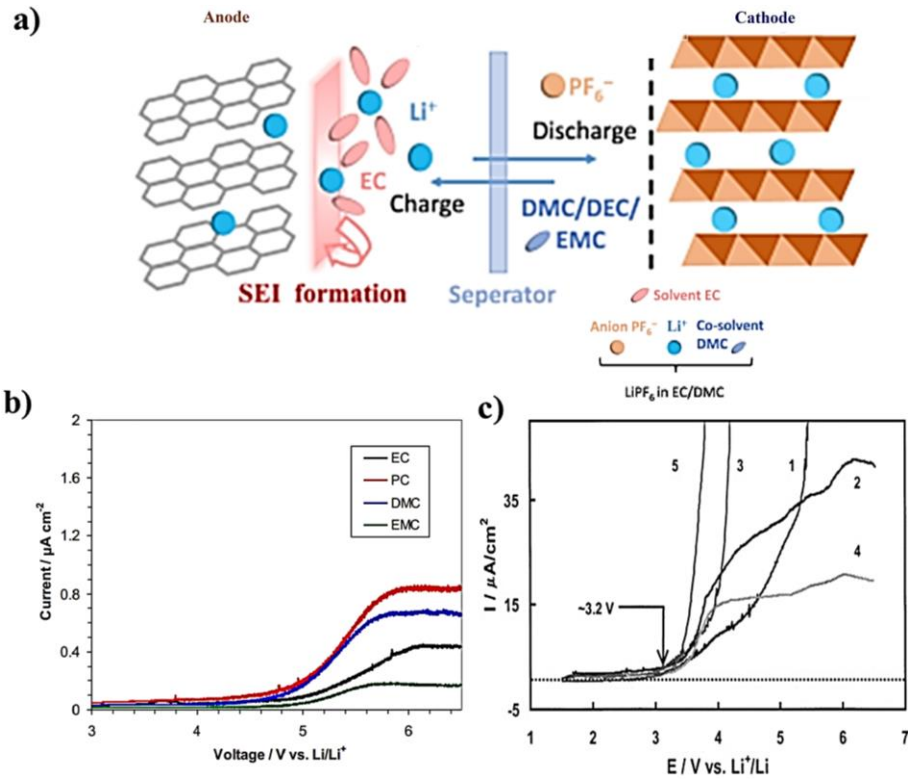

Figure 1. 30: a) Scheme depicting various components of electrolytes with electrodes, reproduced with permission,[225] copyright 2020, Nature. LSV curves of b) half-cells using electrolytes of 1.0 M $LiPF_6$ in carbonate solvents (EC, PC, DMC and EMC) at a scan rate of 0.1 mV/s with Al working electrodes. Reproduced with permission, [227] copyright 2012, Elsevier. c) half cells with Al in 1:1 EC/DME solutions with 1M of (1) $LiClO_4$, (2) $LiPF_6$, (3) $LiN(SO_2CF_3)_2$, (4) $LiBF_4$, and (5) CF_3SO_3Li from first sweep at 5 mV/s. Reproduced with permission,[228] copyright 2002, Elsevier.

for forming stable layer, i.e. SEI on electrodes and 8.) least flammable.[48, 49] Most commonly used solvents are organic-based aliphatic ethers, carbonates, *etc*. and some have been developed via incorporation of more electron-withdrawing substituents such as fluorine, cyano or sulfone groups, *etc*. The most widely used and still popular organic solvents are ethylene carbonate (EC) and propylene carbonate (PC) which are cyclic and offer high dielectric constant but higher viscosity compared to linear carbonates like dimethyl carbonate (DMC), diethyl carbonate (DEC) or ethyl methyl carbonates. Such linear carbonates provide lower viscosity hence higher mobility and conductivity of ions along with good compromise in thermal and chemical properties, refer their properties listed in Table 1.1.[48, 226, 229]

In addition to those characteristics, EC gained great attention due to its ability to form SEI film at the anode at the potential 0.8 V versus Li/Li^+ and 4.8 V versus platinum electrode on the cathode side via its decomposition at the interface.[227, 230] Figure 1.30b shows a comparative linear sweep voltammetry (LSV) plot for carbonate solvents with 1.0 M $LiPPF_6$ against Al-working electrode.[227] The oxidative potential with Al-substrate was found to be higher (> 5 V vs Li/Li^+) than the Pt-electrode for all the carbonates (slightly higher for EC and EMC). EC has comparatively lower ionic conductivity and higher melting point than PC, but still remains in utilization due to inability of PC to form stable film at the electrodes.[53] The mentioned challenges were addressed by forming the solvent blends by combining linear and cyclic carbonates to reach the compromise of viscosity and conductivity with good film formation.[48, 231] While ether-based solvents like 1,2-dimethoxyethane (DME), 1,3-dioxolane (DOL) show better reduction durability with good film forming capability with Li-metal anodes, they are prone to oxidation at lower voltage of < 4 V vs Li/Li^+,[232] which shifts more attention on carbonates and their derivatives.

Besides pure carbonates, electron withdrawing groups attached on organic solvents (e.g. fluorinated ethylene carbonate, FEC), have shown better properties concerning safety and SEI formation ability. The effect of the decomposed products from these electrons withdrawing group is discussed in more details in the SEI section. In line with similar research, other solvents like fluorinated carbamates[233] and sulfonamides,[234] fluorine sulfone derivatives[235, 236] nitriles[237, 238] are also widely studied owing to the need for high ESW electrolytes for high voltage cathodes in the market.

1.3.3.2 Lithium salts

The charge carrier availability for transport is governed by the dissociation of a salt in an organic solvent mixture. The state of an electrolyte is analyzed by the synergic effect and properties of salt and solvent mixture. Commercially, the most widely used

electrolytes are the mixture of EC with DMC, DEC or EMC with $LiPF_6$. The anions of the lithium salt play a crucial role as they undergo decomposition with anode and

Solvent	LUMO [eV]	HOMO [eV]	Melting point, T_m [°C]	Boiling point, T_b [°C]	Flash point, T_f [°C]	Dielectric constant, ε
EC (ethylene carbonate)	1.089	−7.924	36.4	248	160	89.78
PC (propylene carbonate)	1.112	−7.870	−48.8	242	132	64.9
DMC (dimethyl carbonate)	1.189	−7.718	4.6	91	0.76	3.11
DEC (diethyl carbonate)	1.254	−7.633	−74.3	126	31	2.81
EMC (ethyl methyl carbonate)	1.222	−7.675	−53	110	23	2.96
FEC (fluoro-ethylene carbonate)	0.696	−8.315	20	210	102	78.4
DME (1,2-dimethoxy ethane)	2.532	−6.695	−58	82.5	0	5.5
DOL (1,3-dioxolane)	3.049	−6.639	−97.2	75.6	1	6.74
TEGDME (tetraethylene glycol dimethyl ether)	2.186	−6.613	−45	216	106	7.9

Table 1. 1: Physical properties of some organic solvents commonly used in rechargeable lithium-ion batteries. Adapted with permission,[229] copyright 2000, Elsevier.

form components of SEI. Some of the well-known lithium salts known for their remarkable properties and observed to form better SEI are as follows: Lithium hexafluorophosphate ($LiPF_6$), lithium hexafluoroarsenate ($LiAsF_6$), lithium bis(trifluoromethanesulfonyl) imide ($LiN(CF_3SO_2)_2$/LiTFSI)), and lithium bis(oxalato) borate ($LiB(C_2O_4)_2$ /LiBOB) (Figure 1.31). Similar to organic solvent, any lithium salt should have: a) environmental benignity and safety, b) chemical inertness to the cell components except beneficial decomposition for SEI, c) thermal stability beyond the range of operational of electrolyte and battery, d) high dissociation into solvent and broader ESW of the anions for oxidation at cathode.[226, 239, 240] All these requirements clearly highlight the importance of a functional group at the anion which controls the quality of SEI. As mentioned above, $LiPF_6$ is a largely used lithium salt in commercial LIB because of its high dissociation in organic carbonates offering high ionic conductivity, good ESW and corrosion protection to Al collector by formation of (oxy-)fluoride layer. Besides beneficial properties, $LiPF_6$ is super sensitive to moisture forming HF while highly toxic products are formed by exposition to solvent and it does suffer from poor thermal stability (> 55 °C). These drawbacks motivated research in development of $LiBF_4$ provides excellent protection of Al-current collector but primarily lacks in conductivity due to poor dissolution in carbonate-based solvents.[241, 242] As far as moisture sensitivity is concerned, $LiClO_4$ is slightly air stable with good ionic conductivity, ESW and good passivation with Al collector. However ClO_4^- is highly oxidizing in nature and prone to heavy explosion if in contact with certain organic compounds in LIB.[243] Few recent studies are also focused on tris(pentafluoroethyl)trifluorophosphate (LiFAP) which is structurally related to $LiPF_6$ but yet superior in chemical and thermal stability due to stabilized phosphorous- fluorine bond.[244-246]

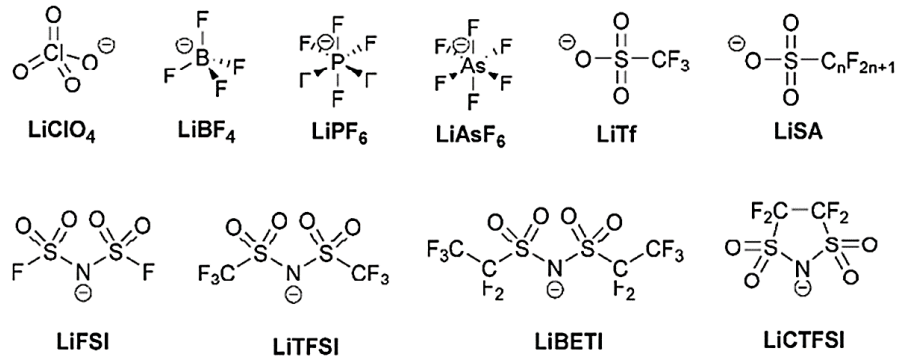

Figure 1. 31: Anion Structure of different lithium salts. Reprinted with permission,[247] copyright 2018, Elsevier.

Two other classes of salts which complete the discussion are chelating borate based lithium and imide based lithium salts. Lithium bis(oxalate)borate (LiBOB), is less toxic, relatively inert to moisture, thermally stable but less ionic conducting than $LiPF_6$.[248, 249] Other borate-based salts were also developed like lithium oxalyldifluoroborate (LiODFB), which offered better conductivity but lower thermal stability than LiBOB.[250, 251] Lithium salts based on imides are highly investigated and the most utilized salt after $LiPF_6$ with LiTFSI as the most representative example. LiTFSI not only offers excellent dissolution, relatively higher chemical and electrochemical inertness but also higher thermal stability.[48, 252, 253] However LiTFSI cannot form a passivation layer against Al–current collector corrosion which is its major drawback.[48, 254] Indeed, Figure 1.30c shows a clear Al dissolution for $LiClO_4$, CF_3SO_3Li, or $LiN(SO_2CF_3)_2$ much higher than for $LiBF_4$ or $LiPF_6$.[228] Subsequent efforts have been taken in playing around the anions with substitution of $-CF_3$ with F to form LIFSI, which resulted in preventing the release of highly toxic HF.[255] Other-imide based salt includes $LiN(SO_2C_2F_5)$ / (LiBETI),[256] (fluorosulfonyl)(nonafluorobutanesulfonyl) imide (LiFNFSI),[257, 258] lithium (fluorosulfonyl)(trifluromethanesulfonyl) imide/(LiFTFSI),[259, 260] and lithium (fluorosulfonyl) (pentafluoroethanesulfonyl)imide(LiFPFSI).[261] For instance, imides like LiBETI and LiFNFSI showed high thermal stability (> 220 ^oC) and ability to prevent anodic aluminum dissolution. Nevertheless, these lithium salts are still in their early phase investigations to match commercial ones.[262] Table 1.2[263] summarizes the qualitative comparison of fundamental properties of salts from best to worst.

1.3.3.3 Additives

Inherent issues with electrolytes require supporting materials, referred as additives, to stabilize the interface and avoid parasitic decomposition. In addition, they can induce interesting properties like flame retardant, over-charging control, *etc*.. The additives play a crucial role in controlling the SEI decomposition in LIB on longer cycling and

Properties	From best → to worst					
Ion mobility	$LiBF_4$	$LiClO_4$	$LiPF_6$	$LiAsF_6$	LiTf	LiTFSI
Ion pair dissociation	LiTFSI	$LiAsF_6$	$LiPF_6$	$LiClO_4$	$LiBF_4$	LiTf
Solubility	LiTFSI	$LiPF_6$	$LiAsF_6$	$LiBF_4$	LiTf	
Thermal stability	LiTFSI	LiTf	$LiAsF_6$	$LiBF_4$	$LiPF_6$	
Chem. inertness	LiTf	LiTFSI	$LiAsF_6$	$LiBF_4$	$LiPF_6$	
SEI formation	$LiPF_6$	$LiAsF_6$	LiTFSI	$LiBF_4$		
Al corrosion	$LiAsF_6$	$LiPF_6$	$LiBF_4$	$LiClO_4$	LiTf	LiTFSI

Table 1. 2: Comparison of fundamental properties of salts from best to worst. Adapted with permission,[263] copyright 2003, Elsevier.

thermal exposure. They are used in quantity less than 10%, beyond that they can be considered as co-solvents. For instance, FEC is used both as co-solvent and additive in electrolyte.[264, 265] They form a stable SEI layer beneath the one formed by decomposition of solvents. The characteristics HOMO and LUMO guide here in determining the role of additives towards SEI via reduction and oxidation potential analysis. Based on their working pathway, additives are identified as reaction-type and SEI-modifier as shown in Figure 1.32. As name suggests, reductive type has higher reduction potential than solvents in LIB and stabilizes SEI layer by discarding the intermediate reduction products of the solvent or incorporation into the films. On contrary SEI modifier in principle affects the thickness and composition of the SEI.[266] Some examples of reductive type additives include vinyl carbonate (VC),[267, 268] vinyl ethylene carbonate (VEC),[269] vinyl ethylene sulfite (VES),[270] FEC,[150,271] or TDI.[267] It has been demonstrated that even 2% Of VC or 0.5% of TDI could greatly enhance the LIB performance in addition to lowering the heat evolution. Anionic receptor like tris(pentafluorophenyl)borane (TPFPB) is an example of SEI modifier additive which can dissolve the species F^-, O_2^- and O_2^{-2} present in SEI.[272]

Since there are high chance of fire in LIB due to internal heating or solvent leak, use of fire retardant additive is an interesting idea. These additives consist of organo-halogen and organophosphorous, or combination of fluorinated organophosphorous (trimethyl phosphate (TMP),[241, 273, 274] triphenyl phosphate (TPP),[275, 276] dimethyl methyl phosphate (DMMP),[277] tributyl phosphate (TBP),[275] or triethyl phosphate (TEP), tris(2,2,2-trifluoroethyl) phosphate (TFP)[278] and bis(2,2,2-trifluoroethyl) methyl phosphate (BMP). These flame retardant additives dissociate into the gas phase and terminate the chain propagating reaction by engaging $OH^{\cdot}$ and $H^{\cdot}$ radicals, or by forming an insulating barrier to ensure the safe LIB.

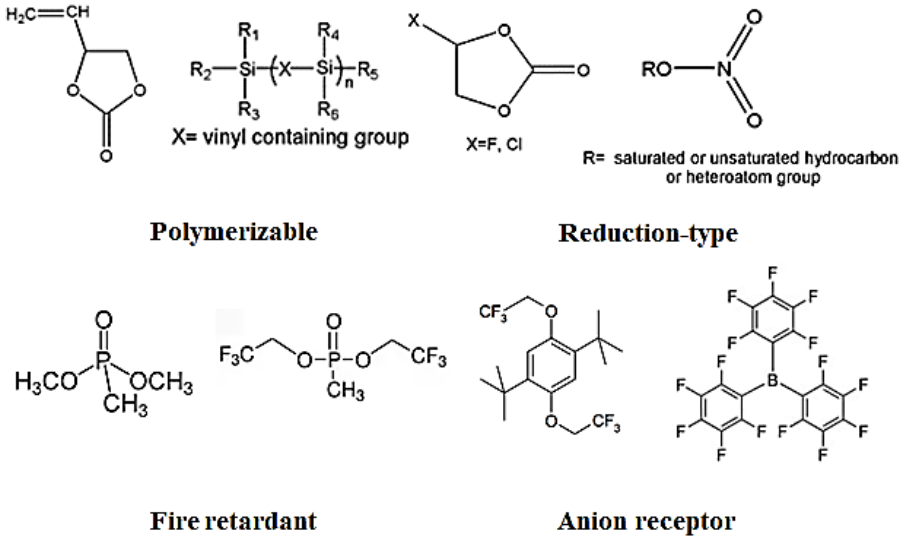

Figure 1. 32: Chemical Structure of various types of functional additives.

Another interesting use of additive is to limit the damages caused by overcharging of LIB. Redox shuttles are proposed to be as an overcharge current shunt which oxidizes when potential reaches higher than a complete charge of cathode. These redox shuttles need to possess good solubility and diffusion coefficient in electrolyte, reversibility with higher oxidative potential, thermally and chemically inertness to the cell components. With first one reported in the 1980s based on iodide (3.25 V), several aromatic redox shuttles have been reported like, 2,5-di-tertbutyl-1,4-dimethoxybenzene (3.96 V vs. Li+ /Li),[279] 2-(pentafluorophenyl)tetrafluoro-1,3,2-benzodioxaborole (4.43 V),[280] 2,5-difluoro-1,4-dimethoxybenzene (4.4 V),[281] 1,4-di-tert-butyl-2,5-bis(2,2,2,-trifluoroethoxy)benzene.[282] This interesting concept also resembles to the shutdown type electrolyte additives which are based on molecules polymerizable at certain potential to form an insulating layer and thus protect over charging.[283, 284]

1.3.3.4 Ionic liquids

Liquid electrolytes have been used in almost all commercial LIB due to their excellent properties, including ionic conductivity, wettability, environment benignity, *etc*. but they suffer from safety, leakage, flammability *etc.*, which motivates the search for alternatives like solid state electrolytes or ionic liquids resembling liquid electrolytes. Ionic liquids are also called molten salts, which are often liquid at room temperature, consisting of asymmetrical cation and delocalized anion. They fill the gap with their low volatility and flammability by using the large and bulky ions in addition to broader ESW. As compared to liquid electrolytes, they possess low melting point and lattice

energy, whereas poor conductivity and high cost. High molecular weight makes them viscous and badly wets some electrodes, leading to higher resistance at the interface. Some of the ionic liquids are based on ammonium and their derivative cations like imidazolium, pyridinium, pyrrolidinium (PYR), piperidinium (PP) with large electron withdrawing anions consisting of BF_4^-, PF_6^-, $[(FSO_2)(CF_3SO_2)N]^-$, $[(CF_3SO_2)(CF_3CO)N]^-$, $[(CF_3SO_2)_2N]^-$, or $[(C_2F_5SO_2)_2N]^-$ *etc.*, as shown in Figure 1.33.[69, 253]

It is observed that imidazolium based ionic liquids are not the best candidates for carbon anodes because of their cation reduction at around ~ 0.7 V versus Li^+/Li.[285, 286] Anions govern the oxidation at high potential which sometime creates trade-off with viscosity due to highly fluorinated ions like tetra-fluoroborates,[287] hexafluorophosphates.[288] Usually ionic liquids based on $TFSI^-$ are more attractive than BF_4^- due to superiority of former in room temperature viscosity (~69 mPa.s for $TFSI^-$ and ~300 mPa.s for BF_4^-). Aliphatic quaternary ammonium cations, namely pyrrolidinium or piperidinium,[289] are also combined with $TFSI^-$ and FSI^- (less viscous) resulting in wider ESW with decent compatibility with Li metal and $LiCoO_2$ electrodes.[290] In an approach to improve the performance and limits the shortcomings, lithium salts are also added sometimes to ionic liquids.[285,286]

The addition of Li-salt increases the viscosity by taking the concentration to 1 M or more, which reflects on a higher transference number and better interfacial stability.[291] However, addition of solvents like carbonates also decreased the viscosity and increased conductivity of ILs at the cost of volatility and flammability.[292, 293] In another study, interesting insights have been found by preparing blends of ILs based on EMI-TFSI with EC-DEC and other carbonates ,which highlighted that the best concentration of ILs with superior conductivity (~10.6 mS cm^{-1}) existed around 60% with viscosity of over 16 mPa s. On top of that, the accordingly obtained IL-LE based electrolyte was still showing low volatility (252% w.r.t to organic solvent) and almost no flammability.[294]

Some ILs, melting above 100 ^oC and comprising fluorosulfonyl-(trifluoromethylsulfonyl) $[(FSO_2)(CF_3SO_2)N]^-$ amide anion have shown interesting results in lithium metal batteries,[293] but they were limited to batteries operating at high temperature. Siloxyl groups have been introduced to ILs for improving the hydrophobicity of tetraalkylammonium cations, e.g. for (trialkyl-siloxy)ethyl group coupled with bis(perfluorosulfonyl)amide (TFSI, FSI, and FTFSI).[295,296, 297] In those cases, the superior ILs with cathodic stability > 5 V (versus Li/Li^+) came out to be those with TFSI due to absence of hydrolysis-sensitive fluorine atom unlike in FSI anion.[298, 299]

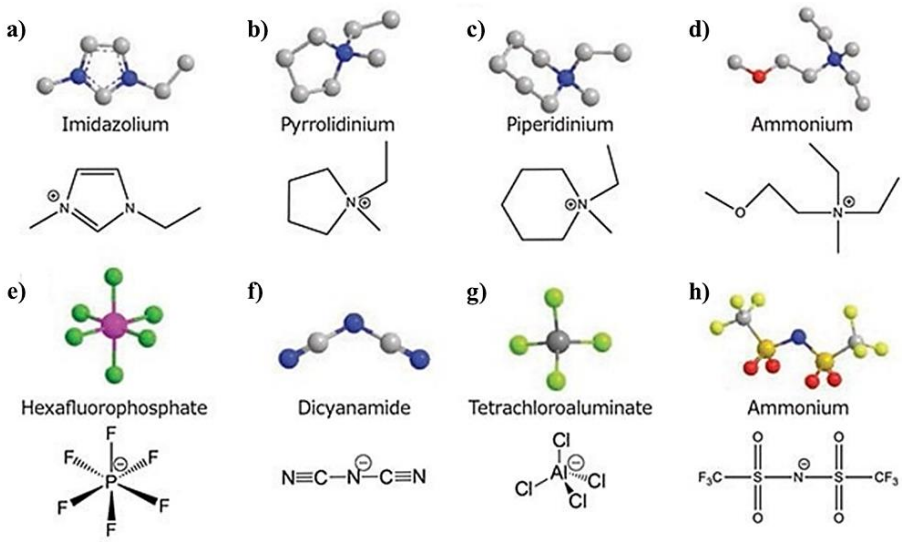

Figure 1. 33: Molecular structure of cations and anions of the RTILs explored in rechargeable batteries, a) Imidazolium cation, b) Pyrrolidinium cation, c) Piperidinium cation, d) Ammonium cation, e) Hexafluorophosphate anion, f) Dicyanamide anion, g) Tetrachloroaluminate anion, and h) Bis(trifluoromethane)sulfonamide anion. Reproduced with permission,[300] copyright 2018, Material matter.

Nevertheless, ILs suffer from poor conductivity and compatibility with some electrodes, like carbon based ones. They do offer a wide window of tunability, functionalization and control over the design with the possibility of blends for stable performance of LIB.

1.4 Solid electrolyte interphase layer

The term SEI referred as solid electrolyte interphase determines the performance and fate of batteries in a longer run. SEI is a passivation layer which results from the reaction/reduction of electrolytes containing solvents, salts and additives with electrodes. As highlighted in the history section, SEI was named by Peled, who identified this layer as electrically insulating and ionically conducting interphase.[57] Various research followed the pursuit later towards the understanding of SEI and its critical role. SEI by nature forms inhomogeneous surface at the cathode with multiple species and is believed to possess certain properties: 1.) it should have an optimum thickness which should not block or slow down Li-diffusion. Generally, it forms in the range of 20 nm to 50 nm thickness in initial cycles but can be thicker (SEM image shows thin SEI in Figure 1.36a). 2.) It should show sufficient mechanical properties (high elasticity) to withstand the volume change in electrodes and prevent dendrite growth in case of lithium metal, 3) It should display stability against decomposition, structure and morphological disturbance because of cell operation. Figure 1.34a shows the Li-ion diffusion from the bulk electrolyte to the anode in three steps;

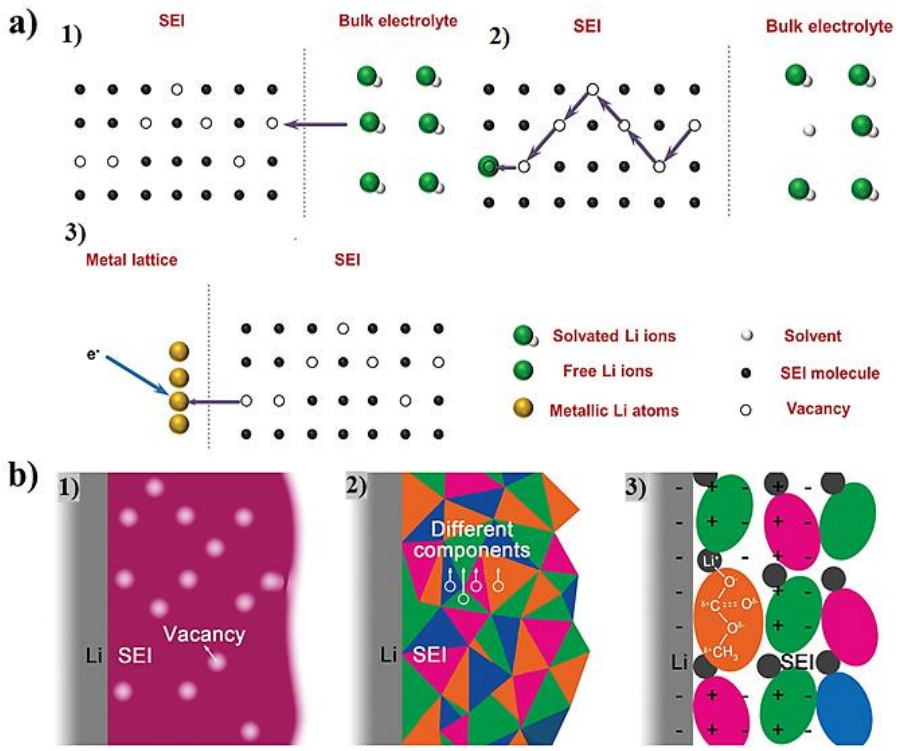

Figure 1. 34: a) A schematic description of Li-ion diffusion from the bulk electrolyte to the anode, 1) The solvated Li ion sheds its solvent molecules and thus has the access to the internal Schottky vacancy of the SEI, 2) The Li ion continuously migrates through the bulk of the SEI by relaying itself in Schottky vacancies, 3) The free Li ion reaches the anode surface and accepts an electron from the current collector, then deposits as Li metal, Reproduced with permission,[301] copyright 2016, Wiley, b) The mechanisms for SEI formation 1) The Peled's model. Reproduced with permission,[57] copyright 1979, Electrochemical Society. 2) Mosaic model. Reproduced with permission,[302] Copyright 1997, Electrochemical Society. 3) Coulombic interaction mechanism. Reproduced with permission,[303] Copyright 1999, Electrochemical Society.

starting from its entrance to internal Schottky vacancy of the SEI, transport from bulk of SEI to reach the anode.[301]The solvent reduces below 1 V (Li/Li^+) and forms SEI via three different popular mechanism as shown in Figure 1.34b: 1) Peled Model, the first explanation of SEI identified by surface reactions and decomposition of components in the layers with Schottky defects for Li migration,[304, 305] 2) Mosaic Model, which stresses mosaic morphology with migration of Li ion through a boundary of multiphase products formed at the anode surface with simultaneous decompositions,[306, 307] 3) the Coulombic interaction mechanism which tells about the alignment of the SEI components with positively charged Li-ion as head and partially positively charged carbon as foot to form double electric layer with strong adhesive ion pairs.[304, 305]The mobility of Li ion via SEI has been already explained in Figure 1.34a. It is speculated that Li ion follows two-layer model of diffusion: pore diffusion

in the outer layer (desolvation also takes place there) and knock-off diffusion in the inner layer. In order to have high mobility, the SEI should be designed to possess a lower energy barrier to dissociate the Li and solvent molecules.[221, 308] It is also being observed that Li-ion diffusion though different components of SEI has different energy barrier, highest with LiF (0.729 eV) and lower for Li_2CO_3 (ranging from 0.227 to 0.491 eV) and Li_2O (0.152 eV), respectively.[309] For the deeper understanding of SEI, several structural models has been proposed for understanding the morphology and structure of the interphase layer: (1) solid electrolyte interphase model,[310, 311] (2) polymer electrolyte interphase (PEI) model,[311, 312] (3) solid polymer layer (SPL) model, (4) compact stratified layer (CSL) model.[313]

In the 1980s, graphite was seen as a potential anode but it faced a serious issue of exfoliation with PC, which was encountered by replacing with EC and dialkyl carbonates. SEI formation at the surface of the graphite was seen to stabilize the cycling efficiency by passivation. Since then composition of SEI is investigated to throw lights on the compatibility of electrode and electrolyte reactions. SEI consists of complex compounds of both organic and inorganic nature in different layers whose quantification change with cycles and are often characterized by ex-situ SEM, EDX, TEM, XPS, IR, NMR, and OEMS.[314-317] For instance, SEI of graphite anode and 1.0M $LiPF_6$ in EC electrolyte was observed to be composed of lithium alkyl carbonate (here, lithium ethylene dicarbonate (LEDC)) and lithium fluoride (LiF) with ethylene as evolved gas and traces of lithium fluorophosphates, $Li_xPF_yO_z$ in the initial formation cycles. Figure 1.35 shows the formation of LIF and LEDC because of direct reduction of solvent and salt with lithium in series of reactions.[318, 319]

The solvent also undergoes reaction with cathode to form CO_2, which converts to Li_2CO_3 on its reaction with Li at the anode side. It is well depicted in Figure 1.35, where LEDC and Li_2CO_3 undergo further reduction to form CO_2, LiF, $LiPOF_2$, LiOR and other hydrocarbons.[320-322] The porous nature of SEI can also be credited to the release of soluble (such as ethers, oligo(ethylene oxide)s, and fluorophosphate) or gaseous (CO_2 and ethylene) products from the reaction of alkyl carbonate, LEDC, with $LiPF_6$.

Subsequently, the SEI composition does not remain the same over aging or longer cycling, further decomposition prevails (shown in Figure 1.36a and 1.36b).[323, 324] With limited understanding, it is observed that the inorganic layer (close to electrode) of SEI increases in concentration due to further reduction of lithium alkyl carbonate with salt, moisture and heat. The quantification of this inorganic layer depends on the type of salts in the electrolyte as highlighted in Figure 1.36c.[325] The composition of SEI is depending on the type of electrolyte and thermal or mechanical conditions of operation.[326, 327] As discussed above, electrolyte is also being used in a mixture of solvents, salts and addition of additives. These combinations are not only targeted for

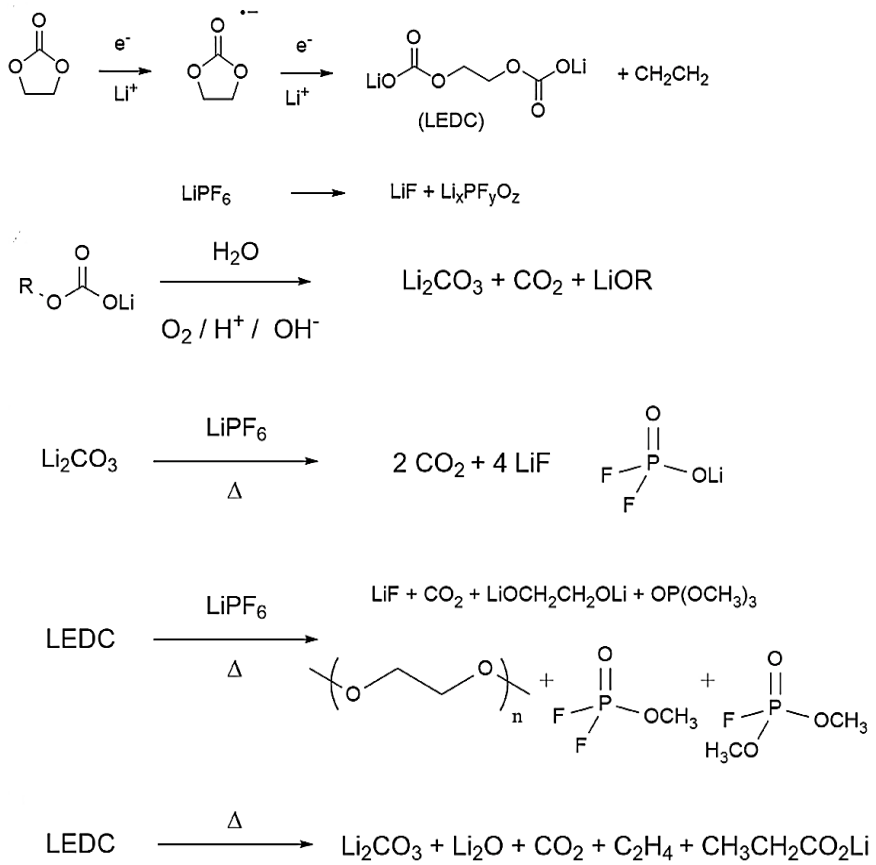

Figure 1. 35: Reaction pathway for the formation of SEI species such as LEDC, Li_2CO_3, Reproduced with permission,[314] copyright 2019, Elsevier.

better electrolyte but also for stable SEI formation which is well documented by the use of EC with additives such as FEC and VC. Interesting findings pointed that FEC is superior to SEI stability than VC due to the formation of more LIF and lower molecular weight poly(VC) in the former, while both decrease the reduction of EC for LEDC and ethylene by forming poly(VC) and Li_2CO_3.[328, 329]

Nevertheless, SEI is a vast research topic which needs to be pursued continuously with new electrodes and electrolytes design and existing complexity. For instance, SEI forming at the Li-metal anode is similar to the graphite, but it offers much more complexity due to dendrite growth, hostless Li-metal and infinite volume change.[57, 330] Unlike graphite, SEI on Li metal contains a lot of species like Li_3N, Li_2O, LiOH, LiI, Li_2S_2/Li_2S and RCOOLi, ROCOLi, COO_2Li, and $ROCO_2Li$ (R = alkyl groups).[307, 331, 332] The elasticity of SEI layer is an important physical parameter for the suppression of dendrite growth and has been believed to inhibit it with shear modulus

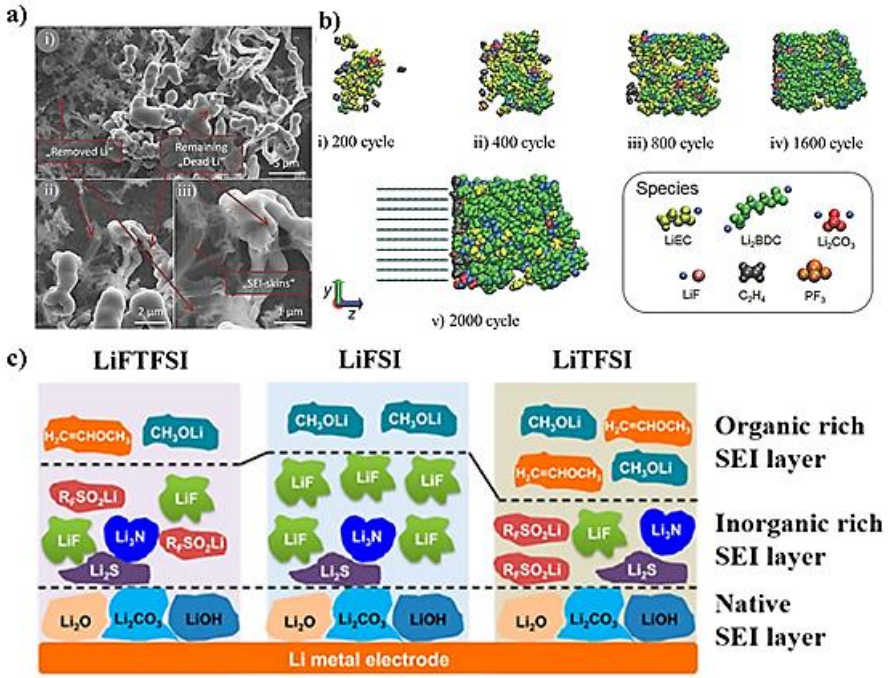

Figure 1. 36: a) SEM image showing appearance of Li dendrites and SEI layer on a Cu electrode after OsO_4 exposure in constant current mode. Reproduced with permission,[323] Copyright 2014, Elsevier. Typical snapshots of the aggregation state changes of reaction product in b) 200th cycle, ii) 400th cycle, iii) 800th cycle, iv) 1600th cycle, and v) 2000th cycle. Reproduced with permission,[324] Copyright 2014, ACS, c) Comparison of SEI layer formation with anion from different FSI based salts, Reproduced with permission,[325] Copyright 2021, Wiley

of (~10^9 Pa).[333, 334] Looking on individual contribution to nucleation of dendritse with varying current densities (as shown in Figure 1.29c), the investigations revealed that LiF/Li interface is less likely to facilitate dendrite growth than Li_2CO_3/Li interfaces due to larger electron tunneling barrier in the former.[335, 336] There are various other ways in which SEI can be stabilized, and those stabilized SEI could prevent underlying challenges in LMB or LIB for higher performance.

Similar to a solid electrolyte layer on the anode, a complex layer forms at the cathode, which is referred as cathode-electrolyte interphase (CEI). It involves the formation of alkyl carbonates, acid-base reactions, nucleophilic reactions, polymerizations and transient metal dissolution from cathodes.[337] The characterizations tools utilized for SEI offer greater complexity for CEI owing to their complexity, mixed signals from various phenomena and sensitivity towards external agents.[338] In an important investigation by Cui *et al.*[339] using cryo-EM characterizations, it is speculated that CEI possesses different distribution and morphology on the electrodes as depicted in Figure 1.37b. However, observation of CEI is not as simple as of SEI. In their work, they form the in situ stable conformal CEI by applying electrochemical shorting. As

depicted in scheme and SEM-images in Figures 1.37c-f, the uniform conformal CEI forms as a result of brief shorting on the NMC particles of ~5-10 nm amorphous in nature. Further analysis revealed that following CEI consists of organic polymers from alkyl carbonate electrolyte. As a result, Li^+ transport was improved with less side reactions from electrode-electrolyte, diminished increment in overpotential for NMC cycling with improved Coulombic efficiency and capacity retention. As mentioned above, the detection of CEI is complex, which also attracts less study on it, in addition to the fact that most of the cathodes lie in the operating voltage of electrolytes.[49] However, it does inspire to discover the upcoming challenges and solutions to innovate, improve and stabilize high voltage cathodes with clear distinction from the need of protecting coating and CEI formation.

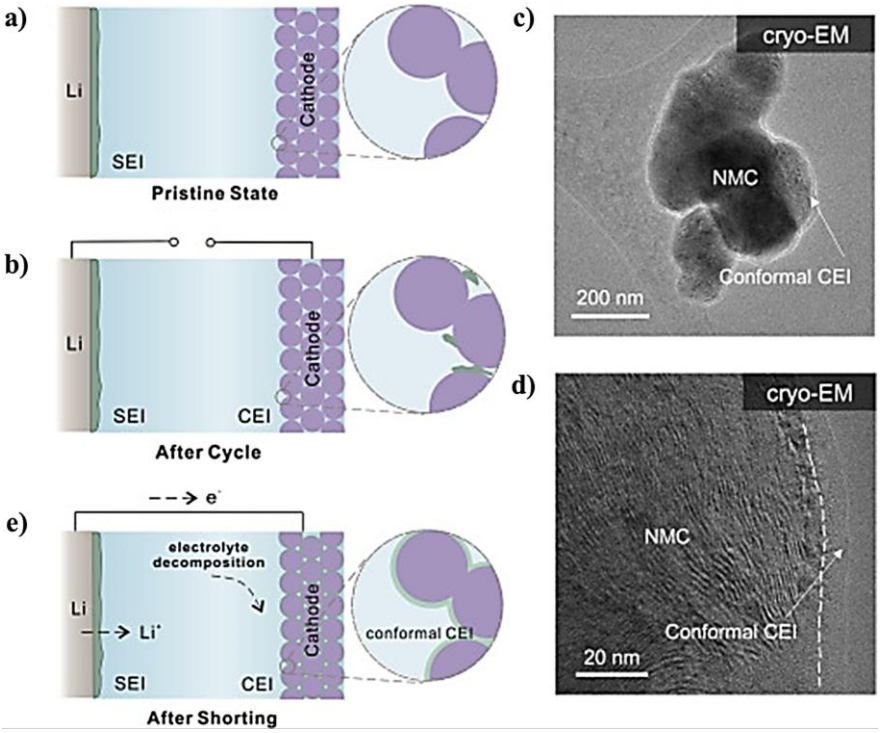

Figure 1.37: Schematics for CEI Formation under Different Conditions, and Cryo-EM Characterization of Conformal CEI (a–c) a) Schematics for positive electrodes in different states: pristine cathodes, b) CEI formed during normal cycling conditions, and c) conformal CEI formed via electrical shorting mechanism. d) and e) Cryo-EM images of conformal CEI formed on NMC-positive electrodes. Reproduced with permission,[339] copyright 2021, Elsevier.

1.5 Environmental challenges

The discovery of lithium batteries cannot be credited to one person, it is the result of a tremendous effort of the thousands of researchers together for more than a century in order to understand the complexity of the battery. With decades of research in material developments, there are well stabilized electrodes and electrolytes in addition to supporting materials and current collectors. Previous sections discussed various classes of electrodes, i.e. cathode or anode which possess unique merits and drawbacks, so is the case for other components. A scheme of a commercial LIB is shown in Figure 1.38 which highlights the environment concern of individual components from cathode to anode including salt *etc*.[340] The processing of raw materials and manufacturing of batteries indulge large emission which is a key concern for reducing emission as well with net zero goals. Beginning with commercial cathodes, most of them are based on toxic transition metals (e.g. Ni, Co, Mn) whose extractions take a lot of effort and energy, after tedious manufacturing processes. Cobalt, which is one of the important metal for cathodes, comes largely from Democratic Republic of Congo by underground mining. The dark side of this mining is brutal, reflected from the worst life conditions of the local population falling into slavery, child labor, toxic health conditions (congenital disabilities) as highlighted in Figure 1.39 (left).[341-343] Therefore, less or non-toxic elements should be ramped up in the existing and future technology processed via a sustainable method for environment and humanity.

In fact, lithium metal extraction is also under criticism due to regional threat to soil degradation, livestock farming and plant life in the locality. One report highlights the

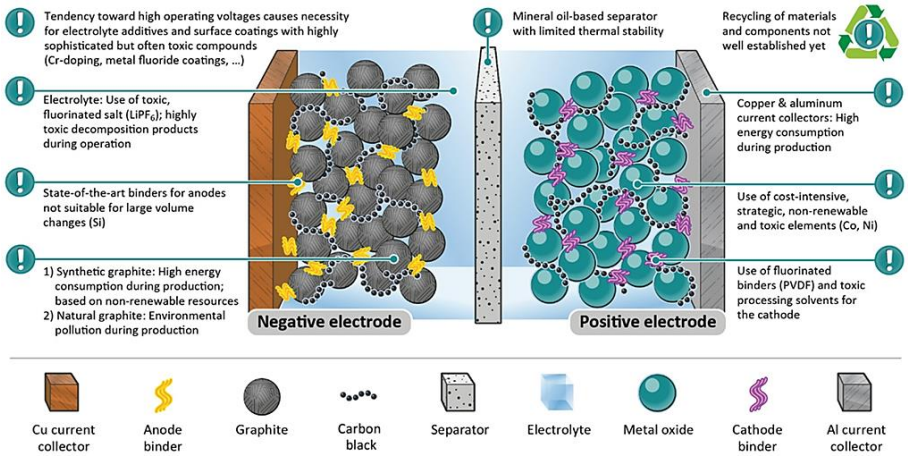

Figure 1. 38: Environmental challenges of current materials and components in SOTA LIB cells. Reproduced with permission,[340] copyright 2020, Wiley.

dark side of the lithium extraction in Chile (Figure 1.39 shows the lithium field), South America and its implication. For instance, 2.2 million liters of water are consumed to produce one ton of lithium affecting local population, ecosystem with fresh water supplies and probable drought.[344] This demand is expected to increase over years, given the high time when major economies are switching to renewable energy storage, specifically in transport-mobility and stationary power grids. It could be noticed from the above discussion on the materials sections that despite the poor performance from the materials based on elements like Fe, Mn, Si, C *etc*, they are actively looked upon.

Figure 1. 39: Left: Image showing Sea of Laborer including woman and children at Shabara, Cobalt mine in Congo exposed to toxic chemicals without any safety regulations. Reprinted with permission.[341] Right: Lithium Fields' in the Salar de Atacama salt flats in northern Chile. Reprinted with permission.[345]

That's solely because of reducing toxicity, dependence on less abundant resources, cost and increasing environment benignity. Other alternatives to these are also being actively searched by researchers, such as organic electrodes, which have been briefly discussed in previous sections. However, organic electrodes cannot match the performance of the inorganic electrodes due to their solubility and other issues, complex synthesis, cell reactions and are limited to lab scale. The current LIB technology uses liquid electrolytes, which proffers a prominent concern with safety measure. The most commonly used carbonate solvents in the presence of moisture are flammable in reaction to lithium (Figure 1.40a). The past accidents are enough to realize that it's not the best candidate to be adapted for higher temperature applications (say EVs) and larger stack with the risk of electrolyte leakage and fire. This requires concrete solution to either improve existing technology, modify or alternatives.

Development of solid-state electrolyte is one of the smart solution which not only intend to improve the performance of batteries, cut the cost, increase sustainability by easier recycling (as huge untreated battery waste is another concern (Figure 1.40b)). This thesis focuses on the development of electrolytes, including solid electrolytes in an attempt to provide alternatives, build an understanding of a certain class of materials.

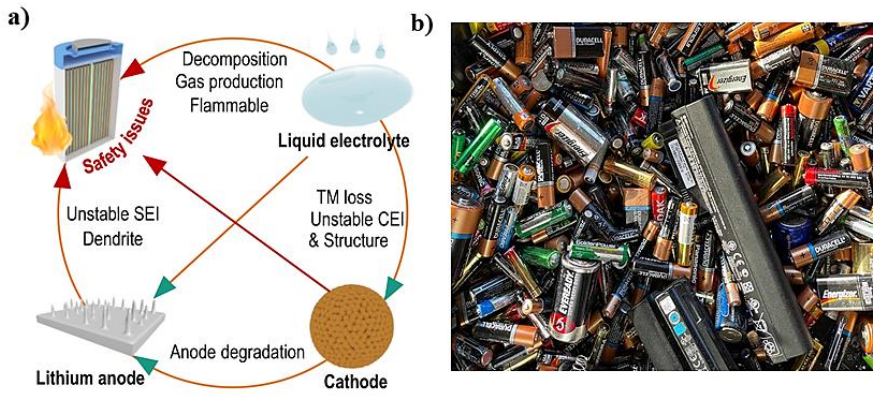

Figure 1. 40: a) Safety hazards induced by using traditional liquid electrolytes. Reproduced with permission,[346] copyright 2022, Nature. b) Battery dumping and waste. Reprinted with permission,[347] copyright (John Cameron), TRVST.

In efforts to make fossil fuel free mobility, every country is setting up the battery industry, highlighting the need for the local supply chain. While the following transport sector with EV has not dominated the market yet, but forecast says, soon it will face a tremendous surge in demand. It is thus crucial to have a brief understanding of LIB life cycle assessment, as depicted in Figure 1.41 (top).[348] With market prediction of Li-ion battery consumption from US$30 billion in 2017 to $100 billion in 2025,[349] the availability of raw materials is worrisome. And thus, industries are wary of finding alternatives, either other technologies or initiate massive recycling plants to create the circular ecosystem of materials and avoid the dry-out.

Second-life of batteries after processing is an interesting idea to exploit the limit of the batteries with existing materials. Figure 1.41 (bottom-left) demonstrates the percentage of recovered material from LIBs on recycling.[350] And recycling all the discarded batteries for material recovery and flowing it for manufacturing would require significant energy. This can be coupled with other renewable energy in the process of decreasing emission. In fact, each step in the LCA can be combined with renewable energy to decarbonize the emissions. While this discussion started more than a decade ago but not enough actions were taken, as highlighted in the circular chart on history of recycling LIBs, Figure 1.41 (bottom-right) since the start of the 21st century.[351] Fortunately, major economies are taking stringent actions on the second life use, recycling and other measures to minimize the unpleasant effect of lithium battery technology.

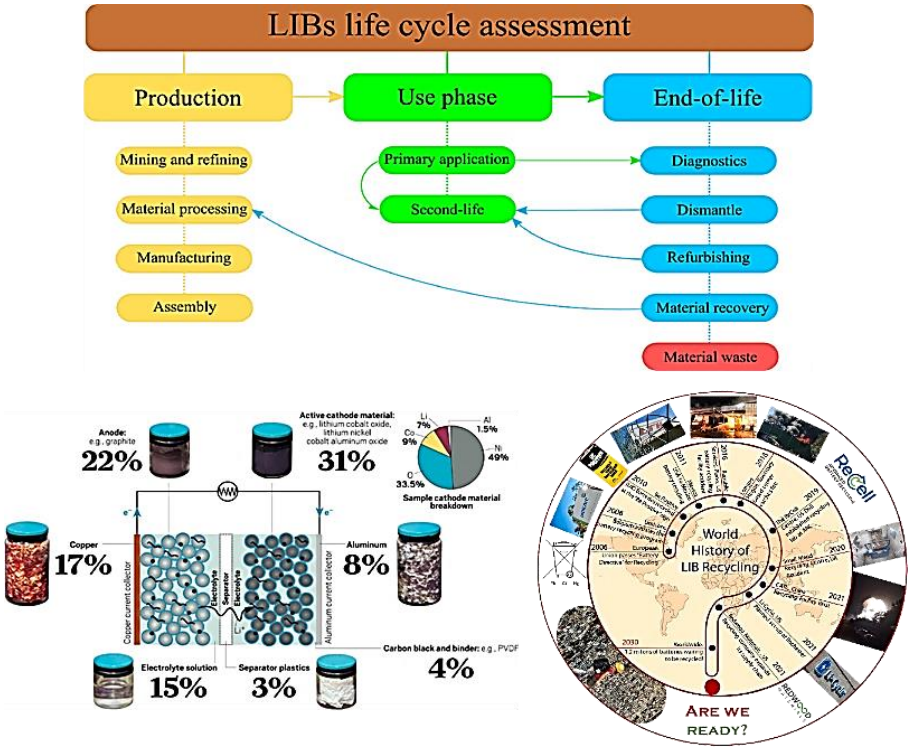

Figure 1. 41: Life cycle assessment of lithium ion batteries (top). Reprinted with permission,[348] copyright 2021, Elsevier. Percentage of material recovered on recycling LIB (Bottom left). Reprinted with permission.[350] Timeline of recycling events globally from in 21st century (Bottom right), Reprinted with permission,[351] copyright 2022, Elsevier.

1.6 Summary

Unfortunate greenhouse gas emission and depleting fossil fuels are alarming louder than ever. This calls upon switchover to renewable energy along with robust energy storage technologies globally. Batteries are the frontrunner in that race which was developed centuries ago. Among them, Lithium battery (LB) technology is the best bet due to their high energy and power density covering a wide range of applications. This revolutionary technology was discovered after a series of other conventional batteries technology such as metal acid, metal hydride or metal alkaline batteries. Unlike other technologies, lithium batteries involved complex research over a half century from materials discovery, optimization, and commercialization with multiple challenges. In our daily life, most of the devices we see around is operated on lithium batteries either smartphone, watches, laptop, *etc*. The transport industry, largely E-vehicle based on LB, is clearly foreseen as the future mobility in the big efforts toward lowering CO_2 emission. However, the increased demand of these devices, along with

the transition of decreasing fossil-fuel reliance on the transport sector, points to an exponential increase in battery production with innovations for superior technology.

The present Lithium-ion battery consists of a cathode, anode, electrolyte, and supporting materials. Each of these components has its own timeline of history over decades before their first commercialization. A LIB operates with shuttling of Li-ion from cathode to anode and vice versa in state of charge and discharge, respectively. While, redox reaction, i.e., oxidation occurs at anode and reduction occurs at cathode. The key characteristics for a full LIB cell stress on high energy and power density, durability, safety, cost effective, robust and sustainability. Since the source of Li-ion is derived from electrodes, which is why they are referred as active materials of the battery, determining the net capacity depending upon the chemistry, composition and weight of the active material. Various classes of electrode materials have been developed so far varying in transport mechanism, chemical and physical structure and properties. Many researchers are now focusing on dual intercalations battery from one to two intercalations hosts in LIB.

Referring to the positive electrode of LIB, cathode, which didn't offer much complexity, unlike anode due to their relatively better thermodynamic stability with electrolyte. Some of the first commercialized cathode materials include LCO, LMO and LFP, *etc*. Also categorized on the basis of transport and crystal structure, they are well classified as layered oxide ($LiCoO_2$, $LiNiO_2$), ternary layered oxide ($LiNiCoO_x$, $LiM_xM_yM_zO_2$), polyanionic (NASICON, olivine ($LiFePO_4$), silicates), conversion cathodes, *etc*. Most of the batteries in the market are based on metal oxides and olivine due to their superior structure. While, high performance in the longer run poses necessary concerns with each of them motivating further developmental efforts. LCO delivers an experimental capacity of ~174 mAh g^{-1} while offering voltage decay and irreversible capacity loss. This sparked the idea of other alternatives like less expensive LNO and LMO which offer a capacity of <140 mAh g^{-1} and > 100 mAh g^{-1} respectively but pose issues like thermodynamic instability, cation mixing and Jahn Teller effect (in case of oxides of Manganese). However, mixing cations turned out to be an interesting idea for the discovery of NMC, NCA cathodes. Away from that, phosphate based polyanionic cathodes like $LiMPO_4$ are gaining much attention after the breakthrough of less toxic $LiFePO_4$ which has already penetrated its place in the market in slow rate capability batteries with a capacity of > 160 mAh g^{-1}. Besides these insertion materials, the conversion cathode is an attractive class of materials due to their high discharge capacity and potential. However, these less expensive materials lag behind due to their lower conductivity, larger volume change, poor reversibility and thus capacity loss. In parallel innovations, many researchers are also looking at more sustainable, inexpensive organic cathodes, such as carbonyl, organosulphur, imine, *etc*.. These are far away from commercialization but offer great potential to be commercialized in the future through extensive research.

Similar to cathode, anode is also classified as insertion, alloying and conversion type materials based on transport/ reaction mechanism. It took more time and effort to achieve a breakthrough in anodes due to a lack of understanding of their chemistry with electrolyte. Carbon-based materials such as coke, graphite and graphene have been explored extensively for decades, which leads to their commercialization with graphite. With lithium cations intercalating into the layers of graphite, it did suffer from exfoliation, which was later addressed by the use of appropriate solvent and understanding of SEI. In addition to carbon, Inorganic oxides such as lithium titanate oxides ($Li_4Ti_5O_{12}$), lithium vanadate oxide (Li_3VO_4) *etc*., present as possible alternates with fast kinetics and rate capabilities than graphite but lower energy than latter. Differing in cell reaction, alloying materials offer much higher capacity and potential range than insertion anodes due to higher number of Li ions uptake. Silicon from group IV and phosphorous from group V offer a high capacity of >2400 mAh g^{-1}, which led Silicon based anode as the next generation cathodes for high-energy-density batteries. Not only in pure element, these cathodes are also synthesized as intermetallic to exploit the synergy of element in tackling inherent issues like volume expansion, irreversibility and capacity loss. When alloying is combined with conversion materials, they offer lower intercalation potential and good reversibility with composites. Above all, the most popular and potential anode is Lithium metal among industrial research in addition to LTO, graphite and silicon. Lithium metal is light with high capacity and energy density, which hopes to revolutionize the Lithium battery technology with solid state electrolyte.

The next section in materials review discusses about the electrolyte which provides the channel for mobility of ions between electrodes. It mostly consists of salts and a media to solvate the salts, and sometime also supported with additives and co-solvents. Commonly used solvents include ethers and carbonates with salts such as LiTFSI, $LiPF_6$, $LiClO_4$. Fluoride containing salts offer relatively better ionic mobility, solubility, SEI formation and thermal stability, which make LiTFSI and $LiPF_6$ popular in commercial application. As mentioned, additives complete the shortcomings of the electrolyte with properties like SEI formation, flammability, broadening electrochemical stability, fire-resistance, *etc*. Since electrolytes are volatile and flammable when in contact with lithium in air, which led the development of room temperature ionic liquids. Ionic liquids are molten salts with cations and delocalized anions such as ammonium-based imidazolium, pyridinium and pyrrolidinium. Nevertheless, they are still behind to match up liquid electrolytes due to their poor conductvity, wettability and affordability.

The operating principle of batteries beyond materials was not focused on the interfaces until 1980s when researcher's effort paid off with understanding of solid electrolyte interphase/SEI. This forms at the surface of the anode following numerous reactions resulting in various layers of organic and inorganic species. SEI proves out

to be beneficial for the battery as it presents the anode with a protective layer between anode and electrolyte limiting unnecessary side reactions. The nature of SEI depends upon electrolyte solvent, salt and the electrodes along with the experiment conditions. SEI at the anode is well studied while SEI at cathode, also referred as CEI, is not much looked upon until now.

The last section of this chapter draws kind attention to the dark reality of lithium battery production, associated environmental as well as human life exploitation in developing and poor countries. The global need for batteries is increasing exponentially, which is putting high pressure on the raw materials and minerals. This unprecedented demand draws alarm on other alternatives and methodologies to not fall behind the target of net zero. Combined with other renewable energies for steps of manufacturing and processing, the neutrality could be achieved. Another major initiative was the massive scale of second life batteries and recycling plants within the local supply chain for avoiding the battery waste and exploit recovered materials as fodder for first life batteries.

Bibliography

1. Total energy consumption. https://yearbook.enerdata.net/total-energy/world-consumption-statistics.html.
2. A Global Breakdown of Greenhouse Gas Emissions by Sector. https://www.visualcapitalist.com/cp/a-global-breakdown-of-greenhouse-gas-emissions-by-sector/.
3. UN climate report: It's 'now or never' to limit global warming to 1.5 degrees. https://news.un.org/en/story/2022/04/1115452.
4. Hannah Ritchie, P. R., Max Roser *Fossil Fuels*; 2021.
5. Pallardy, R. *IPCC Report Analysis: The Top Five Measures to Halve Emissions by 2030*; 2022.
6. Dunn, B.; Kamath, H.; Tarascon, J.-M., Electrical Energy Storage for the Grid: A Battery of Choices. *Science* **2011,** *334* (6058), 928-935.
7. Winter, M.; Brodd, R. J., What Are Batteries, Fuel Cells, and Supercapacitors? *Chemical Reviews* **2004,** *104* (10), 4245-4270.
8. Shao, Y.; El-Kady, M. F.; Sun, J.; Li, Y.; Zhang, Q.; Zhu, M.; Wang, H.; Dunn, B.; Kaner, R. B., Design and Mechanisms of Asymmetric Supercapacitors. *Chemical Reviews* **2018,** *118* (18), 9233-9280.
9. Heilbron, J. L., Electricity in the 17th and 18th Centuries: A Study of Early Modern Physics. University of California Press.: California, 1979; p 309.
10. Buchholz, K., Nikola producing battery-electric trucks, fuel-cell EVs coming. *Sar.org* 2023-04-25, 2023.
11. Eurobat, Avicenne study: "EU battery demand and supply (2019-2030) in a global context" shows that in the next decade lead and lithium batteries are critical to clean energy transition. 2021.
12. How 4 leading companies are tackling supply chain emissions. https://www.weforum.org/agenda/2022/11/scope3-supply-chain-emissions-cop27-ikea-philips-zf-unilever/#:~:text=Tackling%20supply%20chain%20emissions%20could,emissions%20in%20their%20supply%20chains. (accessed 16/08/2023).
13. Norway-2022, Executive summary. *IEA, Paris* **2022**.
14. Hertz, Was Tesla The First Electric Car? 2023; Vol. 2023.
15. Porsche Gamechanger: how Ferdinand Porsche designed the first-ever hybrid car. https://www.porsche.com/stories/innovation/gamechanger-how-ferdinand-porsche-designed-first-hybrid-car.
16. Jakob Fleischmann, P. S., Martin Linder, Mikael Hanicke, Evan Horetsky, Dina Ibrahim, Sören Jautelat, Lukas Torscht *Battery 2030: Resilient, sustainable, and circular*; January 16, 2023.
17. Chen, T.; Jin, Y.; Lv, H.; Yang, A.; Liu, M.; Chen, B.; Xie, Y.; Chen, Q., Applications of Lithium-Ion Batteries in Grid-Scale Energy Storage Systems. *Transactions of Tianjin University* **2020,** *26* (3), 208-217.
18. Mcturk, E., A Brief History of Electric Vehicles. 2019; Vol. 2023.
19. Ley, H.; Konig, E., Spectra of solutions of important acids of elements of the sulfur group. *Z. Chem. B* **1938,** *14*, 365-87.
20. Society, E.; Dubpernell, G.; Westbrook, J. H., *Selected Topics in the History of Electrochemistry: Written Symposium : Papers*. Electrochemical Society.
21. Pavlov, D., Invention and Development of the Lead–Acid Battery. 2017; pp 3-32.
22. Volta, A., On the electricity exited by the mere contact of conducting substances of different kind, letter to the Right Hon. Sir Joseph Banks, KBPRS, Philos. *Trans* **1800,** *2*, 430.
23. Trasatti, S., 1799-1999: Alessandro Volta's' electric pile'-Two hundred years, but it doesn't seem like it. *Journal of electroanalytical chemistry* **1999,** *460* (1-2), 1-4.
24. Chen, A.; Qu, C.; Shi, Y.; Shi, F., Manufacturing Strategies for Solid Electrolyte in Batteries. *Frontiers in Energy Research* **2020,** *8*.
25. Leclanche, G., New Form of Galvanic Battery. *Compt. rend* **1866,** *83*, 54-56.
26. Scrosati, B., History of lithium batteries. *Journal of Solid State Electrochemistry* **2011,** *15* (7), 1623-1630.
27. Liang, Y.; Zhao, C.-Z.; Yuan, H.; Chen, Y.; Zhang, W.; Huang, J.-Q.; Yu, D.; Liu, Y.; Titirici, M.-M.; Chueh, Y.-L.; Yu, H.; Zhang, Q., A review of rechargeable batteries for portable electronic devices. *InfoMat* **2019,** *1* (1), 6-32.
28. Park, J. K., *Principles and Applications of Lithium Secondary Batteries*. Wiley: 2012.
29. Holze, R., Handbook of battery materials. Daniel C, B., Ed. Springer: 2012; Vol. 16.
30. Crompton, T., In *Battery Reference Book*, Elsevier: 2000; Vol. Third edition.
31. May, G. J.; Davidson, A.; Monahov, B., Lead batteries for utility energy storage: A review. *Journal of Energy Storage* **2018,** *15*, 145-157.

32. Linden, D.; Reddy, T., *Handbook of Batteries*. McGraw-Hill Education: 2001.
33. DeCicco, J.; James Kliesch, B. S. M. S., *Aceee's Green Book: The Environmental Guide to Cars and Trucks*. American Council for an Energy Efficient Economy: 2001.
34. Ericson, B.; Hu, H.; Nash, E.; Ferraro, G.; Sinitsky, J.; Taylor, M. P., Blood lead levels in low-income and middle-income countries: a systematic review. *The Lancet Planetary Health* **2021,** *5* (3), e145-e153.
35. MEPs ban cadmium from power tool batteries and mercury from button cells. European Parliament, 2013.
36. Tian, Y.; Zeng, G.; Rutt, A.; Shi, T.; Kim, H.; Wang, J.; Koettgen, J.; Sun, Y.; Ouyang, B.; Chen, T. J. C. r., Promises and challenges of next-generation "beyond Li-ion" batteries for electric vehicles and grid decarbonization. *Chemical Reviews* **2020,** *121* (3), 1623-1669.
37. Au, H.; Crespo-Ribadeneyra, M.; Titirici, M.-M., Beyond Li-ion batteries: performance, materials diversification, and sustainability. *One Earth* **2022,** *5* (3), 207-211.
38. Singh, A. N.; Islam, M.; Meena, A.; Faizan, M.; Han, D.; Bathula, C.; Hajibabaei, A.; Anand, R.; Nam, K. W., Unleashing the Potential of Sodium-Ion Batteries: Current State and Future Directions for Sustainable Energy Storage. *Advanced Functional Materials* **2023,** *33* (46), 2304617.
39. Huang, Z.-X.; Gu, Z.-Y.; Heng, Y.-L.; Ang, E. H.; Geng, H.-B.; Wu, X.-L., Advanced layered oxide cathodes for sodium/potassium-ion batteries: Development, challenges and prospects. *Chemical Engineering Journal* **2023,** *452*, 139438.
40. Sada, K.; Darga, J.; Manthiram, A., Challenges and Prospects of Sodium-Ion and Potassium-Ion Batteries for Mass Production. *Advanced Energy Materials* **2023,** *13* (39), 2302321.
41. Canepa, P.; Sai Gautam, G.; Hannah, D. C.; Malik, R.; Liu, M.; Gallagher, K. G.; Persson, K. A.; Ceder, G., Odyssey of Multivalent Cathode Materials: Open Questions and Future Challenges. *Chemical Reviews* **2017,** *117* (5), 4287-4341.
42. Tian, Y.; Zeng, G.; Rutt, A.; Shi, T.; Kim, H.; Wang, J.; Koettgen, J.; Sun, Y.; Ouyang, B.; Chen, T.; Lun, Z.; Rong, Z.; Persson, K.; Ceder, G., Promises and Challenges of Next-Generation "Beyond Li-ion" Batteries for Electric Vehicles and Grid Decarbonization. *Chemical Reviews* **2021,** *121* (3), 1623-1669.
43. Ponrouch, A.; Bitenc, J.; Dominko, R.; Lindahl, N.; Johansson, P.; Palacin, M. R., Multivalent rechargeable batteries. *Energy Storage Materials* **2019,** *20*, 253-262.
44. Weeks, M. E.; Larson, M. E., J. A. Arfwedson and his services to chemistry. *Journal of Chemical Education* **1937,** *14* (9), 403.
45. *Journal of Science and the Arts*. Journal of Science and the Arts

1818.
46. Placke, T.; Kloepsch, R.; Dühnen, S.; Winter, M., Lithium ion, lithium metal, and alternative rechargeable battery technologies: the odyssey for high energy density. *Journal of Solid State Electrochemistry* **2017,** *21* (7), 1939-1964.
47. Winter, M.; Barnett, B.; Xu, K., Before Li Ion Batteries. *Chemical Reviews* **2018,** *118* (23), 11433-11456.
48. Xu, K., Nonaqueous Liquid Electrolytes for Lithium-Based Rechargeable Batteries. *Chemical Reviews* **2004,** *104* (10), 4303-4418.
49. Xu, K., Electrolytes and Interphases in Li-Ion Batteries and Beyond. *Chemical Reviews* **2014,** *114* (23), 11503-11618.
50. Harris, W. S. In *Electrochemical Studies In Cyclic Esters*, 1958.
51. Bauman, H. G.; Chilton, J. E.; Cook, G. M., *New Cathode-Anode Couples Using Nonaqueous Electrolyte*. Lockheed Missiles Space Co Inc, Defense Technical Information Center: Sunnyvale CA.

, 1963.
52. Bauman, H. F.; Chilton, J. E.; Hultquist, A. E. In *Lithium Anode Limited Cycle Battery Investigation*, Center, DD (ed.), 1966.
53. Fong, R.; von Sacken, U.; Dahn, J. R., Studies of Lithium Intercalation into Carbons Using Nonaqueous Electrochemical Cells. *Journal of The Electrochemical Society* **1990,** *137* (7), 2009.
54. Wagner, M.; Raimann, P.; Trifonova, A.; Möller, K.; Besenhard, J.; Winter, M., Electrolyte Decomposition Reactions on Tin and Graphite-Based Anodes are Different. *Electrochemical and Solid State Letters* **2004,** *7*.
55. Tasaki, K.; Goldberg, A.; Winter, M., On the difference in cycling behaviors of lithium-ion battery cell between the ethylene carbonate- and propylene carbonate-based electrolytes. *Electrochimica Acta* **2011,** *56*, 10424-10435.

56. Wagner, M.; Albering, J.; Möller, K.; Besenhard, J. O.; Winter, M., XRD evidence for the electrochemical formation of Li+(PC)yCn- in PC-based electrolytes. *Electrochemistry Communications* **2005,** *7*, 947–952.
57. Peled, E., The Electrochemical Behavior of Alkali and Alkaline Earth Metals in Nonaqueous Battery Systems—The Solid Electrolyte Interphase Model. *Journal of The Electrochemical Society* **1979,** *126* (12), 2047-2051.
58. Armand, M., Chabagno, J.M., and Duelot, M In *Polymer solid electrolytes*, Second International Meeting on Solid Electrolytes, St. Andrews, Scotland, St. Andrews, Scotland, 1978.
59. Read, J. A.; Cresce, A. V.; Ervin, M. H.; Xu, K., Dual-graphite chemistry enabled by a high voltage electrolyte. *Energy & Environmental Science* **2014,** *7* (2), 617-620.
60. Inaba, M.; Kawatate, Y.; Funabiki, A.; Jeong, S.-K.; Abe, T.; Ogumi, Z., STM study on graphite/electrolyte interface in lithium-ion batteries: solid electrolyte interface formation in trifluoropropylene carbonate solution. *Electrochimica Acta* **1999,** *45* (1), 99-105.
61. Whittingham, M. S., Chemistry of intercalation compounds: Metal guests in chalcogenide hosts. *Progress in Solid State Chemistry* **1978,** *12* (1), 41-99.
62. Whittingham, M. S., The Role of Ternary Phases in Cathode Reactions. *Journal of The Electrochemical Society* **1976,** *123* (3), 315.
63. Hever, K. O., A Solid-State Electrochemical Cell Based on Ion Conductive Ceramics. *Journal of The Electrochemical Society* **1968,** *115* (8), 830.
64. Hever, K., Ion Mobility in Crystals of a Mixed-Alkali Ferrite: K x Na1− x Fe7 O 11. *Journal of The Electrochemical Society* **1968,** *115* (8), 826.
65. Armand, M. B., Intercalation Electrodes. In *Materials for Advanced Batteries*, Murphy, D. W.; Broadhead, J.; Steele, B. C. H., Eds. Springer US: Boston, MA, 1980; pp 145-161.
66. Lazzari, M.; Scrosati, B., A Cyclable Lithium Organic Electrolyte Cell Based on Two Intercalation Electrodes. *Journal of The Electrochemical Society* **1980,** *127* (3), 773.
67. Rao, B. M. L.; Francis, R. W.; Christopher, H. A., Lithium-Aluminum Electrode. *Journal of The Electrochemical Society* **1977,** *124* (10), 1490.
68. Mizushima, K.; Jones, P.; Wiseman, P.; Goodenough, J. B., LixCoO2 (0< x<-1): A new cathode material for batteries of high energy density. *Materials Research Bulletin* **1980,** *15* (6), 783-789.
69. Thackeray, M. M.; Johnson, P. J.; de Picciotto, L. A.; Bruce, P. G.; Goodenough, J. B., Electrochemical extraction of lithium from LiMn2O4. *Materials Research Bulletin* **1984,** *19* (2), 179-187.
70. Nagaura, T. A. In *Lithium Ion Rechargeable Battery*, Oral Presentation in the Third International Rechargeable Battery Seminar, Deerfield Beach, FL, March 5−7, 1990; Deerfield Beach, FL, 1990.
71. Japan pivotal in advancing energy storage and conversion materials. Phys.org: 2017; Vol. 2023.
72. Peljo, P.; Girault, H. H., Electrochemical potential window of battery electrolytes: the HOMO–LUMO misconception. *Energy Environmental Science* **2018,** *11* (9), 2306-2309.
73. Desilvestro, J.; Haas, O., Metal Oxide Cathode Materials for Electrochemical Energy Storage: A Review. *Journal of The Electrochemical Society* **1990,** *137* (1), 5C.
74. Morzilli, S.; Bonino, F.; Scrosati, B., Characteristics of the lithium electrode in organic and polymeric electrolytes. *Electrochimica Acta* **1987,** *32* (6), 961-964.
75. Euler, K. J., Thermokraft von Batteriebraunstein. *Naturwissenschaften* **1980,** *67* (11), 561-562.
76. Tarascon, J. M.; Armand, M., Issues and challenges facing rechargeable lithium batteries. *Nature* **2001,** *414* (6861), 359-367.
77. Lee, W.; Muhammad, S.; Sergey, C.; Lee, H.; Yoon, J.; Kang, Y.-M.; Yoon, W.-S., Advances in the Cathode Materials for Lithium Rechargeable Batteries. *Angewandte Chemie International Edition* **2020,** *59* (7), 2578-2605.
78. Cram, D. J.; Cram, J. M., Host-Guest Chemistry. *Science* **1974,** *183* (4127), 803-809.
79. Mohamed, N.; Allam, N. K., Recent advances in the design of cathode materials for Li-ion batteries. *RSC Advances* **2020,** *10* (37), 21662-21685.
80. Van der Ven, A.; Ceder, G., Lithium Diffusion in Layered Lix CoO2. *Electrochemical and Solid-State Letters* **2000,** *3* (7), 301.
81. Lu, X.; Sun, Y.; Jian, Z.; He, X.; Gu, L.; Hu, Y.-S.; Li, H.; Wang, Z.; Chen, W.; Duan, X.; Chen, L.; Maier, J.; Tsukimoto, S.; Ikuhara, Y., New Insight into the Atomic Structure of Electrochemically Delithiated O3-Li(1–x)CoO2 ($0 \leq x \leq 0.5$) Nanoparticles. *Nano Letters* **2012,** *12* (12), 6192-6197.
82. Amatucci, G. G.; Tarascon, J. M.; Klein, L. C., CoO2, The End Member of the Lix CoO2 Solid Solution. *Journal of The Electrochemical Society* **1996,** *143* (3), 1114.
83. Wang, K.; Wan, J.; Xiang, Y.; Zhu, J.; Leng, Q.; Wang, M.; Xu, L.; Yang, Y., Recent advances and historical developments of high voltage lithium cobalt oxide materials for rechargeable Li-ion batteries. *Journal of Power Sources* **2020,** *460*, 228062.

84. Shen, X.; Zhang, X.-Q.; Ding, F.; Huang, J.-Q.; Xu, R.; Chen, X.; Yan, C.; Su, F.-Y.; Chen, C.-M.; Liu, X.; Zhang, Q., Advanced Electrode Materials in Lithium Batteries: Retrospect and Prospect. *Energy Material Advances 2021*.
85. Yoon, W.-S.; Kim, K.-B.; Kim, M.-G.; Lee, M.-K.; Shin, H.-J.; Lee, J.-M.; Lee, J.-S.; Yo, C.-H., Oxygen Contribution on Li-Ion Intercalation−Deintercalation in LiCoO2 Investigated by O K-Edge and Co L-Edge X-ray Absorption Spectroscopy. *The Journal of Physical Chemistry B* **2002,** *106* (10), 2526-2532.
86. Jiang, Y.; Qin, C.; Yan, P.; Sui, M., Origins of capacity and voltage fading of LiCoO2 upon high voltage cycling. *Journal of Materials Chemistry A* **2019,** *7* (36), 20824-20831.
87. Zhou, A.; Liu, Q.; Wang, Y.; Wang, W.; Yao, X.; Hu, W.; Zhang, L.; Yu, X.; Li, J.; Li, H., Al2O3 surface coating on LiCoO2 through a facile and scalable wet-chemical method towards high-energy cathode materials withstanding high cutoff voltages. *Journal of Materials Chemistry A* **2017,** *5* (46), 24361-24370.
88. Yoon, C. S.; Jun, D.-W.; Myung, S.-T.; Sun, Y.-K., Structural Stability of LiNiO2 Cycled above 4.2 V. *ACS Energy Letters* **2017,** *2* (5), 1150-1155.
89. Goodenough, J. B.; Wickham, D. G.; Croft, W. J., Some magnetic and crystallographic properties of the system Li+xNi++1−2xni+++xO. *Journal of Physics and Chemistry of Solids* **1958,** *5* (1), 107-116.
90. Dyer, L. D.; Borie, B. S., Jr.; Smith, G. P., Alkali Metal-Nickel Oxides of the Type MNiO2. *Journal of the American Chemical Society* **1954,** *76* (6), 1499-1503.
91. Dahn, J. R.; Fuller, E. W.; Obrovac, M.; von Sacken, U., Thermal stability of LixCoO2, LixNiO2 and λ-MnO2 and consequences for the safety of Li-ion cells. *Solid State Ionics* **1994,** *69* (3), 265-270.
92. Yano, A.; Shikano, M.; Ueda, A.; Sakaebe, H.; Ogumi, Z., LiCoO2 Degradation Behavior in the High-Voltage Phase Transition Region and Improved Reversibility with Surface Coating. *Journal of The Electrochemical Society* **2017,** *164* (1), A6116.
93. Mohan, P.; Kalaignan, G. P., Electrochemical behaviour of surface modified SiO2-coated LiNiO2 cathode materials for rechargeable lithium-ion batteries. *Nanosci Nanotechnol* **2013,** *13* (4), 2765-70.
94. Kato, M.; Hayashi, T.; Hasegawa, G.; Lu, X.; Miyazaki, T.; Matsuda, Y.; Kuwata, N.; Kurihara, K.; Kawamura, J., Electrochemical properties of LiCoO2 thin film surface modified by lithium tantalate and lithium niobate coatings. *Solid State Ionics* **2017,** *308*, 54-60.
95. Cho, J.; Kim, T.-J.; Kim, Y. J.; Park, B., High-Performance ZrO2-Coated LiNiO2 Cathode Material. *Electrochemical and Solid-State Letters* **2001,** *4* (10), A159.
96. Ammundsen, B.; Desilvestro, J.; Groutso, T.; Hassell, D.; Metson, J. B.; Regan, E.; Steiner, R.; Pickering, P. J., Formation and Structural Properties of Layered LiMnO2 Cathode Materials. *Journal of The Electrochemical Society* **2000,** *147* (11), 4078.
97. Croguennec, L.; Pouillerie, C.; Mansour, A. N.; Delmas, C., Structural characterisation of the highly deintercalated LiNiO phases (with ≤ 0.30). *Journal of Materials Chemistry* **2001,** *11* (1), 131-141.
98. Yoon, W.-S.; Balasubramanian, M.; Yang, X.-Q.; Fu, Z.; Fischer, D. A.; McBreen, J., Soft X-Ray Absorption Spectroscopic Study of a LiNi0.5Mn0.5 O 2 Cathode during Charge. *Journal of The Electrochemical Society* **2004,** *151* (2), A246.
99. Deb, A.; Bergmann, U.; Cramer, S.; Cairns, E., Local structure of LiNi0.5Mn0.5O2 cathode material probed by in situ x-ray absorption spectroscopy. *Journal of Applied Physics* **2006,** *99*, 063701.
100. Ohzuku, T.; Makimura, Y., Layered Lithium Insertion Material of LiCo1/3Ni1/3Mn1/3O2 for Lithium-Ion Batteries. *Chemistry Letters - CHEM LETT* **2001,** *1*, 642-643.
101. Rossen, E.; Jones, C. D. W.; Dahn, J. R., Structure and electrochemistry of LixMnyNi1−yO2. *Solid State Ionics* **1992,** *57* (3), 311-318.
102. Julien, C. M.; Mauger, A. NCA, NCM811, and the Route to Ni-Richer Lithium-Ion Batteries *Energies* [Online], 2020.
103. Mori, D.; Kobayashi, H.; Shikano, M.; Nitani, H.; Kageyama, H.; Koike, S.; Sakaebe, H.; Tatsumi, K., Bulk and surface structure investigation for the positive electrodes of degraded lithium-ion cell after storage test using X-ray absorption near-edge structure measurement. *Journal of Power Sources - J POWER SOURCES* **2009,** *189*, 676-680.
104. Jung, S.-K.; Gwon, H.; Hong, J.; Park, K.-Y.; Seo, D.-H.; Kim, H.; Hyun, J.; Yang, W.; Kang, K., Understanding the Degradation Mechanisms of LiNi0.5Co0.2Mn0.3O2 Cathode Material in Lithium Ion Batteries. *Advanced Energy Materials* **2014,** *4* (1), 1300787.
105. Padhi, A.; Nanjundaswamy, K. S.; Goodenough, J., Phospho-Olivines as Positive-Electrode Materials for Rechargeable Lithium Batteries. *Journal of The Electrochemical Society* **1997,** *144*, 1188-1194.

106. Ohzuku, T.; Takeda, S.; Iwanaga, M., Solid-state redox potentials for Li[Me1/2Mn3/2]O4 (Me: 3d-transition metal) having spinel-framework structures: a series of 5 volt materials for advanced lithium-ion batteries. *Journal of Power Sources* **1999,** *81-82*, 90-94.
107. Zhong, Q.; Bonakdarpour, A.; Zhang, M.; Gao, Y.; Dahn, J. R., Synthesis and Electrochemistry of LiNix Mn2 − x O 4. *Journal of The Electrochemical Society* **1997,** *144* (1), 205.
108. House, R. A.; Bruce, P. G., Lightning fast conduction. *Nature Energy* **2020,** *5* (3), 191-192.
109. Goodenough, J. B.; Park, K.-S., The Li-Ion Rechargeable Battery: A Perspective. *Journal of the American Chemical Society* **2013,** *135* (4), 1167-1176.
110. Gong, Z.; Yang, Y., Recent advances in the research of polyanion-type cathode materials for Li-ion batteries. *Energy & Environmental Science* **2011,** *4* (9), 3223-3242.
111. Xiang, J.; Wei, Y.; Zhong, Y.; Yang, Y.; Cheng, H.; Yuan, L.; Xu, H.; Huang, Y., Building Practical High-Voltage Cathode Materials for Lithium-Ion Batteries. *Advanced Materials* **2022,** *34* (52), 2200912.
112. Ghosh, S.; Bhattacharjee, U.; Bhowmik, S.; Martha, D. S. K., A Review on High-Capacity and High-Voltage Cathodes for Next-Generation Lithium-ion Batteries. *Journal of Energy and Power Technology* **2022,** *04* (01), 002.
113. Li, Z.; Zhang, D.; Yang, F., Developments of lithium-ion batteries and challenges of LiFePO4 as one promising cathode material. *Journal of Materials Science* **2009,** *44* (10), 2435-2443.
114. Fergus, J. W., Recent developments in cathode materials for lithium ion batteries. *Journal of Power Sources* **2010,** *195* (4), 939-954.
115. Ellis, B. L.; Lee, K. T.; Nazar, L. F., Positive Electrode Materials for Li-Ion and Li-Batteries. *Chemistry of Materials* **2010,** *22* (3), 691-714.
116. Mohamed, N.; Allam, N. K., Recent advances in the design of cathode materials for Li-ion batteries. *RSC Advances*

2020, *10* (37), 21662-21685.
117. Nguyen, M. T.; Pham, T. L.; Tuyen, H. T. K.; Dai, H. N.; Le, M. L. P., Effect of conductive carbon additives and negative/positive capacity ratio on graphite/LiFePO4 full-cells performance. *Energy Storage* **2023,** *n/a* (n/a), e449.
118. Sun, S.; Guan, T.; Shen, B.; Leng, K.; Gao, Y.; Cheng, X.; Yin, G., Changes of Degradation Mechanisms of LiFePO4/Graphite Batteries Cycled at Different Ambient Temperatures. *Electrochimica Acta* **2017,** *237*, 248-258.
119. Herstedt, M.; Stjerndahl, M. r.; Nytén, A.; Gustafsson, T. r.; Rensmo, H.; Siegbahn, H.; Ravet, N.; Armand, M.; Thomas, J.; Edström, K., Surface Chemistry of Carbon-Treated LiFePO[sub 4] Particles for Li-Ion Battery Cathodes Studied by PES. *Electrochemical and Solid-State Letters* **2003,** *6*, A202.
120. Recham, N.; Chotard, J. N.; Jumas, J. C.; Laffont, L.; Armand, M.; Tarascon, J. M., Ionothermal Synthesis of Li-Based Fluorophosphates Electrodes. *Chemistry of Materials* **2010,** *22* (3), 1142-1148.
121. Nagahama, M.; Hasegawa, N.; Okada, S., High Voltage Performances of Li2NiPO4F Cathode with Dinitrile-Based Electrolytes. *Journal of The Electrochemical Society* **2010,** *157* (6), A748.
122. Julien, C.; Mauger, A.; Ait-Salah, A.; Massot, M.; Gendron, F.; Zaghib, K., Nanoscopic Scale Studies of LiFePO4 as Cathode Material in Lithium-ion Batteries for HEV Application. *Ionics* **2007,** *13*, 395-411.
123. Delacourt, C.; Poizot, P.; Levasseur, S.; Masquelier, C., Size Effects on Carbon-Free LiFePO4 Powders: The Key to Superior Energy Density. *Electrochemical and Solid-State Letters* **2006,** *9* (7), A352.
124. Marques Hobold, G.; Khurram, A.; Gallant, B., Operando Gas Monitoring of Solid Electrolyte Interphase Reactions on Lithium. *Chemistry of Materials* **2020**.
125. Whittingham, M. S., Lithium Batteries and Cathode Materials. *Chemical Reviews* **2004,** *104* (10), 4271-4302.
126. Delacourt, C.; Laffont, L.; Bouchet, R.; Wurm, C.; Leriche, J. B.; Morcrette, M.; Tarascon, J. M.; Masquelier, C., Toward Understanding of Electrical Limitations (Electronic, Ionic) in LiMPO4 (M = Fe , Mn) Electrode Materials. *Journal of The Electrochemical Society* **2005,** *152* (5), A913.
127. Yamada, A.; Iwane, N.; Harada, Y.; Nishimura, S.-i.; Koyama, Y.; Tanaka, I., Lithium Iron Borates as High-Capacity Battery Electrodes. *Advanced Materials* **2010,** *22* (32), 3583-3587.
128. Legagneur, V.; An, Y.; Mosbah, A.; Portal, R.; Le Gal La Salle, A.; Verbaere, A.; Guyomard, D.; Piffard, Y., LiMBO3 (M=Mn, Fe, Co):: synthesis, crystal structure and lithium deinsertion/insertion properties. *Solid State Ionics* **2001,** *139* (1), 37-46.
129. Pizarro-Sanz, J. L.; Dance, J. M.; Villeneuve, G.; Arriortua-Marcaida, M. I., The natural and synthetic tavorite minerals: Crystal chemistry and magnetic properties. *Materials Letters* **1994,** *18* (5), 327-330.

130. Barker, J.; Saidi, M. Y.; Swoyer, J. L., Electrochemical Insertion Properties of the Novel Lithium Vanadium Fluorophosphate, LiVPO4 F *Journal of The Electrochemical Society* **2003,** *150* (10), A1394.
131. Wang, X.; Gu, W.; Lee, J. T.; Nitta, N.; Benson, J.; Magasinski, A.; Schauer, M. W.; Yushin, G., Carbon Nanotube–CoF2 Multifunctional Cathode for Lithium Ion Batteries: Effect of Electrolyte on Cycle Stability. *Small* **2015,** *11* (38), 5164-5173.
132. Pereira, N.; Badway, F.; Wartelsky, M.; Gunn, S.; Amatucci, G. G., Iron Oxyfluorides as High Capacity Cathode Materials for Lithium Batteries. *Journal of The Electrochemical Society* **2009,** *156* (6), A407.
133. Liu, C.; Neale, Z. G.; Cao, G., Understanding electrochemical potentials of cathode materials in rechargeable batteries. *Materials Today* **2016,** *19* (2), 109-123.
134. Recham, N.; Chotard, J. N.; Dupont, L.; Delacourt, C.; Walker, W.; Armand, M.; Tarascon, J. M., A 3.6 V lithium-based fluorosulphate insertion positive electrode for lithium-ion batteries. *Nature Materials* **2010,** *9* (1), 68-74.
135. Barpanda, P.; Chotard, J.-N.; Recham, N.; Delacourt, C.; Ati, M.; Dupont, L.; Armand, M.; Tarascon, J.-M., Structural, Transport, and Electrochemical Investigation of Novel AMSO4F (A = Na, Li; M = Fe, Co, Ni, Mn) Metal Fluorosulphates Prepared Using Low Temperature Synthesis Routes. *Inorganic Chemistry* **2010,** *49* (16), 7401-7413.
136. Barpanda, P.; Recham, N.; Chotard, J.-N.; Djellab, K.; Walker, W.; Armand, M.; Tarascon, J.-M., Structure and electrochemical properties of novel mixed Li(Fe1−xMx)SO4F (M = Co, Ni, Mn) phases fabricated by low temperature ionothermal synthesis. *Journal of Materials Chemistry* **2010,** *20* (9), 1659-1668.
137. Meethong, N.; Kao, Y.-H.; Carter, W. C.; Chiang, Y.-M., Comparative Study of Lithium Transport Kinetics in Olivine Cathodes for Li-ion Batteries. *Chemistry of Materials* **2010,** *22* (3), 1088-1097.
138. Gong, Z. L.; Li, Y. X.; Yang, Y., Synthesis and electrochemical performance of Li2CoSiO4 as cathode material for lithium ion batteries. *Journal of Power Sources* **2007,** *174* (2), 524-527.
139. Lyness, C.; Delobel, B.; Armstrong, A. R.; Bruce, P. G., The lithium intercalation compound Li2CoSiO4 and its behaviour as a positive electrode for lithium batteries. *Chemical Communications* **2007,** (46), 4890-4892.
140. Jafta, C. J.; Hilger, A.; Sun, X.-G.; Geng, L.; Li, M.; Risse, S.; Belharouak, I.; Manke, I., A Multidimensional Operando Study Showing the Importance of the Electrode Macrostructure in Lithium Sulfur Batteries. *ACS Applied Energy Materials* **2020,** *3* (7), 6965-6976.
141. Weret, M. A.; Su, W.-N.; Hwang, B. J., Strategies towards High Performance Lithium-Sulfur Batteries. *Batteries & Supercaps* **2022,** *5* (8), e202200059.
142. Wu, F.; Yushin, G., Conversion cathodes for rechargeable lithium and lithium-ion batteries. *Energy & Environmental Science* **2017,** *10* (2), 435-459.
143. Yu, S.-H.; Feng, X.; Zhang, N.; Seok, J.; Abruña, H. D., Understanding Conversion-Type Electrodes for Lithium Rechargeable Batteries. *Accounts of Chemical Research* **2018,** *51* (2), 273-281.
144. Zhang, S.; Ueno, K.; Dokko, K.; Watanabe, M., Recent Advances in Electrolytes for Lithium–Sulfur Batteries. *Advanced Energy Materials* **2015,** *5* (16), 1500117.
145. Andre, D.; Kim, S.-J.; Lamp, P.; Lux, S. F.; Maglia, F.; Paschos, O.; Stiaszny, B., Future generations of cathode materials: an automotive industry perspective. *Journal of Materials Chemistry A* **2015,** *3* (13), 6709-6732.
146. Alt, H.; Binder, H.; Köhling, A.; Sandstede, G., Investigation into the use of quinone compounds-for battery cathodes. *Electrochimica Acta* **1972,** *17* (5), 873-887.
147. Ren, L.; Su, L.; Chen, X., Influence of DC conductivity of PPy anode on Li/PPy secondary batteries. *Journal of Applied Polymer Science* **2008,** *109* (6), 3458-3460.
148. Lu, Y.; Hou, X.; Miao, L.; Li, L.; Shi, R.; Liu, L.; Chen, J., Cyclohexanehexone with Ultrahigh Capacity as Cathode Materials for Lithium-Ion Batteries. *Angewandte Chemie International Edition* **2019,** *58* (21), 7020-7024.
149. Peng, C.; Ning, G.-H.; Su, J.; Zhong, G.; Tang, W.; Tian, B.; Su, C.; Yu, D.; Zu, L.; Yang, J.; Ng, M.-F.; Hu, Y.-S.; Yang, Y.; Armand, M.; Loh, K. P., Reversible multi-electron redox chemistry of π-conjugated N-containing heteroaromatic molecule-based organic cathodes. *Nature Energy* **2017,** *2* (7), 17074.
150. Sang, P.; Si, Y.; Fu, Y., Polyphenyl polysulfide: a new polymer cathode material for Li–S batteries. *Chemical Communications* **2019,** *55* (33), 4857-4860.
151. Wang, S.; Li, F.; Easley, A. D.; Lutkenhaus, J. L., Real-time insight into the doping mechanism of redox-active organic radical polymers. *Nature Materials* **2019,** *18* (1), 69-75.

152. Poizot, P.; Dolhem, F.; Gaubicher, J., Progress in all-organic rechargeable batteries using cationic and anionic configurations: Toward low-cost and greener storage solutions? *Current Opinion in Electrochemistry* **2018,** *9*, 70-80.
153. Janoschka, T.; Hager, M. D.; Schubert, U. S., Powering up the Future: Radical Polymers for Battery Applications. *Advanced Materials* **2012,** *24* (48), 6397-6409.
154. Takayuki, M.; Takayuki, K.; Toyonari, S.; Masaharu, S., High-performance Lithium Secondary Batteries Using Cathode Active Materials of Triquinoxalinylenes Exhibiting Six Electron Migration. *Chemistry letters* **2011,** *40* (7), 750-752.
155. Wu, Q.; Yang, L.; Wang, X.; Hu, Z., Mesostructured carbon-based nanocages: an advanced platform for energy chemistry. *Science China Chemistry* **2020,** *63* (5), 665-681.
156. Oubaha, H.; Gohy, J.-F.; Melinte, S., Carbonyl-Based π-Conjugated Materials: From Synthesis to Applications in Lithium-Ion Batteries. *ChemPlusChem* **2019,** *84* (9), 1179-1214.
157. Jouhara, A.; Dupré, N.; Gaillot, A.-C.; Guyomard, D.; Dolhem, F.; Poizot, P., Raising the redox potential in carboxyphenolate-based positive organic materials via cation substitution. *Nature Communications* **2018,** *9* (1), 4401.
158. Gu, S.; Bai, Z.; Majumder, S.; Huang, B.; Chen, G., Conductive metal–organic framework with redox metal center as cathode for high rate performance lithium ion battery. *Journal of Power Sources* **2019,** *429*, 22-29.
159. Yang, A.; Wang, X.; Lu, Y.; Miao, L.; Xie, W.; Chen, J., Core-shell structured 1,4-benzoquinone@TiO2 cathode for lithium batteries. *Journal of Energy Chemistry* **2018,** *27* (6), 1644-1650.
160. Han, X.; Chang, C.; Yuan, L.; Sun, T.; Sun, J., Aromatic Carbonyl Derivative Polymers as High-Performance Li-Ion Storage Materials. *Advanced materials* **2007,** *19* (12), 1616-1621.
161. Renault, S.; Geng, J.; Dolhem, F.; Poizot, P., Evaluation of polyketones with N-cyclic structure as electrode material for electrochemical energy storage: case of pyromellitic diimide dilithium salt. *Chemical Communications* **2011,** *47* (8), 2414-2416.
162. Lyu, H.; Sun, X.-G.; Dai, S., Organic cathode materials for lithium-ion batteries: Past, present, and future. *Advanced Energy Sustainability Research* **2021,** *2* (1), 2000044.
163. Yuan, C.; Wu, Q.; Li, Q.; Duan, Q.; Li, Y.; Wang, H.-g., Nanoengineered ultralight organic cathode based on aromatic carbonyl compound/graphene aerogel for green lithium and sodium ion batteries. *ACS Sustainable Chemistry & Engineering* **2018,** *6* (7), 8392-8399.
164. Heiska, J.; Nisula, M.; Karppinen, M., Organic electrode materials with solid-state battery technology. *Journal of Materials Chemistry A* **2019,** *7* (32), 18735-18758.
165. Lin, Z.; Liu, T.; Ai, X.; Liang, C., Aligning academia and industry for unified battery performance metrics. *Nature Communications* **2018,** *9* (1), 5262.
166. Lu, J.; Chen, Z.; Pan, F.; Cui, Y.; Amine, K., High-Performance Anode Materials for Rechargeable Lithium-Ion Batteries. *Electrochemical Energy Reviews* **2018,** *1* (1), 35-53.
167. Zhou, L.; Zhang, K.; Hu, Z.; Tao, Z.; Mai, L.; Kang, Y.-M.; Chou, S.-L.; Chen, J., Recent Developments on and Prospects for Electrode Materials with Hierarchical Structures for Lithium-Ion Batteries. *Advanced Energy Materials* **2018,** *8* (6), 1701415.
168. Winter, M.; Besenhard, J. O.; Spahr, M. E.; Novák, P., Insertion Electrode Materials for Rechargeable Lithium Batteries. *Advanced Materials* **1998,** *10* (10), 725-763.
169. Yan, J.; Zhang, J.; Su, Y.-C.; Zhang, X.-G.; Xia, B.-J., A novel perspective on the formation of the solid electrolyte interphase on the graphite electrode for lithium-ion batteries. *Electrochimica Acta* **2010,** *55*, 1785-1794.
170. Satoh, A.; Takami, N.; Ohsaki, T., Electrochemical intercalation of lithium into graphitized carbons. *Solid State Ionics* **1995,** *80* (3), 291-298.
171. Reddy, A. L. M.; Srivastava, A.; Gowda, S. R.; Gullapalli, H.; Dubey, M.; Ajayan, P. M., Synthesis Of Nitrogen-Doped Graphene Films For Lithium Battery Application. *ACS Nano* **2010,** *4* (11), 6337-6342.
172. Ai, W.; Luo, Z.; Jiang, J.; Zhu, J.; Du, Z.; Fan, Z.; Xie, L.; Zhang, H.; Huang, W.; Yu, T., Nitrogen and Sulfur Codoped Graphene: Multifunctional Electrode Materials for High-Performance Li-Ion Batteries and Oxygen Reduction Reaction. *Advanced Materials* **2014,** *26* (35), 6186-6192.
173. Cheng, Q.; Okamoto, Y.; Tamura, N.; Tsuji, M.; Maruyama, S.; Matsuo, Y., Graphene-Like-Graphite as Fast-Chargeable and High-Capacity Anode Materials for Lithium Ion Batteries. *Scientific Reports* **2017,** *7* (1), 14782.
174. Shi, H., Coke vs. graphite as anodes for lithium-ion batteries. *Journal of Power Sources* **1998,** *75* (1), 64-72.
175. Wang, G. X.; Bradhurst, D. H.; Dou, S. X.; Liu, H. K., Spinel Li[Li1/3Ti5/3]O4 as an anode material for lithium ion batteries. *Journal of Power Sources* **1999,** *83* (1), 156-161.

176. Amine, K.; Belharouak, I.; Chen, Z.; Tran, T.; Yumoto, H.; Ota, N.; Myung, S.-T.; Sun, Y.-K., Nanostructured Anode Material for High-Power Battery System in Electric Vehicles. *Advanced Materials* **2010,** *22* (28), 3052-3057.
177. Zhu, Z.; Cheng, F.; Chen, J., Investigation of effects of carbon coating on the electrochemical performance of Li4Ti5O12/C nanocomposites. *Journal of Materials Chemistry A* **2013,** *1* (33), 9484-9490.
178. Khan, F.; Oh, M.; Kim, J. H., N-functionalized graphene quantum dots: Charge transporting layer for high-rate and durable Li4Ti5O12-based Li-ion battery. *Chemical Engineering Journal* **2019,** *369*, 1024-1033.
179. Nzereogu, P. U.; Omah, A. D.; Ezema, F. I.; Iwuoha, E. I.; Nwanya, A. C., Anode materials for lithium-ion batteries: A review. *Applied Surface Science Advances* **2022,** *9*, 100233.
180. Yang, Y.; Li, Z.; Zhang, R.; Ding, Y.; Xie, H.; Liu, G.; Fan, Y.; Yang, Z.; Liu, X., Polydopamine-derived N-doped carbon-coated porous TiNb2O7 microspheres as anode materials with superior rate performance for lithium-ion batteries. *Electrochimica Acta* **2021,** *368*, 137623.
181. Li, H.; Liu, X.; Zhai, T.; Li, D.; Zhou, H., Li3VO4: A Promising Insertion Anode Material for Lithium-Ion Batteries. *Advanced Energy Materials* **2013,** *3* (4), 428-432.
182. Channu, V. S. R.; Holze, R.; Walker, E. H.; Wicker, S. A.; Kalluru, R. R.; Williams, Q. L.; Walters, W., Synthesis and Characterization of Lithium Vanadates for Electrochemical Applications. *International Journal of Electrochemical Science* **2010,** *5* (9), 1355-1366.
183. West, A. R.; Glasser, F. P., Preparation and crystal chemistry of some tetrahedral Li3PO4-type compounds. *Journal of Solid State Chemistry* **1972,** *4* (1), 20-28.
184. Yu, X.-Y.; Yu, L.; Lou, X. W., Metal Sulfide Hollow Nanostructures for Electrochemical Energy Storage. *Advanced Energy Materials* **2016,** *6* (3), 1501333.
185. Speirs, J.; Contestabile, M.; Houari, Y.; Gross, R., The future of lithium availability for electric vehicle batteries. *Renewable and Sustainable Energy Reviews* **2014,** *35*, 183-193.
186. Liang, B.; Liu, Y.; Xu, Y., Silicon-based materials as high capacity anodes for next generation lithium ion batteries. *Journal of Power Sources* **2014,** *267*, 469-490.
187. Park, C.-M.; Kim, J.-H.; Kim, H.; Sohn, H.-J., Li-alloy based anode materials for Li secondary batteries. *Chemical Society Reviews* **2010,** *39* (8), 3115-3141.
188. Esmanski, A.; Ozin, G. A., Silicon inverse-opal-based macroporous materials as negative electrodes for lithium ion batteries. *Advanced Functional Materials* **2009,** *19* (12), 1999-2010.
189. Beattie, S. D.; Loveridge, M. J.; Lain, M. J.; Ferrari, S.; Polzin, B. J.; Bhagat, R.; Dashwood, R., Understanding capacity fade in silicon based electrodes for lithium-ion batteries using three electrode cells and upper cut-off voltage studies. *Journal of Power Sources* **2016,** *302*, 426-430.
190. Hatchard, T. D.; Dahn, J. R., In situ XRD and electrochemical study of the reaction of lithium with amorphous silicon. *Journal of the Electrochemical Society* **2004,** *151* (6), A838-A842.
191. Yoshio, M.; Tsumura, T.; Dimov, N., Electrochemical behaviors of silicon based anode material. *Journal of Power Sources* **2005,** *146* (1), 10-14.
192. Yao, Y.; McDowell, M. T.; Ryu, I.; Wu, H.; Liu, N.; Hu, L.; Nix, W. D.; Cui, Y., Interconnected Silicon Hollow Nanospheres for Lithium-Ion Battery Anodes with Long Cycle Life. *Nano Letters* **2011,** *11* (7), 2949-2954.
193. Su, X.; Wu, Q.; Li, J.; Xiao, X.; Lott, A.; Lu, W.; Sheldon, B. W.; Wu, J., Silicon-Based Nanomaterials for Lithium-Ion Batteries: A Review. *Advanced Energy Materials* **2014,** *4* (1), 1300882.
194. Tamura, N.; Ohshita, R.; Fujimoto, M.; Kamino, M.; Fujitani, S., Advanced Structures in Electrodeposited Tin Base Negative Electrodes for Lithium Secondary Batteries. *Journal of The Electrochemical Society* **2003,** *150* (6), A679.
195. Wen, C. J.; Huggins, R. A., Thermodynamic Study of the Lithium-Tin System. *Journal of The Electrochemical Society* **1981,** *128* (6), 1181.
196. Dailly, A.; Ghanbaja, J.; Willmann, P.; Billaud, D., Lithium insertion into new graphite–antimony composites. *Electrochimica Acta* **2003,** *48* (8), 977-984.
197. He, X.; Pu, W.; Wang, L.; Ren, J.; Jiang, C.; Wan, C., Synthesis of nano Sb-encapsulated pyrolytic polyacrylonitrile composite for anode material in lithium secondary batteries. *Electrochimica Acta* **2007,** *52* (11), 3651-3653.
198. Morales, J.; Sánchez, L., Improving the Electrochemical Performance of SnO2 Cathodes in Lithium Secondary Batteries by Doping with Mo. *Journal of The Electrochemical Society* **1999,** *146* (5), 1640.
199. Chen, W. X.; Lee, J. Y.; Liu, Z., The nanocomposites of carbon nanotube with Sb and SnSb0.5 as Li-ion battery anodes. *Carbon* **2003,** *41* (5), 959-966.
200. Fuller, C. S.; Severiens, J. C., Mobility of Impurity Ions in Germanium and Silicon. *Physical Review* **1954,** *96* (1), 21-24.

201. Xianming, W.; Nishina, T.; Uchida, I., Lithium alloy formation at bismuth thin layer electrode and its kinetics in propylene carbonate electrolyte. *Journal of Power Sources* **2002,** *104* (1), 90-96.
202. Liang, H.; Liu, X.; Gao, D.; Ni, J.; Li, Y., Reduced graphene oxide decorated with Bi2O2.33 nanodots for superior lithium storage. *Nano Research* **2017,** *10* (11), 3690-3697.
203. Cabana, J.; Monconduit, L.; Larcher, D.; Palacín, M. R., Beyond Intercalation-Based Li-Ion Batteries: The State of the Art and Challenges of Electrode Materials Reacting Through Conversion Reactions. *Advanced Materials* **2010,** *22* (35), E170-E192.
204. Zhang, L.; Wu, H. B.; Lou, X. W., Iron-Oxide-Based Advanced Anode Materials for Lithium-Ion Batteries. *Advanced Energy Materials* **2014,** *4* (4), 1300958.
205. Yuan, C.; Wu, H. B.; Xie, Y.; Lou, X. W., Mixed Transition-Metal Oxides: Design, Synthesis, and Energy-Related Applications. *Angewandte Chemie International Edition* **2014,** *53* (6), 1488-1504.
206. Xiao, Y.; Hwang, J.-Y.; Belharouak, I.; Sun, Y.-K., Superior Li/Na-storage capability of a carbon-free hierarchical CoSx hollow nanostructure. *Nano Energy* **2017,** *32*, 320-328.
207. Rui, K.; Wen, Z.; Lu, Y.; Jin, J.; Shen, C., One-Step Solvothermal Synthesis of Nanostructured Manganese Fluoride as an Anode for Rechargeable Lithium-Ion Batteries and Insights into the Conversion Mechanism. *Advanced Energy Materials* **2015,** *5* (7), 1401716.
208. Bresser, D.; Passerini, S.; Scrosati, B., Leveraging valuable synergies by combining alloying and conversion for lithium-ion anodes. *Energy & Environmental Science* **2016,** *9* (11), 3348-3367.
209. Mueller, F.; Bresser, D.; Chakravadhanula, V. S. K.; Passerini, S., Fe-doped SnO2 nanoparticles as new high capacity anode material for secondary lithium-ion batteries. *Journal of Power Sources* **2015,** *299*, 398-402.
210. Wang, X.; Wang, J.; Chen, Z.; Yang, K.; Zhang, Z.; Shi, Z.; Mei, T.; Qian, J.; Li, J.; Wang, X., Yolk-double shell Fe3O4@ C@ C composite as high-performance anode materials for lithium-ion batteries. *Journal of Alloys Compounds* **2020,** *822*, 153656.
211. Wu, H. B.; Zhang, G.; Yu, L.; Lou, X. W., One-dimensional metal oxide-carbon hybrid nanostructures for electrochemical energy storage. *Nanoscale Horizons* **2016,** *1* (1), 27-40.
212. Qi, J.; Lai, X.; Wang, J.; Tang, H.; Ren, H.; Yang, Y.; Jin, Q.; Zhang, L.; Yu, R.; Ma, G.; Su, Z.; Zhao, H.; Wang, D., Multi-shelled hollow micro-/nanostructures. *Chemical Society Reviews* **2015,** *44* (19), 6749-6773.
213. Gachot, G.; Grugeon, S.; Armand, M.; Pilard, S.; Guenot, P.; Tarascon, J.-M.; Laruelle, S., Deciphering the multi-step degradation mechanisms of carbonate-based electrolyte in Li batteries. *Journal of Power Sources* **2008,** *178* (1), 409-421.
214. Zhang, W.-M.; Hu, J.-S.; Guo, Y.-G.; Zheng, S.-F.; Zhong, L.-S.; Song, W.-G.; Wan, L.-J., Tin-Nanoparticles Encapsulated in Elastic Hollow Carbon Spheres for High-Performance Anode Material in Lithium-Ion Batteries. *Advanced Materials* **2008,** *20* (6), 1160-1165.
215. León, B.; Corredor, J.; Tirado, J.; Perez Vicente, C., On the Mechanism of the Electrochemical Reaction of Tin Phosphide with Lithium. *Journal of The Electrochemical Society* **2006,** *153*, A1829-A1834.
216. Oh, H.-J.; Jo, C.-H.; Yoon, C. S.; Yashiro, H.; Kim, S.-J.; Passerini, S.; Sun, Y.-K.; Myung, S.-T., Nickel oxalate dihydrate nanorods attached to reduced graphene oxide sheets as a high-capacity anode for rechargeable lithium batteries. *NPG Asia Materials* **2016,** *8* (5), e270-e270.
217. Yoon, T.; Chae, C.; Sun, Y.-K.; Zhao, X.; Kung, H. H.; Lee, J. K., Bottom-up in situ formation of Fe3O4 nanocrystals in a porous carbon foam for lithium-ion battery anodes. *Journal of Materials Chemistry* **2011,** *21* (43), 17325-17330.
218. Park, C. M.; Sohn, H. J., Black Phosphorus and its Composite for Lithium Rechargeable Batteries. *Advanced Materials* **2007,** *19* (18), 2465-2468.
219. Qian, J.; Wu, X.; Cao, Y.; Ai, X.; Yang, H., High Capacity and Rate Capability of Amorphous Phosphorus for Sodium Ion Batteries. *Angewandte Chemie International Edition* **2013,** *52* (17), 4633-4636.
220. Hughes, T., Beyond Li-ion – batteries for transportation. SEIMENS: 2018; Vol. 2023.
221. Cheng, X.-B.; Zhang, R.; Zhao, C.-Z.; Zhang, Q., Toward Safe Lithium Metal Anode in Rechargeable Batteries: A Review. *Chemical Reviews* **2017,** *117* (15), 10403-10473.
222. He, Y.; Hu, H., Analysis of lithium ion concentration and stress in the solid electrolyte interphase on the graphite anode. *Physical Chemistry Chemical Physics* **2015,** *17* (36), 23565-23572.
223. Kushima, A.; So, K. P.; Su, C.; Bai, P.; Kuriyama, N.; Maebashi, T.; Fujiwara, Y.; Bazant, M. Z.; Li, J., Liquid cell transmission electron microscopy observation of lithium metal growth and dissolution: Root growth, dead lithium and lithium flotsams. *Nano Energy* **2017,** *32*, 271-279.
224. Pei, A.; Zheng, G.; Shi, F.; Li, Y.; Cui, Y., Nanoscale nucleation and growth of electrodeposited lithium metal. *Nano letters* **2017,** *17* (2), 1132-1139.
225. Xie, J.; Lu, Y.-C., A retrospective on lithium-ion batteries. *Nature Communications* **2020,** *11* (1), 2499.

226. Kalhoff, J.; Eshetu, G. G.; Bresser, D.; Passerini, S., Safer Electrolytes for Lithium-Ion Batteries: State of the Art and Perspectives. *ChemSusChem* **2015,** *8* (13), 2154-2175.
227. Xu, W.; Chen, X.; Ding, F.; Xiao, J.; Wang, D.; Pan, A.; Zheng, J.; Li, X. S.; Padmaperuma, A. B.; Zhang, J.-G., Reinvestigation on the state-of-the-art nonaqueous carbonate electrolytes for 5 V Li-ion battery applications. *Journal of Power Sources* **2012,** *213*, 304-316.
228. Zhang, S. S.; Jow, T. R., Aluminum corrosion in electrolyte of Li-ion battery. *Journal of Power Sources* **2002,** *109* (2), 458-464.
229. Song, J.; Wang, Y.; Wan, C., Conductivity study of porous plasticized polymer electrolytes based on poly (vinylidene fluoride) a comparison with polypropylene separators. *Journal of The Electrochemical Society* **2000,** *147* (9), 3219.
230. Jiang, J.; Dahn, J. R., Effects of solvents and salts on the thermal stability of LiC6. *Electrochimica Acta* **2004,** *49* (26), 4599-4604.
231. Tarascon, J. M.; Guyomard, D., New electrolyte compositions stable over the 0 to 5 V voltage range and compatible with the Li1+xMn2O4/carbon Li-ion cells. *Solid State Ionics* **1994,** *69* (3), 293-305.
232. Ue, M.; Sasaki, Y.; Tanaka, Y.; Morita, M., Nonaqueous Electrolytes with Advances in Solvents. In *Electrolytes for Lithium and Lithium-Ion Batteries*, Jow, T. R.; Xu, K.; Borodin, O.; Ue, M., Eds. Springer New York: New York, NY, 2014; pp 93-165.
233. J. Kalhoff, D. B., M. Bolloli, F. Alloin, J.-Y. Sanchez, S. Passerini, *EP 14 306 218.0* **2014**.
234. J. Kalhoff, D. B., M. Bolloli, F. Alloin, J.-Y. Sanchez, S. Passerini, *EP 15 305 097.6* **2015**.
235. Xu, K.; Angell, C. A., Sulfone-Based Electrolytes for Lithium-Ion Batteries. *Journal of The Electrochemical Society* **2002,** *149* (7), A920.
236. Watanabe, Y.; Kinoshita, S.-i.; Wada, S.; Hoshino, K.; Morimoto, H.; Tobishima, S.-i., Electrochemical properties and lithium ion solvation behavior of sulfone–ester mixed electrolytes for high-voltage rechargeable lithium cells. *Journal of Power Sources* **2008,** *179* (2), 770-779.
237. Duncan, H.; Salem, N.; Abu-Lebdeh, Y., Electrolyte Formulations Based on Dinitrile Solvents for High Voltage Li-Ion Batteries. *Journal of The Electrochemical Society* **2013,** *160* (6), A838.
238. Isken, P.; Dippel, C.; Schmitz, R.; Schmitz, R. W.; Kunze, M.; Passerini, S.; Winter, M.; Lex-Balducci, A., High flash point electrolyte for use in lithium-ion batteries. *Electrochimica Acta* **2011,** *56* (22), 7530-7535.
239. Tasaki, K.; Kanda, K.; Nakamura, S.; Ue, M., Decomposition of LiPF6and Stability of PF 5 in Li-Ion Battery Electrolytes: Density Functional Theory and Molecular Dynamics Studies. *Journal of The Electrochemical Society* **2003,** *150* (12), A1628.
240. Mauger, A.; Julien, C. M.; Paolella, A.; Armand, M.; Zaghib, K., A comprehensive review of lithium salts and beyond for rechargeable batteries: Progress and perspectives. *Materials Science and Engineering: R: Reports* **2018,** *134*, 1-21.
241. Zhang, S. S.; Xu, K.; Jow, T. R., Study of LiBF4 as an Electrolyte Salt for a Li-Ion Battery. *Journal of The Electrochemical Society* **2002,** *149* (5), A586.
242. Ue, M.; Mori, S., Mobility and Ionic Association of Lithium Salts in a Propylene Carbonate-Ethyl Methyl Carbonate Mixed Solvent. *Journal of The Electrochemical Society* **1995,** *142* (8), 2577.
243. Newman, G. H.; Francis, R. W.; Gaines, L. H.; Rao, B. M. L., Hazard Investigations of LiClO4 / Dioxolane Electrolyte. *Journal of The Electrochemical Society* **1980,** *127* (9), 2025.
244. Dougassa, Y. R.; Jacquemin, J.; El Ouatani, L.; Tessier, C.; Anouti, M., Viscosity and Carbon Dioxide Solubility for LiPF6, LiTFSI, and LiFAP in Alkyl Carbonates: Lithium Salt Nature and Concentration Effect. *The Journal of Physical Chemistry B* **2014,** *118* (14), 3973-3980.
245. Gnanaraj, J. S.; Zinigrad, E.; Levi, M. D.; Aurbach, D.; Schmidt, M., A comparison among LiPF6, LiPF3(CF2CF3)3 (LiFAP), and LiN(SO2CF2CF3)2 (LiBETI) solutions: electrochemical and thermal studies. *Journal of Power Sources* **2003,** *119-121*, 799-804.
246. Aravindan, V.; Gnanaraj, J.; Madhavi, S.; Liu, H.-K., Lithium-Ion Conducting Electrolyte Salts for Lithium Batteries. *Chemistry – A European Journal* **2011,** *17* (51), 14326-14346.
247. Mauger, A.; Julien, C.; Paolella, A.; Armand, M.; Zaghib, K., A comprehensive review of lithium salts and beyond for rechargeable batteries: Progress and perspectives. *Materials Science Engineering: R: Reports* **2018,** *134*, 1-21.
248. Barthel, J.; Wühr, M.; Buestrich, R.; Gores, H. J., A New Class of Electrochemically and Thermally Stable Lithium Salts for Lithium Battery Electrolytes: I . Synthesis and Properties of Lithium bis[1,2-benzenediolato(2-)-O,O′]borate. *Journal of The Electrochemical Society* **1995,** *142* (8), 2527.
249. Xu, K.; Zhang, S.; Jow, T. R.; Xu, W.; Angell, C. A., LiBOB as Salt for Lithium-Ion Batteries:A Possible Solution for High Temperature Operation. *Electrochemical and Solid-State Letters* **2002,** *5* (1), A26.
250. Shui Zhang, S., An unique lithium salt for the improved electrolyte of Li-ion battery. *Electrochemistry Communications* **2006,** *8* (9), 1423-1428.

251. Zhang, Z.; Chen, X.; Li, F.; Lai, Y.; Li, J.; Liu, P.; Wang, X., LiPF6 and lithium oxalyldifluoroborate blend salts electrolyte for LiFePO4/artificial graphite lithium-ion cells. *Journal of Power Sources* **2010,** *195* (21), 7397-7402.
252. Dudley, J. T.; Wilkinson, D. P.; Thomas, G.; LeVae, R.; Woo, S.; Blom, H.; Horvath, C.; Juzkow, M. W.; Denis, B.; Juric, P.; Aghakian, P.; Dahn, J. R., Conductivity of electrolytes for rechargeable lithium batteries. *Journal of Power Sources* **1991,** *35* (1), 59-82.
253. Kalhoff, J.; Bresser, D.; Bolloli, M.; Alloin, F.; Sanchez, J.-Y.; Passerini, S., Enabling LiTFSI-based Electrolytes for Safer Lithium-Ion Batteries by Using Linear Fluorinated Carbonates as (Co)Solvent. *ChemSusChem* **2014,** *7* (10), 2939-2946.
254. Zhang, X.; Winget, B.; Doeff, M.; Evans, J. W.; Devine, T. M., Corrosion of Aluminum Current Collectors in Lithium-Ion Batteries with Electrolytes Containing LiPF6. *Journal of The Electrochemical Society* **2005,** *152* (11), B448.
255. Han, H.-B.; Zhou, S.-S.; Zhang, D.-J.; Feng, S.-W.; Li, L.-F.; Liu, K.; Feng, W.-F.; Nie, J.; Li, H.; Huang, X.-J.; Armand, M.; Zhou, Z.-B., Lithium bis(fluorosulfonyl)imide (LiFSI) as conducting salt for nonaqueous liquid electrolytes for lithium-ion batteries: Physicochemical and electrochemical properties. *Journal of Power Sources* **2011,** *196* (7), 3623-3632.
256. Krause, L. J.; Lamanna, W.; Summerfield, J.; Engle, M.; Korba, G.; Loch, R.; Atanasoski, R., Corrosion of aluminum at high voltages in non-aqueous electrolytes containing perfluoroalkylsulfonyl imides; new lithium salts for lithium-ion cells. *Journal of Power Sources* **1997,** *68* (2), 320-325.
257. Kanamura, K., Anodic oxidation of nonaqueous electrolytes on cathode materials and current collectors for rechargeable lithium batteries. *Journal of Power Sources* **1999,** *81-82*, 123-129.
258. Han, H.; Guo, J.; Zhang, D.; Feng, S.; Feng, W.; Nie, J.; Zhou, Z., Lithium (fluorosulfonyl)(nonafluorobutanesulfonyl)imide (LiFNFSI) as conducting salt to improve the high-temperature resilience of lithium-ion cells. *Electrochemistry Communications* **2011,** *13* (3), 265-268.
259. Matsumoto, H.; Terasawa, N.; Umecky, T.; Tsuzuki, S.; Sakaebe, H.; Asaka, K.; Tatsumi, K., Low Melting and Electrochemically Stable Ionic Liquids Based on Asymmetric Fluorosulfonyl(trifluoromethylsulfonyl)amide. *Chemistry Letters* **2008,** *37* (10), 1020-1021.
260. Moretti, A.; Jeong, S.; Giffin, G. A.; Jeremias, S.; Passerini, S., Li-doped N-methoxyethyl-N-methylpyrrolidinium fluorosulfonyl-(trifluoromethanesulfonyl)imide as electrolyte for reliable lithium ion batteries. *Journal of Power Sources* **2014,** *269*, 645-650.
261. Han, H.-B.; Zhou, Y.-X.; Liu, K.; Nie, J.; Huang, X.-J.; Armand, M.; Zhou, Z.-B., Efficient Preparation of (Fluorosulfonyl)(pentafluoroethanesulfonyl)imide and Its Alkali Salts. *Chemistry Letters* **2010,** *39* (5), 472-474.
262. Chen, Z.; Liu, J.; Jansen, A. N.; GirishKumar, G.; Casteel, B.; Amine, K., Lithium Borate Cluster Salts as Redox Shuttles for Overcharge Protection of Lithium-Ion Cells. *Electrochemical and Solid-State Letters* **2010,** *13* (4), A39.
263. Tasaki, K.; Kanda, K.; Nakamura, S.; Ue, M., Decomposition of LiPF6 and stability of PF5 in Li-Ion battery electrolytes. Density functional theory and molecular dynamics studies. *Journal of the Electrochemical Society* **2003,** *150* (12), A1628-A1636.
264. McMillan, R.; Slegr, H.; Shu, Z. X.; Wang, W., Fluoroethylene carbonate electrolyte and its use in lithium ion batteries with graphite anodes. *Journal of Power Sources* **1999,** *81-82*, 20-26.
265. Benmayza, A.; Lu, W.; Ramani, V.; Prakash, J., Electrochemical and Thermal Studies of LiNi0.8Co0.15Al0.015O2 under Fluorinated Electrolytes. *Electrochimica Acta* **2014,** *123*, 7-13.
266. Chen, Z.; Amine, K., Tris(pentafluorophenyl) Borane as an Additive to Improve the Power Capabilities of Lithium-Ion Batteries. *Journal of The Electrochemical Society* **2006,** *153* (6), A1221.
267. Eshetu, G. G.; Grugeon, S.; Gachot, G.; Mathiron, D.; Armand, M.; Laruelle, S., LiFSI vs. LiPF6 electrolytes in contact with lithiated graphite: Comparing thermal stabilities and identification of specific SEI-reinforcing additives. *Electrochimica Acta* **2013,** *102*, 133-141.
268. Zhang, S. S., A review on electrolyte additives for lithium-ion batteries. *Journal of Power Sources* **2006,** *162* (2), 1379-1394.
269. Xu, S.-D.; Zhuang, Q.-C.; Wang, J.; Xu, Y.-Q.; Zhu, Y.-B., New Insight into Vinylethylene Carbonate as a Film Forming Additive to Ethylene Carbonate-Based Electrolytes for Lithium- Ion Batteries. *International Journal of Electrochemical Science* **2013,** *8* (6), 8058-8076.
270. Yao, W.; Zhang, Z.; Gao, J.; Li, J.; Xu, J.; Wang, Z.; Yang, Y., Vinyl ethylene sulfite as a new additive in propylene carbonate-based electrolyte for lithium ion batteries. *Energy & Environmental Science* **2009,** *2* (10), 1102-1108.
271. Liu, B.; Li, B.; Guan, S., Effect of Fluoroethylene Carbonate Additive on Low Temperature Performance of Li-Ion Batteries. *Electrochemical and Solid-State Letters* **2012,** *15* (6), A77.
272. Zheng, J.; Xiao, J.; Gu, M.; Zuo, P.; Wang, C.; Zhang, J.-G., Interface modifications by anion receptors for high energy lithium ion batteries. *Journal of Power Sources* **2014,** *250*, 313-318.

273. Xu, K.; Ding, M. S.; Zhang, S.; Allen, J. L.; Jow, T. R., An Attempt to Formulate Nonflammable Lithium Ion Electrolytes with Alkyl Phosphates and Phosphazenes. *Journal of The Electrochemical Society* **2002,** *149* (5), A622.
274. Yao, X. L.; Xie, S.; Chen, C. H.; Wang, Q. S.; Sun, J. H.; Li, Y. L.; Lu, S. X., Comparative study of trimethyl phosphite and trimethyl phosphate as electrolyte additives in lithium ion batteries. *Journal of Power Sources* **2005,** *144* (1), 170-175.
275. Hyung, Y. E.; Vissers, D. R.; Amine, K., Flame-retardant additives for lithium-ion batteries. *Journal of Power Sources* **2003,** *119-121*, 383-387.
276. Shim, E.-G.; Nam, T.-H.; Kim, J.-G.; Kim, H.-S.; Moon, S.-I., Electrochemical performance of lithium-ion batteries with triphenylphosphate as a flame-retardant additive. *Journal of Power Sources* **2007,** *172* (2), 919-924.
277. Xiang, H. F.; Xu, H. Y.; Wang, Z. Z.; Chen, C. H., Dimethyl methylphosphonate (DMMP) as an efficient flame retardant additive for the lithium-ion battery electrolytes. *Journal of Power Sources* **2007,** *173* (1), 562-564.
278. Xu, K.; Zhang, S.; Allen, J. L.; Jow, T. R., Evaluation of Fluorinated Alkyl Phosphates as Flame Retardants in Electrolytes for Li-Ion Batteries: II. Performance in Cell. *Journal of The Electrochemical Society* **2003,** *150* (2), A170.
279. Chen, J.; Buhrmester, C.; Dahn, J. R., Chemical Overcharge and Overdischarge Protection for Lithium-Ion Batteries. *Electrochemical and Solid-State Letters* **2005,** *8* (1), A59.
280. Chen, Z.; Amine, K., Bifunctional electrolyte additive for lithium-ion batteries. *Electrochemistry Communications* **2007,** *9* (4), 703-707.
281. Taggougui, M.; Carré, B.; Willmann, P.; Lemordant, D., 2,5-Difluoro-1,4-dimethoxybenzene for overcharge protection of secondary lithium batteries. *Journal of Power Sources* **2007,** *174* (2), 1069-1073.
282. Moshurchak, L. M.; Lamanna, W. M.; Bulinski, M.; Wang, R. L.; Garsuch, R. R.; Jiang, J.; Magnuson, D.; Triemert, M.; Dahn, J. R., High-Potential Redox Shuttle for Use in Lithium-Ion Batteries. *Journal of The Electrochemical Society* **2009,** *156* (4), A309.
283. Shima, K.; Shizuka, K.; Ue, M.; Ota, H.; Hatozaki, T.; Yamaki, J.-I., Reaction mechanisms of aromatic compounds as an overcharge protection agent for 4V class lithium-ion cells. *Journal of Power Sources* **2006,** *161* (2), 1264-1274.
284. Xiao, L.; Ai, X.; Cao, Y.; Yang, H., Electrochemical behavior of biphenyl as polymerizable additive for overcharge protection of lithium ion batteries. *Electrochimica Acta* **2004,** *49* (24), 4189-4196.
285. Arai, J.; Matsuo, A.; Fujisaki, T.; Ozawa, K., A novel high temperature stable lithium salt (Li2B12F12) for lithium ion batteries. *Journal of Power Sources* **2009,** *193* (2), 851-854.
286. Armand, M.; Johansson, P., Novel weakly coordinating heterocyclic anions for use in lithium batteries. *Journal of Power Sources* **2008,** *178* (2), 821-825.
287. Wang, C.-H.; Yeh, Y.-W.; Wongittharom, N.; Wang, Y.-C.; Tseng, C.-J.; Lee, S.-W.; Chang, W.-S.; Chang, J.-K., Rechargeable Na/Na0.44MnO2 cells with ionic liquid electrolytes containing various sodium solutes. *Journal of Power Sources* **2015,** *274*, 1016-1023.
288. M. Ue, A. M., K. Omata, S. Nakamura Book of Abstracts of the 41st Battery Symposium in Japan, 2000; p p. 292.
289. MacFarlane, D. R.; Meakin, P.; Sun, J.; Amini, N.; Forsyth, M., Pyrrolidinium Imides: A New Family of Molten Salts and Conductive Plastic Crystal Phases. *The Journal of Physical Chemistry B* **1999,** *103* (20), 4164-4170.
290. H. Sakaebe, H. M., H. Ohno (Ed.), Electrochemical Aspect of Ionic Liquid. Springer: Hoboken, NJ, 2005.
291. Yoon, H.; Best, A. S.; Forsyth, M.; MacFarlane, D. R.; Howlett, P. C., Physical properties of high Li-ion content N-propyl-N-methylpyrrolidinium bis(fluorosulfonyl)imide based ionic liquid electrolytes. *Physical Chemistry Chemical Physics* **2015,** *17* (6), 4656-4663.
292. Matsumoto, H.; Sakaebe, H.; Tatsumi, K.; Kikuta, M.; Ishiko, E.; Kono, M., Fast cycling of Li/LiCoO2 cell with low-viscosity ionic liquids based on bis(fluorosulfonyl)imide [FSI]−. *Journal of Power Sources* **2006,** *160* (2), 1308-1313.
293. Wongittharom, N.; Wang, C.-H.; Wang, Y.-C.; Fey, G. T.-K.; Li, H.-Y.; Wu, T.-Y.; Lee, T.-C.; Chang, J.-K., Charge-storage performance of Li/LiFePO4 cells with additive-incorporated ionic liquid electrolytes at various temperatures. *Journal of Power Sources* **2014,** *260*, 268-275.
294. Guerfi, A.; Dontigny, M.; Charest, P.; Petitclerc, M.; Lagacé, M.; Vijh, A.; Zaghib, K., Improved electrolytes for Li-ion batteries: Mixtures of ionic liquid and organic electrolyte with enhanced safety and electrochemical performance. *Journal of Power Sources* **2010,** *195* (3), 845-852.
295. Koželj, M.; Guerfi, A.; Zaghib, K., Silylated quaternary ammonium salts – ionic liquids with hydrophobic cations. *Journal of Materials Chemistry A* **2014,** *2* (38), 15964-15971.

296. Vilčnik, A.; Jerman, I.; Šurca Vuk, A.; Koželj, M.; Orel, B.; Tomšič, B.; Simončič, B.; Kovač, J., Structural Properties and Antibacterial Effects of Hydrophobic and Oleophobic Sol−Gel Coatings for Cotton Fabrics. *Langmuir* **2009,** *25* (10), 5869-5880.
297. S. Yamazaki, M. T., M. Usui 2010.
298. Sun, J.; Forsyth, M.; MacFarlane, D. R., Room-Temperature Molten Salts Based on the Quaternary Ammonium Ion. *The Journal of Physical Chemistry B* **1998,** *102* (44), 8858-8864.
299. Zhou, Z.-B.; Matsumoto, H.; Tatsumi, K., Low-Melting, Low-Viscous, Hydrophobic Ionic Liquids: Aliphatic Quaternary Ammonium Salts with Perfluoroalkyltrifluoroborates. *Chemistry – A European Journal* **2005,** *11* (2), 752-766.
300. Meng-Chang Lin, H. C., Hongjie Dai, Ionic Liquids Based Electrolytes for Rechargeable Batteries. *Material Matters* **2018,** *13.1*.
301. Cheng, X.-B.; Zhang, R.; Zhao, C.-Z.; Wei, F.; Zhang, J.-G.; Zhang, Q., A Review of Solid Electrolyte Interphases on Lithium Metal Anode. *Advanced Science* **2016,** *3* (3), 1500213.
302. Peled, E.; Golodnitsky, D.; Ardel, G., Advanced model for solid electrolyte interphase electrodes in liquid and polymer electrolytes. *Journal of the Electrochemical Society* **1997,** *144* (8), L208.
303. Ein-Eli, Y., A New Perspective on the Formation and Structure of the Solid Electrolyte Interface at the Graphite Anode of Li-Ion Cells. *Electrochemical solid-state letters* **1999,** *2* (5), 212.
304. Ein-Eli, Y.; McDevitt, S. F.; Laura, R., The Superiority of Asymmetric Alkyl Methyl Carbonates. *Journal of The Electrochemical Society* **1998,** *145* (1), L1.
305. Ein-Eli, Y., A New Perspective on the Formation and Structure of the Solid Electrolyte Interface at the Graphite Anode of Li - Ion Cells. *Electrochemical and Solid-State Letters* **1999,** *2* (5), 212.
306. Kanamura, K.; Shiraishi, S.; Takehara, Z. i., Electrochemical Deposition of Very Smooth Lithium Using Nonaqueous Electrolytes Containing HF. *Journal of The Electrochemical Society* **1996,** *143* (7), 2187.
307. Kanamura, K.; Tamura, H.; Shiraishi, S.; Takehara, Z. i., XPS Analysis of Lithium Surfaces Following Immersion in Various Solvents Containing LiBF4. *Journal of The Electrochemical Society* **1995,** *142* (2), 340.
308. Shi, S.; Lu, P.; Liu, Z.; Qi, Y.; Hector, L. G., Jr.; Li, H.; Harris, S. J., Direct calculation of Li-ion transport in the solid electrolyte interphase. *J Am Chem Soc* **2012,** *134* (37), 15476-87.
309. Chen, Y.; Ouyang, C.; Song, L.; Sun, Z., Electrical and Lithium Ion Dynamics in Three Main Components of Solid Electrolyte Interphase from Density Functional Theory Study. *Journal of Physical Chemistry C* **2011,** *115*, 7044-7049.
310. Peled, E.; Lombardi, A.; Schlaikjer, C. R., Lithium Alloy-Thionyl Chloride Cells: Performance and Safety Aspects. *Journal of The Electrochemical Society* **1983,** *130* (6), 1365.
311. Garreau, M., Cyclability of the lithium electrode. *Journal of Power Sources* **1987,** *20* (1), 9-17.
312. Thevenin, J., Passivating films on lithium electrodes. An approach by means of electrode impedance spectroscopy. *Journal of Power Sources* **1985,** *14* (1), 45-52.
313. Thevenin, J. G.; Muller, R. H., Impedance of Lithium Electrodes in a Propylene Carbonate Electrolyte. *Journal of The Electrochemical Society* **1987,** *134* (2), 273.
314. Heiskanen, S. K.; Kim, J.; Lucht, B. L., Generation and Evolution of the Solid Electrolyte Interphase of Lithium-Ion Batteries. *Joule* **2019,** *3* (10), 2322-2333.
315. Aurbach, D.; Markovsky, B.; Shechter, A.; Ein-Eli, Y.; Cohen, H., A Comparative Study of Synthetic Graphite and Li Electrodes in Electrolyte Solutions Based on Ethylene Carbonate-Dimethyl Carbonate Mixtures. *Journal of The Electrochemical Society* **1996,** *143* (12), 3809.
316. Zhang, B.; Metzger, M.; Solchenbach, S.; Payne, M.; Meini, S.; Gasteiger, H. A.; Garsuch, A.; Lucht, B. L., Role of 1,3-Propane Sultone and Vinylene Carbonate in Solid Electrolyte Interface Formation and Gas Generation. *The Journal of Physical Chemistry C* **2015,** *119* (21), 11337-11348.
317. Louli, A. J.; Ellis, L. D.; Dahn, J. R., Operando Pressure Measurements Reveal Solid Electrolyte Interphase Growth to Rank Li-Ion Cell Performance. *Joule* **2019,** *3* (3), 745-761.
318. Nie, M.; Chalasani, D.; Abraham, D. P.; Chen, Y.; Bose, A.; Lucht, B. L., Lithium Ion Battery Graphite Solid Electrolyte Interphase Revealed by Microscopy and Spectroscopy. *The Journal of Physical Chemistry C* **2013,** *117* (3), 1257-1267.
319. Liu, T.; Lin, L.; Bi, X.; Tian, L.; Yang, K.; Liu, J.; Li, M.; Chen, Z.; Lu, J.; Amine, K.; Xu, K.; Pan, F., In situ quantification of interphasial chemistry in Li-ion battery. *Nature Nanotechnology* **2019,** *14* (1), 50-56.
320. Aurbach, D.; Ein-Eli, Y.; Chusid, O.; Carmeli, Y.; Babai, M.; Yamin, H., The Correlation Between the Surface Chemistry and the Performance of Li-Carbon Intercalation Anodes for Rechargeable 'Rocking-Chair' Type Batteries. *Journal of The Electrochemical Society* **1994,** *141* (3), 603.
321. Wang, A.; Kadam, S.; Li, H.; Shi, S.; Qi, Y., Review on modeling of the anode solid electrolyte interphase (SEI) for lithium-ion batteries. *NPJ Computational Materials* **2018,** *4* (1), 15.

322. Cao, C.; Abate, I. I.; Sivonxay, E.; Shyam, B.; Jia, C.; Moritz, B.; Devereaux, T. P.; Persson, K. A.; Steinrück, H.-G.; Toney, M. F., Solid Electrolyte Interphase on Native Oxide-Terminated Silicon Anodes for Li-Ion Batteries. *Joule* **2019,** *3* (3), 762-781.
323. Zier, M.; Scheiba, F.; Oswald, S.; Thomas, J.; Goers, D.; Scherer, T.; Klose, M.; Ehrenberg, H.; Eckert, J., Lithium dendrite and solid electrolyte interphase investigation using OsO4. *Journal of Power Sources* **2014,** *266*, 198-207.
324. Takenaka, N.; Suzuki, Y.; Sakai, H.; Nagaoka, M., On Electrolyte-Dependent Formation of Solid Electrolyte Interphase Film in Lithium-Ion Batteries: Strong Sensitivity to Small Structural Difference of Electrolyte Molecules. *The Journal of Physical Chemistry C* **2014,** *118* (20), 10874-10882.
325. Chen, X.; Xie, J.; Zhao, X.; Zhu, T., Electrochemical Compatibility of Solid-State Electrolytes with Cathodes and Anodes for All-Solid-State Lithium Batteries: A Review. *Advanced Energy and Sustainability Research* **2021,** *2* (5), 2000101.
326. Yoon, T.; Milien, M. S.; Parimalam, B. S.; Lucht, B. L., Thermal Decomposition of the Solid Electrolyte Interphase (SEI) on Silicon Electrodes for Lithium Ion Batteries. *Chemistry of Materials* **2017,** *29* (7), 3237-3245.
327. Young, B. T.; Heskett, D. R.; Nguyen, C. C.; Nie, M.; Woicik, J. C.; Lucht, B. L., Hard X-ray Photoelectron Spectroscopy (HAXPES) Investigation of the Silicon Solid Electrolyte Interphase (SEI) in Lithium-Ion Batteries. *ACS Applied Materials & Interfaces* **2015,** *7* (36), 20004-20011.
328. Nie, M.; Demeaux, J.; Young, B. T.; Heskett, D. R.; Chen, Y.; Bose, A.; Woicik, J. C.; Lucht, B. L., Effect of Vinylene Carbonate and Fluoroethylene Carbonate on SEI Formation on Graphitic Anodes in Li-Ion Batteries. *Journal of The Electrochemical Society* **2015,** *162* (13), A7008.
329. Michan, A. L.; Parimalam, B. S.; Leskes, M.; Kerber, R. N.; Yoon, T.; Grey, C. P.; Lucht, B. L., Fluoroethylene Carbonate and Vinylene Carbonate Reduction: Understanding Lithium-Ion Battery Electrolyte Additives and Solid Electrolyte Interphase Formation. *Chemistry of Materials* **2016,** *28* (22), 8149-8159.
330. Peled, E.; Straze, H., The Kinetics of the Magnesium Electrode in Thionyl Chloride Solutions. *Journal of The Electrochemical Society* **1977,** *124* (7), 1030.
331. Xiong, S.; Xie, K.; Diao, Y.; Hong, X., On the role of polysulfides for a stable solid electrolyte interphase on the lithium anode cycled in lithium–sulfur batteries. *Journal of Power Sources* **2013,** *236*, 181-187.
332. Lu, Y.; Tu, Z.; Shu, J.; Archer, L. A., Stable lithium electrodeposition in salt-reinforced electrolytes. *Journal of Power Sources* **2015,** *279*, 413-418.
333. Monroe, C.; Newman, J., The Impact of Elastic Deformation on Deposition Kinetics at Lithium/Polymer Interfaces. *Journal of The Electrochemical Society* **2005,** *152*, A396-A404.
334. Goodenough, J., Energy Storage Materials: A Perspective. *Energy Storage Materials* **2015,** *1*, ENSM_2015_34.
335. Liu, Z.; Qi, Y.; Lin, Y. X.; Chen, L.; Lu, P.; Chen, L. Q., Interfacial Study on Solid Electrolyte Interphase at Li Metal Anode: Implication for Li Dendrite Growth. *Journal of The Electrochemical Society* **2016,** *163* (3), A592.
336. Lin, Y.-X.; Liu, Z.; Leung, K.; Chen, L.-Q.; Lu, P.; Qi, Y., Connecting the irreversible capacity loss in Li-ion batteries with the electronic insulating properties of solid electrolyte interphase (SEI) components. *Journal of Power Sources* **2016,** *309*, 221-230.
337. Aurbach, D.; Markovsky, B.; Salitra, G.; Markevich, E.; Talyossef, Y.; Koltypin, M.; Nazar, L.; Ellis, B.; Kovacheva, D., Review on electrode–electrolyte solution interactions, related to cathode materials for Li-ion batteries. *Journal of Power Sources* **2007,** *165* (2), 491-499.
338. Schroder, K. W.; Celio, H.; Webb, L. J.; Stevenson, K. J., Examining Solid Electrolyte Interphase Formation on Crystalline Silicon Electrodes: Influence of Electrochemical Preparation and Ambient Exposure Conditions. *The Journal of Physical Chemistry C* **2012,** *116* (37), 19737-19747.
339. Zhang, Z.; Yang, J.; Huang, W.; Wang, H.; Zhou, W.; Li, Y.; Li, Y.; Xu, J.; Huang, W.; Chiu, W.; Cui, Y., Cathode-Electrolyte Interphase in Lithium Batteries Revealed by Cryogenic Electron Microscopy. *Matter* **2021,** *4* (1), 302-312.
340. Dühnen, S.; Betz, J.; Kolek, M.; Schmuch, R.; Winter, M.; Placke, T., Toward Green Battery Cells: Perspective on Materials and Technologies. *Small Methods* **2020,** *4* (7), 2000039.
341. Smith, J., The shaming images that show where our iPhones, laptops and Tesla cars really come from: The truth about the Congolese mines where kids are paid $2-a-day to dig for cobalt. 30 January 2023, 2023.
342. Gross, T. *How 'modern-day slavery' in the Congo powers the rechargeable battery economy*; February 1, 2023, 2023.
343. Kara, S., *Cobalt Red : How the Blood of the Congo Powers Our Lives*. St. Martin's Press: 2023; p 288.

344. Frédéric Simon, P. M., Facing water stress: Chile's lithium industry under scrutiny in Atacama Desert. Euractiv: 2023.
345. Campbell, M., South America's 'lithium fields' reveal the dark side of our electric future. 01/02/2022, 2022.
346. Chang, Z.; Yang, H.; Zhu, X.; He, P.; Zhou, H., A stable quasi-solid electrolyte improves the safe operation of highly efficient lithium-metal pouch cells in harsh environments. *Nature Communications* **2022,** *13* (1), 1510.
347. Okafor, J., Environmental Impact Of Battery Production And Disposal. TRVST: 2022; Vol. 2023.
348. Costa, C. M.; Barbosa, J. C.; Gonçalves, R.; Castro, H.; Campo, F. J. D.; Lanceros-Méndez, S., Recycling and environmental issues of lithium-ion batteries: Advances, challenges and opportunities. *Energy Storage Materials* **2021,** *37*, 433-465.
349. *Lithium-ion batteries need to be greener and more ethical*; Nature: 29 June 2021, 2021.
350. Jacoby, M., It's time to get serious about recycling lithium-ion batteries. July 14, 2019.
351. Shekhar, A. R.; Parekh, M. H.; Pol, V. G., Worldwide ubiquitous utilization of lithium-ion batteries: What we have done, are doing, and could do safely once they are dead? *Journal of Power Sources* **2022,** *523*, 231015.

Chapter 2 Polymer-based electrolytes

Abstract

The key components of batteries referring to electrodes and electrolyte, are already discussed in chapter 1 covering the state of art of materials and research. The contextual focus of discussion was attempted in line with the background of Lithium-ion batteries based on liquid electrolytes in the previous chapter. While current research trends largely revolve around safe, sustainable and high performing solid-state batteries. That takes us to the adoption of lithium metal anode with safer solid or quasi-solid electrolytes and high voltage cathodes. In this chapter, a detailed introduction to the polymer electrolytes has been attempted with advantages and disadvantages highlighting their performance in lithium metal batteries. One of the important discovery, poly(ethylene oxide) based polymers as cation conductors boasted varieties of polymer electrolytes investigations such as polycarbonates, poly(vinyl difluoride), polyurethanes, *etc*. Engineering polymers for targeted properties gained significant interest via techniques such as copolymerization, block, grafting and blending polymers. An ideal electrolyte requires good conductivity, broad voltage window and other electrochemical properties which led to the development of gel polymer electrolytes and hybrid electrolytes with inorganic particles. Given most of those electrolytes are sourced from environment unfriendly

precursors, important efforts are simultaneously going on polymers derived from bio-based sources such as cellulose, gum and vegetables. The last section of this chapter focuses on that aspect which is also the crux of this thesis.

2.1 Introduction to non-liquid electrolytes

The all solid-state battery constitutes cell components entirely solid, specifically referring to solid electrolytes. A brief and yet necessary discussion has been explained in Chapter 1 in materials section for electrolytes, salts, solvents which established our basic understanding prior to diving into solid state electrolytes. In short, current LIB technology needs to be revolutionized which suggested the use for safer solid-state electrolytes (SSEs) with reactive lithium metal anode for high energy density and power density application. SSE enhances the safety of the battery from both leakage and thermal hazard, limiting dendrite growth, provide flexibility, robustness and easier recycling. They are not only limited to lithium metal batteries but also lithium polysulfide and lithium oxygen batteries as future alternatives in the domain of lithium battery technology.[1-4] In a boost towards other metal-based batteries such as sodium, potassium and magnesium batteries, many researchers are simultaneously working on solid state electrolyte integrated cells for safe and alternate solutions to existing ones.[5] The fossil fuels free based mobility for vehicles, aviation and marine industry bets on high performance all solid-state batteries using high voltage cathodes and anodes such as lithium metal, silicon-and sulfide based ones. Figure 2.1 demonstrates the relation of energy density with the amount of solid electrolyte composition versus liquid.[6]

From the beginning, both inorganic solid electrolytes (ISEs) and organic solid polymer electrolytes (SPEs) are actively looked upon. ISEs have relatively more chemically and thermal stability with the high ionic conductivity at RT. Nevertheless, they are crystalline in nature providing ordered Li- ion transport channels and thus transference number equals to unity. There are different categories of ISE like garnet-type, perovskite type, NASICON, LISICON, ceramic oxides (LLZO, Al_2O_3) *etc*.[7-11] However, they suffer from a serious issue of brittleness and interfacial compatibility. On contrary to ISEs, SPEs proffer better interfacial contact with electrodes, a high degree of flexibility on deformation and easy processability. It is not to be ignored that SPEs are lighter, scalable, cheaper, no or less toxic. In general, most of them cannot compete well in terms of ionic conductivity and transference number when compared to ISEs.[12] But the wide range of structural control and tunablity for the desired properties with available polymerization techniques make SPEs more interesting candidates.

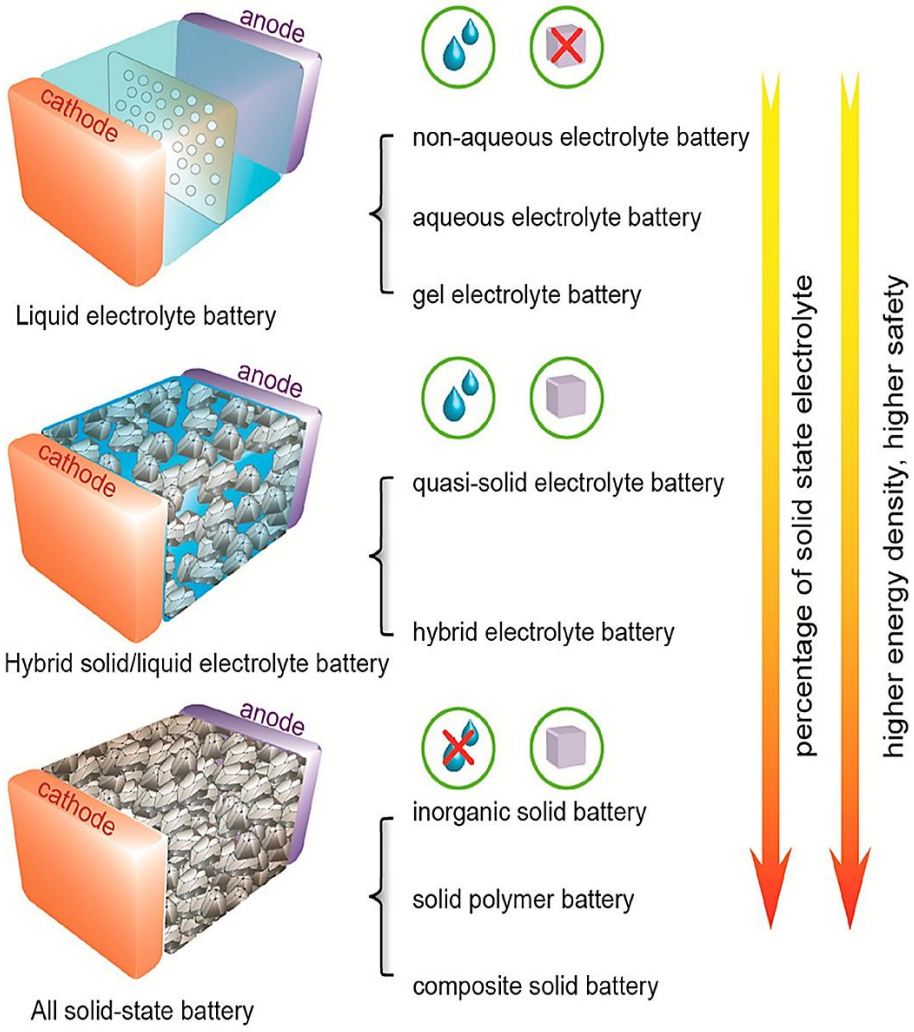

Figure 2. 1: Schematic illustration of the classification of prevailing lithium batteries. Three types of batteries can be classified based on the amount of liquid and percentage of SSE in the assembled batteries. Reproduced with permission,[6] copyright 2021, ACS.

2.1.1 Polymer electrolytes

The first report of a polymer as SPE for Li ion conduction was demonstrated by Armand *et al*. in 1978,[13] after the successful discovery of alkali metal salts dissolution in poly(ethylene oxide) as conductive material in 1973 by Fenton and Wright.[14, 15] This discovery of the PEO-LiTFSI system is marked as a breakthrough and opened a wholesome gateway to other SPEs. Even after 50 years, it is still considered as a hot topic of research. It comes in the category of dry SPEs which has been discussed in

subsequent sections. Around the same time period, Feuillade *et al.* developed in 1975 quasi-solid state gel polymer electrolytes (GPEs) by introducing organic plasticizers into the polymer-salt binary system.[16] Keeping the lower conductivity of SPEs in mind, composite electrolytes were formulated in a series of steps using active and inactive fillers. For instance, Skaarup[17] and Wieczorek[18] investigated in their work that addition of Li_3N (active) and Al_2O_3 (inactive) fillers contribute to the increased conductivity relative to pristine PEO. A detailed plot reviewing and showcasing the state-of-the-art electrolytes developed over 50 years has been depicted with their conductivity in Figure 2.2a.[19]

Each development in the structural framework of the electrolyte is dedicated to obtain properties defined above in a single material. Within the years of understanding of batteries materials, their operation and failure mechanisms, it became very clear that an electrolyte should possess a stabilized interface with lower interfacial resistance, higher storage modulus *etc.*, in addition to ionic conductivity, higher oxidation stability and transference number.

A Radar chart has been depicted in Figure 2.3 for comparative overview of electrolytes from liquid to solid.[20] Targeting these properties, several polymer electrolytes have been designed and reported so far based on different strategies which

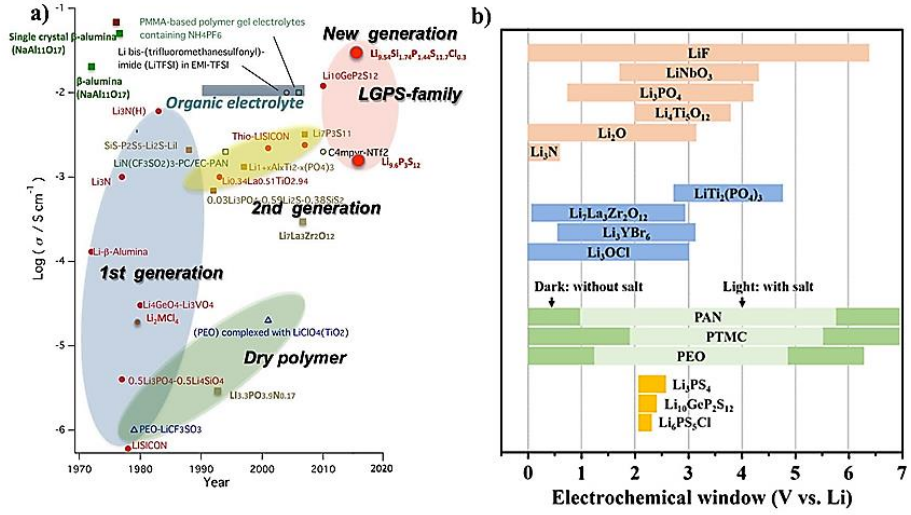

Figure 2. 2: A brief history of innovation of lithium super ionic conducting electrolytes over several decades. Reproduced with permission,[19] copyright 2016, Wind power engineering & development. b) Electrochemical windows of various electrolytes (PEO:Poly(ethylene oxide), PTMC: Poly(trimethylene carbonate) and PAN: Polyacrylonitrile) and lithium salts. Reproduced with permission,[21] copyright 2021, Wiley.

fall into categories as explained below. Given the development in the high voltage cathodes for higher energy density, ESW plays a key role in designing the electrolyte and adapting to the right salt within voltage window as shown in Figure 2.2b for some common polymers.[21] However, a background on the characteristics of the polymer electrolyte is equally important for smart selection of monomers and other polymeric functionalities.

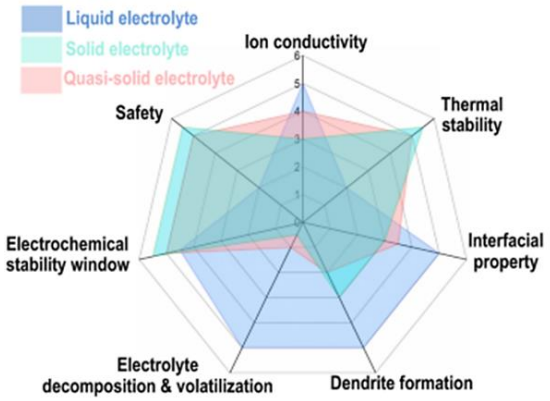

Figure 2. 3: Radar chart for comparative advantages within respective electrolytes. Reproduced with permission,[20] copyright 2022, Nature.

2.1.2 Characteristics of polymer electrolytes

2.1.2.1 Electrochemical characteristics

2.1.2.1.1 Ion transfer / conductivity:

Unlike ISE, SPE conducts via dissolution of ions by forming polymer-salt complexes. Polymers with polar groups such as — O—, — S—, — N—, — P—, C=O, and C=N are credited to dissolve lithium salts. In general, higher conductivity is attributed to a higher number of mobile ions dissolved in the polymer matrix. Yet another established fact about dissociation of salts is that the lattice energy of the salt should be relatively low with a higher dielectric constant of the polymer.[22] In thermal analysis of the polymer, glass transition temperature (T_g) of the polymer is often considered as an important parameter since the ionic transport takes place in amorphous regions above T_g. The mechanism can be explained as polar groups coordinated lithium ions migrate from one to another coordination site along with segmental motion of polymer chains or hopping between chains via free volume (as a result of local segmental motion)

under electric field. This is one of the simplest theory given by Cohen and Turnbull in 1959.[23] However, this model does not involve the microscopic behaviour like dielectric relaxation, effect of molecular weight in transport properties *etc*. Beside this theory, a newer concept of ion conductivity was diverted from the former one stating the ionic conductivity through ordered and static crystalline phase can be greater than amorphous phase above T_g of the material.[24] This has been explained in the schematic model expressing that a cylindrical tunnel evolves from the pair of folded PEO chains constituting the crystalline phase of P(EO) $_6$-LiX (X=PF_6, AsF_6, SbF_6) as shown in Figure 2.4a and 2.4b.

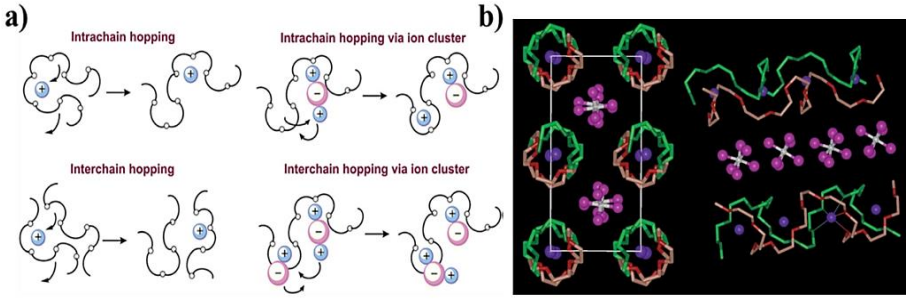

Figure 2. 4: a) Mechanism of ion transport in PEO. Reproduced with permission,[25] copyright 2015, RSC. b) Structure of PEO along the chain axis showing rows of Li^+ ions from top view (left) and structure showing the relative position of the chains and their conformation (hydrogen not shown) (where, blue spheres, lithium; white spheres, arsenic; pink spheres, fluorine; light green, carbon in chain 1; dark green, oxygen in chain 1; light red, carbon in chain 2; dark red, oxygen in chain 2 and thin lines indicate coordination around the Li^+ cation) (right). Reproduced with permission,[24] copyright 2001, Nature.

The coordinated lithium within the tunnel moves from one site to another without any segmental motion while anions sit outside these tunnels in inter-chain space.[24, 26-28] The validation of this new model was not initially successful by Wesley and Stefano in their ionic conductivity analysis of the same crystalline SPEs $P(EO)_6$-LiX (X=PF_6, AsF_6, SbF_6).[29, 30] This is why more investigations are required to validate this model.

The ionic conductivity in composite polymer electrolytes follows different mechanism due to the Lewis acid-base interactions. It is found that the polymer phase acts as ion transport media via dipole-dipole interactions. The Lewis acid groups of fillers and Li-ion compete to formation of complexes with the polymer host and with the anions of the salt while the hydrogen bonds between fillers and polymer host increase the free volume and fast transport by disturbing the chains. Therefore, those Lewis-base interactions avail more charge carriers for higher conductivity via promoting decoupling of polymer-ions for more dissociation. The interaction of

inorganic filler with polymer follows thus multiple ways, as discussed above and briefly depicted in Figure 2.5.

Focusing on the effect of temperature on-ion transfer, there are two popular models referred as Arrhenius type and Vogal–Fulcher–Tamman (VFT) type.[31] Arrhenius type is usually applied when the conductivity follows linear behaviour fitted using equation 2.1,

$$\sigma = \sigma_o \mathrm{e}^{-\frac{E_\alpha}{k_\mathrm{b} T}} \qquad 2.1$$

Where σ is the ionic conductivity, σ_o is the pre-exponential factor which is related to the number of charge carriers E_α is activation energy and k_b is Boltzmann constant. The slope of the equation is used to calculate the activation energy of the salt in SPE. An SPE following Arrhenius type is supposed to have conductivity from ion hopping decoupled from the polymer chain breathing.[32] It is widely applied in both ISEs and SPEs. As far as VFT type is concerned, it was developed mostly for the diffusion process in disordered and glass materials. Unlike Arrhenius type, the logarithmic plot of $\sigma\ vs\ \frac{1}{T}$ comes non-linear, indicating the combined effect of ion hopping and breathing/segmental motion above T_g of SPE applied in gel polymer electrolytes and ionic liquids too. The equation for VFT is expressed as in equation 2.2:

$$\sigma T^{1/2} = A\mathrm{e}^{-\frac{B}{(T-T_0)}} \qquad 2.2$$

With B as pseudo activation energy for the conductivity equivalent to ratio of activation energy and Boltzmann's constant, T_0 is equilibrium glass transition temperature, temperature ($T_0 \cong T_g - 50$ K), T_g is the glass transition temperature.[32-34] These models are well utilized for investigation of conductivity for current research investigations. However, beside them there are various models aligning well with different electrolyte systems due to their ionic conductivity dependence on amorphous phase, cation size, ion pairing, dielectric constant, *etc*. These are the configurational entropy model,[35] Angels decoupling theory,[36] amorphous phase model,[37] effective medium theory[38] and Williams, Landel, and Ferry theory[39] (similar to VFT).

2.1.2.1.2 Transference number

The ionic transport is the key parameter for an electrolyte. However, Li cations complex well with polar groups of polymers, leaving away the mobile anions which contribute significantly to the unnecessary conductivity, causing the concentration gradients, larger at high discharge currents. This leads to low lithium transfer number

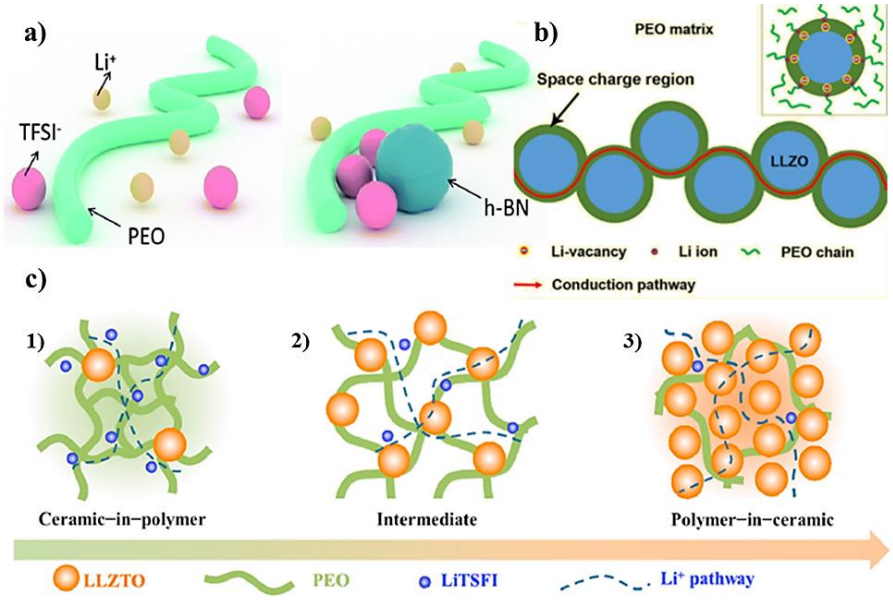

Figure 2.5: Schematic illustration of a) PEO/LiTFSI solid polymer electrolyte (left) and PEO/LiTFSI/h-BN composite solid electrolyte membrane (right), Reproduced with permission,[40] copyright 2020, RSC, b) fast ionic conduction pathway along the space charge regions, Reproduced with permission,[41] copyright 2019, ACS, and c) PEO-LLZTO CSE: (1) "ceramic-in-polymer"; (2) "intermediate"; (3) "polymer-in-ceramic", Reproduced with permission,[42] copyright 2018, Elsevier.

(for instance ~ 0.2 for PEO) which is detrimental for the battery cycling leading to higher polarization, degradation, and cell failure. Addressing this concern requires design of high transference number (t_{Li^+}) polymer electrolyte that is influenced by various internal as well external parameters. A choice of polymer to possess high t_{Li^+} can be based on polarity, Lewis acidity-basicity, donor number, ionic affinity and segmental motion.[43] Anions complex with Lewis acidic sites, which points at the requirement of Lewis acid polymers such as polymers with boron and phosphorous atoms, increasing t_{Li^+} significantly by affecting the interaction, as illustrated in Figure 2.5a.[40, 44] Higher segmental motion contributes toward superior Li-ion transport in addition to large intra-chain Li-ion diffusion. Segmental motion with lower T_g coupled with lower crystallinity is a crucial parameter as observed in a comparison of PEO and PPC.[45] Unlike the former, polarity and donor number do hold a straight relation with ionic conductivity and t_{Li^+}, meaning it should be in proper range to have balanced dissociation and electrostatic interaction for facile mobility.

Besides polymeric parameters, lithium salts and inorganic fillers influence t_{Li^+} as well. The size of anions relates directly to the increased dissociation and restricted

mobility in the order of $LiBF_4$ < $LiClO_4$ < LiFSI < LiTFSI < LiBOB < LiBNMB. Nevertheless, the concentration of salts in some electrolytes influences higher cationic transports.[46] Addition of inorganic fillers (referred as additives as well) is a popular and interesting approach for composite electrolytes which integrates various desired properties into the polymer. Again, Lewis acid-base interactions in fillers and others clearly enhance the mobility depending on the dielectric constant, surface state, structure and concentration. In few investigations, it is demonstrated that vacancies on the surface provide a pathway for the fast hopping of Li^+.[47] Figure 2.5b and 2.5c depict the Li^+ mobility in composite electrolytes along with space charge region and effect of concentration on transport pathway. With ranging concentration of fillers, contribution of transport largely shifts from random walk (in polymer) to mobility through contact percolation and percolation via interface.[48, 49]

2.1.2.1.3 Redox stability

An electrochemically stable electrolyte is a primary criterion for an ion-host channel between electrodes. It is crucial to have information on the reduction and oxidation of an electrolyte with voltage for the estimation of an electrochemical stability window (ESW). Similar to conventional electrolytes as depicted in Figure 1.12 in chapter 1, the energy gap in the polymer electrolyte should not exceed the difference of electrochemical potential of anode (μ_A) and cathode (μ_C) (with $\mu_C$and μ_A within the HOMO and LUMO of the electrolyte).[50] The ESW can be measured by voltammetry techniques (discussed in Chapter 4) and optical spectroscopy techniques as well as computational calculations. A polymer electrolyte undergoing side reactions (can be indicated with Faradaic current in I-V curve) at a certain voltage range is detrimental to its application with cathode and anode in charge-discharge processes.

In reports, it is often referred as an oxidation stability of polymer electrolyte considering its default compatibility with lithium metal. Usually, linear sweep voltammetry is performed for this investigation to evaluate the higher oxidation voltage limit for selecting the cathode within the voltage window. There are various strategies to increase the ESW of an electrolyte via analysis of its decomposition combined with theoretical experiments. This could be achieved by limiting the reactive groups, interfacial engineering, blending of polymers, addition of additives/fillers and their concentrations. For an instance, PEO possesses lower oxidation potential (≤ 3.8 V versus Li/Li^+), while its blending/copolymer/additives with other polymers and inorganic fillers have observed to enhance to ≥ 4.5 V.[51-53] These higher ESWs (> 4.5 V versus Li/Li^+) are beneficial for some emerging and future high voltage cathodes implying high-energy-density batteries.

2.1.2.2 Mechanical characteristics

Mechanical properties hold an equally important position for realizing the goal of all solid-state batteries. An electrolyte with good mechanical properties not only eases the processing and compatibility with anode and cathode but also safety, packaging, flexibility and robustness. It is highlighted by some researchers that lithium dendrites can be prevented with optimum toughness and shear modulus (G' > 0.1 GPa) along with reduced current densities.[54, 55] There is a recurrent trade off observed in conductivity and mechanical properties. A polymer needs to have flexible and mobile chains for facile mobility of ions in addition to free standing and toughness for preventing rupture or dendrites.

There exist well explored approaches to enhance the mechanical properties of PE involving inclusion of hard segments/stiff groups by crosslinking, grafting, star polymer, blending, additives/ fillers along with utilizing a framework. Employing these methodologies, shear modulus of 0.1 GPa with 10^{-3} S cm^{-1} has been recorded for a star polymer.[56] Cross-linked SPEs have shown great potential with higher toughness and decent conductivity.[57] Beyond polymer design with blending, some researchers combined a PVDF-based polymer electrolyte within an electro-spinned framework, increasing tensile strength from 3.9 MPa to 11.5 MPa.[58]

2.1.2.3 Thermal properties

By nature, liquid electrolytes are subjected to high evaporation, flammability, thermal runaway. Those thermal disadvantages are expected to be addressed by solid state electrolytes. Polymer electrolytes have a relatively lower thermal degradation temperature than inorganic solid electrolytes. With increasing temperature, a polymer undergoes various phase transformations which not only affect the physical nature (mechanical properties) of the material but also influence electrochemical properties. The temperatures of concern from the thermal scan are glass transition (T_g), melting temperature (T_m) and crystallization temperature (T_c) and decomposition temperature (T_d) which are often investigated via techniques like differential scanning calorimetry, differential mechanical analysis, Thermo-gravimetric analysis, *etc*. A polymer above T_g undergoes a deformational transition from the glassy state to the rubbery state, where those chains possess segmental motion. The decomposition temperature of a SPE should be higher than 150 ^oC which is assumed to be the operating temperature limitation.

Again, these thermal properties can be tailored by polymer engineering, utilizing additives/fillers, and plasticizers. Polymers such as PMMA, PTFE, PAN, *etc*, known for high-temperature resistance, are used. A blend of PAN/PVC/LiTFSI showed high thermal stability up to 315 ^{o}C as reported by Ramesh and co-workers.[59] A copolymer electrolyte, a poly(arylene ether sulfone) backcone grafted with PEG side-schains exhibited both efficient Li-metal cycling with high ionic conductivity of 8.97 x 10^{-4} S cm^{-1} and excellent initial decomposition temperature of ~ 430 ^{o}C.[60] A composite electrolyte of LLTO with PVDF delivered thermal stability until 410 ^{o}C as well as stable Li-cell cycling for more than 200 cycles.[61] As highlighted, the right strategies and composition of SPEs should be adopted to counter the trade-off associated with electrochemical, mechanical, and thermal properties.

2.2 Solid polymer electrolytes

2.2.1 Dry-solid polymer electrolytes

First few reported polymer electrolytes come in the category of dry-solid polymer electrolytes (dry-SPEs) which consist of a polymer matrix and salts. The polymer matrix consisting of a polyether which dissolves lithium salts via complexation, has strong donor character. It is important to have an information on the dissolution of different lithium salts for efficient transport in polymers. Among the widely used lithium salts, their dissociation in polyethers lies in the following order; $LiN(CF_3SO_2)_2$ > $LiAsF_6$ > $LiPF_6$ > $LiClO_4$ > $LiBF_4$ > $LiCF_3SO_3$ and ion mobility in the order of $LiBF_4$>$LiClO_4$ >$LiPF_6$ >$LiAsF_6$> $LiCF_3SO_3$> $LiN(CF_3SO_2)_2$.[62, 63] LiTFSI is the best candidate for dissociation with less ion mobility as obtained from the trend highlighted in Table 2.1 for polypropylene oxide (PPO),[64-66] poly[bis(methoxy-ethoxy-ethoxy-)phosphazene] (MEEP),[67-69] polysiloxane (PSi),[70-72] *etc*. but it offers other disadvantages as discussed in Chapter 1.

In dry-SPEs, the ions transport is believed to take place in the amorphous regions above T_g with chain segmental motion. This is why, higher amorphous phase content with reduced/lower T_g of a polymer electrolyte could result in higher conductivity.[73-75] The concentration of the salt in the polymer affects not only transport properties but also the mechanical nature of polymer along with T_g. Poly(ethylene oxide) (PEO) is considered one of the best candidates when it comes to the dissolution of lithium salts with other interesting merits. Most of the reports suggest that the ionic mobility for PEO occurs in their amorphous phase with a limited contribution from crystalline, as explained in the previous section.

Polymer electrolyte	Conductivity (S cm^{-1})	Temperature (°C)
$P(EO)_{20}/LiBF_4$	6.32×10^{-7}	27
$P(EO)_{20}/LiClO_4$	2.78×10^{-7}	27
PEO/5 wt% $LiPF_6$	1.20×10^{-6}	25
PEO/11.1 wt% $LiAsF_6$	1.43×10^{-4}	25
$P(EO)_{20}/LiCF_3SO_3$	1.88×10^{-9}	27
PEO/15 wt% $LiCF_3SO_3$	1.00×10^{-6}	RT[a]
$P(EO)_{24}/LiN(CF_3SO_2)_2$	3.84×10^{-4}	50
P(PO)/10 mol% $LiClO_4$	$>10^{-4}$	50
MEEP/10 wt% $LiCF_3SO_3$	1.00×10^{-5}	25
MEEP/25 wt% $LiCF_3SO_3$	2.70×10^{-5}	30
$P(Si)_{32}/LiN(CF_3SO_2)_2$	4.50×10^{-4}	25

[a] Room temperature.

Table 2. 1: Dry SPEs with different Li-salts and their conductivity values. Reprinted with permission,[76] copyright 2016, Elsevier.

It is usually crystalline below 65 °C which limits room temperature conductivity to $10^{-8} \sim 10^{-6}$ S cm^{-1}. The mechanical strength of PEO varies from 1 MPa to 15 MPa with a high dielectric constant of $\varepsilon \sim 5$ in the amorphous phase.[77, 78] The PEO chain ends with hydroxyl group, which also lower oxidation stability and reduces interfacial properties despite having conducting ether units for lithium coordination.[79, 80] Several other homopolymers have been successfully demonstrated as SPEs such as (PAN),[81] poly(methyl methacrylate) (PMMA),[82] poly(vinyl chloride) (PVC),[83] and poly(vinylidene fluoride) (PVDF),[84] polycarbonate,[85, 86] polyester,[87] (refer Figure 2.6 for the chemical structures). Functional homopolymers are always utilized in designing other innovative polymers with modifications via grafting,[88] crosslinking,[89] copolymerization,[90] plasticizers,[91] blending,[92] inorganic fillers.[33]

2.2.2 Polymer in salt

As the title suggests, polymer in salt refers to a small amount of polymer matrix into salt or related mixture which has usually more than 50 wt% of salt loading. This idea developed to facilitate the electrolyte with a higher concentration of charge carriers with fast and efficient transport properties and a polymer for superior mechanical properties. First reported by Angell,[93, 94] those kinds of SPEs are also called rubbery electrolytes due to their rubber like nature credited to lower T_g. With higher charge carrier number, they possess higher transference number and sufficient SEI stabilizing species at the electrolyte-electrode interface. They are categorized into single-salt, binary-salt and ternary-salt, *etc*., based on types of salt. For instance, an acrylonitrile

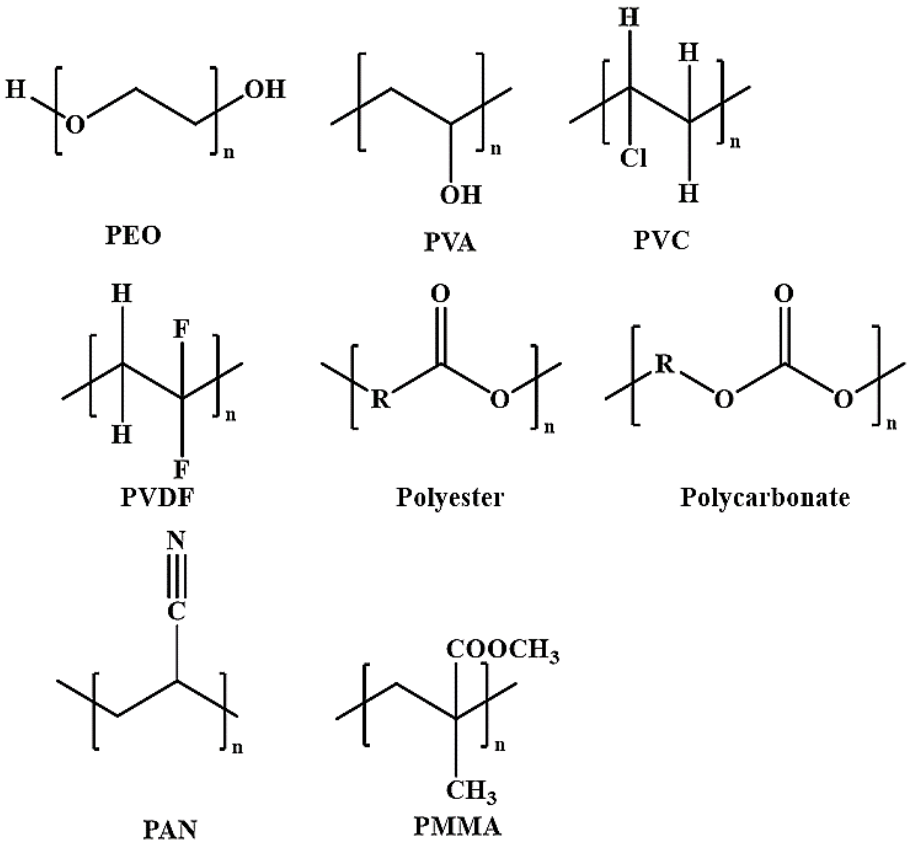

Figure 2. 6: Structure of different classes of polymers explored as electrolytes in lithium batteries.

and butyl acrylate copolymer (poly(AN-co-BuA)) was mixed with $LiBF_4$-LiDBOB as binary salt, and a conductivity to ~10^{-5} S cm higher than in a single salt was observed.[95] A ternary-salt system containing $LiClO_4$-$LiNO_3$-LiOAc and PEO was reported to exhibit conductivity around 10^{-3} S cm^{-1} at ambient temperature.[96] Those rubbery electrolytes have often been subjected to aging analysis to check on salt precipitation. This precipitation, depending upon the type of salt, results in lowered ionic conductivity and increased T_g of the SPE. Figure 2.7a (left) shows the relation of conductivity with T_g upon salt concentration for poly(AN-co-BuA) based electrolytes. The SEM image of the electrolyte film after 365 days confirms crystallites of salt, as in Figure 2.7a (right).[97] In another study, the blend of poly(ethylene carbonate) (PEC) and poly(vinylidene fluoride-co-hexafluoropropylene) (PVDF-HFP) with 80 wt.% LiTFSI demonstrated higher ionic conductivity (1.08×10^{-4} S cm^{-1} at 30 ºC for FPEC80/50 as indicated in Figure 2.7b-left) along with broad ESW of > 4.5 V (vs. Li/Li^+).[98]

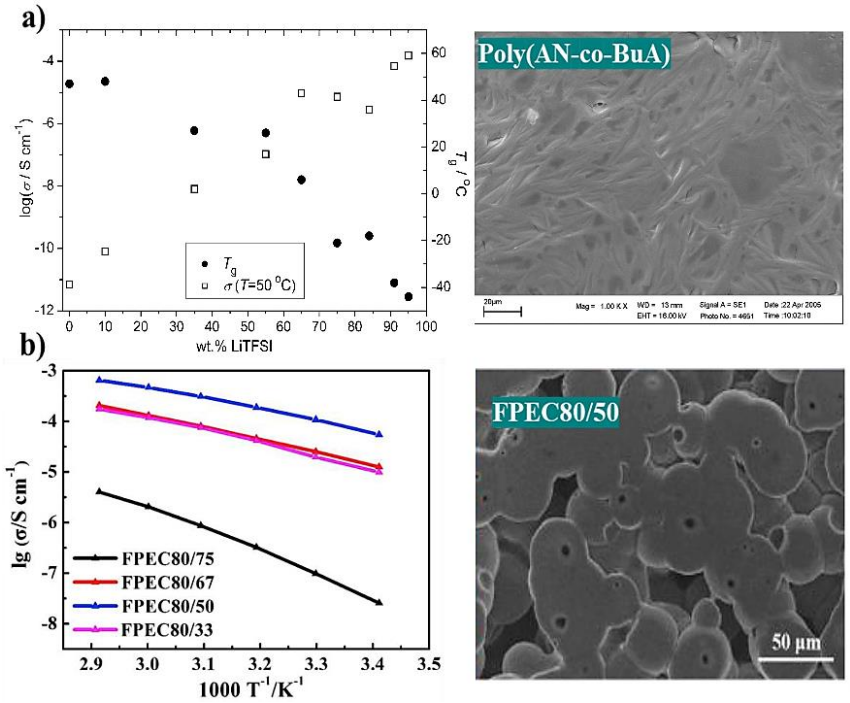

Figure 2. 7: a) Ionic conductivity (at 50 °C) and the T_g for the electrolyte composed of poly(AN-co-BuA) and LiTFSI for freshly prepared electrolyte films (left) and SEM images of poly(AN-co-BuA) and 91 wt.% of LiTFSI based electrolyte, aged 365 days (right). Reproduced with permission,[97] copyright 2015, Elsevier. b) Temperature dependent conductivity of FPEC80/50 with different ratio of PVDF-HFP (left) and SEM image of FPEC80/50 surface (right). Reproduced with permission,[98] copyright 2018, Elsevier.

The transport mechanism for the ions in polymer in salt electrolytes is linked with ionic aggregation/clusters. There have been combined arguments involving percolation paths through a polymeric matrix with ionic clusters decoupled from segmental motion.[99-101] In another study by Bushkova,[102] the authors proposed that, beyond a critical concentration, single clusters combine to form an infinite cluster for fast cationic transport. The shortcoming is the limitation in the mechanical properties due to the lower content of the polymer matrix, which could be overcome either by using a very high-molecular-weight polymer or by the formation of a network by crosslinking. Polymeric networks have been seen as interesting candidates due to their

ion-trapping mechanism beneficial for both mechanical and electrochemical properties for the SPEs.

2.2.3 Single lithium ion conducting polymer electrolytes

Usually, in SPEs, the salt is solvated by the polymer matrix and avails both cation as anion for the mobility in the matrix as a result of the applied electric field. The implication of both mobile cation and anion results in a concentration gradient due to anion gathering at the anode which results in the higher interfacial resistance and lower conductivity.[98] In contrast, a single lithium ion conducting electrolyte consists of an anion blocked by a covalent linkage. Therefore the concentration gradient can be addressed by restricting/blocking the anion and only allowing cation transport. One approach was by anchoring anions to the polymer units and thus lithium hops from anion to another anion at different polymeric unit. The second strategy is the introduction of anion receptor that hinders the anionic mobility by specific interaction.[76] A third approach lies in the use of cross-linked polymer network where anions are restricted in the network trap. These approaches lead to higher cationic transport number (> 0.5) than conventional bi-ion (cation and anion) based SPEs.

More work has been conducted on the polymeric lithium salt approach for the development of SLIC than anionic receptors over years due to the former giving more freedom of control on structural design and synthesis. Given the wider choice of polymers, SLIC polymers have extended not only to homopolymers but also to copolymers and hybrid polymers.[103] Ciu and coworkers reported homopolymers of poly(lithium 2-acrylamido-2-methylpropanesulfonic acid) (LiPAMPS) (Figure 2.8a) whose AMPS monomeric units contain sulfone acid groups and double bond for radical polymerization with themselves or other monomers.[104] The combination of PEO linear chain and lithium poly(4-styrene sulfonyl(trifluoromethylsulfonyl) imide) (LiPSTFSI, Figure 2.8b) resulted in ionic conductivity of 10^{-5} S cm^{-1} with t_{Li+} close to unity as demonstrated by Meziane *et al.*[105] Other Lewis acids like carboxylic acid and borontrifluoride diethyl ether have been actively investigated involving, poly(lithium carboxylate)-type salts,[106] poly(lithium sorbate) (Poly(Li-Sorb, Figure 2.8c) and poly(lithium muconate) (Poly(Li-Muco, Figure 2.8d),[107] lithium oxalate polyacrylic acid borate (LiOPAAB, Figure 2.8e)[102] and lithium poly(vinyl alcohol) oxalate borate (LiPVAOB, Figure 2.8f),[103] respectively. Boronate units contribute towards higher t_{Li+} and mechanical stability. One of the most researched polymer lithium salt is polyimide, motivated by LiTFSI and its strong electron-withdrawing group. These polyimide anion lithium salts based SLIC have shown excellent

electrochemical properties due to their higher dissociation and t_{Li^+} such as poly(perfluoroalkylsulfonyl)imide (LiPFSI, Figure 2.8i),[108] poly(2-oxo-1-difluoroethylene sulfonylimide lithium) (LiPEI, Figure 2.8g), and poly(5-oxo-3-oxy-4-trifluoromethyl-1,2,4-pentafluoropentylene sulfonylimide lithium) (LiPPI, Figure 2.8h).[109] SLICs based on polymer lithium salts have proven to possess superior cycling capabilities in full cell measurements.

An interesting approach is the design of a block copolymer integrated with polymeric salt anion bonded units. A diblock copolymer comprising poly(lithium methacrylate-co-oligoethylene glycol methacrylate) ion conducting block (P(MALi-co-OEGMA)) with a polystyrene block (PS) was reported by Gohy and coworkers.[110] The macromolecular design allowed the self-standing film to attain the attractive ionic conductivities of up to 2 x 10^{-5} S cm^{-1} at RT with ESW up to 4.5 V *vs.* Li^+/Li. A self-assembled polyanionic BAB triblock copolymers (P(STFSILi)-b-PEO-b-P(STFSILi) (Figure 2.9a) was synthesized with potential mechanical (~10 MPa) and transport

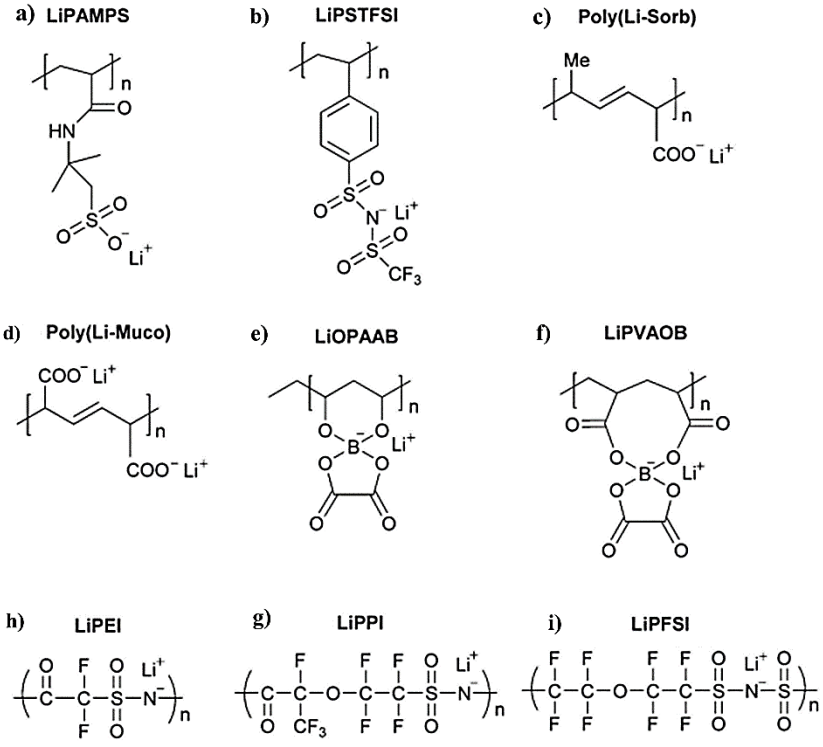

Figure 2.8: Molecular structures of well reported single lithium ion conducting polymer electrolytes.

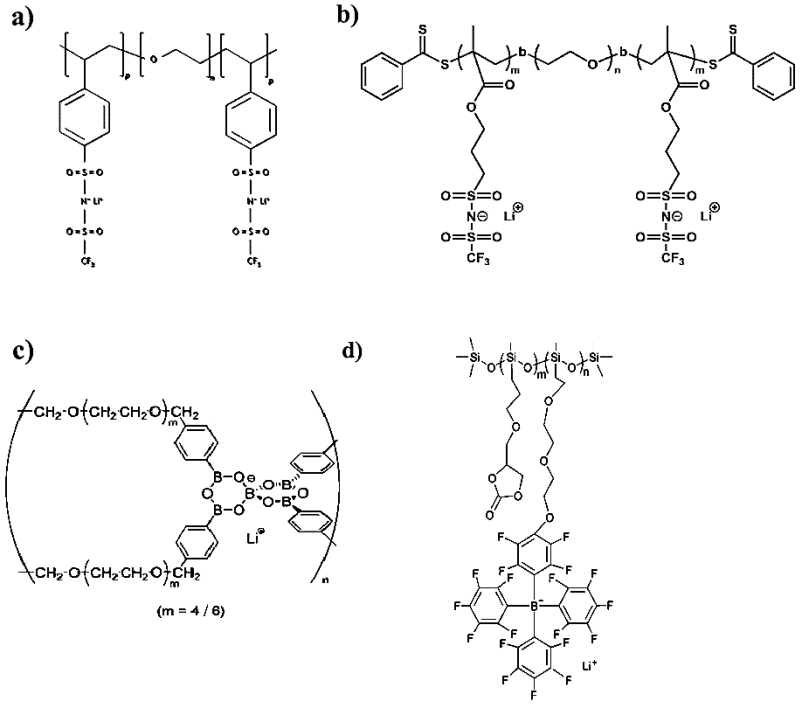

Figure 2. 9: Structure of triblock copolymers based on SLIC electrolyte, a) P(STFSILi)-b-PEO-b-P(STFSILi)[111] and b) Poly(LiMTFSI)-b-PEO-b-poly(LiMTFSI).[112] Structure of inorganic–organic hybrid polymer electrolyte c) poly(lithium tetraarylpentaborate)s[113] and d) lithium tris(perfluorophenyl)(2,3,5,6-tetrafluoro-4-(2-(2-(vinyloxy)ethoxy)ethoxy)phenyl) borate.[114]

properties (1.3 x 10^{-5} S cm^{-1} at 60 °C, t_{Li^+}> 0.85).[111] Another triblock copolymer poly(LiMTFSI)-b-PEO-b-poly(LiMTFSI) (Figure 2.9b) was developed via reversible addition-fragmentation chain transfer polymerization (RAFT) polymerization with polytrifluoromethyl sulfonimide lithium outer blocks and PEO inner block. It exhibited improved ionic conductivity of ~10^{-4} S cm^{-1}, $t_{Li^+}$of 0.91 with low T_g of -55 °C and 51% of crystallinity.[112]

Hybrid copolymers based on organic and inorganic units are attempted as well to exploit the involved synergy in the class of polymers like polysiloxane, borosiloxane, organoboron, aluminate polymers covering large polymeric topologies. Nishihara *et al.*[113] developed an organoborate polymer, poly(lithium tetraarylpentaborate), combined with hexathylene glycol (Figure 2.9c) and resulting in a conductivity of 5 x 10^{-5} S cm^{-1} at 60 °C. Cyclic carbonates (CCs) as side chains have also been explored in SLIC by Colby and coworkers[114] for CCs and lithium tris(perfluorophenyl)(2,3,5,6-tetrafluoro-4-(2-(2-(vinyloxy)ethoxy)ethoxy)phenyl) borate (Figure 2.9d) side chains

reaching conductivities up to ~10^{-7} S cm^{-1}. A thermally stable star shaped polymer was reported consisting of polyhedral oligomeric silsesquioxane-polyethylene oxide and poly((4-styrene sulfonyl) (POSS-PEO-PSTF) and a conductivity of ~10^{-5} S cm^{-1} was reached at 60 °C.[115]

Anionic receptors

On contrary to anchoring the anion to the polymer backbone, anionic receptors trap anions to form single lithium ion conductors. Further, they initiate dissociation of salt for cationic mobility, resulting in higher t_{Li^+}. They are classified into two groups, one is Lewis acid type and other is calixarene. Boron atom carrying molecules such as boroxine rings combined with oligoether side chains have been used as anionic receptors due to their Lewis acid nature.[76] SPEs with boroxine rings-oligomer ether significantly improved the conductivity to 1.6 x 10^{-5} S cm^{-1} at 30 °C with t_{Li^+} of 0.82 and ESW up to ~4.9 V vs Li/Li^+.[116, 117] Calixarenes are desired due to their high anion complexation selectivity. In addition of calix[4]arene (C4P) to PEO-LiX complexes, t_{Li^+} *is* increased from 0.77 to 1.0 with calixarene concentration increasing from 25 mol% to 100 mol% as investigated by Scrosati *et al.*[118, 119] However, calix[2]-p-benzo[4]pyrrole (CBP) when added to PEO-based electrolytes increased the t_{Li^+} and interfacial properties but not ionic conductivity.[120]

2.2.4 Hybrid and composite copolymer electrolytes

Hybrid polymer electrolytes are categorized into organic/inorganic copolymers and composite polymer electrolytes (following the addition of active or passive inorganic fillers). They add necessary properties, such as higher thermal stability and strong chain movement (higher amorphous phase and lower T_g). Polyhedral oligomeric silsesquioxanes (POSS/ $R\text{-}SiO_{1.5})_n$, where R: organofunctional group and n= 6, 8 or 10) are nano-structured hybrid building blocks containing nano-sized silicon/oxygen cores with organic groups surrounding them.[121] They offer the flexibility towards copolymerization, grafting and blending as evident from the reports on synthesis of poly (ethylene glycol) methyl ether methacrylate (PEGMA),3-(3,5,7,9,11,13,15-heptaisobutylpentacyclo[9.5.1.13,9.15,15.17,13] octasiloxane-1-yl) propyl methacrylate (MA-POSS), and ethylene glycol dimethacrylate (EGDMA) with hyper-branched and linear graft topology (Figure 2.10a and 2.10b).[122, 123] It was observed the hyper branched possesses higher conductivity than the linear graft. For example, PEG-functionalized POSS/star-shaped polymer P(PEGMA-r-MA-POSS) was obtained with a high conductivity of ~10^{-5} S cm^{-1} at 30 °C and ESW >4.2 V vs Li/Li^+.[124, 125]

Polysiloxane based polymers offer high molecular chain flexibility and structural synthetic control but lack in lithium salt solvation units and thus demand modification. Polysiloxane combined with cyclic carbonate propylene carbonate and comb-shaped PEO (Figure 2.10c) resulted in a bifunctional polymer demonstrating higher conductivity of 1.5 x 10^{-4} S cm^{-1} (with PC/PEO: 6:4).[126] Blends of PMMA as polymer matrix and polysiloxane comb propyloxy methoxytriethylene glycol (PS_x) (Figure 2.10d) as the ion conductor were prepared by solution casting with a semi-interpenetrating network by Cznotka *et al.*[127] which recorded high conductivity of 3.1 x 10^{-6} S cm^{-1}. Organic/inorganic hybrid copolymers improve the SPEs in various parameters as highlighted above, but some strategies can be adopted to increase the solvation of salts by addition of highly polar groups, by modifying into SLIC (as discussed in SLIC section), *etc*.

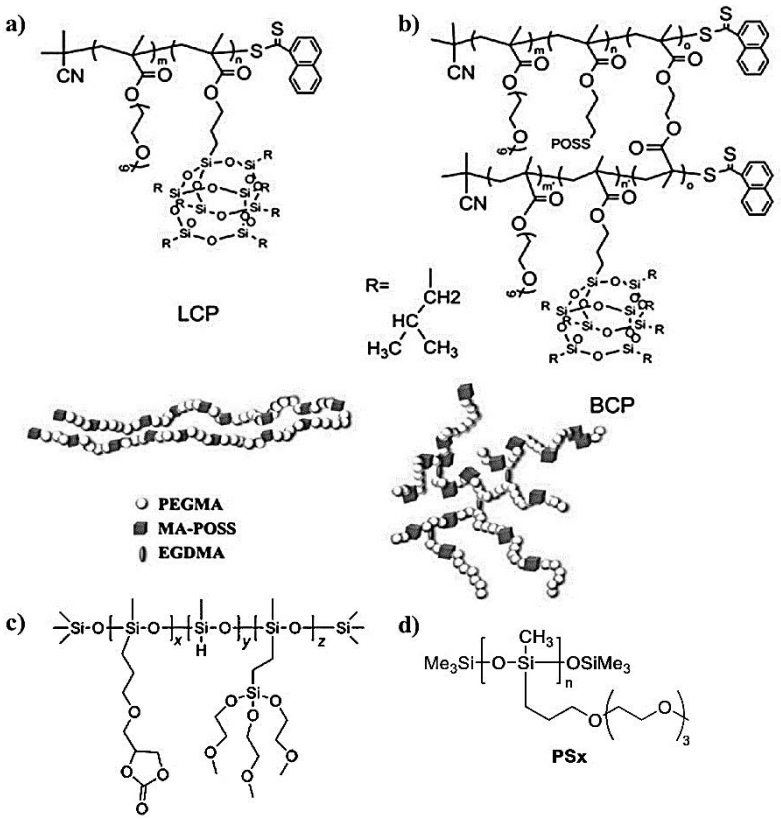

Figure 2. 10: a) Linear (LCPs), b) branched (BCPs)-graft copolymers synthesized via RAFT polymerization, respectively[122, 123] c) CC and Combed Poly(ethylene oxide) grafted on Polysiloxane,[126] d) Polysiloxane comb propyloxy methoxytriethylene glycol (PSx).[127]

Hybrid SPE

Many researchers believe that a hybrid SSE will be an efficient and optimum solution to the issues underlying with SPE or ISE alone. As mentioned above, another approach for hybrid electrolytes is the introduction of inorganic fillers under the missing characteristics in SPEs. As far as transport is concerned, Figure 2.5 shows the scheme of ion conductivity pathways for filler and polymer composite with different concentrations. It was reported quite earlier in 1982 by Weston in his effort to improve the mechanical stability of PEO, led by the addition of α-alumina.[128] These fillers, while moving with SPE, suppress the crystallinity of the polymers by increasing the amorphous phase.[37, 129] Based on their ion conductivity, they are categorized into active fillers and passive fillers, irrespective of their net contribution to the electrolyte. Well known Passive fillers are divided into oxide ceramics such as Al_2O_3,[130, 131] SiO_2,[132-134] TiO_2,[135] ZrO_2,[135] Y_2O_3,[136] $LiAlO_2$,[137] ferroelectric ceramics i.e. $BaTiO_3$, $PbTiO_3$, $LiNbO_3$, *etc*.,[138, 139] and clay-based fillers such as halloysite,[140, 141] palygorskite,[142, 143] vermiculite.[144, 145]

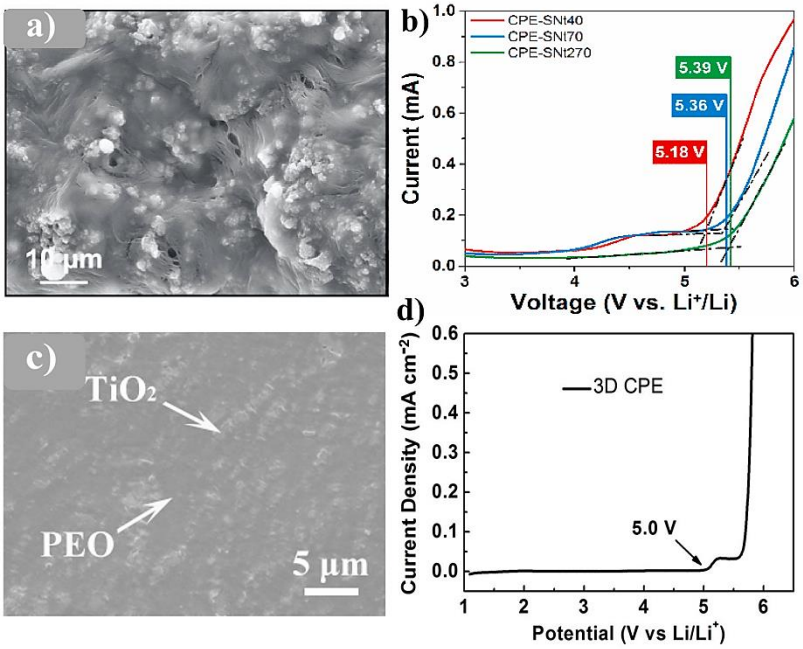

Figure 2. 11: a) SEM images of randomly distributed bumps of silica nanotubes (SNt) in CPE, b) LSV curves of CPE-SNt40, CPE-SNt70 and CPE-SNt270, Reproduced with permission,[146] copyright 2021, Elsevier. c) SEM image of the CPE based on PEO-TiO_2 and d) LSV curve of the 3D CPE at a sweep rate of 1.0 mV s^{-1}, Reproduced with permission,[147] copyright 2020, ACS.

CPE based on silica nanotubes with random distribution as shown in SEM image (Figure 2.11a) recorded excellent conductivity of 4.35×10^{-4} S cm^{-1} with ESW as high as ~ 5.39 V for longer nanotubes (as depicted in Figure 2.11b).[146] Additionally, the effect of TiO_2 covered within PEO layers was also explored which delivered promising oxidation voltage of ~5 V with conductivity of 0.69×10^{-4} S cm^{-1} at 30 ^{o}C when incorporated into PEO electrolyte (Figure 2.11c and 2.11d).[147] Ferroelectric ceramics undergo polarization and thus interact with polymer chains to lower the interfacial impedance. For examples, nanoparticles based $BaTiO_3$ mixed with PEO demonstrated the elevation in the conductivity to 2×10^{-5} S cm^{-1} at 25 ^{o}C as reported by Cai *et al.*[148] Lastly, clay-based fillers provide large interfacial contact area with the polymer due to their nanoparticle/lamellar morphology resulting in higher salt solvation.[149] Composite with clay such as nanosheets of montmorillonite polyethyelene carbonate/LiFSI has improved the conductivity of to 3.5×10^{-4} at RT with oxidation stability to 4.6 V (versus Li/Li^{+}).[150]

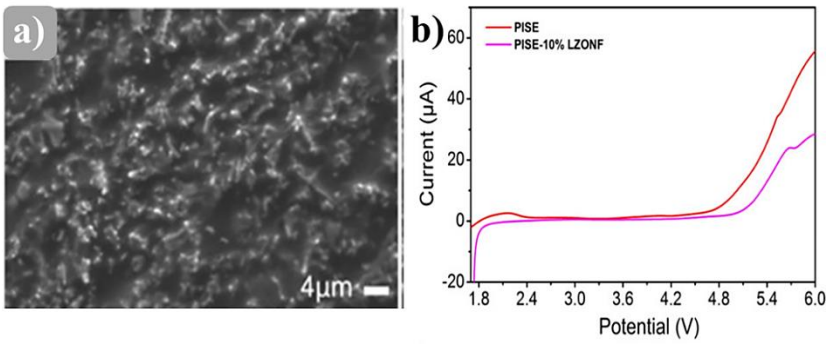

Figure 2. 12: a) SEM images of PISE reinforced with 10% LLZTO NFs and b) Electrochemical stability of the fabricated electrolytes Reproduced with permission,[151] copyright 2020, ACS.

Active fillers were discovered later than passive fillers but they gained huge attention due to their individual contribution to the ionic conductivity. They include various ISEs like garnet-type ISEs,[10, 152] perovskite-structured ISEs,[153, 154] NASICON which, upon mixing with SPE, possesses an advantage of high ionic conductivity, interfacial stability and flexibility.[155] It is observed that active fillers with concentration lower than 20 wt% (ceramics in polymer) provide a higher concentration of free Li ions in the interfacial regions than passive fillers and to the overall ionic conductivity when the concentration gets higher than 50 wt% (polymer in ceramics). Several CPEs have been investigated based on the type of active fillers like $Li_{6.75}La_3Zr_{1.75}Ta_{0.25}O_{12}$ (SEM image shown in Figure 2.12a for $Li_{6.75}La_3Zr_{1.75}Ta_{0.25}O_{12}$ (LLZTO)), $Li_{1.3}Al_{0.3}Ti_{1.7}(PO_4)_3$, and $Li_{0.35}La_{0.55}TiO_3$ when incorporated to PEO/LiTFSI led the improvement

in the conductivity to 2.13×10^{-4}, 2.5×10^{-5}, and 8.8×10^{-5} S cm^{-1} at RT, respectively. The addition of fillers demonstrated higher ESW > 5 V vs Li/Li^{+} as depicted in Figure 2.12b with and without LLZTO nanofiber (LZONF).[151, 154, 156] CPEs possess high ionic conductivity and large ESW which mark them as potential candidates for higher voltage cathodes and thus high energy and power density batteries.

2.3 Gel Polymer electrolytes

Gel polymer electrolytes as name suggest are ionic conductors with a physical state like gel, between solid and liquid, first proposed by Feuillade *et al.*[16] A polymer matrix swollen in liquid as plasticizer forms a gel loaded with lithium salts and additives (in some cases). GPEs provide better ionic conductivity and wettability with the electrodes than SPEs. Most commonly used polymer matrices include PEO, PAN, PMMA and poly(vinylidene fluoride-co-hexafluoropropylene)v(PVDF-HFP) which have been used with plasticizers like propylene carbonate (PC), ethylene carbonate (EC), dimethyl carbonate (DMC), and diethyl carbonate (DEC), ethers (tetraethylene glycol dimethyl ether (TEGDME),1,2-dioxolane (DOL) and dimethoxymethane (DME), and ionic liquids.[33, 157] Unlike SPEs, ion transport in GPEs takes place in swollen gelled or liquid phase while the polymer matrix provides mechanical support.[158] Plasticizers increase the amorphous phase, ion pair dissociation for higher ionic conductivity. GPEs found their way to the market than ahead of SPEs due to their lower safety risk than liquid electrolytes (LEs) via quasi-solid state and compromised characteristics between SPEs and LEs. Despite an edge to LEs in anti-leakage and safety, they still pose a high risk of fire and offer poor thermal stability owing to their high organic solvent content.

3.3.1 Methods of preparation

GPEs could be prepared by two approaches, one by physical (phase separation) and the other by chemical preparation (uniform). In the physical method, a porous polymer membrane is synthesized and swelled in LE with Li-salt to form GPE. This results in three phases in the GPE, liquid electrolyte, solvent-swollen gel electrolyte and polymer matrix. The key parameters include high porosity and small pore diameter, which could lead to high uptake of LE without much overflow or leakage.[159] It is observed that a single polymer matrix often could not cater all the needed properties despite plasticizer, which in turn requires blending, copolymerization, crosslinking or compounding.[160-163] However, chemical preparation of GPE looks more appealing as it involves in situ polymerization methods of monomers/cross-linkers such as acrylate

esters,[164, 165,166] by initiators (like azo compounds, AIBN,[167] or benzoyl peroxide[168]) dissolved in LE. For the in-situ process, polymerization of monomers takes place along with immobilization of LE in pores, resulting in cross-linked structures within the fabricated cells driven either by UV radiation, thermal, electrochemical assistance or electron beam radiation source. The precursors in these processes should have adequate viscosity for wetting electrodes.[76, 169] There exist other techniques including conventional solution inverted phase method,[170] electrospinning method,[171] and foaming technology.[172] For example, a GPE was prepared with poly(vinyl alcohol) oxalate borate electro spun PVDF composite membrane with 1 mol L^{-1} $LiPF_6$ based electrolyte exhibiting superior performance than LE with 0.26 mS cm^{-1} conductivity and 0.58 of t_{Li^+}.[171]

Wang *et al.* synthesized highly microporous (as shown in SEM image in Figure 2.13a) SLIC based on aromatic poly(arylene ether)s with pendant lithium perfluoroethyl sulfonates. It recorded very high conductivity of 3.1 x 10^{-3} S cm^{-1} at RT with a unity transference number on respective solvent saturation, depicted in Figure 2.13b.[173] Thermal crosslinking of poly(ethylene glycol) methyl ether acrylate (PEGMEA) and poly(ethylene glycol) diacrylate (PEGDA) was reported in polypropylene separators for a GPE referred as GFPS (gel filled polypropylene separator). The GFPS-supported GPE membrane presented a good porosity as observed in SEM image, Figure 2.13c and best conductivity of 1.12 x 10^{-3} S cm^{-1} for 14.3 wt% ether content (as shown in Figure 2.13d).

2.3.2 Plasticizers

There are quite a few low molar mass plasticizers explored and their performance are compared in polymer matricesw involving, poly(ethylene glycol) dimethyl ether (PEGDME),[174, 175] borate esters-type such as PEG-borate ester,[176] (tris(2-(2-methoxyethoxy)ethyl) borate (B2), tris(2-(2-methoxyethoxy)ethoxy)ethyl) borate) (B3),[70] phthalate-type such as dibutyl phthalate (DBP),[177, 178] dimethyl phthalate (DMP),[179, 180] 2-dioxy phthalate (DOP),[181] and succinonitrile (SN).[182, 183]One of the report highlighted that conductivity and salt diffusion coefficients of the plasticized electrolyte fall best for PEGDME, following the order, PEGDME>PC>EC.[184] Organic solvents are usually used in combinations as plasticizers. As reported by Choi *et al.*,[185] mixed solvents swelling PAN matrices in 1 M solution of $LiPF_6$ align with following conductivity order: EC/DMC/DEC(1:1:1) > EC/DC(1:1) > EC/EMC(1:1) > EC/DEC(1:1) > EC/DMC(2:1). PVDF- LiPVAOB based GPE soaked in 1 mol L^{-1} $LiPF_6$ solution in EC/DMC/EMC demonstrated good cycling performance with LFP

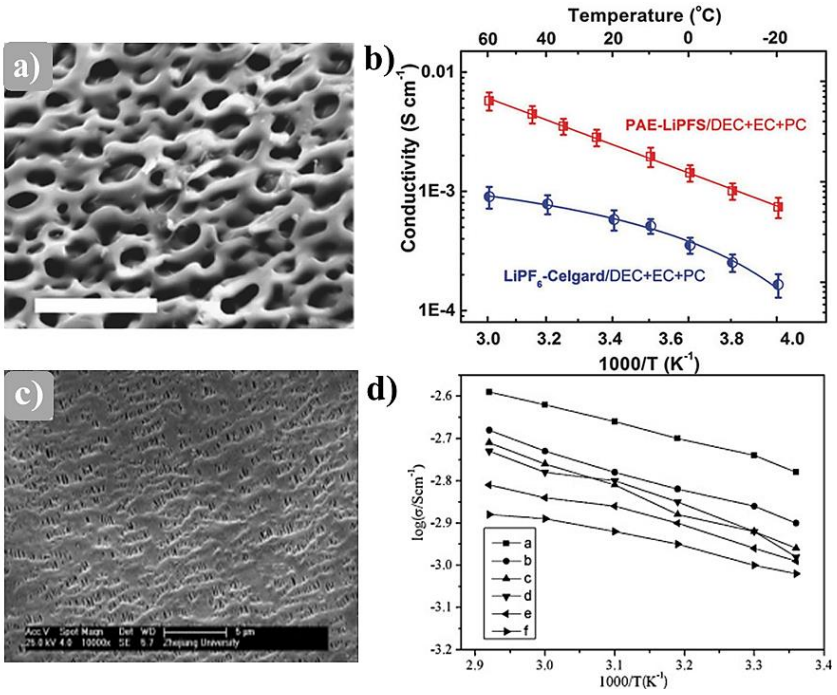

Figure 2. 13: a) Surface view SEM image of the SLIC GPE porous membrane based on aromatic poly(arylene ether)s with pendant lithium perfluoroethyl sulfonates, (scale bars- 2 µm) b) Temperature dependent ionic conductivity of GPE saturated by DEC + EC + PC (1:1:1 by vol, 92 wt%) in comparison to the conventional Celgard 2500 separator saturated by 1 M $LiPF_6$ in DEC + EC + PC (1:1:1 by volume). Reproduced with permission,[173] copyright 2016, ACS. c) SEM image of GFPS based GPE and d) Conductivity vs. temperature for GPE with various formulations, where "a-f" represents different weight proportion for PEGMEA and PEGDA. Reproduced with permission,[166] copyright 2011, Elsevier.

cathode via improved conductivity of 0.26 x 10^{-3} S cm^{-1} at RT relative to celgard and LiPVAOB as observed in Figure 2.14a and 2.14b.[171] However, organic solvents have low vaporization point, thermal stability and higher flammability which opens the room for potential alternatives like ionic liquids. Those are also called as room temperature molten salts consisting of bulky organic cations and inorganic large delocalized anions. They bring in interesting features like non-flammability, higher chemical, thermal and electrochemical stability (also explained in details in electrolyte section of Chapter 1).

A series of RTIL containing pyrrolidinium-based cations and TFSI anion[186] has been investigated by Passerini *et al*[187] who initiated the RTIL incorporation into SPEs. GPEs based on N-alkyl-N-methylpyrrolidinium bistrifluoromethanesulfonyl imide (PYR_1ATFSI, A = C_nH_{2n+1} with n ranging from 1 to 10) show a higher conductivity of 2.7 × 10^{-4} S cm^{-1} at RT for P(VDF-HFP)/LiTFSI/PYR_{13}TFSI which is two-three

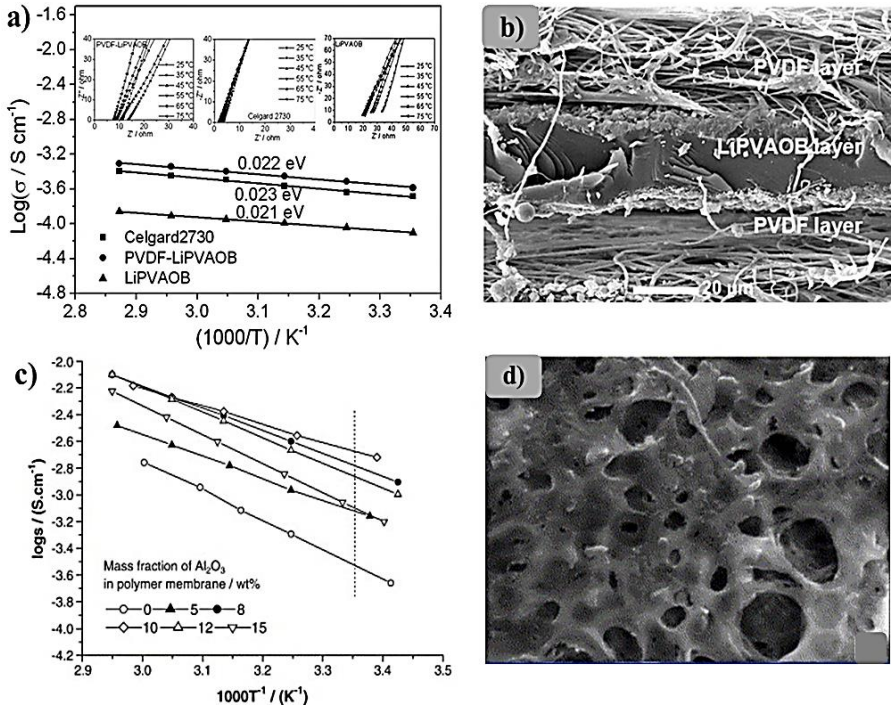

Figure 2. 14: a) Arrhenius plots of the PVDF-LiPVAOB GPE, LiPVAOB and the Celgard 2730 saturated with 1 M $LiPF_6$ organic electrolyte wit Impedance plots of the conductivity data at different temperatures, b) SEM images for the cross-section of the PVDF-LiPVAOB composite membrane. Reproduced with permission,[171] copyright 2014, Wiley. c) Log σ vs 1000/ T curves of P(VDF-HFP) polymer electrolyte filled with various amounts of Al_2O_3 nanoparticles and d) SEM surface images of P(VDF-HFP) membrane filled with 10% Al_2O_3 content. Reproduced with permission,[188] copyright 2005, Elsevier.

orders of magnitude higher than IL-free SPEs.[189] Raghavan *et al.*[190] used three ILs 1-ethyl-3-methylimidazolium TFSI (EMImTFSI), 1-propyl-3-methylimidazolium TFSI (PMImTFSI), and 1-butyl-3-methylimidazolium TFSI (BMImTFSI) in PVdF-HFP matrix, which resulted in the high conductivity ranges $2.4\times10^{-3} \sim 4.5\times10^{-3}$ S cm^{-1} at 25 °C.

2.3.3 Inorganic fillers

The bottleneck for GPEs lies in finding the right balance of the plasticizer and polymer matrix without compromising the ionic conductivity and mechanical flexibility, which itself is a real challenge. Besides approaches like crosslinking and blending, the introduction of inorganic fillers (such as TiO_2, Al_2O_3, SiO_2, MgO *etc.*) for composite polymer electrolytes is an interesting and yet easy approach to address this concern. In an investigation by Kumar *et al.*, it was postulated that space charge layers existing on boundaries of ceramic grains overlap with increasing grain concentration for ionic

transport pathways.[191] Reports on SiO_2 based GPE revealed that addition of SiO_2 into polymer matrices improved the ionic conductivity, deducing submicron sized particles led to better results than nano-sized ones.[192, 193] Further, it was concluded that particle agglomeration and phase separation in the polymer matrices are caused due to higher surface energy of inorganic particles. Thus, it requires surface modification to improve its interaction with the organic component and enhance dispersion.[193] This was validated by Walkowiak *et al.*, who synthesized GPEs with modified SiO_2 (modified SiO_2 with vinylene, glycidoxy, mercapto, chloropropyl, octyl, methacryl and amino functional groups) which increased the conductivity by two orders of magnitude (~10^{-2} S cm^{-1} at 20 °C) compared to unmodified SiO_2.[193] Nanoparticles of aluminium oxide (Al_2O_3) used in P(VDF-HFP), PAN matrices *etc*. act as solid plasticizers. Their Lewis acid surface groups contribute to higher conductivity via reducing ion-pair formation and their optimum concentration is evaluated at 10 wt% which showed 1.95×10^{-3} S cm^{-1} conductivity in porous P(VDF-HFP) with Al_2O_3 (as depicted in Figure 2.14c and 2.14d). [188,194, 195] Rutile TiO_2 has been believed to improve the interfacial conductivity and transport properties.[196] Besides other fillers have exhibited potential performance while incorporated into GPE, such as $Al(OH)_3$,[197] ZrO_2,[198] clay fillers,[199] and carbon-based allotropes like CNT.[200]

2.4 Cyclic Carbonate and Poly(hydroxyurethane)

2.4.1 Carbon dioxide capture and its utility

The level of carbon dioxide has been increasing in the atmosphere drastically by 49% as compared to 33% of pre-industrial era.[201] This imbalance has not only affected the various living domains on earth but has been in the epicentre of climate change and natural disasters. The climate change accompanies the melting of glaciers, unpredicted floods, drought, and forest fire, extinction of terrestrial and aquatic life.[202] It is a global concern which has to be tackled with strategic and collective effort for the planet instead of a particular geographic location. Well, various research domains are active in progress for cutting down the CO_2 emission along with political decisions referenced to climate change accord and conference, COP global, *etc*.[203] Addressing this, two approaches are well known: carbon capture and storage (CCS)[204] and carbon capture and utilisation (CCU) as depicted in Figure 2.15.[205,206, 207] In the first approach, the CO_2 is captured from source point, purified and pressurized for storage to underground or oil fields. Indeed, this entire process is expensive and borne by product manufacturers and consumers indirectly. While other approach is more appealing and sustainable, as CO_2 in CCU is utilized for chemical and biological

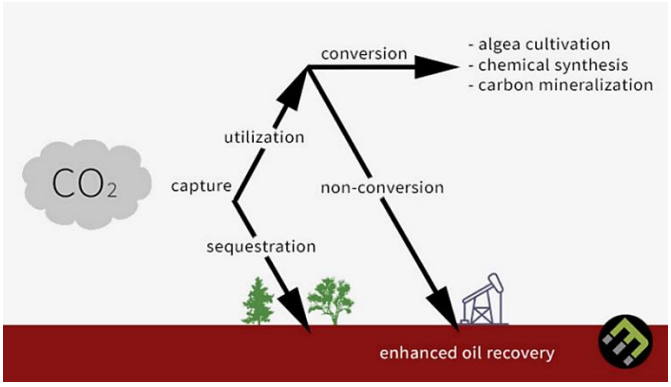

Figure 2.15: Reprinted with permission,[205] copyright 2020, eco-nnect.com.

synthesis of chemical and fuels. This makes the waste CO_2 a valuable resource. Using these captured CO_2 for synthesis of cyclic carbonate (CC) is common and yet interesting synthetic pathway as together with methane production, they take up of utilization of 25% waste carbon dioxide produced annually.[208]

2.4.2 Cyclic carbonate-based electrolytes

There are various pathways towards the synthesis of CC as shown in Figure 2.16[209] i.e., co-cyclization between alkenes or alkynes and carbon dioxide,[210-212] electrochemical reactions,[213, 214] transesterification of a hydroxyl reactant (or polyhydroxyl) with dialkyl carbonates (diethyl or dimethyl carbonates)[215-217] with basic catalysts.[218] The reaction of CO_2 with epoxides in the presence of catalyst for the formation of CC[219] or polycarbonate[220] has been explored since its discovery around 1958. Since then, CCs have been synthesized commercially for catering the needs for battery industry, polar aprotic solvents, gas separation, synthesis of polymers like polycarbonate,[221, 222] poly(hydroxyurethane),[223] *etc*. Additional advantage lies in biomass precursors which are used for CC, such as cellulose, sorbitol, and glucose. However, CC/linear carbonates are among the most preferred organic molecules in electrolytes after ethers because of their higher lithium ion solvation ability. The brief discussion on LEs based on carbonates has been already documented in the organic solvent section of Chapter 1. While in this section, we are focusing more on the design and synthesis of carbonates and their significance in correlation with the ionic conductor. Both linear and CC have been investigated extensively for their parametrical distinct properties such as viscosity, dielectric constant, melting and boiling point *etc*. (detailed comparison shown in Table 1.1 of Chapter 1). These properties are linked to the size and shape of carbonates, i.e., bigger

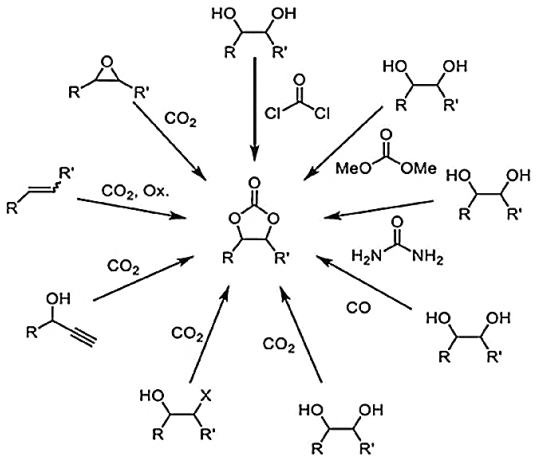

Figure 2. 16: Synthetic routes for the formation of CCs. Reprinted with permission,[209] copyright 2022, Springer.

molecules of alkyl carbonates lead to higher boiling point due to higher Van der Waals interactions. The higher dielectric constant in the CC directs towards increased phase transition point, viscosity and therefore better solvation than linear/alkyl carbonates due to higher dipole-dipole forces.[224] However, CC provides better solvation structure than linear carbonates and the solvated lithium ions desolvate at interfaces to diffuse and decompose other components to contribute to SEI. SEI originating from linear carbonates does not prevent electrolytic decomposition (at anode) and co-intercalation of the lithium ion solvation shell while CC provides better stability.[225] Nevertheless, the optimum electrolyte into the market has been credited to mixtures of carbonates to counter mutual trade off and exploit the synergy as individual cannot fulfil all the requirements.

In general, both metal-based and organic catalysts are exploited for synthesis of CC but in this section, we are discussing on organocatalysts as they lower the toxicity level of the reaction. As far as the mechanism of the synthesis is concerned, the reaction can proceed via epoxide activation, CO_2 activation or both activations. The most common is epoxide activation which starts with Lewis acid coordination from catalyst and thus ring opening by a nucleophile in step a.[226] In step b, the reaction of alkoxide intermediate with CO_2 leads to the formation of five membered CC in step c as shown in Figure 2.17.[226] The respective cis and trans isomers could be detected by NMR analysis. Within carbonates, further modifications are often performed involving fluorination such FEC, FEMC *etc*. for higher polar groups and SEI stabilizing species.[227-230] Despite all these interesting features, most of the low molecular weight CCs are flammable, offer poor thermal stability, release some

gaseous products on combustion and are in the liquid phase. It is thus necessary to find alternatives or overcome these issues by changing the source of synthesis of the CC/phase, or polymerization via main or side chain units, *etc*.

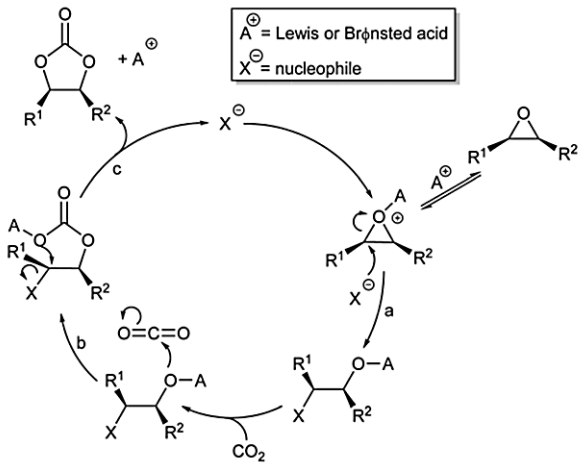

Figure 2.17: Epoxide activation mechanism for CC synthesis. Reproduced with permission,[226] copyright 2021, RSC.

2.4.3 Polymerization of CC

2.4.3.1 Side Chain CC copolymers

The idea of higher dielectric constant, better ionic conductivity and SEI stabilizing species encouraged CCs attachment to polymer backbone as side chains/pendant groups and polycarbonates as explained in section above. A GPE based on a polymer matrix resulting from the copolymerization of a CC methacrylate with oligo(ethylene glycol) methyl ether methacrylate (Figure 2.18a) was synthesized with the conductivity of 2.3 x 10^{-3} S cm^{-1} at 25 ^{o}C.[231] Colby *et al.* incorporated CCs in polysiloxane-based SLIC-SPEs containing novel borates (Figure 2.18b) via one-pot hydrosilylation reaction with anions anchored for SLIC (also discussed above in SLIC section).[232, 233] In a detailed study, hyperbranched polyacetals (HBPAs as in Figure 2.18d) bearing CCs were synthesized in series of steps via polycondensation and transesterification which delivered SPEs with conductivity of 8.2 × 10^{-9} to 2.1 × 10^{-3} S cm^{-1} at 23–80 ^{o}C.[234] Gohy *et al.* investigated SPEs based on CC trifluoromethacrylate and vinylidene fluoride units (Figure 2.18c)[235] and random copolymers of *n*-butylacrylate and CC bearing acrylate (Figure 2.18e).[236] Copolymers composed of polyether segments and linear carbonates were reported by Mecerreyes

and co-workers.[237] The influence of the incorporation of CCs within the chains (as in Figure 2.18f) was also studied by Detrembleur and co-workers.[238]

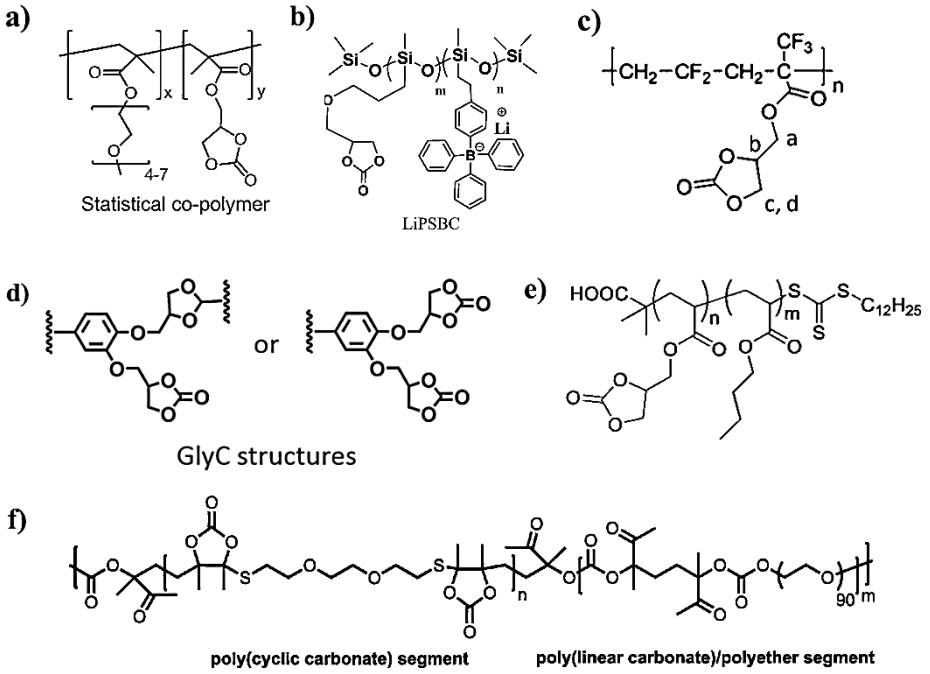

Figure 2. 18: Various classes of polymer electrolytes bearing CC as side or main chain functional groups, a) Statistical co-polymer of OEGMA and CCMA,[231] b) LiPSBC, polysiloxane single-ion conductors,[233] c) Fluorinated copolymer of VDF and MAF-cyCB,[235] d) Hyperbranched polyacetals (HBPAs) bearing CC terminals,[234] e) Copolymers of CC Acrylate and n-butylacrylate,[236] and f) Polycarbonates bearing linear CC linkages.[238] Reproduced from respective reports.

2.4.3.2 Polycarbonates

The polymerization of CC for polycarbonates has been observed around 1969 by Koinuma.[239] Later this polymer was also demonstrated as a potential ionic conductor for metal ions (such as poly(vinylene car-bonate) (PVC), poly(ethylene carbonate) (PEC), poly(propylene carbonate) (PPC), and poly(trimethylene carbonate) (PTMC)). The first report by Shriver *et al.*[240] on the synthesis of poly(vinylene carbonate) (PVIC) using 0.3 wt% benzoyl peroxide (BPO) and poly((1,3-dioxolan-2-one-4,5-diyloxalate (PVICOX) with silver oxalate and dibromoethylene carbonate showed remarkable properties with conductivity of ~10^{-4} and 4 × 10^{-4} S cm^{-1}, respectively. Tominaga *et al.* designed various PECs based polymers in series of their investigation like, macroporous polyimide-supported PEC/LiFSI (4:1) exhibiting conductivity of

1.6×10^{-5} S cm^{-1} at 30 °C.[241] They observed that addition of the side groups enhances the conductivity due to fast local and segmental motion by modifying PEC with methoxyethyl side groups.[242, 243] In an interesting attempt, they combined IL, SiO_2 fibre to the PEC-LiTFSI for a CPE as represented in Figure 2.19a (left). However, the flexible membrane had a poor conductivity of ~10^{-7} S cm with higher T_g with no melting and crystallization temperature, as observed in DSC, Figure 2.19a (right).[244] The reaction of propylene oxide with CO_2 gives PPC, which has been widely used in SPEs. With superior segmental motion from PPC, many composites have been explored such as novel rigid frame (cellulose nonwoven) reinforced PPC-SPE which demonstrated good cycling in $LiFePO_4$/Li pouch cell at 20 °C.[245, 246] Blends of PPC for composites like PVDF-PPC and PEO-PPC[247] have efficiently worked out by lowering the T_g and crystallinity.

Inspired by the positive interfacial effect of vinylene carbonate additive on SEI, a novel poly(vinylene carbonate) based solid polymer electrolyte was prepared via a facile in situ polymerization process. The obtained poly(vinylene carbonate)/PVCA SPE transparent film possesses a superior electrochemical stability window up to 4.5 V versus Li/Li^+ and considerable ionic conductivity of 9.82×10^{-5} S cm^{-1} at 50 °C as shown in Figure 2.19b. As reported, the higher conducvity might be due to hindrance effect weakening the interaction of Li^+ with oxygen atom in C-O-C, conversely favoring of Li^+-O=C and segmental motion along with the Li^+ coupling/decoupling with oxygen atom in C=O.[248] In a recent study, a poly(carbonate-b-ether-b-carbonates) were developed which possessed elastomeric properties with decent ionic conductivity with goal to alleviate volume change in cathode.[249]

2.4.3.3 Polyurethane/poly(hydroxy urethanes)

Various classes of polymers have been designed over half century for SPEs but none of them could cater all the sought-after key properties. This has motivated the search of all in one superior SPEs for desired parameters for years. Polyurethanes (PU) first introduced by Otto *et al.*[250] in 1940 present great candidature due to high degree of control on structure, optimum flexibility, compatibility for composite synthesis and with surfaces. Generally, PU can be produced by the reaction of polyols and isocyanate monomers containing at least two reacting groups for the repetition of the urethane linkage.[251, 252] Other monomers which are the main focus of our work and this thesis involve CC and amines/hydroxyl to PU or poly(hydroxy urethanes)(PHU).[251] PU and PHU differ by an additional hydroxyl group at each urethane linkage for PHU, which forms hydrogen bonds with other polar groups in the polymer. These polymers are multifunctional in nature for various product

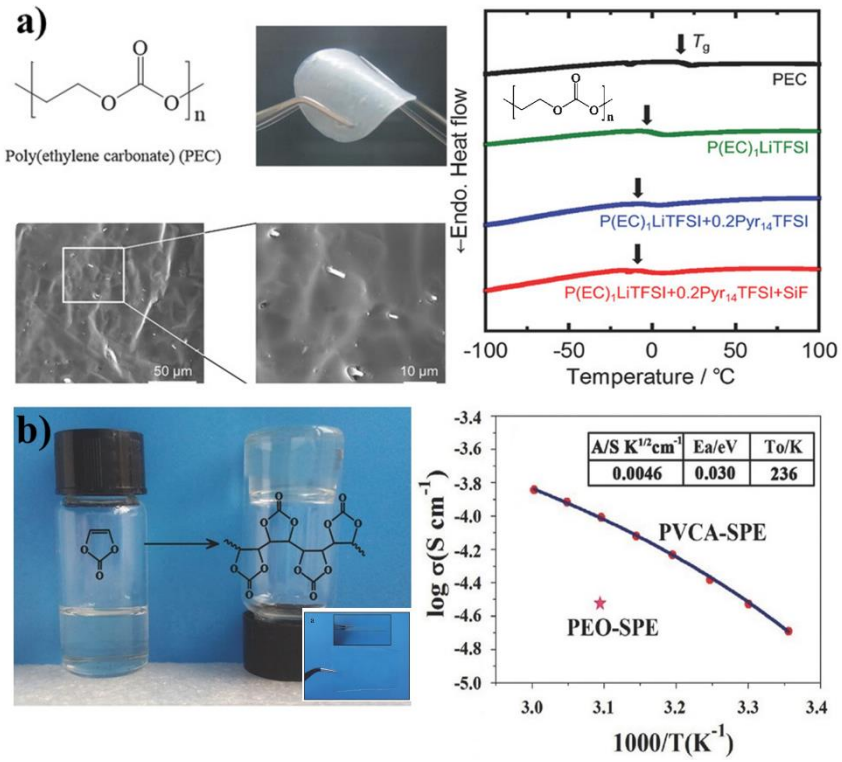

Figure 2. 19: a) Chemical structure and SEM image morphology of PEC based CPE with IL and SiF (left), and Comparative DSC exotherms of CPEs. Reproduced with permission,[244] copyright 2018, Wiley. b) Typical image of in situ polymerization of VC into PVCA-SPE transparent film (left), Arrhenius plot for ionic conductivity of PVCA-SPE. Reproduced with permission,[248] copyright 2017, Wiley.

manufacturing due to their good healing and adhesive characteristics to surfaces. This makes their market-size bigger in paint and coating manufacturing besides gaining popularity in the domain of SPEs. PU as an SPE has attracted quite a few attentions due to their compatibility with other polymers, ability to interact with inorganic particles for desired properties and their inter-chain hydrogen bonds as discussed in the reviews.[253, 254]

2.4.3.3.1 Design of PU

For a long time, the classical method of PU synthesis involving isocyanates has been flourished and used until now. Besides polyols and isocyanates, chain extenders such as diols, binary amines or hydrazines are used to increase the molecular weight of PU as listed in Table 2.2.[254] This pathway includes diisocyanates production through

Hetschel method involving the rearrangement of compounds with electron deficiency at the nitrogen atom (nitrenes).[255] However, despite the optimized method, it raises an alarming question on toxicity and environment friendly approach due to the use of phosgene and amines. Addressing this, various alternative approaches have been developed for the synthesis of non-isocyanate polyurethanes (NIPUs) such as, copolymerization of aziridines with carbon dioxide,[256, 257] transurethanization between a carbamate and a diol, azide condensation,[258, 259] the copolymerization of 2,2-dimethyltrimethylene carbonate with tetramethylene urea[260, 261] and ROP of CC with amines.[262]

2.4.3.3.2 Isocyanate-based PUs.

Isocyanate-based PUs with polyether groups in the main chain or side chains have been widely investigated due to a high degree of coordination of oxygen to lithium ions. One of the first reports on polyether-based PU SPE loaded with $LiClO_4$ (SPE ([Li]/ [PO]= 0.04) demonstrated conductivity of ~ 10^{-8} S cm^{-1} at 40 ^oC following Arrhenius behaviour with temperature.[263]

Polyols	Isocyanate	Chain extenders	Catalysts
Contributing flexible segments, and providing flexibility for PU.	Responsible for reactivity and rigidity of PUs.	For structural engineering of the PU molecular and to offer mechanical support.	To speed up reaction rate and lower reaction temperature.
Polyether (Aliphatic linear polyether) 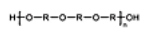 (Aromatic polyether) 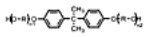	Toluene-2,6-diisocyanate (TDI) 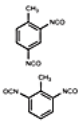	1,4-butanediol (BDO) Ethylenediamine (EDA) 	Dimethylcyclohexylamine (DMCHA) 
Polyester 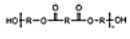	4,4'-methylenebis (phenyl isocyanate) (MDI) 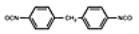	cyclohexane dimethanol (CHDA) 	Dimethylethanolamine (DMEA) 
Polycarbonate 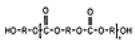	1,5-naphtylene diisocyanate (NDI) 	Trimethylolpropane (TMP) 	Bismuth 2-ethylhexanoate (BEHA) 
Acrylic 	5-isocyanato-1-(isocyanatomethyl)-1,3,3-trimethylcyclo-hexane (IPDI) 	hydroquinone bis(2-hydroxyethyl) ether (HQEE) 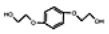	Dibutyltindilaurate (DBTDL) 
Polybutadiene 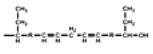	4,4'-methylenebis (cyclohexylisocyanate) (HMDI) 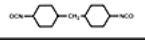	dimethyl propionic acid (DMPA) 	Triethylenediamine (DABCO) 

Table 2. 2: List of commonly used monomers and catalyst for the synthesis of PU. Reprinted with permission,[188] copyright 2005, Elsevier.

Moved by this, significant improvement was achieved over years by exploiting polyether segments from different polymers. For instance, polydioxanone (PDXL) based PU (PDXL-PU) with $LiClO_4$ achieved three orders of magnitude of enhancement in the conductivity (2×10^{-5} S cm^{-1}) at RT with as low T_g as -51.75 °C.[264] In a fundamental study, it was verified that the ionic conductivity decreases with an increase in the content of the hard segment and branching in the polymer due to lower free volume availability and lesser ion-pair and aggregate formation, respectively.[265, 266] A waterborne PU (WPU) was synthesized using PEG, diethylene (DEG), hexamethylene diisocyanate (HDI), and dimethyl propionic (DMPA) by Junjie *et al.*[267] in the series of reaction steps and with the semi-crystalline nature of films as indicated in Figure 2.20a and 2.20b. The WPU-SPE loaded with 20% LiTFSI assembled with LFP displayed excellent performance when cycled at 0.1C with conductivity of 5.14×10^{-5} S cm^{-1} at 25 °C as shown in Figure 2.20c. PU has shown high compatibility in blending with PEO and a report confirms that an electrospun

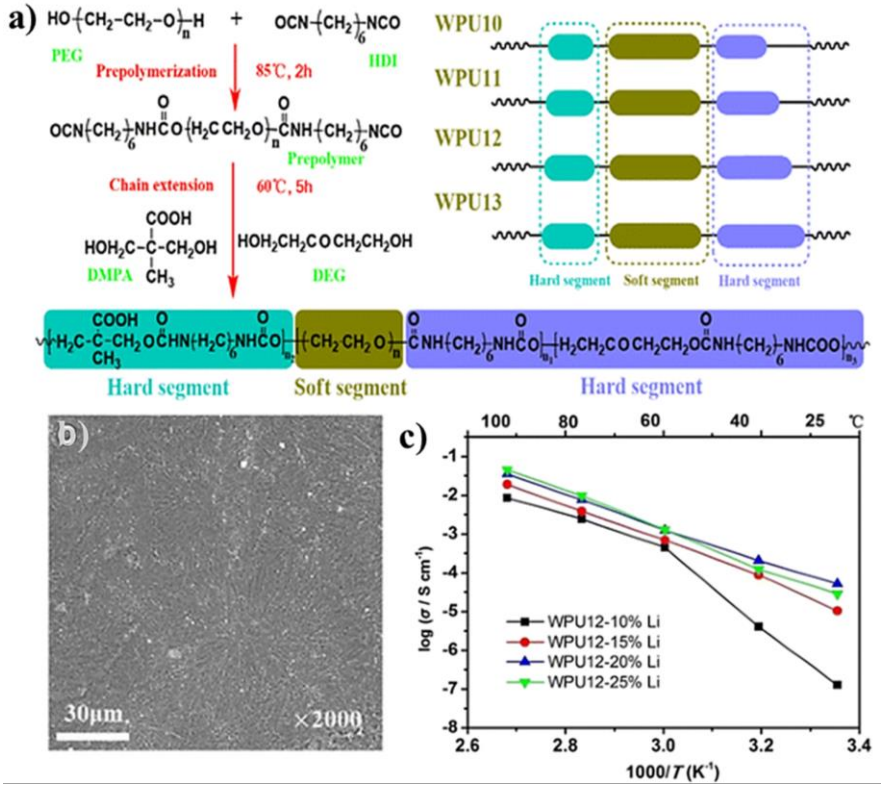

Figure 2.20: a) Schematic representation of synthesis of WPU, b) SEM image of WPU film and c) Temperature dependent ionic conductivity of WPU with LiTFSI Reproduced with permission,[267] copyright 2018, Springer.

membrane of PEO/PU blend polymer lowered the crystallinity and exhibited fibrous nature reaching the conductivity of ~10^{-3} S cm^{-1}.[268] With further progress, a 3D block copolymer electrolyte, referred as PH-BCPE, was developed by reacting hexamethylene diisocyanate trimer (HDIt) and PEG and showed ESW > 4.65 V and conductivity, ~5.7 × 10^{-4} S cm^{-1} at 55 °C. The fabricated battery with PH-BCPE showed superior performance with LFP at a high rate of 1 C for more than 100 cycles.[269] Besides SPE, they have shown interesting performance on addition of plasticizers. For instance, PC based PU possessed higher conductivity in comparsion to other plasticizers screened, respectively.[270]

Polycarbonates, as discussed above, possess highly amorphous nature, dielectric constant and oxidation stability whose addition to PU could benefit the SPE. In a detailed study, a polycarbonate-based PU (PCPU) was synthesized by step-growth polymerization of HDI, DEG and polycarbonatediol (PCDL). The effect of hard segment was analyzed by varying from 8 to 14% in PCPU, indicating that thermal stability decreased and mechanical stability increased with an increase in hard segments. The PCPU-LiTFSI SPE delivered 1.12 × 10^{-4} S cm^{-1}, ESW > 4.5 V *vs.* Li/Li^+ at 80 °C with a specific capacity of 134 mAh g^{-1} at 1 C for LFP cells. Figure 2.21 shows PCPU films with chemical structure and variable temperature dependent conductivity measurements.[271] While PCPU has a higher redox window but it lags behind in matching the conductivity to PEO. For this reason, alternative polyesters and polysiloxanes have also been looked upon actively. With lower T_g, higher thermal and chemical stability, polysiloxane-based PU was designed using poly(dimethylsiloxane) (PDMS) with conductivity recorded at 1.05 × 10^{-5} S cm^{-1} at 30 °C.[272]

Unlike linear, cross-linked polymers possess superior temperature and mechanical stability. With high control on crosslinking density and structure, it's entrancing to extend their investigation in batteries for the longer run. PU derived from acrylates are expected to show higher compatibility with electrodes due to their in-situ polymerization and interaction. Santhosh et al. developed PU acrylates by end-capping a hexamethylene diisocyanate (HDI)/PEG-based prepolymer with hydroxy butyl methacrylate (HBMA), which showed a high degradation temperature of 400 °C but a lower conductivity of < 10^{-8} S cm^{-1}.[273] Nevertheless, the concept of integrating a single lithium ion conductor has also clubbed quite attentively with anions such sulfonic,[274] sulfonyl imide,[275] carboxylic,[276] phosphonic,[277] *etc*., within PU structural framework. While the subtle limitations in SLIC-based PU remain the same, i.e. ionic conductivity of isophorone diisocyanate (IPDI)-SLIC-based SPE was recorded at ~8.91 × 10^{-7} S cm^{-1} at 30 °C which needs to be improved.[278]

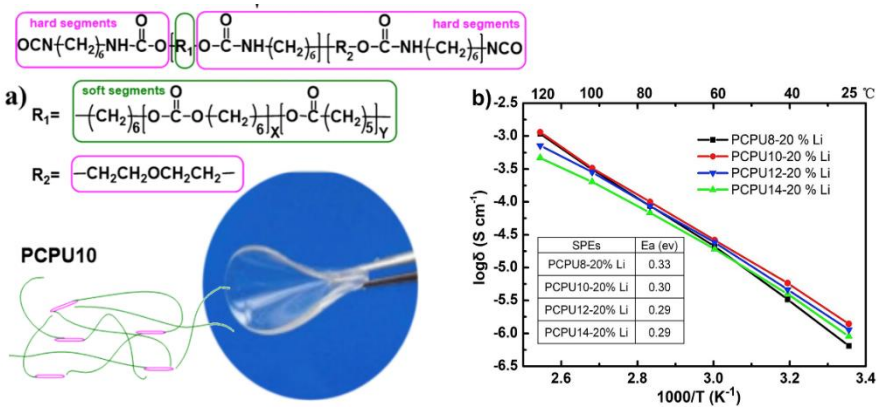

Figure 2. 21: a) Schematic representation of PCPU synthesis and the soft and hard domains of PCPU with different hard segments content, image of PCPU10-20% Li membrane before cycling. b) Temperature dependence of ionic conductivity of PCPU-based SPEs. Reproduced with permission,[271] copyright 2018, Elsevier.

Blends and Composite PU/PHU

Among alternative pathways to address the trade-off and integrate desired properties, one facile method is the blending and composite development. The polar groups in PU already facilitate its interaction with other polymers or inorganic elements involving hydrogen bonds from -NH and -OH units. PEO has been one of the first preference for blending due to the oxygen donor atoms and soft segments, as discussed in above section. PEO blended PU (3:1) was synthesized showing no crystallinity and good conductivity of 5.3×10^{-4} S cm^{-1} (60 °C) which on further cycling experiments exhibited promising specific capacity and retention with LFP-Li cells.[279] In a report, Wen *et al*. developed a composite polymer electrolyte consisting of thermoplastic polyurethane (TPU) with polyacrylonitrile (PAN). They explained the possibility of dipolar interactions of C=O group of PU with C≡N, which affects varyingly on T_g of hard and soft segments. As a result of this interaction, hydrogen bonding with the polymer also gets affected while overall conductivity was recorded to be higher than PU alone.[280]

As discussed in the previous sections, inorganic fillers fill the gap in drawbacks by bringing higher conductivity, thermal stability, *etc*. This does not leave PU to lag behind without exploiting the beneficial interaction with PU repeatable units. The most commonly used filler, SiO_2, has been explored in few reports indicating positive outcomes of the composites.[281, 282] Fang *et al*.[281] incorporated hydrophilic SiO_2 ($uSiO_2$) and hydrophobic SiO_2 ($mSiO_2$) into poly(ether-urethane) network polymer

(PUN), respectively. They are assumed to elevate the Lewis acid-base interactions between $uSiO_2$, polymer matrix and lithium salts while increasing the amorphous phase. As a result, 20 times improvement compared to the pristine SPE was obtained with 1.15×10^{-5} S cm^{-1} ($mSiO_2$) and 1.02×10^{-5} S cm^{-1} ($uSiO_2$) at 30 °C as depicted in Figure 2.22. Titanium oxide (TiO_2) was incorporated into electrospun PU-PVDF GPE which clearly led to the improved conductivity i.e. 4.8×10^{-3} S cm^{-1} and 3.2×10^{-3} S cm^{-1} at ambient temperature, respectively with and without TiO_2.[283] Although, a thorough understanding of hybrid electrolytes still remains unclear with change in host polymer and their interaction with inorganic fillers. Hybrid SPE based on $Li_7La_3Zr_2O_{12}$ (LLZO) powders (with 5 wt% of LLZO) was designed and tested as a SPE for LFP-Li cells, indicating a high potential for further prospects.[284] Nevertheless, both PU blends and composites are not as studied as PEO, which limits any conclusion at this stage.

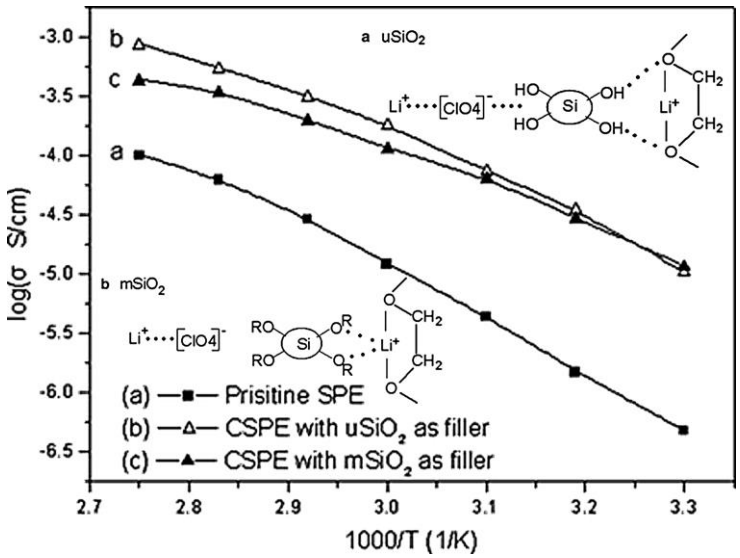

Figure 2. 22: Temperature dependent ionic conductivity for pristine PUN /Li ClO_4 SPE, PUN /$uSiO_2$/ Li ClO_4 CSPE, Inset: Pictorial model of the surface interaction between two forms of dispersed fumed silica filler and the PUN-$LiClO_4$ electrolyte complex. Reproduced with permission,[281] copyright 2007, Springer.

2.4.3.3.3 Non-isocyanate urethanes

PU has been synthesized via various approaches in lieu of polymers and their composites for diverse application. However, as explained above, majority of them still involves isocyanate monomers and phosgene, which itself is of grave concern due to their toxicity and unsustainability.[285] Due to the huge market demand in various sectors, it's inevitably evident to observe the surge in alternatives, i.e. less or nontoxic

PU/ non-isocyanate PU (NIPU) with improved properties and facile synthesis. Unlike urethane linkage in PU, NIPU comprises primary or secondary hydroxyl in urethane units, which is why it is also referred as poly(hydroxyurethane) (PHU) with first patent was published in 1950.[286] The hydroxyl group adds an advantage of post-functionalization for other reaction and synthesis. However, it is still debatable whether PHU is more thermally stable than PU.[287] NIPU could be obtained by ring opening polymerization, polycondensation, polyaddition and rearrangement as depicted in Figure 2.23.[288]

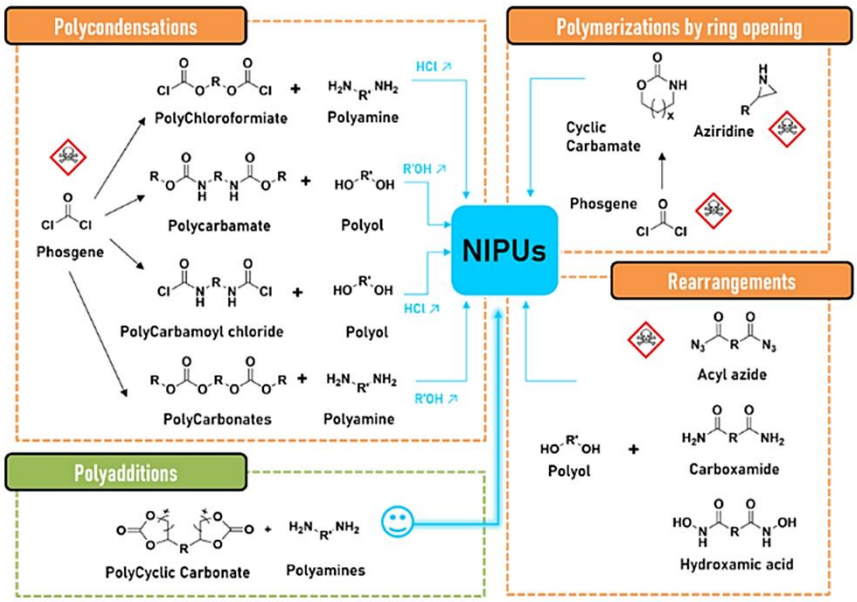

Figure 2. 23: Different pathway for the synthesis of non-isocyanate polyurethanes. Reproduced with permission,[288] copyright 2005, Elsevier.

Ring opening polymerization uses aliphatic cyclic carbamates[289, 290] or aziridines[286, 291, 292] with cyclic carbamates (generally 6-7 membered cyclic carbamates) with the support of catalysts (such as sodium hydride or N-acetyl caprolactam). It uses phosgene gas, like conventional PU in most of the cases.[292] Polycondensation involves various monomers for the synthesis of NIPU following transurethanization pathway. It involves a reaction between polychloroformate and polyamine, polycarbamate and polyol, polycarbamoyl chloride and polyol, and polycarbonate and polyamine difunctional carbamate for obtaining PHU.[293] However, additional steps involve the formation of polycarbamates or polycarbonates. This method is not very popular due to longer reaction time, catalyst requirement and side products.[294, 295] Rearrangement reaction involves established acyl azides (Curtius

rearrangement), carboxamides (Hoffman rearrangement) or hydroxamic azides (Lossen rearrangement) for NIPU.[296, 297] However, all these methods rely on toxic monomers or catalysts for the synthesis of NIPU.

NIPU/PHU via polyaddition

As highlighted in Figure 2.23, polyaddition is considered to be the cleanest pathway for non-toxic synthesis of the NIPU at a large scale as well. The reactions of cyclic carbonates and amines are well investigated systems due to their facile availability, easy handling and storage, high solvation, boiling point for the reactions. The synthesis of both monomers involving multi-functional CC via epoxide and CO_2 using organocatalysts (discussed in sections above) and polyamines from fatty diacids marks the high environment friendly character.[298] It was discovered by Endo and coworkers that the reactivity of CCX (X represents the number of atoms in the ring) lies in the order of CC7 > CC6 >CC5.[299] However, further studies indicated that CC5 and CC6 possess similar reactivity. This could be due to the strain of the seven-membered cyclic carbonate which is greater than the strain of the six- and five-membered cyclic carbonate rings.[300] Despite lower reactivity, CC5 is more favoured among CCs which is related to its nontoxic and easier production. Over the years, various methods and parameters were discovered to increase the reactivity of CC5 and for polymerization at milder conditions. Figure 2.24a demonstrates the trend in time-dependent reaction of CC with side groups.

The side groups act as an electron-withdrawing group on the CC and thus increase the electrophilicity of the carbonyl, which in turn enhances the chance of nucleophilic attack by amines.[301] Derived from some investigations by Lamarzelle *et al.*[302] and Tomita *et al.*[303], substituents follow a certain order in reactivity: R = Me < H < Ph < CH_2OH < CF_3 which was observed to be crucial for predicting the extent of ring opening. In support of this argument, they found that CC5 with ester, CF_3 and double bond showed higher reactivity while equivalent to CC6 in case of ester substituent. The nucleophilic amines also determine the rate of reaction in order of their reactivity with aromatic and sterically hindered amines to be least reactive as shown in the Figure 2.24b.[300] However, elevated temperature increases the yield with the possibility of side reactions such urea, in-situ CO_2 formation, carbonation of amine, amidification and oxazolidinone formation by dehydration.[302, 304, 305] Another approach consists in the use of catalyst for the aminolysis reaction via three pathways as depicted in Figure 2.25a: 1) increasing the electrophilicity of the carbonyl at CC, 2) nucleophilicity of amine and 3) opening of CC with a nucleophilic catalyst.[306] These catalysts include enzymes, Lewis acids, bases *etc*, with well utilized 1,5,7-

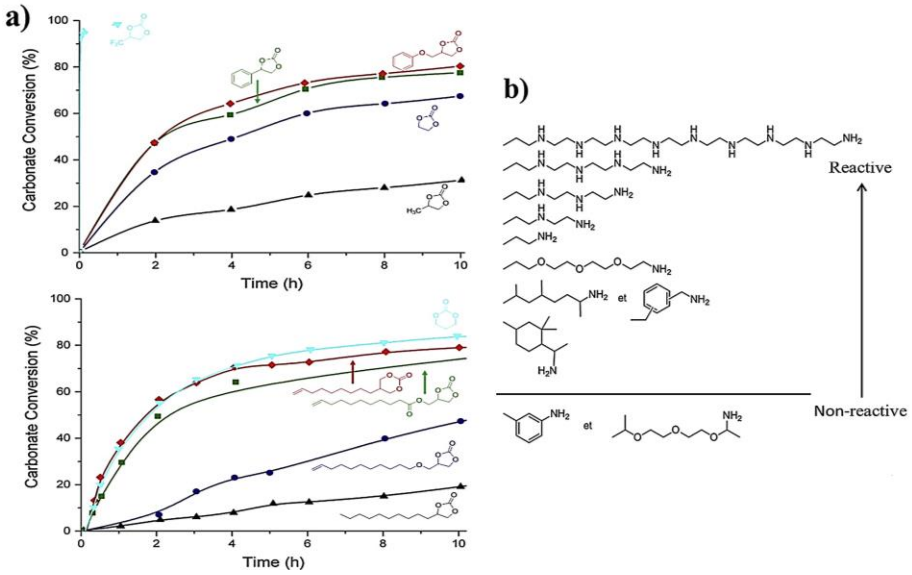

Figure 2. 24: a) Time-conversion curves in the reaction with CC5 carrier of different substituents and hexylamine at 70 °C, 1 mol L^{-1} in DMSO-d6 (top left) and CC5 or CC6 carrier of different substituents (aliphatic, ether or ester) and hexylamine at 50 °C, 1 mol L^{-1} in DMO-d6 (bottom left); b) Reactivity of various amines toward ether-CC5 at room temperature. Reproduced with permission,[299, 302, 307] copyright 2016 (RSC), 2001 (Wiley) and 2004 (Wiley), respectively.

triazabicyclo[4.4.0]dec-5-ene (TBD), 1,8-Diazabicyclo(5.4.0)undec-7-ene (DBU) and thiourea *etc*.[218, 308, 309]

The synthesis of NIPU via aminolysis is promising and isocyanate-free methods largely involvering opening of CC with an amine.[262] The mechanism involves three steps as shown in Figure 2.25b tetrahedral intermediate formation via attack of carbonyl in step I, attack of amine on tetrahedral with removal of protonin step II and, in the last step, the carbon-oxygen bond is broken along with H^+ combining with alkoxy ions to give PHU.[306] Unlike in PU, urethane with hydroxyl groups in PHU could offer higher chemical resistance to non-polar solvents due to probable intra- and inter-molecular hydrogen bonds with carbamate.[295, 310] Steblyanko *et al.* described that during PHU formation, secondary alcohol is preferred over primary due to lower energy potential of the former in correlation with reactivity factors explained above.[311]

One of the major concerns in PHU synthesis lies in the limited reaction and thus reduced molar masses. It could be explained via two reasons: 1) as the reaction undergoes, the viscosity increases and thus extent of reaction decreases (due to lower diffusion of monomers) which in turns requires temperature to decrease the viscosity,[312] 2) due to stoichiometric unbalance between monomers. The reaction

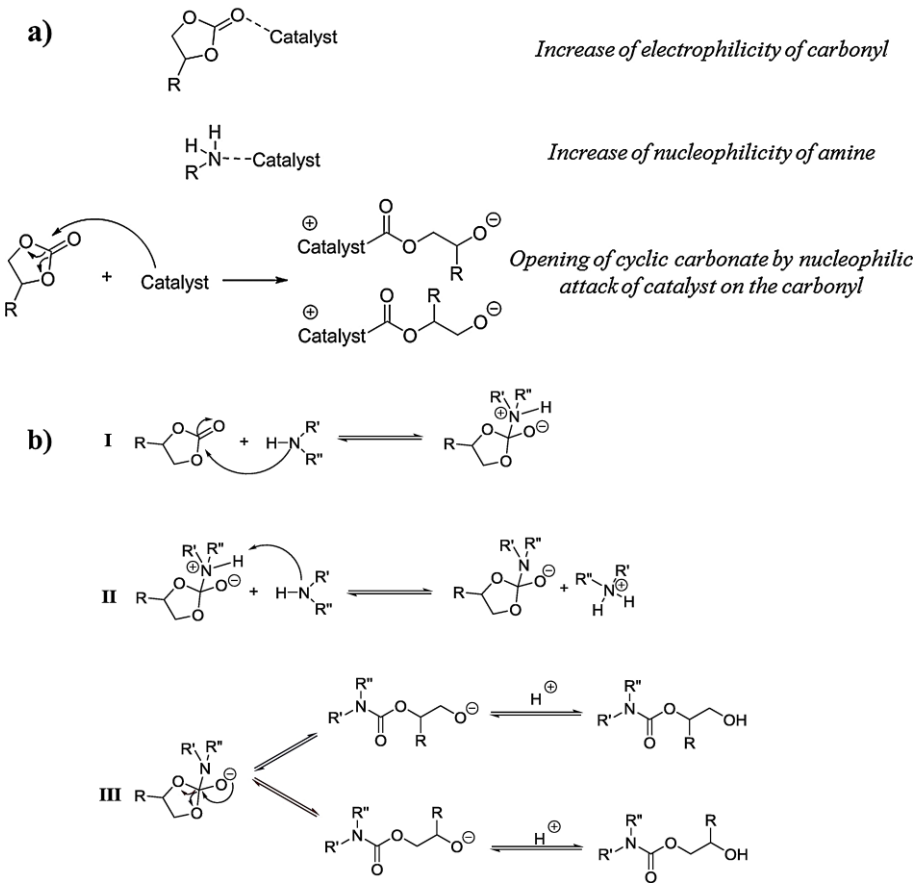

Figure 2. 25: a) Different catalytic mechanisms of cyclic carbonate aminolysis, and b) Mechanism of CC/amine reaction. Reproduced with permission,[306] copyright 2017, Elsevier.

scheme in Figure 2.26 shows the reactions between CC5 and amine. Undesired side reactions can consume the monomer, which leads to a limited reaction to PHU formation.[306] Nevertheless, the initial parameters influencing the reaction yield are structure and functionality of the monomer and catalyst, followed by reaction conditions like temperature, *etc.*

For an instance, Carre and coworkers reported the catalyst-free PHU formation from the reaction of dimer-based diamines (DDA) and sebacic biscyclocarbonate (SB-Bis CC) highlighting the role in amine functionalities (2.0 to 2.2).[313] The limited reaction leading to reduced molar mass also paved the way for involving other monomers for forging the targeted properties. One such approach was recorded for the synthesis of PHU by crosslinking of partially carbonated epoxide monomers. Figovsky *et al.*[314] developed this technique by indulging two reactions together: aminolysis of CC

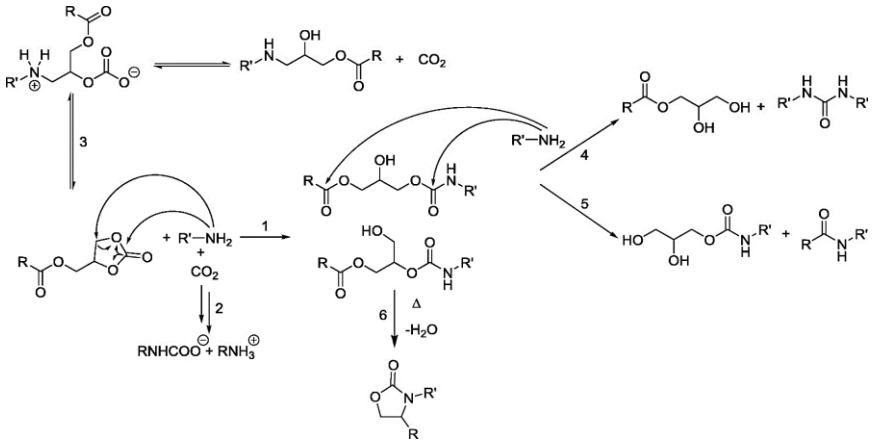

Figure 2. 26: Possible reactions between 5-membered CC and amine: (1) classic aminolysis, (2) carbonation of amine, (3) CO_2-in-situ formation, (4) urea formation by trans-urethanization, (5) amidification reaction and (6) oxazolidinone formation by dehydration. Reproduced with permission,[306] copyright 2000, Wiley.

of CC and ring opening of epoxide monomers. This partial carbonation of the epoxide monomer enhanced the mechanical properties of PHU and expanded its commercial application for materials like fibres, *etc*.[306, 315]

CC formation upon coupling of CO_2 in epoxide has been the most preferred choice as monomer for PHU. Targeting diverse applications, PHUs have so far largely aimed industrial markets involving porous foams, adhesives, coatings, wearables, *etc*. However, they are gaining increasing attention in sensors and energy sector with polymer electrolytes with potential competition to conventional polymer electrolytes. Detrembleur and coworkers have developed a variety of PHUs and their composites for adhesive and coating applications involving CC synthesis from epoxide to PHU via facile aminolysis.[316, 317, 318, 319] In one of those reports, they synthesized PHU adhesives from tri CC/diamine/amino-telechelic poly(dimethylsiloxane) formulation containing various amounts of native, epoxy- or CC functionalized ZnO.[316] Li and coworkers[320] reported a new bio-based CC (derived from renewable diphenolic acid and carbon dioxide) with ethylenediamine (EDA), diethylenetriamine (DETA), and isophoronediamine (IPDA), corresponding to PHU-EDA, PHU-DETA, and PHU-IPDA, respectively for greener water-borne coatings. A photoluminescent linear PHU was prepared from siloxane-bridged carbonate copolymerized with diamines such as 1,6-hexanediamine (HDA) and ethylenediamine EDA for potential LED application.[321] For years, PU has been already researched widely in electrolytes with their composites showing exceptional properties and potential improvement with a high degree of control on structure, whereas very few studies have been conducted on

PHU based electrolytes. Moreover, most of the PHU based electrolytes reports are sourced to bio-derived precursors such as vegetable oil (which are discussed in the next section).

2.5 Bio-based polymer electrolytes

Naturally derived polymers are eco-friendly and smart choices due to their less hazardous impact, right from their formation, design and processing. They are categorized into three different classes based on source and synthesis, 1.) directly extracted from biomass (cellulose, gelatin and natural rubber), 2) those produced directly by microorganisms (e.g. bacterial cellulose and gellan gum) and 3.) those chemically synthesized from bio-derived monomers (e.g. polylactic acid and vegetable oil based) as represented in the flowchart of Figure 2.27.[322, 323] These polymers or their sources such as starch,[324] cellulose,[325-327] chitosan, lignin, natural gums, proteins, furfurals, fatty acid derived oils *etc*., have been constantly picked for their functionality not only as additives, binders and electrolytes but also as electrodes.[328-331] Most of them possess high polar groups such as, -O, -N, =O, -S *etc*. which facilitate salt solvation and cationic transport efficiently with optimum control on structural design and modification.

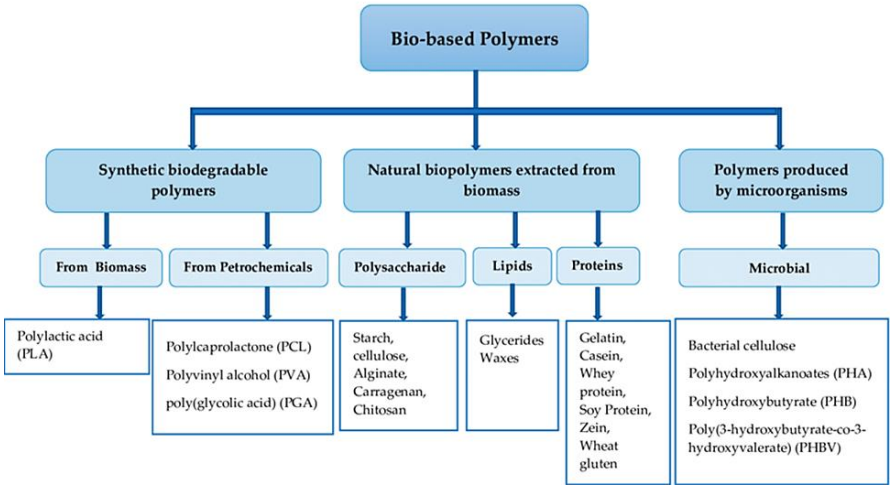

Figure 2. 27: Classification of biodegradable polymers based on their source. Reproduced with permission,[323] copyright 2022, MDPI.

2.5.1 Polymers extracted from biomass and microorganisms

Gums belonging to the class of polysaccharides are lucrative choices due to their many oxygen units and properties like adhesive, binding and mechanical resistance. Differing in origin and structure, variety of gums have been discovered suitable for electrolytes such as carrageenan, agar, pectin, guar, Arabic gum *etc*. Guar gum based GPE with $LiClO_4$ and glycerol was synthesized and exhibited a conductivity of 2.2×10^{-3} S cm^{-1} with $LiClO_4$ and glycerol at RT as shown in Figure 2.28a.[332] Naturally occurring rubbers possess high elasticity and adhesion like gums but they lack polar groups for Li-solvation which shifts their dependence as supporting material.

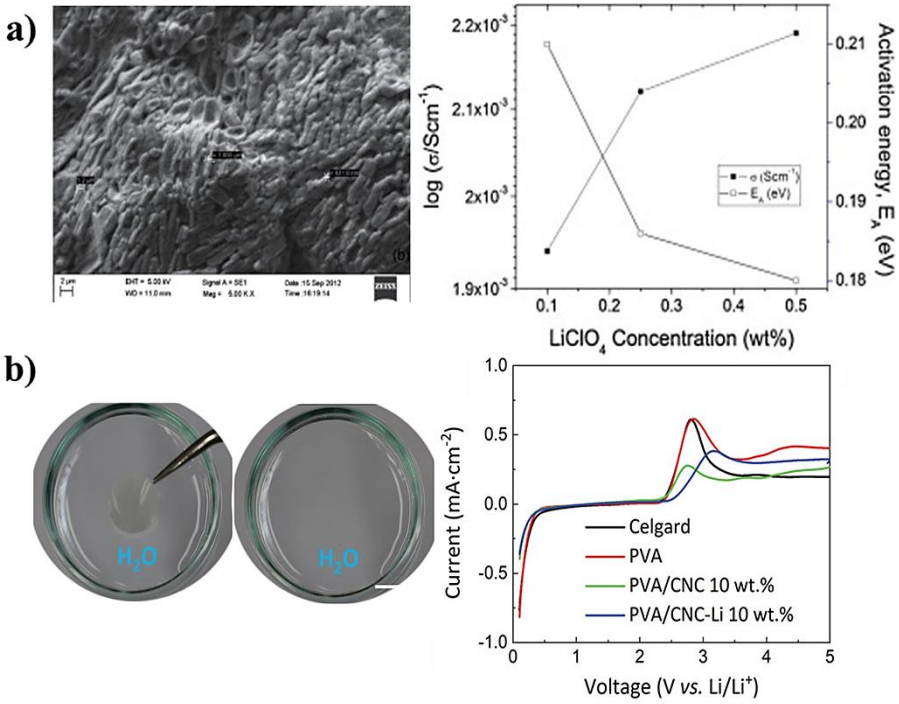

Figure 2. 28: a) SEM images of guar gum based GPE at magnification scale of 2 µm (left) and logarithmic conductivity and activation energy as a function of $LiClO_4$ concentration at RT. Reproduced with permission,[332] copyright 2014, Elsevier. b) Optical photographs demonstrating the transiency of a PVA/CNC-Li 10 wt% membrane (Ø = 11 mm) in deionized water at RT over a time period of 6 s. The scale bar is 11 mm (left) Linear sweep voltammetry for ESW at a scan rate of 10 mV s^{-1}. Reproduced with permission,[333] copyright 2021, Wiley.

Due to their lower T_g and highlighted characteristics, they were blended with PEO via solution casting method and the obtained SPE showed a conductivity in the range of ~10^{-6} S cm^{-1} at RT.[334] Many reports can be found on chitosan-based binders and electrolytes despite their higher crystallinity and low ionic conductivity due to their free amine and carboxyl group available for modification. SPE based on chitosan-poly(aminopropyltriethoxysilane)/PEO was designed by Fuentes *et al.*[335] which delivered the conductivity of ~10^{-5} S cm^{-1}. However, it was observed to enhance the performance of chitosan-based electrolytes when incorporated with plasticizers into a GPE.[336]

Cellulose, being the most abundant biomass, has been in the center of interest with excellent outcomes.[9] In an interesting report, a GPE was synthesized by combining cellulose nanocrystals and poly(vinyl alcohol) (PVA/CNC) membranes. The electrolyte delivered a conductivity of 3.08 x 10^{-3} mS cm^{-1} with ultrawide ESW of ~5.5 V and significant performance for lithium assembled cells as depicted in Figure 2.28b.[333] Kale *et al.* combined cellulose triacetate with poly(polyethylene glycol methacrylate) p(PEGMA) using photo polymerization for a transparent film based GPE as shown in Figure 2.29a. They obtained a high conductivity of 1.8 x 10^{-3} S cm^{-1} (Figure 2.29b), > 5 V of ESW and excellent cycling with LFP-Li cells.[337] Besides modification and polymer blending, entrancing attempts were also made on cellulose via incorporating inorganic fillers like Boron nitride to exploit the synergy of the composite.[338] In addition, integrating metal organic framework (MOF) particles along the cellulose fibers through an in situ approach was reported by Zhou *et al.* as depicted in Figure 2.29c and 2.29d.[339] This approach of MOF-cellulose fiber-GPE delivered high t_{Li^+} of 0.88, oxidation limit of ~ 5.1 V and superior cycling at C-rate of 3 C.[340]

Bacterial cellulose derived as a result of metabolism in bacteria has been reported as a riveting candidate for composite and gel polymer electrolytes. BC-based GPEs such as poly(methyl vinyl ether-alt-maleic anhydride) plus propylene carbonate/lithium difluoro(oxalato) borate (BCP-PMM) have been synthesized which outperformed liquid electrolytes. Those GPEs recorded lower overpotential and high compatibility with lithium metal and higher voltage cathodes (4.45 V vs. $LiCoO_2$) as confirmed by cycling experiments.[325, 326]

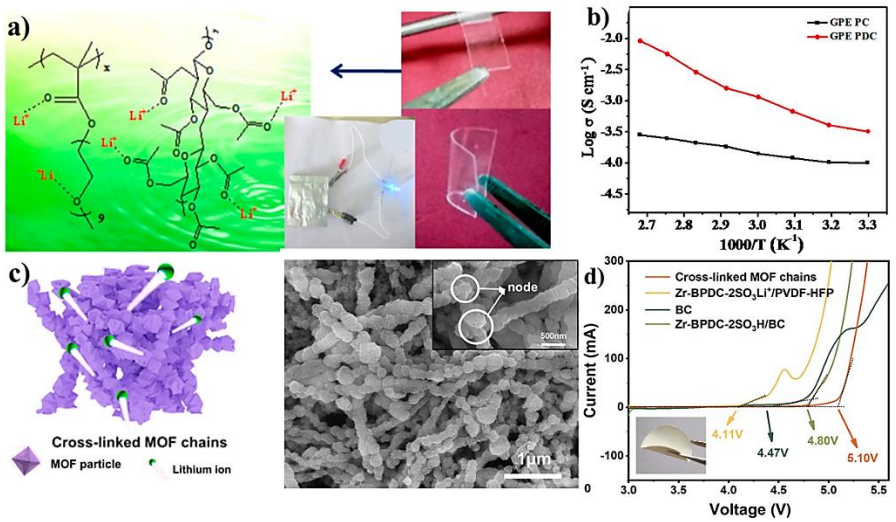

Figure 2. 29: a) Structure of polymer showing Lithium ions transfer through the coordination sites of ether and carbonyl functional groups (left), Photograph of a flexible and transparent polymer, bendable GPE film and flexible Li ion battery with $LiFePO_4$/GPE PC/graphite. (right); b) Temperature dependent ionic conductivities of the GPE with PC and PDC, respectively, reproduced with permission,[337] copyright 2017, ACS. c) Illustration of the SE Based on Cross-Linked MOF Chains (left), SEM image of the cross-linked MOF membrane (topview-right); and d) LSV profiles of the Li|SEs|SS asymmetric cell (Inset: Photograph of the cross-linked MOF chains membrane). Reproduced with permission,[340] copyright 2021, ACS.

2.5.2 Polymers chemically synthesized from bio-derived monomers

Under the category of polymer chemically synthesized from bio-derived monomers, there is complete freedom to modify the structure, introduce functionality, and target certain properties in the final polymer. Bio-derived sources like sugar, wood (cellulose, lignin), lactides, vegetable oil, have served as monomers for the design of polymers via particular synthetic approach. Poly(lactic) acids (PLA) are derived from two routes: ring opening of lactide or polycondensation of lactic acid.[322] Their monomers are produced naturally via a fermentation process of sugar feedstock like dextrose. The conductivity of pure PLA based electrolyte was reported to be very low, around 9.46 x 10^{-12} S cm^{-1} at RT.[341] This was followed by further development toward the synthesis of PLA blended with poly(3-hydroxybutyrate) (PHB) by electrospinning method which delivered the conductivity of 1.5 x 10^{-5} S cm^{-1} at RT as GPE after the incorporation of liquid electrolyte.[342] Later, Stephano *et al.*[343] combined the Pyr_{14}TFSI ionic liquid with a ternary polymer electrolyte based on PLA loaded with LiTFSI. The solvent free electrolyte recorded decent conductivity of 2.1 x 10^{-4} S cm^{-1} at 60 °C. In

some other reports, the addition of inorganic fillers such as Al_2O_3 also has demonstrated the improvement of the net conductivity (2.07×10^{-5} S cm^{-1}) with the later acting as Lewis acid filler.[344]

2.5.2.1 Bio-based PU/PHU

Bio-waste derived glycerol is used for the conversion to CC due to two functional units: a primary OH and a 2-oxo-1,3-dioxolane (ODO) group. A fully bio-based PHU was reported from the ring opening polyaddition reaction of diglycerol dicarbonate with various amines without using a catalyst at milder conditions targeting the coating industry.[345, 346] Starch and sugar derived molecules such as ISO (1,4:3,6-dianhydrosorbitol),[347] erythritol,[348] 2,5-furandicarboxylic acid (FDCA),[349] *etc*. were strategically converted into CC in two or multiple steps via epoxidation as a prepolymer for environmentally friendly PHU.[350] Naturally occurring aromatic and non-aromatic compounds from wood were attempted to polymerize PHU with derivates like lignin,[351] tannins,[352] terpenes,[353] *etc*. In a study, tannin molecules were carbonated with dimethyl carbonate and thereafter reacted with diamine to form PU.[352] One of the exciting class of bio-derived monomers for PHU is vegetable oil.

Vegetable and other non-edible oils being used as monomers for various polymers are a potential alternative for the industry manufacturing, coatings, cosmetics to energy materials. Triglyceride containing oils include usually soybean, palm, sunflower, linseed, rapseed, jatropha, castor oil *etc*.[322] They are attractive choices due to their easy availability and abundance, along with their renewability. With diverse functional groups such as unsaturated bond, hydroxyl, epoxy units *etc*., they can be converted to targeted functionality on controlled reaction. Polyols derived from vegetable oils have been reacted with diisocyanates for the formation of PU to develop membranes.[251, 354,354, 355] Palm kernel oil based PU as SPE was obtained from the palm kernel oil polyol and 2,4-methylene diphenyl diisocyanate (2,4' MDI) which showed the conductivity of 7.6×10^{-4} S cm^{-1} at RT on plasticization with EC as shown in Figure 2.30b.[356] Rayung *et al.*[357] modified Jatropha oil by epoxidation and hydroxylation reaction. Further, the as-synthesized polyol was reacted with isocyanates for PU. The electrolyte prepared by solution casting method with the addition of $LiClO_4$, exhibited conductivity of 1.29×10^{-4} S cm^{-1} at RT with T_g as low as ~ -25 ^oC for PU-25$LiClO_4$ as shown in Figure 2.30c and 2.30d. Non edible castor oil has been modified for its utilization toward bio-based polymer electrolytes in some reports as well.[358-360] Salmiah and coworkers in their investigation, developed PU-SPE and provided comparative data on the conductivity of Li^+ and Na^+ ions (1.78×10^{-6} S cm^{-1} and 4.28×10^{-7} S cm^{-1} at RT) from 30% of LiI and NaI salts, respectively.

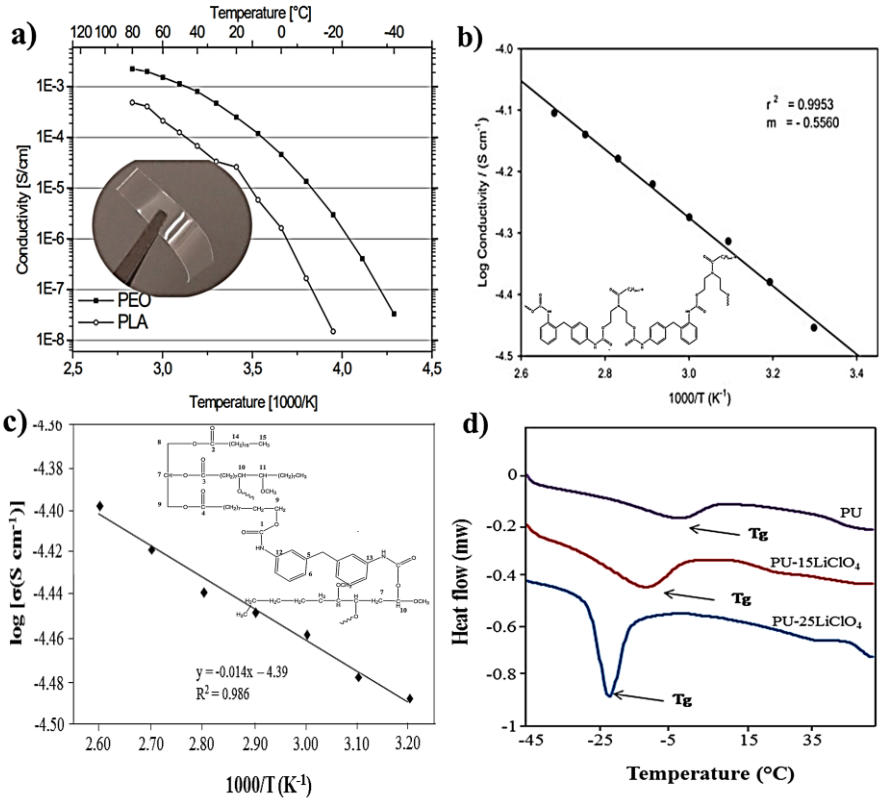

Figure 2. 30: a) Comparative ionic conductivity of the PEO-based and PLA-based electrolytes both at a molar composition of (polymer– LiTFSI–$Pyr_{14}TFSI$) = (20:2:4) (Inset: ternary SPE based on PLA, molar composition (LA units/LiTFSI/Pyr14TFSI)=(10:1:1) after hot-pressing (same composition) Reproduced with permission,[343] copyright 2016, Wiley. b) Temperature dependent conductivity of PU-25 wt.% LiI SPE (Inset: Structure of as synthesized PU), Reproduced with permission,[356] copyright 2014, Elsevier. c) Temperature dependent conductivity of PU-25$LiClO_4$ (Inset: Structure of PU based on NMR spectra), and d) DSC thermograms of PU, PU-15$LiClO_4$, and PU-25$LiClO_4$. Reproduced with permission,[357] copyright 2021, MDPI.

The polymerization was performed on the polyol from castor oil with 4,4-methylene diphenyl diisocyanate (4,4' MDI).[359]

Focusing on other NIPU investigations, castor oil fatty acid was dehydrated prior to carbonation with CO_2 for PHU,[361] polycarbamate (developed from soybean oil-based alkyl polyol and epoxidized sucrose soyate polyol) was crosslinked with 1,4-cyclohexanedicarboxaldehyde and 2,5-diformylfuran (DFF) to obtain PHU.[362] Epoxidation is one of the most popularly utilized method for oil based fatty acids. Furthermore, epoxidized soybean oil (ESBO) and epoxidized linseed oil are carbonated to get CC for PHU on the ring opening addition with amine. However,

PHUs are hardly exploited as electrolytes despite the recent development into CC monomers modified from vegetable oil. This thesis is a consolidated effort in that direction that aims to discover electrolytes from CC to PHU, as well as the synergic effect with blends.

2.6 Summary and conclusion

The electrolyte is a complimentary component of a battery, supporting its operation primarily by providing an ion transport channel between electrodes. A superior electrolyte not only provides good ionic conductivity, broad voltage window, high compatibility with electrodes and other electrochemical properties but also possesses physical characteristics such as flexibility, non-leakage, robustness, lightweight, and safety from flammability. The conventional liquid electrolyte falls behind in a few of these electrochemical parameters such as broad ESW, transference number and above highlighted physical characteristics pointing at the improvement or alternatives. Solid state electrolytes, specifically discussed polymer electrolytes here, have shown huge potential in line with their counterpart inorganic solid electrolytes. With first few investigations of PE (ex. PEO) as lithium conductor were carried in the 1990s, although it did not gain speed due to their lower conductivities and other shortcomings compared to liquid electrolyte. However, it gained much interest and attention for LB technology requiring high voltage cathode and high-capacity anodes (such as lithium, silicon) to revolutionize the transport industry.

Polymer electrolytes are discussed based on the physical phase, solid polymer electrolytes, gel polymer electrolytes and hybrids. Solvent-free PEs referred as dry-solid polymer electrolyte possess lower conductivity than others but facile handling and flexibility. Exploiting various polymeric synthetic techniques such as copolymerization, blending and grafting, researchers have reported quite a few high exceptional performing electrolytes with good cycling at room temperature. An interesting approach is to blend polymer in salt for higher cationic mobility and transport. While the ion concentration gradient was addressed by anchoring the anions to polymer chains and formalized as a single lithium ion conducting polymer electrolyte. However, these SLIC PEs possess lower conductivity despite transference number nearly unity. Mixing polymer electrolytes with inorganic entities are also studied by many researchers with goals to target properties such as decreasing crystallinity, increasing Lewis-acid based interactions and thermal stability. There are two methodologies for such materials, one is the copolymer of organic and inorganic chains such as PSx, POSS *etc*. and another is addition of inorganic fillers, either active

fillers (LLZO, LATP, NASICON) or passive fillers (Al_2O_3, SiO_2, $LiAlO_2$, TiO_2). They are indeed expected to improve the conductivity and exploit the synergy of polymer and ceramic particles.

A good compromise between the desired electrochemical properties superior to liquid electrolyte and mechanical properties of polymer electrolyte was attempted by adopting the use of gel polymer electrolytes. GPEs offer good wettability, ionic transport, higher flexibility with less leakage and other interesting advantages. They are either synthesized via soaking the polymer in an appropriate electrolyte solution or by in-situ polymerization with liquid electrolyte immobilized in the pores of the GP. There are sufficient reports on GPEs with the use of plasticizers, inorganic fillers in order to improve the mechanical strength for restricting dendrite growth and increased flexibility. They found their way ahead in the market for commercialization compared to dry SPE due to the intermediate characteristics between SPE and LE.

Further in this chapter, the discussion focuses on a specific class of monomers and polymers, i.e. CC and poly(hydroxyurethane), as of this thesis is concerned. Carbonate-based solvents are very entrancing for electrolytes due to their good solvation, high dielectric constant, tunable viscosity, evaporation temperature range and ability to form beneficial species in SEI. There are various pathways to synthesize CC with or without utilizing carbon dioxide via co-cyclization, electrochemical and transesterification. Sufficient reports have highlighted the crucial role of carbonate groups as main or side groups in improving the performance. While the polycarbonates from the CC monomer demonstrated good conductivity in their pristine as well in copolymers.

Another polymer, polyurethane, has gained much attention due to its tunable structure with presence of soft and hard segments. PU-based electrolytes show high conductivity and superior mechanical properties but demand alternatives due to their higher toxic footprints. Therefore, poly(hydroxyurethane)/non-isocyanate poly(urethane) research avoids the use of toxic catalysts by employing polyaddition of CCs with amines. These materials are proving to be a sustainable PU alternative for paints, coatings, adhesives and wearables. However, the novel idea developing PHUs using bio-derived monomers seems fascinating and has been hardly reported by any researchers for LB polymer electrolytes. Material development utilizing toxic chemicals and approaches is ambiguous to the environment friendly technology. Thus, more and more efforts towards bio-derived materials should be attempted in order to tackle these imbalances. And one such effort is the work performed in this thesis.

Bibliography

1. Gao, Z.; Sun, H.; Fu, L.; Ye, F.; Zhang, Y.; Luo, W.; Huang, Y., Promises, Challenges, and Recent Progress of Inorganic Solid-State Electrolytes for All-Solid-State Lithium Batteries. *Advanced materials (Deerfield Beach, Fla.)* **2018,** *30* (17), e1705702.
2. Bruce, P. G.; Freunberger, S. A.; Hardwick, L. J.; Tarascon, J.-M., Li–O2 and Li–S batteries with high energy storage. *Nature Materials* **2012,** *11* (1), 19-29.
3. Mauger, A.; Armand, M.; Julien, C. M.; Zaghib, K., Challenges and issues facing lithium metal for solid-state rechargeable batteries. *Journal of Power Sources* **2017,** *353*, 333-342.
4. Li, F.; Kitaura, H.; Zhou, H., The pursuit of rechargeable solid-state Li–air batteries. *Energy & Environmental Science* **2013,** *6* (8), 2302-2311.
5. Placke, T.; Kloepsch, R.; Dühnen, S.; Winter, M., Lithium ion, lithium metal, and alternative rechargeable battery technologies: the odyssey for high energy density. *Journal of Solid State Electrochemistry* **2017,** *21* (7), 1939-1964.
6. Chen, R.; Li, Q.; Yu, X.; Chen, L.; Li, H., Approaching Practically Accessible Solid-State Batteries: Stability Issues Related to Solid Electrolytes and Interfaces. *Chemical Reviews* **2020,** *120* (14), 6820-6877.
7. Wang, X.; Zhai, H.; Qie, B.; Cheng, Q.; Li, A.; Borovilas, J.; Xu, B.; Shi, C.; Jin, T.; Liao, X.; Li, Y.; He, X.; Du, S.; Fu, Y.; Dontigny, M.; Zaghib, K.; Yang, Y., Rechargeable solid-state lithium metal batteries with vertically aligned ceramic nanoparticle/polymer composite electrolyte. *Nano Energy* **2019,** *60*, 205-212.
8. Xu, H.; Chien, P.-H.; Shi, J.; Li, Y.; Wu, N.; Liu, Y.; Hu, Y.-Y.; Goodenough, J. B., High-performance all-solid-state batteries enabled by salt bonding to perovskite in poly(ethylene oxide). *Proceedings of the National Academy of Sciences* **2019,** *116* (38), 18815-18821.
9. Chen, W.; Yu, H.; Lee, S.-Y.; Wei, T.; Li, J.; Fan, Z., Nanocellulose: a promising nanomaterial for advanced electrochemical energy storage. *Chemical Society Reviews* **2018,** *47* (8), 2837-2872.
10. Li, Y.; Xu, B.; Xu, H.; Duan, H.; Lü, X.; Xin, S.; Zhou, W.; Xue, L.; Fu, G.; Manthiram, A.; Goodenough, J. B., Hybrid Polymer/Garnet Electrolyte with a Small Interfacial Resistance for Lithium-Ion Batteries. *Angewandte Chemie (International ed. in English)* **2017,** *56* (3), 753-756.
11. Zhao, Y.; Wu, C.; Peng, G.; Chen, X.; Yao, X.; Bai, Y.; Wu, F.; Chen, S.; Xu, X., A new solid polymer electrolyte incorporating Li10GeP2S12 into a polyethylene oxide matrix for all-solid-state lithium batteries. *Journal of Power Sources* **2016,** *301*, 47-53.
12. Yu, X.; Manthiram, A., A review of composite polymer-ceramic electrolytes for lithium batteries. *Energy Storage Materials* **2021,** *34*, 282-300.
13. Armand, M., Chabagno, J.M., and Duelot, M In *Polymer solid electrolytes*, Second International Meeting on Solid Electrolytes, St. Andrews, Scotland, St. Andrews, Scotland, 1978.
14. Fenton, D. E.; Parker, J. M.; Wright, P. V., Complexes of alkali metal ions with poly(ethylene oxide). *Polymer* **1973,** *14* (11), 589.
15. Wright, P. V., Electrical conductivity in ionic complexes of poly(ethylene oxide). *British Polymer Journal* **1975,** *7* (5), 319-327.
16. Feuillade, G.; Perche, P., Ion-conductive macromolecular gels and membranes for solid lithium cells. *Journal of Applied Electrochemistry* **1975,** *5* (1), 63-69.
17. Skaarup, S.; West, K.; Zachau-Christiansen, B., Mixed phase solid electrolytes. *Solid State Ionics* **1988,** *28-30*, 975-978.
18. Marcinek, M.; Syzdek, J.; Marczewski, M.; Piszcz, M.; Niedzicki, L.; Kalita, M.; Plewa-Marczewska, A.; Bitner, A.; Wieczorek, P.; Trzeciak, T.; Kasprzyk, M.; P.Łężak; Zukowska, Z.; Zalewska, A.; Wieczorek, W., Electrolytes for Li-ion transport – Review. *Solid State Ionics* **2015,** *276*, 107-126.
19. Dvorak, P., Solid electrolytes open doors to solid-state batteries. Windpower Engineering & Development: 2016; Vol. 2023.
20. Chang, Z.; Yang, H.; Zhu, X.; He, P.; Zhou, H., A stable quasi-solid electrolyte improves the safe operation of highly efficient lithium-metal pouch cells in harsh environments. *Nature Communications* **2022,** *13* (1), 1510.
21. Chen, X.; Xie, J.; Zhao, X.; Zhu, T., Electrochemical Compatibility of Solid-State Electrolytes with Cathodes and Anodes for All-Solid-State Lithium Batteries: A Review. *Advanced Energy and Sustainability Research* **2021,** *2* (5), 2000101.
22. Young, W.-S.; Kuan, W.-F.; Epps, I. I. I. T. H., Block copolymer electrolytes for rechargeable lithium batteries. *Journal of Polymer Science Part B: Polymer Physics* **2014,** *52* (1), 1-16.
23. Cohen, M. H.; Turnbull, D., Molecular Transport in Liquids and Glasses. *The Journal of Chemical Physics* **2004,** *31* (5), 1164-1169.

24. Gadjourova, Z.; Andreev, Y. G.; Tunstall, D. P.; Bruce, P. G., Ionic conductivity in crystalline polymer electrolytes. *Nature* **2001,** *412* (6846), 520-523.
25. Xue, Z.; He, D.; Xie, X., Poly(ethylene oxide)-based electrolytes for lithium-ion batteries. *Journal of Materials Chemistry A* **2015,** *3* (38), 19218-19253.
26. MacGlashan, G. S.; Andreev, Y. G.; Bruce, P. G., Structure of the polymer eleotrolyte poly(ethylene oxide)6:LiAsF6. *Nature* **1999,** *398* (6730), 792-794.
27. Zhang, C.; Staunton, E.; Andreev, Y. G.; Bruce, P. G., Raising the Conductivity of Crystalline Polymer Electrolytes by Aliovalent Doping. *Journal of the American Chemical Society* **2005,** *127* (51), 18305-18308.
28. Lilley, S. J.; Andreev, Y. G.; Bruce, P. G., Ionic Conductivity in Crystalline PEO6:Li(AsF6)1-x(SbF6)x. *Journal of the American Chemical Society* **2006,** *128* (37), 12036-12037.
29. Henderson, W. A.; Passerini, S., Ionic conductivity in crystalline–amorphous polymer electrolytes – P(EO)6:LiX phases. *Electrochemistry Communications* **2003,** *5* (7), 575-578.
30. Henderson, W. A.; Brooks, N. R.; Young, V. G., Single-Crystal Structures of Polymer Electrolytes. *Journal of the American Chemical Society* **2003,** *125* (40), 12098-12099.
31. Garca-Coln, L. S.; del Castillo, L. F.; Goldstein, P., Theoretical basis for the Vogel-Fulcher-Tammann equation. *Physical Review B* **1989,** *40* (10), 7040-7044.
32. Ratner, M. A.; Johansson, P.; Shriver, D. F., Polymer Electrolytes: Ionic Transport Mechanisms and Relaxation Coupling. *MRS Bulletin* **2000,** *25* (3), 31-37.
33. Quartarone, E.; Mustarelli, P., Electrolytes for solid-state lithium rechargeable batteries: recent advances and perspectives. *Chemical Society Reviews* **2011,** *40* (5), 2525-2540.
34. Agrawal, R. C.; Pandey, G. P., Solid polymer electrolytes: materials designing and all-solid-state battery applications: an overview. *Journal of Physics D: Applied Physics* **2008,** *41* (22), 223001.
35. Gibbs, J. H.; DiMarzio, E. A., Nature of the Glass Transition and the Glassy State. *The Journal of Chemical Physics* **2004,** *28* (3), 373-383.
36. Angell, C. A., Recent developments in fast ion transport in glassy and amorphous materials. *Solid State Ionics* **1986,** *18-19*, 72-88.
37. Wieczorek, W.; Such, K.; Wyciślik, H.; Płocharski, J., Modifications of crystalline structure of peo polymer electrolytes with ceramic additives. *Solid State Ionics* **1989,** *36* (3), 255-257.
38. Nan, C.-W.; Smith, D. M., A.c. electrical properties of composite solid electrolytes. *Materials Science and Engineering: B* **1991,** *10* (2), 99-106.
39. Williams, M. L.; Landel, R. F.; Ferry, J. D., The Temperature Dependence of Relaxation Mechanisms in Amorphous Polymers and Other Glass-forming Liquids. *Journal of the American Chemical Society* **1955,** *77* (14), 3701-3707.
40. Li, Y.; Zhang, L.; Sun, Z.; Gao, G.; Lu, S.; Zhu, M.; Zhang, Y.; Jia, Z.; Xiao, C.; Bu, H.; Xi, K.; Ding, S., Hexagonal boron nitride induces anion trapping in a polyethylene oxide based solid polymer electrolyte for lithium dendrite inhibition. *Journal of Materials Chemistry A* **2020,** *8* (19), 9579-9589.
41. Li, Z.; Huang, H.-M.; Zhu, J.-K.; Wu, J.-F.; Yang, H.; Wei, L.; Guo, X., Ionic Conduction in Composite Polymer Electrolytes: Case of PEO:Ga-LLZO Composites. *ACS Applied Materials & Interfaces* **2019,** *11* (1), 784-791.
42. Chen, S.; Wen, K.; Fan, J.; Bando, Y.; Golberg, D., Progress and future prospects of high-voltage and high-safety electrolytes in advanced lithium batteries: from liquid to solid electrolytes. *Journal of Materials Chemistry A* **2018,** *6* (25), 11631-11663.
43. Jia, M.; Khurram Tufail, M.; Guo, X., Insight into the key factors in high Li+ transference number composite electrolytes for solid lithium batteries. *ChemSusChem* **2023,** *16* (2), e202201801.
44. Rojaee, R.; Cavallo, S.; Mogurampelly, S.; Wheatle, B. K.; Yurkiv, V.; Deivanayagam, R.; Foroozan, T.; Rasul, M. G.; Sharifi-Asl, S.; Phakatkar, A. H., Highly-cyclable room-temperature phosphorene polymer electrolyte composites for Li metal batteries. *Advanced Functional Materials* **2020,** *30* (32), 1910749.
45. Chen, R.; Qu, W.; Guo, X.; Li, L.; Wu, F., The pursuit of solid-state electrolytes for lithium batteries: from comprehensive insight to emerging horizons. *Materials Horizons* **2016,** *3* (6), 487-516.
46. Takahashi, K.; Kurosaki, H.; Hashimoto, S.; Takenouchi, K.; Kamada, T.; Nakamura, H., 483 Efficacy of Radiofrequency Hyperthermia in Symptoms of Knee Osteoarthritis. *Osteoarthritis and Cartilage* **2011,** *19*, S224-S225.
47. Wu, N.; Chien, P. H.; Qian, Y.; Li, Y.; Xu, H.; Grundish, N. S.; Xu, B.; Jin, H.; Hu, Y. Y.; Yu, G., Enhanced surface interactions enable fast Li+ conduction in oxide/polymer composite electrolyte. *Angewandte Chemie International Edition* **2020,** *59* (10), 4131-4137.

48. Chen, L.; Li, Y.; Li, S.-P.; Fan, L.-Z.; Nan, C.-W.; Goodenough, J. B., PEO/garnet composite electrolytes for solid-state lithium batteries: From "ceramic-in-polymer" to "polymer-in-ceramic". *Nano Energy* **2018,** *46*, 176-184.
49. Zaman, W.; Hortance, N.; Dixit, M. B.; De Andrade, V.; Hatzell, K. B., Visualizing percolation and ion transport in hybrid solid electrolytes for Li–metal batteries. *Journal of Materials Chemistry A* **2019,** *7* (41), 23914-23921.
50. Chen, L.; Venkatram, S.; Kim, C.; Batra, R.; Chandrasekaran, A.; Ramprasad, R., Electrochemical stability window of polymeric electrolytes. *Chemistry of Materials* **2019,** *31* (12), 4598-4604.
51. Tang, S.; Lan, Q.; Xu, L.; Liang, J.; Lou, P.; Liu, C.; Mai, L.; Cao, Y.-C.; Cheng, S., A novel cross-linked nanocomposite solid-state electrolyte with super flexibility and performance for lithium metal battery. *Nano Energy* **2020,** *71*, 104600.
52. Shi, Y.; Chen, Y.; Liang, Y.; Andrews, J.; Dong, H.; Yuan, M.; Ding, W.; Banerjee, S.; Ardebili, H.; Robertson, M. L.; Cui, X.; Yao, Y., Chemically inert covalently networked triazole-based solid polymer electrolytes for stable all-solid-state lithium batteries. *Journal of Materials Chemistry A* **2019,** *7* (34), 19691-19695.
53. Wang, Q.; Liu, X.; Cui, Z.; Shangguan, X.; Zhang, H.; Zhang, J.; Tang, K.; Li, L.; Zhou, X.; Cui, G., A fluorinated polycarbonate based all solid state polymer electrolyte for lithium metal batteries. *Electrochimica Acta* **2020,** *337*, 135843.
54. Monroe, C.; Newman, J., The impact of elastic deformation on deposition kinetics at lithium/polymer interfaces. *Journal of The Electrochemical Society* **2005,** *152* (2), A396.
55. Barai, P.; Higa, K.; Srinivasan, V., Effect of initial state of lithium on the propensity for dendrite formation: a theoretical study. *Journal of The Electrochemical Society* **2016,** *164* (2), A180.
56. Glynos, E.; Petropoulou, P.; Mygiakis, E.; Nega, A. D.; Pan, W.; Papoutsakis, L.; Giannelis, E. P.; Sakellariou, G.; Anastasiadis, S. H., Leveraging molecular architecture to design new, all-polymer solid electrolytes with simultaneous enhancement in modulus and ionic conductivity. *Macromolecules* **2018,** *51* (7), 2542-2550.
57. Khurana, R.; Schaefer, J. L.; Archer, L. A.; Coates, G. W., Suppression of lithium dendrite growth using cross-linked polyethylene/poly (ethylene oxide) electrolytes: a new approach for practical lithium-metal polymer batteries. *Journal of the American Chemical Society* **2014,** *136* (20), 7395-7402.
58. Hu, J.; He, P.; Zhang, B.; Wang, B.; Fan, L.-Z., Porous film host-derived 3D composite polymer electrolyte for high-voltage solid state lithium batteries. *Energy Storage Materials* **2020,** *26*, 283-289.
59. Ramesh, S.; Ng, H. M., An investigation on PAN–PVC–LiTFSI based polymer electrolytes system. *Solid State Ionics* **2011,** *192* (1), 2-5.
60. Tian, Z.; Kim, D., Solid electrolyte membranes prepared from poly(arylene ether sulfone)-g-poly(ethylene glycol) with various functional end groups for lithium-ion battery. *Journal of Membrane Science* **2021,** *621*, 119023.
61. Li, B.; Su, Q.; Yu, L.; Wang, D.; Ding, S.; Zhang, M.; Du, G.; Xu, B., Li0.35La0.55TiO3 Nanofibers Enhanced Poly(vinylidene fluoride)-Based Composite Polymer Electrolytes for All-Solid-State Batteries. *ACS Applied Materials & Interfaces* **2019,** *11* (45), 42206-42213.
62. Ahmad, S., RETRACTED ARTICLE: Polymer electrolytes: characteristics and peculiarities. *Ionics* **2009,** *15* (3), 309-321.
63. Choudhary, S.; Sengwa, R. J., Effect of different anions of lithium salt and MMT nanofiller on ion conduction in melt-compounded PEO–LiX–MMT electrolytes. *Ionics* **2012,** *18* (4), 379-384.
64. Tominaga, Y.; Mizumo, T.; Ohno, H., Ionic conductivity of PPO-sulfonamide salt hybrids and their network polymers. *Polymers for Advanced Technologies* **2000,** *11* (8-12), 524-528.
65. Vachon, C.; Labreche, C.; Vallee, A.; Besner, S.; Dumont, M.; Prud'homme, J., Microphase Separation and Conductivity Behavior of Poly(propylene oxide)-Lithium Salt Electrolytes. *Macromolecules* **1995,** *28* (16), 5585-5594.
66. Andersson, D.; Carlsson, P.; Engberg, D.; Torell, L. M.; Börjesson, L.; McGreevy, R. L.; Howells, W. S., Modelling of segmental dynamics in polymer electrolyte PPO-LiClO4, by surface fitting of quasi-elastic neutron scattering data. *Physica B: Condensed Matter* **1999,** *266* (1), 126-130.
67. Blonsky, P. M.; Shriver, D. F.; Austin, P.; Allcock, H. R., Complex formation and ionic conductivity of polyphosphazene solid electrolytes. *Solid State Ionics* **1986,** *18-19*, 258-264.
68. Paulsdorf, J.; Burjanadze, M.; Hagelschur, K.; Wiemhöfer, H. D., Ionic conductivity in polyphosphazene polymer electrolytes prepared by the living cationic polymerization. *Solid State Ionics* **2004,** *169* (1), 25-33.
69. Luther, T. A.; Stewart, F. F.; Budzien, J. L.; LaViolette, R. A.; Bauer, W. F.; Harrup, M. K.; Allen, C. W.; Elayan, A., On the Mechanism of Ion Transport through Polyphosphazene Solid

Polymer Electrolytes: NMR, IR, and Raman Spectroscopic Studies and Computational Analysis of 15N-Labeled Polyphosphazenes. *The Journal of Physical Chemistry B* **2003,** *107* (14), 3168-3176.
70. Karatas, Y.; Banhatti, R. D.; Kaskhedikar, N.; Burjanadze, M.; Funke, K.; Wiemhöfer, H.-D., Synthesis and Modeling of Polysiloxane-Based Salt-in-Polymer Electrolytes with Various Additives. *The Journal of Physical Chemistry B* **2009,** *113* (47), 15473-15484.
71. Snyder, J. F.; Ratner, M. A.; Shriver, D. F., Ion conductivity of comb polysiloxane polyelectrolytes containing oligoether and perfluoroether sidechains. *Journal of the Electrochemical Society* **2003,** *150* (8), A1090-A1094.
72. Hooper, R.; Lyons, L.; Mapes, M.; Schumacher, D.; Moline, D.; West, R., Highly Conductive Siloxane Polymers. *Macromolecules* **2001,** *34*, 931-936.
73. Sengwa, R. J.; Dhatarwal, P.; Choudhary, S., Role of preparation methods on the structural and dielectric properties of plasticized polymer blend electrolytes: Correlation between ionic conductivity and dielectric parameters. *Electrochimica Acta* **2014,** *142*, 359-370.
74. Murakami, S.; Ueda, K.; Kitade, T.; Ikeda, Y.; Kohjiya, S., Control on the structure of poly(oxyethylene) with tri(oxyethylene) side chains for a polymer solid electrolyte. *Solid State Ionics* **2002,** *154-155*, 399-406.
75. Jannasch, P., Synthesis of Novel Aggregating Comb-Shaped Polyethers for Use as Polymer Electrolytes. *Macromolecules* **2000,** *33* (23), 8604-8610.
76. Long, L.; Wang, S.; Xiao, M.; Meng, Y., Polymer electrolytes for lithium polymer batteries. *Journal of Materials Chemistry A* **2016,** *4* (26), 10038-10069.
77. Moreno, M.; Quijada, R.; Santa Ana, M. A.; Benavente, E.; Gomez-Romero, P.; González, G., Electrical and mechanical properties of poly (ethylene oxide)/intercalated clay polymer electrolyte. *Electrochimica Acta* **2011,** *58*, 112-118.
78. Kumar, M.; Sekhon, S. S., Role of plasticizer's dielectric constant on conductivity modification of PEO–NH4F polymer electrolytes. *European Polymer Journal* **2002,** *38* (7), 1297-1304.
79. Bruce, P. G., Structure and electrochemistry of polymer electrolytes. *Electrochimica Acta* **1995,** *40* (13), 2077-2085.
80. Ito, Y.; Kanehori, K.; Miyauchi, K.; Kudo, T., Ionic conductivity of electrolytes formed from PEO-LiCF3SO3 complex low molecular weight poly(ethylene glycol). *Journal of Materials Science* **1987,** *22*, 1845-1849.
81. Liu, B.; Huang, Y.; Cao, H.; Zhao, L.; Huang, Y.; Song, A.; Lin, Y.; Li, X.; Wang, M., A novel porous gel polymer electrolyte based on poly(acrylonitrile-polyhedral oligomeric silsesquioxane) with high performances for lithium-ion batteries. *Journal of Membrane Science* **2018,** *545*, 140-149.
82. Shukla, N.; Thakur, A. K., Role of salt concentration on conductivity optimization and structural phase separation in a solid polymer electrolyte based on PMMA-LiClO4. *Ionics* **2009,** *15* (3), 357-367.
83. Ramesh, S.; Winie, T.; Arof, A. K., Investigation of mechanical properties of polyvinyl chloride–polyethylene oxide (PVC–PEO) based polymer electrolytes for lithium polymer cells. *European Polymer Journal* **2007,** *43* (5), 1963-1968.
84. Zhang, X.; Han, J.; Niu, X.; Xin, C.; Xue, C.; Wang, S.; Shen, Y.; Zhang, L.; Li, L.; Nan, C.-W., High Cycling Stability for Solid-State Li Metal Batteries via Regulating Solvation Effect in Poly(Vinylidene Fluoride)-Based Electrolytes. *Batteries & Supercaps* **2020,** *3* (9), 876-883.
85. Zhao, Y.; Bai, Y.; Li, W.; An, M.; Bai, Y.; Chen, G., Design Strategies for Polymer Electrolytes with Ether and Carbonate Groups for Solid-State Lithium Metal Batteries. *Chemistry of Materials* **2020,** *32* (16), 6811-6830.
86. Zhang, J.; Yang, J.; Dong, T.; Zhang, M.; Chai, J.; Dong, S.; Wu, T.; Zhou, X.; Cui, G., Aliphatic Polycarbonate-Based Solid-State Polymer Electrolytes for Advanced Lithium Batteries: Advances and Perspective. *Small* **2018,** *14* (36), 1800821.
87. Wu, I. D.; Chang, F.-C., Determination of the interaction within polyester-based solid polymer electrolyte using FTIR spectroscopy. *Polymer* **2007,** *48* (4), 989-996.
88. Watanabe, M.; Hirakimoto, T.; Mutoh, S.; Nishimoto, A., Polymer electrolytes derived from dendritic polyether macromonomers. *Solid State Ionics* **2002,** *148* (3), 399-404.
89. Porcarelli, L.; Gerbaldi, C.; Bella, F.; Nair, J. R., Super Soft All-Ethylene Oxide Polymer Electrolyte for Safe All-Solid Lithium Batteries. *Scientific Reports* **2016,** *6*.
90. Devaux, D.; Glé, D.; Phan, T. N. T.; Gigmes, D.; Giroud, E.; Deschamps, M.; Denoyel, R.; Bouchet, R., Optimization of Block Copolymer Electrolytes for Lithium Metal Batteries. *Chemistry of Materials* **2015,** *27* (13), 4682-4692.
91. Fan, L. Z.; Hu, Y. S.; Bhattacharyya, A. J.; Maier, J., Succinonitrile as a Versatile Additive for Polymer Electrolytes. *Advanced Functional Materials* **2007,** *17* (15), 2800-2807.

92. An, S. Y.; Jeong, I. C.; Won, M.-S.; Jeong, E. D.; Shim, Y.-B., Effect of additives in PEO/PAA/PMAA composite solid polymer electrolytes on the ionic conductivity and Li ion battery performance. *Journal of Applied Electrochemistry* **2009,** *39* (9), 1573-1578.
93. Angell, C.; Liu, C.; Sanchez, E., Rubbery solid electrolytes with dominant cationic transport and high ambient conductivity. *Nature* **1993,** *362* (6416), 137-139.
94. Angell, C. A.; Xu, K.; Zhang, S. S.; Videa, M., Variations on the salt-polymer electrolyte theme for flexible solid electrolytes. *Solid State Ionics* **1996,** *86-88*, 17-28.
95. Zygadło-Monikowska, E.; Florjańczyk, Z.; Kubisa, P.; Biedroń, T.; Tomaszewska, A.; Ostrowska, J.; Langwald, N., Mixture of LiBF4 and lithium difluoro(oxalato)borate for application as a new electrolyte for lithium-ion batteries. *Journal of Power Sources* **2010,** *195* (18), 6202-6206.
96. Fan, J.; Angell, C. A., The preparation, conductivity, viscosity and mechanical properties of polymer electrolytes and new hybrid ionic rubber electrolytes. *Electrochimica Acta* **1995,** *40* (13), 2397-2400.
97. Łasińska, A. K.; Marzantowicz, M.; Dygas, J. R.; Krok, F.; Florjańczyk, Z.; Tomaszewska, A.; Zygadło-Monikowska, E.; Żukowska, Z.; Lafont, U., Study of ageing effects in polymer-in-salt electrolytes based on poly(acrylonitrile-co-butyl acrylate) and lithium salts. *Electrochimica Acta* **2015,** *169*, 61-72.
98. Zhao, Y.; Bai, Y.; Bai, Y.; An, M.; Chen, G.; Li, W.; Li, C.; Zhou, Y., A rational design of solid polymer electrolyte with high salt concentration for lithium battery. *Journal of Power Sources* **2018,** *407*, 23-30.
99. Mishra, R.; Baskaran, N.; Ramakrishnan, P.; Rao, K., Lithium ion conduction in extreme polymer in salt regime. *Solid State Ionics* **1998,** *112* (3-4), 261-273.
100. Kao, H.-M.; Chao, S.-W.; Chang, P.-C., Multinuclear Solid-State NMR, Self-Diffusion Coefficients, Differential Scanning Calorimetry, and Ionic Conductivity of Solid Organic− Inorganic Hybrid Electrolytes Based on PPG− PEG− PPG Diamine, Siloxane, and Lithium Perchlorate. *Macromolecules* **2006,** *39* (3), 1029-1040.
101. Forsyth, M.; Jiazeng, S.; Macfarlane, D. R., Novel high salt content polymer electrolytes based on high Tg polymers. *Electrochimica Acta* **2000,** *45* (8-9), 1249-1254.
102. Bushkova, O. V.; Zhukovsky, V. M.; Lirova, B. I.; Kruglyashov, A. L., Fast ionic transport in solid polymer electrolytes based on acrylonitrile copolymers. *Solid State Ionics* **1999,** *119* (1), 217-222.
103. Zhang, H.; Li, C.; Piszcz, M.; Coya, E.; Rojo, T.; Rodriguez-Martinez, L. M.; Armand, M.; Zhou, Z., Single lithium-ion conducting solid polymer electrolytes: advances and perspectives. *Chemical Society Reviews* **2017,** *46* (3), 797-815.
104. Cui, W.-W.; Tang, D.-Y., Electrospun poly(lithium 2-acrylamido-2-methylpropanesulfonic acid) fiber-based polymer electrolytes for lithium-ion batteries. *Journal of Applied Polymer Science* **2012,** *126* (2), 510-518.
105. Meziane, R.; Bonnet, J.-P.; Courty, M.; Djellab, K.; Armand, M., Single-ion polymer electrolytes based on a delocalized polyanion for lithium batteries. *Electrochimica Acta - ELECTROCHIM ACTA* **2011,** *57*.
106. Heishi, M.; Niwa, H.; Uno, T.; Kubo, M.; Itoh, T., Polymer electrolytes based on polyanionic lithium salts. *Electrochimica Acta* **2013,** *114*, 54-59.
107. Itoh, T.; Mitsuda, Y.; Ebina, T.; Uno, T.; Kubo, M., Solid polymer electrolytes composed of polyanionic lithium salts and polyethers. *Journal of Power Sources* **2009,** *189* (1), 531-535.
108. Shi, Q.; Xue, L.; Qin, D.; Du, B.; Wang, J.; Chen, L., Single ion solid-state composite electrolytes with high electrochemical stability based on a poly(perfluoroalkylsulfonyl)-imide ionene polymer. *Journal of Materials Chemistry A* **2014,** *2* (38), 15952-15957.
109. Watanabe, M.; Tokuda, H.; Muto, S., Anionic effect on ion transport properties in network polyether electrolytes. *Electrochimica Acta* **2001,** *46* (10), 1487-1491.
110. Rolland, J.; Poggi, E.; Vlad, A.; Gohy, J.-F., Single-ion diblock copolymers for solid-state polymer electrolytes. *Polymer* **2015,** *68*, 344-352.
111. Bouchet, R.; Maria, S.; Meziane, R.; Aboulaich, A.; Lienafa, L.; Bonnet, J.-P.; Phan, T. N. T.; Bertin, D.; Gigmes, D.; Devaux, D.; Denoyel, R.; Armand, M., Single-ion BAB triblock copolymers as highly efficient electrolytes for lithium-metal batteries. *Nature materials* **2013,** *12* (5), 452-457.
112. Porcarelli, L.; Aboudzadeh, M. A.; Rubatat, L.; Nair, J. R.; Shaplov, A. S.; Gerbaldi, C.; Mecerreyes, D., Single-ion triblock copolymer electrolytes based on poly(ethylene oxide) and methacrylic sulfonamide blocks for lithium metal batteries. *Journal of Power Sources* **2017,** *364*, 191-199.
113. Nishihara, Y.; Miyazaki, M.; Tomita, Y.; Kadono, Y.; Takagi, K., Synthesis and ion conductive characteristics of inorganic–organic hybrid polymers bearing a tetraarylpentaborate unit. *Journal of Polymer Science Part A: Polymer Chemistry* **2008,** *46* (23), 7913-7918.

114. Liang, S.; Chen, Q.; Choi, U. H.; Bartels, J.; Bao, N.; Runt, J.; Colby, R. H., Plasticizing Li single-ion conductors with low-volatility siloxane copolymers and oligomers containing ethylene oxide and cyclic carbonates. *Journal of Materials Chemistry A* **2015,** *3* (42), 21269-21276.
115. Cao, P.-F.; Wojnarowska, Z.; Hong, T.; Carroll, B.; Li, B.; Feng, H.; Parsons, L.; Wang, W.; Lokitz, B. S.; Cheng, S.; Bocharova, V.; Sokolov, A. P.; Saito, T., A star-shaped single lithium-ion conducting copolymer by grafting a POSS nanoparticle. *Polymer* **2017,** *124*, 117-127.
116. Mehta, M. A.; Fujinami, T.; Inoue, S.; Matsushita, K.; Miwa, T.; Inoue, T., The use of boroxine rings for the development of high performance polymer electrolytes. *Electrochimica acta* **2000,** *45* (8-9), 1175-1180.
117. Mehta, M. A.; Fujinami, T., Novel inorganic–organic polymer electrolytes – preparation and properties. *Solid State Ionics* **1998,** *113-115*, 187-192.
118. Blazejczyk, A.; Wieczorek, W.; Kovarsky, R.; Golodnitsky, D.; Peled, E.; Scanlon, L. G., Novel Solid Polymer Electrolytes with Single Lithium-Ion Transport. *Journal of The Electrochemical Society* **2004,** *151*, A1762.
119. Blazejczyk, A.; Szczupak, M.; Wieczorek, W.; Cmoch, P.; Appetecchi, G. B.; Scrosati, B.; Kovarsky, R.; Golodnitsky, D.; Peled, E., Anion-Binding Calixarene Receptors: Synthesis, Microstructure, and Effect on Properties of Polyether Electrolytes. *Chemistry of Materials* **2005,** *17* (6), 1535-1547.
120. Barthel, J.; Buestrich, R.; Gores, H. J.; Schmidt, M.; Wühr, M., A New Class of Electrochemically and Thermally Stable Lithium Salts for Lithium Battery Electrolytes: IV. Investigations of the Electrochemical Oxidation of Lithium Organoborates. *Journal of The Electrochemical Society* **1997,** *144* (11), 3866.
121. Wang, F.; Lu, X.; He, C., Some recent developments of polyhedral oligomeric silsesquioxane (POSS)-based polymeric materials. *Journal of Materials Chemistry* **2011,** *21* (9), 2775-2782.
122. Shim, J.; Kim, D.-G.; Lee, J. H.; Baik, J. H.; Lee, J.-C., Synthesis and properties of organic/inorganic hybrid branched-graft copolymers and their application to solid-state electrolytes for high-temperature lithium-ion batteries. *Polymer Chemistry* **2014,** *5* (10), 3432-3442.
123. Shim, J.; Kim, D.-G.; Kim, H. J.; Lee, J. H.; Baik, J.-H.; Lee, J.-C., Novel composite polymer electrolytes containing poly(ethylene glycol)-grafted graphene oxide for all-solid-state lithium-ion battery applications. *Journal of Materials Chemistry A* **2014,** *2* (34), 13873-13883.
124. Kim, D.-G.; Shim, J.; Lee, J. H.; Kwon, S.-J.; Baik, J.-H.; Lee, J.-C., Preparation of solid-state composite electrolytes based on organic/inorganic hybrid star-shaped polymer and PEG-functionalized POSS for all-solid-state lithium battery applications. *Polymer* **2013,** *54* (21), 5812-5820.
125. Kim, D.-G.; Sohn, H.-S.; Kim, S.-K.; Lee, A.; Lee, J.-C., Star-shaped polymers having side chain poss groups for solid polymer electrolytes; synthesis, thermal behavior, dimensional stability, and ionic conductivity. *Journal of Polymer Science Part A: Polymer Chemistry* **2012,** *50* (17), 3618-3627.
126. Li, J.; Lin, Y.; Yao, H.; Yuan, C.; Liu, J., Tuning Thin-Film Electrolyte for Lithium Battery by Grafting Cyclic Carbonate and Combed Poly(ethylene oxide) on Polysiloxane. *ChemSusChem* **2014,** *7* (7), 1901-1908.
127. Cznotka, E.; Jeschke, S.; Vettikuzha, P.; Wiemhöfer, H.-D., Semi-interpenetrating polymer network of poly(methyl methacrylate) and ether-modified polysiloxane. *Solid State Ionics* **2015,** *274*, 55-63.
128. Weston, J. E.; Steele, B. C. H., Effects of inert fillers on the mechanical and electrochemical properties of lithium salt-poly(ethylene oxide) polymer electrolytes. *Solid State Ionics* **1982,** *7* (1), 75-79.
129. Croce, F.; Appetecchi, G. B.; Persi, L.; Scrosati, B., Nanocomposite polymer electrolytes for lithium batteries. *Nature* **1998,** *394* (6692), 456-458.
130. Kwon, S. J.; Jung, B. M.; Kim, T.; Byun, J.; Lee, J.; Lee, S. B.; Choi, U. H., Influence of Al2O3 nanowires on ion transport in nanocomposite solid polymer electrolytes. *Macromolecules* **2018,** *51* (24), 10194-10201.
131. Pradeepa, P.; Sowmya, G.; Edwinraj, S.; Fareetha Begum, G.; Ramesh Prabhu, M., Influence of Al2O3 on the structure and electrochemical properties of PVAc / PMMA based blend composite polymer electrolytes. *Materials Today: Proceedings* **2016,** *3* (6), 2187-2196.
132. Xu, Z.; Yang, T.; Chu, X.; Su, H.; Wang, Z.; Chen, N.; Gu, B.; Zhang, H.; Deng, W.; Zhang, H.; Yang, W., Strong Lewis Acid–Base and Weak Hydrogen Bond Synergistically Enhancing Ionic Conductivity of Poly(ethylene oxide)@SiO2 Electrolytes for a High Rate Capability Li-Metal Battery. *ACS Applied Materials & Interfaces* **2020,** *12* (9), 10341-10349.
133. Zhu, Y.; Cao, J.; Chen, H.; Yu, Q.; Li, B., High electrochemical stability of a 3D cross-linked network PEO@ nano-SiO 2 composite polymer electrolyte for lithium metal batteries. *Journal of Materials Chemistry A* **2019,** *7* (12), 6832-6839.

134. Zhou, D.; Liu, R.; He, Y.-B.; Li, F.; Liu, M.; Li, B.; Yang, Q.-H.; Cai, Q.; Kang, F., SiO2 Hollow Nanosphere-Based Composite Solid Electrolyte for Lithium Metal Batteries to Suppress Lithium Dendrite Growth and Enhance Cycle Life. *Advanced Energy Materials* **2016,** *6* (7), 1502214.
135. Ketabi, S.; Lian, K., The effects of SiO2 and TiO2 nanofillers on structural and electrochemical properties of poly(ethylene oxide)–EMIHSO4 electrolytes. *Electrochimica Acta* **2015,** *154*, 404-412.
136. Liu, W.; Lin, D.; Sun, J.; Zhou, G.; Cui, Y., Improved lithium ionic conductivity in composite polymer electrolytes with oxide-ion conducting nanowires. *ACS nano* **2016,** *10* (12), 11407-11413.
137. Mastragostino, M.; Soavi, F.; Zanelli, A., Improved composite materials for rechargeable lithium metal polymer batteries. *Journal of power sources* **1999,** *81*, 729-733.
138. Shanmukaraj, D.; Wang, G. X.; Murugan, R.; Liu, H. K., Ionic conductivity and electrochemical stability of poly(methylmethacrylate)–poly(ethylene oxide) blend-ceramic fillers composites. *Journal of Physics and Chemistry of Solids* **2008,** *69* (1), 243-248.
139. Sun, H.; Takeda, Y.; Imanishi, N.; Yamamoto, O.; Sohn, H. J., Ferroelectric materials as a ceramic filler in solid composite polyethylene oxide-based electrolytes. *Journal of The Electrochemical Society* **2000,** *147* (7), 2462.
140. Zeng, S.; Reyes, C.; Liu, J.; Rodgers, P. A.; Wentworth, S. H.; Sun, L., Facile hydroxylation of halloysite nanotubes for epoxy nanocomposite applications. *Polymer* **2014,** *55* (25), 6519-6528.
141. Pongsuk, P.; Pumchusak, J., Effects of Halloysite Nanotubes on Ionic Conductivity, Morphology, Crystallinity and Mechanical Properties of PEO-based Solid Polymer Electrolyte. *Materials Today: Proceedings* **2019,** *17*, 1956-1963.
142. Wang, W.; Dong, W.; Tian, G.; Sun, L.; Wang, Q.; Hui, A.; Mu, B.; Wang, A., Highly efficient self-template synthesis of porous silica nanorods from natural palygorskite. *Powder Technology* **2019,** *354*, 1-10.
143. Xu, J.; Wang, W.; Wang, A., Effect of squeeze, homogenization, and freezing treatments on particle diameter and rheological properties of palygorskite. *Advanced Powder Technology* **2014,** *25* (3), 968-977.
144. Tang, W.; Tang, S.; Zhang, C.; Ma, Q.; Xiang, Q.; Yang, Y.-W.; Luo, J., Simultaneously Enhancing the Thermal Stability, Mechanical Modulus, and Electrochemical Performance of Solid Polymer Electrolytes by Incorporating 2D Sheets. *Advanced Energy Materials* **2018,** *8* (24), 1800866.
145. Tang, W.; Tang, S.; Guan, X.; Zhang, X.; Xiang, Q.; Luo, J., High-Performance Solid Polymer Electrolytes Filled with Vertically Aligned 2D Materials. *Advanced Functional Materials* **2019,** *29* (16), 1900648.
146. Hu, J.; Wang, W.; Zhu, X.; Liu, S.; Wang, Y.; Xu, Y.; Zhou, S.; He, X.; Xue, Z., Composite polymer electrolytes reinforced by hollow silica nanotubes for lithium metal batteries. *Journal of Membrane Science* **2021,** *618*, 118697.
147. Chen, W.; Xiong, X.; Zeng, R.; Jiang, L.; Chen, Z.; Xiao, Z.; Qie, L.; Yu, F.; Huang, Y., Enhancing the Interfacial Ionic Transport via in Situ 3D Composite Polymer Electrolytes for Solid-State Lithium Batteries. *ACS Applied Energy Materials* **2020,** *3* (7), 7200-7207.
148. Zhang, Y.; Wang, X.; Feng, W.; Zhen, Y.; Zhao, P.; Li, L.; Cai, Z., The effects of the size and content of BaTiO 3 nanoparticles on solid polymer electrolytes for all-solid-state lithium-ion batteries. *Journal of Solid State Electrochemistry* **2019,** *23*, 749-758.
149. Zhang, Y.; Zhao, Y.; Gosselink, D.; Chen, P., Synthesis of poly (ethylene-oxide)/nanoclay solid polymer electrolyte for all solid-state lithium/sulfur battery. *Ionics* **2015,** *21*, 381-385.
150. Chen, L.; Li, W.; Fan, L.-Z.; Nan, C.-W.; Zhang, Q., Intercalated Electrolyte with High Transference Number for Dendrite-Free Solid-State Lithium Batteries. *Advanced Functional Materials* **2019,** *29* (28), 1901047.
151. Fan, R.; Liu, C.; He, K.; Ho-Sum Cheng, S.; Chen, D.; Liao, C.; Li, R. K. Y.; Tang, J.; Lu, Z., Versatile Strategy for Realizing Flexible Room-Temperature All-Solid-State Battery through a Synergistic Combination of Salt Affluent PEO and Li6.75La3Zr1.75Ta0.25O12 Nanofibers. *ACS Applied Materials & Interfaces* **2020,** *12* (6), 7222-7231.
152. Li, L.; Deng, Y.; Chen, G., Status and prospect of garnet/polymer solid composite electrolytes for all-solid-state lithium batteries. *Journal of Energy Chemistry* **2020,** *50*, 154-177.
153. Xu, H.; Chien, P.-H.; Shi, J.; Li, Y.; Wu, N.; Liu, Y.; Hu, Y.-Y.; Goodenough, J. B., High-performance all-solid-state batteries enabled by salt bonding to perovskite in poly(ethylene oxide). **2019,** *116* (38), 18815-18821.
154. Bae, J.; Li, Y.; Zhang, J.; Zhou, X.; Zhao, F.; Shi, Y.; Goodenough, J. B.; Yu, G., A 3D Nanostructured Hydrogel-Framework-Derived High-Performance Composite Polymer Lithium-Ion Electrolyte. *Angewandte Chemie (International ed. in English)* **2018,** *57* (8), 2096-2100.

155. Wang, X.; Zhai, H.; Qie, B.; Cheng, Q.; Li, A.; Borovilas, J.; Xu, B.; Shi, C.; Jin, T.; Liao, X., Rechargeable solid-state lithium metal batteries with vertically aligned ceramic nanoparticle/polymer composite electrolyte. *Nano Energy* **2019,** *60*, 205-212.
156. Yu, X.; Manthiram, A., A long cycle life, all-solid-state lithium battery with a ceramic–polymer composite electrolyte. *ACS Applied Energy Materials* **2020,** *3* (3), 2916-2924.
157. Zhou, D.; Shanmukaraj, D.; Tkacheva, A.; Armand, M.; Wang, G., Polymer Electrolytes for Lithium-Based Batteries: Advances and Prospects. *Chem* **2019,** *5* (9), 2326-2352.
158. Cheng, X.; Pan, J.; Zhao, Y.; Liao, M.; Peng, H., Gel Polymer Electrolytes for Electrochemical Energy Storage. *Advanced Energy Materials* **2018,** *8* (7), 1702184.
159. Wang, X.; Gong, C.; He, D.; Xue, Z.; Chen, C.; Liao, Y.; Xie, X., Gelled microporous polymer electrolyte with low liquid leakage for lithium-ion batteries. *Journal of Membrane Science* **2014,** *454*, 298-304.
160. Li, G.; Li, Z.; Zhang, P.; Zhang, H.; Wu, Y., Research on a gel polymer electrolyte for Li-ion batteries. *Pure Applied Chemistry* **2008,** *80* (11), 2553-2563.
161. Baskakova, Y. V.; Ol'ga, V. Y.; Efimov, O. N., Polymer gel electrolytes for lithium batteries. *Russian Chemical Reviews* **2012,** *81* (4), 367.
162. Stephan, A. M., Review on gel polymer electrolytes for lithium batteries. *European polymer journal* **2006,** *42* (1), 21-42.
163. Song, J. Y.; Wang, Y. Y.; Wan, C. C., Review of gel-type polymer electrolytes for lithium-ion batteries. *Journal of Power Sources* **1999,** *77* (2), 183-197.
164. Kim, H.; Choi, G.; Moon, S.; Kim, S., Electrochemical properties of Li ion polymer battery with gel polymer electrolyte based on polyurethane. *Journal of applied electrochemistry* **2003,** *33*, 491-496.
165. Ha, H.-J.; Kil, E.-H.; Kwon, Y. H.; Kim, J. Y.; Lee, C. K.; Lee, S.-Y., UV-curable semi-interpenetrating polymer network-integrated, highly bendable plastic crystal composite electrolytes for shape-conformable all-solid-state lithium ion batteries. *Energy & Environmental Science* **2012,** *5* (4), 6491-6499.
166. Li, H.; Ma, X.-T.; Shi, J.-L.; Yao, Z.-K.; Zhu, B.-K.; Zhu, L.-P., Preparation and properties of poly(ethylene oxide) gel filled polypropylene separators and their corresponding gel polymer electrolytes for Li-ion batteries. *Electrochimica Acta* **2011,** *56* (6), 2641-2647.
167. Rao, M. M.; Liu, J. S.; Li, W. S.; Liang, Y.; Zhou, D. Y., Preparation and performance analysis of PE-supported P(AN-co-MMA) gel polymer electrolyte for lithium ion battery application. *Journal of Membrane Science* **2008,** *322* (2), 314-319.
168. Kim, H.-S.; Shin, J.-H.; Moon, S.-I.; Yun, M.-S., Electrochemical properties of poly (tetra ethylene glycol diacrylate)-based gel electrolytes for lithium-ion polymer batteries. *Journal of power sources* **2003,** *119*, 482-486.
169. Kim, H.-S.; Moon, S.-I., Synthesis and electrochemical performances of di (trimethylolpropane) tetraacrylate-based gel polymer electrolyte. *Journal of power sources* **2005,** *146* (1-2), 584-588.
170. Zhang, J.; Sun, B.; Huang, X.; Chen, S.; Wang, G., Honeycomb-like porous gel polymer electrolyte membrane for lithium ion batteries with enhanced safety. *Scientific Reports* **2014,** *4*.
171. Zhu, Y.; Xiao, S.; Shi, Y.; Yang, Y.; Hou, Y.; Wu, Y., A Composite Gel Polymer Electrolyte with High Performance Based on Poly(Vinylidene Fluoride) and Polyborate for Lithium Ion Batteries. *Advanced Energy Materials* **2014,** *4* (1), 1300647.
172. Zhang, H.; Zhang, P.; Li, G.; Wu, Y.; Sun, D., A porous poly (vinylidene fluoride) gel electrolyte for lithium ion batteries prepared by using salicylic acid as a foaming agent. *Journal of Power Sources* **2009,** *189* (1), 594-598.
173. Oh, H.; Xu, K.; Yoo, H. D.; Kim, D. S.; Chanthad, C.; Yang, G.; Jin, J.; Ayhan, I. A.; Oh, S. M.; Wang, Q., Poly(arylene ether)-Based Single-Ion Conductors for Lithium-Ion Batteries. *Chemistry of Materials* **2016,** *28* (1), 188-196.
174. Kim, Y.-T.; Smotkin, E., The effect of plasticizers on transport and electrochemical properties of PEO-based electrolytes for lithium rechargeable batteries. *Solid State Ionics* **2002,** *149*, 29-37.
175. Kim, H.; Oh, B.; Kang, Y., Preparation and electrochemical properties of nonwoven reinforced solid polymer electrolytes. *Polymer Bulletin* **2000,** *44*, 509-515.
176. Paillard, E.; Toulgoat, F.; Arvai, R.; Iojoiu, C.; Cointeaux, L.; Medebielle, M.; Alloin, F.; Langlois, B.; Sanchez, J. Y., Syntheses of a wide family of new aryl based perfluorosulfonimide lithium salts. Electrochemical performances of the related polymer electrolytes. *Journal of Fluorine Chemistry* **2011,** *132* (12), 1213-1218.
177. Johan, M. R.; Fen, L. B., Combined effect of CuO nanofillers and DBP plasticizer on ionic conductivity enhancement in the solid polymer electrolyte PEO–LiCF 3 SO 3. *Ionics* **2010,** *16*, 335-338.

178. Mathew, C. M.; Karthika, B.; Ulaganathan, M.; Rajendran, S., Electrochemical analysis on poly (ethyl methacrylate)-based electrolyte membranes. *Bulletin of Materials Science* **2015,** *38*, 151-156.
179. Rajendran, S.; Sivakumar, M.; Subadevi, R., Li-ion conduction of plasticized PVA solid polymer electrolytes complexed with various lithium salts. *Solid State Ionics* **2004,** *167* (3-4), 335-339.
180. Rajendran, S.; Mahendran, O., Experimental investigations on plasticized PMMA/PVA polymer blend electrolytes. *Ionics* **2001,** *7*, 463-468.
181. Klongkan, S.; Pumchusak, J., Effects of nano alumina and plasticizers on morphology, ionic conductivity, thermal and mechanical properties of PEO-LiCF3SO3 solid polymer electrolyte. *Electrochimica Acta* **2015,** *161*, 171-176.
182. Wu, X.-L.; Xin, S.; Seo, H.-H.; Kim, J.; Guo, Y.-G.; Lee, J.-S., Enhanced Li+ conductivity in PEO–LiBOB polymer electrolytes by using succinonitrile as a plasticizer. *Solid State Ionics* **2011,** *186* (1), 1-6.
183. Echeverri, M.; Kim, N.; Kyu, T., Ionic conductivity in relation to ternary phase diagram of poly (ethylene oxide), succinonitrile, and lithium bis (trifluoromethane) sulfonimide blends. *Macromolecules* **2012,** *45* (15), 6068-6077.
184. Kim, Y.-T.; Smotkin, E. S., The effect of plasticizers on transport and electrochemical properties of PEO-based electrolytes for lithium rechargeable batteries. *Solid State Ionics* **2002,** *149* (1-2), 29-37.
185. Choi, S.; Kim, J.; Jo, S.; Lee, W.; Kim, Y.-R., Electrochemical and spectroscopic properties of electrospun PAN-based fibrous polymer electrolytes. *Journal of the Electrochemical Society* **2005,** *152* (5), A989.
186. Shin, J.-H.; Henderson, W. A.; Passerini, S., PEO-Based Polymer Electrolytes with Ionic Liquids and Their Use in Lithium Metal-Polymer Electrolyte Batteries. *Journal of The Electrochemical Society* **2005,** *152* (5), A978.
187. Shin, J.-H.; Henderson, W. A.; Passerini, S., Ionic liquids to the rescue? Overcoming the ionic conductivity limitations of polymer electrolytes. *Electrochemistry Communications* **2003,** *5* (12), 1016-1020.
188. Li, Z.; Su, G.; Wang, X.; Gao, D., Micro-porous P(VDF-HFP)-based polymer electrolyte filled with Al2O3 nanoparticles. *Solid State Ionics* **2005,** *176* (23), 1903-1908.
189. Ye, H.; Huang, J.; Xu, J. J.; Khalfan, A.; Greenbaum, S. G., Li Ion Conducting Polymer Gel Electrolytes Based on Ionic Liquid/PVDF-HFP Blends. *Journal of The Electrochemical Society* **2007,** *154* (11), A1048.
190. Raghavan, P.; Zhao, X.; Choi, H.; Lim, D.-H.; Kim, J.-K.; Matic, A.; Jacobsson, P.; Nah, C.; Ahn, J.-H., Electrochemical characterization of poly (vinylidene fluoride-co-hexafluoro propylene) based electrospun gel polymer electrolytes incorporating room temperature ionic liquids as green electrolytes for lithium batteries. *Solid State Ionics* **2014,** *262*, 77-82.
191. Kumar, B., Heterogeneous electrolytes: Variables for and uncertainty in conductivity measurements. *Journal of power sources* **2008,** *179* (1), 401-406.
192. Osińska, M.; Walkowiak, M.; Zalewska, A.; Jesionowski, T., Study of the role of ceramic filler in composite gel electrolytes based on microporous polymer membranes. *Journal of Membrane Science* **2009,** *326* (2), 582-588.
193. Zalewska, A.; Walkowiak, M.; Niedzicki, L.; Jesionowski, T.; Langwald, N., Study of the interfacial stability of PVdF/HFP gel electrolytes with sub-micro-and nano-sized surface-modified silicas. *Electrochimica acta* **2010,** *55* (4), 1308-1313.
194. Croce, F.; Persi, L.; Scrosati, B.; Serraino-Fiory, F.; Plichta, E.; Hendrickson, M., Role of the ceramic fillers in enhancing the transport properties of composite polymer electrolytes. *Electrochimica Acta* **2001,** *46* (16), 2457-2461.
195. Li, Z.; Su, G.; Wang, X.; Gao, D., Micro-porous P (VDF-HFP)-based polymer electrolyte filled with Al2O3 nanoparticles. *Solid State Ionics* **2005,** *176* (23-24), 1903-1908.
196. Kim, K. M.; Ko, J. M.; Park, N.-G.; Ryu, K. S.; Chang, S. H., Characterization of poly (vinylidenefluoride-co-hexafluoropropylene)-based polymer electrolyte filled with rutile TiO2 nanoparticles. *Solid State Ionics* **2003,** *161* (1-2), 121-131.
197. Stephan, A. M.; Nahm, K., Review on composite polymer electrolytes for lithium batteries. *Polymer* **2006,** *47* (16), 5952-5964.
198. Subramania, A.; Sundaram, N. K.; Priya, A. S.; Kumar, G. V., Preparation of a novel composite micro-porous polymer electrolyte membrane for high performance Li-ion battery. *Journal of Membrane Science* **2007,** *294* (1-2), 8-15.
199. Meneghetti, P.; Qutubuddin, S.; Webber, A., Synthesis of polymer gel electrolyte with high molecular weight poly (methyl methacrylate)–clay nanocomposite. *Electrochimica Acta* **2004,** *49* (27), 4923-4931.

200. Xiao, W.; Li, X.; Guo, H.; Wang, Z.; Li, Y.; Yang, B., Preparation and physicochemical performances of poly [(vinylidene fluoride)-co-hexafluoropropylene]-based composite polymer electrolytes doped with modified carbon nanotubes. *Polymer international* **2014,** *63* (2), 307-314.
201. Krause, L. J.; Lamanna, W.; Summerfield, J.; Engle, M.; Korba, G.; Loch, R.; Atanasoski, R., Corrosion of aluminum at high voltages in non-aqueous electrolytes containing perfluoroalkylsulfonyl imides; new lithium salts for lithium-ion cells. *Journal of Power Sources* **1997,** *68* (2), 320-325.
202. Kanamura, K., Anodic oxidation of nonaqueous electrolytes on cathode materials and current collectors for rechargeable lithium batteries. *Journal of Power Sources* **1999,** *81-82*, 123-129.
203. Nation, U. For a livable climate:Net-zero commitments must be backed by credible action. https://www.un.org/en/climatechange/net-zero-coalition#:~:text=To%20keep%20global%20warming%20to,reach%20net%20zero%20by%202050.
204. Zahasky, C.; Krevor, S., Global geologic carbon storage requirements of climate change mitigation scenarios. *Energy & Environmental Science* **2020,** *13* (6), 1561-1567.
205. Traversone, V., Carbon Capture Storage vs Carbon Capture Utilization. *Cimate news* 2020.
206. Burkart, M. D.; Hazari, N.; Tway, C. L.; Zeitler, E. L., Opportunities and Challenges for Catalysis in Carbon Dioxide Utilization. *ACS Catalysis* **2019,** *9* (9), 7937-7956.
207. Dabral, S.; Schaub, T., The use of carbon dioxide (CO2) as a building block in organic synthesis from an industrial perspective. *Advanced Synthesis Catalysis* **2019,** *361* (2), 223-246.
208. Subramanian, S.; Song, Y.; Kim, D.; Yavuz, C. T., Redox and Nonredox CO2 Utilization: Dry Reforming of Methane and Catalytic Cyclic Carbonate Formation. *ACS Energy Letters* **2020,** *5* (5), 1689-1700.
209. Nasirov, F.; Nasirli, E.; Ibrahimova, M., Cyclic carbonates synthesis by cycloaddition reaction of CO2 with epoxides in the presence of zinc-containing and ionic liquid catalysts. *Journal of the Iranian Chemical Society* **2022,** *19* (2), 353-379.
210. Patai, S., *The Chemistry of the Thiol Group*. Wiley: 1974.
211. Adams, H.; Bell, R.; Cheung, Y.-Y.; Jones, D. N.; Tomkinson, N. C. O., The cleavage of meso-epoxides with homochiral thiols: synthesis of (+)- and (−)-trans-1-mercaptocyclohexan-2-ol. *Tetrahedron: Asymmetry* **1999,** *10* (21), 4129-4142.
212. Besse, V.; Foyer, G.; Auvergne, R.; Caillol, S.; Boutevin, B., Access to nonisocyanate poly(thio)urethanes: A comparative study. *Journal of Polymer Science Part A: Polymer Chemistry* **2013,** *51* (15), 3284-3296.
213. Ochiai, B.; Nakayama, J.-i.; Mashiko, M.; Kaneko, Y.; Nagasawa, T.; Endo, T., Synthesis and crosslinking reaction of poly(hydroxyurethane) bearing a secondary amine structure in the main chain. *Journal of Polymer Science Part A: Polymer Chemistry* **2005,** *43* (23), 5899-5905.
214. Kihara, N.; Nakawaki, Y.; Endo, T., Preparation of 1,3-Oxathiolane-2-thiones by the Reaction of Oxirane and Carbon Disulfide. *The Journal of Organic Chemistry* **1995,** *60* (2), 473-475.
215. Helou, M.; Miserque, O.; Brusson, J.-M.; Carpentier, J.-F.; Guillaume, S. M., Organocatalysts for the Controlled "Immortal" Ring-Opening Polymerization of Six-Membered-Ring Cyclic Carbonates: A Metal-Free, Green Process. *Chemistry – A European Journal* **2010,** *16* (46), 13805-13813.
216. Annunziata, L.; Diallo, A. K.; Fouquay, S.; Michaud, G.; Simon, F.; Brusson, J. M.; Carpentier, J. F.; Guillaume, S. M., α,ω-Di(glycerol carbonate) telechelic polyesters and polyolefins as precursors to polyhydroxyurethanes: An isocyanate-free approach. *Green Chemistry* **2014,** *16* (4), 1947-1956.
217. Nijenhuis, A. J.; Grijpma, D. W.; Pennings, A. J., Lewis acid catalyzed polymerization of L-lactide. Kinetics and mechanism of the bulk polymerization. *Macromolecules* **1992,** *25* (24), 6419-6424.
218. Dobrzynski, P.; Pastusiak, M.; Bero, M., Less toxic acetylacetonates as initiators of trimethylene carbonate and 2,2-dimethyltrimethylene carbonate ring opening polymerization. *Journal of Polymer Science Part A: Polymer Chemistry* **2005,** *43* (9), 1913-1922.
219. Shaikh, R. R.; Pornpraprom, S.; D'Elia, V., Catalytic Strategies for the Cycloaddition of Pure, Diluted, and Waste CO2 to Epoxides under Ambient Conditions. *ACS Catalysis* **2018,** *8* (1), 419-450.
220. Huang, J.; Worch, J. C.; Dove, A. P.; Coulembier, O., Update and challenges in carbon dioxide-based polycarbonate synthesis. *ChemSusChem* **2020,** *13* (3), 469-487.
221. Azechi, M.; Matsumoto, K.; Endo, T., Anionic ring-opening polymerization of a five-membered cyclic carbonate having a glucopyranoside structure. *Journal of Polymer Science Part A: Polymer Chemistry* **2013,** *51* (7), 1651-1655.
222. Haba, O.; Tomizuka, H.; Endo, T., Anionic Ring-Opening Polymerization of Methyl 4,6-O-Benzylidene-2,3-O- carbonyl-α-d-glucopyranoside: A First Example of Anionic Ring-Opening

Polymerization of Five-Membered Cyclic Carbonate without Elimination of CO2. *Macromolecules* **2005,** *38* (9), 3562-3563.
223. Blattmann, H.; Fleischer, M.; Bähr, M.; Mülhaupt, R., Isocyanate-and phosgene-free routes to polyfunctional cyclic carbonates and green polyurethanes by fixation of carbon dioxide. *Macromolecular rapid communications* **2014,** *35* (14), 1238-1254.
224. Luo, D.; Li, M.; Zheng, Y.; Ma, Q.; Gao, R.; Zhang, Z.; Dou, H.; Wen, G.; Shui, L.; Yu, A.; Wang, X.; Chen, Z., Electrolyte Design for Lithium Metal Anode-Based Batteries Toward Extreme Temperature Application. *Advanced Science* **2021,** *8* (18), 2101051.
225. Jiang, J.; Dahn, J. R., Effects of solvents and salts on the thermal stability of LiC6. *Electrochimica Acta* **2004,** *49* (26), 4599-4604.
226. Guo, L.; Lamb, K. J.; North, M., Recent developments in organocatalysed transformations of epoxides and carbon dioxide into cyclic carbonates. *Green Chemistry* **2021,** *23* (1), 77-118.
227. Su, C.-C.; He, M.; Cai, M.; Shi, J.; Amine, R.; Rago, N. D.; Guo, J.; Rojas, T.; Ngo, A. T.; Amine, K., Solvation-protection-enabled high-voltage electrolyte for lithium metal batteries. *Nano Energy* **2022,** *92*, 106720.
228. Aurbach, D.; Markevich, E.; Salitra, G., High energy density rechargeable batteries based on Li metal anodes. The role of unique surface chemistry developed in solutions containing fluorinated organic co-solvents. *Journal of the American Chemical Society* **2021,** *143* (50), 21161-21176.
229. Wang, Z.; Sun, Z.; Shi, Y.; Qi, F.; Gao, X.; Yang, H.; Cheng, H.-M.; Li, F., Ion-Dipole Chemistry Drives Rapid Evolution of Li Ions Solvation Sheath in Low-Temperature Li Batteries. *Advanced energy materials* **2021,** *11* (28), 2100935.
230. Markevich, E.; Salitra, G.; Chesneau, F.; Schmidt, M.; Aurbach, D., Very Stable Lithium Metal Stripping–Plating at a High Rate and High Areal Capacity in Fluoroethylene Carbonate-Based Organic Electrolyte Solution. *ACS Energy Letters* **2017,** *2* (6), 1321-1326.
231. Tillmann, S. D.; Isken, P.; Lex-Balducci, A., Gel polymer electrolyte for lithium-ion batteries comprising cyclic carbonate moieties. *Journal of Power Sources* **2014,** *271*, 239-244.
232. Liang, S.; Choi, U. H.; Liu, W.; Runt, J.; Colby, R. H., Synthesis and lithium ion conduction of polysiloxane single-ion conductors containing novel weak-binding borates. *Chemistry of Materials* **2012,** *24* (12), 2316-2323.
233. Choi, U. H.; Liang, S.; O'Reilly, M. V.; Winey, K. I.; Runt, J.; Colby, R. H., Influence of solvating plasticizer on ion conduction of polysiloxane single-ion conductors. *Macromolecules* **2014,** *47* (9), 3145-3153.
234. Matsukizono, H.; Matsumoto, K.; Endo, T., Multifunctional cyclic carbonates comprising hyperbranched polyacetals: Synthesis and applications to polymer electrolytes and networked polymer materials. *Journal of Polymer Science Part A: Polymer Chemistry* **2019,** *57* (23), 2295-2303.
235. Boujioui, F.; Zhuge, F.; Damerow, H.; Wehbi, M.; Améduri, B.; Gohy, J.-F., Solid polymer electrolytes from a fluorinated copolymer bearing cyclic carbonate pendant groups. *Journal of Materials Chemistry A* **2018,** *6* (18), 8514-8522.
236. Boujioui, F.; Damerow, H.; Zhuge, F.; Gohy, J. F.; Physics, Solid Polymer Electrolytes Based on Copolymers of Cyclic Carbonate Acrylate and n-Butylacrylate. *Macromolecular Chemistry* **2020,** *221* (6), 1900556.
237. Meabe, L.; Huynh, T. V.; Lago, N.; Sardon, H.; Li, C.; O'Dell, L. A.; Armand, M.; Forsyth, M.; Mecerreyes, D., Poly (ethylene oxide carbonates) solid polymer electrolytes for lithium batteries. *Electrochimica Acta* **2018,** *264*, 367-375.
238. Ouhib, F.; Meabe, L.; Mahmoud, A.; Grignard, B.; Thomassin, J.-M.; Boschini, F.; Zhu, H.; Forsyth, M.; Mecerreyes, D.; Detrembleur, C., Influence of the cyclic versus linear carbonate segments in the properties and performance of CO2-sourced polymer electrolytes for lithium batteries. *ACS Applied Polymer Materials* **2020,** *2* (2), 922-931.
239. Inoue, S.; Koinuma, H.; Tsuruta, T., Copolymerization of carbon dioxide and epoxide. *Journal of Polymer Science Part B: Polymer Letters* **1969,** *7*, 287-292.
240. Wei, X.; Shriver, D. F., Highly conductive polymer electrolytes containing rigid polymers. *Chemistry of materials* **1998,** *10* (9), 2307-2308.
241. Kimura, K.; Yajima, M.; Tominaga, Y., A highly-concentrated poly (ethylene carbonate)-based electrolyte for all-solid-state Li battery working at room temperature. *Electrochemistry Communications* **2016,** *66*, 46-48.
242. Nakamura, M.; Tominaga, Y., Utilization of carbon dioxide for polymer electrolytes [II]: Synthesis of alternating copolymers with glycidyl ethers as novel ion-conductive polymers. *Electrochimica acta* **2011,** *57*, 36-39.
243. Tominaga, Y.; Shimomura, T.; Nakamura, M., Alternating copolymers of carbon dioxide with glycidyl ethers for novel ion-conductive polymer electrolytes. *Polymer* **2010,** *51* (19), 4295-4298.

244. Kimura, K.; Matsumoto, H.; Hassoun, J.; Panero, S.; Scrosati, B.; Tominaga, Y., A QuaternaryPoly(ethylene carbonate)-Lithium Bis(trifluoromethanesulfonyl)imide-Ionic Liquid-Silica Fiber Composite Polymer Electrolyte for Lithium Batteries. *Electrochimica Acta* **2015,** *175*, 134-140.
245. Zhang, J.; Yue, L.; Hu, P.; Liu, Z.; Qin, B.; Zhang, B.; Wang, Q.; Ding, G.; Zhang, C.; Zhou, X., Taichi-inspired rigid-flexible coupling cellulose-supported solid polymer electrolyte for high-performance lithium batteries. *Scientific reports* **2014,** *4* (1), 6272.
246. Zhang, J.; Zhao, J.; Yue, L.; Wang, Q.; Chai, J.; Liu, Z.; Zhou, X.; Li, H.; Guo, Y.; Cui, G.; Chen, L., Safety-Reinforced Poly(Propylene Carbonate)-Based All-Solid-State Polymer Electrolyte for Ambient-Temperature Solid Polymer Lithium Batteries. *Advanced Energy Materials* **2015,** *5* (24), 1501082.
247. Yu, X. Y.; Xiao, M.; Wang, S. J.; Zhao, Q. Q.; Meng, Y. Z., Fabrication and characterization of PEO/PPC polymer electrolyte for lithium-ion battery. *Journal of applied polymer science* **2010,** *115* (5), 2718-2722.
248. Chai, J.; Liu, Z.; Ma, J.; Wang, J.; Liu, X.; Liu, H.; Zhang, J.; Cui, G.; Chen, L., In Situ Generation of Poly (Vinylene Carbonate) Based Solid Electrolyte with Interfacial Stability for LiCoO2 Lithium Batteries. *Advanced Science* **2017,** *4* (2), 1600377.
249. Gregory, G. L.; Gao, H.; Liu, B.; Gao, X.; Rees, G. J.; Pasta, M.; Bruce, P. G.; Williams, C. K., Buffering Volume Change in Solid-State Battery Composite Cathodes with CO2-Derived Block Polycarbonate Ethers. *Journal of the American Chemical Society* **2022,** *144* (38), 17477-17486.
250. Bayer, O., Das Di-Isocyanat-Polyadditionsverfahren (Polyurethane). *Angewandte Chemie* **2006,** *59*, 257-272.
251. Karimi, M. B.; Khanbabaei, G.; Sadeghi, G. M. M., Vegetable oil-based polyurethane membrane for gas separation. *Journal of Membrane Science* **2017,** *527*, 198-206.
252. Akindoyo, J. O.; Beg, M. D. H.; Ghazali, S.; Islam, M. R.; Jeyaratnam, N.; Yuvaraj, A. R., Polyurethane types, synthesis and applications – a review. *RSC Advances* **2016,** *6* (115), 114453-114482.
253. Misenan, M. S. M.; Khiar, A. S. A.; Eren, T., Polyurethane-based polymer electrolyte for lithium ion batteries: a review. *Polymer International* **2022,** *71* (7), 751-769.
254. Lv, Z.; Tang, Y.; Dong, S.; Zhou, Q.; Cui, G., Polyurethane-based polymer electrolytes for lithium Batteries: Advances and perspectives. *Chemical Engineering Journal* **2022,** *430*, 132659.
255. Król, P., Synthesis methods, chemical structures and phase structures of linear polyurethanes. Properties and applications of linear polyurethanes in polyurethane elastomers, copolymers and ionomers. *Progress in Materials Science* **2007,** *52* (6), 915-1015.
256. Ihata, O.; Kayaki, Y.; Ikariya, T., Aliphatic Poly(urethane−amine)s Synthesized by Copolymerization of Aziridines and Supercritical Carbon Dioxide. *Macromolecules* **2005,** *38* (15), 6429-6434.
257. Ihata, O.; Kayaki, Y.; Ikariya, T., Synthesis of Thermoresponsive Polyurethane from 2-Methylaziridine and Supercritical Carbon Dioxide. *Angewandte Chemie International Edition* **2004,** *43* (6), 717-719.
258. Palaskar, D. V.; Boyer, A.; Cloutet, E.; Alfos, C.; Cramail, H., Synthesis of Biobased Polyurethane from Oleic and Ricinoleic Acids as the Renewable Resources via the AB-Type Self-Condensation Approach. *Biomacromolecules* **2010,** *11* (5), 1202-1211.
259. More, A. S.; Gadenne, B.; Alfos, C.; Cramail, H., AB type polyaddition route to thermoplastic polyurethanes from fatty acid derivatives. *Polymer Chemistry* **2012,** *3* (6), 1594-1605.
260. Neffgen, S.; Keul, H.; Höcker, H., Cationic Ring-Opening Polymerization of Trimethylene Urethane: A Mechanistic Study. *Macromolecules* **1997,** *30* (5), 1289-1297.
261. Schmitz, F.; Keul, H.; Höcker, H., Copolymerization of 2,2-dimethyltrimethylene carbonate with tetramethylene urea: a new route to the polyurethane. *Polymer* **1998,** *39* (14), 3179-3186.
262. Maisonneuve, L.; Lamarzelle, O.; Rix, E.; Grau, E.; Cramail, H., Isocyanate-Free Routes to Polyurethanes and Poly(hydroxy Urethane)s. *Chemical Reviews* **2015,** *115* (22), 12407-12439.
263. Watanabe, M.; Oohashi, S.; Sanui, K.; Ogata, N.; Kobayashi, T.; Ohtaki, Z., Morphology and ionic conductivity of polymer complexes formed by segmented polyether poly(urethane urea) and lithium perchlorate. *Macromolecules* **1985,** *18* (10), 1945-1950.
264. Zhu, W.; Yang, B.; Wang, X.; Wang, L.; Tang, X.; Yang, C., Structure and ionic conductive properties of polydioxolane–polyurethane-based electrolytes. *Journal of applied polymer science* **2002,** *83* (1), 103-111.
265. Wen, T.-C.; Du, Y.-L.; Digar, M., Compositional effect on the morphology and ionic conductivity of thermoplastic polyurethane based electrolytes. *European Polymer Journal* **2002,** *38* (5), 1039-1048.

266. Hong, L.; Shi; Tang, Conductivities and Spectroscopic Studies of Polymer Electrolytes Based on Linear Polyurethane and Hybrid and Copolymer of Linear and Hyperbranched Polyurethanes. *Macromolecules* **2003,** *36* (13), 4989-4994.
267. Ren, N.; Song, Y.; Tao, C.; Cong, B.; Cheng, Q.; Huang, Y.; Xu, G.; Bao, J., Effect of the soft and hard segment composition on the properties of waterborne polyurethane-based solid polymer electrolyte for lithium ion batteries. *Journal of Solid State Electrochemistry* **2018,** *22* (4), 1109-1121.
268. Parveen, J. S.; Majeed, S. A., Poly (ethylene oxide)/Polyurethane based gel polymer electrolytes for lithium batteries. *International Journal of Scientific Engineering Research* **2013,** *4* (12).
269. Lin, Z.; Guo, X.; Yang, Y.; Tang, M.; Wei, Q.; Yu, H., Block copolymer electrolyte with adjustable functional units for solid polymer lithium metal battery. *Journal of Energy Chemistry* **2021,** *52*, 67-74.
270. Tian, L. y.; Zhu, W. h.; Tang, X., Polymer gel electrolytes based on thermoplastic polyurethane. *Journal of applied polymer science* **2003,** *90* (9), 2310-2315.
271. Bao, J.; Shi, G.; Tao, C.; Wang, C.; Zhu, C.; Cheng, L.; Qian, G.; Chen, C., Polycarbonate-based polyurethane as a polymer electrolyte matrix for all-solid-state lithium batteries. *Journal of Power Sources* **2018,** *389*, 84-92.
272. Wu, F.; Li, Y. J.; Chen, R. J.; Chen, S., Preparation and characterization of a mixing soft-segment waterborne polyurethane polymer electrolyte. *Chinese Chemical Letters* **2009,** *20* (1), 115-118.
273. Santhosh, P.; Gopalan, A.; Vasudevan, T.; Lee, K.-P., Evaluation of a cross-linked polyurethane acrylate as polymer electrolyte for lithium batteries. *Materials Research Bulletin* **2006,** *41* (6), 1023-1037.
274. Visser, S. A.; Cooper, S. L., Comparison of the physical properties of carboxylated and sulfonated model polyurethane ionomers. *Macromolecules* **1991,** *24* (9), 2576-2583.
275. Porcarelli, L.; Manojkumar, K.; Sardon, H.; Llorente, O.; Shaplov, A. S.; Vijayakrishna, K.; Gerbaldi, C.; Mecerreyes, D., Single Ion Conducting Polymer Electrolytes Based On Versatile Polyurethanes. *Electrochimica Acta* **2017,** *241*, 526-534.
276. Polizos, G.; Kyritsis, A.; Pissis, P.; Shilov, V. V.; Shevchenko, V. V., Structure and molecular mobility studies in novel polyurethane ionomers based on poly(ethylene oxide). *Solid State Ionics* **2000,** *136-137*, 1139-1146.
277. Kakati, D. K.; George, M. H., Polyurethane ionomers containing phosphate groups. *Polymer* **1993,** *34* (20), 4319-4324.
278. Fei, Y.; Liu, S.; Long, Y.; Lu, L.; He, Y.; Ma, X.; Deng, Y., New single lithium ion conducting polymer electrolyte derived from delocalized tetrazolate bonding to polyurethane. *Electrochimica Acta* **2019,** *299*, 902-913.
279. Tao, C.; Gao, M.-H.; Yin, B.-H.; Li, B.; Huang, Y.-P.; Xu, G.; Bao, J.-J., A promising TPU/PEO blend polymer electrolyte for all-solid-state lithium ion batteries. *Electrochimica Acta* **2017,** *257*, 31-39.
280. Wen, T.-C.; Kuo, H.-H.; Gopalan, A., Studies on Composite Electrolytes Composed of Thermoplastic Polyurethane and Polyacrylonitrile. *Macromolecules* **2001,** *34* (9), 2958-2963.
281. Wang, X. J.; Zhang, H. P.; Kang, J. J.; Wu, Y. P.; Fang, S. B., Novel composite polymer electrolytes based on poly(ether-urethane) network polymer and fumed silicas. *Journal of Solid State Electrochemistry* **2007,** *11* (1), 21-26.
282. Jiang, G.; Maeda, S.; Yang, H.; Saito, Y.; Tanase, S.; Sakai, T., All solid-state lithium-polymer battery using poly(urethane acrylate)/nano-SiO2 composite electrolytes. *Journal of Power Sources* **2005,** *141* (1), 143-148.
283. Wu, N.; Cao, Q.; Wang, X.; Chen, Q., Study of a novel porous gel polymer electrolyte based on TPU/PVdF by electrospinning technique. *Solid State Ionics* **2011,** *203* (1), 42-46.
284. Yu, R.; Bao, J.-J.; Chen, T.-T.; Zou, B.-K.; Wen, Z.-Y.; Guo, X.-X.; Chen, C.-H., Solid polymer electrolyte based on thermoplastic polyurethane and its application in all-solid-state lithium ion batteries. *Solid State Ionics* **2017,** *309*, 15-21.
285. Varma, D. R.; Guest, I., The Bhopal accident and methyl isocyanate toxicity. *Journal of toxicology and environmental health* **1993,** *40* (4), 513-29.
286. R.D. Lundberg, M. D. R. Carbon dioxide polymers. 1970-08-11, 1970.
287. Nohra, B.; Candy, L.; Blanco, J.-F.; Guerin, C.; Raoul, Y.; Mouloungui, Z., From Petrochemical Polyurethanes to Biobased Polyhydroxyurethanes. *Macromolecules* **2013,** *46* (10), 3771-3792.
288. Błażek, K.; Datta, J., Renewable natural resources as green alternative substrates to obtain bio-based non-isocyanate polyurethanes-review. *Critical Reviews in Environmental Science and Technology* **2019,** *49* (3), 173-211.
289. Drechsel, E. K. Polymerization of cyclic carbamates, . 1957.
290. Neffgen, S.; Keul, H.; Höcker, H., Cationic ring-opening polymerization of trimethylene urethane: A mechanistic study. *Macromolecules* **1997,** *30* (5), 1289-1297.

291. Soga, K.; Chiang, W.-Y.; Ikeda, S., Copolymerization Of Carbon Dioxide With Propyleneimine *J Polym Sci Part A-1 Polym Chem* **1974,** *12* (1), 121-131.
292. Ihata, O.; Kayaki, Y.; Ikariya, T., Synthesis of Thermoresponsive Polyurethane from 2-Methylaziridine and Supercritical Carbon Dioxide. *Angewandte Chemie - International Edition* **2004,** *43* (6), 717-719.
293. Błażek, K.; Datta, J.; Technology, Renewable natural resources as green alternative substrates to obtain bio-based non-isocyanate polyurethanes-review. *Critical Reviews in Environmental Science* **2019,** *49* (3), 173-211.
294. Wu, Z.; Cai, W.; Chen, R.; Qu, J., Synthesis and properties of ambient-curable non-isocyanate polyurethanes. *Progress in Organic Coatings* **2018,** *119*, 116-122.
295. Kathalewar, M. S.; Joshi, P. B.; Sabnis, A. S.; Malshe, V. C., Non-isocyanate polyurethanes: from chemistry to applications. *RSC Advances* **2013,** *3* (13), 4110-4129.
296. Unverferth, M.; Kreye, O.; Prohammer, A.; Meier, M. A., Renewable Non-Isocyanate Based Thermoplastic Polyurethanes via Polycondensation of Dimethyl Carbamate Monomers with Diols. *Macromolecular rapid communications* **2013,** *34* (19), 1569-1574.
297. Kreye, O.; Wald, S.; Meier, M. A., Introducing catalytic lossen rearrangements: sustainable access to carbamates and amines. *Advanced Synthesis Catalysis* **2013,** *355* (1), 81-86.
298. Pelckmans, M.; Renders, T.; Van de Vyver, S.; Sels, B. F., Bio-based amines through sustainable heterogeneous catalysis. *Green Chemistry* **2017,** *19* (22), 5303-5331.
299. Tomita, H.; Sanda, F.; Endo, T., Polyaddition of bis(seven-membered cyclic carbonate) with diamines: A novel and efficient synthetic method for polyhydroxyurethanes. *Journal of Polymer Science, Part A: Polymer Chemistry* **2001,** *39* (23), 4091-4100.
300. Ochiai, B.; Matsuki, M.; Miyagawa, T.; Nagai, D.; Endo, T., Kinetic and computational studies on aminolysis of bicyclic carbonates bearing alicyclic structure giving alicyclic hydroxyurethanes. *Tetrahedron* **2005,** *61* (7), 1835-1838.
301. Garipov, R. M.; Sysoev, V. A.; Mikheev, V. V.; Zagidullin, A. I.; Deberdeev, R. Y.; Irzhak, V. I.; Berlin, A. A., Reactivity of cyclocarbonate groups in modified epoxy-amine compositions. *Doklady Physical Chemistry* **2003,** *393* (1-3), 289-292.
302. Lamarzelle, O.; Durand, P.-L.; Wirotius, A.-L.; Chollet, G.; Grau, E.; Cramail, H., Activated lipidic cyclic carbonates for non-isocyanate polyurethane synthesis11Electronic supplementary information (ESI) available: Abbreviations, kinetic data, ESI, NMR, MALDI-TOF, DSC, TGA spectra of different compounds. See DOI: 10.1039/c5py01964h. *Polymer Chemistry* **2016,** *7* (7), 1439-1451.
303. Tomita, H.; Sanda, F.; Endo, T., Model reaction for the synthesis of polyhydroxyurethanes from cyclic carbonates with amines: Substituent effect on the reactivity and selectivity of ring-opening direction in the reaction of five-membered cyclic carbonates with amine. *Journal of Polymer Science, Part A: Polymer Chemistry* **2001,** *39* (21), 3678-3685.
304. Bürgel, T.; Fedtke, M.; Franzke, M., Reaction of cyclic carbonates with amines: Linear telechelic oligomers. *Polymer Bulletin* **1993,** *30* (2), 155-162.
305. Besse, V.; Camara, F.; Méchin, F.; Fleury, E.; Caillol, S.; Pascault, J.-P.; Boutevin, B., How to explain low molar masses in PolyHydroxyUrethanes (PHUs). *European Polymer Journal* **2015,** *71*, 1-11.
306. Cornille, A.; Auvergne, R.; Figovsky, O.; Boutevin, B.; Caillol, S., A perspective approach to sustainable routes for non-isocyanate polyurethanes. *European Polymer Journal* **2017,** *87*, 535-552.
307. Diakoumakos, C. D.; Kotzev, D. L. In *Non-Isocyanate-Based Polyurethanes Derived upon the Reaction of Amines with Cyclocarbonate Resins*, Macromolecular Symposia, Wiley Online Library: 2004; pp 37-46.
308. Kobayashi, S.; Kikuchi, H.; Uyama, H., Lipase-catalyzed ring-opening polymerization of 1,3-dioxan-2-one. *Macromolecular Rapid Communications* **1997,** *18* (7), 575-579.
309. Lambeth, R. H.; Henderson, T. J., Organocatalytic synthesis of (poly)hydroxyurethanes from cyclic carbonates and amines. *Polymer* **2013,** *54* (21), 5568-5573.
310. Figovsky, O.; Shapovalov, L.; Leykin, A.; Birukova, O.; Potashnikova, R., Advances in the field of nonisocyanate polyurethanes based on cyclic carbonates. *Lviv Polytechnic Publishing House* **2013**.
311. Steblyanko, A.; Choi, W.; Sanda, F.; Endo, T., Addition of five-membered cyclic carbonate with amine and its application to polymer synthesis. *Journal of Polymer Science, Part A: Polymer Chemistry* **2000,** *38* (13), 2375-2380.
312. Fleischer, M.; Blattmann, H.; Mülhaupt, R., Glycerol-, pentaerythritol- and trimethylolpropane-based polyurethanes and their cellulose carbonate composites prepared via the non-isocyanate route with catalytic carbon dioxide fixation. *Green Chemistry* **2013,** *15* (4), 934-942.

313. Carré, C.; Bonnet, L.; Avérous, L., Original biobased nonisocyanate polyurethanes: solvent-and catalyst-free synthesis, thermal properties and rheological behaviour. *RSC Advances* **2014,** *4* (96), 54018-54025.
314. Figovsky, O. L.; Shapovalov, L. D., Features of reaction amino-cyclocarbonate for production of new type nonisocyanate polyurethane coatings. *Macromolecular Symposia* **2002,** *187*, 325-332.
315. Figovsky, O. L., Hybrid nonisocyanate polyurethane network polymers and composites formed therefrom. Google Patents: 2000.
316. Panchireddy, S.; Thomassin, J. M.; Grignard, B.; Damblon, C.; Tatton, A.; Jerome, C.; Detrembleur, C., Reinforced poly(hydroxyurethane) thermosets as high performance adhesives for aluminum substrates. *Polymer Chemistry* **2017,** *8* (38), 5897-5909.
317. Panchireddy, S.; Grignard, B.; Thomassin, J.-M.; Jerome, C.; Detrembleur, C., Bio-based poly(hydroxyurethane) glues for metal substrates. *Polymer Chemistry* **2018,** *9* (19), 2650-2659.
318. Panchireddy, S.; Grignard, B.; Thomassin, J.-M.; Jerome, C.; Detrembleur, C., Catechol Containing Polyhydroxyurethanes as High-Performance Coatings and Adhesives. *ACS Sustainable Chemistry & Engineering* **2018,** *6* (11), 14936-14944.
319. Grignard, B.; Thomassin, J. M.; Gennen, S.; Poussard, L.; Bonnaud, L.; Raquez, J. M.; Dubois, P.; Tran, M. P.; Park, C. B.; Jerome, C.; Detrembleur, C., CO2-blown microcellular non-isocyanate polyurethane (NIPU) foams: from bio- and CO2-sourced monomers to potentially thermal insulating materials. *Green Chemistry* **2016,** *18* (7), 2206-2215.
320. Ma, Z.; Li, C.; Fan, H.; Wan, J.; Luo, Y.; Li, B.-G., Polyhydroxyurethanes (PHUs) Derived from Diphenolic Acid and Carbon Dioxide and Their Application in Solvent- and Water-Borne PHU Coatings. *Industrial & Engineering Chemistry Research* **2017,** *56* (47), 14089-14100.
321. Liu, B.; Wang, Y.-L.; Bai, W.; Xu, J.-T.; Xu, Z.-K.; Yang, K.; Yang, Y.-Z.; Zhang, X.-H.; Du, B.-Y., Fluorescent linear CO2-derived poly(hydroxyurethane) for cool white LED. *Journal of Materials Chemistry C* **2017,** *5* (20), 4892-4898.
322. Rayung, M.; Aung, M. M.; Azhar, S. C.; Abdullah, L. C.; Su'ait, M. S.; Ahmad, A.; Jamil, S. N. A. M., Bio-based polymer electrolytes for electrochemical devices: Insight into the ionic conductivity performance. *Materials Horizons* **2020,** *13* (4), 838.
323. Baghi, F.; Gharsallaoui, A.; Dumas, E.; Ghnimi, S., Advancements in Biodegradable Active Films for Food Packaging: Effects of Nano/Microcapsule Incorporation. *Foods* **2022,** *11* (5), 760.
324. Pawlicka, A.; Machado, G.; Guimaraes, K.; Dragunski, D., *Solid polymeric electrolytes obtained from modified natural polymers*. SPIE: 2003; Vol. 5136.
325. Dong, T.; Zhang, J.; Xu, G.; Chai, J.; Du, H.; Wang, L.; Wen, H.; Zang, X.; Du, A.; Jia, Q.; Zhou, X.; Cui, G., A multifunctional polymer electrolyte enables ultra-long cycle-life in a high-voltage lithium metal battery. *Energy & Environmental Science* **2018,** *11* (5), 1197-1203.
326. Xu, D.; Wang, B.; Wang, Q.; Gu, S.; Li, W.; Jin, J.; Chen, C.; Wen, Z., High-Strength Internal Cross-Linking Bacterial Cellulose-Network-Based Gel Polymer Electrolyte for Dendrite-Suppressing and High-Rate Lithium Batteries. *ACS Applied Materials & Interfaces* **2018,** *10* (21), 17809-17819.
327. Xiao, S.; Wang, F.; Yang, Y.; Chang, Z.; Wu, Y., An environmentally friendly and economic membrane based on cellulose as a gel polymer electrolyte for lithium ion batteries. *RSC Advances* **2014,** *4* (1), 76-81.
328. Huber, G. W.; Iborra, S.; Corma, A., Synthesis of Transportation Fuels from Biomass: Chemistry, Catalysts, and Engineering. *Chemical Reviews* **2006,** *106* (9), 4044-4098.
329. Zhu, Y.; Romain, C.; Williams, C. K., Sustainable polymers from renewable resources. *Nature* **2016,** *540* (7633), 354-362.
330. Yu, B.-C.; Park, K.; Jang, J.-H.; Goodenough, J. B., Cellulose-based porous membrane for suppressing Li dendrite formation in lithium–sulfur battery. *ACS Energy Letters* **2016,** *1* (3), 633-637.
331. Shuai, L.; Amiri, M. T.; Questell-Santiago, Y. M.; Héroguel, F.; Li, Y.; Kim, H.; Meilan, R.; Chapple, C.; Ralph, J.; Luterbacher, J. S., Formaldehyde stabilization facilitates lignin monomer production during biomass depolymerization. *Science* **2016,** *354* (6310), 329-333.
332. Sudhakar, Y. N.; Selvakumar, M.; Bhat, D. K., Tubular array, dielectric, conductivity and electrochemical properties of biodegradable gel polymer electrolyte. *Materials Science and Engineering: B* **2014,** *180*, 12-19.
333. Mittal, N.; Ojanguren, A.; Cavasin, N.; Lizundia, E.; Niederberger, M., Transient Rechargeable Battery with a High Lithium Transport Number Cellulosic Separator. *Advanced Functional Materials* **2021,** *31* (33), 2101827.
334. Yoshizawa, M.; Marwanta, E.; Ohno, H., Preparation and characteristics of natural rubber/poly(ethylene oxide) salt hybrid mixtures as novel polymer electrolytes. *Polymer* **2000,** *41* (26), 9049-9053.

335. Fuentes, S.; Retuert, P. J.; González, G., Lithium ion conductivity of molecularly compatibilized chitosan–poly(aminopropyltriethoxysilane)–poly(ethylene oxide) nanocomposites. *Electrochimica Acta* **2007,** *53* (4), 1417-1421.
336. Yamagata, M.; Soeda, K.; Ikebe, S.; Yamazaki, S.; Ishikawa, M., Chitosan-based gel electrolyte containing an ionic liquid for high-performance nonaqueous supercapacitors. *Electrochimica Acta* **2013,** *100*, 275-280.
337. Nirmale, T. C.; Karbhal, I.; Kalubarme, R. S.; Shelke, M. V.; Varma, A. J.; Kale, B. B., Facile Synthesis of Unique Cellulose Triacetate Based Flexible and High Performance Gel Polymer Electrolyte for Lithium Ion Batteries. *ACS Applied Materials & Interfaces* **2017,** *9* (40), 34773-34782.
338. Liu, M.; Zhang, S.; Li, G.; Wang, C.; Li, B.; Li, M.; Wang, Y.; Ming, H.; Wen, Y.; Qiu, J.; Chen, J.; Zhao, P., A cross-linked gel polymer electrolyte employing cellulose acetate matrix and layered boron nitride filler prepared via in situ thermal polymerization. *Journal of Power Sources* **2021,** *484*, 229235.
339. Zhang, Z.; Yang, J.; Huang, W.; Wang, H.; Zhou, W.; Li, Y.; Li, Y.; Xu, J.; Huang, W.; Chiu, W.; Cui, Y., Cathode-Electrolyte Interphase in Lithium Batteries Revealed by Cryogenic Electron Microscopy. *Matter* **2021,** *4* (1), 302-312.
340. Zeng, Q.; Wang, J.; Li, X.; Ouyang, Y.; He, W.; Li, D.; Guo, S.; Xiao, Y.; Deng, H.; Gong, W., Cross-linked chains of metal–organic framework afford continuous ion transport in solid batteries. *ACS Energy Letters* **2021,** *6* (7), 2434-2441.
341. Chew, K.; Ng, T.; How, Z., Conductivity and microstructure study of PLA-based polymer electrolyte salted with lithium perchloride, LiClO4. *Int J Electrochem Sci* **2013,** *8* (5).
342. Osinska-Broniarz, M.; Gieparda, W.; Wesolek, D.; Martyla, A.; Przekop, R.; Sierczynska, A., Preparation and Characterization of Gel Polymer Electrolytes based on Electrospun PLA/PHB Membranes for Lithium-Ion Batteries. *ECS Transactions* **2015,** *70* (1), 79.
343. Osada, I.; Hosseini, S. M.; Jeong, S.; Passerini, S., Novel Ternary Polymer Electrolytes Based on Poly(lactic acid) from Sustainable Sources. *ChemElectroChem* **2017,** *4* (3), 463-467.
344. Chew, K., Development of novel bio-degradable electrolyte based on polylactide (PLA) for lithium rechargeable battery. *Advanced Materials Research* **2014,** *853*, 270-275.
345. Tryznowski, M.; Świderska, A.; Gołofit, T.; Żołek-Tryznowska, Z., Wood adhesive application of poly(hydroxyurethane)s synthesized with a dimethyl succinate-based amide backbone. *RSC Advances* **2017,** *7* (48), 30385-30391.
346. van Velthoven, J. L. J.; Gootjes, L.; van Es, D. S.; Noordover, B. A. J.; Meuldijk, J., Poly(hydroxy urethane)s based on renewable diglycerol dicarbonate. *European Polymer Journal* **2015,** *70*, 125-135.
347. Rose, M.; Palkovits, R., Isosorbide as a Renewable Platform chemical for Versatile Applications—Quo Vadis? *ChemSusChem* **2012,** *5* (1), 167-176.
348. Schmidt, S.; Gatti, F. J.; Luitz, M.; Ritter, B. S.; Bruchmann, B.; Mülhaupt, R., Erythritol Dicarbonate as Intermediate for Solvent- and Isocyanate-Free Tailoring of Bio-Based Polyhydroxyurethane Thermoplastics and Thermoplastic Elastomers. *Macromolecules* **2017,** *50* (6), 2296-2303.
349. Zhang, L.; Luo, X.; Qin, Y.; Li, Y., A novel 2,5-furandicarboxylic acid-based bis(cyclic carbonate) for the synthesis of biobased non-isocyanate polyurethanes. *RSC Advances* **2017,** *7* (1), 37-46.
350. Carré, C.; Ecochard, Y.; Caillol, S.; Avérous, L., From the Synthesis of Biobased Cyclic Carbonate to Polyhydroxyurethanes: A Promising Route towards Renewable Non-Isocyanate Polyurethanes. *ChemSusChem* **2019,** *12* (15), 3410-3430.
351. Salanti, A.; Zoia, L.; Orlandi, M., Chemical modifications of lignin for the preparation of macromers containing cyclic carbonates. *Green Chemistry* **2016,** *18* (14), 4063-4072.
352. Thébault, M.; Pizzi, A.; Essawy, H. A.; Barhoum, A.; Van Assche, G., Isocyanate free condensed tannin-based polyurethanes. *European Polymer Journal* **2015,** *67*, 513-526.
353. Schimpf, V.; Ritter, B. S.; Weis, P.; Parison, K.; Mülhaupt, R., High Purity Limonene Dicarbonate as Versatile Building Block for Sustainable Non-Isocyanate Polyhydroxyurethane Thermosets and Thermoplastics. *Macromolecules* **2017,** *50* (3), 944-955.
354. Lee, A.; Deng, Y., Green polyurethane from lignin and soybean oil through non-isocyanate reactions. *European Polymer Journal* **2015,** *63*, 67-73.
355. Daud, F.; Ahmad, A.; Haji Badri, K., An Investigation on the Properties of Palm-Based Polyurethane Solid Polymer Electrolyte. *International Journal of Polymer Science* **2014,** *2014*, 1-5.
356. Su'Ait, M.; Ahmad, A.; Badri, K.; Mohamed, N.; Rahman, M.; Ricardo, C. A.; Scardi, P., The potential of polyurethane bio-based solid polymer electrolyte for photoelectrochemical cell application. *International Journal of Hydrogen Energy* **2014,** *39* (6), 3005-3017.

357. Mustapa, S. R.; Aung, M. M.; Rayung, M., Physico-Chemical, Thermal, and Electrochemical Analysis of Solid Polymer Electrolyte from Vegetable Oil-Based Polyurethane. *Polymers* **2021,** *13* (1), 132.
358. Ibrahim, S.; Ahmad, A.; Mohamed, N. S., Synthesis and characterization of castor oil-based polyurethane for potential application as host in polymer electrolytes. *Bulletin of Materials Science* **2015,** *38* (5), 1155-1161.
359. Ibrahim, S.; Ahmad, A.; Mohamed, N. S., Characterization of Novel Castor Oil-Based Polyurethane Polymer Electrolytes. *Polymers* **2015,** *7* (4), 747-759.
360. Oshinowo, M.; Runge, J. R.; Piccini, M.; Marken, F.; Buchard, A., Crosslinked xylose-based polyester as a bio-derived and degradable solid polymer electrolyte for Li+-ion conduction. *Journal of Materials Chemistry A* **2022,** *10* (12), 6796-6808.
361. Pathak, R.; Kathalewar, M.; Wazarkar, K.; Sabnis, A., Non-isocyanate polyurethane (NIPU) from tris-2-hydroxy ethyl isocyanurate modified fatty acid for coating applications. *Progress in Organic Coatings* **2015,** *89*, 160-169.
362. Silbert, S. D.; Serum, E. M.; LaScala, J.; Sibi, M. P.; Webster, D. C., Biobased, nonisocyanate, 2K polyurethane coatings produced from polycarbamate and dialdehyde cross-linking. *ACS Sustainable Chemistry Engineering* **2019,** *7* (24), 19621-19630.

Chapter 3 A brief introduction to the Electrochemical techniques

Abstract

A technical background in electrochemistry is equally important to lead the investigations of materials for battery application. This chapter targets a brief discussion on such necessary techniques to be applied for the polymer electrolytes developed in this thesis. Coin cells and Swagelok cells setups have been widely adopted for cell testing either for conductivity or above open circuit potential experiments. The non-destructive impedance spectroscopy as result of AC signal is a quite decisive experiment for electrolytes and electrodes prior to prototypes. The redox behavior of materials is analyzed via voltammetry techniques with respect to reference material. It gives both qualitative and quantitative understanding of the reversibility and compatibility of a material. A specific transference number measurement is performed for electrolytes to study ionic transport with the same cell setup applied for time-dependent charge-discharge stripping and plating. However, for full cell prototypes, potential limitation of constant current cycling is applied for the performance of cells with assembled components.

3.1 Introduction to Electrochemistry

The understanding of electrochemistry combined with electronic and chemical phenomena has proved to be the holygrail in the history of batteries. It explains both heterogeneous chemical reactions (electron transfer) and homogeneous reactions at the interfaces and bulk for various domains of science. The fundamental concept and principal led to the understanding of various puzzles and life-changing inventions for years. In correlation with batteries, its history has been very forbearing with various milestone which have been briefly discussed in Chapter 1. Over the years, materials innovation relied on electrochemical techniques for their targeted properties and thus validation in the device. With high performing potentiostat and simplified logarithmic analysis, complex processes in liquid, solid and gaseous analytes can be differentiated and concerned mechanism can be attributed. In this Chapter 3, the particular focus has been directed to the methods and techniques commonly applied for the electrochemical characterization of electrolytes (solid polymer electrolytes) and their understanding.

3.2 Cell setup and testing

The fundamental characterization on battery material is based on the cells fabricated with coin cells, Swagelok, pressure-controlled cells, *etc*. Among all, the most popularly used setups are the coin cell and Swagelok due to their design, safety and reusability (for Swagelok), respectively. The small level cell testing conducted on coin cells provides the proof of concept further extended to pouch cells and grid scale cells for the large-scale studies and analysis. The Swagelok cell consists of two/three symmetrical stainless-steel current collectors at a particular separation, i.e. two electrodes shown in Figure 3.1a. The design varies from one manufacturer to the other within the same framework. The coin cell consists of components like cap, cans, spacer and wave spring, which are typically depicted in Figure 3.1b. However, the pouch cell consists of sandwiched electrodes and electrolyte assembly of either multi-layered electrodes or rolled ones which largely used Celgard as a separator soaked with liquid electrolyte for lithium-ion batteries, as shown in Figure 3.1c. Cell assemblies described above for materials of interest are often investigated in following cell setups, such as symmetric cells, half cells and full cells based on the type of electrodes of either two electrodes or three electrodes. The accuracy and prediction of distinct phenomena and mechanism utilizing the state of art of established electrochemical techniques depend significantly on the right selection of cell configuration as highlighted in Figure 3.2 along with respective equivalent circuit.[1]

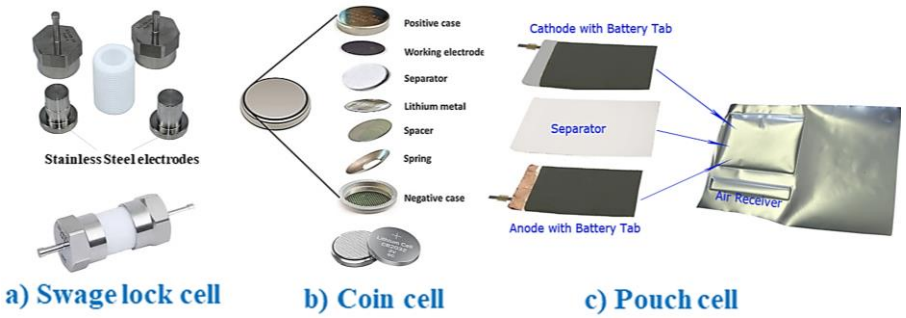

Figure 3. 1: Image illustrating components of major type of commonly utilized cells for battery prototypes: a) Swagelok cell,[2] b) Coin cell,[3] and c) Pouch cell,[4] Reproduced from following reference as cited.

For example, an electrode under analysis should be chosen in half-cell setup with two electrodes (for lower current densities) and three electrodes (reference and counter electrode (RE and CE) coupled with working electrode separately for voltage and current, respectively).[1] For conductivity measurements, blocking electrodes with stainless steel||stainless steel or with gold, are assembled with the target material. A non-blocking symmetric cell consists of same electrode, Li||Li, graphite||graphite or lithiated electrode||lithiated electrode (pseudo symmetric-cell). The cell in this case is operated for cell voltage analysis because of charge/discharge. However, half-cell is used to determine electrode potential (WE) in accordance with the reference electrode (RE). In addition, the full cell operates on the cell voltage/potential of combined electrodes (N and P: negative and positive, as shown in Figure 3.2). A cell fabricated with Li metal and electrode is rather labeled as Li-metal cell instead of half-cell due its influence on the net cell voltage.

3.3 Electrical impedance spectroscopy

Electrical impedance spectroscopy is a powerful, non-destructive transient technique which was established itself as a primary measurement for understanding the time-dependent processes of the electrochemical systems. With widespread application involving corrosion of metals and alloys, electrochemical bio-sensors, batteries, catalysis *etc*. EIS is performed to measure impedance due to existing species and multiple reacting species with their distinctive contribution. EIS uses a small amplitude signal (current or voltage) as periodic perturbation to the target the electrochemical system. The output signal thus follows the evaluation of the transfer function referred as electrochemical impedance, Z expressed as equation 3.1.

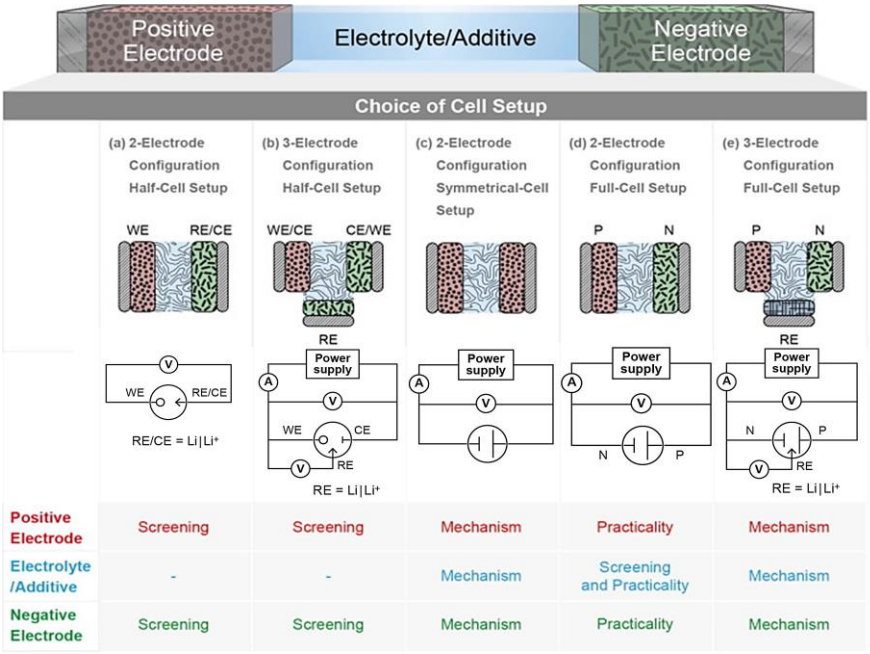

Figure 3. 2: An overall scheme guiding the choice of cell setup with their electrical circuit for the screening and investigation on the desired component of a cell. Reproduced with permission,[1] copyright 2020, Elsevier.

$$Z\,(\omega) = \frac{\tilde{V}(\omega)}{\tilde{I}(\omega)} = \left|\frac{\tilde{V}(\omega)}{\tilde{I}(\omega)}\right| \,(\cos\Phi(\omega) + j sin\Phi(\omega)) = Z_r + jZ_j \qquad 3.1$$

where ω is angular frequency which relates to f by multiplication factor of 2π, Φ is the phase angle between input and output signal and j = $\sqrt{-1}$ is an imaginary number. Frequency dependent impedance Z has two components, real (Z_r/Z`) and imaginary(Z_j /Z") impedance from resistance and reactance of capacitor and inductor, respectively. Mathematically, Kramers-König relation comply with EIS measurement under the assumption of linear and stable system. The amplitude of perturbation voltage is often applied 5-10 mV and up to 1 V in case of high impedance materials.[5, 6] The best setup for EIS can be attributed to four electrode configurations where, two reference electrodes connected for potential and two others for current. However, three electrodes and two electrodes configurations are being adopted largely for batteries and fuel cells. The choice of each electrode and their parameters are not explained here in details as the large focus is emphasized on the EIS of lithium ion batteries with WE and CE. Furthermore, among various principles of EIS instrument, frequency response analyzer (FRA)[7, 8] are the most well-known before Lissajous curves (Figure

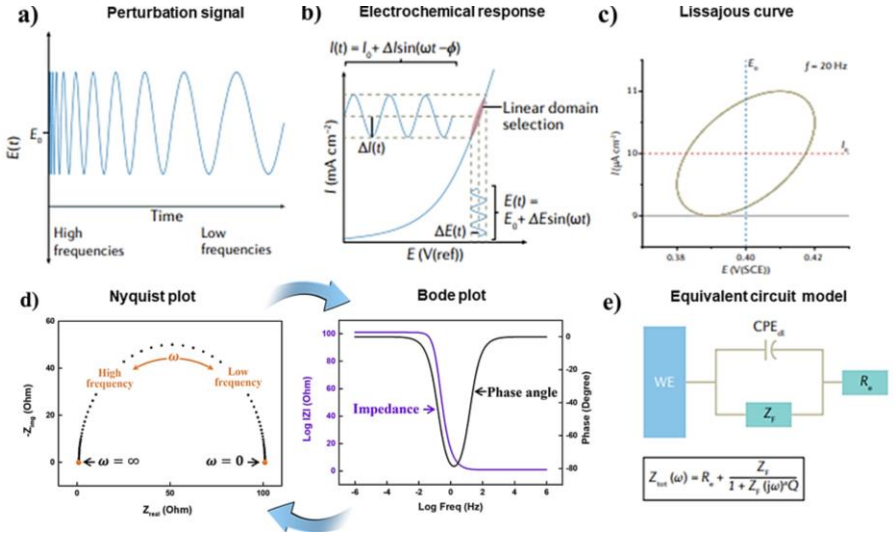

Figure 3. 3: a) AC Perturbation signal with time and frequency, b) Electrochemical response of applied AC signal corresponding to current and voltage and vice versa, c) Lissajous curve (current as a function of potential) plotted from the results presented in a), d) Nyquist to Bode plot transformation, e) Equivalent circuit model of the cell as depicted in a), Reproduced with permission,[6,9] from Nature and Journal of Electrochemical Science and Technology.

3.3c).[6,10] FRA uses orthogonal sine and cosine signals for impedance corresponding to each characteristic frequency. The impedance of cell constitutes of consolidated contribution from resistive, inductive and capacitive component. It depends on various external parameters like, within the cell, wire (twisted or parallel), contact leads, holders, and temperature control. At the lower current and lower frequencies, the electric noise from the environment should be shielded by using Faraday cage.[6, 11]

There are other key parameters such as amplitude signals, frequency range and number of cycles which control the quality of spectra. The EIS with perturbation signal as current signal is referred as Galvanostatic electrical impedance spectroscopy (GEIS) and as voltage signal corresponds to potentiostatic electrical impedance spectroscopy (PEIS). GEIS is usually employed for corrosion or other high energy electrochemical device application where the lower impedance is recorded with high current, while on contrary PEIS is quite favorable for larger impedance electrochemical systems. The magnitude of applied perturbation signal always assured the linearity in accordance with better signal-to-noise ratio. Frequency range is an important parameter to detect the multiple processes which could vary from different states and type of material. The measurement starts from the higher frequency to lower frequency under the assumption of the idea of scanning short period process. With this, the processes occurring at longer time (lower frequency)

are detected subsequently with minimal effect in case of system disturbance by current overload or noisy signals. Periodic EIS over some delay in cycles has been an interesting approach for analysis of real-time process in the system or aging.

The measured data are represented in plots, like Nyquist impedance (as shown in Figure 3.3d left), admittance, Bode plot (as shown in Figure 3.3d right), and black plot depending the parametric interest. Admittance plot is a representation of capacitive behavior at higher frequency and complex capacitance format for the capacitive behavior of the dielectric systems. While Nyquist plot (for mass transfer and kinetic behavior) presents real (Z_r) and imaginary impedance (Z_j) on X and Y-axis respectively with each data point corresponding to unique frequency. Bode plot (frequency dependent behavior) usually depicts phase angle (Φ) and impedance (Z) on the Y-axis with frequency on X-axis. Another representation by the Lissajous curve is significant for understanding the phase difference between input and output signal. The shape of the ellipse and its distortion highlight the nature of perturbation and output signal (Figure 3.3c). However, there is relatively wider acceptance of the Nyquist plot and Bode plot than others, due to their direct representation of impedance.

3.3.1 Impedance of a battery

PEIS is performed as a preliminary experiment for analysis of each component of battery material towards conductivity measurement of distinct entities and processes as well. Bode plot is often referred when the interest lies in the phenomena associated with the unique frequency concerning the impedance of system. Nyquist plot, unlike Bode plot, differentiates the complex impedance into real and imaginary to establish a clear representation of processes and components of the cell. Each Nyquist plot corresponds to an electronic circuit based on the curve fitting. The semi-circle at the higher frequency comprises capacitive behavior (number of semi-circles correspond to number of capacitors) and 45^o slope at lower frequency from the diffusion of ions referred as Warburg diffusion component. An ideal EIS spectra and equivalent circuit based on each component and their understanding has been depicted in Figure 3.4 (A-G).[12] Focusing on the LIB, a typical Nyquist plot has been illustrated in Figure 3.5a, demonstrating the combined impedance of an assembled Li-ion cell which can be splitted into a contribution from different components with compromised accuracy. Ideally, 5 physical processes have been attempted in this Nyquist plot to demonstrate, 1) Li-ion conduction of a porous electrode in the electrolyte, 2) Li ion conduction through SEI films, 3) Intercalation/deintercalation of electrode-electrolyte interface

4.) Li-ion diffusion in electrode phase and 5.) Li-ion diffusion in electrolyte phase.[6,13] As explained above, the semi-circle evolves from the contribution of capacitive behavior either due to electric double layer or geometric capacitor from the system. But this semi-circle is far from perfect in most of the cases and is rather observed as an arc. This anomaly is fitted by addition of an electronic component called constant phase element (CPE).[14] To make it more clear, a scheme of a full LIB cell is depicted in Figure 3.5b which highlights the electrical circuit of each component in series combination with CPE.[15] Therefore, the wiser option is the analysis of each component distinctly with a two or three electrodes setup for a relatively accurate and precise evaluation of a system without interferences. Following the background, the impedance of electrolyte is discussed as our main interest for the evaluation of conductivity.

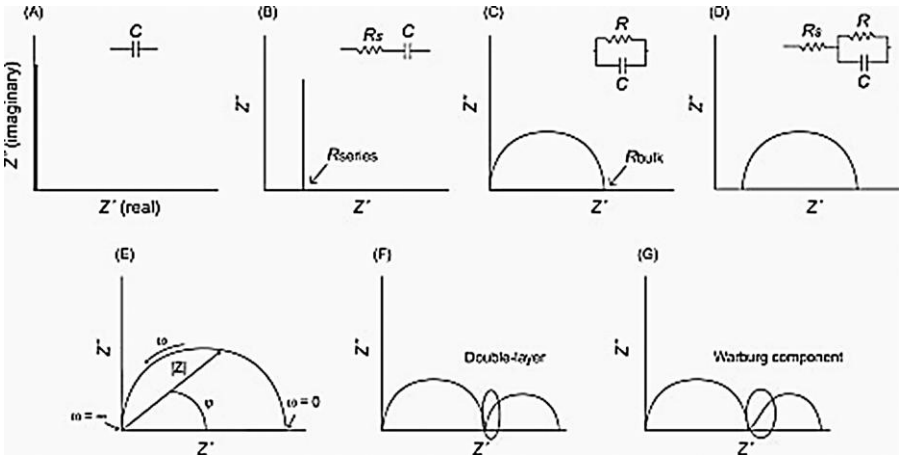

Figure 3. 4: An ideal representation of Nyquist plot in accordance with possible equivalent circuits. Reprinted with permission,[12] copyright 2018, Elsevier.

3.3.2 Conductivity of an electrolyte

An electrolyte serves as an ion channel media between two electrodes and should be electrically insulating. Lower is the hindrance in the mobility better is the net ionic conductivity and transport. Therefore, being one of the most crucial parameters for an electrolyte, conductivity is calculated via impedance obtained from PEIS. A symmetric cell with blocking electrodes is used for the EIS measurement as shown in Figure 3.5c left. The blocking electrodes (gold, silver and stainless steel) restrict the electron transfer/faradaic reactions. A typical EIS of an electrolyte sandwiched between electrodes possesses resistive and capacitive behavior without anomaly. The equivalent circuit employs the series combination of R_s with R_b and C_b in parallel and

C_D. The resistors R_s and R_b correspond to solution resistance and electrolyte bulk resistance, respectively. However, C_b and C_D correspond to geometric capacitor due to charges on the electrodes and double layer capacitor corresponding to charge layer at electrode-electrolyte interface. The capacitive behavior is subjected to frequency, which determines its appearance based on the frequency range. As indicated in Figure 3.5c,[16] the respective electric circuit could be simplified as series combination of impedance labeled as Z, Z_b and Z_D following equations 3.2 to 3.5 below.

$$\frac{1}{Z_b} = \frac{1}{R_b} + \frac{1}{1/i\omega C_b} \quad 3.2$$

$$Z_b = \frac{R_b}{1 + i\omega C_b R_b} \quad 3.3$$

$$Z_D = \frac{1}{i\omega C_D} \quad 3.4$$

$$Z = Z_b + Z_D \quad 3.5$$

$$\sigma = \frac{l}{R_b A} \quad 3.6$$

Therefore, depending on the frequency, when $\omega \rightarrow 0$ then impedance becomes purely resistive, sum of solution and bulk resistance. At high frequency $\omega \rightarrow \infty$, then the bulk impedance approaches to zero and net impedance equals to R_s. As far conductivity of electrolyte is concerned, bulk electrolyte is calculated from Z-fit where imaginary impedance gets zero. The ionic conductivity of an electrolyte is calculated by using the equation 3.6 which depends on parameters such as area and thickness of electrolyte films in addition to experimental conditions. These conductivity data are aligned with a suitable model as described in the ionic conductivity section of Chapter 2 for understanding the mechanism of transport. The EIS measurements are also employed in transference number in combination with other methods in addition to time dependent aging analysis of sample which is explained in subsequent sections.

3.4 Voltammetry

The voltammetry is a remarkable technique within electrochemistry for the study of the analyte via output current in response to varied input voltage. The generated voltammogram highlights the underlying reactions via the exchange of electrons and other transfer phenomena. Depending on the investigations required, voltammetry has been classified into different categories based on the distinct input signal/voltage and type of electrodes (in some cases). They include cyclic voltammetry (CV), linear

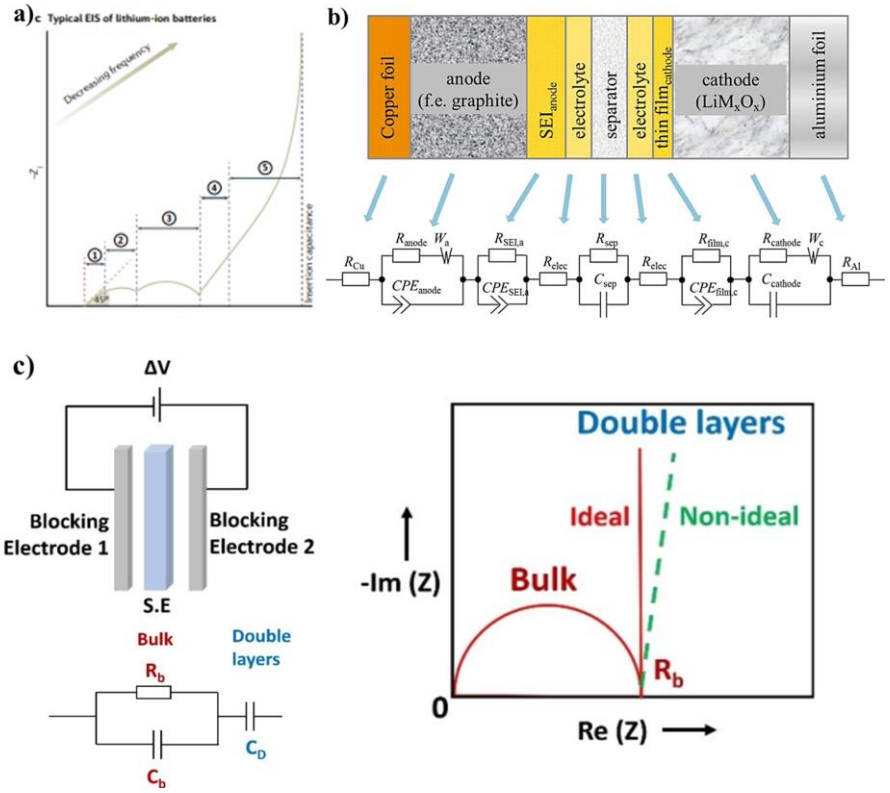

Figure 3. 5: a) A typical EIS spectra of LIB depicting physical processes along its trajectory and b) Scheme of a LIB full cell and associated LCR component in equivalent circuit corresponding to each cell component. c) A scheme of symmetric cell with a solid electrolyte for conductivity measurement (left), corresponding Nyquist plot for the impedance (right). Reproduced with permission,[6,15,16] copyright, 2021 Nature, 2016 Wiley, 2019 Wiley, respectively.

sweep voltammetry (LSV), polargraph stair-case voltammetry, polarography, pulse voltammetry, chronoamperometry (CA) *etc*. Among these, most applied methods are CV and LSV for qualitative understanding of reactions at the working electrodes and CA for the stability of the working electrode. Electron transfer is a thermodynamic process between electrodes or two entities to achieve stable energy levels (also depicted in introduction section). Typically, voltammetry uses three electrodes involving RE, WE and CE, besides two and four electrodes setups. However, for lithium batteries, two electrodes are used with Li/Li^+ as RE and CE together excluding some setups such as Swagelok which facilitates the 3-electrode experiments as well.

3.4.1 Cyclic voltammetry

As the term suggests, CV is cyclic in nature with both forward and reverse scans in the loop to understand the redox processes. It is considered as a crucial technique for analyzing any chemical reactions undergoing reduction and oxidation phenomena. However, CV is quite sensitive and can be performed in both solid state and solution phase at the surface of WE. It requires terminal voltage (E_1 and E_2) with scan rate (v=(dE/dt)) which determines the rate of potential applied linearly with time as shown in Figure 3.6a. The terminal voltage is chosen with a speculation of electrode reactions occurring in that potential window with zero current at vertex potential. Usually, a slow scan rate is chosen in the range of 0.1 -10 mV s^{-1} as integral capacity at a particular scan rate is close to the theoretical capacity of the electrode.[14] As a result, the voltammogram records shapes of Gauss-type peak for single electron concerning oxidation and reduction with reversible nature of analyte, as illustrated in Figure 3.6b.

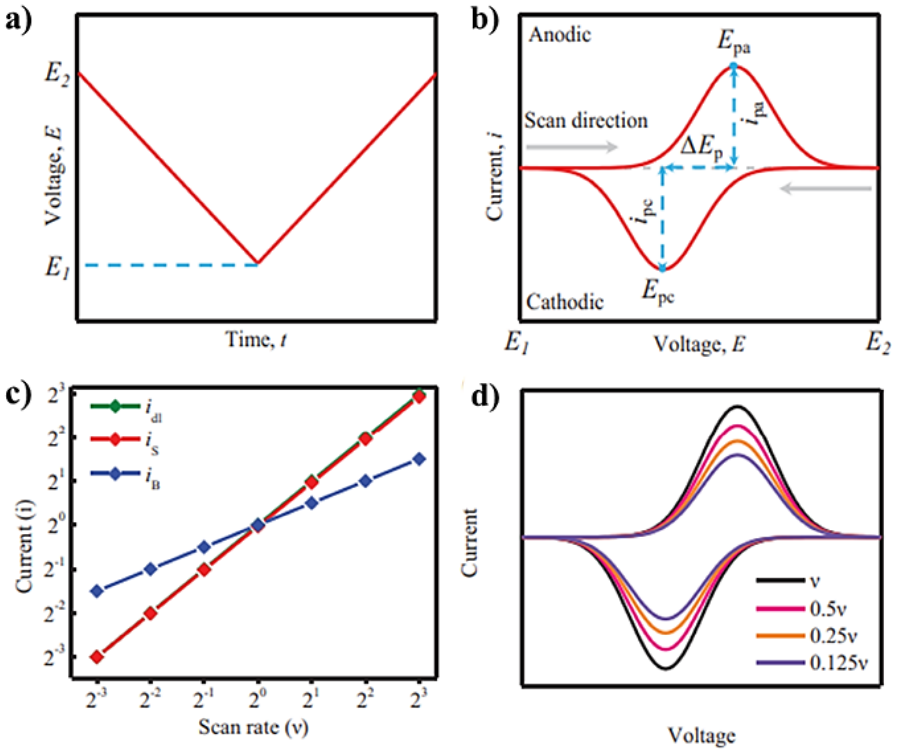

Figure 3. 6 : Illustration of a) Cyclic voltammetry plot for voltage versus time, b) I-V plot: Current response versus voltage curves and c) Possible current response modes during CV with scan rate; d) I-V plot: Voltammograms at various scan rates. Reproduced with permission,[14] copyright 2019, Wiley.

In the window of limiting potential, voltage (E_{pa} and E_{pc}) corresponding to anodic peak current in oxidation/forward scan and cathodic peak current in reduction/reverse scan are analyzed primarily. The reversibility of any redox process is evaluated from the ratio of these peak currents and difference of voltage corresponding to peak currents. The current–voltage response in battery system is not attributed to only Faradaic process, they also include non-Faradaic process like diffusion, intercalation etc. However some of these processes are not reversible in nature. In a study of one-side electrode, RE is used due to their fixed potential, say Li-metal, in the case of evaluation of any cathode for LIB. As far current response is concerned, three modes of current contribute to net current namely, non-Faradaic double layer current (i_{dl}), Faradaic surface and bulk current (i_b and i_S) as shown in Figure 3.c.[14] The square root of scan rate is directly related to the current due to diffusion of charge carriers through the bulk of electrodes. The area covered by the voltammogram is also directly related to the square root of scan rate and increases with the increase in scan rate, depicting

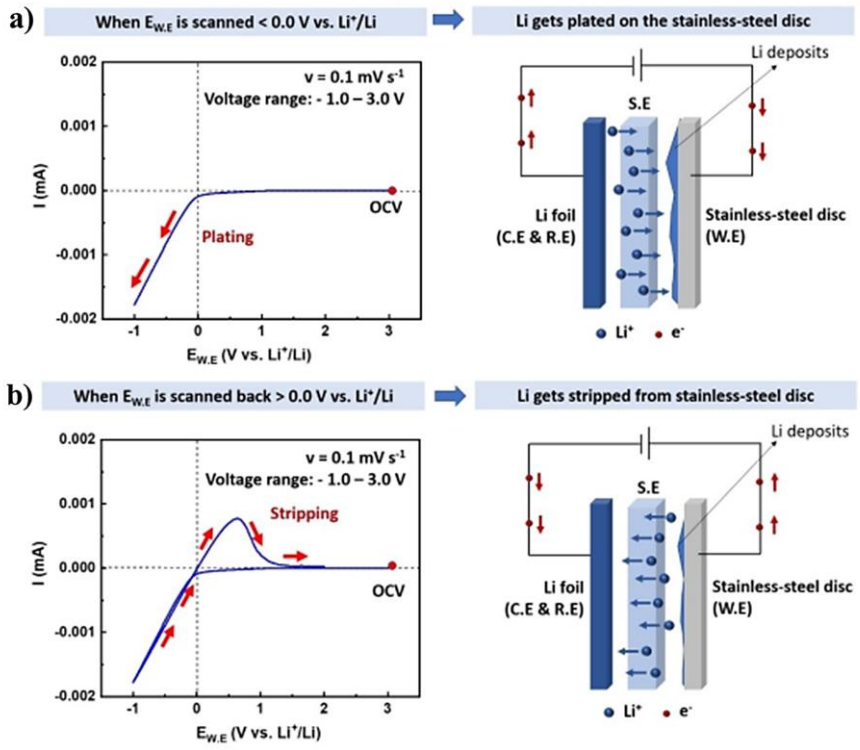

Figure 3. 7: Demonstration of cyclic voltammogram (left) for a solid electrolyte (SE) based Lithium/stainless steel cell as depicted (right), a) when the voltage < 0.0 V vs. Li^+/Li, and b) when the voltage > 0.0 V vs. Li^+/Li. Reproduced with permission,[16] copyright 2019, Wiley.

higher capacitive behavior, as indicated in Figure 3.7d. This scan rate based voltammogram is used to find the diffusion coefficient of ions. Nevertheless, CV curves can also be converted to voltage vs capacity profiles to obtain voltage plateau of oxidation and reduction corresponding to charge–discharge at constant current. CV has also been used to demonstrate the extent of stripping and plating in an asymmetric cell with stainless steel disc/copper- Lithium cells. In a typical experiment, voltage is applied from open circuit potential to -1 V at a lower scan rate (0.1 mV s^{-1}) to SS-Li cells. As a result of applied potential, the lithium plating is observed at the onset of 0 V, which is later stripped from SS on the reverse scan at the potential of E > 0 V onwards as demonstrated in Figure 3.7.[16] The quantitative analysis of this stripping and plating and calculation of Coulombic efficiency explains the reversibility, side reactions along with stability and compatibility versus RE.

3.4.2 Linear sweep voltammetry and anodic stability

Linear sweep voltammetry (LSV) is a subset of cyclic voltammetry which excludes the reverse scan. It uses the similar parameters and principles as cyclic voltammetry for calculation of oxidation potential limit of an analyte. The cell for LSV measurement resembled the one with Li-metal as RE and WE sandwiching electrolyte. Basically, this method involves an oxidation sweep to analyze the anode stability in a wide range of potential, which labels the experiment as anodic stability of an electrolyte. There have been two approaches which were often employed for determination of ESW of an electrolyte. In a simple step, potential is swept linearly from lower potential (0.5 V) to higher potential (target potential of cathode) at a particular scan rate, as highlighted in Figure 3.8a.[17] While in the second approach, potential is swept from open-circuit potential (OCP) to higher potential and from OCP to lower potential, respectively, for two cells at the same scan rate. As a result of applied potential, both Faradaic and non-Faradaic currents are recorded as demonstrated in Figure 3.8b. The sudden increase in the current at higher voltage indicates the Faradaic reaction at the voltage, which is usually described as cut-off voltage for ESW, as shown in Figure 3.8c and 3.8d.[17,18] The recorded oxidation potential provides a validation on the safe and stable utilization of the electrolyte below that voltage with minimum or no decomposition. In addition to the effect of scan rate as observed in Figure 3.8d, area and thickness of electrolyte, current collector materials and cell temperature also affect the current response of the cell in the LSV spectra.[19, 20]

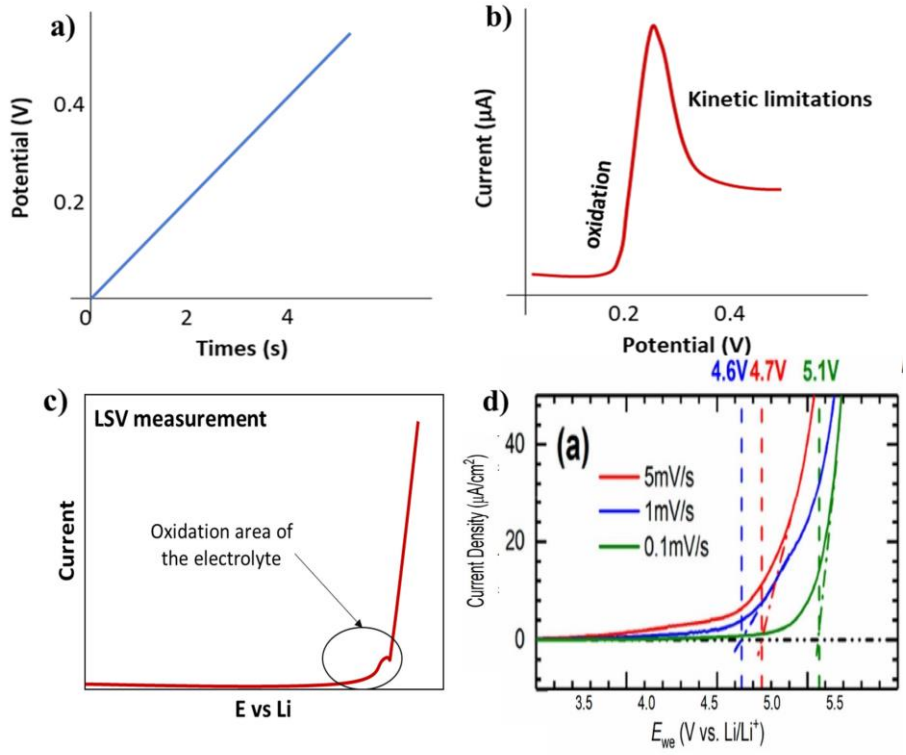

Figure 3. 8: a) Voltage profile with time for linear sweep voltammetry, b) I-V plot: Current-voltage profile for LSV, c) Example of "stability thresholds" determined by onset potential, and d) Effect of scan rate on threshold potential or PEO:LiTFSI (O/Li = 10) from 3.5 to 5.5 V vs. Li^+/Li at RT from LSV. Reproduced with permission,[17, 18] copyright 2021 MDPI and 2021 ACS.

The phenomena of diffusion in liquid electrolytes occurs from bulk towards electrode, which restricts the accurate evaluation of limiting current. Therefore, three electrodes are recommended to be used for LSV in the case of LE based cells, while the third electrode is dipped in the liquid. However, in solid state electrolyte the oxidized species remain under detection range and thus a large area of polymer electrolyte is often desired for legitimate calculation of ESW.[18, 21] To avoid overestimation of onset potential at higher scan rate, lower scan rate such as 0.1 mV s^{-1} is applied.[17]

3.5 Transference number

Transference number t_{M^+} (M: cation) is not a technique as such but a parameter concerning the magnitude of transport of ions within the electrolyte. It quantifies the number of ions available for the mobility within electrolyte. Besides ionic conductivity and diffusion, transference number is one of the important criteria for an electrolyte to predict high performance in a longer run. This dimensionless quantity is often calculated for cations in metal-ion batteries decoupled with ionic conductivity. An electrolyte can possess high ionic conductivity and yet low transference number despite any contradictions. A full cell with higher t_{M^+}electrolyte undergoes superior cycling with minimal capacity decay than one with lower t_{M^+} While the transport mechanism of ions differs from one phase of electrolyte to another, which is why one model does not fit well for all the systems. Therefore, quite a few models have been proposed over time with improved accuracy and limits. Conventionally, the $t_{Li^+}$was calculated by the ratio current at steady state (I_{SS}) and initial current (I_o) as in equation 3.7.

$$t_{Li^+} = \frac{I_{ss}}{I_o} \tag{3.7}$$

$$t_{Li^+} = \frac{I_{ss}(\Delta V - I_o R_{in,0})}{I_o(\Delta V - I_o R_{in,SS})} \tag{3.8}$$

However, questions were raised on the accuracy of this method due to the unavoidable mobility of counter ions and thus new methods were developed using electrochemistry as well as NMR technique. The NMR technique used pulsed field gradient NMR experiment on the mobile ions (^{7}Li and ^{19}F) to calculate their self-diffusion coefficients.

The most popularly used method is a combination of DC polarization (chronoamperometry) and AC impedance spectroscopy, developed by Bruce-Vincent.[22, 23] The cell assembly comprises electrolyte in symmetrical 2-electrodes Li-Li cell and is subjected to constant potential of, ΔV~10-50 mV for certain period. It is well recommended to stabilize the open circuit potential of the cell prior to the measurement with stable measurement temperature condition. The impedance of the cells is performed before and after the polarization at similar parameters as represented in Figure 3.9a and 3.9d with equivalent circuit indicated in Figure 3.9b.[16] As a result of applied potential, the system achieves a stable state where the current response normalizes to constant value, referred as steady state, as shown in Figure 3.9c. The steady state is achieved via cationic migration and diffusion towards a

negatively polarized electrode and conflicted anionic migration and diffusion towards positive polarized electrode on applied potential. It takes account of interfacial resistance and thus the equation 3.8 ($R_{in,0}$and $R_{SS,0}$ are initial and steady state interfacial resistance) is derived from conventional equation 3.7 under the consideration of various other phenomena and approximation.

The correct estimation of transference number has always been a matter of discussion, with researchers reporting negative or higher than unity t_{Li^+}. The dilute solution theory has been the basis of this method, which approximates infinite dilution.[24] Modified equations and approximation tend to find a better compromise according to the type of electrolyte.[25] The trade-off between transference number and ionic conductivity has been a major issue for some time, which is attempted to be overcome by immobilizing anions and providing efficient channels for cations.

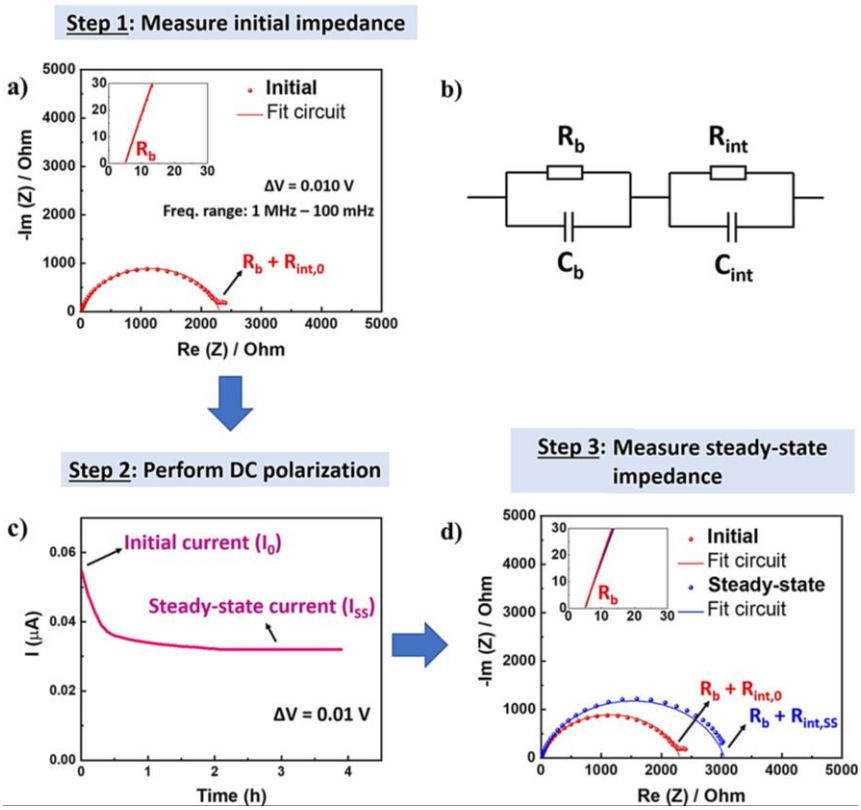

Figure 3. 9: Illustration for estimation of the transference number. a) Nyquist plot showing the initial impedance of the LI-Li symmetric cell, b) Equivalent circuit for corresponding cell, c) DC polarization: Chronoamperometry for achieving the steady-state condition, and d) Comparative Nyquist for the initial and steady-state impedances. Insets: R_b: bulk resistance in (a) and (d). Reproduced with permission,[16] copyright 2019, Wiley.

3.6 Galvanostatic cycling

Galvanostatic cycling is a technique to measure the reversibility of any materials by applying constant current and analyzing the voltage response of the cell. It is one of the most interesting method which is employed to investigate the capacity, differential capacity, potential, stability, rate capability, diffusion coefficient and other measurement with modified Galvanostatic techniques. In CV, the output current response to applied voltage is reciprocated in voltage-capacity profile from the CV resembling charge and discharge of the cell. Similar to that, Galvanostatic charge and discharge profiles can be transformed to differential capacity versus voltage plot with information on oxidation and reduction peaks. This method can also be utilized on both 2 and 3-electrodes cells either for half-cell or full cell. It facilitates control over time, charge and voltage, targeting specific properties with applied current as explained in the subsequent section.

3.6.1 Potential limited charge-discharge

As the term suggests, it corresponds to Galvanostatic charge-discharge with constant current and cut-off voltage (potential limits). This method is largely utilized for the testing of battery prototypes involving analysis of electrodes in half cell and full cell, their performance and compatibility with electrolyte and other materials in cell assembly. Here, cell undergoes charge-discharge in defined voltage limits on time limits to generate various data like voltage profile with current, capacity (gravimetric and volumetric capacity), rate capabilities, Coulombic efficiency, *etc*. The voltage profile with time indicates the speed of electrochemical cells reactions and phenomena in the state of charge-discharge. These Galvanostatic charge-discharge profiles uncover various information right from the electrodes, electrolytes, effects of binders and additive with controlled analysis. The ideal charge-discharge of a cell is shown in the Figure 3.10. The voltage plateaus are often plotted with specific capacity to indicate the oxidation and reduction voltage of electrodes and their corresponding capacities (Figure 3.10b). The plot indicates capacity in certain cycles and its evolution with longer cycling. The capacity of an electrode is calculated by following equation 3.9, where Q_F is the Faradic capacity, M molar mass of the electrode, and F the Faradic constant. The polarization/overpotential is evaluated from voltage difference in respective charge-discharge curves ($E_C - E_D$). An electrolyte with lower conductivity possesses higher polarization/overpotential than a higher ionic conductivity electrolyte similar to overpotential analysis below,

$$Q_F = \frac{nF}{M} \quad 3.9$$

For testing of battery prototypes, few other analysis are represented as capacity retention plot, cyclic stability in addition to voltage profiles. It corresponds to an evaluation of capacity with cycle number in combination with Coulombic efficiency for each cycle. Coulombic efficiency is defined as the percentage of ratio of discharge/charge (the cell is subjected to charge first). It is an important parameter to measure the loss of lithium ions in subsequent charge-discharge for a longer cycling cell. There is also other terminology for evaluation of efficiency of the cells, like round trip efficiency, which uses the ratio of discharge to charge energy capacity. From a cyclic stability plot, one can found the capacity retention of cells with information on the CE. As already stated, higher current density leads to higher overpotential, which is also a subject of investigations for full cells (GC curve). The rate capability plot determines the cell performance depending on fast or slow charge-discharge rate and its ability to perform at various current densities without failure (CR curve) as shown in Figure 3.10c. An ideal electrolyte with a higher ionic conductivity and transference number should facilitate negligible change in aggravated polarization and deliver more or less equivalent specific capacity at higher C-rate. Galvanostatic cycling with potential limitation is more for full battery test or for electrodes screening, while it also provides qualitative information regarding compatibility of electrolytes. Galvanostatic intermittent titration techniques (GITT), a modified GPCL, is an interesting approach for the calculation of apparent diffusion coefficient in electrodes with some approximations. It is based on the splitting of the charge-discharge into multiple small-time steps in combination with relaxation to equilibrium in each charge and discharge as shown in Figure 3.10d. All these methods are standardized and are translated to other metal-ion batteries technology with some major or minor changes based on parameters.

3.6.2 Time dependent charge-discharge

For a time-dependent charge-discharge, constant current is applied to record the voltage response within a limited time of charge-discharge. This is often performed with a fixed amount of charge supply for analyzing the performance of the cell over time. One such necessary experiment referred to is stripping and plating of metal-ions within a symmetrical non-blocking electrode cell. The electrolyte is sandwiched with lithium metal foil, same as the cell assembly for transference number measurement explained above. The Li-Li cell is subjected to constant current for a certain time (say

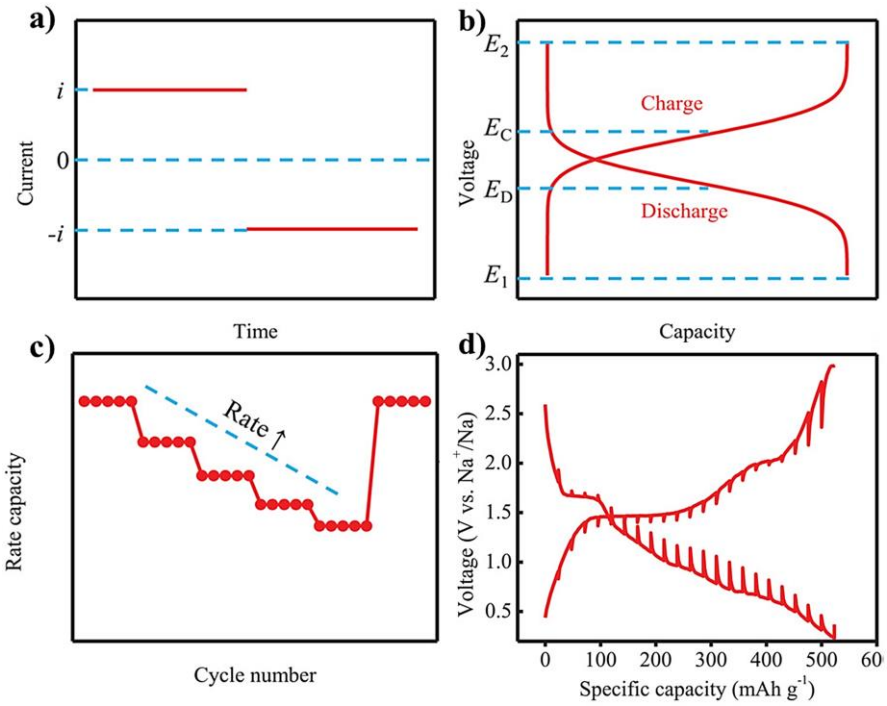

Figure 3. 10: Galvanostatic charge-discharge methods a) Charge and discharge: Constant current with time; b) Voltage response versus capacity curves with potential limitation E1 and E2, and c) Rate capability illustrating change in capacity with cycle number and current densities, and d) Galvanostatic intermittent titration charge-discharge: Voltage profile with specific capacity. Reproduced with permission, [14] copyright 2019, Wiley.

1 h) in the course of each charge and discharge, as depicted in Figure 3.11a. The resulting voltage profile explains about overpotential in the respective process in each cycle. It is the nature of overpotential evolution that defines the stability of the electrolyte, efficient mobility of cations, decomposition reactions and impedance associated with other phenomena.

The overpotential depends highly on ionic conductivity and interfacial resistance of the electrolyte, which may vary with electrolyte decomposition at the metal surface. The electrolyte with higher ionic conductivity results in lower potential and same is observed for lower interfacial resistance.[26] In correlation to that, higher current densities lead to higher polarization and overpotential (for example, 0.05–0.5 V vs. Li^+/Li for current densities of 0.05–0.2 mA cm^{-2}).[16, 27] Usually during longer cycling, interface stabilizes, SEI forms and thus constant overpotential is recorded but initial cycles are attributed to early reactions, decomposition of electrolyte, change in surface morphology, *etc*. The surface morphology resulting from cycling is illustrated in

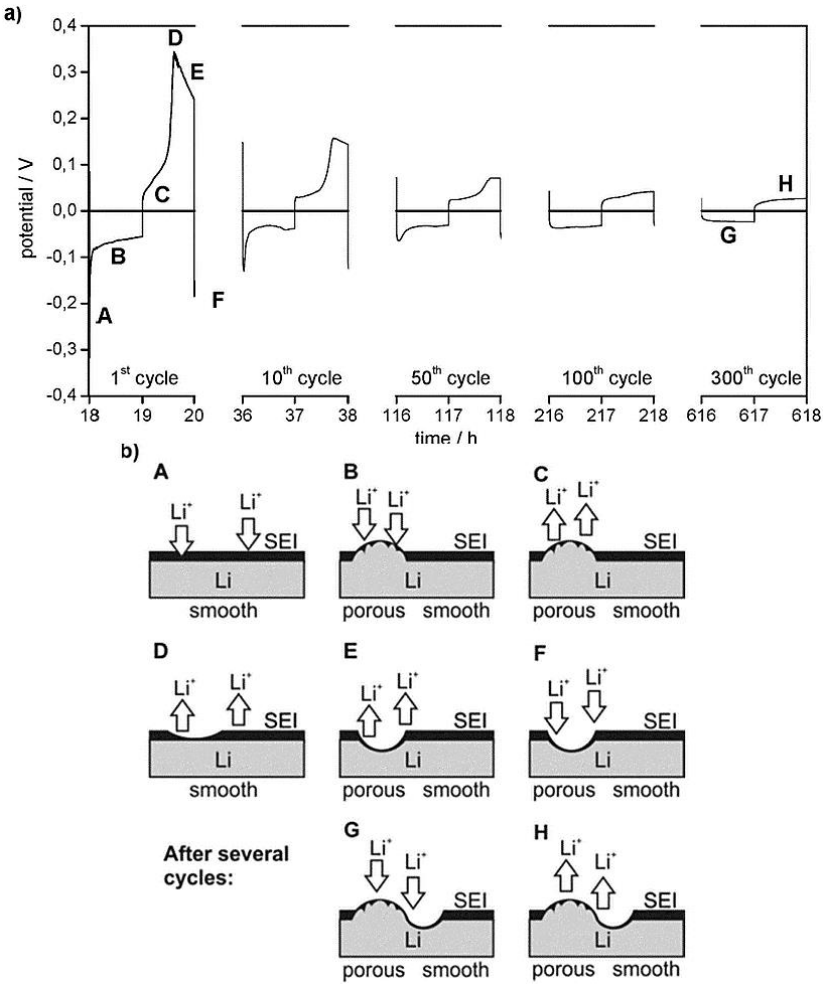

Figure 3. 11: Time dependent Galvanostatic charge-dicharge. a) Overpotential profiles of subsequent lithium plating/stripping processes in Li/Li symmetrical cells with selected region A-H for respective cycles. Reproduced with permission,[28] copyright 2019, Wiley.

Figure 3.11b, corresponding to respective cycles of interest from Figure 3.11a. The highest overpotential at specific constant current density is often observed during the initial cycle due to the kinetic hindrance at the Li-surface (region A), while several other processes occur in transition. Those include deposition of new lithium ions on old ones (region B), first higher rate of dissolution/stripping of fresh deposited lithium (region C) and lower rate of dissolution/stripping of old deposited lithium (region D) underneath fresh ones in region A. The decreased overpotential in region E combines the effect of processes like induction of porosity, in homogeneous dissolution and dendrite formation while subsequent stripping-plating leads to constant overpotential

as depicted in regions G and H. The order of charge and discharge affects the morphology of the lithium metal surface in terms of porosity and dendritic growth which was experimentally depicted.[28]

The stripping and plating are smart and rapid methodologies for the prediction of the potential of a target electrolyte's compatibility and success in a full cell for repeated charge-discharge. The overpotential analysis with Li-Li cells at respective current density range gives an understanding of the extent of high polarization with electrodes, decomposition of electrolyte, SEI formation, and transport efficiency. The post-mortem analysis as a result of stripping and plating via microscopic and spectroscopic tools leads to the crucial findings for tackling the underlying challenges, the design of materials with superior electrochemical parameters, and the tuning of the measurement conditions.

3.7 Summary

The basic understanding of electrochemical analysis is important for prediction and evaluation of proof of concepts of battery materials. In this chapter, a brief discussion of the techniques specifically developed for electrolytes and full cells is presented to build the background. The first step lies in the selection of the cell setup, ranging from 2-electrodes to 3-electrodes with half-cell to full cell. These materials don't follow Ohm's law for the current and corresponding voltage or vice versa. Therefore, a key experiment for the evaluation of contribution to conductivity is often performed via impedance spectroscopy. Frequency dependent Nyquist plots indicates impedance and individual contribution through equivalent electronic circuit corresponding to the capacitor, resistor or inductor.

A material undergoes a redox process as a result of electron transfer led by potential difference. The redox behavior of an electrolyte is expected to be the opposite of electrodes with irreversibility and weak coordination. The popular voltammetry technique, either cyclic or linear in multiple scan rates is conducted to record the current response at each corresponding voltage in the forward or backward scan, respectively. Voltammetry is a powerful technique which not only tells about oxidation and reduction of analyte but also provides yet crucial information on other properties such as reactivity, conductivity, diffusion, and charge storage. The operating voltage, also referred to as the electrochemical stability window (ESW) of an electrolyte, is calculated via linear sweep voltammetry analysis. An ESW tells about the compatibility of the electrolyte-electrode via potential matching for their cycling.

The electrolyte acts as a channel for ionic transport and mobility. Therefore, the number of mobile ions between electrodes is investigated by transference number analysis. It combines the DC polarization and impedance spectroscopy to calculate the actual number of mobile cations and anions. Furthermore, charge-discharge nature of a cell largely depends on its configuration, electrodes and electrolytes. A cell is subjected to galvanostatic cycling, either with time or potential limitations. Time-dependent constant current cycling is usually performed with symmetrical metal-metal non-blocking electrodes to assess the overpotential reactions over time at the interface (referred as SEI or CEI) with exhaustive stripping and plating of metal ions. On the contrary, a full cell consisting of commercial cathodes and anodes is subjected to potential limitation at constant current and is analyzed for its capacity on respective current-rate. Many other techniques have been developed or already existed besides those explained above for the material evaluation, such as dielectric constant, intermittent technique for diffusion, self-discharge, *etc*. With instrumental advancement, quite a few of these techniques are coupled with spectroscopy and microscopy to analyze the structural changes aligned with electrochemical experiments.

Bibliography

1. Nölle, R.; Beltrop, K.; Holtstiege, F.; Kasnatscheew, J.; Placke, T.; Winter, M., A reality check and tutorial on electrochemical characterization of battery cell materials: How to choose the appropriate cell setup. *Materials Today* **2020,** *32*, 131-146.
2. Swagelock cell. https://www.tmaxcn.com/swagelok-type-cell-for-lithium-ion-battery_p853.html.
3. Zülke, A.; Li, Y.; Keil, P.; Burrell, R.; Belaisch, S.; Nagarathinam, M.; Mercer, M. P.; Hoster, H. E., High-Energy Nickel-Cobalt-Aluminium Oxide (NCA) Cells on Idle: Anode- versus Cathode-Driven Side Reactions. *Batteries & Supercaps* **2021,** *4* (6), 934-947.
4. Formed Pouch Cell. https://www.mtixtl.com/FormedPouchCellCase-EQ-PLiB-54560.aspx.
5. Vivier, V.; Orazem, M. E., Impedance Analysis of Electrochemical Systems. *Chemical Reviews* **2022,** *122* (12), 11131-11168.
6. Wang, S.; Zhang, J.; Gharbi, O.; Vivier, V.; Gao, M.; Orazem, M. E., Electrochemical impedance spectroscopy. *Nature Reviews Methods Primers* **2021,** *1* (1), 41.
7. Wellstead, P. *Frequency Response Analysis* 1983.
8. Gabrielli, C. *Identification of electrochemical processes by frequency response Analysis*; Universite P et M Curie: 3 March 1998, 1998.
9. Choi, W.; Shin, H.-C.; Kim, J. M.; Choi, J.-Y.; Yoon, W.-S., Modeling and Applications of Electrochemical Impedance Spectroscopy (EIS) for Lithium-ion Batteries. *J. Electrochem. Sci. Technol* **2020,** *11* (1), 1-13.
10. Lissajous, J. A., Mémoire sur l'étude optique des mouvements vibratoires. *Annales de Chemie et de Physique* **1857,** *3* (51), 147-231.
11. Van Ingelgem, Y.; Tourwe, E.; Blajiev, O.; Pintelon, R.; Hubin, A., Advantages of Odd Random Phase Multisine Electrochemical Impedance Measurements. *Electroanalysis* **2009,** *21*, 730-739.
12. Ellis, C. L.; Smith, E.; Javaid, H.; Berns, G.; Venkataraman, D., Ion migration in hybrid perovskites: Evolving understanding of a dynamic phenomenon. In *Perovskite Photovoltaics*, Elsevier: 2018; pp 163-196.
13. Li, Z.; Ge, H.; Zhang, J., Analytical Solution to the Impedance of Electrode/Electrolyte Interface in Lithium-Ion Batteries. *Journal of The Electrochemical Society* **2015,** *162*, A7037-A7048.
14. Yang, X.; Rogach, A. L., Electrochemical Techniques in Battery Research: A Tutorial for Nonelectrochemists. *Advanced Energy Materials* **2019,** *9* (25), 1900747.
15. Westerhoff, U.; Kurbach, K.; Lienesch, F.; Kurrat, M., Analysis of Lithium-Ion Battery Models Based on Electrochemical Impedance Spectroscopy. *Energy Technology* **2016,** *4* (12), 1620-1630.
16. Deivanayagam, R.; Cheng, M.; Wang, M.; Vasudevan, V.; Foroozan, T.; Medhekar, N. V.; Shahbazian-Yassar, R., Composite Polymer Electrolyte for Highly Cyclable Room-Temperature Solid-State Magnesium Batteries. *ACS Applied Energy Materials* **2019,** *2* (11), 7980-7990.
17. Méry, A.; Rousselot, S.; Lepage, D.; Dollé, M., A Critical Review for an Accurate Electrochemical Stability Window Measurement of Solid Polymer and Composite Electrolytes. *Materials* **2021,** *14* (14), 3840.
18. Li, Z.; Zhao, Y.; Tenhaeff, W. E., Determining the Absolute Anodic Stability Threshold of Polymer Electrolytes: A Capacity-Based Electrochemical Method. *Chemistry of Materials* **2021,** *33* (6), 1927-1934.
19. Asakura, R.; Duchêne, L.; Kühnel, R.-S.; Remhof, A.; Hagemann, H.; Battaglia, C., Electrochemical Oxidative Stability of Hydroborate-Based Solid-State Electrolytes. *ACS Applied Energy Materials* **2019,** *2* (9), 6924-6930.
20. Dewald, G. F.; Ohno, S.; Kraft, M. A.; Koerver, R.; Till, P.; Vargas-Barbosa, N. M.; Janek, J.; Zeier, W. G., Experimental Assessment of the Practical Oxidative Stability of Lithium Thiophosphate Solid Electrolytes. *Chemistry of Materials* **2019,** *31* (20), 8328-8337.
21. Cao, X.; Cheng, J.; Zhang, X.; Zhou, D.; Tong, Y., Composite Polymer Electrolyte based on Liquid Crystalline Copolymer with High-temperature Stability and Bendability for All-solid-state Lithium-ion Batteries. *International Journal of Electrochemical Science* **2020,** *15* (1), 677-695.
22. Evans, J.; Vincent, C. A.; Bruce, P. G., Electrochemical measurement of transference numbers in polymer electrolytes. *Polymer* **1987,** *28* (13), 2324-2328.
23. Bruce, P. G.; Vincent, C. A., Steady state current flow in solid binary electrolyte cells. *Journal of Electroanalytical Chemistry and Interfacial Electrochemistry* **1987,** *225* (1), 1-17.
24. Chintapalli, M.; Timachova, K.; Olson, K. R.; Mecham, S. J.; Devaux, D.; DeSimone, J. M.; Balsara, N. P., Relationship between Conductivity, Ion Diffusion, and Transference Number in Perfluoropolyether Electrolytes. *Macromolecules* **2016,** *49* (9), 3508-3515.

25. Pesko, D. M.; Timachova, K.; Bhattacharya, R.; Smith, M. C.; Villaluenga, I.; Newman, J.; Balsara, N. P., Negative Transference Numbers in Poly(ethylene oxide)-Based Electrolytes. *Journal of The Electrochemical Society* **2017,** *164* (11), E3569.
26. Oh, P.; Lee, H.; Park, S.; Cha, H.; Kim, J.; Cho, J., Improvements to the Overpotential of All-Solid-State Lithium-Ion Batteries during the Past Ten Years. *Advanced Energy Materials* **2020**.
27. Liu, Y.; Lin, D.; Liang, Z.; Zhao, J.; Yan, K.; Cui, Y., Lithium-coated polymeric matrix as a minimum volume-change and dendrite-free lithium metal anode. *Nature Communications* **2016,** *7* (1), 10992.
28. Liu, H.; Cheng, X.-B.; Xu, R.; Zhang, X.-Q.; Yan, C.; Huang, J.-Q.; Zhang, Q., Plating/Stripping Behavior of Actual Lithium Metal Anode. *Advanced Energy Materials* **2019,** *9* (44), 1902254.

Chapter 4 Objective

Abstract

This thesis serves two targets in one step, by combining the green and sustainable material into safer solid polymer electrolytes (SPEs). In this chapter, we briefly address the need for SPEs after a detailed discussion on lithium batteries and their components in the previous chapter. Further, the proposed tasks in the project have been presented in three subsequent chapters. A glimpse of the techniques and tools to be used in the project has been highlighted in the last section.

4.1 Core of the research

The clean energy transition can only be bestowed globally if energy storage devices are revolutionized on a bigger and macroscopic level involving transport and the power grid sector. Lithium batteries, an exciting technology, have been the first choice owing to their energy and power density compared to conventional batteries in the market. The quest to improve lithium battery technology remains a hot topic in the academic and industrial research community towards affordability, sustainability and environment friendliness. The state-of-the-art materials and their performance fulfil the energy needs of micro and semi-macro devices which use inorganic electrodes and organic electrolytes.[1] To pace up the next-generation devices and their efficiency, new electrodes and compatible electrolytes have been undergoing constant innovation. Besides that, the current technology also poses serious concerns apart from the incapacity to meet the demand for high performance. Therefore, it justifies the clear need to discover new electrodes with higher capacity, faster and higher cycling efficiency along cost effectiveness. However, electrolytes equally need to be looked upon as they provide channels for ion shuttles. Nevertheless, higher performance with a good compromise in safety could not be achieved without revisiting the existing materials and their modification.

Due to some concerns, such as leakage with liquid electrolytes, and flammability with lithium, the idea of shifting from liquid to gel or solid electrolytes tends more tempting. However, this not only enhances the safety but also opens its accessibility to a wide range of electrodes for superior performance.[2, 3] Electrolytes, specifically solid polymer electrolytes and composite polymer electrolytes as depicted in Figure 4.1, are smart choices in shifting towards safe, sustainable and cost-effective alternatives to liquid electrolytes. SPE provides lightweight, flexibility, and robustness to the electrolyte-electrode sandwich films. The major drawback underlying SPEs is their slower diffusion of Li^+ ions and conductivity at room and lower temperatures, indicating a large ion transport activation barrier. The trade-off between mechanical and electrochemical properties is one of the key challenges in SPEs. A wide interest also has emerged in interface engineering for lowering interfacial resistance by using surface polymer coatings or catholyte to lower the interfacial resistance. Nevertheless, it remains a top priority to focus on the flexibility and fast kinetics of Li-ion in SPEs at both bulk and interface of the electrolyte-electrode in all solid-state batteries (ASSBs). Away from the technical shortcomings, one of the major worries is the environmental benignity of the materials, either be it for liquid electrolyte-based or solid-state lithium batteries. While most battery

materials are largely based on toxic and hazardous chemicals, it questions the credibility of green and clean energy on a mass approach. Given high toxic footprint at each level of production, each component of the batteries has to be looked for alternatives, synthesized via a greener approach with minimal hazardous materials. This thesis thrives to contribute in that direction with an emphasis on the electrolyte. Solid polymer electrolytes derived or sourced via green /naturally occurring materials will not only fulfil the drawback of LE but also complement the lower toxicity. They not only lower the total cost but also ease the handling and manufacturing process. The last section of Chapter 1 throws light on the impact of hazardous materials in state-of-the-art LIBs.

Addressing the need of hour, stressing an environment-friendly solid electrolyte, it is speculated that bio-derived cyclic carbonate-based monomers could be interesting candidates for polymerization. These functional molecules provide a great control on the tuneability of the targeted structure and properties. Polycarbonates are already well-investigated systems as inspired by low molecular weight carbonates-based liquid electrolytes. Interesting properties like solvation, dielectric constant and freedom to be grafted as a side chain in a polymer make carbonates widely accepted.[4] Another interesting but least explored polymer is poly(hydroxyurethane), which inspired our investigation.

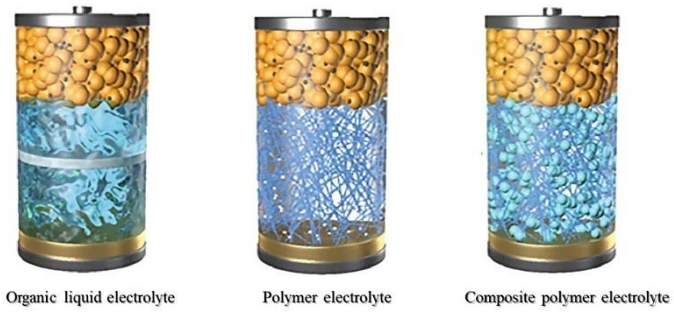

Figure 4.1: Representation of lithium batteries with different type of electrolytes. Reproduced with permission,[2] copyright 2023, Springer.

4.2 The project

This thesis involves research activities carried out in the frame of the BRIDGE-FUSE project funded by INNOVIRIS, Brussels, Belgium. As one of the key members of the consortium, the key tasks of UCLouvain involved the green electrolyte design, development, and validation at the coin cell level. Following the theme, the project

focuses on the synthesis of the bio-based electrolytes via a non-toxic and green approach via facile polymerization techniques. Our investigation on polymer electrolytes is largely focused on molecules with cyclic carbonate functionality and their blend in the first section. The choice of cyclic carbonates is motivated by the commercial liquid electrolytes, mostly consisting of a mixture of cyclic and acyclic carbonates. The carbonate contains one carbonyl oxygen and two oxygens covalently linked with single-bond carbon, which are crucial for solvation and transport of Li-ion in trade with viscosity and dielectric constant of the molecules. The project is split into three sections as highlighted. Chapter 5 is based on unopened cyclic carbonate rings, and Chapter 6 discusses ring-opened cyclic carbonates leading to poly(hydroxyurethane) networks. Finally, composite polymer electrolytes comprising inorganic fillers are described in Chapter 7 (as depicted in Figure 4.2). The thesis intends to demonstrate PHU and cyclic carbonate based polymers which offer significant potential and have not been investigated as electrolytes for lithium metal batteries.

The first section (Chapter 5) involves the preparation and demonstration of bio-based cyclic carbonated soybean oil (CSBO) electrolytes with highly dissociated lithium salt. The ionic conductivity is assured via interaction of lithium ions with oxygens from carbonates and esters in CSBO. The novel synthetic route for CSBO is sustainable, produced at the kilo-gram scale and has been developed by our collaborator, at CERM from ULiège, who provided the CSBO stock required for the

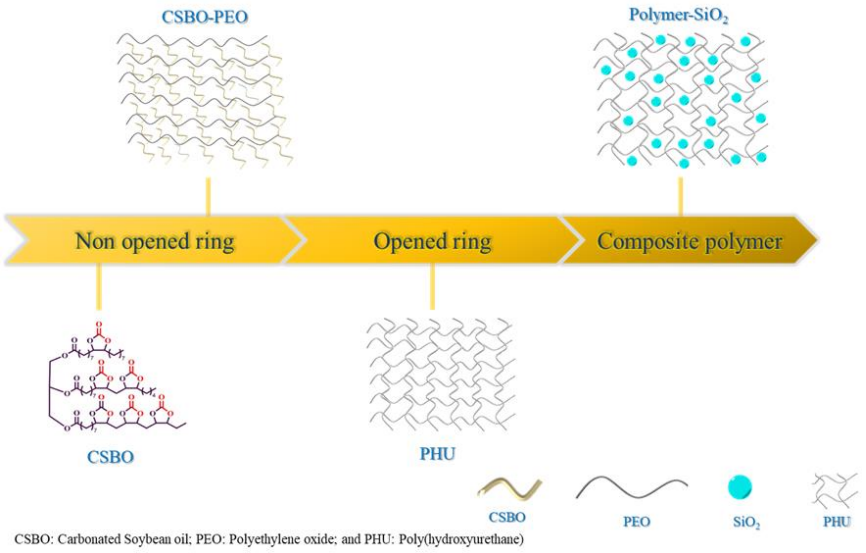

Figure 4.2: Flow diagram of polymers designed in the project from CBSO to PHU with schematics.

realization of this thesis. Our study involves experiments on the viability of the CSBO-based electrolytes for their mechanical properties, and thermal analysis for crystallinity and stability at higher temperatures. Finally, the material is tested in full-cell prototypes with various parameters and conditions followed by a fundamental understanding of primary electrochemical properties.

The further roadmap in the thesis is targeted at tuning the mechanical properties of CSBO along the lines of improving the ionic conductivity. The task is to be carried out by screening various polymers or cross-linkers which are also intended to improve the existing performance besides conductivity. Two possibilities have been highlighted here: a) preparing blends with CSBO and b) preparing networks by complete/partial ring opening of the cyclic carbonates. In the first approach, a physical blend is targeted by incorporating a mechanically superior polymer with a large number of ether units for lithium-ion coordination. CSBO's viscous nature blended with poly(ethylene oxide) (PEO) is chosen for the compromised adhesive properties as represented in Figure 4.3 (left). A comparative investigation has been proposed for a better understanding of the utilization of PEO into the composite.

Carrying forward, the next step explores second possibilities as presented above. The cyclic carbonate ring of CSBO will be opened to form poly(hydroxyurethane) (PHU) networks in a series of analogues, as indicated in Figure 4.3 (right). PHU has been a popular material for the coating and paint industry because of its good binding and adhesive nature. Poly(ethylene glycol) terminated-amine (PEGTA) is chosen as a cross-linker due to its high reactivity towards cyclic carbonates. Also, a mixture of cross-linkers is proposed for controlling the cross-linking density and rigidity of the PHU network. The PHU networks under consideration are thus composed of carbamate bonds and ethylene oxide groups, which are speculated to bring decent mechanical and conductivity properties, respectively.

The last section is intended to explore the possibility of composite polymer electrolytes by incorporation of silicon dioxide nanoparticles and to analyze the synergic effect of fillers into our polymers on fundamental properties. The goal is to utilize the functional groups, modify the glass transition temperature, decrease PEO crystallinity and increase the lithium ions transport.

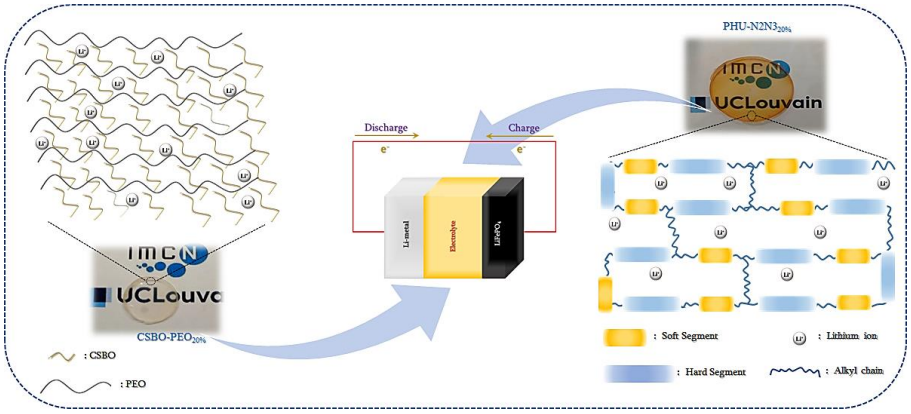

Figure 4.3: Scheme of CSBO-PEO and PHU with their picture as solid polymer electrolyte for lithium metal batteries.

In addition to the design and synthesis of polymer electrolytes, our task also involves their validation by characterization and testing in real prototypes. Structural characterization such as infrared spectroscopy has been a major tool for identification with thermal measurements to qualitatively describe the state and stability of the materials. As far as electrochemistry is concerned, various experiments have to be performed with specific cell configurations. Keeping in mind about low toxicity of $LiFePO_4$ (LFP), the latter is to be used in almost all the full metal batteries testing for the cycling measurements.

There are multiple interfaces in the full cell, which is a large domain of research playing a crucial role in its performance. Thus, interfacial investigation via techniques such as X-ray photoemission spectroscopy (XPS) has been included in the list of crucial measurements. With all these highlighted tasks, we attempt to provide alternatives to hefty, expensive and complex polymer electrolytes with our bio-sourced polymer electrolytes for lithium metal batteries.

Bibliography

1. Sun, Y.-K., Promising All-Solid-State Batteries for Future Electric Vehicles. *ACS Energy Letters* **2020,** *5* (10), 3221-3223.
2. Liang, H.; Wang, L.; Wang, A.; Song, Y.; Wu, Y.; Yang, Y.; He, X., Tailoring Practically Accessible Polymer/Inorganic Composite Electrolytes for All-Solid-State Lithium Metal Batteries: A Review. *Nano-Micro Letters* **2023,** *15* (1), 42.
3. Janek, J.; Zeier, W. G., A solid future for battery development. *Nature Energy* **2016,** *1* (9), 16141.
4. Xia, S.; Wu, X.; Zhang, Z.; Cui, Y.; Liu, W., Practical Challenges and Future Perspectives of All-Solid-State Lithium-Metal Batteries. *Chem* **2019,** *5* (4), 753-785.

Chapter 5.1 Bio-based solid electrolytes bearing cyclic carbonates

Abstract

Green resources for lithium-based batteries excite many researchers due to their eco-friendly nature. In this work, we report on a sustainable bio-based solid-state electrolyte based on carbonated soybean oil (CSBO) obtained by organocatalyzed coupling of CO_2 to epoxidized soybean oil. CSBO coupled with lithium bis(trifluoromethanesulfonyl)imide salt on a bio-based cellulose separator resulted in free standing membranes. Those membranes on electrochemical measurements exhibit ionic conductivity of ~ 10^{-3} S cm^{-1} at 100 ºC and ~10^{-6} S cm^{-1} at room temperature with wide electrochemical stability window (up to 4.6 V *vs.* Li/Li^+), transference number up to 0.39 at RT. Further investigations on the galvanostatic charge-discharge of $LiFePO_4$ cathodes with CSBO-based electrolyte membranes and lithium metal anodes, deliver the gravimetric capacity of 112 mAh g^{-1} and 157 mAh g^{-1} at RT and 60 ºC, respectively, providing a promising direction to further develop bio-based solid electrolytes for a sustainable solid-state lithium batteries.

5.1.1 Introduction

Energy storage devices like metal-ion, metal-air and other classes of batteries have revolutionized our modern life by entering in numerous everyday life and industrial applications ranging from portable electronic devices, electric vehicles and stationary power grids, just to name a few. In this context, lithium-ion batteries are of much interest for more than three decades owing to their high energy density (250 Wh Kg^{-1}) and durability. Until now, the market is dominated by lithium-ion batteries based on conventional liquid electrolytes with lithium ions shuttling between cathodes like $LiFePO_4$ (LFP), $LiCoO_2$ (LCO), *etc*, and anodes based on graphite and silicon,[1] although lithium metal based anodes with their lower potential and higher capacity (3860 mAh g^{-1}) have drawn researchers' interest for a longer time.[2,3] Lithium metal anodes exposed to liquid electrolytes soaked in separators pose major issues like safety, electrolyte leakage, dendrites growth ultimately resulting in short-circuit, intense heating and flammability.[4-6] That's why there is a strong need and increasing market demand for solid-state batteries containing solid electrolytes (SEs) as a potential alternative.[7,8] SEs can provide not only high energy and power density, but may also enhance the safety and durability of batteries.[9] In addition to the design of new solid electrolytes, a large number of studies are also being dedicated to the understanding of the long cycling cells failure via interfacial studies and thus engineering interfaces for beneficial solid electrolyte interface (SEI) species either by surface treatments and computational predictions.[10-12] For example, self-healing materials and coatings gained focus on preventing physical and chemical damage and achieving sustainability, lower environmental impact over the lifetime and better acceptability.[13-16]

As lithium-metal batteries are maturing with time, the clock ticks not only on the improvement of existing Li-ion cells but also beyond Li-ion batteries technologies keeping in mind that the former poses issues like stability, Li-limited reserve and recycling.[17-20] Alternatives like sodium, potassium, magnesium-based batteries, just to name a few, have been actively looked upon.[21-24] Sustainable materials have also reached momentum for the fabrication of the next generation of batteries. For instance, sustainable gel-polymer/solid-state electrolytes are being developed to overcome the hurdles of safety, stability and dendrite growth.[25-28] Recently, Bella and

co-workers designed lignin-based membranes by crosslinking of a pre-oxidized Kraft lignin matrix with an ethoxylated difunctional oligomer. Those gel polymer electrolytes (GPEs) exhibited decent conductivity of 10^{-3} S cm^{-1} and > 4 V stability window with K^+.[29] However, it's still early to compare the market reality of other metal-ion batteries to lithium-based ones due to insufficient understanding of those new technologies. All-solid-state batteries based on lithium are thus still a strong bet for high energy and power density immediate future needs toward a clean energy path.[26]

Upon discovery of poly(ethylene oxide) (PEO) as an ion conductor by Wright[30] and Armand[31], PEO based solid polymer electrolytes (SPEs) got a lot of attention since they allow efficient dissolution and dissociation of lithium salts, ionic transport due to the so-called ion-hopping mechanism and the typical viscoelastic properties of polymers for the formation of free-standing membranes. However, PEO-based devices have demonstrated low to moderate performance in long run due to their low lithium transference number (< 0.2) and limited electrochemical stability window (< 4 V).[32] Moreover, PEO-based batteries need to operate at temperatures higher than the melting point of PEO (around 60 °C) since lithium ions transport is considerably slow-down in crystalline PEO domains. Research is thus now directed towards developing new SPEs outperforming PEO-based systems.

In recent years, electrolytes based on amorphous polycarbonates mimicking low molar mass carbonated liquid electrolytes have emerged as alternatives to PEO due to their lithium ions transport properties, high transference number, good electrochemical stabilities and tailored mechanical properties. Generally, cyclic carbonates were introduced as side-chains in polymers, while linear carbonates were incorporated in the polymer backbone. As a typical example, Chai *et al.* polymerized vinylene carbonate to obtain a linear polymer with cyclic carbonate in the polymer backbone.[33] Lex-Balducci *et al.* copolymerized a methacrylate bearing cyclic carbonate side-chains with oligo(ethylene glycol) methacrylate and prepared gel polymer electrolytes by swelling the accordingly obtained copolymers in a carbonate-based electrolyte.[34,35]

We investigated SPEs based on cyclic carbonate trifluoromethacrylate and vinylidene fluoride units[36] and random copolymers of n-butylacrylate and cyclic carbonate bearing acrylate.[37] Zhang *et al.* described a linear poly(propylene carbonate) providing an ionic conductivity of 10^{-4} S/cm at room temperature.[38] Tominaga *et al.* synthesized linear poly(ethylene carbonate) that was further integrated in a hybrid membrane reaching an ionic conductivity of 10^{-5} S/cm at 30 °C.[39,40] In another study, Tominaga *et al.* combined carbonate and ether units in a copolymer, which was obtained by copolymerization of ethylene oxide with CO_2.[41] Copolymers composed of polyether segments and linear carbonates were reported by Mecerreyes *et al.*[42] The influence of the incorporation of cyclic carbonates within the chains was also studied by the same group.[43] The quest for environment-friendly electrolytes has motivated researchers to investigate "green" polymers in SPEs.[44] These polymers include poly(lactic acid)[45,46] and poly(urethane)s due to their high degree of tuneability in mechanical properties and conductivity as highlighted in recent reviews and articles.[13,47-50] In this context, polymers based on vegetable oils with long fatty acids,[51-53] cellulose,[54] gums [55] and others similar bio-derivatives,[56,57] are of high interest as potential ion conductors owing to their ether and carbonyl functional groups.

Motivated by the urgent need of more sustainable materials for battery applications, we designed a novel bio- and CO_2-based solid electrolyte derived from soybean oils bearing cyclic carbonate units on triglyceride fatty acid segments and CO_2 (as shown in Scheme 1). The cyclic carbonated soybean oil (CSBO) is not only conferring a sustainable character to the electrolyte for lithium-ion battery, but it is also environmentally safe, easy to process and easily accessible at the multiKg scale.[58] In addition, a high density of polar cyclic carbonate units can improve the salt dissolution and reduce the activation energy for ion hopping from one polar group to another.[59] We investigate the influence of the electrolyte system loaded with different amounts of LiTFSI, characterized for electrochemical and thermal properties. We also demonstrate the galvanostatic charge-discharge of LFP and lithium metal coin cell with our bio-based CSBO solid electrolyte.

5.1.2 Material and methods

Epoxidized soybean oil (ESBO) was kindly donated by Vandeputte Oleochemicals (Belgium). Carbon dioxide (CO_2, N48) was supplied by Air Liquide. 1,3-bis (2 hydroxyhexafluroisopropyl) benzene was purchased from Fluorochem. Tetrabutylammonium bromide (TBABr, > 99%), bis(trifluoromethane)sulfonimide lithium (LiTFSI) and cellulose separator (TF48-50 (50 µm x 66 mm)) were purchased from Sigma Aldrich and TOB, respectively. Propylene carbonate (PC) was purchased from Sigma Aldrich. All reactants and catalysts were used as received, without any further purification.

5.1.2.1 Characterization techniques

FTIR spectroscopy*:* FTIR measurements were carried out on a Nicolet IS5 spectrometer (Thermo Fisher Scientific) equipped with a diamond attenuated transmission reflectance (ATR) device, 32 scans were recorded for each sample for different batches over the range of 4000-500 cm^{-1} with a normal resolution of 4 cm^{-1} and spectra were analysed with the ONIUM^{TM} software.

DSC: DSC analysis was carried out on a Q1000 TA Instruments using standard aluminium pans, calibrated with indium and nitrogen was used as a purge gas. The samples were analysed at a heating rate of 10 °C min^{-1} over a temperature range from −80 °C to 200 °C under N_2 atmosphere and the analysis was repeated more three times. For all spectra, second heating and cooling was plotted and analysed.

TGA: TGA was carried out using a Q500 from TA Instruments. Thermal degradation of samples was measured at a heating rate of 20 °C min^{-1} over the temperature range of 0 to 600 ºC under a N_2 atmosphere.

Rheology*:* Rheological properties of samples were measured on an ARES (Advanced Rheometric Expansion System) Rheometric Scientific rheometer, equipped by two parallel plates geometry at a frequency (1 Hz), a strain (1%) and the measurements were carried out at 25 ºC. The evolutions of storage modulus and complex viscosity were monitored as a function of angular frequency.

XPS*:* XPS was performed using an SSI X-Probe (SSX 100/206) photoelectron spectrometer from Surface Science Instruments equipped with a monochromatized Al Kα (200 W) X-ray source. The batteries were disassembled and samples were mounted on an XPS sample holder in a glovebox prior to transferring to the XPS vacuum chamber in the flux of argon atmosphere. All of the binding energies were calculated according to the C– (C, H) component of the C 1s peak fixed at 284.8 eV. Data analysis was carried out using CasaXPS software. For the survey scan, a 1.0 eV step size was used and a 0.1 eV step size was used for high-resolution scans for all elements with 150 energy steps. Multiple samples were analysed to validate data.

5.1.2.2 Electrochemical analysis

Electrochemical analysis of potentiostatic electrochemical impedance spectroscopy (PEIS), linear sweep voltammetry (LSV), chronoamperometry (CA) and galvanostatic cycling potential limitation (GCPL) were carried out on Biologic BCS-COM and VMP3 multichannel potentiostats using CR2032 coin cells.

PEIS: Ionic conductivity of CSBO SEs was determined by PEIS for symmetric stainless steel (SS|SE|SS) coin cells in the frequency range of 7 MHz – 50 mHz, with applied single sinusoidal A.C. excitation voltage of 10 mV. The temperature dependence measurements were carried out from 20 ºC to 100 ºC by gradually increasing temperature at the rate of 0.33 ºC min^{-1}. One hour was waited between each measurement to reach an equilibrium state. The experiments were repeated for more than two time on several cells over two or more different batches to optimise and avoid any errors.

LSV: Measurements were performed at various temperatures on asymmetric CR2032 coin cell as (Li|$CSBO_{x\%}$-SE|Al), (Li|$CSBO_{x\%}$-SE|Al-C|) and (Li|$CSBO_{x\%}$-SE|SS), over the potential range of 0 – 5 V (*vs.* Li/Li^+) at the scan rate of 0.5 mV s^{-1} at 30 ºC and 60 ºC over few times.

$\boldsymbol{t_{Li^+}}$*:* Transference number measurements were carried out on symmetric lithium metal cells (Li|$CSBO_{x\%}$-SE|Li) fabricated over various membranes by following the Bruce-Vincent method. Chronoamperometry with D.C. voltage of 10 mV was

performed followed by PEIS measurements in the frequency range of 7 MHz – 50 mHz, at 10 mV of A.C. excitation voltage at 30 ºC and 60 ºC. PEIS measurements were recorded before and after steady-state (before and after polarization).

GCPL: Galvanostatic charge-discharge cycling and rate capabilities measurement for the LFP|$CSBO_{x\%}$-SE|Li and LFP|$CSBO_{x\%}$-SE-PX|Li cells were tested with a Biologic BCS-COM cycler for various batches of electrolytes at different temperatures with and without propylene carbonate. The slurries for the cathodes were prepared from $LiFePO_4$, Super P, poly(vinylidene difluoride) (PVDF), CSBO and N-methyl pyrrolidone (NMP) via grinding using a mortar pestle and were further casted on carbon-coated Al-foils using the doctor-blade technique. The coated slurries were then dried in an air oven for more than 6 h at 60 ºC prior to vacuum drying at 120 ºC for more than 24 h. The cathode components were maintained in the weight ratio of 7:2:1 and 5:2:1:2 for LFP, Super P and PVDF without CBSO and with CBSO slurries, respectively after several trials. The cathodes and anodes were cut into disks of 14 mm diameter for the electrolyte membranes of 16 mm in diameter for the cell assembly.

5.1.3 Synthesis

5.1.3.1 Synthesis of carbonated soybean oil (CSBO)

Bio-based cyclic carbonated soybean oil (CSBO) was synthesised by reacting supercritical CO_2 with epoxidized soybean oil (ESBO) using a bicomponent organocatalytic system that combined tetrabutylammonium bromide (TBAB) as catalyst and 1,3-bis(2-hydroxyhexafluroisopropyl) benzene (HFI) as an activator as reported.[60-63] The coupling reaction was performed at 100 ºC and 100 bar using 2.5 wt% of organocatalyst (TBAB/HFI molar ratio of 1) for 10 h. These optimised reaction conditions ensured the fast and full conversion of epoxy into corresponding cyclic carbonates.

In a typical experiment, ESBO (30 g), TBAB (0.75 g, 2.32 mmol) and HFI (0.57 mL, 2.32 mmol) were introduced in an 80 mL high-pressure cell equipped with a mechanical stirrer. The cell was closed, the temperature and pressure were

equilibrated at 100 ºC and 100 bar for 10 h. After reaction, the pressure was released through the outlet and a viscous product was recovered.

The conversion of the epoxide (ESBO) into cyclic carbonates (CSBO) was investigated by ^{1}H NMR spectroscopy (Figure S5.1.1) by the disappearance of the characteristic peaks of epoxides, –CH–O– and –CH_2–O– at 2.7 and 3.2 ppm, respectively. New peaks attributed to –CH–O–C(=O)O– and –CH_2–O-C(=O)O– cyclic carbonates appeared at 4.5 and 5.0 ppm, respectively. The formation of cyclic carbonates was further confirmed by FTIR (Figure S5.1.2) by the disappearance of the characteristic band of the epoxy groups of ESBO at 914 cm^{-1} and the presence of a new band at 1790 cm^{-1} corresponding to the carbonyl group of CSBO.

5.1.3.2 Preparation of solid electrolytes (SEs)

SEs were prepared from CSBO loaded with various amount of LiTFSI by a one-pot process. Prior to preparing the formulation, CSBO was degassed by thermal treatment at 70 ºC overnight in a vacuum oven to remove trapped impurities. CSBO (1.0 g, 0.8 mmol, cyclic carbonate average content per molecule = 6, molar mass approximated to 1250 g mol^{-1})[64-68] was dissolved in DMC or THF (0.75 mL) and loaded with different amounts of LiTFSI (0-50 wt% labelled in subscript). The obtained viscous solutions were drop-casted on cellulose support and then dried in a vacuum oven at 60 ºC for more than 12 h and later at 60 ºC for 5 h in the glove box. The cellulose support allowed the formation of self-standing SE membranes containing 9.9 wt% of $CSBO_{50\%}$-SE (50% represent wt% of LiTFSI). All the structural, thermal and mechanical characterization was performed on polymers without separator.

5.1.4 Results and Discussion

5.1.4.1 Mechanical and thermal properties of CSBO-LiTFSI composites

The synthesis and chemical structure of CSBO-LITFSI are depicted in Scheme 5.1.1. The successful transformation of epoxide groups into carbonate ones was evidenced by ^{1}H NMR (Figure S5.1.1) and FTIR (Figure S2) spectroscopies. All the investigated CSBO-LiTFSI samples behaved as viscous liquids with a slight shear thinning behaviour.[69] The influence of LiTFSI salt concentration on the shear behaviour was

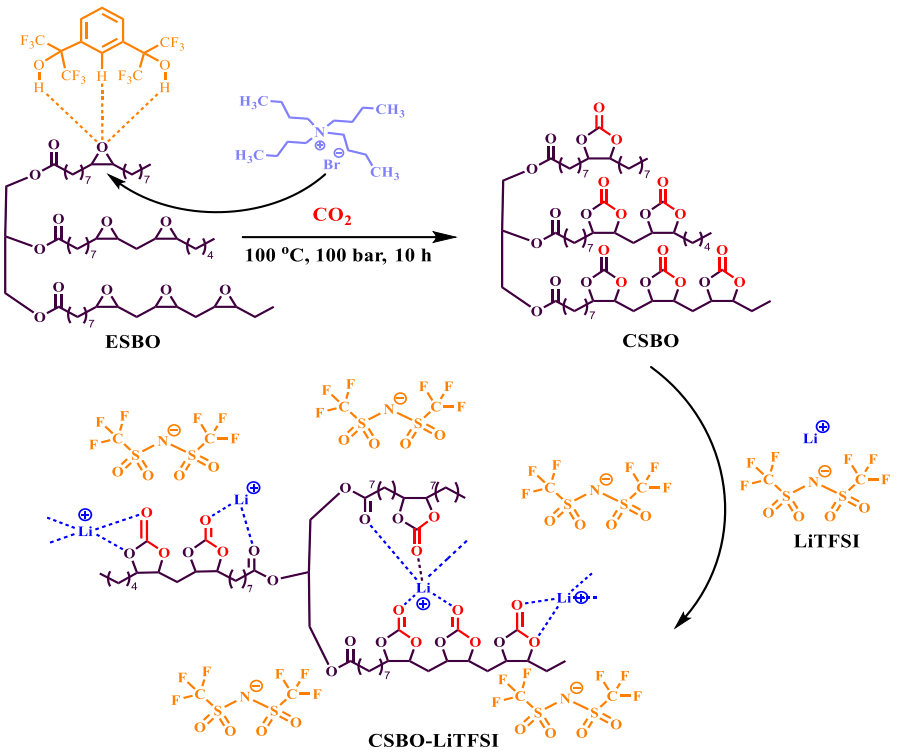

Scheme 5.1.1: Synthesis of carbonated soybean oil (CSBO) along with CSBO molecule interacting with LiTFSI.

investigated by measuring the complex viscosity at a frequency of 1 Hz (Figure 5.1.1a). The complex viscosity significantly increased with the amount of added LiTFSI. We assume that the interactions between Li^+ ions and cyclic carbonates groups in CSBO allow not only efficient dissolution of LiTFSI in CSBO but also intermolecular interactions between CSBO molecules and stiffening of the CSBO molecules, both resulting in an increased viscosity. The amorphous nature of CSBO-LiTFSI samples was confirmed by differential scanning calorimetry (DSC) (Figure S5.1.3). Indeed, CSBO-LiTFSI samples only show a T_g, whose value is almost linearly increasing with the amount of added LiTFSI (Figure 5.1.1b). This can be related to the decreased mobility of aliphatic soft segments in CSBO with higher LiTFSI salt content in line with inter- and intramolecular Li^+/carbonate interactions as discussed above.

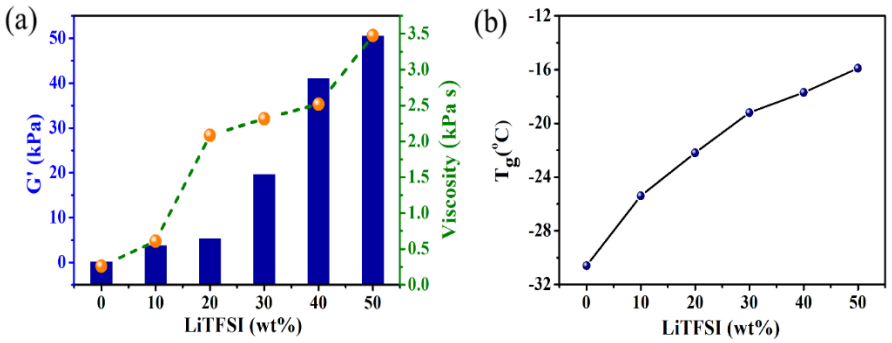

Figure 5.1.1: a) Storage modulus and viscosity at 25 °C and b) Glass temperatures (T_g) of CSBO-LiTFSI solid electrolytes with varying LiTFSI content (without cellulose paper).

In addition, the T_g remains always well below 0 °C even for the highest LiTFSI loading (50 wt%). A low T_g is essential for the adhesive nature of the material, which in turn facilitates good contact and wettability with the electrode interface.[60,70] Nevertheless, since CSBO-LiTFSI mixtures are highly viscous liquids, they are too soft to form self-supporting membranes and to be used as such in state batteries. This is the reason why solid electrolyte membranes (see further electrochemical characterizations) have been formed by casting the CSBO-LiTFSI mixtures directly in cellulose/filter paper, the latter playing the role of a mechanically supporting membrane or separator (see experimental section). Cellulose has indeed been selected as bio-based supporting materials.

Thermogravimetric analysis (TGA) was performed to evaluate the thermal stability of CSBO-LiTFSI samples. There was almost no weight loss beyond ~144 °C and ~193.33 °C for $CSBO_{40\%-50\%}$ (the numbers in subscript indicate the wt% of added LiTFSI and $CSBO_{0\%-30\%}$, respectively (Figure 5.1.2).

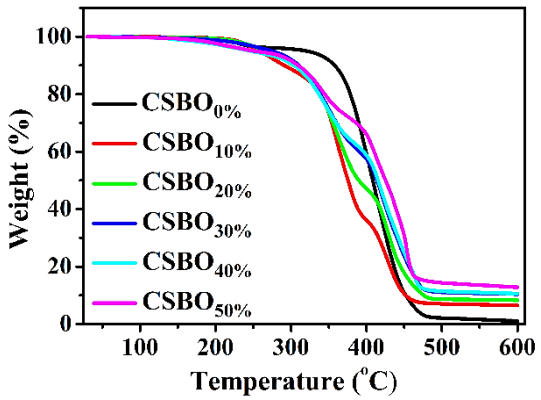

Figure 5.1.2: Thermogravimetric analysis of CSBO-LiTFSI ($CSBO_{x\%}$: x represent wt% of LiTFSI) samples.

This initial weight loss prior to major decomposition can be attributed to the release of moisture traces trapped by the LiTFSI salt. The major decomposition starts at around ~260 ºC for the CSBO-LiTFSI samples and continues till ~475 ºC. It is worth noting that the major decomposition was delayed at ~330 ºC for the CSBO sample with no added LiTFSI. This can be explained by the weakening of C-O bonds in the carbonate groups as a result of O-Li^+ coordination.[71] Moreover, the introduction of LiTFSI in CSBO leads to a more complicated decomposition pathway compared to pure CSBO (Figure 5.1.2).

5.1.4.2 Ionic conductivity of CSBO-LiTFSI solid electrolytes

The temperature-dependent ionic conductivities of cellulose paper supported CSBO-LiTFSI solid electrolytes (SEs) with LiTFSI content varying from 10 to 50 wt% were investigated by PEIS and displayed in the form of Nyquist plots as shown, in Figure 5.1.3a at 20 ºC (and Figure S5.1.4 for 60 ºC). The ionic conductivities (σ) of CSBO-based SEs were calculated using the following equation:

$$\sigma = \frac{l}{RS}$$

where R is bulk electrolyte ohmic resistance from AC impedance, l and S are the thickness and the surface area of the analysed polymer electrolyte thin film, respectively. As expected, the ionic conductivities of SEs were substantially increased with increasing temperature (20 – 100 ºC) due to the enhanced mobility of fatty acid chain segments and charge carriers. The sample loaded with 50 wt% LITFSI displays the best value of ionic conductivity (≈ 10^{-3} S cm^{-1} at 100 ºC and ≈ 10^{-6} S cm^{-1} at 20 ºC), as depicted in Figure 5.1.3b. The obtained ionic conductivity data were averaged over 4-5 different membranes measurements and were plotted with less than 4% error. As already pointed above, our electrolyte system based on CSBO is able to dissolve a high amount of salts. The results are in agreement with previous studies on polyether or polyester- based polycarbonates that provided the highest ionic conductivity at 30 ºC temperature. The conductivity data have also been fitted by using the Vogel–Fulcher-Tamman (VFT) equation over the temperature range of 20-100 ºC, where A is the pre-exponential factor, T is the absolute temperature, T_0 is the Vogel scaling temperature at which the free volume disappears or at which free entropy becomes zero, T_0 is related to T_g by T_g-50 K following an approximation,[74] E_α is the

Table 5.1.1: Activation energy and pre-exponential factor as calculated from the slope of VFT plots.

$CSBO_{LiTFSI}$ (wt%)	T_g (°C)	R^2	ln$A$	E_a (kJ/mol)
10%	-25.4	0.999	0.289	11.24
20%	-22.2	0.999	0.427	11.28
30%	-19.2	0.997	0.475	10.63
40%	-17.7	0.992	0.588	9.52
50%	-15.9	0.992	0.524	9.22

pseudoactivation energy of ion transport and k_b is Boltzmann constant:

$$\sigma T^{1/2} = A\mathrm{e}^{-\frac{E_\alpha}{k_b (T-T_0)}}$$

VFT model has been applied in order to demonstrate the effect of segmental motion on the overall conductivity above the glass transition temperature.[75, 76] The activation energy calculated from the slope of VFT plot is found to decrease with an increase in the salt content as shown in Figure 5.1.3d. This could be explained by the fact that, at higher salt content, ionic conductivity is not only solely based on ion-hopping of Li^+ ions from neighbouring carbonate groups, but also from diffusion of free ions dissolved in the fatty acid segments. The coupled effect of hopping and segmental motion in our system at a high percentage of salt could explain why less energy is required for the transport of ions under those conditions. Figure 5.1.3d shows the trend of activation energy, E_a and ionic conductivity as a function of the weight percentage of LiTFSI salt derived from the results plotted in Figure 5.1.3b and 5.1.3c. Table 5.1.1 shows the E_a calculated for the CSBO-LiTFSI SEs with various LiTFSI loading along with the pre-exponential factor and R^2 as corresponding fitting coefficient.

5.1.4.3 Linear sweep voltammetry (LSV) of CSBO-LiTFSI solid electrolytes

LSV measurements have been performed to investigate the electrochemical stability window (ESW) of the investigated of CSBO-LiTFSI SEs. The fabrication of the cell for LSV measurements is pictured in Figure 5.1.4a. The measurements were recorded on a wide voltage window of 0-5 V to probe the ESW with a scan rate of 0.5 mV/s versus Li/Li^+ at RT and 60 °C. The results reported in Figure 5.1.4b reveals that

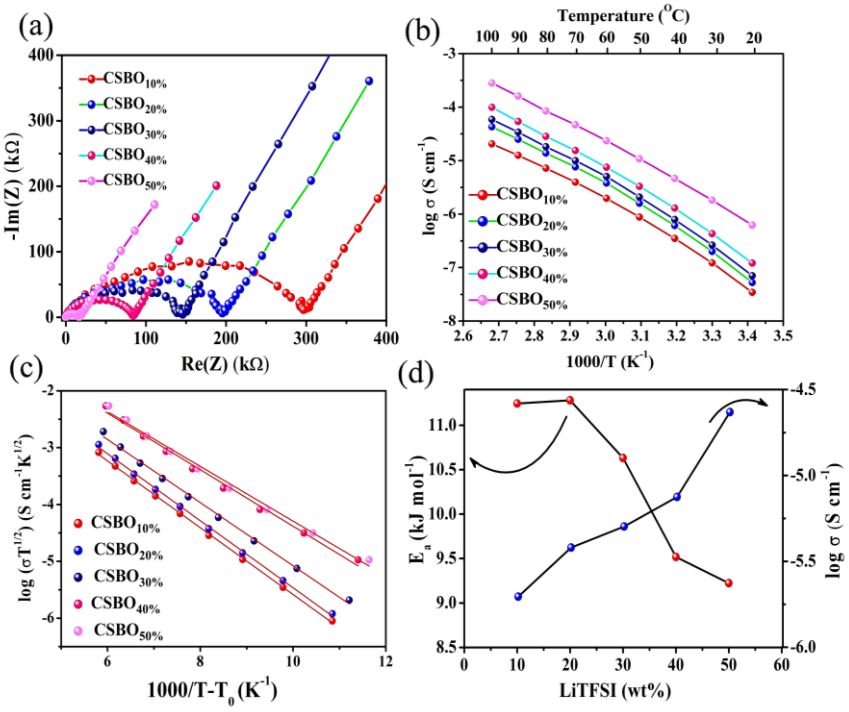

Figure 5.1.3: a) Nyquist plots of CSBO as a result of PEIS at 20 ºC. b) Temperature dependent ionic conductivity for CSBO-LiTFSI SEs (depicted as $CSBO_{x\%}$, x : wt.% of LiTFSI)). c) Temperature dependent ionic conductivity using the VFT model. d) Y1 axis as activation energy, E_a, derived using VFT equation from ionic conductivity plot and Y2 axis as conductivity at 60 ºC versus the weight percentage of LiTFSI in the SE.

CSBO-LiTFSI SEs were electrochemically stable over 4.8 V and 4.6 V (vs. Li/Li^+) at RT and 60 ºC, respectively. However, a slight higher cut off current density has been observed in the case of $CSBO_{50\%}$ owing to higher salt content. In addition, the ESW of CSBO-LiTFSI SEs was significantly decreased with increasing temperature along with increased cut-off current density for higher LiTFSI loading. The electrolyte decomposition at higher voltage was also cross-checked by changing the electrode from Al to Al-carbon foil and pure stainless-steel spacer (see experimental section), as shown in the Supporting Information section (Figure S5.1.5). From all these data, we did not evidence any Al corrosion with LiTFSI even at the higher potential of 4.5-5.0 V. The high ESW indicates the electrolyte compatibility with Li-electrodes and no oxidation was observed on the cathodic side. Consequently, bio-based CSBO-LiTFSI SEs appeared as promising electrolytes compared to PEO-based SPE for

lithium metal batteries in the operational window of most of standard commercial cathode materials.[77,78]

5.1.4.4 Transference number of CSBO-LiTFSI solid electrolytes

The lithium transference number(t_{Li^+}) of a symmetric Li|$CSBO_{50\%}$-SE|Li cells was determined by AC impedance combined with DC polarization. The t_{Li^+} value was calculated using Bruce-Vincent method,[79, 80] following the equation:

$$t_{Li^+} = \frac{I_{ss}(V - I_o R_o)}{I_o(V - I_{ss} R_{ss})} \quad (5.1.3)$$

where V is the DC applied potential, I_o and I_{ss} are the initial and steady state currents recorded with R_o and R_{ss} as initial and steady-state interfacial resistances from PEIS measurements at an AC sinusoidal voltage of 10 mV. Figure 5.1.4c shows that the polarization as a result of constant potential of 10 mV changes the interfacial resistance from 7350 to 7749 Ω, while current varies from an initial value of 1.26 μA to a stabilized value of 0.91 μA. The t_{Li^+} of $CSBO_{50\%}$ was then calculated to be 0.39±.0.03 at 30 ºC (t_{Li^+}= 0.31 ± 0.03 at 60 ºC as in Figure S5.1.5d), in agreement with results previously reported by Han.[73] This value is comparable to the commercial liquid electrolytes (0.31) and higher than PEO based polymer electrolytes (0.2).[81] A high t_{Li^+} is indeed a crucial parameter for the long-term cycling of batteries, allowing efficient diffusion and lower Coulombic efficiency loss.

5.1.4.5 Stripping and plating experiments for CSBO-LiTFSI solid electrolytes

The time-dependent voltage profile was investigated on symmetric Li|$CSBO_{50\%}$-SE|Li cell using galvanostatic cyclic measurements at current densities of 0.4 μA cm^{-2} at RT. Reversible plating/stripping of Li–metal was carried out for a prolonged time for an individual plating or stripping steps with charge and discharge for 1 h each at RT for Li-symmetric cells and was recorded an average overpotential in the range of 150 mV to 200 mV during initial cycles. As it can be observed in Figure 5.1.4d, a slight overpotential is associated with the bulk resistance of the electrolyte and electrolyte/electrode interface.[82] As a result of multiple cycling, the SEI layer stabilizes and facilitates the mobility of Li^+ ions at the interfaces. Steady-state was

observed to be achieved in less than 100 h with more or less constant overpotential. These constant values are mirroring a high Coulombic efficiency and reversibility in the electrochemical process with efficient Li-ion transport and stable interface that minimizes dendrites formation and growth.

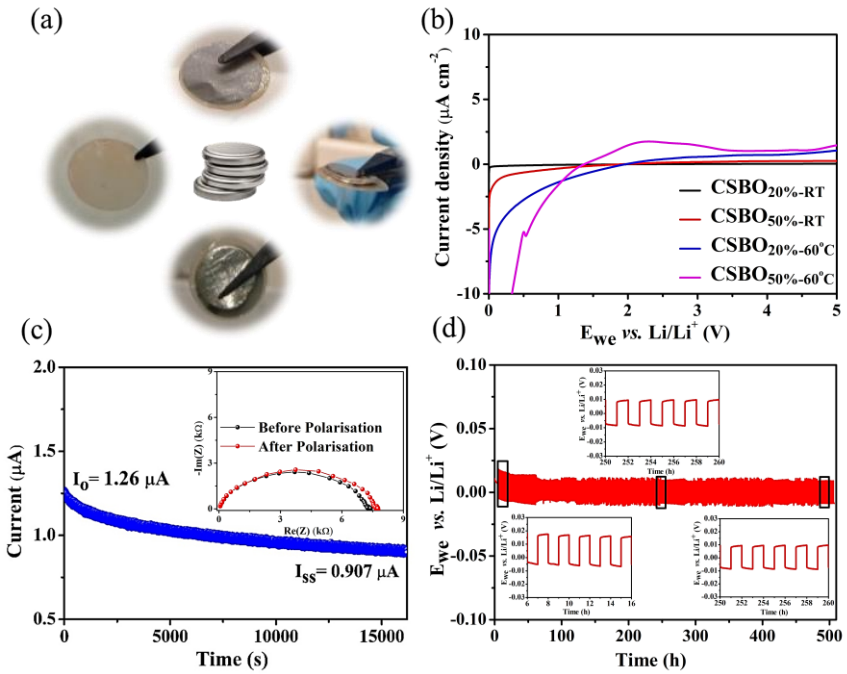

Figure 5.1.4: a) Cell fabrication for LSV measurements. b) Linear sweep voltametry of the CSBO$_{20\%}$-SE and CSBO$_{50\%}$-SE at RT and 60 ºC with Al and lithium electrodes. c) Chronoampereometry measurement at 10 mV for CBSO$_{50\%}$-SE with Nyquist plots for PEIS before and after polarization in the inset at RT. d) Galvanostatic charge-dicharge for stripping and plating of lithium in Li|CBSO$_{50\%}$-SE|Li symmetric cell with three enlarged plots at respective time demonstrating the constant over potential in the inset.

The constant overpotentials also confirm the formation of a stable and conducting SEI beneficial for a long cycling life of the cells.[1] As a result of minor fluctuations in cell temperature at RT, a slight increase in the overpotential is however recorded in day-night measurements. With these results, the good interfacial compatibility of the CSBO-LiTFSI SEs with Li-metal was revealed.

5.1.4.6 Li-metal batteries based on CSBO-LiTFSI solid electrolytes

In order to probe the applicability of our bio-based CSBO-LiTFSI SEs in all solid-state lithium metal batteries, battery prototypes constituting of a cathode based on $LiFePO_4$ (LFP), an anode of metal Li and CSBO-LiTFSI solid electrolytes have been constructed (abbreviated as LFP|$CSBO_{x\%}$-SE|Li) and their galvanostatic cycling performances have been measured at various temperatures with different concentration of salt loaded CSBO electrolytes over multiple batch of samples. The cathode has been formulated from LFP as electroactive material, carbon as conducting agent, PVDF as binder and CSBO as catholyte for ion transport (see experimental part). CSBO-LiTFSI/cellulose SEs have been used as electrolyte membrane. It is clearly supported by the PEIS measurements on the Li metal battery prototypes (Figure 5.1.5a) that CSBO-LiTFSI/cellulose SEs with higher LiTFSI content are characterized by a higher conductivity and will lead to better performance for the battery. Indeed, the $CSBO_{50\%}$-SE with the highest LiTFSI content shows a semi-circle in the Nyquist plot that correlates with an electric double layer capacitive behaviour (Figure 5.1.5a). The enhancement in the diffusion of Li^+ ion in the electrolyte to electrode interface for this electrolyte can be noted from the inclination of Warburg impedance away from the real resistance axis (subset of Figure 5.1.5a). In contrast, it was observed that the cells made with CSBO-LiTFSI/cellulose SEs with lower LiTFSI content ($CSBO_{20\text{-}40\%}$) could not deliver decent specific capacity at RT at 0.1C rate due to insufficient lithium-ion conductivity and transport.

Figure 5.1.5b shows galvanostatic charge-discharge voltage profile of the LFP |$CSBO_{50\%}$-SE| Li cell with obtained capacity of 124 mAh g^{-1} and 112 mAh g^{-1} in 1st charge and discharge cycle, respectively, at the 0.1C-rate at RT. The oxidation and reduction plateau for LFP has been observed at 3.52 V and 3.32 V approximately without significant polarisation in subsequent 26th and 100th cycles. However, galvanostatic charge-discharge curves at different C-rates show a drastic polarisation at a higher current density. Similarly, the change in oxidation potential, ΔE_{OO} and change in reduction potential, ΔE_{RR} for the corresponding charge-charge and discharge-discharge at 0.1C and 1C were observed to increase by 0.47 V and 0.51 V, respectively.The ΔE_{OR} between oxidation and reduction increased from 0.15 V at 0.1C to 1.18 V at 1C, as seen in Figure 5.1.5c.

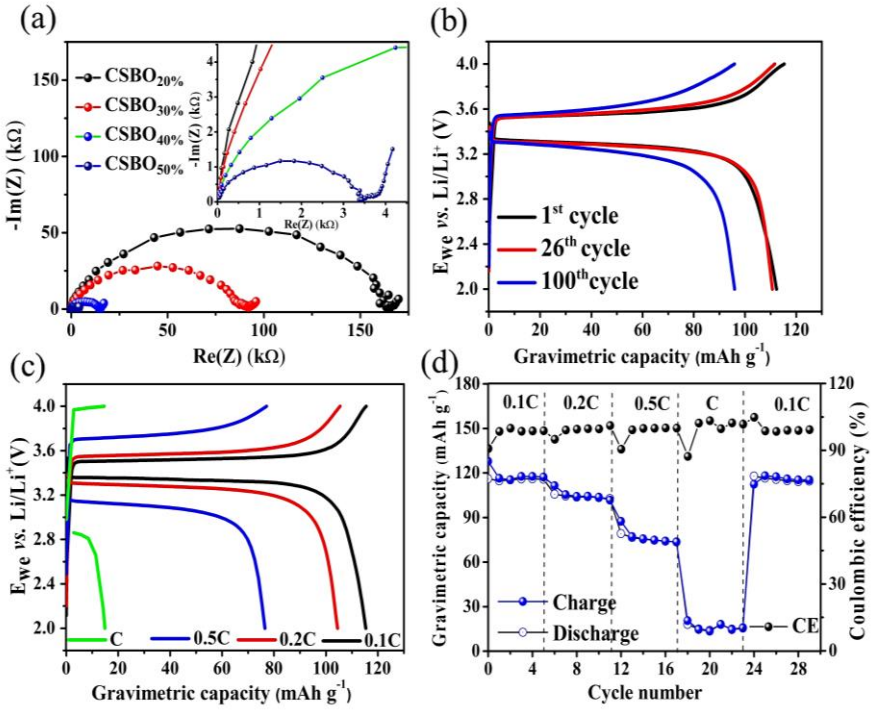

Figure 5.1.5: a) Nyquist plot of Li|CSBO$_{x\%}$-SE|LFP at RT with enlarged PEIS of Li|CSBO$_{50\%}$-SE|LFP. b) Galvanostatic charge-discharge voltage profile at 0.1C, c) Galvanostatic charge-discharge voltage profile at different C-rate and d) Rate capability plot of Li|CSBO$_{50\%}$ -SE|LFP at RT.

This phenomenon correlates to nothing, but the poor conductivity at the interface between electrode and electrolyte. Nonetheless the charge-discharge at RT is achievable due to current density in rate capability plot measurements (Figure 5.1.5d), indicating that the cell regains back its capacity at 0.1C rate even after a significant capacity loss at 1C rate. The capacity retention was calculated to be 83% for long term cycling with a capacity of 96 mAh g^{-1} at the 100th cycle, as shown in Figure 5.1.6d.

Although the experimental capacity for LFP obtained for the LFP|CSBO$_{50\%}$-SE|Li cell is not reaching the theoretical capacity of LFP, it constitutes a very promising result in the context of solid-state lithium metal batteries without the use of plasticizers, additives or elevated temperature.[83,84] In order to increase the performance of our system, we first increase the temperature of operation of our LFP|CSBO$_{50\%}$-SE|Li cell. As shown in Figure 5.1.6a, the increase in charging and discharging time with increasing temperature is self-explanatory. As the temperature increases, the mobility

of fatty chain segments in CSBO along with the increased mobility of ions contribute to the improvement of the overall experimental capacity. With the LFP|$CSBO_{50\%}$-SE|Li cell, we are able to achieve a discharge capacity as high as 157 mAh g^{-1} at 60 ^{o}C in comparison to 151 mAh g^{-1} and 112 mAh g^{-1} at 40 ^{o}C and RT, respectively (also refer Figure S5.1.6 for rate capability and capacity retention at 60 ^{o}C).

Another possibility to increase the cell performance is by addition of organic solvent in the SE. Here, we have selected propylene carbonate (PC) because PC is fully miscible with the CSBO-LiTFSI-SE. The targeted role of the PC is to enhance mobility by decreasing viscositthus nd transport of ions.[85, 86, 87] Figure S5.1.7c shows the effect of the amount of PC on charge-discharge performance at 0.1C. According to the data shown in Figure S5.1.7, it seems that an added ~5 wt% of PC to $CSBO_{50\%}$ (5 µL of PC by volume, represented by P5) is sufficient to significantly increase the cell performance. Figure 5.1.6c shows galvanostatic charge-discharge curves for the LFP|$CSBO_{50\%}$-SE|Li cell (without P5) and Li|$CBSO_{50\%}$-P5|LFP with P5. Although there is no enhanced capacity during the first cycle due of the presence of PC, a visible improvement in the capacity can be observed for the 100th cycle for the $CBSO_{50\%}$-P5 cell. In addition, the ΔE_O and ΔE_R for LFP were found to be decreased upon addition of PC from 3.52 to 3.47 V and 3.37 V to 3.32 V for oxidation and reduction respectively. Moreover, during the subsequent 100th cycle, the $\Delta E_{OO}/\Delta E_{RR}$ in respective charge or discharge is observed to be around 0.02 V for $CBSO_{50\%}$-SE and less than 0.005 V for $CSBO_{50\%}$-SE-P5. This is also fully supported by a lower electrolytic bulk resistance recorded in the PEIS measurements of the respective cells a shown in Figure S5.1.6. Figure 5.1.6d shows the comparison in the capacity retention of the $CSBO_{50\%}$-SE and $CSBO_{50\%}$-P5 cells. The capacity retention is enhanced from 83% to 96% with P5 Coulombic efficiencies for both ranging in between 99%-100%. In contrast, there is no improvement in the overall capacity with P5 in compare to P10 and P20 (P10, P20 correspond to 9.7 wt% and 17.8 wt% of PC, 10 µl and 20 µl of PC by volume for $CSBO_{20\%}$) as recorded (refer supporting information, Figure S5.1.7 and S5.1.8).

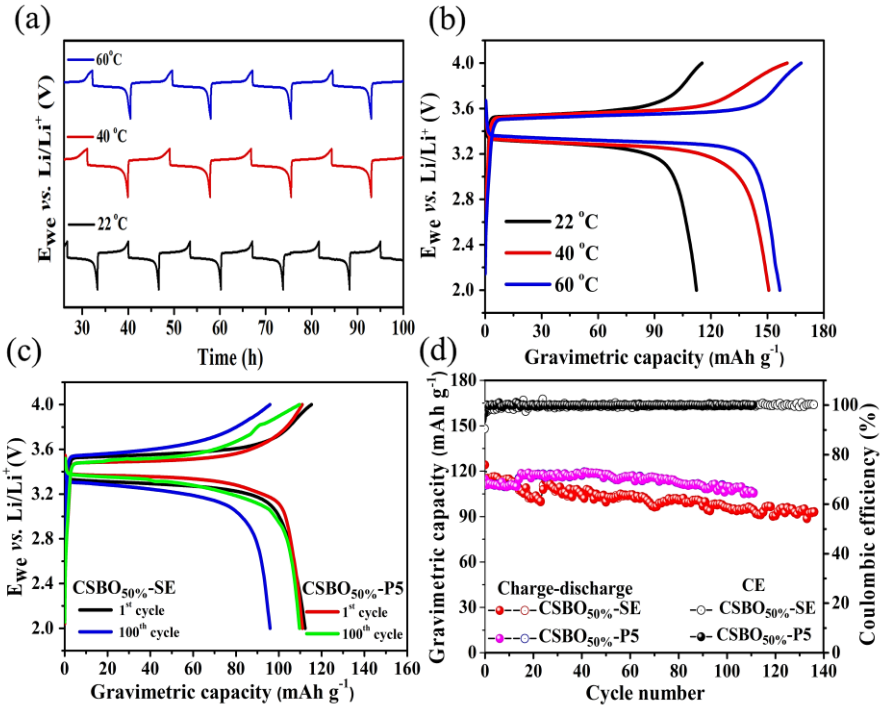

Figure 5.1.6: Galvanostatic charge-discharge voltage profile with respect to a) time and b) with gravimetric capacity at 0.1C for Li|CSBO$_{50\%}$-SE|LFP at variable temperature. c) Galvanostatic charge-discharge voltage profile with gravimetric capacity for 1st and 100th cycle and d) Capacity retention plot with cycle number for Li|CSBO$_{50\%}$-SE|LFP and Li|CSBO$_{50\%}$-P5|LFP (P5 represent PC) at 0.1C at RT.

5.1.4.7 Post-cycling XPS analysis of electrode interfaces

For a stable electrolyte, minimal growth of dendrite or its suppression (if any) are crucial parameters for a longer performance of the battery. The active formation of lithium fluoride (LiF) in a solid electrolyte interface (SEI) layer as a result of the decomposition of LiTFSI serves the purpose of ensuring efficient Li-ion mobility while limiting the dendrite growth.[88, 89] Therefore, XPS measurements on the surface of the Li anode and LFP cathode for Li|CSBO$_{50\%}$-SE|LFP cells were performed to probe the interfacial composition after galvanostatic charge-discharge for more than 100 cycles at 0.1C. The C 1s peak at 284.8 eV was used as a reference to calibrate the binding energy.[90] The major C and O elements could not be ignored from the XPS chamber or atmosphere and hence can also correspond to adventitious carbon. The

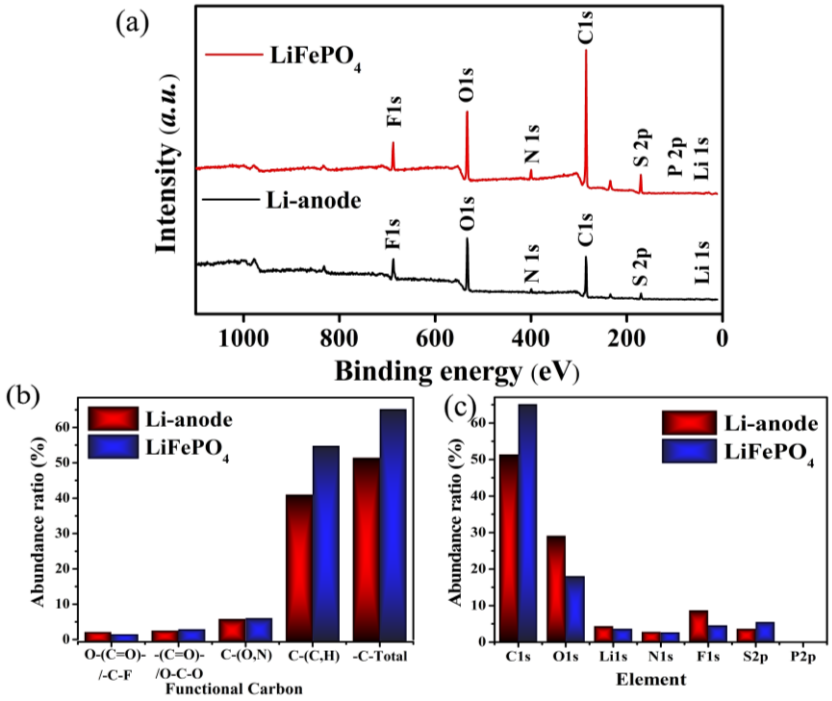

Figure 5.1.7: a) Survey spectrum of LFP cathode and lithium metal anode after cycling for more than 100 cycles of Li|CSBO$_{50\%}$-SE|LFP. b) Bar charts showing the abundance ratio percentage of functional carbon and c) elements from their surface.

survey spectra detected the desired elements like C, O, Li, F, N, S and P originating from the SEI layer or the other constituents from electrodes, as shown in Figure 5.1.7a. The abundance ratio percentage of functional carbons and elements has been presented through the bar charts in Figures 5.1.7b and 5.1.7c.

The C1s spectra in both samples can be attributed to C-C/C-H, C-O/N and O-C-O/C=O with the binding energy of ~284.8 eV, 286.3 eV and 287.8 eV, respectively. Other O-(C=O)-/-C-F functional species have been detected at 289.54 eV and 289.98 eV for Li-metal surface and LFP with a shift of 0.44 eV, as shown in Figures 5.1.8a and 5.1.8d. As a result of prolonged cycling, a significant amount of 2.6% LiF species in the F1s spectra (Figure 5.1.8b) at the binding energy of 684.8 eV was detected at the surface of the Li anode, in agreement with the formation of a stable SEI interface.[91] While 6.1% and 4.6% -CF_3 derived from LiTFSI were recorded at 687.6 eV and 687.8 eV for Li anode and LFP cathode, respectively (Figure 5.1.7c and Table S5.1.1). The

S2p spectra in Figure 5.1.8c and 5.1.8d show the characteristic peaks of sulfone (–SO_x) from LiTFSI for both electrodes. The HR-XPS of O1s could not be deconvoluted owing to overlapped peaks which may correspond to the following species, S-O (LiTFSI), O-(C=O)-O, O-(C=O)-C, C-OH and C-(SO_2) (Figure S5.1.9, also showing Li1s, N1S and P2p XPS spectra). These insights complemented the good performance of our bio-based CSBO-SE based Li-metal batteries by confirming the presence of LiF species for a stable SEI.

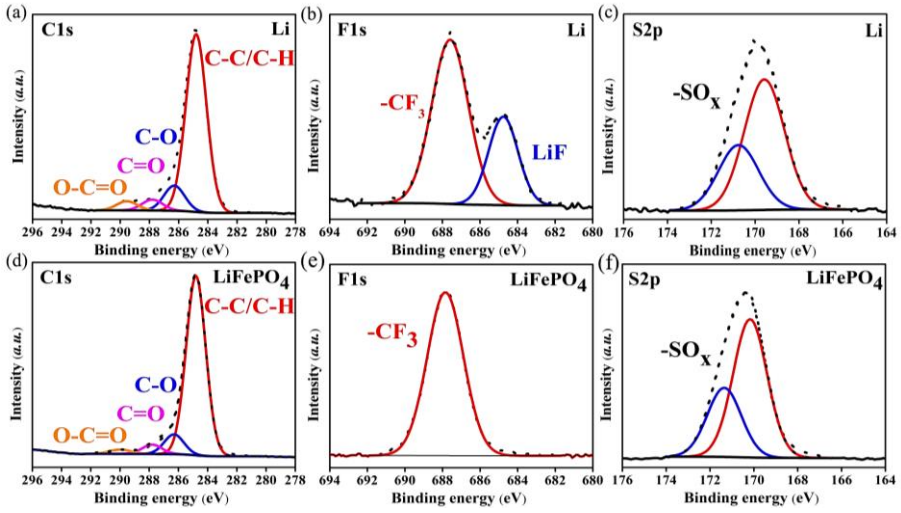

Figure 5.1.8: HR-XPS of a) and d) Carbon (C1s), b) and e) Fluorine (F1s) and c) and f.) Sulphur (S2p) for lithium metal and LFP surface of cycled Li|$CSBO_{50\%}$-SE|LFP cell, respectively.

5.1.5 Conclusion

In this contribution, we have disclosed an approach to develop solid electrolytes from bio-based starting materials (namely carbonated soybean oil and cellulose) and CO_2 using a green chemistry approach. The carbonated soybean oil was capable of dissolving lithium salts, thanks to its high dielectric constant resulting from the presence of cyclic carbonate groups. As anticipated, the ionic conductivities of CSBO-LiTFSI SEs were substantially increased with the amount of added salt due to the increased number of charge carriers and temperature due to the enhanced mobility of chain segments. A maximum ionic conductivity of ca. 10^{-3} S cm^{-1} was obtained for $CSBO_{50\%}$ at 100 °C and 10^{-6} S cm^{-1} at 20 °C. Electrochemical stability window up to

4.8 V (*vs.* Li/Li^+) and lithium-ion transference number up to 0.39 ± 0.03 were obtained for the $CSBO_{50\%}$-based SE at RT. However, our fundamental understanding of ionic transport in this system remains limited. Further electrochemical studies like galvanostatic charge-discharge measurements confirmed the stable SEI layer formation in subsequent stripping and plating. The CSBO-LiTFSI SEs were then incorporated in lithium metal battery cells using LFP as cathode material. The accordingly obtained cell can deliver up to 112 mAh g^{-1} of discharge capacity at 0.1C, RT. The capacity of the cell was further shown to improve with parameters like elevated temperature and addition of PC to 156 mAh g^{-1} close to the theoretical capacity. Further, XPS analysis on the Li-metal and LFP surface highlighted the stable SEI formation and decomposition of electrolyte. Our findings are paving the way towards bio-based and more environmentally friendly solid-state batteries operating at RT with the aim of high energy density.

Bibliography

1. M. D. Murbach, D. T. Schwartz, *J. Electrochem. Soc.* **2018**, *165*, A297.
2. M. Armand, J. -M. Tarascon, *Nature*. **2008**, *451*, 652.
3. J. W. Choi, D Aurbach, *Nat. Rev. Mater*. **2016**, *1*, 16013.
4. A. Manthiram, X. Yu, S. Wang, *Nat. Rev. Mater*. **2017**, *2*, 16103.
5. K. J. Harry, D. T. Hallinan, D. Y. Parkinson, A. A. MacDowell, N. P. Balsara, *Nat. Mater*. **2014**, *13*, 69.
6. C. Wacker, *Annual Report, Fraunhofer ISIT*, Itzehoe, Germany, **2004** (https://www.ise.fraunhofer.de/content/dam/ise/en/documents/annual_reports/ISE_JB04_e_Complete_screen.pdf).
7. Y. Yamada, J. Wang, S. Ko, E. Watanabe, A. Yamada, *Nat. Energy* **2019**, *4*, 269–280.
8. J. Lopez, D. G. Mackanic, Y. Cui, Z. Bao, *Nat. Rev. Mater*. **2019**, *4*, 312–330.
9. S. Choudhury, S. Stalin, D. Vu, A. Warren, Y. Deng, P. Biswal, L. A. Archer, *Nat. Commun.* **2019**, *10*, 4398.
10. J. Dai, C. Yang, C. Wang, G. Pastel, L. Hu, *Adv. Mater*. **2018**, *30*, 1802068.
11. L. P. Li, W. Y. Liu, H. Y. Dong, Q. Y. Gui, Z. Q. Hu, Y. Y. Li, J. P. Liu, *Adv. Mater*. **2021**, *33*, 2004959.
12. L. Bekaert, A. Raj, J.-F. Gohy, A. Hubin, F. D. Proft, M. H. Mamme, *J. Phys. Chem. C* **2022**, *126*, 8227−8237.
13. F. Elizalde, J. Amici, S. Trano, G. Vozzolo, R. Aguirresarobe, D. Versaci, S. Bodoardo, D. Mecerreyes, H. Sardon, F. Bella, *J. Mater. Chem. A*, **2022**, *10*, 12588-12596.
14. X. Guo, Y. Ding, L. Xue, L. Zhang, C. Zhang, J. B. Goodenough, G. Yu, *Adv. Funct. Mater*. **2018**, *28*, 1804649.
15. R. Narayan, C. Laberty-Robert, J. Pelta, J. -M. Tarascon, R. Dominko, *Adv. Energy Mater*. **2022**, *12*, 2102652.
16. D. H. Cho, K. G. Cho, S. An, M. S. Kim, H. W. Oh, J. Yeo, W. C. Yoo, K. Hong, M. Kim, K. H. Lee, *Energy Storage Materials* **2022**, *45*, 323-331.
17. Y. Gao, Z. Pan, J. Sun, L. Zhaolin, W. John, *Nano-Micro Lett.* **2022,** *14*, 94.
18. Y. Tian, G. Zeng, A. Rutt, T. Shi, H. Kim, J. Wang, J. Koettgen, Y. Sun, B. Ouyang, T. Chen, Z. Lun, Z. Rong, K. Persson, G. Ceder, *Chem. Rev.* **2021**, *121, 3*, 1623–1669.
19. J. Amici, C. Torchio, D. Versaci, D. Dessantis, A. Marchisio, F. Caldera, F. Bella, C. Francia, S. Bodoardo, *Polymers* **2021**, *13(10)*, 1625.
20. H. Oubaha, J.-F. Gohy, S. Melinte, *ChemPlusChem* **2019**, *84*, 1179.
21. J. Hassoun, B. Scrosati, *J. Electrochem. Soc.* **2015**, *162*, A2582.
22. K. Kubota, M. Dahbi, T. Hosaka, S. Kumakura, S. Komaba, *Chem. Rec.* **2018**, *18*, 459.
23. Y. Liang, H. Dong, D. Aurbach Y. Yao, *Nat Energy* **2020**, *5*, 646–656.
24. A. M. Abakumov, S. S. Fedotov, E. V. Antipov, J. -M. Tarascon, *Nat Commun* **2020**, *11*, 4976.
25. S. Ferrari, M. Falco, A. B. Muñoz-García, M. Bonomo, S. Brutti, M. Pavone, C. Gerbaldi, *Adv. Energy Mater.* **2021**, *11*, 2100785.
26. S. Tang, W. Guo, Y. Fu, *Adv. Energy Mater*. **2021**, *11*, 2000802.
27. E. Manarin, F. Corsini, S. Trano, L. Fagiolari, J. Amici, C. Francia, S. Bodoardo, S. Turri, F. Bella, G. Griffini, *ACS Applied Polymer Materials* **2022**, *4, 5*, 3855-3865.
28. J. Wang, X. Liu, H. Jia, P. Apostol, X. Guo, F. Lucaccioni, X. Zhang, Q. Zhu, C. Morari, J. -F. Gohy, A. Vlad, *ACS Energy Lett.* **2022**, *7, 2*, 668–674.
29. S. Trano, F. Corsini, G. Pascuzzi, E. Giove, L. Fagiolari, J. Amici, C. Francia, S. Turri, S. Bodoardo, G. Griffini, F. Bella, *ChemSusChem* **2022**, *15*, e2022002.
30. D. E. Fenton, J. M. Parker, P. V. Wright, *Polymer* **1973**, *14*, 589.
31. M. Armand, *Solid State Ionics* **1983**, *9-10*, 745-754.
32. W. H. Meyer, *Adv. Mater.* **1998**, *10*, 439–448.
33. J. Chai, Z. Liu, J. Zhang, J. Sun, Z. Tian, Y. Ji, K. Tang, X. Zhou, G. Cui, *ACS Appl. Mater. Interfaces* **2017**, *9*, 17897.
34. S. D. Tillmann, P. Isken, A. Lex-Balducci, *J. Power Sources* **2014**, *271*, 239.
35. S. D. Tillmann, P. Isken, A. Lex-Balducci, *J. Phys. Chem. C* **2015**, *119*, 14873.
36. F. Boujioui, F. Zhuge, H. Damerow, M. Wehbi, B. Améduri, J.-F. Gohy, *J. Mater. Chem. A* **2018**, *6*, 8514.
37. F. Boujioui, H. Damerow, F. Zhuge, J.-F. Gohy, *Macromol. Chem. Phys.* **2020**, *221*, 1900556.
38. J. Zhang, J. Zhao, L. Yue, Q. Wang, J. Chai, Z. Liu, X. Zhou, H. Li, Y. Guo, G. Cui, L. Chen, *Adv. Energy Mater.* **2015**, *5*, 1501082.
39. K. Kimura, M. Yajima, Y. Tominaga, *Electrochem. commun.* **2016**, *66*, 46.
40. Y. Tominaga, V. Nanthana, D. Tohyama, *Polym. J.* **2012**, *44*, 1155.
41. T. Morioka, K. Nakano, Y. Tominaga, *Macromol. Rapid Commun.* **2017**, *38*, 1600652.
42. L. Meabe, T. V. Huynh, N. Lago, H. Sardon, C. Li, L. A. O'Dell, M. Armand, M. Forsyth, D. Mecerreyes, *Electrochim. Acta* **2018**, *264*, 367.
43. F. Ouhib, L. Meabe, A. Mahmoud, B. Grignard, J.-M. Thomassin, F. Boschini, H. Zhu, M. Forsyth, D. Mecerreyes, C. Detrembleur, *ACS Appl. Polym. Mater.* **2020**, *2*, 922−931.
44. M. Rayung, M. M. Aung, S. C. Azhar, L. C. Abdullah, M. S. Su'ait, A. Ahmad, N. A. Md Jamil, *Materials* **2020**, *13(4)*, 838.

45. K. W. Chew, T. C. Ng, Z. H. How, *Int. J. Electrochem. Sci.* **2013**, *8*, 6354 – 6364.
46. I. Osada, S. M. Hosseini, S. Jeong, S. Passerini, *ChemElectroChem* **2017**, *4*, 463.
47. Z. Lv, Y. Tang, S. Dong, Q. Zhou, G. Cui, *Chemical Engineering Journal* **2022**, *430*, 132659.
48. M. S. M. Misenan, A. S. A. Khiarb, T. Eren, *Polym Int* **2022**, *71*, 751–769.
49. C. Carré, Y. Ecochard, S. Caillol, L. Avérous, *ChemSusChem* **2019**, *12*, 3410 – 3430.
50. N. Ren, Y. Song, C. Tao, B. Cong, Q. Cheng, Y. Huang, G. Xu, J. Bao, *J. Solid State Electrochem.* **2018**, *22*, 1109–1121.
51. S. Ibrahim, A. Ahmad, N. S. Mohamed, *Polymers* **2015**, *7(4)*, 747-759.
52. S. R. Mustapa, M. M. Aung, M. Rayung, *Polymers* **2021**, *13(1)*, 132.
53. M. Oshinowo, J. R. Runge, M. Piccini, F. Marken, A. Buchard, *J. Mater. Chem. A* **2022**, *10*, 6796-6808.
54. L. Zhang, H. Gao, G. Jin, S. Liu, J. Wu, H. Wu, Y. Yang, Q. Wang, S. Wang, *ChemNanoMat* **2022**, e202200142.
55. R. Alves, A. F. Marijuan, L. C. Arias, R. Gonçalves, M. M. Silva, F. J. D. Campo, C. M. Costa, S. L. Mendez, *ACS Appl. Mater. Interfaces* **2022**, *14(13)*, 15494-15503.
56. C.W. Liew, S. Ramesh, *Cellulose* **2013**, *20*, 3227–3237.
57. A. S. A. Khiar, A. K. Arof, *Ionics* **2010**, *16*, 123–129.
58. L. Poussard, J. Mariage, B. Grignard, C. Detrembleur, C. Jérôme, C. Calberg, B. Heinrichs, J. De Winter, P. Gerbaux, J. M. Raquez, L. Bonnaud, P. Dubois, *Macromolecules* **2016**, *49*, 2162–2171.
59. X. Wei, D. F. Shriver, *Chem. Mater.* **1998**, *10*, 2307–2308.
60. B. Scrosati, C.A. Vincent, *MRS Bulletin* **2000**, *25*, 28–30.
61. S. Panchireddy, J.-M. Thomassin, B. Grignard, C. Damblon, A. Tatton, C. Jerome, C. Detrembleur, *Polym. Chem.* **2017**, *8*, 5897–5909.
62. S. Gennen, M. Alves, R. Méreau, T. Tassaing, B. Gilbert, C. Detrembleur, C. Jerome, B. Grignard, *ChemSusChem* **2015**, *8*, 1845-1849.
63. M. Alves, B. Grignard, S. Gennen, R. Mereau, C. Detrembleur, C. Jérôme, T. Tassaing, *Catal. Sci. Technol.* **2015**, *5*, 4636–4643.
64. M. Alves, B. Grignard, S. Gennen, C. Detrembleur, C. Jerome, T. Tassaing, *RSC Adv.* **2015**, *5*, 53629–53636.
65. G. Karmakar, P. Ghosh, *ACS Sustain. Chem. Eng.* **2016**, *4*, 775–781.
66. A. Ghosal, O. U. Rahman, S. Ahmad, *Ind. Eng. Chem. Res.* **2015**, *54*, 12770–12787.
67. M. Sacristán, J. C. Ronda, M. Galià, V. Cádiz, *Biomacromolecules* **2009**, *10*, 2678–2685.
68. C. Zhang, Y. Xia, R. Chen, S. Huh, P. A. Johnston, M. R. Kessler, *Green Chem.* **2013**, *15*, 1477–1484.
69. S. S. Gupta, N. Solanki, A. T. M. Serajuddin, *AAPS PharmSciTech* **2016**, *17*, 148–157.
70. R. C. Agrawal, G. P. Pandey, *J. Phys. D.* **2008**, *4*, 3715–3725.
71. P. L.Kuo, W. J. Liang, T. Y. Chen, *Polymer* **2003**, *44*, 2957–2964.
72. J. Mindemark, B. Sun, E. Törmä, D. Brandell, *J. Power Sources* **2015**, *298*, 166–170.
73. L. Meabe, N. Lago, L. Rubatat, C. Li, A. J. Müller, H. Sardon, M. Armand, D. Mecerreyes, *Electrochim. Acta* **2017**, *237*, 259–266.
74. J.R. MacCallum, C.A. Vincent Eds., *Polymer Electrolyte Reviews 1*, Elsevier, London, **1987,** 23.
75. N.K. Karan, D.K. Pradhan, R. Thomas, B. Natesan, R.S. Katiyar, *Solid State Ionics* **2008**, *179*, 689–696.
76. T. Miyamoto, K.J. Shibayama, K. *J. Appl. Phys.* **1973**, *44*, 5372.
77. J. Xi, X. Qiu, M. Cui, X. Tang, W. Zhu, L. Chen, *J. Power Sources* **2006**, *156*, 581.
78. Y.R. Zhao, Z. Huang, S.J. Chen, B. Chen, J. Yang, Q. Zhang, F. Ding, Y.H. Chen, X.X. Xu, *Solid State Ionics* **2016**, *295*, 65–71.
79. J. Evans, C. A. Vincent, P. G. Bruce, *Polymer* **1987**, *28*, 2324**.**
80. P.G. Bruce, C.A. Vincent, *J. Electroanal. Chem. Interfacial Electrochem.* **1987**, *225*, 1-17.
81. S. Han, *Sci. Rep.* **2019**, *9*, 5555.
82. M. Rosso, C. Brissot, A. Teyssot, M. Dollé, L. Sannier, J. -M. Tarascon, R. Bouchet, S. Lascaud, *Electrochim. Acta* **2006**, *51*, 5334–5340.
83. R. Bouchet, S. Maria, R. Meziane, A. Aboulaich, L. Lienafa, J. P. Bonnet, T. N. T. Phan, D. Bertin, D. Gigmes, D. Devaux, R. Denoyel, M. Armand, *Nat. Mater.* **2013**, *12*, 452-457.
84. R. Meziane, J. P. Bonnet, M. Courty, K. Djellab, M. Armand, *Electrochim. Acta* **2011**, *570*, 14-19.
85. Z. Y. Cui, Y. Y. Xu, L. P. Zhu, J. Y. Wang, Z. Y. Xi, B. K. Zhu, *J. Membr. Sci.* **2008**, *325*, 957.
86. L. L. Liu, Z. H. Li, Q. L. Xia, Q. Z. Xiao, G. T. Lei, X. D. Zhou, *Ionics* **2012**, *18*, 275-281.
87. R. Khurana, J.L. Schaefer, L.A. Archer, G.W. Coates, *J. Am. Chem. Soc.* **2014**, *136*, *20*, 7395–7402.
88. K.N. Wood, G. Teeter, *ACS Appl. Energy Mater.* **2018**, *1*, 4493–4504.
89. P. Shi, L. Zhang, H. Xiang, X. Liang, Y. Sun, W. Xu, *ACS Appl. Mater. Interfaces* **2018**, *10*, 22201−22209.
90. S. Leroy, H. Martinez, R. Dedryvere, D. Lemordant, D. Gonbeau, *Appl. Surf. Sci.* **2007**, *253*, 4895−4905.
91. R. Grissa, V. Fernandez, N. Fairley, J. Hamon, N. Stephant, J. Rolland, R. Bouchet, M. Lecuyer, M. Deschamps, D. Guyomard, *ACS Appl. Energy Mater.* **2018**, *1*, 5694−5702

Supporting Information

Bio-based solid electrolytes bearing cyclic carbonates

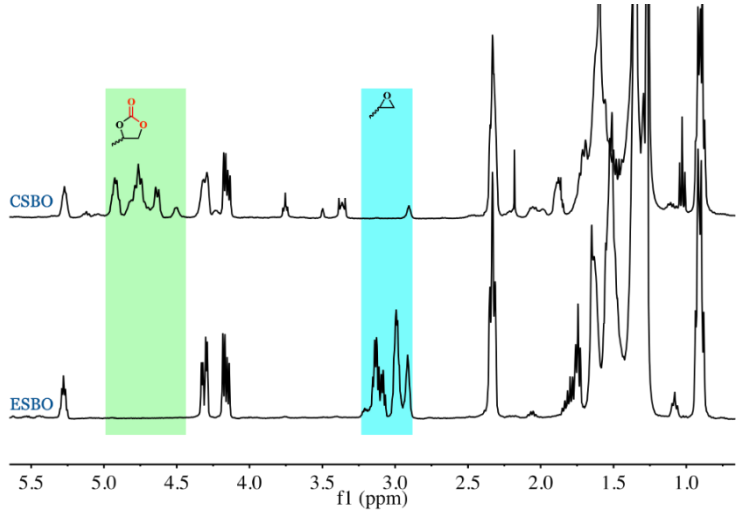

Figure S5.1.1: ^{1}H NMR spectra of epoxidized soybean oil (ESBO) and cyclic carbonated soybean oil (CSBO).

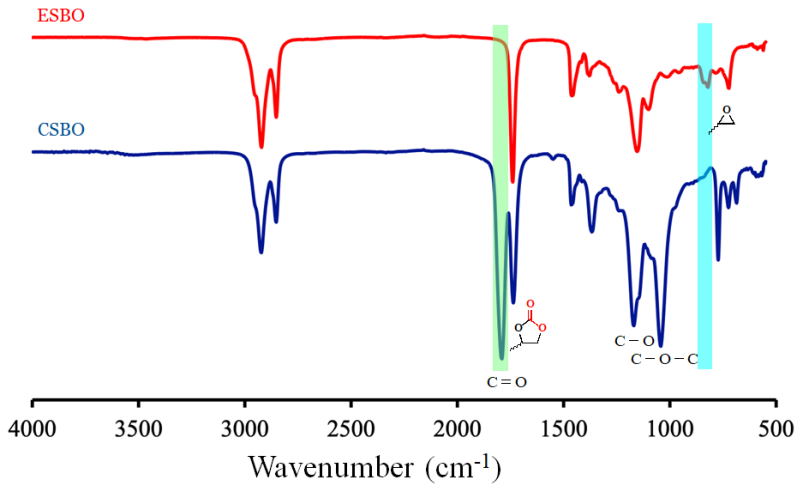

Figure S5.1.2: FTIR spectra of epoxidized soybean oil (ESBO) and cyclic carbonated soybean oil (CSBO).

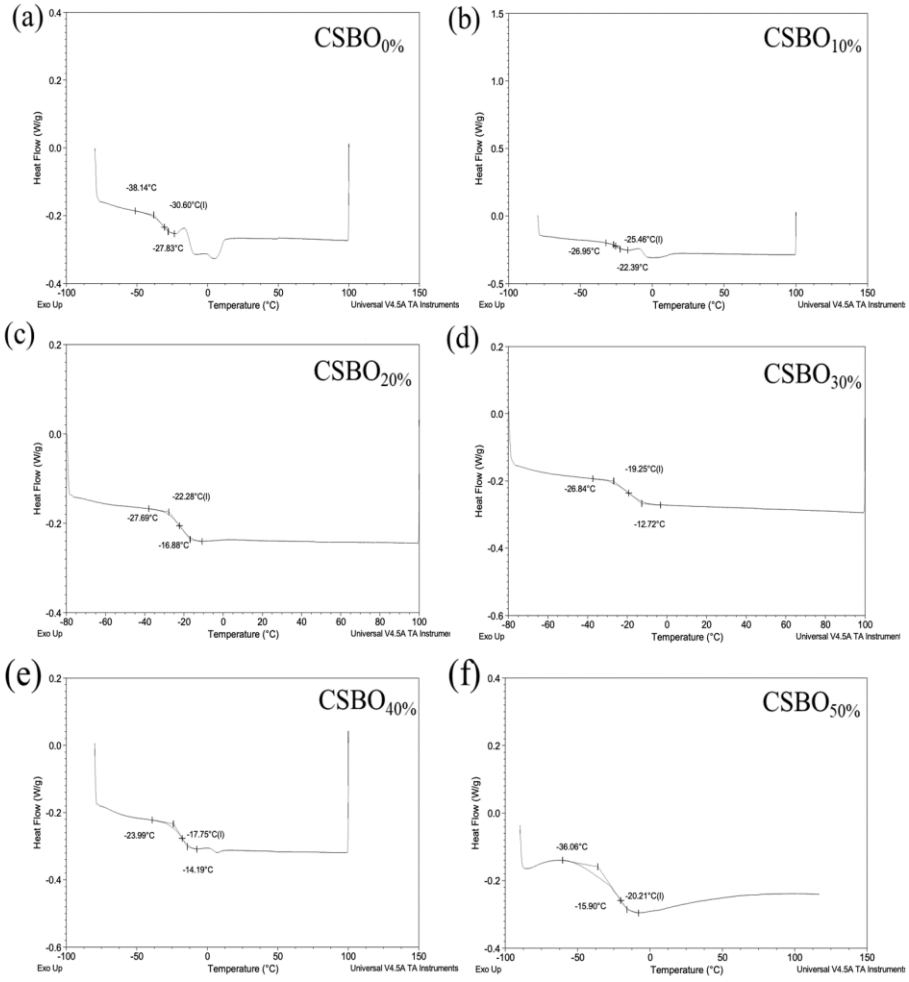

Figure S5.1.3: Differential scanning calorimetry heating curve (exo up) of a) $CBSO_{0\%}$, b) $CBSO_{10\%}$, c) $CBSO_{20\%}$, d) $CBSO_{30\%}$, e) $CBSO_{40\%}$ and f) $CBSO_{50\%}$, respectively.

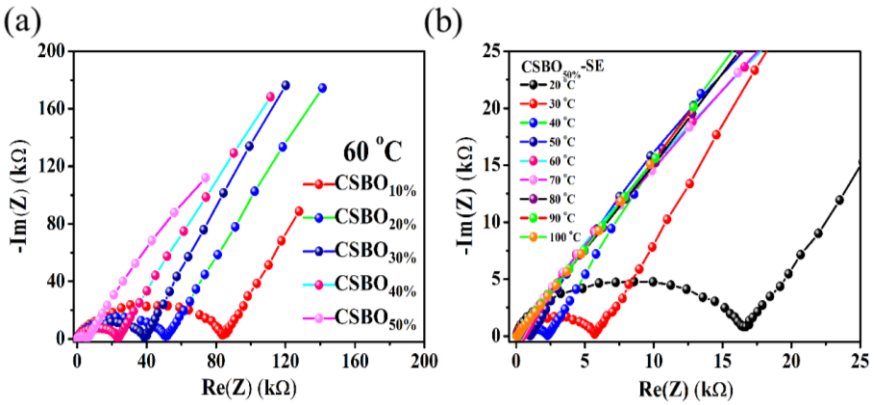

Figure S5.1.4: Nyquist plot of a) SS|CBSO$_{x\%}$-SE|SS symmetric cell at 60 ºC and b) SS|CBSO$_{50\%}$-SE|SS at different temperature for PEIS, respectively.

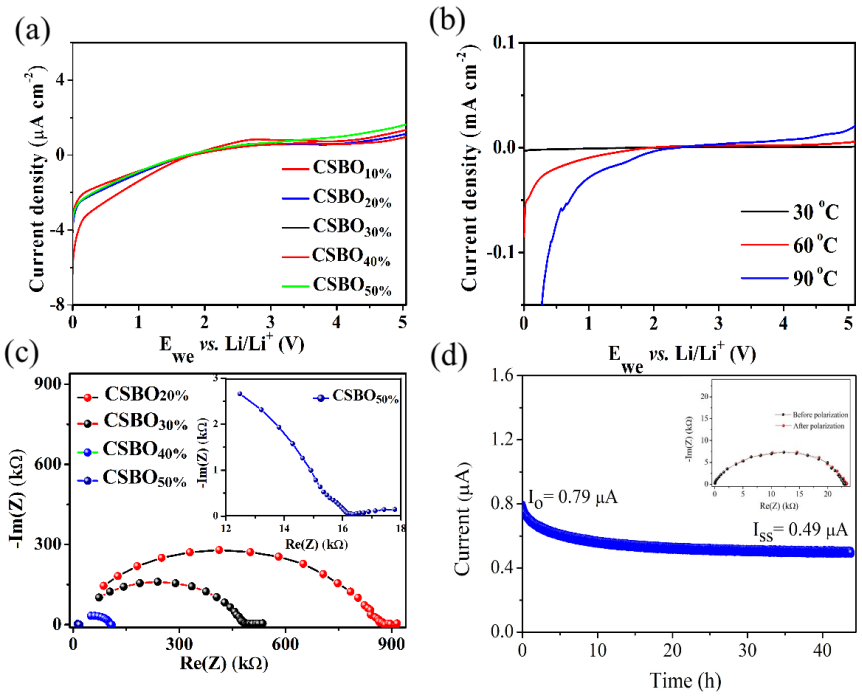

Figure S5.1.5: a) Linear sweep voltametry of the Li|CBSO-SE|SS at 30 ºC and b) Li|CBSO$_{20\%}$-SE|SS at 30 ºC, 60 ºC and 90 ºC, respectively. c) Nyquist plot of Li|CBSO$_{x\%}$-SE|Li symmetric cell with enlarged PEIS of Li|CBSO$_{50\%}$-SE|Li at inset and d) Chronoampereometry measurement at 10 mV for CBSO$_{30\%}$ with Nyquist plots for PEIS before and after polarization in the inset at 60 ºC.

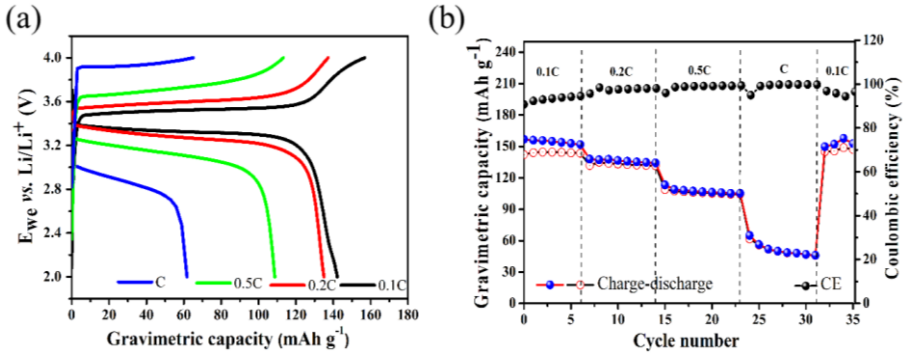

Figure S5.1.6: a) Galvanostatic charge-discharge voltage profile with gravimetric capacity at different C-rate and b) Rate capability plot of Li|CSBO$_{50\%}$ -SE|LFP at 60 ºC.

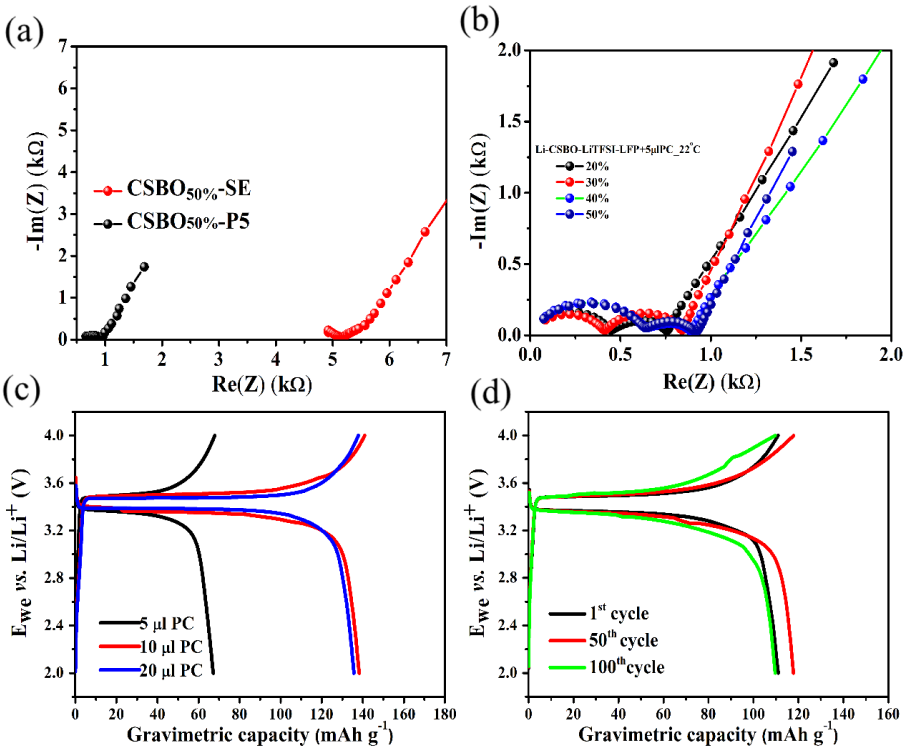

Figure S5.1.7: Nyquist plot of a) Li|CSBO$_{50\%}$-SE|LFP with and without P5 and b) Li|CSBO$_{x\%}$-P5|LFP at RT, respectively. Galvanostatic charge-discharge voltage profile gravimetric capacity, c) Li|CSBO$_{20\%}$-SE|LFP with P5, P10 and P20, d) Li|CSBO$_{50\%}$-P5|LFP at RT with 0.1C.

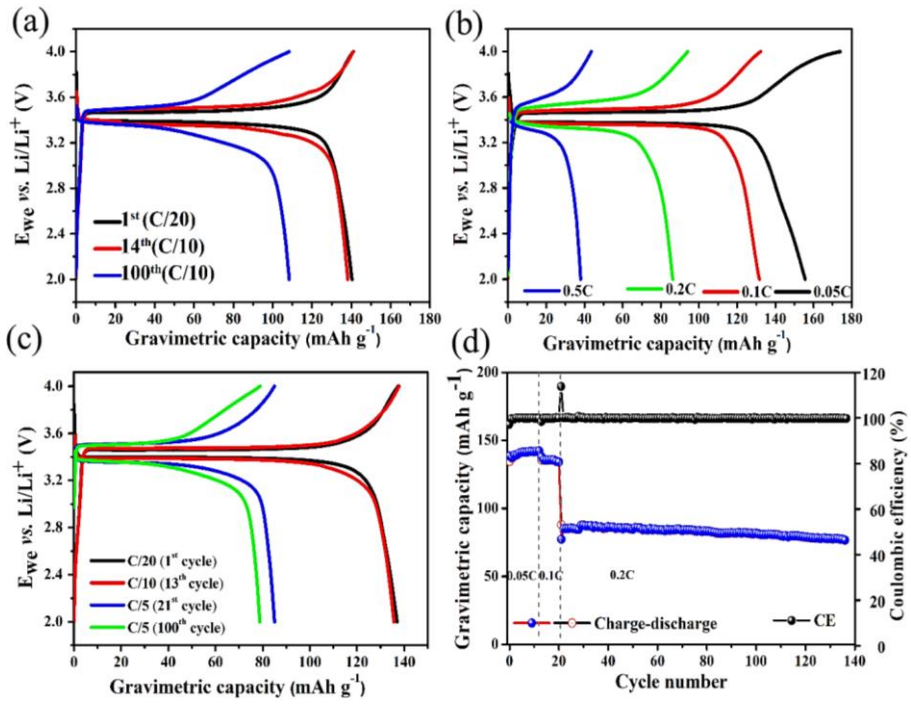

Figure S5.1.8: Galvanostatic charge-discharge voltage profile with gravimetric capacity, a) at following charge and discharge of 1st, 14th and 100th, b) at different C-rate of Li|$CSBO_{20\%}$ -P10|LFP and c) at different C-rate and following cycles for Li|$CSBO_{20\%}$ -P20|LFP d) Capacity retention plot with cycle number for Li|$CSBO_{20\%}$ -P20|LFP (all at RT).

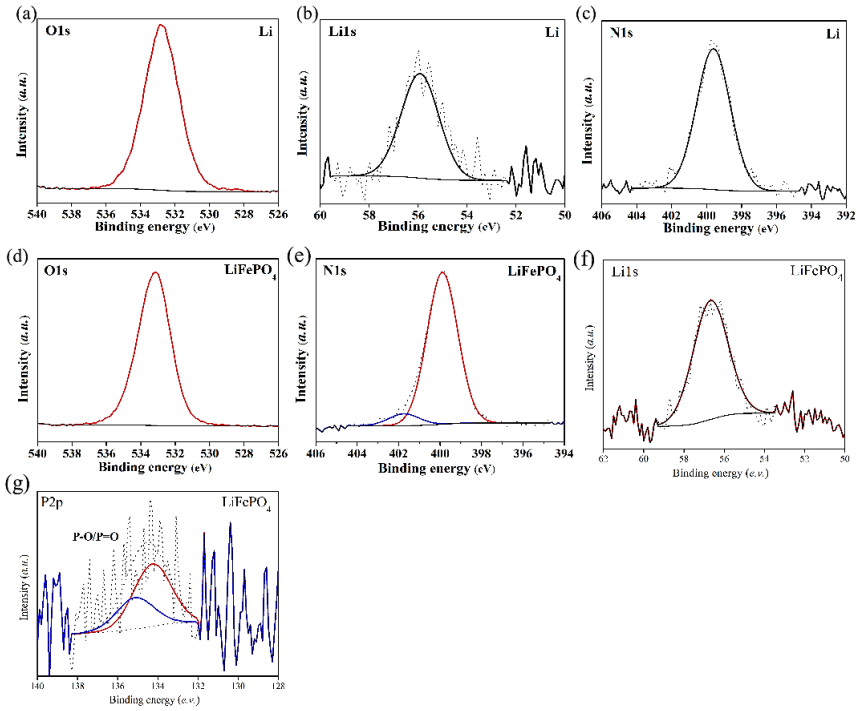

Figure S5.1.9: HR-XPS of a) and d) Oxygen (O1s), b) and e) Nitrogen (N1s), c) and f) Lithium (L1s), g) Phosphorous (P2p) for lithium metal and LFP surface of cycled Li|CSBO$_{50\%}$-SE|LFP cell, respectively.

Table S5.1.1: Quantization table of XPS analysis of electrodes post-cycling indicating, BE, FWHM and abundance ratio %.

		F 1s			O 1s	N 1s			C 1s						S $2p_{3/2}$	P $2p_{3/2}$	Si 2p	Li 1s
		F-C	F-Li	F tot.		$\underline{N}H^+$-(C,H)	$\underline{N}$-(C,H)	N tot.	O=$\underline{C}$-O, $\underline{C}$-F	$\underline{C}$=O, O-$\underline{C}$-O	$\underline{C}$-(O,N)	$\underline{C}$-(C,H)	C tot.	Sulphate	Phosphate	$\underline{Si}^{(IV)}$		
	BE	687.59	684.76		532.89		399.61		289.54	287.8	286.3	284.8		169.58			55.93	
Li anode	FWHM	2.295	1.858		2.336		2.272		1.664	1.664	1.664	1.664		2.169			1.812	
	A%	6.06	2.638	8.698	29.118		2.767	2.767	2.123	2.511	5.802	40.968	51.404	3.637			4.375	
	BE	687.85			533.19	401.74	399.89		289.98	287.8	286.3	284.8		170.17	134.27	102.3	56.68	
Al/C-LFP	FWHM	2.279			2.216	1.75	1.75		1.751	1.576	1.576	1.576		1.825	2.2	1.896	2.044	
	A%	4.563		4.563	18.042	0.195	2.495	2.69	1.455	2.868	6.043	54.78	65.146	5.49	0.054	0.398	3.617	

Chapter 5.2 Carbonated Soybean oil blends with poly(ethylene oxide)

Abstract

While poly(ethylene oxide) (PEO) based solid-state batteries have been a frontrunner in the polymer electrolyte research, they do present unavoidable trade-offs. Many polymer blends have been demonstrated as better alternatives to pure polymers exhibiting superior electrochemical and mechanical properties but are less environmentally friendly. In our project, we have developed blends of PEO and soybean-derived carbonated soybean oil (CSBO) by a facile blending approach. The physical blend of PEO and CSBO with lithium bis(trifluoromethane sulfonyl)imide salt results in free-standing membranes combining the ether and cyclic carbonate functionalities in the blend. It confers increased amorphous phase and adhesive nature to the polymer blend owing to CSBO, in addition to better interface with electrodes. With the conductivity of 3.3 x 10^{-5} S cm^{-1} at room temperature, a broad electrochemical stability window (ESW > 4.2 V versus Li/Li^{+}) is observed with high stability versus lithium metal electrodes as inferred from stripping and plating experiments (for cycling time > 300 h). Subsequently, the lithium ferrophosphate ($LiFePO_4$)/polymer blend/lithium metal battery prototypes deliver 108.2 mAh g^{-1} of

discharge capacity with high Coulombic efficiency at 0.1C and 60 ºC in the first cycle. Here, the trade-offs in PEO have addressed with bio-derived carbonates-containing molecules contributing towards sustainable materials development for higher energy density.

5.2.1 Introduction

The serendipitous discovery and thereafter continuous arduous effort led to the successful revolution of lithium-based batteries involving lithium-ion, lithium metal, lithium-sulfur and lithium-air batteries as promising future alternatives.[1,2] Lithium batteries have bartered the fate of energy storage technology for clean energy largely because of their high energy and power density in high-performance electronics from small watches, mobile phones to large stationary power grids. Unlike prosaic batteries, lithium batteries tendered a lot of complications in the long run. It took years of development to realize the underlying issues and come up with a series of optimized electrodes and electrolytes. From the alloying to intercalation, electrodes based on TiS_2, MoS_2, LCO, LMO, LFP, NMC, and lithium sulfides have been seen as a grail for the cathode materials.[3,4] On the contrary, the anode was not equally looked upon limiting it to lithium metal, carbonaceous graphite, silicon and other alloys due to their complex compatibility with electrolytes.[5] Contemporary technology is referred to as Li-ion and Li-metal batteries, with the latter using Li-metal as an anode.[6] The quest to reach the newer milestone of energy density with adequate cost and safety continues to spark a strong interest in bringing more innovations in the matured and existing technology. Commercial Li-ion batteries consist of bulky cathode and anode (except lithium metal) as highlighted above with separators soaked in non-aqueous liquid electrolytes. Thus, this higher weight lowers total energy density but also poses a risk of electrolyte leakage, flammability, inflexibility, and complex recycling just to name a few.[7,8] In addition, typically used ether/ester-based liquid electrolytes also offer limited electrochemical stability (ESW) to match up with high voltage cathodes.[4]

However, LIB research still gained momentum solely because of its cost-effective anode and higher safety compared to metallic lithium. The original idea of lithium metal as an anode was never dropped in the research area due to its high capacity (3860 mAh g^{-1}) and lightweight (energy density ~ 250 Wh Kg^{-1}). However, the major obstacle has always been the safety of the battery due to high reactivity, Li-dendrite growth, processing and lack of infrastructure, limiting its commercial use.[9,10] The solid-state battery (SSB) based on lithium metal has been eyed upon with huge expectation overcoming all the underlying hurdles associated with li-metal for

superior performance. It facilitates lightweight, robustness, flexibility, thermal safety, and recyclability to lithium metal battery (LMB) in addition to upheaval in the long life and high performance of the cells.[11,12] Having all these advantages, the quest for superior solid-state electrolytes has been active for decades even before commercial LIB came into the market. From 1980 and onwards, SSEs such as ceramic-based conductors and organic polymer electrolytes gained momentum. Armand, Wright and co-workers efforts led to the discovery of a Li^+/Na^+-polymer complexes as potential ion conductors.[13,14] Their revolutionary discovery of poly(ethylene oxide) (PEO) based solid polymer electrolytes (SPEs) paved the long road of utilizing polymer chemistry for electrolytes. Ether units responsible for oxygen coordination and conduction mechanism were one of the crucial findings during those times. The great deal of tuneability in the structure and mechanical properties retains its top preference for most polymers for energy storage applications. Moreover, designing an electrolyte with good ionic conductivity, wide electrochemical stability window (ESW), high transference number, decent interface compatibility and high dielectric constant with superior mechanical and thermal properties remains a challenge until now.[15,16] Addressing this concern, various classes of PEO-based polymers and their alternatives,[17,18] have been investigated via smart approaches like grafting[19-21], block copolymers,[22-24] networks, blends[25-27], single lithium-ion conducting,[28-30] gel polymers,[31,32] and hybrids.[27,33,34] Potential polymers such as polyesters,[35,36] polycarbonates,[37-39] polyalcohols,[40, 41] polyurethanes,[42-44] polysiloxanes[45, 46] have been designed with functionality involving ether, ester and carbonate analogous to nonaqueous solvents for overruling issues accompanying PEO-based electrolytes (ESW<3.9 V, t_{Li+} < 0.2). SPEs congruent to high voltage cathodes need to be designed repealing the trade-offs in hand with sustainability.

For the last few years, stretched interest towards alternatives for non-green and toxic materials has escalated the research in bio-sourced materials. Organic electrodes and electrolytes are widely attempted to be designed via eco-friendly processes. Several reports can be found on vegetable oils[47,48], cellulose[49], and gum[50] derived cation conductors for potential energy storage applications. Cyclic carbonates are quite appropriate for lithium-ion coordination and dissolution due to their superior dielectric constant (normally ≈ 60–70 for carbonate vs less than 10 for EO at room

temperature).[51,52] Coupling cyclic carbonate functionality and ethylene oxide units in co-polymers and blend has also been an interesting approach. Tominaga *et al*. synthesized linear poly (ethylene carbonate) that was further integrated into hybrid membrane reaching an ionic conductivity of ~10^{-5} S cm^{-1} at 30 °C.[39,53] Our research group investigated SPEs based on cyclic carbonate trifluoro methacrylate and vinylidene fluoride units[54] and random copolymers of n-butyl acrylate and cyclic carbonate-bearing acrylate.[55] Xue *et al.* reported borate-based porous polymer electrolytes containing cyclic carbonates wth ionic conductivity of 1.32×10^{-3} S cm^{-1} at 30 °C.[56] An intense amount of work is also directed toward understanding the interfaces which guide the design of electrolytes. On those trails, interfacial engineering, chain end modification, coating stabilized polymers are being studied.[57-59]

Therefore, taking up the challenge to improve the existing PEO by combining it with bio-derived molecules, we report here the blend of PEO and carbonated soybean oil (CSBO). CBSO-PEO blends were prepared by mixing CBSO and PEO with the synthesis of CSBO reported elsewhere as shown in the overall Scheme S5.2.1.[60] Cyclic carbonates with their viscous nature plasticize the PEO and are speculated to facilitate blend formation with less crystallinity of PEO and overcome the trade-offs in electrochemical properties. Herein, we investigated the various CSBO-PEO and pristine PEO membranes by performing spectroscopic and electrochemical measurements. With the ability of monomer scale up for both CSBO and PEO, we can highlight the great prospects of Soybean oil derived-PEO blends.

5.2.2 Materials and methods

Epoxidized soybean oil (ESBO) was obtained from Vandeputte Oleochemicals (Belgium). Carbon dioxide (CO_2, N48) was supplied by Air Liquide. 1,3-bis (2 hydroxyhexafluroisopropyl) benzene was purchased from Fluorochem. Poly(ethylene oxide) (M_w~1000k), tetrabutylammonium bromide (TBABr,>99%), bis(trifluoromethane)sulfonimide lithium (LiTFSI) and cellulose separator (TF48-50 (50 µm x 66 mm)) were purchased from Sigma Aldrich and TOB, respectively. Propylene carbonate (PC) was purchased from Sigma Aldrich. All reactants and

catalysts were used as received, without any further purification. Deuterated chloroform ($CDCl_3$) used for NMR spectroscopy was purchased from Eurisotop.

Note: Refer the Chapter 5.1 for characterization and electrochemical techniques.

5.2.3 Experimental section

5.2.3.1 Synthesis of CSBO-PEO and electrolyte films

The procedure of synthesis of CBSO has been followed as highlighted in experimental section 5.1.3.1 of Chpater 5.1 .CSBO-PEO blends were synthesized by mixing various amounts of CSBO and PEO (CSBO:PEO_x (y:z) y and z are the wt% of CSBO and PEO, respectively and x is the wt% of added LiTFSI) in a vial using acetonitrile solvent. The mixtures were stirred for > 6 h and then drop-cast on Teflon molds respectively and later transferred to the vacuum oven. They were maintained at 70 ^oC for ≥ 24 h in a dynamic vacuum. The CSBO-PEO SPEs were prepared following a similar procedure with LiTFSI (by wt% to CBSO-PEO) added to the CSBO-PEO mixtures prior to solvent evaporation. The dried membranes were peeled off from the molds respectively in the glove box as depicted in Scheme 5.2.1. All the structural and thermal characterization was performed on polymers without separator. In addition to free-standing blend membranes, the polymer solutions were also drop-cast on the cellulose paper for separator supported membranes. Both films were cut in a diameter of 16 mm, each which possesses a thickness of 50-200 μm.

5.2.4 Results and discussion

The CSBO-PEO blends were prepared as shown in Scheme 5.2.1 via blending. The free-standing polymer blends and cellulose supported membranes were assured solvent-free by sufficient drying in the vacuum oven at >24 h at 70 ^oC. The cellulose support was utilized to control the thickness and avoid short-circuit at higher temperature above the melting point of the investigated electrolytes. Each CSBO unit possesses six cyclic carbonates but not all of them are equally accessible to lithium-ion coordination owing to the structure and steric hindrance highlighting the need of additional lithium-conducting functionality. Therefore, we synthesized the blends in various formulations following percentages of PEO varying from 100% to 50% by

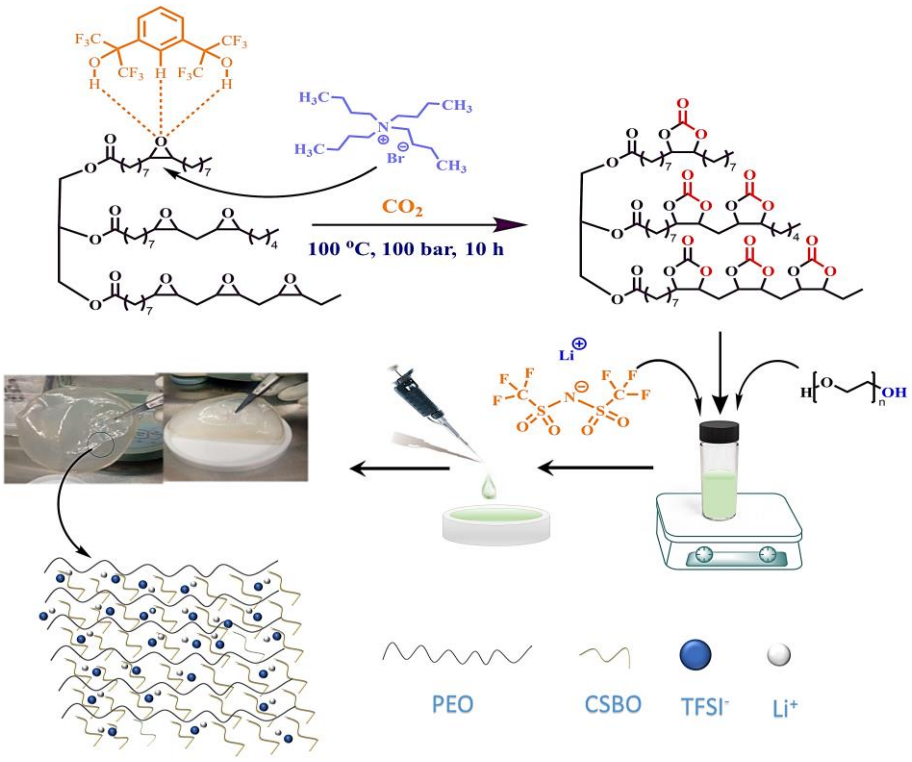

Scheme 5.2.1: Synthesis of carbonated soybean oil (CSBO) and its composite with PEO along with rough scheme of molecular chains interacting with LiTFSI.

weight, as shown in Figure 5.2.1. The pale color of the accordingly obtained blends is credited to the increasing content of CSBO. The physical nature of viscous oily CSBO did not allow less than 40% of PEO in the blend for the self-standing membrane. CSBO with 50wt% LiTFSI demonstrated amorphous and adhesive nature as reported in our previous work,[47] which was utilized for improving the performance of pristine PEO. The blends were observed to be softer and more flexible as compared to pristine PEO with and without LiTFSI.

5.2.4.1 Fourier transform infra-red spectroscopy

Fourier transform infra-red spectroscopy measurements of the blends were recorded as shown in Figure 5.2.2. The carbonyl (O=C-) of CC rings was not opened as confirmed from the stretching band at 1796 cm^{-1} for pure CBSO with shift to 1801 cm^{-1} for CSBO-PEO (10:90). Another carbonyl corresponding to the ester groups of

Figure 5.2.1: Images of CSBO:PEO (y:z) SPEs with 20% wt LiTFSI.

CSBO was detected at 1739 cm^{-1} with a slight shift at 1741 cm^{-1} for all the blends. The broadening of the peaks at 1280 cm^{-1} and 1240 cm^{-1} for CSBO-PEO (40:60 and 50:50, respectively) can be explained by a lower availability of C-O ether units than for other samples (Figure 5.2.2a).

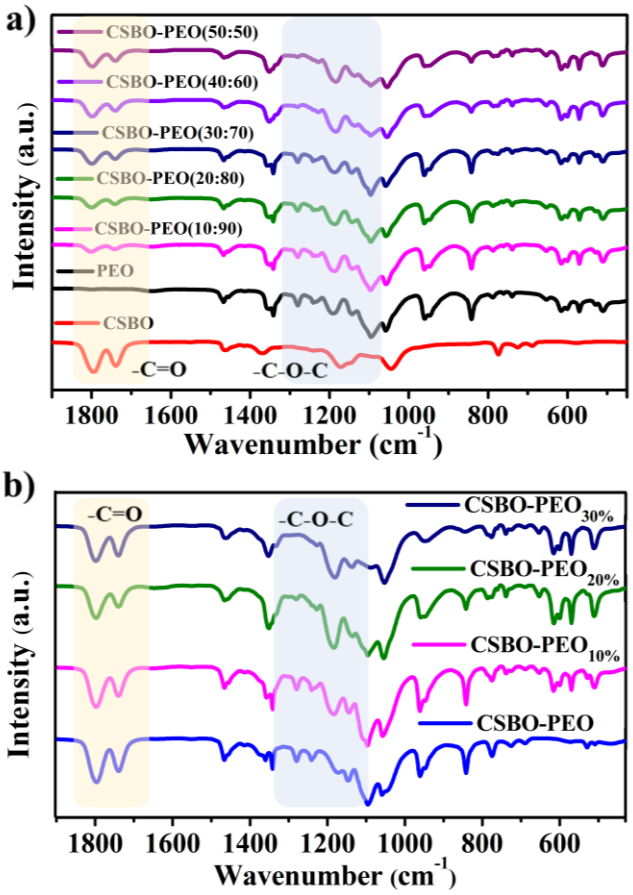

Figure 5.2.2: a) Comparative IR spectra of CSBO, PEO and composites with various formulations, respectively with 20wt% of LiTFSI ; and b) IR of CSBO-PEO (50:50 wt%) composites with LiTFSI (by wt%).

The characteristic peaks for LiTFSI were observed at 1188 cm^{-1} from SO_2 asymmetric stretching.[62,63] Further focusing on the IR spectra of CSBO-PEO (50:50) with added salt, broadening in the signals was observed with an increase in salt concentration which also resulted in increased softness of the blend. As shown in the highlighted region of Figure 5.2.4b, C=O around 1800 cm^{-1}, a shift towards lower frequency could be witnessed as salt concentration increases due to Li-ion interaction with carbonyl. While dissociation of LiTFSI was assured superior in all samples ranging from 10wt% to 30wt%.

5.2.4.2 Thermal measurements

Thermal stability underlying phase changes is a crucial investigation for designing an electrolyte. The lower is the glass transition temperature (T_g), the higher chain segmental motion in the polymer.[64] Differential scanning calorimetry has been performed for measuring T_g, melting temperature (T_m) and crystallization temperature (T_c) of the investigated samples as listed in Table 5.2.1. All the curves of the samples shown in Figure 5.2.3a contain 20wt% of LiTFSI. Almost all the samples demonstrated T_g around ~ -34 ºC except CSBO-PEO (50:50%) with -48 ºC. The T_m continued to decrease from 62.9 ºC to 45.5 ºC for 100wt% PEO to 50wt% PEO loading in the blend. (Table 5.2.1). Further analysis were performed for the CSBO-PEO (50:50 wt%) vs. salt concentration. Both T_m and T_g decrease with increasing salt concentration (Figure 5.2.3b). The T_g decreased from -10.8 ºC to -45.5 ºC from 10wt% to 20wt% of added salt. For CSBO-PEO (50:50wt%) loaded with 30wt% LITFSI, the crystalline behaviour disappears owing to the high salt concentration with an increase in T_g to -36.7 ºC.

Most of these polymer electrolytes showed T_g below 0 °C like CSBO electrolytes, as reported before.[47] The CBSO-PEO (50:50wt%) blend was investigated for thermal degradation with and without salt, as shown in Figure 5.2.3c.Initial increment beyond 100% weight can be attributed to the decomposition of adsorbed water. The decomposition of PEO starts at 185.4 ºC while for PEO-LiTFSI at 199.4 ºC in one and two phases, respectively. The degradation temperature was increased with added LiTFSI for PEO and vice versa for CSBO-PEO blend. However, the decomposition (T_d) for CSBO-PEO starts at 293ºC and decreased to 238 ºC with addition of salt in a

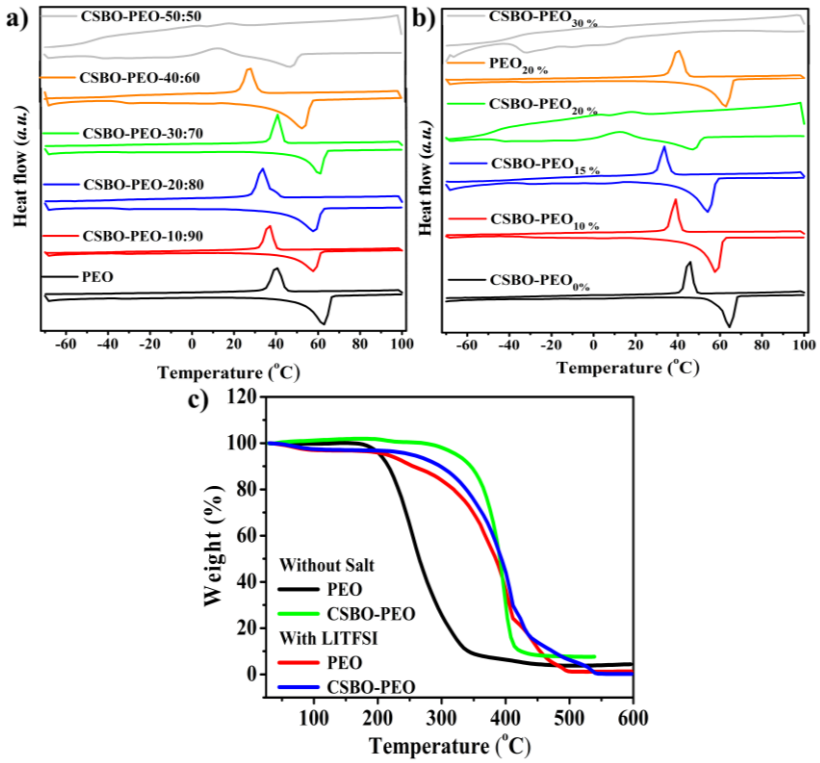

Figure 5.2.3: DSC thermograms of SPE films, a) different compositions of CSBO: PEO (y:z) with LITFSI (x: 20%); b) CSBO-PEO (y:z=50:50 wt%) with LiTFSI (x wt%); and c) Thermogravimetric analysis of PEO and CSBO-PEO (y:z=50:50 wt%) with and without LiTFSI, respectively.

reverse trend with two and three phases, respectively. The decomposition of salt could be observed beyond 400 ºC for both blend and pure PEO. Nevertheless, it is assured that the reported electrolyte could be utilized safely for the cell operation safely beyond 238 ºC without decomposition.

5.2.4.3 Ionic conductivity

The ionic conductivities of SPEs were obtained from Nyquist plots by performing potential electrical impedance spectroscopy (PEIS) at various temperatures with 10wt% to 20wt% of added LiTFSI as shown in Figure 5.2.4a. Equation 5.2.1 has been used for the calculation of the ionic conductivities (σ):

$$\sigma = \frac{l}{RS} \tag{5.2.1}$$

Table 5.2.1: DSC (T_{in} and T_{off} are the inset and offset temperature to find the T_g) and TGA data (decomposition temperature: T_d) of SPEs with all temperature value indicated in degree Celsius.

Samples-LiTFSI (wt%) CSBO:PEO (1:1 wt%)	T_m	T_c	T_{off}	T_{in}	T_g	T_d
$PEO_{20\%}$	62.9	40.7	-37.9	-31.3	-34.6	199.4
CSBO-$PEO_{0\%}$	64.6	46.0	-13.9	-7.6	-10.8	293.1
CSBO-$PEO_{10\%}$	57.6	39.0	-38.8	-21.6	-30.2	
CSBO-$PEO_{15\%}$	54.2	33.6	-37.6	-29.1	-33.3	
CSBO-$PEO_{20\%}$	47.2	17.8	-49.1	-42.0	-45.5	238.2
CSBO-$PEO_{30\%}$			-42.0	-31.5	-36.7	

where *R* is bulk electrolyte Ohmic resistance from AC impedance, *l* and *S* are the thickness and the surface area of the analysed polymer electrolyte film, respectively. The CSBO-$PEO_{20\%}$ film showed a conductivity of 1.28 x 10^{-5} S cm^{-1} yet lesser than the pure PEO electrolyte with 2.26 x 10^{-5} S cm^{-1} at room temperature. In all the blend samples, the conductivity was increased with temperature until 80 ^{o}C (Figure 5.2.4b) and the error in conductivity values were analysed to be less than 5%. The conductivity follows another linear regime from 60^{o}C onwards which could be explained by the melting of the polymer as highlighted in DSC exo curves. At elevated temperature CSBO-PEO with lower salt concentration outperform CSBO-$PEO_{20\%}$ slightly. This could be explained by the higher ion pairing and ion concentration gradient in a higher salt concentrated electrolyte. Nevertheless, the 20wt% LiTFSI amount was chosen for both blend and pure PEO with conductivity of 1.18 x 10^{-4} S cm^{-1} and 3.69 x 10^{-4} S cm^{-1}, respectively at 60 ^{o}C, for charge and discharge experiments owing to balance between the mechanical stability and charge carriers.

Moreover, the conductivity of SPEs did not seem to align well with Arrhenius behaviour following a linear regime upon the inverse of temperature. Therefore, the following data have also been fitted by using the Vogel–Fulcher-Tamman (VFT) equation (equation 5.2.2) over the temperature range of 30-80 ^{o}C,

$$\sigma T^{1/2} = A e^{-\frac{E_\alpha}{k_b (T - T_0)}} \quad (5.2.2)$$

where, A is the pre-exponential factor, *T* is the absolute temperature, T_0 is the Vogel

scaling temperature at which the free volume disappears or at which free entropy becomes zero, T_0 is related to T_g by T_g-50 K following an approximation, E_α is the pseudo-activation energy of ion transport and k_b is Boltzmann constant.[65,66] This model could be often informative on unravelling the effect of segmental motion on the overall conductivity above T_g.[67] Like Arrhenius, VFT plots also show nonlinear behaviour which have been fit into two components i.e. 20 ^oC – 60 ^oC (region 1) and 60 ^oC – 80 ^oC (region 2). The activation energy calculated from the slope of VFT plot and equation (5.2.2) is observed to decrease with salt concentration for CSBO-PEO SPEs as obtained from in Figure 5.2.4c. The lowest E_{a1} of -14.26 kJ/mol for CSBO-$PEO_{15\%}$ was calculated higher than $PEO_{20\%}$-SPE at -15.42 kJ/mol within same temperature range. However, clear increasing trend in E_{a2} was witnessed in higher temperature region above melting, in the order of $PEO_{20\%}$ (-4.91 kJ/mol) < CSBO-$PEO_{10\%}$ (-5.63 kJ/mol) < CSBO-$PEO_{15\%}$ (-8.01 kJ/mol) < CSBO-$PEO_{20\%}$ (-9.18 kJ/mol) favouring chain and ion mobility with less hindrance. The structure of CSBO indicates that all cyclic carbonate rings are not equidistant from each others and could block the Li ions due to both carbonyl and ether oxygen coordination. That could support that the inclusion of CSBO in the PEO matrix lowered mobility of Li ions preventing their fast release for hopping. Nevertheless, the investigated CSBO-PEO blend SPEs highlighted the combined conductivity of PEO and CSBO, which is far higher than pristine $CSBO_{20\%}$ based SPE as reported earlier,[47] despite the shift in the physical state of the electrolyte from oily CSBO to solid CSBO-PEO films. This is clearly evidenced by the diffusion of free ions dissolved in the fatty acid segments and chain segmental motion of CSBO within long linear chain of PEO. Table S5.2.1 in supporting information shows the E_{a1} and E_{a2} calculated for the SPEs along with the pre-exponential factor and R^2 as corresponding fitting coefficient.

5.2.4.4 Linear sweep voltammetry of SPEs

The electrochemical stability window (ESW) of SPEs was investigated by performing linear sweep voltammetry (LSV). The pure $PEO_{20\%}$ and CSBO-$PEO_{20\%}$ SPEs were submitted to a constant scan rate of 1 mV/s in the range of 0-5 V versus Li/Li^+ at 60 ^oC as shown in Figure 5.2.4d. A lithium metal chip and aluminium foil were chosen as anode and cathode, respectively. The CSBO-$PEO_{20\%}$ sample showed a broad oxidative potential of > 4.2 V compared to < 4 V for the SPE based on pure PEO.

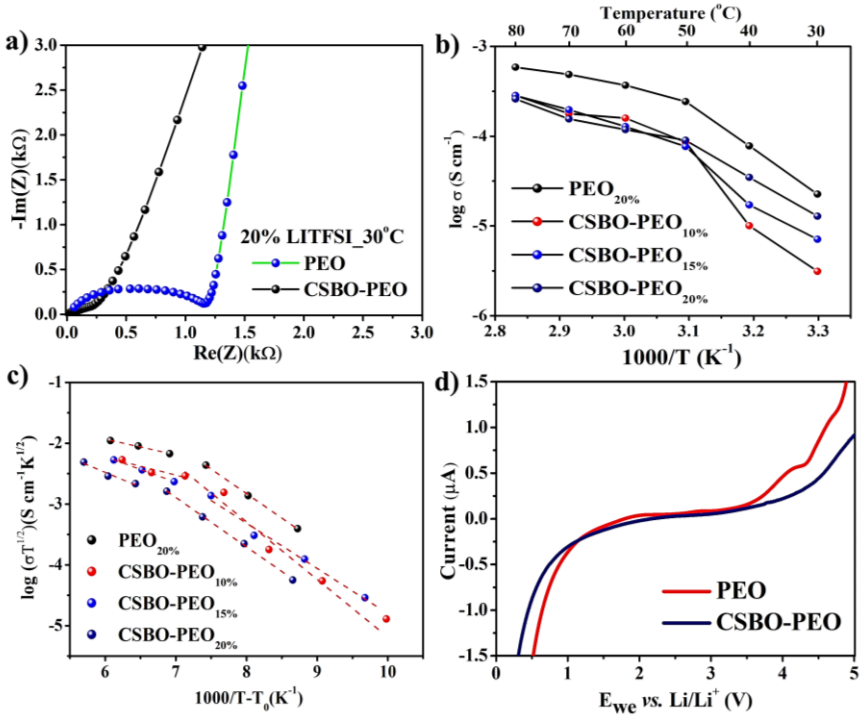

Figure 5.2.4: a) Nyquist plot of symmetric cells as a result of PEIS at 30 °C; b) Temperature dependent ionic conductivity CSBO-PEO (y:z:50:50 wt%) in comparison to $PEO_{20\%}$ (subscript indicates wt% LiTFSI); c) Temperature dependent ionic conductivity using the VFT model; d) Linear sweep voltammetry comparison of PEO and CSBO-PEO composite with 20% LiTFSI at 60°C, respectively.

There was no noticeable redox peak observed for both SPEs in the lower voltage range. The following analysis confirmed that inclusion of CSBO led to the decrease in oxidation of PEO with lithium metal boosting the lithium electrolyte interface compatibility. Partial degradation of CSBO in contact with lithium metal is believed to play a key role in the formation of a stable SEI and could also prevent or decrease further degradation of PEO. Moreover with a slight compromise in the conductivity, we could be able to achieve higher ESW and hence offer interesting electrolyte candidates for higher voltage cathodes.

5.2.4.5 Transference number

A high t_{Li^+} is advantageous for long-term cycling batteries, allowing efficient Li ions transport and lower Coulombic efficiency loss. The transference number(t_{Li^+}) of lithium cations in non-blocking Li|SPE|Li cells was determined by AC impedance

combined with DC polarization. The t_{Li^+} value was calculated using Bruce-Vincent method,[68,69] following equation 5.2.3:

$$t_{Li^+} = \frac{I_{ss}(V - I_0 R_0)}{I_0(V - I_{ss} R_{ss})} \quad (5.2.3)$$

where, V is the DC applied potential, I_0 and I_{ss} are the initial and steady state currents recorded with R_o and R_{ss} as initial and steady-state interfacial resistances from PEIS measurements at an AC sinusoidal voltage of 10 mV. The chronoamperometry plot is shown in Figures 5.2.5a and 5.2.5b with impedance before and after polarization for both SPEs at 60 °C. The current values cannot be numerically compared due to different thickness of both SPEs. As a result of constant potential of 10 mV, the interfacial resistance decreased from 712.7 to 658.9 Ω, while current varies from an initial value of 11.17 µA to a stabilized value of 5.23 µA, which led to the calculation of the t_{Li^+} to be 0.15 ± 0.04 for PEO films. While t_{Li^+} of the CSBO-PEO SPE was calculated to be 0.36 ±.0.04 at 60 °C from Figure 5.2.5b with interfacial resistance increasing from 2025.8 to 2087.4 Ω and initial current from 0.92 µA to 0.37 µA of steady-state current.

5.2.4.6 Aging study and stripping-plating

The PEIS measurement as a function of time is recorded to track the effect of reactive species at the electrode surface. This is often performed at open circuit potential (OCP) to analyse the effect of aging at the bulk and interface level. For solid-state batteries, another interesting investigation revolves around the absence or minimal formation of lithium dendrites, which also motivates the mechanical investigation of the solid-state electrolytes. We performed aging analysis via Nyquist plots as shown in Figures 5.2.5c and 5.2.5d at RT and OCP after equilibrating both cells at 60 °C. The resistance was dropped in case of CSBO-PEO after prolonged heating due to the change in the thickness of the electrolyte membrane while this phenomenon was less pronounced in case of the PEO membrane. The percentage increase in electrolytic resistance and interfacial resistance from day 1 to day 14 was 138.6% and 171.8% for PEO, respectively. However, it was recorded to be 151.7% and 136.9% in the case of

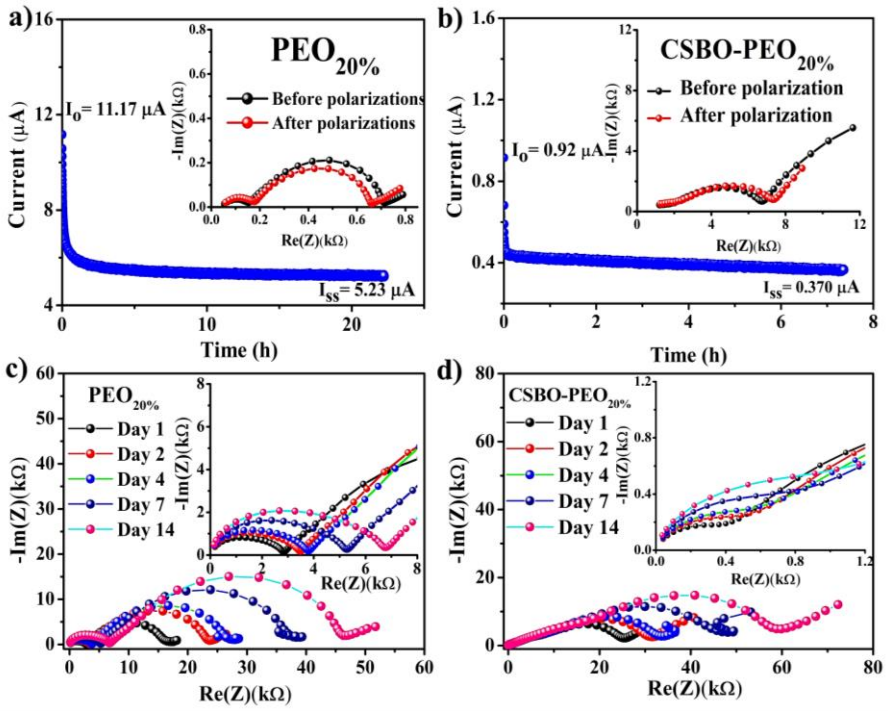

Figure 5.2.5: a) and b) Transference number measurement using chronoamperometry (DC polarization) followed by AC PEIS as demonstrated inset; c) and d) Aging studies: PEIS with time at open circuit potential (OCP) of both Li|$PEO_{20\%}$|Li cell and Li|CSBO-$PEO_{20\%}$|Li cells, respectively (CSBO:PEO=50:50wt%, subscript indicating x wt% of LiTFSI) (magnified plot in the inset).

CSBO-PEO (refer to Table S5.2.2 for resistance values). The less pronounced semi-circle in the latter case could be attributed to imperfect geometrical capacitive behaviour within the bulk of electrolyte of the soft CSBO-PEO membrane. The increase in electrolyte resistance can be related to the higher reactivity of carbonates in the blend membrane. However, the lower percentage increase in interfacial resistance compared to the PEO membrane can be attributed to the formation of an optimized SEI at the lithium metal surface in the presence of CSBO, as discussed before.

The stability of lithium metal and dendrites formation have been also qualitatively studied via long-term stripping and plating of lithium for a symmetric Li|SPE|Li cell. Galvanostatic charge-discharge for 1 h each was performed for each cell held at 60 ^{o}C

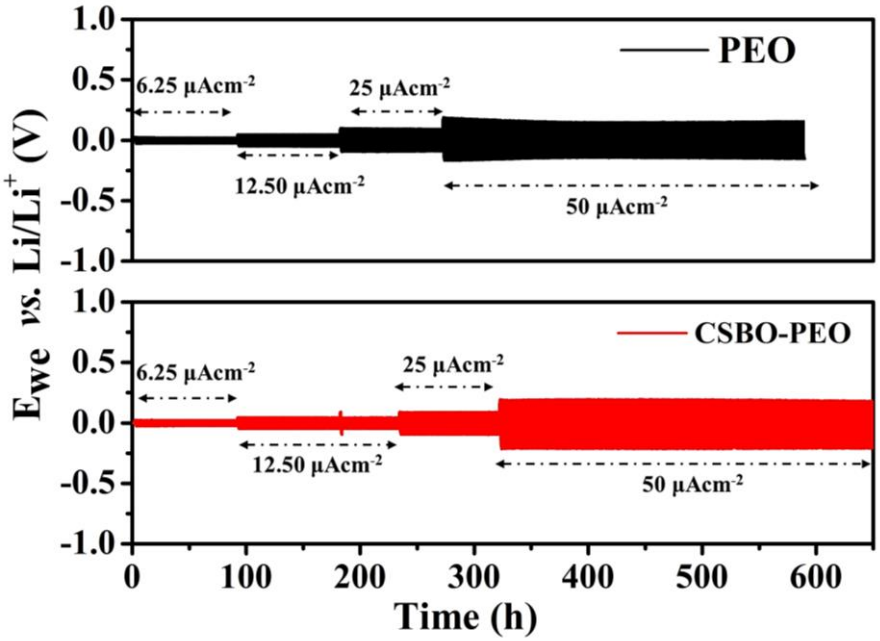

Figure 5.2.6: a) Galvanostatic charge-discharge voltage profile for stripping-plating at various current densities at 60 ºC with Li|SPE|Li symmetric cells, respectively (CSBO:PEO=50:50wt%, both SPEs with 20wt% LiTFSI).

in climate chamber followed by 6 h of rest at the current densities of 6.25 µA cm^{-2}, 12.5 µA cm^{-2}, 25 µA cm^{-2} and 50 µA cm^{-2} for more than 45 cycles each, respectively. Both SPE-based cells recorded similar net overpotential of ~25 mV and ~23 mV for PEO and CSBO-PEO, respectively, which increased consistently to ~45 mV and ~47 mV at 12.5 µA cm^{-2}. Upon further increment in the current density to 50 µA cm^{-2}, a trivial elevation of overpotential to ~190 mV was observed as shown in Figure 5.1.6. The constant overpotential recorded over more than 300 cycles hints at the formation of a stable passivation layer constituting SEI. With these findings, it could be speculated that the investigated SPEs could facilitate high Coulombic efficiency and reversibility of lithium-ion transport across the electrolyte. Moreover, with stripping and plating experiment of lithium with both SPEs at mentioned current densities, it is still not clear to discriminate the effect of CSBO into the CBSO-PEO blend.

5.2.4.7 Li-metal battery prototypes

The lithium metal batteries have been fabricated using LFP cathodes, lithium metal anodes and the investigated SPEs. In case of full metal cells, we have incorporated PEO and CSBO-PEO membranes on sustainable cellulose separators for the controlled thickness and transport channel. We have demonstrated charge-discharge of LFP-based cells on both SPEs between cut-off voltages of 4 to 2 V at 60 ^{o}C via constant current cycling also called galvanostatic charge–discharge and have presented a comparative study as depicted in Figure 5.2.7. With the CSBO-PEO SPEs, specific discharge capacities of 108 mAh g^{-1}, 105 mAh g^{-1} and 99 mAh g^{-1} were achieved for 1st, 100th and 250th cycles at 0.1C, respectively. On contrary, SPEs based on PEO at 0.1 C delivered 90 mAh g^{-1} ,103 mAh g^{-1} and 74 mAh g^{-1} corresponding to 1st, 50th and 100th discharge cycles and they further continued to decay as shown in Figure 5.2.7b. Despite the performances of CSBO-PEO SPEs were superior to pure PEO SPEs, higher polarisations were observed in former than later. Polarizations of < ~0.3 V and ~0.1 V were recorded during the first cycle, while they decreased to ~0.28 V and~0.06 V in subsequent 100th cycles for CSBO-PEO and PEO SPEs, respectively. The lower polarization in case of PEO SPEs can be supported by their slightly higher conductivity and the decrement of the overpotentials could be credited to the stabilization of the SEI at the lithium metal. The capacity fading was clearly observed in case of PEO SPEs after 25 cycles onward with calculated capacity retention of <80% after 125 cycles whereas 93.4% were recorded for CSBO-PEO SPEs after 200 cycles.

While the CSBO-PEO demonstrated almost no cycling at higher current density of 1C and 2C, it delivered specific discharge capacities of 54 mAh g^{-1}, 108 mAh g^{-1} and 122 mAh g^{-1} at the C-rates of 0.5 C, 0.1C and 0.05C, respectively (Figure 5.2.7c). The rate capability plot as shown in Figure 5.2.7d highlights the cells recover their capacity despite failure and cycling at every higher current rate while they were cycled again at 0.1C and 0.05 C respectively after 25 cycles. The same cell was continued to run at 0.1C as shown in Figure 5.2.7b for longer cycles, and it can be noted that the superior performance was recorded resembling to real-testing condition. The Coulombic efficiency was more than 98% during most of the cycles, which supports the efficient mobility of lithium. We also tested LFP cells with our SPEs without cellulose support

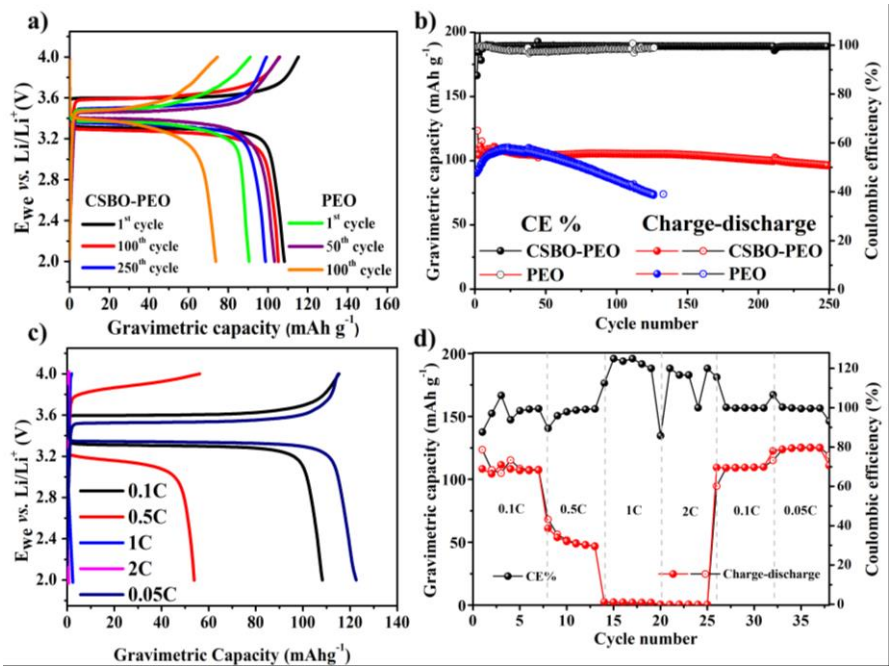

Figure 5.2.7: a) Galvanostatic charge-discharge voltage profiles for Li|SPE@CP|LFP cells based on PEO and CSBO-PEO SPEs at 0.05C, 60 ºC during following cycles; b) Capacity retention plot with cycle number 0.05C at 60 ºC; c) Galvanostatic charge-discharge voltage profiles at different C-rates; and d) Rate capability plot with different C-rates for for Li|CSBO-$PEO_{20\%}$@CP|LFP, (whereas, for both PEO and CSBO:PEO=50:50wt% supported on cellulose separator, with 20 wt% of LiTFSI).

at lower temperature of 40 ºC in climate chamber at 0.1 C which witnessed slightly higher polarization of 0.37 V during the initial cycle. In the first cycles, a lower capacity of 40 mAh g^{-1} was obtained, while it kept on increasing and was calculated to be 80 mAh g^{-1} for the 100th cycle at 0.1C rate. The capacity was observed to be increasing and remained constant after 60 cycles to 150 cycles of charge-discharge with excellent Coulombic efficiency as shown in supporting information Figure S5.2.1.

5.2.4.8 Post-cycling XPS analysis on interfaces

A qualitative yet comparative investigation has been attempted on SPEs cycled cells based on either PEO or PEO-CSBO blend in a Li|SPE@CP|LFP cell configuration. Both SPEs based cells were cycled for >100 cycles at 0.1C at 60 ºC prior to post-mortem analysis. HR-XPS measurements were performed on the surface of cycled Li-

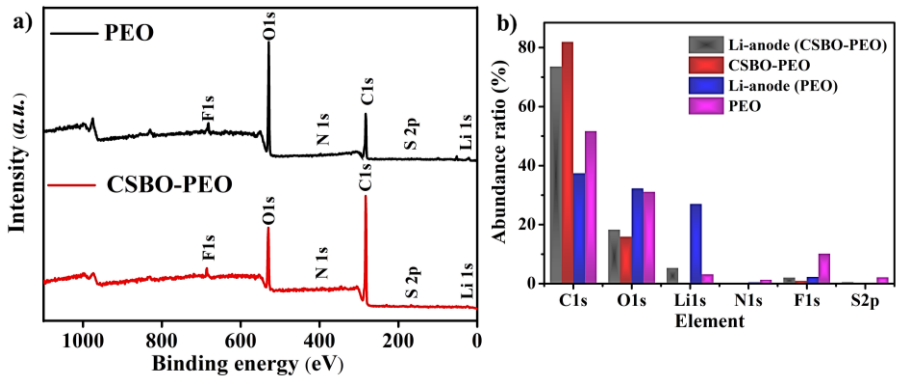

Figure 5.2.8: a) Survey spectrum of Li-anode of PEO and CSBO-PEO SPE based Li-LFP cells after 100+ cycling and b) Abundance ratio percentage of surface elements constituting SEI for Li-anode and corresponding SPE films.

metal and SPEs from PEO and CSBO-PEO based cells. The abundance percentage highlighted the majority of carbon and oxygen elements in both SPEs as well as in survey spectra (Figures 5.2.8a and 5.2.8b). However, a lower percentage of carbon is detected for the PEO cell relatively with higher lithium content meaning the SEI of the PEO cell contains less carbon species including adventitious carbon due to lower reactivity than the CSBO-PEO blend. On the other hand, a higher amount of fluorine is detected for the PEO than for the blend one indicating more decomposition of LiTFSI. The HR-XPS spectra for comparative Li-metal surfaces have been depicted in Figure 5.2.9.

HR-XPS of C1s indicates peaks at 284.8 eV, 286.4 eV, 287.7 eV, 288.7 eV, 289.7 eV for C-C/C-H, C-O/N, O-C-O/C=O, O-C=O, and CO_3^{2-}, respectively in the PEO cell and at 284.8 eV, 286.4 eV, 287.8 eV, 289.1 eV, and 290.4 eV corresponding to C-C/C-H, C-O/N, O-C-O/C=O, CO_3^{-2}, and - (O-C=O)-O-, respectively for the CSBO-PEO cell.[57] Those results confirm that organic carbonates in CSBO have a higher reactivity towards lithium metal than PEO and largely contribute to the formation of stable SEI in case of the CSBO-PEO cell. As far as the F1s spectra are concerned, the PEO cell recorded higher decomposition of LiTFSI to LiF (1.9% at 684.7 eV and 0.2% of CF_3 at 688.5 eV, Figure 5.2.9e) compared to the CSBO-PEO cell (0.5% of LiF at 684.6, 1.5% of CF_3 at 688.5 eV, Figure 5.2.9b).[70] Higher CF_3 content in the CSBO-PEO cell might be credited to lower LiTFSI decomposition (as well as catalyst

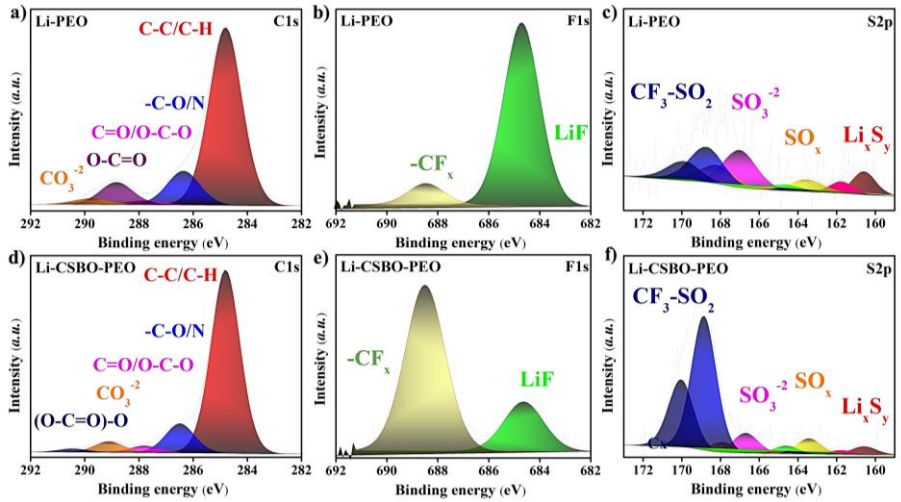

Figure 5.2.9: HR-XPS of a.) and d.) Carbon, b.) and e.) Fluorine and c.) and f.) Sulphur for lithium anode surface of PEO and CSBO-PEO cells after cycling with LFP, respectively.

involved in synthesis of CSBO) due to $TFSI^-$ ion trapped around CC rings resulting in lower concentration gradient at the surface as highlighted above. The Sulphur, S2p from SEI of both SPEs is deconvoluted into four species in double splitting involving CF_3-SO_2, SO_4^{-2}, SO_x and Sulphides in the B.E of ~168.7 eV–160.6 eV respectively (Figure 5.2.9c and 5.2.9f) evolving from LiTFSI.[71]

Other elemental HR-XPS of N1s, O1s and Li1s has been provided in the supporting information, Figure S5.2.2. Again, higher fluoride content was detected in case of the PEO cell with more $–CF_3$ than LiF due to limited reactivity of LiTFSI and higher concentration gradients as contrary to the CSBO-PEO blend cell. To summarize, we discovered that addition of CSBO to PEO decreases the reactivity of PEO chains which benefits the superior Li-transport, broadened ESW along with a stable SEI layer at the anode.

5.2.5 Conclusion

In summary, we have reported here blend electrolyte membranes from carbonated soybean oil and poly(ethylene oxide) via facile blending approach. CBSO-PEO blends offered lower rigidity, slight adhesiveness and thus good interfacial contact with electrodes compare to PEO. With our structural analysis, we confirmed the cyclic carbonates remain integrated as rings without being opened by hydroxyl groups of

PEO chains. Due to the oily nature of CBSO, CBSO-PEO blends possess lower melting temperatures and yet similar glass transition temperatures as of PEO in addition to extended degradation temperatures. Coin cells were fabricated both via self-standing membranes of both polymers and cellulose supported polymers with controlled thickness for electrochemical measurements. The inclusion of CSBO molecules didn't result in the increase in the conductivity of blend membranes but rather offered crucial properties like, extension of electrochemical stability window to > 4.2 V for blends in relative < 3.9 V for PEO versus Li/Li^+. The presence of carbonated moieties is believed to contribute to the beneficial decomposition of the electrolytes at the electrodes for SEI, and to lower the reaction of PEO chains with lithium metal. In our investigation, we found that the transference number was increased to more than double for the CSBO-PEO blend which is supposed to significantly improve the charge-discharge performance of the further investigated LFP-based cells. Our blend delivered stable cycling of LFP cathodes with lithium metal beyond 250+ cycles with as high capacity as 122 mAh g^1 on contrary to capacity fading in case of PEO-LFP cells. In the post-mortem analysis, the lithium metal reactivity and the resulting decomposed electrolytic species were confirmed as well as the crucial role of CSBO decomposition in forming a stable SEI and in preventing further PEO decomposition. The attempts to increase the green footprint and sustainability of the electrolyte was successfully achieved in our work and would encourage more efforts in future in line with state of art polymer electrolytes to match the required expectations of solid-state batteries with high energy and power density.

Bibliography

1. Benveniste, G.; Rallo, H.; Canals Casals, L.; Merino, A.; Amante, B., Comparison of the state of Lithium-Sulphur and lithium-ion batteries applied to electromobility. *Journal of Environmental Management* **2018,** *226*, 1-12.
2. Aurbach, D.; McCloskey, B. D.; Nazar, L. F.; Bruce, P. G., Advances in understanding mechanisms underpinning lithium–air batteries. *Nature Energy* **2016,** *1* (9), 16128.
3. Armand, M.; Axmann, P.; Bresser, D.; Copley, M.; Edström, K.; Ekberg, C.; Guyomard, D.; Lestriez, B.; Novák, P.; Petranikova, M.; Porcher, W.; Trabesinger, S.; Wohlfahrt-Mehrens, M.; Zhang, H., Lithium-ion batteries – Current state of the art and anticipated developments. *Journal of Power Sources* **2020,** *479*, 228708.
4. Winter, M.; Barnett, B.; Xu, K., Before Li Ion Batteries. *Chemical Reviews* **2018,** *118* (23), 11433-11456.
5. Ji, L.; Lin, Z.; Alcoutlabi, M.; Zhang, X., Recent developments in nanostructured anode materials for rechargeable lithium-ion batteries. *Energy & Environmental Science* **2011,** *4* (8), 2682-2699.
6. Li, J.; Cai, Y.; Wu, H.; Yu, Z.; Yan, X.; Zhang, Q.; Gao, T. Z.; Liu, K.; Jia, X.; Bao, Z., Polymers in Lithium-Ion and Lithium Metal Batteries. *Advanced Energy Materials* **2021,** *11* (15), 2003239.
7. Etacheri, V.; Marom, R.; Elazari, R.; Salitra, G.; Aurbach, D., Challenges in the development of advanced Li-ion batteries: a review. *Energy & Environmental Science* **2011,** *4* (9), 3243-3262.
8. Deng, D., Li-ion batteries: basics, progress, and challenges. *Energy Science & Engineering* **2015,** *3* (5), 385-418.
9. Su, L.; Manthiram, A., Lithium-Metal Batteries via Suppressing Li Dendrite Growth and Improving Coulombic Efficiency. *Small Structures* **2022,** *3* (10), 2200114.
10. Aslam, M. K.; Niu, Y.; Hussain, T.; Tabassum, H.; Tang, W.; Xu, M.; Ahuja, R., How to avoid dendrite formation in metal batteries: Innovative strategies for dendrite suppression. *Nano Energy* **2021,** *86*, 106142.
11. Takada, K., Progress and prospective of solid-state lithium batteries. *Acta Materialia* **2013,** *61* (3), 759-770.
12. Varzi, A.; Raccichini, R.; Passerini, S.; Scrosati, B., Challenges and prospects of the role of solid electrolytes in the revitalization of lithium metal batteries. *Journal of Materials Chemistry A* **2016,** *4* (44), 17251-17259.
13. Armand, M., The history of polymer electrolytes. *Solid State Ionics* **1994,** *69* (3), 309-319.
14. Payne, D. R.; Wright, P. V., Morphology and ionic conductivity of some lithium ion complexes with poly(ethylene oxide). *Polymer* **1982,** *23* (5), 690-693.
15. Grundish, N. S.; Goodenough, J. B.; Khani, H., Designing composite polymer electrolytes for all-solid-state lithium batteries. *Current Opinion in Electrochemistry* **2021,** *30*, 100828.
16. Agrawal, R. C.; Pandey, G. P., Solid polymer electrolytes: materials designing and all-solid-state battery applications: an overview. *Journal of Physics D: Applied Physics* **2008,** *41* (22), 223001.
17. Xue, Z.; He, D.; Xie, X., Poly(ethylene oxide)-based electrolytes for lithium-ion batteries. *Journal of Materials Chemistry A* **2015,** *3* (38), 19218-19253.
18. Yue, L.; Ma, J.; Zhang, J.; Zhao, J.; Dong, S.; Liu, Z.; Cui, G.; Chen, L., All solid-state polymer electrolytes for high-performance lithium ion batteries. *Energy Storage Materials* **2016,** *5*, 139-164.
19. Wright, P. V., Polymer electrolytes—the early days. *Electrochimica Acta* **1998,** *43* (10), 1137-1143.
20. Murata, K.; Izuchi, S.; Yoshihisa, Y., An overview of the research and development of solid polymer electrolyte batteries. *Electrochimica Acta* **2000,** *45* (8), 1501-1508.
21. Meng, N.; Lian, F.; Cui, G., Macromolecular Design of Lithium Conductive Polymer as Electrolyte for Solid-State Lithium Batteries. *Small* **2021,** *17* (3), 2005762.
22. Ghosh, A.; Wang, C.; Kofinas, P., Block Copolymer Solid Battery Electrolyte with High Li-Ion Transference Number. *Journal of The Electrochemical Society* **2010,** *157*, A846-A849.
23. Young, W.-S.; Kuan, W.-F.; Epps, I. I. I. T. H., Block copolymer electrolytes for rechargeable lithium batteries. *Journal of Polymer Science Part B: Polymer Physics* **2014,** *52* (1), 1-16.
24. Rolland, J.; Brassinne, J.; Bourgeois, J. P.; Poggi, E.; Vlad, A.; Gohy, J. F., Chemically anchored liquid-PEO based block copolymer electrolytes for solid-state lithium-ion batteries. *Journal of Materials Chemistry A* **2014,** *2* (30), 11839-11846.
25. Manuel Stephan, A.; Nahm, K. S., Review on composite polymer electrolytes for lithium batteries. *Polymer* **2006,** *47* (16), 5952-5964.
26. Ngai, K. S.; Ramesh, S.; Ramesh, K.; Juan, J. C., A review of polymer electrolytes: fundamental, approaches and applications. *Ionics* **2016,** *22* (8), 1259-1279.
27. Tang, S.; Guo, W.; Fu, Y., Advances in Composite Polymer Electrolytes for Lithium Batteries and Beyond. *Advanced Energy Materials* **2021,** *11* (2), 2000802.
28. Gao, J.; Wang, C.; Han, D.-W.; Shin, D.-M., Single-ion conducting polymer electrolytes as a key jigsaw piece for next-generation battery applications. *Chemical Science* **2021,** *12* (40), 13248-13272.
29. Zhu, J.; Zhang, Z.; Zhao, S.; Westover, A. S.; Belharouak, I.; Cao, P.-F., Single-Ion Conducting Polymer Electrolytes for Solid-State Lithium–Metal Batteries: Design, Performance, and Challenges. *Advanced Energy Materials* **2021,** *11* (14), 2003836.
30. Zhang, H.; Li, C.; Piszcz, M.; Coya, E.; Rojo, T.; Rodriguez-Martinez, L. M.; Armand, M.; Zhou, Z., Single lithium-ion conducting solid polymer electrolytes: advances and perspectives. *Chemical Society Reviews* **2017,** *46* (3), 797-815.
31. Manuel Stephan, A., Review on gel polymer electrolytes for lithium batteries. *European Polymer Journal* **2006,** *42* (1), 21-42.
32. Zhu, M.; Wu, J.; Wang, Y.; Song, M.; Long, L.; Siyal, S. H.; Yang, X.; Sui, G., Recent advances in gel polymer electrolyte for high-performance lithium batteries. *Journal of Energy Chemistry* **2019,** *37*, 126-142.
33. Liang, J.; Luo, J.; Sun, Q.; Yang, X.; Li, R.; Sun, X., Recent progress on solid-state hybrid electrolytes for solid-state lithium batteries. *Energy Storage Materials* **2019,** *21*, 308-334.

34. Fan, P.; Liu, H.; Marosz, V.; Samuels, N. T.; Suib, S. L.; Sun, L.; Liao, L., High Performance Composite Polymer Electrolytes for Lithium-Ion Batteries. *Advanced Functional Materials* **2021,** *31* (23), 2101380.
35. Mindemark, J.; Törmä, E.; Sun, B.; Brandell, D., Copolymers of trimethylene carbonate and ε-caprolactone as electrolytes for lithium-ion batteries. *Polymer* **2015,** *63*, 91-98.
36. Lin, C.-K.; Wu, I. D., Investigating the effect of interaction behavior on the ionic conductivity of Polyester/LiClO4 blend systems. *Polymer* **2011,** *52* (18), 4106-4113.
37. Mindemark, J.; Lacey, M. J.; Bowden, T.; Brandell, D., Beyond PEO—Alternative host materials for Li+-conducting solid polymer electrolytes. *Progress in Polymer Science* **2018,** *81*, 114-143.
38. Zhang, J.; Yang, J.; Dong, T.; Zhang, M.; Chai, J.; Dong, S.; Wu, T.; Zhou, X.; Cui, G., Aliphatic Polycarbonate-Based Solid-State Polymer Electrolytes for Advanced Lithium Batteries: Advances and Perspective. *Small* **2018,** *14* (36), 1800821.
39. Kimura, K.; Yajima, M.; Tominaga, Y., A highly-concentrated poly(ethylene carbonate)-based electrolyte for all-solid-state Li battery working at room temperature. *Electrochemistry Communications* **2016,** *66*, 46-48.
40. Every, H. A.; Zhou, F.; Forsyth, M.; MacFarlane, D. R., Lithium ion mobility in poly(vinyl alcohol) based polymer electrolytes as determined by 7Li NMR spectroscopy. *Electrochimica Acta* **1998,** *43* (10), 1465-1469.
41. Zhu, Y. S.; Wang, X. J.; Hou, Y. Y.; Gao, X. W.; Liu, L. L.; Wu, Y. P.; Shimizu, M., A new single-ion polymer electrolyte based on polyvinyl alcohol for lithium ion batteries. *Electrochimica Acta* **2013,** *87*, 113-118.
42. Lv, Z.; Tang, Y.; Dong, S.; Zhou, Q.; Cui, G., Polyurethane-based polymer electrolytes for lithium Batteries: Advances and perspectives. *Chemical Engineering Journal* **2022,** *430*, 132659.
43. Misenan, M. S. M.; Khiar, A. S. A.; Eren, T., Polyurethane-based polymer electrolyte for lithium ion batteries: a review. *Polymer International* **2022,** *71* (7), 751-769.
44. Raj, A.; Grignard, B.; Detrembleur, C.; Gohy, J.-F., Polyhydroxy Urethanes and Carbonates Bearing Bio-Based Solid Electrolyte for Solid-State Lithium Batteries. *ECS Meeting Abstracts* **2022,** *MA2022-02* (4), 493.
45. Lin, Y.; Li, J.; Lai, Y.; Yuan, C.; Cheng, Y.; Liu, J., A wider temperature range polymer electrolyte for all-solid-state lithium ion batteries. *RSC Advances* **2013,** *3* (27), 10722-10730.
46. Wang, Q.; Zhang, H.; Cui, Z.; Zhou, Q.; Shangguan, X.; Tian, S.; Zhou, X.; Cui, G., Siloxane-based polymer electrolytes for solid-state lithium batteries. *Energy Storage Materials* **2019,** *23*, 466-490.
47. Raj, A.; Panchireddy, S.; Grignard, B.; Detrembleur, C.; Gohy, J.-F., Bio-Based Solid Electrolytes Bearing Cyclic Carbonates for Solid-State Lithium Metal Batteries. *ChemSusChem* **2022,** *15* (18), e202200913.
48. Kai Ling, C.; Aung, M. M.; Rayung, M.; Chuah Abdullah, L.; Lim, H. N.; Mohd Noor, I. S., Performance of Ionic Transport Properties in Vegetable Oil-Based Polyurethane Acrylate Gel Polymer Electrolyte. *ACS Omega* **2019,** *4* (2), 2554-2564.
49. Wang, S.; Zhang, L.; Zeng, Q.; Liu, X.; Lai, W.-Y.; Zhang, L., Cellulose Microcrystals with Brush-Like Architectures as Flexible All-Solid-State Polymer Electrolyte for Lithium-Ion Battery. *ACS Sustainable Chemistry & Engineering* **2020,** *8* (8), 3200-3207.
50. Padil, V. V. T.; Ramesh, M. V.; Cheong, J. Y., Comprehensive review on gum-based electrolytes for energy applications: current status and future projection. *Materials Today Chemistry* **2023,** *28*, 101373.
51. Payne, R.; Theodorou, I. E., Dielectric properties and relaxation in ethylene carbonate and propylene carbonate. *The Journal of Physical Chemistry* **1972,** *76* (20), 2892-2900.
52. Chernyak, Y., Dielectric Constant, Dipole Moment, and Solubility Parameters of Some Cyclic Acid Esters. *Journal of Chemical & Engineering Data* **2006,** *51* (2), 416-418.
53. Tominaga, Y.; Nanthana, V.; Tohyama, D., Ionic conduction in poly(ethylene carbonate)-based rubbery electrolytes including lithium salts. *Polymer Journal* **2012,** *44* (12), 1155-1158.
54. Boujioui, F.; Zhuge, F.; Damerow, H.; Wehbi, M.; Améduri, B.; Gohy, J.-F., Solid polymer electrolytes from a fluorinated copolymer bearing cyclic carbonate pendant groups. *Journal of Materials Chemistry A* **2018,** *6* (18), 8514-8522.
55. Boujioui, F.; Damerow, H.; Zhuge, F.; Gohy, J.-F., Solid Polymer Electrolytes Based on Copolymers of Cyclic Carbonate Acrylate and n-Butylacrylate. *Macromolecular Chemistry and Physics* **2020,** *221* (6), 1900556.
56. Zhou, B.; Zhou, Y.; Lai, L.; Chen, Z.; Li, J.; Jiang, Y.; Liu, J.; Wang, Z.; Xue, Z., Fabrication of Borate-Based Porous Polymer Electrolytes Containing Cyclic Carbonate for High-Performance Lithium Metal Batteries. *ACS Applied Energy Materials* **2021,** *4* (9), 9582-9593.
57. Bekaert, L.; Raj, A.; Gohy, J.-F.; Hubin, A.; De Proft, F.; Mamme, M. H., Assessing the Long-Term Reactivity to Achieve Compatible Electrolyte–Electrode Interfaces for Solid-State Rechargeable Lithium Batteries Using First-Principles Calculations. *The Journal of Physical Chemistry C* **2022,** *126* (19), 8227-8237.
58. Raj, A.; Grignard, B.; Detrembleur, C.; Gohy, J. F., Extending Electrochemical Stability Window As a Result of Carbonate-Ketone Side Chain Modified Polyethylene Glycol Electrolytes for Lithium Batteries. *ECS Meeting Abstracts* **2022,** *MA2022-01* (2), 254.
59. Adenusi, H.; Chass, G. A.; Passerini, S.; Tian, K. V.; Chen, G., Lithium Batteries and the Solid Electrolyte Interphase (SEI)—Progress and Outlook. *Advanced Energy Materials* **2023,** *13* (10), 2203307.
60. Panchireddy, S.; Grignard, B.; Thomassin, J.-M.; Jérôme, C.; Detrembleur, C., Bio-based poly(hydroxyurethane) glues for metal substrates. *Polymer Chemistry* **2018,** *9*, 2650.
61. Leroy, S.; Martinez, H.; Dedryvère, R.; Lemordant, D.; Gonbeau, D., Influence of the lithium salt nature over the surface film formation on a graphite electrode in Li-ion batteries: An XPS study. *Applied Surface Science* **2007,** *253* (11), 4895-4905.
62. Rey, I.; Lassègues, J. C.; Grondin, J.; Servant, L., Infrared and Raman study of the PEO-LiTFSI polymer electrolyte. *Electrochimica Acta* **1998,** *43* (10), 1505-1510.
63. Wong, D. H. C.; Vitale, A.; Devaux, D.; Taylor, A.; Pandya, A. A.; Hallinan, D. T.; Thelen, J. L.; Mecham, S. J.; Lux, S. F.; Lapides, A. M.; Resnick, P. R.; Meyer, T. J.; Kostecki, R. M.; Balsara, N. P.; DeSimone, J. M., Phase Behavior and Electrochemical Characterization of Blends of Perfluoropolyether, Poly(ethylene glycol), and a Lithium Salt. *Chemistry of Materials* **2015,** *27* (2), 597-603.

64. Golodnitsky, D.; Strauss, E.; Peled, E.; Greenbaum, S., Review—On Order and Disorder in Polymer Electrolytes. *Journal of The Electrochemical Society* **2015,** *162* (14), A2551.
65. M.A. Ratner, i. J. R. M., C.A. Vincent Eds, In *Polymer Electrolyte Reviews 1*, Elsevier: Londen, 1987.
66. Karan, N. K.; Pradhan, D. K.; Thomas, R.; Natesan, B.; Katiyar, R. S., Solid polymer electrolytes based on polyethylene oxide and lithium trifluoro- methane sulfonate (PEO–LiCF3SO3): Ionic conductivity and dielectric relaxation. *Solid State Ionics* **2008,** *179* (19), 689-696.
67. Miyamoto, T.; Shibayama, K., Free-volume model for ionic conductivity in polymers. *Journal of Applied Physics* **2003,** *44* (12), 5372-5376.
68. Evans, J.; Vincent, C. A.; Bruce, P. G., Electrochemical measurement of transference numbers in polymer electrolytes. *Polymer* **1987,** *28* (13), 2324-2328.
69. Bruce, P. G.; Vincent, C. A., Steady state current flow in solid binary electrolyte cells. *Journal of Electroanalytical Chemistry and Interfacial Electrochemistry* **1987,** *225* (1), 1-17.
70. Grissa, R.; Fernandez, V.; Fairley, N.; Hamon, J.; Stephant, N.; Rolland, J.; Bouchet, R.; Lecuyer, M.; Deschamps, M.; Guyomard, D.; Moreau, P., XPS and SEM-EDX Study of Electrolyte Nature Effect on Li Electrode in Lithium Metal Batteries. *ACS Applied Energy Materials* **2018,** *1* (10), 5694-5702.
71. Chu, H.; Noh, H.; Kim, Y.-J.; Yuk, S.; Lee, J.-H.; Lee, J.; Kwack, H.; Kim, Y.; Yang, D.-K.; Kim, H.-T., Achieving three-dimensional lithium sulfide growth in lithium-sulfur batteries using high-donor-number anions. *Nature Communications* **2019,** *10* (1), 188.

Supporting Information

Carbonated Soybean oil blends with poly(ethylene oxide)

Table S5.2.1: Activation energy and pre-exponential factor as calculated from the two region linear fitting of VFT plots (region 1 and region 2 correspond to lower (20 ºC – 50 ºC) and higher temperature (60 ºC – 80 ºC), respectively).

CSBO-PEO (1:1)	**Adj. R_1^2**	**Adj. R_2^2**	**lnA_1**	**lnA_1**	***E_{a1}* (kJ-mol^{-1})**	***E_{a2}* (kJ-mol^{-1})**
PEO	0.99	0.99	5.03	-0.39	-15.43	-4.91
10%	0.91	0.75	4.29	-0.47	-19.79	-5.63
15%	0.98	0.99	2.64	0.29	-14.26	-8.01
20%	0.99	0.92	2.79	0.39	-15.54	-9.18

Table S5.2.2: Aging analysis: Interfacial (R_{in}) and bulk (R_b) resistance of the symmetric Li-Li cells at OCP.

Day	**at OCP**			
	$PEO_{20\%}$		$CSBO\text{-}PEO_{20\%}$	
	R_b	R_{in}	R_b	R_{in}
1st	2836.3	17185.1	362.4	25266.8
2nd	3489.1	23686.8	431.8	31579.0
4th	3798.7	27933.7	530.5	33645.4
7th	5283.4	38322.6	857.5	48160.4
14th	6768.6	46708.4	912.0	59863.9

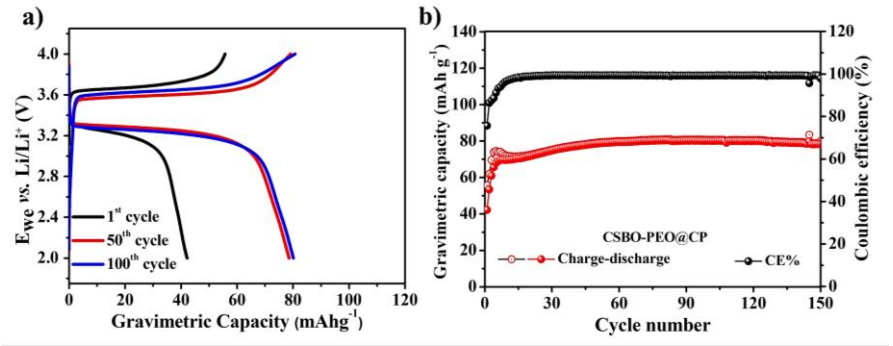

Figure S5.2.1: a) Galvanostatic charge-discharge voltage profile with gravimetric capacity at following charge and discharge of 1st, 50th and 100th at 0.1C and b) Capacity retention plot with cycle number for Li|CSBO-PEO$_{20\%}$ |LFP at 40 ºC.

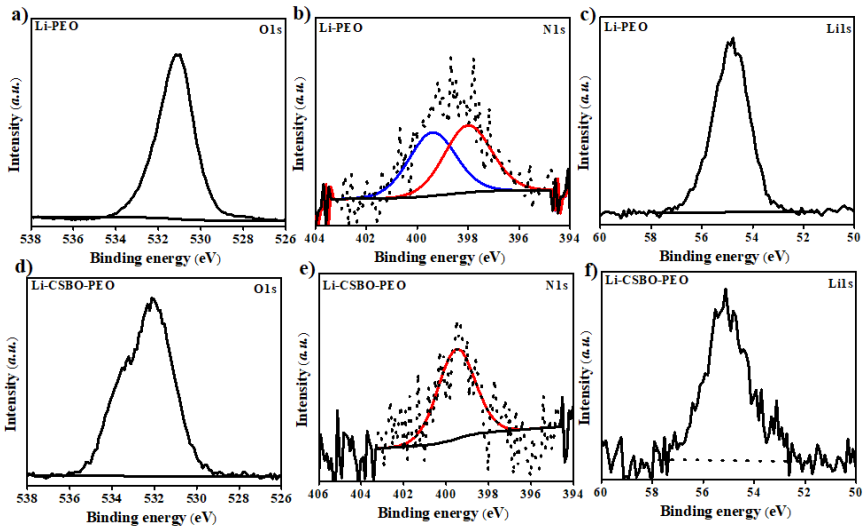

Figure S5.2.2: HR-XPS of a) and d) Oxygen (O1s), b) and e) Nitrogen (N1s), c) and f) Lithium (L1s), for li-anode surface of cell based on PEO and CSBO-PEO, respectively.

Chapter 6.1 Bio-derived cyclic carbonates bearing poly(hydroxyurethane)-based networks

Abstract

While there is constantly increasing research on poly(ethylene oxide) (PEO) based polymers, we aim at PEO alternatives such as poly(hydroxyurethane)s (PHUs) that are sustainable and environmentally friendly. PHUs, owing to their high degree of structural tunability, can be interesting candidates for solid polymer electrolytes (SPEs). Here, we synthesize bio-based PHU networks by reacting carbonated soybean oil (CSBO) with oligo(ethylene glycol) chains functionalized at both ends with amines as cross-linkers via an isocyanate and catalyst free pathway. The presence of polyether and triglyceride (in CSBO) segments in the network provides the PHU with soft segments while urethane linkages result in hard segments. The low T_g and high thermal stability of the resulting PHU networks widespread their application at elevated temperature without melting and significant degradation. In addition, the PHU networks show remarkable adhesive properties to the surface of metals, speculating better interfacial contact and stability. The electrochemical investigations of the SPEs obtained from PHU networks exhibit decent ionic conductivity (> 10^{-4} S cm^{-1} at 60 ^{o} C), electrochemical stability window (ESW > 4.5 V *vs.* Li/Li^{+}) and

transport properties. Lithium ferrophosphate($LiFePO_4$) cells with PHU networks based SPEs also show promising charge-discharge (> 100 mAh g^1 at 60 ^{o}C) with Li-metal anode.

6.1.1 Introduction

We cannot initiate and carry out an immediate action towards changing our energy habits in our daily life today without batteries. Battery technologies based on lithium are already front runner in the race of energy storage catering to the needs of consumers from small button cells in watches to large pack pouch and grid cells in heavy devices and electric vehicles (EV).[1] In the coming few years, the projection of EV market is expected to boom, replacing fossil fuel-based vehicles.[2] While Lithium ion battery technology is already matured enough, the underlying challenges also multiply with up-scaling of batteries packs. The conventional liquid-based lithium batteries pose serious safety concerns witnessed over the past few years right from small devices to electric vehicles.[3,4] This led to the strong emphasis on solid-state electrolytes based lithium batteries which not only offer safety but also lightweight, easy stack and packaging, recyclability, thermal stability and high energy density with longer cycles.[5,6] Solid-state electrolytes offer wide electrochemical stability window (ESW) which makes them suitable candidate for high voltage cathodes like $LiCoO_2$ (LCO) and $LiNi_xMn_yCo_{1-x-y}O_2$ (NMC) *etc.*[7, 8] Furthermore, solid-state electrolytes (SSEs) are suitable for application with lithium metal anodes which offer capacity as high as 3860 mAh g^{-1} and energy density ~ 250 Wh Kg^{-1} with possibility of dendrite-free mechanism.[9] Although all solid-state batteries (ASSBs) have their own technical challenges and hurdles which need to be addressed via materials research and development. Indeed, SSEs offer lower conductivity ranging from 10^{-3} to 10^{-6} S cm^{-1} at room temperature (RT) along with poor interfacial contacts with electrodes. This leads to higher interfacial resistance for charge transfer and less lithium ions available for the transport.

Researchers have developed or are developing several strategies and materials to address these key issues. The most conventional ways to deal with these issues require higher temperature for enhanced wettability and free volume to polymer chains for faster mobility. The goal of developing fully solvent-free solid polymer electrolytes with conductivity equivalent to liquid electrolytes at RT is one such milestone that motivates as well as haunts many researchers. While the very first discovered PEO-LITFSI.[10] SPEs does not perform up to the mark owing to their semi-crystalline,

narrow ESW (< 3.9 V *vs.* Li/Li^+), low transference number (< 0.2) and unstable SEI species, researchers have explored various classes of alternate polymers like polycarbonates (PCs),[11-13] polyesters,[14] poly(methylmethacrylate) (PMMA),[15,16] polyacrylonitrile (PAN),[17,18] polysiloxanes (PSEs),[19] and their derivatives. Although most of them suffer from one or more issues, as highlighted above. This is why, methodologies like copolymerization[20], blending[21,22], hybrids with inorganic fillers,[23] gel polymers,[17] have been popular in the trends to achieve targeted functionalities.

Polyurethanes (PUs), first discovered by Otto[24] in 1937, have been seen as a major industrial candidate in the paint and coating industry.[25] The crucial properties which make them distinct from above polymers are flexibility, adhesive, mechanical strength and compatibility with other polymers or inorganic particles.[26] The novel characteristic of PU-based polymers is the presence of both soft and hard segments, which makes them an attracting candidate for SPEs. While the presence of polyether acting as soft segment is important for lithium coordination, the carbamate groups are acting as hard segments contributing toward mechanical properties. One of the first investigations on PUs for Li-ions conduction was reported by Ohtaki and co-workers[27] in 1985 for polyether-containing PUs (PEUUs) with conductivity of ~10^{-7} S cm^{-1} at 60 ^oC. In subsequent years, many PU-based polyethers (PE) were reported as highlighted in recent reviews.[26,28,29] Another study by Hong *et al.*[30] demonstrated that the conductivity of hyperbranched PU (1.51 x 10^{-5} S cm^{-1}) was observed to be superior compared to linear PU (2.7 x 10^{-7} S cm^{-1}) due to less formation of ion pair aggregates. It has been shown that PU-based polymer networks are even performing better. In this respect, Santhosh *et al.*[31] who largely focused on acrylate-based PU (PUA) with a conductivity of $<10^{-8}$ S cm^{-1} at RT, demonstrated that the parent PUA networks had better conductivity because of increased free volume available for chain segments mobility.[32-34] In addition, PU-based networks are actively explored for self-healing properties[35] and single lithium ion conducting behavior[36] in SPEs. Poly(hydroxy urethane)s (PHUs) differs from PUs by the presence of an hydroxyl group in the urethane unit and are also considered as interesting candidates for SPEs. So far, most of PUs are developed via catalyst-led reactions, largely with isocyanate monomers. Therefore, non-isocyanate PUs (NIPUs)/PHUs have found their strong place due to their facile synthesis, sustainability and cost effectiveness.[37] Referring to bio-sourced

materials, quite a few investigations on vegetable oils for PUs such as jatropha and castor oil-based monomers[38,39] have been reported in the past few years. Although, there are almost no reports on NIPU/PHU based on bio-derived sources for Li-ion conduction so far, which motivated us to look for sustainable and yet high performing PHU SPEs.

In this work, we focus on synthesis of non-isocyanate and catalyst-free PHU via reaction of bio-based carbonated soybean oil (CSBO) bearing carbonates with amine-terminated oligo(ethylne glycol) crosslinkers. The effect of Li^+ and $TFSI^-$ ions on the accordingly obtained PHU networks is studied from physical as well as electrochemical point of view. Further, lithium metal battery prototypes with LFP and PHU-SPEs are investigated. Finally, we also probe the interface between PHU-SPEs and the Li-metal surface as a result of cycling using XPS.

6.1.2 Materials and methods

Epoxidized soybean oil (ESBO) was obtained from Vandeputte Oleochemicals (Belgium). Carbon dioxide (CO_2, N48) was supplied by Air Liquide. 1,3-bis (2 hydroxyhexafluroisopropyl) benzene was purchased from Fluorochem. Poly(ethylene glycol) bis(3-aminopropyl) terminated (PEGTA)(M_w~1500) and 4,7,10-trioxa-1,13-tridecanediamine (M_w~220.31), 2,2′-(ethylenedioxy) bis (ethylamine) (M_w~ 148.2), lithium metal foil (99.9%), lithium battery-grade, lithium bis(trifluoromethanesulfonyl) imide (LiTFSI), lithium iron phosphate ($LiFePO_4$), poly(vinylidene fluoride) and Super-P were purchased from Sigma-Aldrich. N-methyl-2-pyrrolidone (NMP) was purchased was bought from Alfa Aesar, tetrahydrofuran from VWR. Deuterated chloroform ($CDCl_3$) used for NMR spectroscopy was purchased from Eurisotop. Cellulose fibre paper was purchased from TOB. All reactants and catalysts were used as received without any further purification.

Note: Refer the Chapter 5.1 for characterization and electrochemical techniques.

6.1.3 Experimental section

6.1.3.1 Synthesis of PHU and PHU-LiTFSI

Before Poly(hydroxyurethane), bio-based cyclic carbonated soybean oil (CSBO) was synthesised by following the approach highlighted in the section 5.1.3.1 of Chapter 5.1. Next, PHU networks were synthesized by polyaddition reaction of CSBO with of poly(ethylene glycol) bis(3-aminopropyl) terminated (PEGTA) (M_w~1500), 4,7,10-trioxa-1,13-tridecanediamine (M_w~220.31) and 2,2′- (ethylenedioxy) bis (ethylamine) (M_w~ 148.2), respectively as demonstrated in Scheme 6.1.1. The ratio of the CSBO to PEGTA was chosen to 1:3 ((y/z=mol/mol) in tetrahydrofuran solvent corresponding to complete ring opening and varied accordingly. The mixture was stirred for > 6 h and then drop casted on cellulose paper and Teflon molds separately followed by transfer to the vacuum oven. The crosslinking reaction was performed by opening of the CC rings of at 70 ºC for >12 h and at 90 ºC for > 24 h in vacuum. The PHU-based solid polymer electrolyte ($PHU_{x,}$ x represents the % LiTFSI added) was prepared following the similar procedure with LiTFSI added to the reaction mixture before polymerization of the CBSO by the cross-linker All the structural and thermal characterization was performed on polymers without separator prior to preparation of film.

6.1.3.2 Preparation of solid polymer electrolytes (SPEs)

For preparation of PHU SPE films, in situ loading of LiTFSI to the PHU reaction mixture was adopted as highlighted in the synthesis section. The reaction mixtures with salt were drop-casted on cellulose paper from 100 to 150 μL. The impregnated membranes were then transferred to a vacuum oven for thermal curing. The cellulose paper was used in the preparation of SPEs to provide the self-standing ability to the films with controlled crosslinking and thickness. Coin 2032-type cells were assembled using free-standing SPE film (70-150 μm) sandwiched between SS|SS, Li|SS, Li|Al/C, Li|Li and Li|LFP electrodes to evaluate electrochemical properties.

6.1.4 Results and discussion

The PHU networks have been obtained by ring-opening of CC rings in CSBO by nucleophilic attack of terminal amino groups of PEGTA via two transient states differing in alpha carbon functionality. The thermal energy drives the reactivity, leaving away the need of catalyst. A dense and hard network was obtained when the lower molar mass PEGTA diamine with M_w~148.2 (N1) was used while the rigidity decreased when the PEGTA molar mass was increased to Mw ~220.3 and 1500 (N2 and N3). The pictures in Figure 6.1.1 shows the physical nature of the three different PHU networks with respective cross-linkers. This behavior can be explained by the increased number of ethylene oxide moieties which essentially contribute to soft segments in contrast to the fixed number of hydroxyl urethanes as hard segments resulting from the reaction of CCs in CSBO with terminal amines of PEGTA (provided that this reaction is quantitative and thus that all the CCs are opened). The PHU SPE films synthesized from low molar mass PEGTA crosslinkers presented free

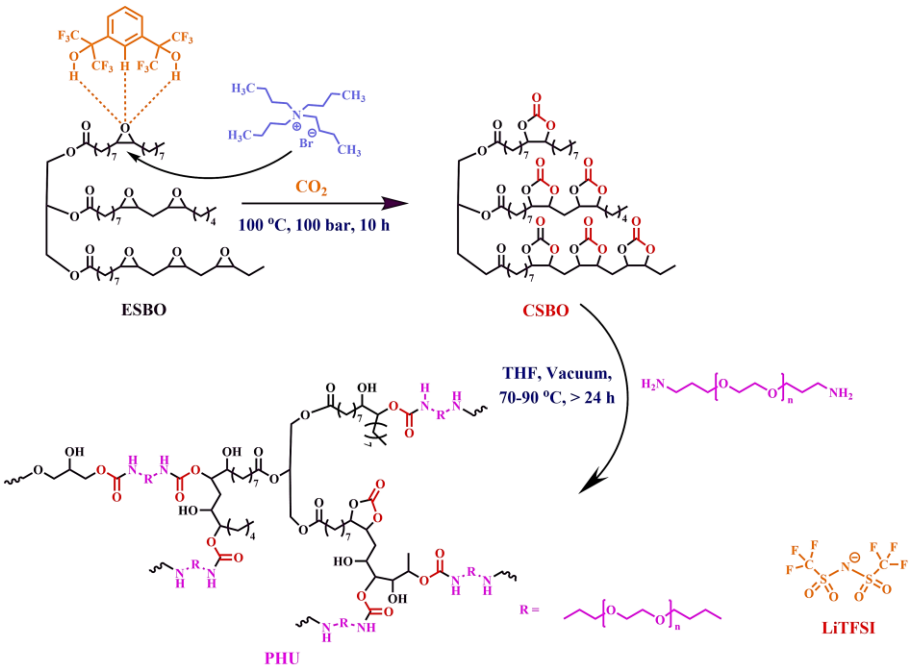

Scheme 6.1.1: Synthesis scheme of poly(hydroxy urethane) (PHU) solid polymer electrolyte networks from epoxidized soybean oil (ESBO) via carbonated soybean oil (CSBO) and with addition of LiTFSI.

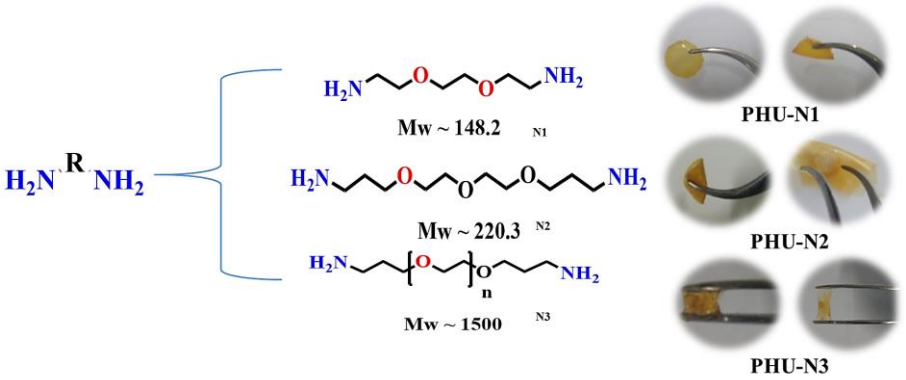

Figure 6.1.1: Comparison of PHU SPE networks with variable crosslinker chain length in presence of LiTFSI.

standing ability, while the one designed with N3 (M_w ~ 1500) required a supporting membrane (cellulose fiber separator was used) when LiTFSI concentration was more than 10wt% in the mixture. Given the higher number of ethylene oxide units, N3 was chosen for further investigations. Subsequently, we attempted to investigate the role of CC rings in PHU by partial controlled ring opening following the stoichiometric ratio in presence of 15 wt% of LiTFSI. The CSBO:PEGTA:1:3 ratio corresponds to the assumption that all six-ring of CSBO are opened by using 1:3 molar ratio of CBSO:PEGTA. Similarly, the CSBO: PEGTA: 2:5 molar ratio targets the opening of 5 CCs rings and so on for other analogues.

6.1.4.1 Fourier transform infra-red spectroscopy

We analyzed the effect of this varying formulation with FTIR spectroscopy (Figures 6.1.2a). The increase in the peak intensity of bands of urethanes around 1716 cm^{-1} and 1539 cm^{-1} can be observed because of PHU-LITFSI network formation. As expected, the rigidity of the obtained PHU SPE network was found to increase with a higher number of carbonate rings opened. We chose the CSBO:PEGTA 1:3 formulation for PHU SPE after validation of its superior conductivity as compared to other analogues. As it can be observed in the FTIR-Spectra of PHU-LiTFSI, the formation of PHU was confirmed by the appearance of a characteristic peak at ~1716 cm^{-1} (C=O urethane) along with a peak at ~1738 cm^{-1} ("ester" part of the urethane group). While the characteristic peak of the CC group around ~1799 cm^{-1} highlights that all the CC rings

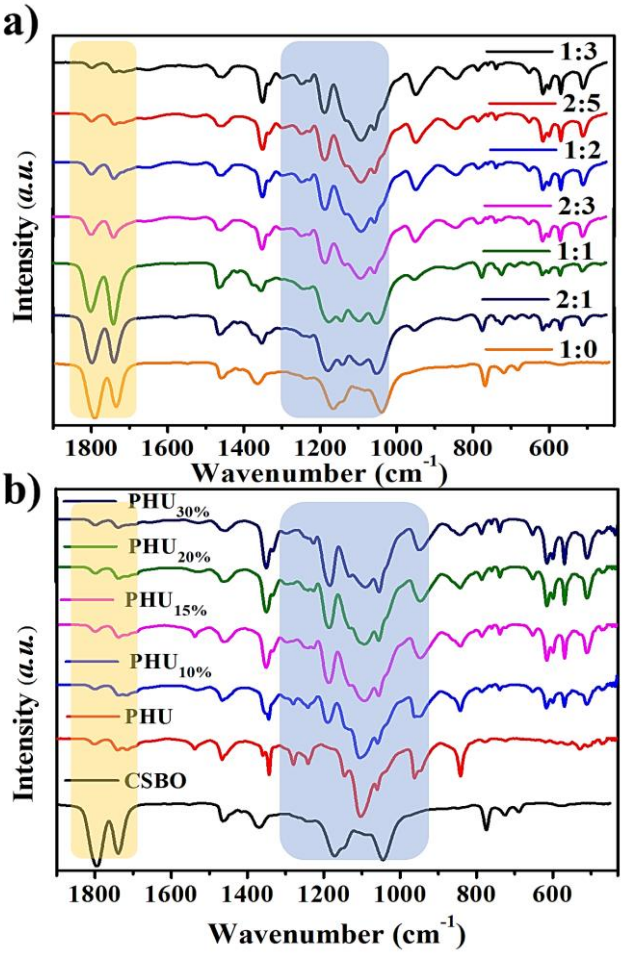

gure 6.1.2: Comparative IR spectra a) PHUs with respective formulations (CSBO:PEGTA:y:z in ol/mol) as of targeted ring opening with 15% of LiTFSI; and b) PHU_x (where, CSBO:PEGTA:y:z=1:3 roughout, x represents the wt% of LITFSI added), respectively.

were not opened as opposite to what we speculated. This could be explained by the unequal accessibility of all carbonate rings and short reaction time. Eventually, it contradicts our assumption on all CC rings opening with the stoichiometric ratio CSBO:PEGTA:1:3. In the case of PHU-LiTSFI, the broad band at ~3474 cm^{-1} characteristic of –OH was recorded with red shift with formation of PHU and blue shift with increasing concentration of LiTFSI at ~1539 cm^{-1} for -N-H for PHU.[40] Here ring opening is driven by PEGTA while it was found to be restricted/hindered with higher concentration of LiTFSI resulting lower crosslinking (Figure 6.1.2b).

6.1.4.2 Thermal Measurements

CSBO, one of the monomers of the PHU, possesses amorphous nature, is oily at RT and shows no transition in DSC thermogram.[41] While PEGTA, which contains ether units and primary amine at both chain ends is solid at RT and shows a melting temperature (T_m) at 50.0 °C and a crystallization temperature (T_c) at 20.1 °C. For a good ionic conducting polymer, it's interesting to have an amorphous nature with low glass temperature (T_g). The comparative DSC thermograms of PHUs have been shown in Figure 6.1.3a in comparison to PEGTA without LiTFSI (summarized in Table 6.1.1). The T_m of 50.1 °C was decreased to 39.7 °C from PEGTA to PHU with T_c of 20.1 °C and 14.1 °C, respectively. The polymer network was screened from 0 wt% to 40 wt% of LiTFSI concentration witnessing the change in the physical the state of the PHU networks from solid to gel-like sticky materials with LiTFSI concentration increasing from 20 wt% onwards. The T_g was detected at -28.2 °C and -46.9 °C for PEGTA and PHU without added LiTFSI, respectively, while it decreased to -40.3 °C, with 10 wt%-LiTFSI for $PHU_{10\%}$. For $PHU_{20\%}$, $PHU_{30\%}$ and $PHU_{40\%}$, T_g was observed at -46.9 °C, -41.1 °C and -33.4 °C, respectively. Subsequent increase in T_g with increase in LiTFSI could be attributed to lower crosslinking with higher salt concentration. PHU networks turned out to be completely amorphous beyond 20wt% salt concentration.

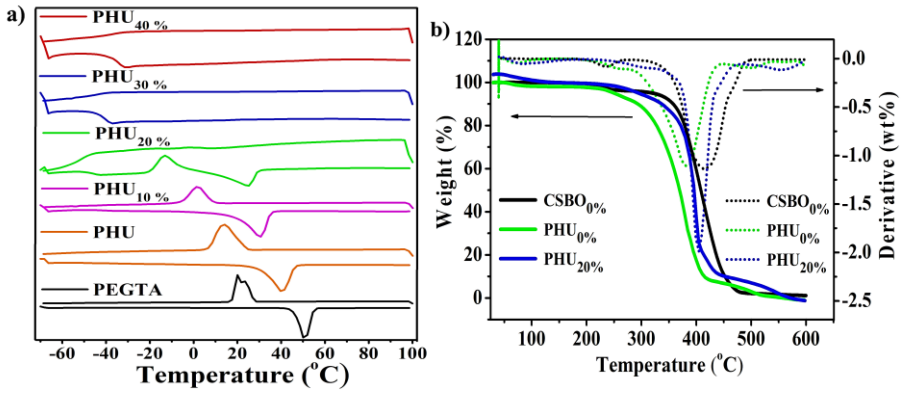

Figure 6.1.3: DSC thermograms (2nd heating and cooling) of PHU_x-SPEs in comparison to $PEGTA_{0\%}$; and b) Thermogravimetric analysis of PHUs with and without LiTFSI, (subscripts indicates the wt% of LiTFSI added, i.e. 0% signifies no LiTFSI).

Table 6.1.1: DSC data of PHU-SPEs with all temperature values indicated in Celsius. (T_{in} and T_{off} are the inset and offset temperature to find the T_g, all temperature values are in degree Celsius)

Sample	T_m	T_c	T_{off}	T_{on}	T_g
PEGTA	50.1	20.1	-41.2	-15.1	-28.2
$PHU_{0\%}$	39.7	14.1	-54.1	-39.6	-46.9
$PHU_{10\%}$	30.7	1.2	-46.1	-34.5	-40.3
$PHU_{15\%}$	30.6	-11.7	-58.6	-38.2	-48.4
$PHU_{20\%}$	25.3	-0.8	-50.9	-42.8	-46.9
$PHU_{30\%}$			-44.4	-37.7	-41.1
$PHU_{40\%}$			-39.8	-31.3	-33.4

In all cases, no T_g was recorded above -30.0 ^oC, which is advantageous for the chain segmental motion and ionic conductivity at service temperatures of batteries.

We performed the thermogravimetric analysis of the samples in N_2 atmosphere for PHUs in comparison with CSBO, as shown in Figure 6.1.3b. Initial increased weight beyond 100% can be attributed to the adsorbed moisture from air. The two-phase decomposition of CSBO was replicated in PHU with a slight shift and narrow band recording onset decomposition temperature at ~172 ^oC, ~199 ^oC, ~217.5 ^oC for $CSBO_{0\%}$, PHU without LiTFSI and PHU with LiTFSI, respectively. However, second/major (around 80%) decomposition starts at the ~284.7 ^oC, 269.5 ^oC and 322.8 ^oC with decomposition temperature peak at 410 ^oC, 378.8 ^oC and 400.1 ^oC for $CSBO_{0\%}$, $PHU_{0\%}$ and $PHU_{20\%}$, respectively. The presence of LiTFSI increased the thermal stability of the polymer electrolyte for PHU networks. As recorded, only one phase was observed with major decomposition, with and without LiTFSI, respectively. The degradation of LiTFSI salt is believed to occur beyond 400 ^oC.

6.1.4.3 Ionic conductivity measurements

The electrochemical investigations of the polymeric networks with LiTFSI were initiated by ionic conductivity measurements by performing potential electrical impedance spectroscopy (PEIS) with PHU networks sandwiched in PTFE ring using symmetric Swagelok and coin cells at various composition and temperature. The

resulting Nyquist plots have been analyzed to find out the electrolytic resistance and therefore ionic conductivity (σ) using equation 6.1.1:

$$\sigma = \frac{l}{R_b S} \quad (6.1.1)$$

where, R_b is bulk electrolyte Ohmic resistance from AC impedance, l and S are the thickness and the surface area of polymer electrolyte, respectively. The effect of the presence of CCs in the PHU network on conductivity has been analyzed by controlling the number of rings opened in a sample containing 15wt% LiTFSI. Figure S6.1.1a shows logarithmic of conductivity with inverse temperature for PHUs containing variable amounts of unopened CCs. At 20 ^{o}C, the PHU (2:3) shows best conductivity of 1.23 x 10^{-5} S cm^{-1} while the sample with the least ring opened shows the worst conductivity of 3.41 x 10^{-6} S cm^{-1}. An increase in the temperature results in higher lithium mobility due to thermal energy and a softening of the network. Beyond 30 ^{o}C onwards, PHU (1:3) with speculative completely opened rings is observed to show higher conductivity with temperature, such as 2.36 x 10^{-4} S cm^{-1} at 60 ^{o}C particularly. The soft nature of network due to unreacted CC rings and a higher number of ether units in PHU (1:3, as highlighted in FTIR) attribute to the superior conductivity at higher temperature relative to other PHU analogues. Therefore, we proceeded with incomplete ring opened PHU (1:3) for further investigation of conductivity versus salt concentration.

Considering the physical limitations faced by the (too) soft PHU (1:3) at salt concentration higher than 10wt% LiTFSI ($PHU_{10\%}$), we adopted the method of in situ crosslinking within fibres of cellulose separator (CP) to facilitate controlled thickness and freestanding flexible membrane. The ionic conductivity obtained for the network at 20 ^{o}C is 6.58 x 10^{-6} S cm^{-1}, which increased to 6.64 x 10^{-5} at 60 ^{o}C (Figure 6.1.4a). However, the higher conductivity was observed for $PHU_{30\%}$ owing to low cross-linked soft network with higher number of charge carriers. For corresponding $PHU_{15\%}$, it can be clearly concluded that the conductivity of the PHU network impregnated into separator was recorded 5.623x10^{-5} S cm^{-1} at 60 ^{o}C lower than PHU without cellulose separator due to restricted mobility of polymeric segments within cellulose fibres (refer Figure S6.1.1b also for comparison). It is therefore noted that the balance

between the right salt loading and crosslinking is the key step for the PHU network-based SPEs.

Another model for conductivity using Vogel-Fulcher-Tamman theory was applied to distinct the effect of chain segmental motion in the temperature range of 20-90 ^{o}C for conductivity data as shown in Figure 6.1.4b using equation 6.1.2 where A is conductivity pre-exponential factor, E_a is the activation energy, and T is the absolute temperature, T_0 is the Vogel scaling temperature at which the free volume disappears or at which free entropy becomes zero following approximation as $T_0 = (T_g - 50\ K)$, E_a is the pseudo-activation energy of ion transport, k_b is Boltzmann constant,[42, 43]

$$\sigma T_{1/2} = Ae^{-\frac{E_a}{K_b}(T-T_0)} \quad (6.1.2)$$

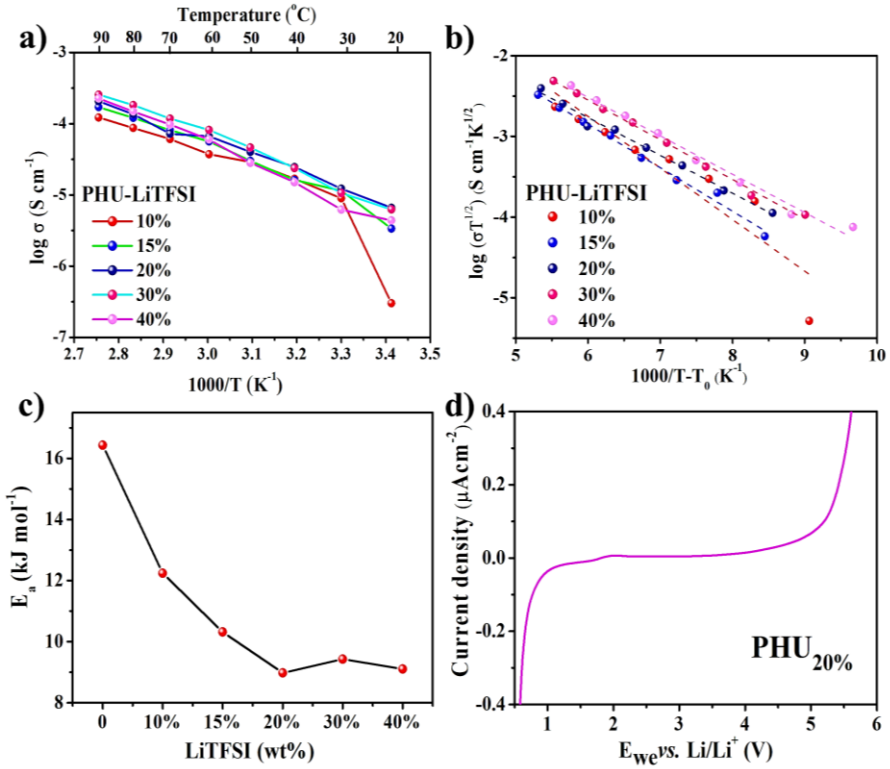

Figure 6.1.4: a) Temperature dependent ionic conductivity for PHU-LiTFSI (10-40 wt%) SPEs; b) Ionic conductivity using the VFT model; c) Activation energy, E_a, derived using VFT equation from ionic conductivity versus LiTFSI (wt%) loaded SPE; and d) Linear sweep voltammetry analysis of PHU-SPE with 20% LiTFSI (depicted as $PHU_{20\%}$).

The plot indicates that the conductivity decreases from higher ($PHU_{40\%}$) to lower ($PHU_{10\%}$) salt loading unlike the trend observed in Arrhenius plot of Figure 6.1.4b. However, the higher LiTFSI loaded PHU demonstrated higher chain segmental motion due to less rigid network in addition to higher charge-carriers, respectively. The mismatch in conductivity values between these two models clearly hints at the decent contribution of chain segmental motion highest in $PHU_{40\%}$ and lowest in $PHU_{10\%}$ at 20 ^{o}C. Pseudo-activation energy was calculated from the slope of the VFT plots, as shown in Figure 6.1.4c. As the salt concentration increases from 10% to 40%, E_a decreased linearly until 20wt%. However, the slight increment in E_a from 30wt% to 40wt% could be related to ion-pair formation due to a higher number of charge carriers. The Y2 axis in E_a plot demonstrated the conductivity values at 60 ^{o}C suggesting an increase in conductivity until the $PHU_{30\%}$ sample and further decrement due to ion-pair aggregates for higher salt loading (refer to Table S6.1.1 for calculated E_a for PHU-SPEs with the pre-exponential factor and R^2 as the corresponding fitting coefficient).

6.1.4.4 Linear sweep voltammetry

With aluminium as cathode and lithium metal as anode, asymmetric cells have been assembled to investigate the electrochemical stability window (ESW) by employing the linear sweep voltammetry technique. Figure 6.1.4d shows that there is no oxidation observed in the voltage range of 1.8 V to > 5.2 V at 60 ^{o}C at the scan rate of 0.5 mV/s for $PHU_{20\%}$. The high oxidative potential facilitates application of our SPEs with high voltage cathodes without electrolyte degradation. A comparative LSV study was performed with PHU-SPEs and salt concentration (Figure S6.1.1d). The cut-off current was observed in the order of increasing salt concentration. Although, higher salt concentrated electrolytes showed narrow ESW with possible degradation of salt aggregates limiting them to 2-4.6 V and 2-3.8 V for $PHU_{30\%}$ and $PHU_{40\%}$, respectively at 60 ^{o}C as shown in Figure S6.1.1d. The $PHU_{15\%}$ demonstrated the higher ESW of > 4.5 V while the onset current was observed in $PHU_{40\%}$ around 4 V.

6.1.4.5 Transference number

The transference number is a key parameter in determining transport properties for the validation of SPEs in batteries. Here, it has been calculated by using Bruce and Vincent method via equation (6.1.3):

$$t_{Li^+} = \frac{I_{ss}(V - I_0 R_0)}{I_0(V - I_{ss} R_{ss})} \quad (6.1.3)$$

Where, V is DC applied potential, I_o and I_{SS} are initial and steady state currents, R_o and R_{ss} are initial and steady state interfacial resistances, respectively.[44] The polarization curve as shown Figure 6.1.5a, has recorded the drop in the I_o from 0.29 µA to I_{ss} of 0.16 µA while the interfacial resistance from 639.7 Ω to 676.1 Ω, respectively. The t_{Li^+} of $PHU_{10\%}$ was calculated to be 0.55 at 60 °C, higher than CBSO (t_{Li^+} = 0.39 for 50 wt% of LiTFSI at 30 °C).[41] The improvement in t_{Li^+} can be attributed to the structural network which allows the Li-ions to hop and restricts the mobility of counter anions leading to reduced concentration gradient. Although it was observed that t_{Li^+} decreased with LiTFSI concentration in the PHU networks from 0.55 to 0.17 with salt concentration as shown in Figure 6.1.5b. Unlike in $PHU_{10\%}$ which has a rigid and compact network, $PHU_{40\%}$ has higher charge carrier concentration which not only hinders the opening of CCs but also promotes ionic gradients and aggregates irrespective of mobility of chains. Nevertheless, it is yet interesting to explore networks with higher conductivity which can also offer promising transference number close alternative to single lithium ion conducting SPEs.

6.1.4.6 Stripping and plating

Beside voltammetry, the reaction and stability of lithium metal with electrolytes are often studied with exhaustive stripping and plating of Li-ions within non-blocking lithium metal symmetrical cells. Time-dependent constant current density charge-discharge technique has been applied for 1 h each to realize the overpotential within cut-off voltage limits. PHU20% SPE was used as an electrolyte sandwiched with lithium metal and was subjected to two different current densities of 5 µA cm-2 and 10 µA cm-2 for almost 200 cycles each at 60 oC, as shown in Figure 6.1.5c. During initial cycles, the overpotential was observed to be ~90 mV, which remained constant

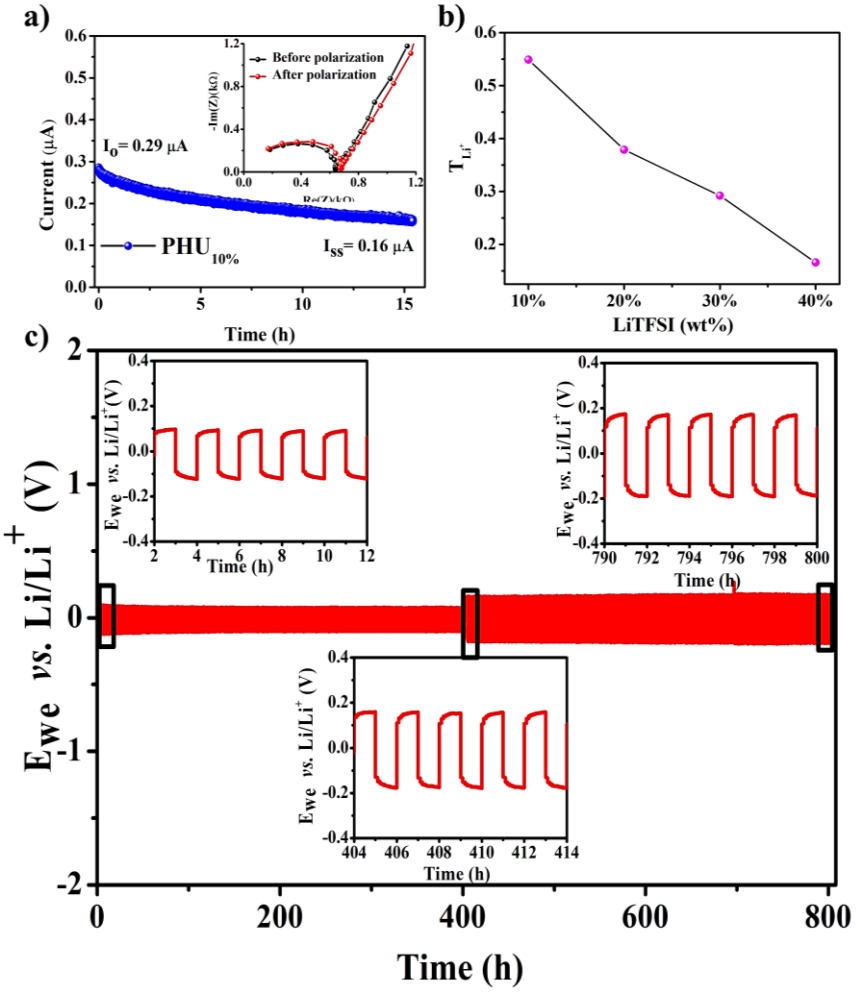

Figure 6.1.5: a) Transference number measurement using chronoamperometry (DC polarization) followed by AC PEIS as demonstrated in inset; b) Transference number versus LiTFSI concentration of PHU-SPE measured at 60 °C; and c) Galvanostatic charge-discharge voltage profile for stripping-plating at following current densities at 60 °C with Li|$PHU_{20\%}$-SPE|Li symmetric cells, respectively with enlarged plots at respective time demonstrating the constant over potential in the inset.

to ~100 mV with an error of less than 4% despite cycling for 400 hours. However, a constant shift in the output potential was obtained when the current density was doubled to 10 μA cm-2 in the subsequent measurement. The recorded overpotential during the 201st cycle was ~160 mV, which remained constant because of long stripping and plating of lithium to ~170 mV with a calculated error of < 6%. The

constant overpotential subjected to current density applied throughout the cycling highlights the efficient lithium mobility, hence higher Coulombic efficiency and stabilized interface. It can be speculated that the electrolytic decomposition is supposed to stabilize the solid electrolyte interphase (SEI) layer with less parasitic reactions and species.

6.1.4.7 Li-metal battery prototypes

The battery prototypes were assembled with lithium ferrophosphate (LFP) as cathode material and lithium metal anode together with PHU_x SPEs in a coin cell assembly. For cycling, galvanostatic cycling with potential limitation (GCPL) was applied at the limit of 2-4 V for the cells maintained at 60 ^{o}C in the climate chamber. The voltage profile with specific capacity shows that with LFP cathodes, we achieved 122.6 mAh g^{-1}, 118.1 mAh g^{-1} and 111.3 mAh g^{-1} of the discharge capacity during 1st, 100th and 200th cycles at 0.1C, respectively. The overpotential (E_{OR} for oxidation and reduction) during 1st cycle was calculated to be ~96.1 mV which decreased to ~56.1 mV and ~65.8 mV in respective 100th and 200th cycles (Figure 6.1.6a), credited to the formation of a stable SEI. The same cell was subjected to higher current density from 0.1C to 2C and then to 0.05C, followed by 0.1C. The cell delivered the discharge capacity of 129.4 mAh g^{-1}, 123.8 mAh g^{-1}, 112.8 mAh g^{-1}, 97.9 mAh g^{-1}, 75.6 mAh g^{-1} and 129.8 mAh g^{-1} at 0.1C, 0.5C, 0.2C, 1C, 2C and 0.05C, respectively (Figure 6.1.6b). At lower C-rate of 0.05C, the recorded polarization overpotential is ~37.9 mV, while ~241.6 mV for 2C.

The long-term exhaustive charge-discharge is demonstrated via a capacity retention plot. In Figure 6.1.6c, the cell was cycled at various high and low current densities without any treatment. A high Coulombic efficiency of > 99% was achieved for almost all cycles, with a capacity retention of 90.8% while long cycling at 0.1C for more than 200 cycles. After cycling for 250 cycles, we applied higher current which subsequently led to capacity drop at respective C-rate but stable cycling was observed at 0.5C on prolonged cycling. The rate capability plot at different C-rate is shown in Figure 6.1.6d for the subsequent charge-discharge at high and low C-rates and was achieved without much capacity fading. The cell recovered it capacity back at 0.1 C without significant increase in polarizations as observed in Figure 6.1.6c. The capacity

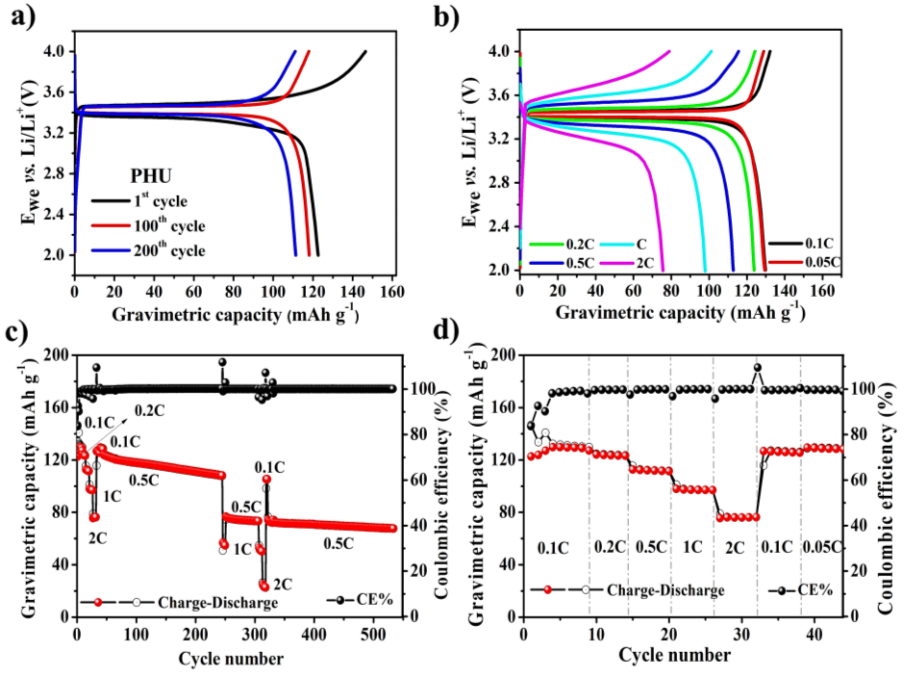

Figure 6.1.6: Galvanostatic charge-discharge voltage profiles a) Gravimetric capacity at 0.1C for respective cycles; b) Gravimetric capacity at variable current densities; c) Global capacity retention plot with cycle number; and d) Rate capability plot for Li|$PHU_{20\%}$-SPE|LFP at 60 °C, respectively.

drops at higher C-rate after hundreds of cycles could be explained by the increased interfacial resistance and parasitic decomposition of the electrolyte. Our bio-derived PHU-SPE based cells demonstrated excellent cycling performance both at lower and higher C-rate in hundreds of cycling.

6.1.4.8 Post-mortem XPS analysis

The stable cycling in full metal battery prototype was investigated via XPS analysis on the surface of the anode and on the PHU SPE facing the anode on the cell cycled for more than > 500 cycles. The surface species at the depth of ~10 nm correspond to solid electrolyte interphase, including the external contamination. The standardised calibration for C 1s peak at 284.8 eV was adopted to fit other spectral binding energies.[45] The scanned elements with their abundance percentage indicated a significant amount of carbon in both Li-metal and PHU SPE surfaces involving the

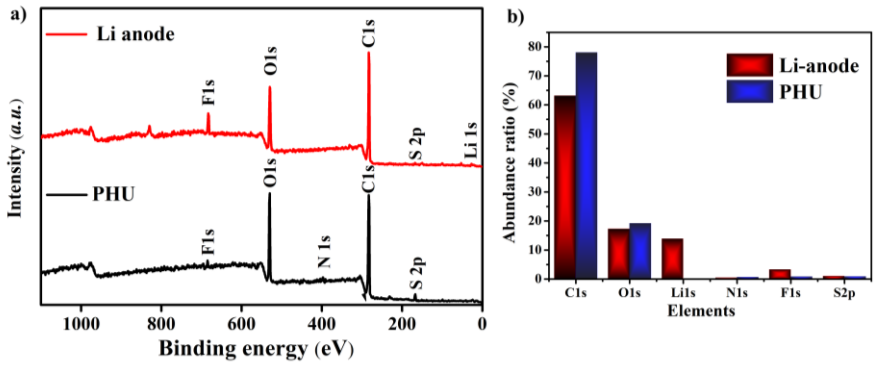

Figure 6.1.7: a) Survey spectrum of surface of cycled Li-anode and PHU SPE of Li|PHU SPE|LFP cells after 500+ cycles and b) Abundance ratio percentage of surface elements constituting SEI for Li-anode and corresponding $PHU_{20\%}$ SPE films.

adventitious carbon. However, no lithium and negligible fluorine constituents was detected on the PHU-SPE surface as highlighted in Figure 6.1.7a and 6.1.7b.

In HR-XPS of C1s, conventional C-C/C-H (284.8 eV), C-O/N (286.4 eV), O-C-O/C=O (287.8 eV) groups were observed on both Li-metal and PHU surfaces. While, inorganic carbonates at ~288.8 eV and ~289.1 eV were detected along with organic carbonates at ~289.8 eV and ~290.7 eV for Li-anode and PHU-SPE, respectively (Figure 6.1.8a and 6.1.8d).[46,47] The high reactivity of LiTFSI led to the significant formation of LiF at the SEI i.e. 2.9% (684.8 eV) and 0.06% (684.6 eV) while $–CF_3$, 0.35% (687.1 eV) and 0.73% (687.4 eV) at Li metal and PHU, respectively (Figure 6.1.8b and 6.1.8e). Further, the S2p signal was convoluted into CF_3-SO_2, SO_3^{-2}, SO_x and Li_xS_y in the range of ~169.4 eV–~160 eV for both sample surfaces (Figure 6.1.7c and 6.1.8f).[48] To elaborate it more, higher percentage of SO_3^{-2} and Li_xS_y was detected at Li-surface while higher CF_3-SO_2 and SO_x was observed at PHU SPE surface. All other elements such as O1s, N1s and Li1s were not convoluted due to overlapping binding energies for probable species in SEI and are depicted in supporting information, Figure S6.1.2. The formation of LIF and speculated absence of dendrite are credited to attribute superior cycling performance of the cell.[49]

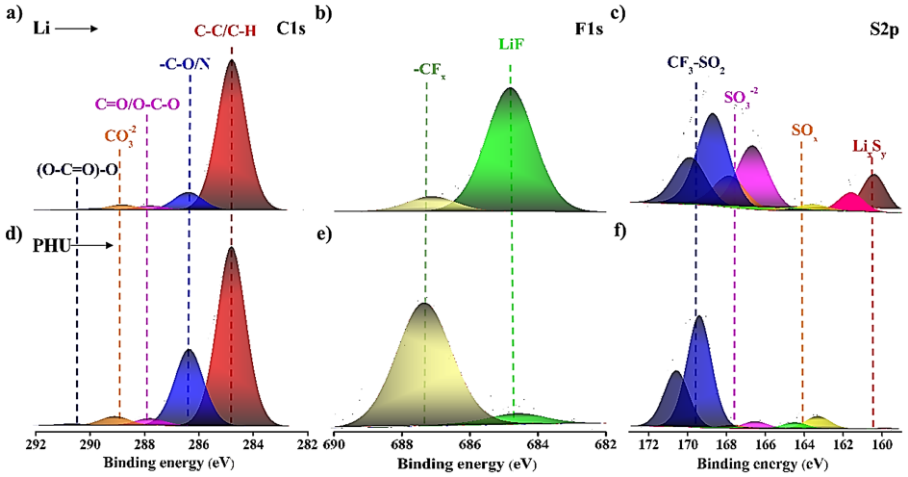

Figure 6.1.8: HR-XPS of a) and d) Carbon, b) and e) Fluorine and c) and f) Sulphur at lithium and $PHU_{20\%}$ film surface after cycling with LFP.

6.1.5 Conclusion

Following the quest for solid-state batteries materials sourced through green-sustainable materials, we designed and synthesised PHUs via facile ring opening reaction of CC rings of CBSO with PEGTA through non-isocyanate and catalyst free approach. The accordingly synthesised PHU networks with polyethers, esters, CCs and carbamate functionalities facilitated the targeted mechanical and electrochemical properties. It was deduced that it was interesting to leave a few CC rings besides carbamate formation for adhesive nature, indirectly contributing to better interface and wettability. The lower T_g also confirmed the contribution of chain segmental motion in addition to charge carrier's mobility. The optimum compromise between crosslinking and salt concentration has been obtained via the utilisation of a cellulose separator. With conductivity of 2.36 x 10^{-4} S cm^{-1}, the optimized PHU-SPEs demonstrated a high oxidation potential ESW > 5 V and t_{Li^+} of 0.55 at 60 °C. The cycling with symmetrical lithium metal cells for > 800 h highlighted the decent compatibility of electrode-electrolyte interface and stable SEI. Further, Li|PHU SPE|LFP cells delivered superior charge-discharge for long cycles with a specific capacity of 122.6 mAh g^{-1} at 0.1C with capacity retention of > 90%. Those interesting full metal batteries cycling experiments were then supported by post-mortem analysis

on the surface of anode and electrolyte via XPS. We reported that monomers sourced through vegetables oil could be interesting candidates for environment friendly polymer electrolytes for all solid-state batteries with high energy density.

Bibliography

1. Armand, M.; Axmann, P.; Bresser, D.; Copley, M.; Edström, K.; Ekberg, C.; Guyomard, D.; Lestriez, B.; Novák, P.; Petranikova, M.; Porcher, W.; Trabesinger, S.; Wohlfahrt-Mehrens, M.; Zhang, H., Lithium-ion batteries – Current state of the art and anticipated developments. *Journal of Power Sources* **2020,** *479*, 228708.
2. Kalhoff, J.; Eshetu, G. G.; Bresser, D.; Passerini, S., Safer Electrolytes for Lithium-Ion Batteries: State of the Art and Perspectives. *ChemSusChem* **2015,** *8* (13), 2154-2175.
3. Etacheri, V.; Marom, R.; Elazari, R.; Salitra, G.; Aurbach, D., Challenges in the development of advanced Li-ion batteries: a review. *Energy & Environmental Science* **2011,** *4* (9), 3243-3262.
4. Deng, D., Li-ion batteries: basics, progress, and challenges. *Energy Science & Engineering* **2015,** *3* (5), 385-418.
5. Takada, K., Progress and prospective of solid-state lithium batteries. *Acta Materialia* **2013,** *61* (3), 759-770.
6. Varzi, A.; Raccichini, R.; Passerini, S.; Scrosati, B., Challenges and prospects of the role of solid electrolytes in the revitalization of lithium metal batteries. *Journal of Materials Chemistry A* **2016,** *4* (44), 17251-17259.
7. Chen, S.; Wen, K.; Fan, J.; Bando, Y.; Golberg, D., Progress and future prospects of high-voltage and high-safety electrolytes in advanced lithium batteries: from liquid to solid electrolytes. *Journal of Materials Chemistry A* **2018,** *6* (25), 11631-11663.
8. Ahniyaz, A.; de Meatza, I.; Kvasha, A.; Garcia-Calvo, O.; Ahmed, I.; Sgroi, M. F.; Giuliano, M.; Dotoli, M.; Dumitrescu, M.-A.; Jahn, M.; Zhang, N., Progress in solid-state high voltage lithium-ion battery electrolytes. *Advances in Applied Energy* **2021,** *4*, 100070.
9. Su, L.; Manthiram, A., Lithium-Metal Batteries via Suppressing Li Dendrite Growth and Improving Coulombic Efficiency. *Small Structures* **2022,** *3* (10), 2200114.
10. Armand, M., The history of polymer electrolytes. *Solid State Ionics* **1994,** *69* (3), 309-319.
11. Mindemark, J.; Lacey, M. J.; Bowden, T.; Brandell, D., Beyond PEO—Alternative host materials for Li+-conducting solid polymer electrolytes. *Progress in Polymer Science* **2018,** *81*, 114-143.
12. Zhang, J.; Yang, J.; Dong, T.; Zhang, M.; Chai, J.; Dong, S.; Wu, T.; Zhou, X.; Cui, G., Aliphatic Polycarbonate-Based Solid-State Polymer Electrolytes for Advanced Lithium Batteries: Advances and Perspective. *Small* **2018,** *14* (36), 1800821.
13. Kimura, K.; Yajima, M.; Tominaga, Y., A highly-concentrated poly(ethylene carbonate)-based electrolyte for all-solid-state Li battery working at room temperature. *Electrochemistry Communications* **2016,** *66*, 46-48.
14. Lin, C.-K.; Wu, I. D., Investigating the effect of interaction behavior on the ionic conductivity of Polyester/LiClO4 blend systems. *Polymer* **2011,** *52* (18), 4106-4113.
15. Ali, U.; Karim, K. J. B. A.; Buang, N. A., A Review of the Properties and Applications of Poly (Methyl Methacrylate) (PMMA). *Polymer Reviews* **2015,** *55* (4), 678-705.
16. Song, J. Y.; Wang, Y. Y.; Wan, C. C., Review of gel-type polymer electrolytes for lithium-ion batteries. *Journal of Power Sources* **1999,** *77* (2), 183-197.
17. Manuel Stephan, A., Review on gel polymer electrolytes for lithium batteries. *European Polymer Journal* **2006,** *42* (1), 21-42.
18. Hu, P.; Chai, J.; Duan, Y.; Liu, Z.; Cui, G.; Chen, L., Progress in nitrile-based polymer electrolytes for high performance lithium batteries. *Journal of Materials Chemistry A* **2016,** *4* (26), 10070-10083.
19. Wang, Q.; Zhang, H.; Cui, Z.; Zhou, Q.; Shangguan, X.; Tian, S.; Zhou, X.; Cui, G., Siloxane-based polymer electrolytes for solid-state lithium batteries. *Energy Storage Materials* **2019,** *23*, 466-490.
20. Rolland, J.; Brassinne, J.; Bourgeois, J. P.; Poggi, E.; Vlad, A.; Gohy, J. F., Chemically anchored liquid-PEO based block copolymer electrolytes for solid-state lithium-ion batteries. *Journal of Materials Chemistry A* **2014,** *2* (30), 11839-11846.
21. Manuel Stephan, A.; Nahm, K. S., Review on composite polymer electrolytes for lithium batteries. *Polymer* **2006,** *47* (16), 5952-5964.
22. Ngai, K. S.; Ramesh, S.; Ramesh, K.; Juan, J. C., A review of polymer electrolytes: fundamental, approaches and applications. *Ionics* **2016,** *22* (8), 1259-1279.
23. Fan, P.; Liu, H.; Marosz, V.; Samuels, N. T.; Suib, S. L.; Sun, L.; Liao, L., High Performance Composite Polymer Electrolytes for Lithium-Ion Batteries. *Advanced Functional Materials* **2021,** *31* (23), 2101380.
24. Bayer, O., Das Di-Isocyanat-Polyadditionsverfahren (Polyurethane). *Angewandte Chemie* **1947,** *59* (9).
25. Das, A.; Mahanwar, P., A brief discussion on advances in polyurethane applications. *Advanced Industrial and Engineering Polymer Research* **2020,** *3* (3), 93-101.
26. Andersson, R.; Hernández, G.; See, J.; Flaim, T. D.; Brandell, D.; Mindemark, J., Designing Polyurethane Solid Polymer Electrolytes for High-Temperature Lithium Metal Batteries. *ACS Applied Energy Materials* **2022,** *5* (1), 407-418.
27. Watanabe, M.; Oohashi, S.; Sanui, K.; Ogata, N.; Kobayashi, T.; Ohtaki, Z., Morphology and ionic conductivity of polymer complexes formed by segmented polyether poly(urethane urea) and lithium perchlorate. *Macromolecules* **1985,** *18* (10), 1945-1950.
28. Lv, Z.; Tang, Y.; Dong, S.; Zhou, Q.; Cui, G., Polyurethane-based polymer electrolytes for lithium Batteries: Advances and perspectives. *Chemical Engineering Journal* **2022,** *430*, 132659.
29. Misenan, M. S. M.; Khiar, A. S. A.; Eren, T., Polyurethane-based polymer electrolyte for lithium ion batteries: a review. *Polymer International* **2022,** *71* (7), 751-769.
30. Hong, L.; Shi; Tang, Conductivities and Spectroscopic Studies of Polymer Electrolytes Based on Linear Polyurethane and Hybrid and Copolymer of Linear and Hyperbranched Polyurethanes. *Macromolecules* **2003,** *36* (13), 4989-4994.
31. Santhosh, P.; Gopalan, A.; Vasudevan, T.; Lee, K.-P., Evaluation of a cross-linked polyurethane acrylate as polymer electrolyte for lithium batteries. *Materials Research Bulletin* **2006,** *41* (6), 1023-1037.

32. Bao, J.; Qu, X.; Qi, G.; Huang, Q.; Wu, S.; Tao, C.; Gao, M.; Chen, C., Solid electrolyte based on waterborne polyurethane and poly(ethylene oxide) blend polymer for all-solid-state lithium ion batteries. *Solid State Ionics* **2018,** *320*, 55-63.
33. Bao, J.; Shi, G.; Tao, C.; Wang, C.; Zhu, C.; Cheng, L.; Qian, G.; Chen, C., Polycarbonate-based polyurethane as a polymer electrolyte matrix for all-solid-state lithium batteries. *Journal of Power Sources* **2018,** *389*, 84-92.
34. Tao, C.; Gao, M.-H.; Yin, B.-H.; Li, B.; Huang, Y.-P.; Xu, G.; Bao, J.-J., A promising TPU/PEO blend polymer electrolyte for all-solid-state lithium ion batteries. *Electrochimica Acta* **2017,** *257*, 31-39.
35. Wu, N.; Shi, Y.-R.; Lang, S.-Y.; Zhou, J.-M.; Liang, J.-Y.; Wang, W.; Tan, S.-J.; Yin, Y.-X.; Wen, R.; Guo, Y.-G., Self-Healable Solid Polymeric Electrolytes for Stable and Flexible Lithium Metal Batteries. *Angewandte Chemie International Edition* **2019,** *58* (50), 18146-18149.
36. Porcarelli, L.; Manojkumar, K.; Sardon, H.; Llorente, O.; Shaplov, A. S.; Vijayakrishna, K.; Gerbaldi, C.; Mecerreyes, D., Single Ion Conducting Polymer Electrolytes Based On Versatile Polyurethanes. *Electrochimica Acta* **2017,** *241*, 526-534.
37. Gomez-Lopez, A.; Elizalde, F.; Calvo, I.; Sardon, H., Trends in non-isocyanate polyurethane (NIPU) development. *Chemical Communications* **2021,** *57* (92), 12254-12265.
38. Das, S.; Pandey, P.; Mohanty, S.; Nayak, S. K., Insight on Castor Oil Based Polyurethane and Nanocomposites: Recent Trends and Development. *Polymer-Plastics Technology and Engineering* **2017,** *56* (14), 1556-1585.
39. Mustapa, S. R.; Aung, M. M.; Rayung, M., Physico-Chemical, Thermal, and Electrochemical Analysis of Solid Polymer Electrolyte from Vegetable Oil-Based Polyurethane. **2021,** *13* (1), 132.
40. Panchireddy, S.; Grignard, B.; Thomassin, J.-M.; Jerome, C.; Detrembleur, C., Bio-based poly(hydroxyurethane) glues for metal substrates. *Polymer Chemistry* **2018,** *9* (19), 2650-2659.
41. Raj, A.; Panchireddy, S.; Grignard, B.; Detrembleur, C.; Gohy, J.-F., Bio-Based Solid Electrolytes Bearing Cyclic Carbonates for Solid-State Lithium Metal Batteries. *ChemSusChem* **2022,** *15* (18), e202200913.
42. Karan, N. K.; Pradhan, D. K.; Thomas, R.; Natesan, B.; Katiyar, R. S., Solid polymer electrolytes based on polyethylene oxide and lithium trifluoro- methane sulfonate (PEO–LiCF3SO3): Ionic conductivity and dielectric relaxation. *Solid State Ionics* **2008,** *179* (19), 689-696.
43. M.A. Ratner, i. J. R. M., C.A. Vincent Eds, In *Polymer Electrolyte Reviews 1*, Elsevier: Londen, 1987.
44. Bruce, P. G.; Vincent, C. A., Steady state current flow in solid binary electrolyte cells. *Journal of Electroanalytical Chemistry and Interfacial Electrochemistry* **1987,** *225* (1), 1-17.
45. Leroy, S.; Martinez, H.; Dedryvère, R.; Lemordant, D.; Gonbeau, D., Influence of the lithium salt nature over the surface film formation on a graphite electrode in Li-ion batteries: An XPS study. *Applied Surface Science* **2007,** *253* (11), 4895-4905.
46. Bekaert, L.; Raj, A.; Gohy, J.-F.; Hubin, A.; De Proft, F.; Mamme, M. H., Assessing the Long-Term Reactivity to Achieve Compatible Electrolyte–Electrode Interfaces for Solid-State Rechargeable Lithium Batteries Using First-Principles Calculations. *The Journal of Physical Chemistry C* **2022,** *126* (19), 8227-8237.
47. Zheng, J.; Yan, P.; Mei, D.; Engelhard, M.; Cartmell, S.; Polzin, B.; Wang, C.; Zhang, J.-G.; Xu, W., Highly Stable Operation of Lithium Metal Batteries Enabled by the Formation of a Transient High-Concentration Electrolyte Layer. *Advanced Energy Materials* **2016,** *6*.
48. Chu, H.; Noh, H.; Kim, Y.-J.; Yuk, S.; Lee, J.-H.; Lee, J.; Kwack, H.; Kim, Y.; Yang, D.-K.; Kim, H.-T., Achieving three-dimensional lithium sulfide growth in lithium-sulfur batteries using high-donor-number anions. *Nature Communications* **2019,** *10* (1), 188.
49. Grissa, R.; Fernandez, V.; Fairley, N.; Hamon, J.; Stephant, N.; Rolland, J.; Bouchet, R.; Lécuyer, M.; Deschamps, M.; Guyomard, D.; Moreau, P., XPS and SEM-EDX Study of Electrolyte Nature Effect on Li Electrode in Lithium Metal Batteries. *ACS Applied Energy Materials* **2018,** *1*.

Supporting Information

Bio-derived cyclic carbonates bearing poly(hydroxyurethane)-based networks

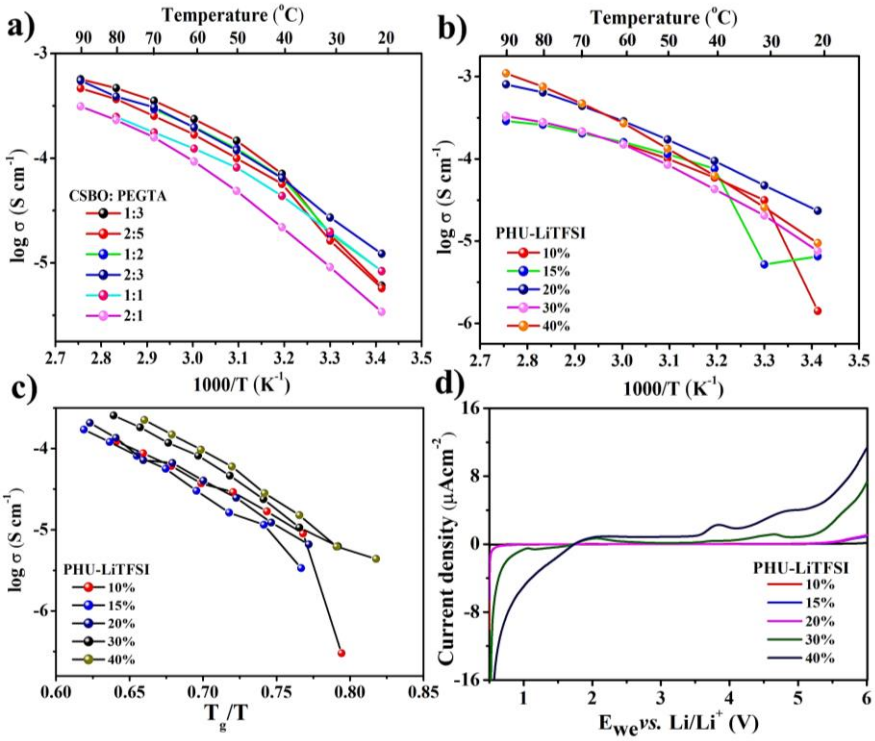

Figure 6.1.1: a) Temperature dependent ionic conductivity for a) stoichiometric controlled PHU-15%LiTFSI SPEs and b) with wt% LiTFSI without cellulose separator; c) Ionic conductivity using the Fox model; d) Linear sweep voltammetry analysis of PHU-SPE with wt% LiTFSI, respectively.

Table S6.1.1: Activation energy and pre-exponential factor as calculated from the slope of VFT plots (x% indicates wt% LiTFSI).

Sample	Adj. R^2	lnA	E_a (kJ-mol^{-1})
PHU-0%	0.7519	-0.10	-16.43
PHU-10%	0.8405	1.08	-12.24
PHU-15%	0.9901	0.38	-10.32
PHU-20%	0.9892	0.04	-8.98
PHU-30%	0.9954	0.40	-9.43
PHU-40%	0.9836	0.34	-9.11

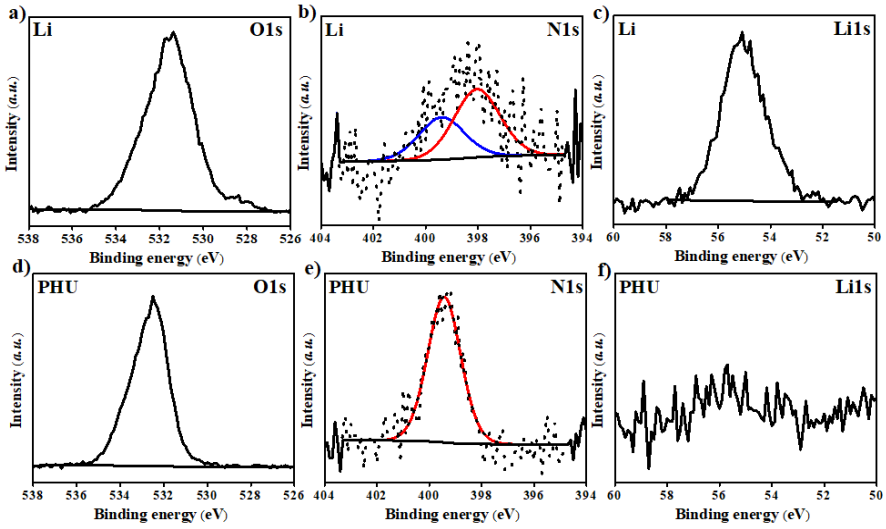

Figure S6.1.2: HR-XPS of a) and d) Oxygen (O1s), b) and e) Nitrogen (N1s), c) and f) Lithium (L1s), for li-anode and PHU electrolyte surface of Li-LFP cell, respectively.

Chapter 6.2 Non-isocyanate poly(hydroxyurethane)-based networks

Abstract

Various classes of polymers incorporating PEG segments have been developed in search of superior properties, stability and compatibility at the device level. Poly(hydroxyurethane) (PHU) networks derived from bio-based monomers propose an interesting alternative, not only targeting sustainability but also tunability in the mechanical and electrochemical properties. Therefore, we report here on the facile synthesis of PHU networks obtained via the ring-opening of cyclic carbonates present on bio-based carbonated soy bean oil by PEG segments of various lengths functionalized at both ends by amines. We also explore the possibility to form PHU-poly(epoxy) mixed networks by additionally incorporating PEG segments functionalized at both ends by epoxides in the reaction mixture. The accordingly obtained polymer networks possess high flexibility and a good interface stability. After salt loading, the SPE membranes based on PHU and PHU-poly(epoxy) mixed networks exhibit ionic conductivities in the range of ~$10^{-4.5}$ to 10^{-5} S cm^{-1} at 60 °C

with oxidation stability > 4.2 V versus Li/Li^+. Further, their long-term compatibility with lithium metal has been investigated in a controlled setup for more than a hundred cycles in stripping and plating experiments. Those results drive the PHU-based networks toward the developmental intent of a functional polymer with a higher degree of control on structure and properties dealing with the trade-off of mechanical and electrochemical properties.

6.2.1 Introduction

Batteries have become a part of our daily life, from small devices to large gadgets with huge potential to revolutionize the transport sector. Various automotive companies are betting on fossil fuel-free electric vehicles, based on lithium batteries. Differing in scale, from coin cells to large grids, lithium batteries have already made their place in the market for more than two decades.[1] However, they are required to outperform their energy density with improved safety and processing. These aspirations can only be achieved with high-energy-density electrodes and safer electrolytes (specifically solid state electrolytes, SSEs). High voltage cathodes development has been progressive throughout the timeline of lithium batteries research with periodic challenges for anodes either with compatibility or stability with electrolytes. Among those, silicon-based materials and lithium metal anodes possess the highest theoretical capacity, with the later showing as much as 3860 mAh g^{-1}.[2] Moreover, they do not sound very promising and safe due to the number of incidents recorded with battery fires or explosions.[3] Therefore, replacing liquid electrolytes with solid ones would not only remove the drawbacks of flammability, leakage, and short-circuit due to dendrite growth and packaging but also provide lithium metal compatibility and a broad voltage window for high-voltage cathodes application as well. In addition, this replacement brings in other remarkable advantages aligning with both electrochemical and mechanical properties. SSE electrolytes are supposed to offer broad oxidation stability (beneficial for high voltage cathodes without electrolyte decomposition), lightweight, flexibility, easy stack, robustness, safety (non-flammable) and thus cost-effective.[2,4] On the contrary, SSEs offer low ionic conductivity and poor interfacial compatibility. So far, inorganic solid electrolytes (ISEs) have outperformed solid polymer electrolytes (SPEs) but the latter excites with good mechanical properties and processability.

Over the years, various classes of polymers have been tested with varying architecture, topology, and size in their pristine or copolymer state. The availability of polar groups for lithium ion complexation via weak coordination is always desired in any polymer as a conduction host. Some of the well-known polymers explored in batteries include PEG,[5,6] polycarbonates,[7,8] polyvinylidene fluoride (PVDF),[9,10] poly(methyl methacrylate),[11,12] polysiloxanes,[13,14] polyurethanes,[15-17], *etc*. While most

of these exhibited potential performance in their investigation, they underperform on other required parameters such as salt solvation or oxidation stability, which demands more polymer engineering. In concern to addressing those trade-offs in one polymer, a variety of synthetic methods and techniques found their way like block copolymers, blends, plasticization, hybrid polymers with inorganic fillers *etc*.[18-20] Higher salt dissociation and mobile charge carriers contribute to higher ionic conductivity and higher transference number. The ability to prevent dendrite growth and form a stable solid electrolyte interphase (SEI) with decent compatibility mark crucial indicators for a good electrolyte. Therefore, a superior battery material relies on material design and development, processing, interfacial engineering and investigation to understand the surface chemistry neck to neck with theoretical assumptions and findings.[21-23]

Poly(hydroxyurethane)s (PHUs), like the parent polyurethanes (PUs), combine soft and hard segments in one polymer. PUs, first discovered by Otto and co-workers[24], are being used in many industrial products, including coatings, paints, adhesives and resins. However, the first report on PUs as SPEs in 1980 highlighted their potential in batteries.[25] The conductivity was speculated to be facilitated by soft segments and mechanical properties via hard segments within the same polymer.[16] In later reports, isocyanate-based PUs have been exploited in various forms involving copolymers, blends, hybrids showing conductivities as low as ~10^{-8} to as high as ~10^{-5} S cm^{-1} at 25 ^{o} C.[26,27] There are some reports on natural oil-based monomers-derived PUs, exhibiting decent Li-ion conduction, such as Jatropha,[28] Palm kernel oil,[29] castor oil.[30]

While PUs were often synthesized via a reaction between diisocyanates and alcohol/polyol in the presence of a catalyst, PHUs are presented as non-isocyanate polyurethanes (NIPUs). They are prepared using different techniques, among them the aminolysis of cyclic carbonates.[31,32] The cyclic carbonates and derived PHUs are gaining more interest due to their highly sustainable synthetic pathway via coupling of CO_2.[8] In Chapter 6.1, we reported the solid PHU-based SPEs on cellulose separator derived from the reaction of carbonates and diamines with the conductivity > 10^{-4} S cm^{-1} and decent performance in Li|PHU SPE|LFP cells at 60 ^{o}C. Referring to a few reports, polymer networks provide better mechanical as well as electrochemical properties on the potential addition of additives, fillers, plasticizers *etc*. Scardi *et al.*

demonstrated that SPEs obtained by reacting palm kernel oil polyol and 2,4-methylene diphenyl diisocynate (2,4' MDI) could reach a conductivity of 7.6 x 10^{-4} S cm^{-1} at RT after plasticization with ethylene carbonate.[29] Taking that inspiration, we intended to design a Plasticized PHU by incorporating epoxy in addition to PHU with the scope of investigations on the effect of unreacted cyclic carbonate in the crosslinked network.

Here, we report a series of SPEs based on PHU, synthesized via catalyst-free addition reaction between carbonated soybean oil (CSBO) bearing on average 6 carbonates and PEG segments of various lengths terminated at both ends by amines (see Scheme 6.2.1) to tune the mechanical and electrochemical properties unlike in Chapter 6.1. The network results from the ring-opening reaction of the cyclic carbonate (CC) rings of CSBO by the nucleophilic amines (Scheme 6.2.1). Since CC rings show good lithium solvation and are widely used in the side chains and main chain of SPEs for their better transport properties,[7,33] it would be desirable to leave some CC rings unopened in the final networks in order to reach superior ionic conductivity in the final SPE. To this aim, we introduce here a competitive ring-opening reaction by adding poly(ethylene glycol) diglycidyl ether (PEGDCE) in the reaction mixture. Since the ring opening reaction induced by nucleophilic amines of PEGTA is expected to be faster with epoxy of PEGDCE than with CCs of CSBO, the resulting network could contain untouched CCs units. By a careful control of the PEGDCE/CSBO stoichiometry, we show that we can preserve a certain amount of unopened CCs units without comprising on the mechanical properties of the final networks since the more reactive PEGDCE/amino-functionalized PEG ring-opening leads to crosslinking nodes at the expense of CSBO/amino-functionalized PEG ones. The lithium metal compatibility with our SPE membrane is finally demonstrated with some interesting findings supported by cycling and post mortem XPS analysis.

6.2.2 Materials and methods

2,2′-(Ethylenedioxy)bis(ethylamine)(M_w~148.20), 4,7,10-trioxa-1,13-tridecanediamine (M_w~ 220.31), poly(ethylene glycol) diglycidyl ether (M_w~500), anhydrous tetrahydrofuran solvent (THF) and lithium battery-grade, lithium bis(trifluoromethanesulfonyl)imide (LiTFSI) are purchased from Sigma-Aldrich.

Poly(ethylene glycol) bis(3-aminopropyl) terminated (PEGTA)(Mw~1500) was bought from Acros organic chemical. Carbonated soybean oil (CSBO) was prepared following a previously published report.[34] Lithium metal foil (99.9%), lithium iron phosphate ($LiFePO_4$), poly(vinylidene fluoride) and Super-P were purchased from TOB chemicals. N-methyl-2-pyrrolidone (NMP) was purchased was bought from Alfa Aesar. Deuterated chloroform ($CDCl_3$) used for NMR spectroscopy was purchased from Eurisotop. All reactants and catalysts were used as received, without any further purification.

Note: Refer the Chapter 5.1 for characterization and electrochemical techniques.

6.2.3 Experimental section

6.2.3.1 Synthesis of Poly(hydroxyurethane) (PHU-NXNY)

Bio-based cyclic carbonated soybean oil (CSBO) was synthesised by coupling of supercritical CO_2 with epoxidised soybean oil (ESBO) as reported somewhere else.[34] As for PHU, the reaction between CSBO and poly(ethylene glycol) bis(3-aminopropyl) terminated (PEGTA), 4,7,10-trioxa-1,13-tridecanediamine (TDD) and 2,2′-(ethylenedioxy)bis(ethylamine) (EDEA) in varied ratio. The ratio of all, EDEA (N1), TDD (N2) and PEGTA (N3) to CSBO was chosen to 3:1 equivalent corresponding to assumption of all ring opening, accordingly.

For the reaction of PHU-N2N3, 90 mg of CSBO (M_n ~ 1250), 81 mg of PEGTA (for 25 mol%, M_n ~ 1500) and 35.69 mg of TDD (75 mol%, M_n ~ 220.31) was taken in a small vial. These were dissolved in anhydrous THF via magnetic stirring at room temperature (RT) for >6 h. The resulting transparent solution was then drop cast on a Teflon mold followed by transfer to the vacuum oven. The temperature of the vacuum oven was set at 70 ^oC for >12 h and later increased to 90 ^oC for >24 h under dynamic vacuum .A similar procedure was followed for other PHU-NXNY and LiTFSI loaded PHU-NXNY (NX: N1, N2, N3) following the addition of salt solution to the initial mixture in case of the latter. After curing, the samples were transferred to the glove box. The reaction is highlighted as depicted in Scheme 6.2.1.

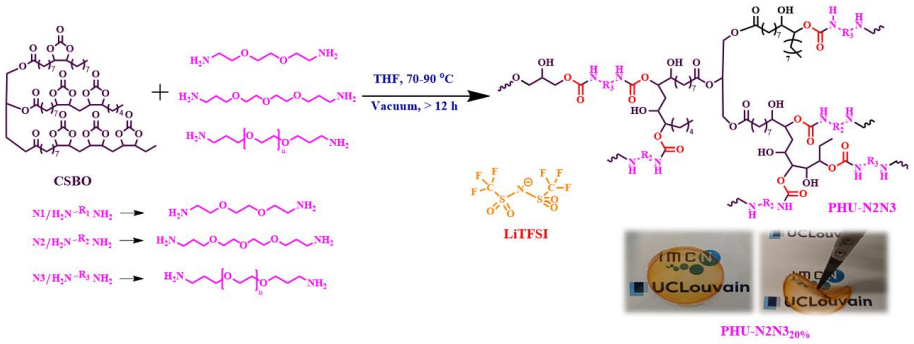

Scheme 6.2.1: Synthesis of poly(hydroxyurethane) analogues with possible network structure, (bottom-right). Pictures of PHU-N2N3 (75 mol% of N2 and 25 mol% of N3) films with 20wt% LiTFSI as labelled in subscript.

6.2.3.2 Synthesis of Poly(hydroxyurethane)-poly(epoxy) mixed networks (PHU-N2N3-Ep)

Poly(ethylene glycol) bis(3-aminopropyl) terminated (PEGTA) and 4,7,10-trioxa-1,13-tridecanediamine (TDD) in mole ratio of 25% and 75% was chosen to react with CSBO to obtain PHU-N2N3 as mentioned above. For the mixed networks, poly(ethylene glycol) diglycidyl ether was added to the reaction mixture required for PHU-N2N3 at various concentrations from 0 to 100 wt% (with respect to CSBO). The most explored composition, (PHU-N2N3-Ep) involved 70 mg of CSBO (M_w~ 1250), 63 mg of PEGTA (for 25 mol%, M_w ~ 1500), 27.75 mg of TDD (75 mol%, M_w ~ 220.31) and 70 mg of PEGDCE (M_w ~ 500. 100 wt% w.r.t. CBSO) dissolved in a small vial with the help of anhydrous THF. Subsequent procedures were similar to those performed above for PHU-N2N3. Refer scheme 6.2.2.

6.2.3.3 Preparation of electrolytes (SPEs)

LiTFSI enforcement to the PHUs network was performed in the first step prior to thermal curing for electrolyte films. The dried films were transferred to the glove box and SPE films were peeled off the Teflon molds and stored in the glove box before cell fabrication and characterization. The thickness of 16 mm punched membranes was measured to be in the range of 100-200 μm. 2032-type coin cells were assembled using those free-standing SPE films sandwiched between SS|SS, SS|Li, Al/Al-C|Li, Li|Li and Li|LFP electrode configurations to evaluate electrochemical analysis.

Scheme 6.2.2: Synthesis of mixed poly(hydroxyurethane)-poly(epoxy) networks with PEGDCE, (bottom-right: picture of PHU-N2N3-Ep films (75 mol% of N2, 25 mol% of N3 and 100 wt% of poly(epoxy) with respect to CBSO)), subscript indicates x-wt% LiTFSI).

6.2.4 Results and discussions

We synthesized PHU and PHU-poly(epoxy) (PHU-Ep) analogues via an isocyanate and catalyst-free, sustainable synthetic approach at mild temperature and reaction conditions. The synthesis of the polymer networks is depicted in Scheme 6.2.1 and 6.2.2, respectively for pristine PHU-NXNY and mixed PHU-NXNY-Ep (refer to experimental section for the meaning of acronyms) involving ring-opened epoxy in addition to hydroxy urethanes crosslinking nodes.

The reaction between CC and diamine follows the ring opening with intermediate steps as highlighted in the reaction mechanism reported elsewhere.[35] PHU-NXNY have been synthesized by a combination of crosslinkers from three diamines in order of their increasing chain length/higher number of ethylene oxide (EO) units, i.e. 2 in EDEA, 3 in TDD, to ~32 units in PEGTA, respectively. Several combinations of PHU-NXNY were formalized with varied mechanical properties and conductivity, as highlighted in Table S6.2.1. The crosslinking reaction (or extent of aminolysis) is not only dependent on the concentration of monomers and reaction time but also on other parameters such as temperature, solvent mixture and interfering agents. A detailed investigation on PHU-N3 bearing unreacted CC units supported on cellulose separator is demonstrated in Chapter 6.1. While here, separator-free SPEs were obtained by using mixtures of crosslinkers of different chain lengths, and with increased softening

in the network with LiTFSI concentration. As reported in Chapter 6.1, PHU-N3 offered good conductivity while poor mechanical properties, which required an increased yield in the ring-opening reaction leading to hydroxy urethanes. Here, a better compromise was obtained with a combination of 75 mol% of TDD (N2) and 25 mol% PEGTA (N3) (as shown in the picture of SPE in Scheme 6.2.1). The higher number of EO units forming soft segments is sourced from PEGTA, which is crucial for Li^+ conduction. In contrast, TDD increases the yield of ring-opening reaction due to its higher accessibility to CC rings contributing directly to an increased number of crosslinking nodes and of urethane hard segments in the network. Combining in varying amounts a long chain crosslinker (PEGTA) to a short one (TDD or EDEA) thus appears as a valuable strategy to finely modulate the mechanical properties of the accordingly obtained networks while not compromising ionic conductivity.

In further attempts, another strategy was designed to investigate the effect of unreacted CC and target higher salt dissociation without losing the free-standing nature of the SPE resulting from network formation (Scheme 6.2.2). This strategy consist in using a competitive, faster, crosslinking reaction beside the ring-opening of CCs by nucleophilic amines. More precisely, we introduced PEG chains bearing epoxides at both ends (PEGDCE), well known to react quantitatively and quickly with amines. Therefore, PEGDCE has been mixed in varying quantities with CSBO and the different amino-functionalized PEG to obtain PHU-NXNY-Ep mixed networks. In those networks, most of crosslinking nodes are believed to essentially originate from the PEGDCE epoxy groups with amino-functionalized PEG while much less should result from the less reactive hydroxy urethane groups from CSBO/amino-functionalized PEG. Practically, the optimized ratio and reaction conditions for PHU-N2N3-Ep were translated from PHU-N2N3 without change. The higher the concentration of epoxy, the lower is the formation of PHU units in the network due to the higher reactivity of PEGTA and TDD towards epoxy. However, the epoxy monomer consists of ~8 EO units as well, which is beneficial for conduction. This step of restricting CC-ring opening and engaging epoxy-aminolysis directly affects the physical properties of PHU at a limited concentration of amines.

6.2.4.1 Fourier transform infra-red spectroscopy

The PHU networks were characterized via IR analysis for the confirmation of crosslinking reaction and other changes in functionalities, as shown in Figure 6.2.1. The carbonyl peak corresponding to CC at 1796 cm^{-1} was retained with a slight shift at 1801 cm^{-1} in PHU-N3 with lower intensity as observed in Figure 6.2.1a. This hints at the incomplete CC ring opening either due to a low concentration of crosslinkers or inaccessible CC rings. However, the CC carbonyl peak almost disappeared in the case of PHU-N2N3 with the appearance of an urethane bond signal at 1701-1696 cm^{-1} and 1713- 1716 cm^{-1} in all PHUs. At higher salt concentration, a broadening in urethane signals was observed as reported in PHUs.[36]

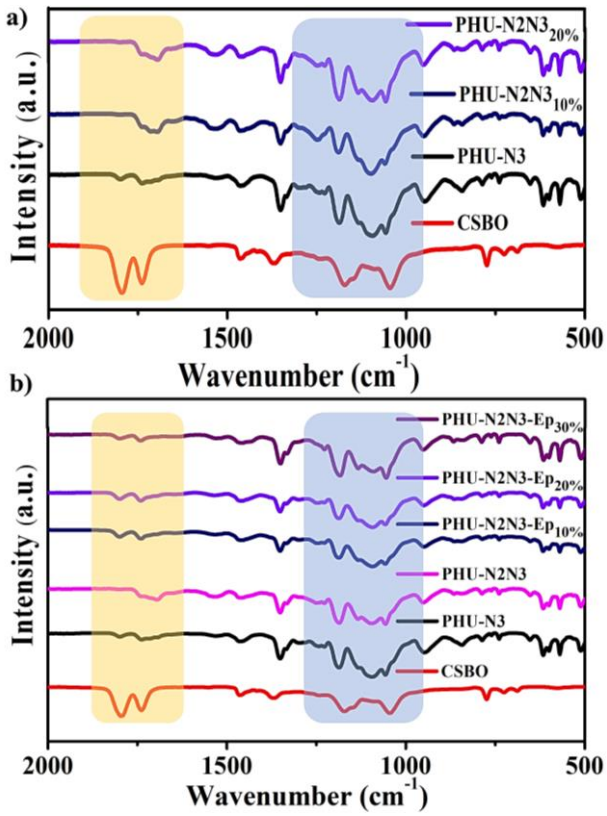

Figure 6.2.1: Comparative IR spectra of PHU analogues with varying formulation, a) PHU-N2N3$_x$; and c) PHU-N2N3-Ep$_x$ in comparison to PHU-N3 and CSBO, respectively (where, 75 mol% of N2, 25 mol% of N3, 100 wt% of poly(epoxy) with respect to CBSO and x wt% of LiTFSI).

The ester signal (-RCOOR-) from CSBO at 1739 cm^{-1} was detected at 1740 cm^{-1} for PHU-N3 and slightly shifted to 1738 cm^{-1} and 1736 cm^{-1} for PHU-$N2N3_{20\%}$ and PHU-$N2N3_{10\%}$, respectively. Other characteristic signals involved –OH stretching at 3451 cm^{-1}, 3380 cm^{-1} and 3390 cm^{-1} while, –NH signal at 1531 cm^{-1}, 1537 cm^{-1}, 1533 cm^{-1} for PHU-N3, PHU-$N2N3_{10\%}$ and PHU-$N2N3_{20\%}$, respectively. The strong aliphatic ether (-C-O) signal was recorded around 1106 cm^{-1} along with C-N stretching in the range of 1250 cm^{-1}-1275 cm^{-1} in corresponding PHU networks.

Similarly, referring to Figures 6.2.1b for PHU-N2N3-Ep, incomplete ring opening of CC was observed in comparative spectra of PHU-N2N3-Ep with PHU-N3. CC, carbonyl (-C=O) peak was marked within 1798-1800 cm^{-1} in addition to the ester (-RCOOR) around 1738-1741 cm^{-1}. While urethane stretching was recorded with higher broadening due to lesser carbamate formation and higher salt concentration in a similar region as of PHU-N2N3. However, there was no strong signal detected from epoxy besides a slightly weak and broadened peak around 880 cm^{-1} specifically for PHU-$N2N3\text{-}Ep_{10\%}$ and PHU-$N2N3\text{-}Ep_{20\%}$. The higher reactivity of epoxy with diamine dominated the crosslinking over reaction of CBSO in the presence of LiTSFI, confirming our hypothesis. The good solvation of LiTFSI was validated from signals in the range around 900-700 cm^{-1}.

6.2.4.2 Thermal measurements

Thermal analysis was performed with DSC and TGA using parameters as mentioned in the experimental section. The polymer melting (T_m), crystallization (T_c) and other phase change temperatures were monitored via DSC in the –70 °C to 100 °C range. Among all precursors, only PEGTA possesses a solid nature while TDD is liquid and PEGDCE and CBSO are viscous fluids at room temperature. CSBO shows a low glass transition temperature (T_g), which increases with salt concentration with no crystallization,[8] whereas, T_m and T_c were recorded at 50.1 °C and 20.1 °C for PEGTA respectively (Figures 6.2.2a and 6.2.2b). A cold crystallization phenomenon was observed in PHU without LiTFSI with T_g at -48.8 °C. However, LiTFSI loaded PHU-N2N3 networks showed only amorphous behaviour with higher T_g of 43.7 °C, -44.2 °C and -40.8 °C respectively for 10%, 15% and 20% LiTFSI wt/wt%. This trend in T_g is predicted to be non-conclusive due to low differences in salt concentration.

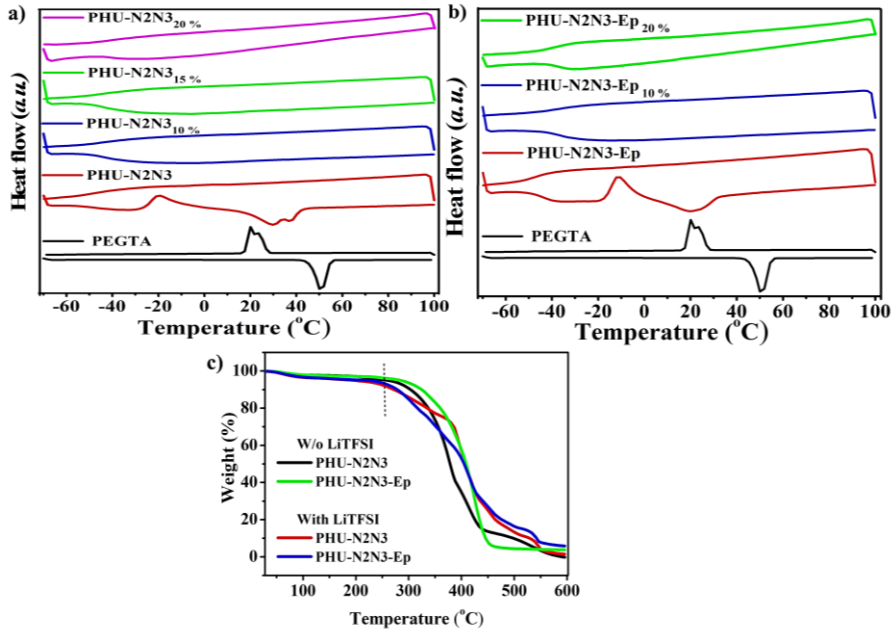

Figure 6.2.2: DSC thermograms of PHU analogues, a) PHU-N2N3 and b) PHU-N2N3-Ep in comparison to PEGTA; and c) Thermogravimetric analysis of PHU-N2N3 and PHU-N2N3-Ep with and without 20 wt% LiTFSI (where, 75 mol% of N2, 25 mol% of N3, 100 wt% of poly(epoxy) with respect to CBSO).

The PHU-N2N3 network with 100wt% of PEGDCE w.r.t to CSBO was subjected to DSC measurements. The network without LiTFSI showed a lower T_g of -43.9 °C relative to PHU-N2N3, while a similar decrement was also observed with LiTFSI, to -37 °C, -37.8 °C and -33.5 °C for PHU-N2N3-$Ep_{10\%}$, PHU-N2N3-$Ep_{20\%}$, and PHU-N2N3-$Ep_{30\%}$ respectively as indicated in Figure 6.2.2b.

Thermal degradation of the networks was analyzed by thermogravimetric analysis measurements in N_2 supply in the temperature range of 30 °C to 600 °C for a comparative analysis of PHU analogues with and without LITFSI (Figure 6.2.2c). The analysis can be split into multiple components as depicted from the derivative of TGA. In the beginning, the slight weight % loss could be correlated to adsorbed moisture for all the samples until 100 °C. Major decomposition for almost all the analogues starts nearly ~250 °C and with polymer without LiTFSI at slightly higher T_d. Among PHU-N2N3 and PHU-N2N3-Ep, higher thermal stability is observed for plasticized

network as evident at higher temperatures, > 500 °C. LiTFSI decomposition was observed around 500 °C in two minor phases for polymer units.

6.2.4.3 Ionic conductivity

Coin/Swagelok cells with PHU networks SPEs membranes were subjected to potentiostatic electrical impedance spectroscopy (PEIS) for conductivity measurement at various temperatures in symmetric blocking cells with stainless steel electrodes. Nyquist plots with real and imaginary impedance were recorded and analyzed for electrolyte resistance. The conductivity (σ) was calculated using equation 6.2.1 which depends on parameters such as length, and area of the film besides resistance from the following equation,

$$\sigma = \frac{l}{R_b S} \tag{6.2.1}$$

$$\sigma T^{1/2} = A e^{-\frac{E_a}{K_b}(T-T_0)} \tag{6.2.2}$$

where, R_b is bulk electrolyte Ohmic resistance from AC impedance, l and S are thickness and the surface area of polymer electrolyte, respectively. Equation 6.2.2 was used for modelling conductivity with VFT behaviour, where A is the conductivity pre-exponential factor, T is the absolute temperature, T_0 is the Vogel scaling temperature at which the free volume disappears or at which free entropy becomes zero following approximation as $T_0 = (T_g\text{-}50\ K)$, E_a is the pseudo-activation energy of ion transport and k_b is Boltzmann constant.[37,38] The conductivity of PHU-N2N3 was compared with various added amount of LITFSI (10-20 wt%) from 0-80 °C and was depicted in the logarithmic conductivity plot with temperature following Arrhenius model (Figure 6.2.3a). PHU-N2N3 exhibited best conductivity of 1.6 x 10^{-4} S cm^{-1} at 80 °C for 20 wt% LITFSI. While at 20 °C, higher conductivity was recorded for PHU-N2N3$_{15\%}$, i.e. 4.07 x 10^{-6} S cm^{-1}. The trend of conductivity versus temperature with certain anomalies could be related to free ion pairs coupled with restricted ion mobility due to crosslinking. While using the VFT model of conductivity, we deduced the higher conductivity trend in PHU-N2N3$_{10\%}$ at lower temperatures and PHU-N2N3$_{20\%}$ at higher temperatures as shown in Figure 6.2.3b.

The conductivity of PHU-N2N3-Ep bearing cyclic carbonate rings was measured with LiTFSI concentration (10-30wt%) as indicated in Figure 6.2.3c. A conductivity of 3.9

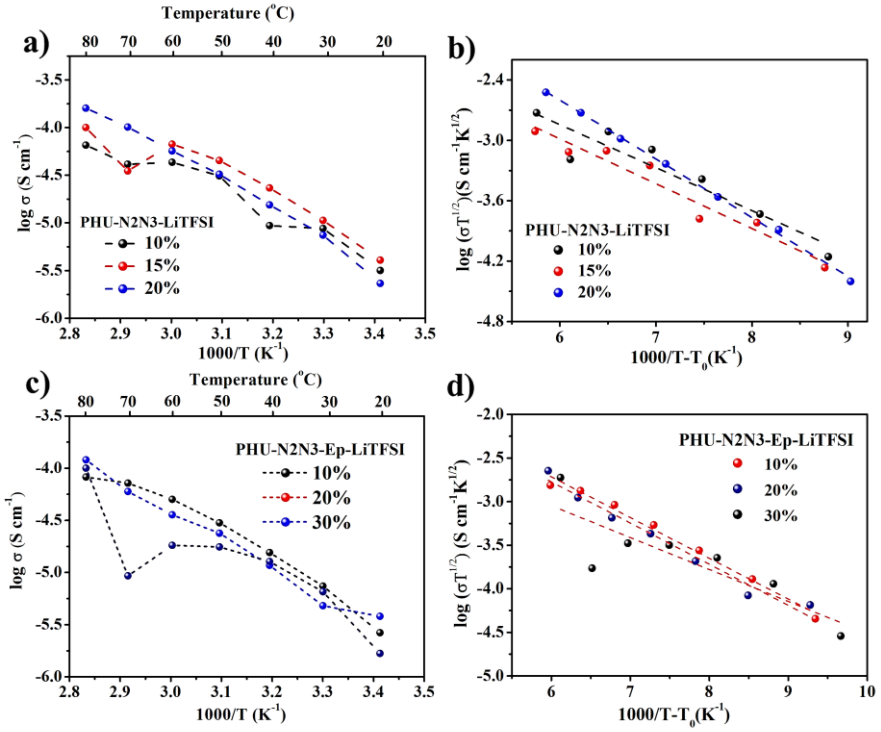

Figure 6.2.3: Temperature dependent ionic conductivity for investigated SPE networks; a) and c) Arrhenius model, b) and d) VFT Model, a) and b) PHU-N2N3-LiTFSI (10-20 wt%); c) and d) PHU-N2N3-Ep-LiTFSI (10-30 wt%), respectively (where, 75 mol% of N2, 25 mol% of N3, 100 wt% of poly(epoxy) with respect to CBSO throughout).

10^{-6} S cm^{-1} at 20 °C was observed for PHU-N2N3-$Ep_{20\%}$. The highest conductivity was obtained at 80 °C to be 1.2 x 10^{-4} S cm^{-1} for PHU-N2N3-$Ep_{20\%}$. For the same salt concentration, PHU-N2N3-$Ep_{20\%}$ exhibited better conductivity than PHU-$N2N3_{20\%}$ until 50 °C and slightly lower conductivity from 60 °C onwards. While aligning the conductivity with VFT model for PHU-poly(epoxy) mixed networks, we did not find much difference as shown in Figure 6.2.3d. We could speculate the higher reaction yield of the oxirane ring resulted in more crosslinking nodes and an increased rigidity in the network, lowering segmental motion. However, it is not clear at this stage if the unreacted CC do exert a positive effect on the overall ionic conductivity and further experiments should be conducted. We can speculate to understand the effect of CC with precise control on quantification ring opened. For further electrochemical measurements, PHU-N2N3-$Ep_{20\%}$ was explored owing to the good compromise in the

conductivity of 4.49 x 10^{-5} S cm^{-1} (at 60 °C), number of charges carrier and mechanical properties.

6.2.4.4 Electrochemical stability window

Oxidation potential limitation for an electrolyte is investigated to find the threshold voltage at which it can channelize ions without decomposition. A wide electrochemical stability window (ESW) at higher voltage allows the higher voltage cathodes to store more reversible energy. ESW as measured using linear scanning voltammetry (LSV) is presented in Figure 6.2.4. At the scan rate of 0.5 mV s^{-1}, the oxidation stability limit of PHU-N2N3$_{20\%}$ was observed to be around E_{ESW} > 4.01 V vs Li/Li^+ with stainless steel cathode. The latter was recorded to be higher in the case of PHU-N2N3-Ep$_{20\%}$ (subscript indicates 20 wt% of LiTFSI for both PHU analogues) i.e. E_{ESW} > 4.24 V vs Li/Li^+ in similar conditions and parameters.

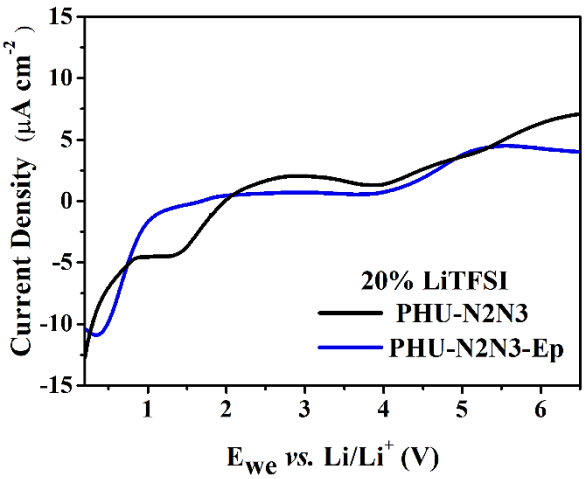

Figure 6.2.4: Linear sweep voltammetry analysis of PHU-based-SPEs with 20% LiTFSI.

6.2.4.5 Stripping and plating

The electrolyte and lithium metal compatibility has been tested via lithium stripping and plating under time-dependent constant current cycling, as represented in Figure 6.2.5a. The voltage-time plot for PHU-N2N3$_{20\%}$ qualitatively explains electrolytic decomposition with lithium metal. Owing to the conductivity of the electrolyte, lower current density has been employed in the range of 0.52 μA cm^{-2} to 4.55 μA cm^{-2} in the cut-off voltage of +2 V to -2 V. The first 2^{nd}-3^{rd} cycles offered huge kinetic hindrance to lithium transport leading to high overpotential to cutoff voltage at 1.3 μA cm^{-2}. Subsequently, a lower current density of 0.52 μA cm^{-2} was applied for almost 100 cycles which recorded a clear decreasing overpotential, i.e. 0.22 V in stripping and -

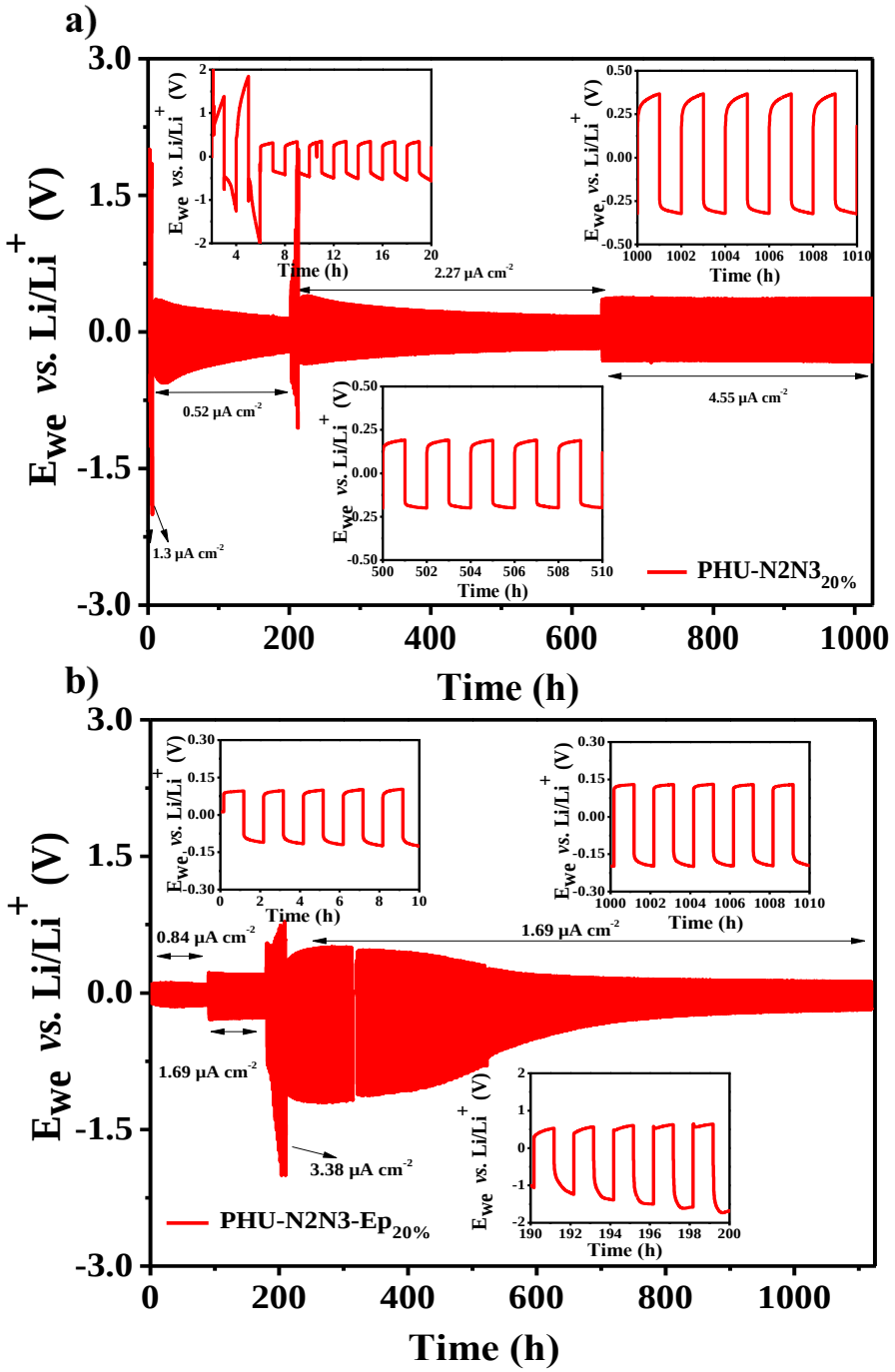

Figure 6.2.5: Galvanostatic charge-discharge voltage profile for stripping-plating at various current densities at 60 °C with Li|PHU-based SPEs|Li symmetric cells, a) PHU-N2N3 and b) PHU-N2N3-Ep, respectively (Insets: magnified plots at respective time demonstrating the constant over potential).

0.3441 V while plating at the 50th cycle. As a result of interfacial stabilization, a reduction in the interfacial resistance could be observed. Furthermore, the overpotential increased drastically when the current density was increased by 4 times, resulting in a stripping voltage of 0.16 V at the 320th cycle. However, despite doubling the current density to 4.55 μA cm^{-2} we did not see much drastic increment in the voltage. The overpotential stabilized from 642 h (321st cycles) onward and recorded over constant values until measured cycles for 1042 h (521 cycles) with stripping-plating of 0.37 V and -0.32 V, respectively. The stable SEI even after a long number of cycles was evident from constant overpotential recorded from 321st cycles onward.

Discussing stripping and plating in PHU-N2N3-Ep$_{20\%}$, higher overpotential was expected in those cells due to relatively lower ionic conductivity. As a result of initial cycling at the current density of 0.84 μA cm^{-2}, the overpotential was ~0.1 V. While for subsequent 45 cycles, almost constant overpotential of ~0.22 V was recorded on the doubling of the current density. However, an abrupt increment to 3.38 μA cm^{-2} led to higher polarization of ~0.7 V and -2 V during charge and discharge, respectively. For remaining long-term cycling, 1.69 μA cm^{-2} was chosen and cycled for more than 400 cycles with constant decreasing overpotential and stabilizing from the 400th cycle onwards at nearly ~0.15 V. Inset in the Figure 6.2.5b shows the voltage profile during the last cycles of the stripping-plating, averaging at ~0.15 V. This supports the efficient transport of lithium ions within the electrolyte and SEI at certain current density. While larger polarization at a relatively higher current explains lower conductivity and parasitic electrolytic decomposition.

6.2.4.6 Post-mortem analysis of cycled cells

The XPS on the Li anode and SPE surfaces for lithium symmetric cells was performed to probe their interfacial composition after stripping and plating for more than 1000 h. The C 1s peak at 284.8 eV was used as a reference to calibrate the binding energy. The survey spectra detected the desired elements like C, O, Li, F, N and S originating from the SEI layer or the decomposition are shown in Figure 6.2.6 for electrolyte films of PHU-N2N3 and PHU-N2N3-Ep. The C1s spectra in both SPEs excluding the adventitious carbon can be attributed to C-C/C-H, C-O/N,

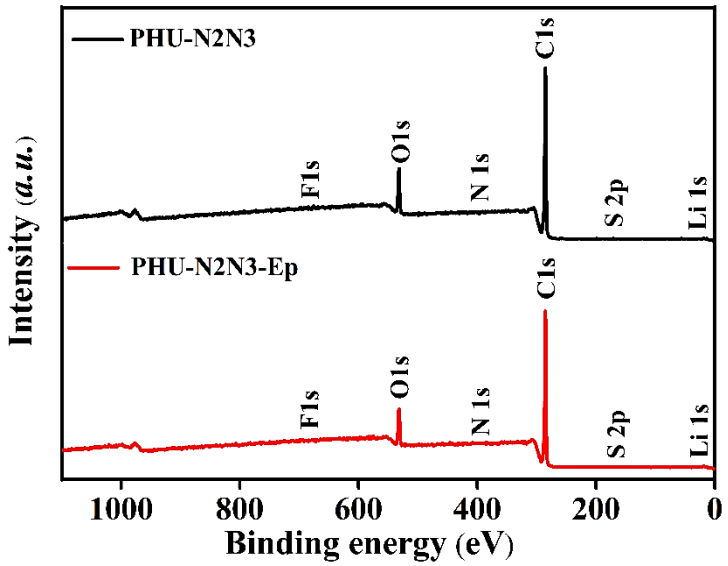

Figure 6.2.6: Survey spectrum of surface of cycled PHU based SPEs from Li-Li cells after 500+ cycles of stripping and plating.

O-C-O/C=O and O-C=O/CO_3^{-2} (inorganic carbonates) with the binding energy of ~ 284.9 eV, 286.3 eV and 287.9 eV and 288.8 for PHU-N2N3 and at ~ 284.8 eV, 286.2 eV and 287.9 eV .and 288.8 for PHU-N2N3-Ep respectively, as shown in Figures 6.2.7a and 6.2.7d. Referred to the simulation performed in our previous report, there is possible C=O formation from carbamate cleavage.[22]

SEI stabilized by LiF formation was detected at 688.2 (0.2%) and 688.3 (0.2%) while -CF_3 corresponding to LiTFSI at 688.2 eV (1.2%) and 688.3 eV (0.3%) in respective PHUs (Figures 6.2.7b and 6.2.7d). From the higher proportion of LiF formation for the films of PHU-N2N3-Ep, it can be deduced that the addition of epoxy to the PHU N2N3 increased the reactivity with lithium and thus higher decomposition. A similar finding has been witnessed as we compare the HR-XPS of S2p for both SPE films in Figures 6.2.7c and 6.2.7f. A sharper signal for SO_x was observed in PHU-N2N3-Ep than in PHU-N2N3. The quantification table can be referred to as supporting information (Figure S6.2.1) along with HR-XPS of other elements, such as O1s, N1s and Li1s. These surface analyses backed the decent stripping and plating experiments over hundreds of cycles due to stable electrolyte decomposition and SEI formation.

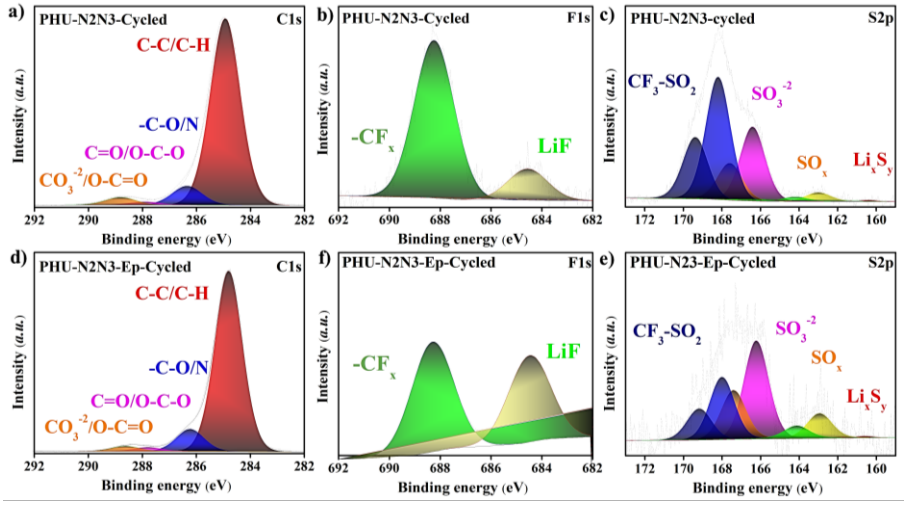

Figure 6.2.7: HR-XPS of a) and c) Carbon, b) and d) Fluorine and e) Sulphur at the surface cycled PHU-based SPE films after stripping and plating with Li-Li cells, respectively

6.2.4.7 Li-metal battery prototypes

Cells with Li metal anodes and LFP cathodes were tested by GCPL technique over the voltage of 2-4 V. Those cells exhibited a discharge capacity of 114.96 mAh g^{-1} at a C-rate of 0.1 C at 60 ^{o}C with the polarization of almost ~0.179 V in the 1st cycle as in Figure 6.2.8a. The polarization drops in the subsequent cycles to ~0.084 V and ~0.0341 V in the 10th cycles and 30th cycle, respectively. This could be credited to the stabilized interface due to the beneficial decomposition of electrolyte at the lithium surface. However, the discharge capacity drop is also observed to 108.79 mAh g^{-1} and 94.63 mAh g^{-1} at the respective 10th and 30th cycle. The capacity-cycle plot shows the fading capacity with increasing Coulombic efficiency (up to ~97.8%) as demonstrated in Figure 6.2.8b. The fading could be also an indication of high diffusion barriers between the electrodes and electrolyte. Nevertheless, a preliminary cycling test on PHU-N2N3-$Ep_{20\%}$ showed the potential performance which could be improved with further focus on these polymers.

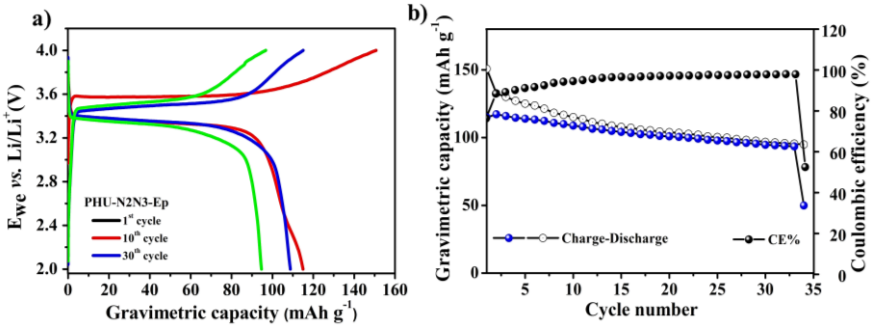

Figure 6.2.8: Galvanostatic charge-discharge voltage profiles, a) Gravimetric capacity at 0.1C for respective cycles; and b) Capacity retention plot with cycle number and Coulombic efficiency for Li|PHU-N2N3-Ep-SPE|LFP at 60 °C, respectively.

6.2.5 Conclusion

More and more emphasis needs to be placed on the innovation of sustainable precursors and approaches for polymer electrolytes given the high concern for the impact of chemicals on clean energy. We have attempted here to address the issue of the environmental footprints by utilizing a bio-based monomer for the synthesis of PHU analogues. We reported a series of PHU and PHU-poly(epoxy) networks as potential solid-state electrolytes from lithium-ion conduction. The self-standing electrolyte films demonstrated good flexibility and interfacial contact, as speculated from low T_g around -40 °C. With high thermal stability, we indicate the absence of polymer degradation in the operating temperature of the batteries. The conductivity of the PHU-N2N3 and PHU-N2N3-Ep remains in the order of 10^{-5} S cm^{-1} for the same LiTFSI concentration. However, PHU-N2N3-Ep showed a higher oxidation potential limitation of > 4.24 V against > 4.01 V versus Li/Li^+ for PHU-N2N3. Further, the long-term stability of those PHU-based SPEs with lithium metal has been confirmed from the exhaustive stripping and plating over 500+ cycles followed by post-mortem analysis, demonstrating constant overpotential. Full metal battery measurement is demonstrated for Li|PHU-N2N3-Ep|LFP cells for their preliminary trials. These investigations on poly(hydroxyurethane)-based polymers derived from bio-sourced monomers are shown to find their way into battery electrolytes credited to their unique properties.

Bibliography

1. Zeng, X.; Li, M.; Abd El-Hady, D.; Alshitari, W.; Al-Bogami, A. S.; Lu, J.; Amine, K., Commercialization of Lithium Battery Technologies for Electric Vehicles. *Advanced Energy Materials* **2019,** *9* (27), 1900161.
2. Boaretto, N.; Garbayo, I.; Valiyaveettil-SobhanRaj, S.; Quintela, A.; Li, C.; Casas-Cabanas, M.; Aguesse, F., Lithium solid-state batteries: State-of-the-art and challenges for materials, interfaces and processing. *Journal of Power Sources* **2021,** *502*, 229919.
3. Hassan, M. K.; Hameed, N.; Hossain, M. D.; Hasnat, M. R.; Douglas, G.; Pathirana, S.; Rahnamayiezekavat, P.; Saha, S. Fire Incidents, Trends, and Risk Mitigation Framework of Electrical Vehicle Cars in Australia *Fire* [Online], 2023.
4. Janek, J.; Zeier, W. G., Challenges in speeding up solid-state battery development. *Nature Energy* **2023,** *8* (3), 230-240.
5. Feng, J.; Wang, L.; Chen, Y.; Wang, P.; Zhang, H.; He, X., PEO based polymer-ceramic hybrid solid electrolytes: a review. *Nano Convergence* **2021,** *8* (1), 2.
6. Zhao, S.; Wu, Q.; Ma, W.; Yang, L., Polyethylene Oxide-Based Composites as Solid-State Polymer Electrolytes for Lithium Metal Batteries: A Mini Review. *Frontiers in Chemistry* **2020,** *8*.
7. Ouhib, F.; Meabe, L.; Mahmoud, A.; Grignard, B.; Thomassin, J.-M.; Boschini, F.; Zhu, H.; Forsyth, M.; Mecerreyes, D.; Detrembleur, C., Influence of the Cyclic versus Linear Carbonate Segments in the Properties and Performance of CO2-Sourced Polymer Electrolytes for Lithium Batteries. *ACS Applied Polymer Materials* **2020,** *2* (2), 922-931.
8. Raj, A.; Panchireddy, S.; Grignard, B.; Detrembleur, C.; Gohy, J.-F., Bio-Based Solid Electrolytes Bearing Cyclic Carbonates for Solid-State Lithium Metal Batteries. *ChemSusChem* **2022,** *15* (18), e202200913.
9. Zhou, S.; Zhong, S.; Dong, Y.; Liu, Z.; Dong, L.; Yuan, B.; Xie, H.; Liu, Y.; Qiao, L.; Han, J.; He, W., Composition and Structure Design of Poly(vinylidene fluoride)-Based Solid Polymer Electrolytes for Lithium Batteries. *Advanced Functional Materials* **2023,** *33* (20), 2214432.
10. Wu, Y.; Li, Y.; Wang, Y.; Liu, Q.; Chen, Q.; Chen, M., Advances and prospects of PVDF based polymer electrolytes. *Journal of Energy Chemistry* **2022,** *64*, 62-84.
11. Pal, P.; Ghosh, A., Investigation of ionic conductivity and relaxation in plasticized PMMA-LiClO4 solid polymer electrolytes. *Solid State Ionics* **2018,** *319*, 117-124.
12. Kurapati, S.; Gunturi, S. S.; Nadella, K. J.; Erothu, H., Novel solid polymer electrolyte based on PMMA:CH3COOLi effect of salt concentration on optical and conductivity studies. *Polymer Bulletin* **2019,** *76* (10), 5463-5481.
13. Wang, Q.; Zhang, H.; Cui, Z.; Zhou, Q.; Shangguan, X.; Tian, S.; Zhou, X.; Cui, G., Siloxane-based polymer electrolytes for solid-state lithium batteries. *Energy Storage Materials* **2019,** *23*, 466-490.
14. Zhang, Q.; Liu, K.; Ding, F.; Liu, X., Recent advances in solid polymer electrolytes for lithium batteries. *Nano Research* **2017,** *10* (12), 4139-4174.
15. Misenan, M. S. M.; Khiar, A. S. A.; Eren, T., Polyurethane-based polymer electrolyte for lithium ion batteries: a review. *Polymer International* **2022,** *71* (7), 751-769.
16. Lv, Z.; Tang, Y.; Dong, S.; Zhou, Q.; Cui, G., Polyurethane-based polymer electrolytes for lithium Batteries: Advances and perspectives. *Chemical Engineering Journal* **2022,** *430*, 132659.
17. Raj, A.; Grignard, B.; Detrembleur, C.; Gohy, J.-F., Poly(hydroxyurethane)s and Carbonates Bearing Bio-Based Solid Electrolyte for Solid-State Lithium Batteries. *ECS Meeting Abstracts* **2022,** *MA2022-02* (4), 493.
18. Yazie, N.; Worku, D.; Gabbiye, N.; Alemayehu, A.; Getahun, Z.; Dagnew, M., Development of polymer blend electrolytes for battery systems: recent progress, challenges, and future outlook. *Materials for Renewable and Sustainable Energy* **2023**.
19. Irfan, M.; Atif, M.; Yang, Z.; Zhang, W., Recent advances in high performance conducting solid polymer electrolytes for lithium-ion batteries. *Journal of Power Sources* **2021,** *486*, 229378.
20. Wang, H.; Sheng, L.; Yasin, G.; Wang, L.; Xu, H.; He, X., Reviewing the current status and development of polymer electrolytes for solid-state lithium batteries. *Energy Storage Materials* **2020,** *33*, 188-215.
21. Park, K. H.; Bai, Q.; Kim, D. H.; Oh, D. Y.; Zhu, Y.; Mo, Y.; Jung, Y. S., Design Strategies, Practical Considerations, and New Solution Processes of Sulfide Solid Electrolytes for All-Solid-State Batteries. *Advanced Energy Materials* **2018,** *8* (18), 1800035.
22. Bekaert, L.; Raj, A.; Gohy, J.-F.; Hubin, A.; De Proft, F.; Mamme, M. H., Assessing the Long-Term Reactivity to Achieve Compatible Electrolyte–Electrode Interfaces for Solid-State Rechargeable Lithium Batteries Using First-Principles Calculations. *The Journal of Physical Chemistry C* **2022,** *126* (19), 8227-8237.
23. Balaish, M.; Gonzalez-Rosillo, J. C.; Kim, K. J.; Zhu, Y.; Hood, Z. D.; Rupp, J. L. M., Processing thin but robust electrolytes for solid-state batteries. *Nature Energy* **2021,** *6* (3), 227-239.
24. Bayer, O., Das Di-Isocyanat-Polyadditionsverfahren (Polyurethane). *Angewandte Chemie* **1947,** *59* (9).
25. Watanabe, M.; Oohashi, S.; Sanui, K.; Ogata, N.; Kobayashi, T.; Ohtaki, Z., Morphology and ionic conductivity of polymer complexes formed by segmented polyether poly(urethane urea) and lithium perchlorate. *Macromolecules* **1985,** *18* (10), 1945-1950.
26. Porcarelli, L.; Manojkumar, K.; Sardon, H.; Llorente, O.; Shaplov, A. S.; Vijayakrishna, K.; Gerbaldi, C.; Mecerreyes, D., Single Ion Conducting Polymer Electrolytes Based On Versatile Polyurethanes. *Electrochimica Acta* **2017,** *241*, 526-534.
27. Zhu, W.; Yang, B.; Wang, X.; Wang, L.; Tang, X.; Yang, C., Structure and ionic conductive properties of polydioxolane–polyurethane-based electrolytes. *Journal of Applied Polymer Science* **2002,** *83* (1), 103-111.
28. Mustapa, S. R.; Aung, M. M.; Rayung, M. Physico-Chemical, Thermal, and Electrochemical Analysis of Solid Polymer Electrolyte from Vegetable Oil-Based Polyurethane *Polymers* [Online], 2021.

29. Su'ait, M. S.; Ahmad, A.; Badri, K. H.; Mohamed, N. S.; Rahman, M. Y. A.; Ricardo, C. L. A.; Scardi, P., The potential of polyurethane bio-based solid polymer electrolyte for photoelectrochemical cell application. *International Journal of Hydrogen Energy* **2014,** *39* (6), 3005-3017.
30. Pathak, R.; Kathalewar, M.; Wazarkar, K.; Sabnis, A., Non-isocyanate polyurethane (NIPU) from tris-2-hydroxy ethyl isocyanurate modified fatty acid for coating applications. *Progress in Organic Coatings* **2015,** *89*, 160-169.
31. Maisonneuve, L.; Lamarzelle, O.; Rix, E.; Grau, E.; Cramail, H., Isocyanate-Free Routes to Polyurethanes and Poly(hydroxyurethane)s. *Chemical Reviews* **2015,** *115* (22), 12407-12439.
32. van Velthoven, J. L. J.; Gootjes, L.; van Es, D. S.; Noordover, B. A. J.; Meuldijk, J., Poly(hydroxyurethane)s based on renewable diglycerol dicarbonate. *European Polymer Journal* **2015,** *70*, 125-135.
33. Tillmann, S. D.; Isken, P.; Lex-Balducci, A., Gel polymer electrolyte for lithium-ion batteries comprising cyclic carbonate moieties. *Journal of Power Sources* **2014,** *271*, 239-244.
34. Panchireddy, S.; Grignard, B.; Thomassin, J.-M.; Jerome, C.; Detrembleur, C., Bio-based poly(hydroxyurethane) glues for metal substrates. *Polymer Chemistry* **2018,** *9* (19), 2650-2659.
35. Cornille, A.; Auvergne, R.; Figovsky, O.; Boutevin, B.; Caillol, S., A perspective approach to sustainable routes for non-isocyanate polyurethanes. *European Polymer Journal* **2017,** *87*, 535-552.
36. Parliament, E., MEPs ban cadmium from power tool batteries and mercury from button cells. 2013.
37. Karan, N. K.; Pradhan, D. K.; Thomas, R.; Natesan, B.; Katiyar, R. S., Solid polymer electrolytes based on polyethylene oxide and lithium trifluoro- methane sulfonate (PEO–LiCF3SO3): Ionic conductivity and dielectric relaxation. *Solid State Ionics* **2008,** *179* (19), 689-696.
38. M.A. Ratner, i. J. R. M., C.A. Vincent Eds, In *Polymer Electrolyte Reviews 1*, Elsevier: Londen, 1987.

Supporting Information

Non-isocyanate poly(hydroxyurethane)-based networks

Table S6.2.1: Conductivity and physical nature relation of PHU with combination of different crosslinkers (ratio indicates mole %).

Ring opened CSBO (15% LiTFSI): diamine	**N3**	**N3-N1 (3:1)**	**N3-N1 (1:1)**	**N3-N1 (1:3)**	**N3-N2 (3:1)**	**N3-N2 (1:1)**	**N3-N2 (1:3)**	**N3-N1-N2 (2:1:1)**
Conductivity	+++++++	++++++	++++++	+++++	++++++	++++++	+++++	++++
Physical nature	Gel like solid (++++)	Gel like solid (+++)	Gel like solid (++)	Solid	Gel like solid (++++)	Gel like solid (+++)	Solid Film	Gel like solid (++)

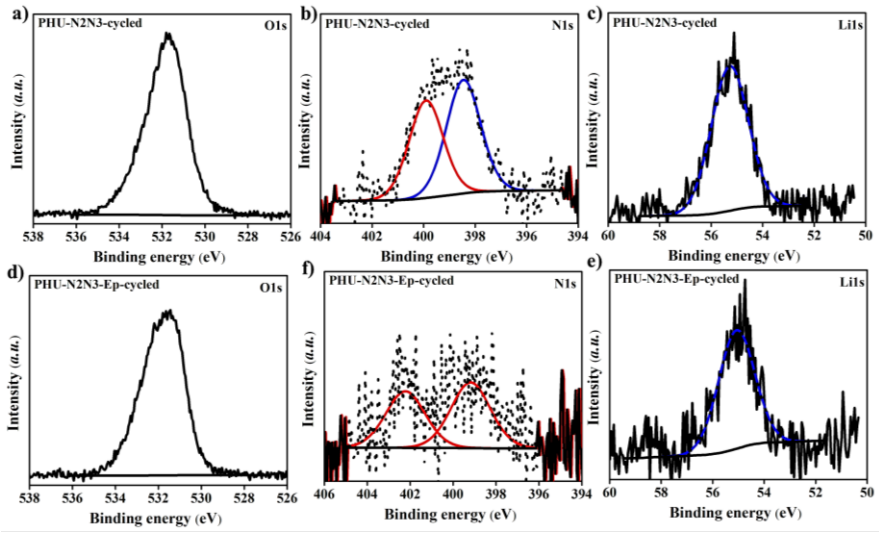

Figure S6.2.2: HR-XPS of a) and d) Oxygen (O1s), b) and e) Nitrogen (N1s), c) and f) Lithium (L1s), at the surface cycled PHU-based SPE films after stripping and plating with Li-Li cells, respectively.

Chapter 7 Composite polymer electrolytes based on silicon dioxide nanoparticles

Abstract

In the coming years, the batteries market size is expected to grow by two-fold with the ongoing development of solid-state electrolyte-based lithium batteries. Following that, composite polymer electrolytes (CPEs) are believed to make lithium metal batteries safer, more efficient, and high-performing by combining organic and inorganic materials. Over the decades, various classes of polymers containing high electronegative atoms have been looked upon for their weak lithium coordination and high lithium ions transport in combination with active and inactive fillers. Within that, bio-sourced polymers are one of the attractive research topics. Poly(hydroxyurethane)s (PHUs) synthesized through a non-isocyanate approach are known for their superior adhesive properties and have been recently explored as solid polymer electrolytes (SPEs) in batteries due to high control over their structural design. Here, we report two types of composite polymer electrolytes. The first CPE is a blend comprising lithium salt loaded poly(ethylene oxide) (PEO) as polymer matrix, bio-based carbonated soybean oil (CSBO) as additive and silicon dioxide nanoparticles as dispersed inorganic material. The second CPE is a lithium salt loaded PHU network prepared from CSBO precursor as polymer matrix entrapping SiO_2

nanoparticles. The synergic effect of the polymer component and SiO_2 facilitated the electrolyte films with good flexibility and high conductivity in the range of ~10^{-4} S cm^{-1} at 80 ºC. The addition of inorganic fillers to the SPEs broadened oxidative potential limitations to > 4.8 V and 4.4 V versus Li/Li^+ for CPEs based on linear PEO and PHU network polymers, respectively. Both CPEs demonstrated decent compatibility with lithium metal as a result of initial constant current and time-dependent charge-discharge, respectively. For instance, the PEO-CSBO-SiO_2-based LFP-Li cell delivered an interesting initial discharge capacity of ~140 mAh g^{-1} at 0.1C, 60 ºC. While PHU-SiO_2 exhibited stable striping and plating for 600+ cycles post stabilization. These composites highlight our consolidated successful attempts to exploit the introduction of passive fillers to the polymeric components for better electrochemical and mechanical properties.

7.1 Introduction

Energy storage complements renewable energy technology, such as solar, wind, and hydropower energy, due to its intermittent and undulating nature. Therefore, the clean energy transition stresses higher energy density and mass grid storage, such as batteries, for our primary needs. One sector that heavily relies on fossil fuels is mobility and transport, which needs to be revolutionized by the extensive switchover to electric vehicles. There comes the discussion of lithium batteries (LBs), which offer higher energy density than other conventional batteries, from small-scale to large-grid storage. In over two decades, LBs have dominated the battery market with higher projections and a surge in electric vehicles demand. However, safe and superior-performing batteries bet on the utilization of solid-state electrolytes with high-capacity electrodes owing to their lightweight, robust flexibility, easy stack and cost-effectiveness.[1,2] While conventional liquid electrolytes pose issues like leakage, decomposition and flammability.[3] One of the major reasons behind solid-state electrolyte push is the consolidated safe utilization of lithium metal for its high capacity (3860 mAh g^{-1}), energy density ~250 Wh Kg^{-1} and high oxidation potential limitations.[2,4] However, solid-state electrolytes present their challenges involving high electrolytic and interfacial resistance which limits its application in a wide range of operating temperature. To tackle those issues, several approaches are being carried out from strategical designing, processing of materials and interfacial understanding and engineering.[1,5] The working and failure mechanism analysis via theoretical and experimental tools has equally become relevant in lithium batteries due to their high complexities.

Over several years of research, it has been highly considered that CPEs proffers more potential prospects than a solid polymer electrolyte (SPE) and an inorganic solid electrolyte (ISE) alone. A hybrid CPE electrolyte combines the superior ionic conductivity, oxidation stability and lower thermal degradation with higher interfacial, mechanical and cost-effective merits of ISE and SPE, respectively.[6,7] The ionic conductivity in SPE is credited to ion hopping from one polar group to another, largely via oxygen coordination and polymer chain segmental motion in particular polymers above their glass transition temperature (T_g).[8,9] While in inorganic electrolytes, the ion transport mechanism is more complex than in SPE. Ion

conduction takes place via defects (from point defects to volume defects) such as Schottky and Frenkel defects involving vacancies and interstitial locations for hopping.[9-11] Based on the type of materials, different principles are applied and thus the mechanism of the pathway varies from the newly proposed paddle wheel to grain boundaries resistance. However, these conductivity pathways do not need to be considered with inorganic passive fillers as they don't contribute to conduction. Passive fillers, such as SiO_2**,** Al_2O_3, ZnO, TiO_2 *etc*., suppress the crystallinity and lower the T_g of the polymer. In addition, they induce Lewis acid-base interactions with lithium salts in the composites.[12,13] As a result, the salt dissociation is improved along with segmental motion and ion transport.[9]

There have been few reports on the CPEs based on silicon dioxide (SiO_2) showing potential outcomes. Nano-sized silicon dioxide particles due to their size, stability, sustainability and cost-effectiveness are a lucrative choice. Cai and co-workers reported poly(ethylene oxide) (PEO) Li salt based CPEs with SiO_2 particles embedded in ethylene carbonate (EC)/propylene carbonate (PC).[13] Particles with different nanostructures and morphology, like nanowires, 3D spheres and mesoporous structures have been investigated and show high compatibility with polymers demonstrating conductivity in the range of 10^{-4}~10^{-5} S cm^{-1} at room temperature (RT).[14-16] Among other approaches, functionalization of SiO_2 nanoparticles is also explored as a smart method to develop beneficial homogeneous interaction between nanoparticles and polymer functional groups. A cross-linked composite gel polymer electrolyte was prepared with mesoporous SiO_2 nanoparticles containing reactive methacrylate groups as cross-linking sites and dispersed into a fibrous polyacrylonitrile membrane.[17] Most of these investigations are largely based on PEO or similar functional polymers. While there are very few reports on passive fillers incorporated into polyurethanes/poly(hydroxyurethane)s (PUs/PHUs), which are looked upon as potential polymer electrolytes owing to their functional groups exhibiting a dual nature of conductivity and mechanical properties. As a typical example, Zhang *et al.*[18] presented a CPE by combining linear PU and $Li_{0.35}La_{0.55}TiO_3$ (LLTO) which exhibited a high conductivity of 3.8 x 10^{-4} S cm^{-1} at ambient temperature.

In the pursuit of sustainable hybrid electrolytes, we investigate here the effect of an inexpensive passive filler, SiO_2, embedded into PEO blended with carbonated soy bean oil (CSBO) and into a PHU network originated from CSBO in extension to our work discussed in previous chapter. We intend to demonstrate the synergetic effect of passive filler interaction with the cyclic carbonates (CCs) rings of CSBO and PHU in terms of conductivity and other characteristic properties. Several formulations have been analyzed with SiO_2 filler and LiTFSI for an optimum CPE compatible with lithium metal.

7.2 Materials and methods

4,7,10-Trioxa-1,13-tridecanediamine (TTD) (Mw ~ 220.31), silicon dioxide (SiO_2, ~10-20 nm), anhydrous tetrahydrofuran and lithium battery-grade, lithium bis(trifluoromethanesulfonyl)imide (LiTFSI) are purchased from Sigma-Aldrich. Poly(ethylene glycol) bis(3-aminopropyl) terminated (PEGTA) (Mw ~1500) was bought from Acros organic chemical. Carbonated soybean oil (CSBO) was prepared as highlighted in a previous report.[19] Lithium metal foil (99.9%), lithium iron phosphate ($LiFePO_4$), poly(vinylidene fluoride) and super-P carbon were purchased from TOB chemicals. N-methyl-2-pyrrolidone (NMP) was purchased was bought from Alfa Aesar. Deuterated chloroform ($CDCl_3$) used for NMR spectroscopy was purchased from Eurisotop. All reactants and catalysts were used as received, without any further purification.

Note: Refer the Chapter 5.1 for characterization and electrochemical techniques.

7.3 Experimental section

7.3.1 Synthesis of CSBO-PEO-SiO_2

Bio-based cyclic carbonated soybean oil (CSBO) was synthesised by coupling of supercritical CO_2 with epoxidised soybean oil (ESBO) as reported somewhere.[19] CSBO-PEO-SiO_2 was prepared by mixing CSBO (50 wt%), PEO (50 wt%), and SiO_2 (x wt% with respect to CSBO+PEO/CPE) in various formulations in a vial using acetonitrile solvent. The mixture was stirred for > 6 h and then drop cast on a Teflon mold and later transferred to the vacuum oven. It was maintained at 70 ^oC for ≥ 24 h in a dynamic vacuum and stored in a glove box. The CSBO-PEO-SiO_2 CPE was

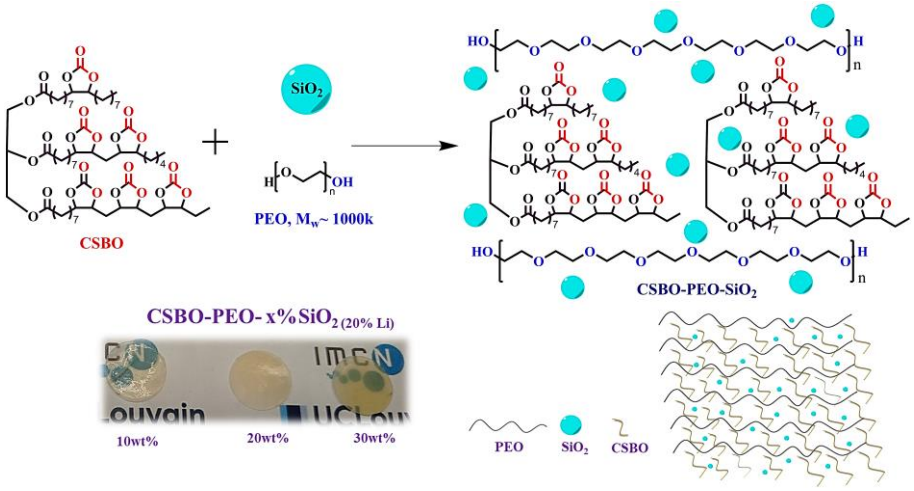

Scheme 7.1: Preparation of blends of CSBO, PEO and SiO_2 (top), Illustration of linear PEO chains hosting CSBO and SiO_2 nanoparticles (bottom-right: LiTFSI is not shown in the structure for the sake of clarity, and bottom-left: picture of 20wt% LiTFSI loaded CPE films with SiO_2 varying from 10wt% to

prepared following a similar procedure with LiTFSI (by wt% with respect to CBSO-PEO) added to the mixture prior to solvent evaporation.

7.3.2 Synthesis of poly(hydroxyurethane) SiO_2 composite (PHU-N2N3-SiO_2)

For PHU-N2N3, a ring-opening reaction between CSBO and bis(3-aminopropyl) terminated poly(ethylene glycol) (PEGTA) and 4,7,10-trioxa-1,13-tridecanediamine (TDD) was conducted in varied ratio with and without SiO_2 (wt/wt% to all monomer). The ratio of TDD (N2) + PEGTA (N3) to CSBO was chosen to be 3:1 mol/mol in tetrahydrofuran solvent corresponding to 6 cyclic carbonate rings. 90 mg of CSBO (M_n ~ 1250), 81 mg of PEGTA (for 25 mol%, M_n ~ 1500) and 35.69 mg of TDD (75 mol%, M_n ~ 220.31) were taken in a small vial with and without SiO_2 (5 to 20 wt% with respect to total monomer wt%). These were dissolved with anhydrous THF via magnetic stirring at RT for > 6 h. The resulting transparent solution was then drop cast on a Teflon mold followed by transfer to the vacuum oven. The temperature of the vacuum oven was set at 70 ^oC for >12h and later increased to 90 ^oC for > 24h with

dynamic vacuum mode. A similar procedure was followed for PHU N2N3-SiO_2 CPE with LITFSI (wt% with respect to PHU-N2N3) solution added to the initial mixture.

7.3.3 Preparation of composite polymer electrolytes films (CPEs)

As indicated above, LiTFSI was added to the mixture prior to blending and curing. The obtained CPE films were peeled off the Teflon molds and stored in the glove box prior to test and characterizations. The thickness of the membrane was recorded to be in the range of 50-250 µm for CBSO-PEO-SiO_2 and 100-200 µm for PHU-N2N3-SiO_2, respectively. 2032-type coin cells were assembled using those 16 mm punched films sandwiched between SS|SS, SS|Li, Al-C|Li, Li|Li and Li|LFP electrode configurations to evaluate electrochemical properties.

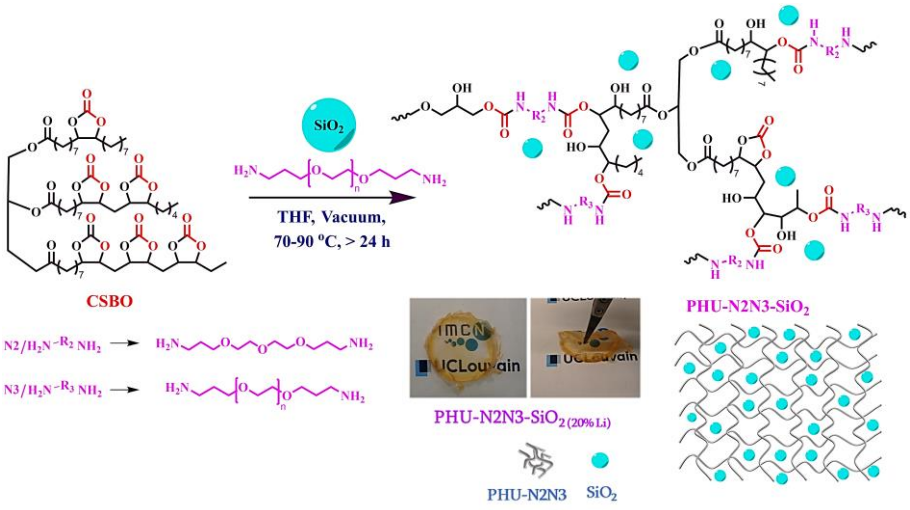

Scheme 7.1: Reaction pathway of PHU-N2N3 formation (75 mol% of N2 and 25% mol %) with SiO_2 nanoparticles (LiTFSI is not shown in the structure for the sake of clarity) along with an illustration of CPE network and transparent film with 20 wt% of SiO_2 and 20 wt% of LiTFSI, as shown in the picture.

7.4 Results and discussion

The challenge of improving the properties of SPEs by combining polymers and inorganic fillers seems easier than reality due to various constraints including, intermolecular interactions and granular boundary interfaces. One of the key issues faced among the CPEs is the inhomogeneous distribution of the inorganic particles.

This is usually tackled by processing the sample using an extruder, blender, *etc*. However, the types of polymers, fillers, and salts, along with their concentration and preparation method, play an equally important role. Here, we screen out two different types of polymers, yet related, further incorporated in CPEs based on the same SiO_2 nanoparticles as passive fillers. The first strategy relies on the preparation of CSBO-PEO-SiO_2-LiTFSI blends by a solvent casting method as shown in Scheme 7.1. This scheme demonstrates the blending of CSBO, SiO_2, LiTFSI and PEO with speculation of the former three entities entrapped within the linear chains of PEO constituting the polymer matrix The pictures in Scheme 7.1 indicated that with higher loading of SiO_2 (wt%), the CPE films became less transparent and adhesive to the surface (adhesion is contributed by the viscous nature of CSBO).

In the second approach, we assimilated the SiO_2 filler into a PHU-N2N3 network resulting from the ring-opening reaction of CSBO with a PEO terminated at both ends with amino groups as depicted in Scheme 7.2. The loading of passive filler was not attempted beyond 20wt% due to dissolution constraint and macroscopically observed particle aggregation. The pictures in Scheme 7.2 show the free-standing flexible CPE film.From a chemical point of view, both approaches are leading to CPEs with rather similar functional groups, i.e. the same SiO_2 passive fillers, LiTFSI salt, PEO segments, and CC rings from CSBO. The main difference is that some of the CC rings of CSBO have been transformed in hydroxyurethane groups to form the crosslinking nodes of the PHU network in the second approach. However, from a topological point of view, the situation is quite different for both systems, i.e. a simple blend based on a linear polymer in the first approach and a polymer network in the second one. The aim of this contribution is to elucidate what is the best approach (simple blends or PHU networks) to obtain CPEs with optimum performance for application in lithium battery, all other parameters being kept almost constant.

7.4.1 Fourier transform infra-red spectroscopy

CPEs with and without LiTFSI were subjected to FTIR spectroscopy for structural analysis. To our assumption, the cyclic carbonate (CC) rings of CSBO did not react with the hydroxyl end-group of PEO, as evidence from the signal at ~1798 cm^{-1} for the carbonyl of CC. While the ester (-RCOOR-) signal was retained at ~ 1740 cm^{-1}

with almost no shift in both CSBO-PEO and CSBO-PEO-SiO_2 as shown in Figure 7.1a. The contribution from C-O stretching and Si-O-Si unit peaks are detected in the composite samples with PEO and SiO_2 in the range of 1050-1100 cm^{-1}. Other characteristic peaks from PEO in the region of 1000-800 cm^{-1} have also been observed in the composite polymers in addition to a peak at ~462 cm^{-1} for -O-Si in composite samples. In Figure 7.1b, we have presented the comparative IR of CPEs with increasing concentration of SiO_2 in the presence of LiTFSI. With SiO_2 (wt%) increment, the intensity of both carbonyl peak from CC ring and ester decreased while Si-O signals (around 1180 cm^{-1} and 462 cm^{-1}) increased in 10wt% to 30wt% SiO_2 loaded CPEs. The SO_2 asymmetric stretching was also observed at 1182 cm^{-1} confirming LiTFSI in all three samples.[20,21] For the FT-IR analysis of PHU-N2N3 CPEs, we observed almost the disappearance of the signal at 1796 cm^{-1} corresponding to CCs from CSBO and the appearance of urethane characteristic peaks around 1695-1697 cm^{-1} and 1712-1716 cm^{-1} (Figure 7.1c). However, the weak peak at 1800 cm^{-1} highlights the presence of a few unreacted CCs from CSBO in the PHU-N2N3 CPEs.

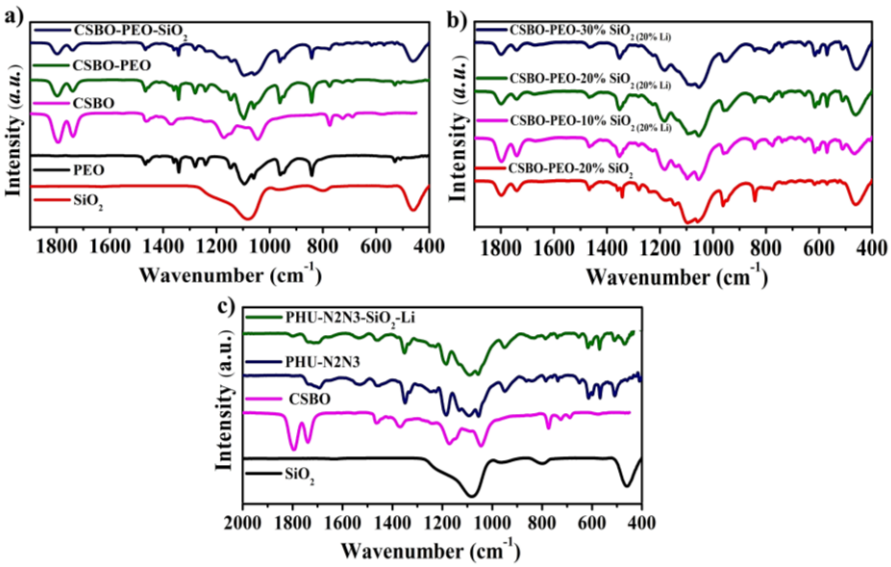

Figure 7.1: Comparative IR spectra of CPEs a) CSBO-PEO-Si-O_2 in relative to blend with filler and monomers; b) CSBO-PEO-x%SiO_2 with and without LiTFSI, respectively; and c) IR of PHU-N2N3 with and without SiO_2 (PHU-N2N3-SiO_2-Li, where 75 mol% of N2 and 25 mol% of N3, 20wt% SiO_2 and 20 wt% LiTFSI throughout correspondingly).

Indeed, the Lewis acid-base interaction of CC and SiO_2 might offer steric hindrance for aminolysis with PEGTA resulting in incomplete ring opening. The ester peak (-RCOOR-) was observed in all samples around 1738 cm^{-1}. The remaining characteristic signals from PHU-N2N3 and its composite with SiO_2 resembled more or less, such as –N-H and C-N stretching around 1534-1535 cm^{-1} and 1250-1275 cm^{-1}, respectively. The characteristic signal of -Si-O peak is measured around ~467 cm^{-1} in the composite, while the Si-O-Si signal supposed to be around 1100 cm^{-1} could not be separated from the organic functional groups overlap. The dissolution of LiTFSI salt was assured by the observation of the SO_2 asymmetric stretching at ~1180 cm^{-1}.

7.4.2 Thermal measurements

Differential scanning calorimetry has been performed to measure the glass transition (T_g), melting temperature (T_m) and crystallization temperature (T_c) of the investigated polymers and composites. Without added LiTFSI, T_g could not be detected while T_m was measured at 62.8 °C, 62.7 °C and 59.4 °C for PEO, CSBO-PEO and CSBO-PEO-SiO_2, respectively (Figure 7.2a). Addition of LiTFSI resulted in a decrease in T_m for the composite samples (compare CSBO-PEO-20%SiO_2 with or without LiTFSI in Figure 7.2a) while a further decrease in T_m was witnessed with increasing the loading in SiO_2 for the same concentration of LiTFSI. Indeed, the CPEs with LITFSI show a decline in T_m to 48.9 °C, 43.7 °C and 38.5 °C from 10wt% to 30wt% of SiO_2 as shown in Figure 7.2a. To our assumption, the addition of SiO_2 and LiTFSI decreased the crystallinity of PEO chains in the composite as expected. The T_g for these CPEs was marked at -49.2 °C, -46.3 °C and -44.8 °C in order of decreasing SiO_2 content for a constant 20wt% LiTFSI. Cold crystallization was also observed in all three samples with LiTFSI around 20 °C between T_g and T_m possibly due to rearrangements in the chains.

For the PHU network-based CPEs, thermal behaviour largely depends on the extent of crosslinking. The precursor PEGTA and SiO_2 possess crystalline nature. The sharp T_m and T_c of PEGTA were recorded at 50.07 °C and 20.06 °C, respectively as indicated in Figure 7.2b. PHU-N2N3 exhibited melting transition temperature of 29.7 °C with T_g at -48.8 °C without LiTFSI as highlighted in Chapter 6.2. While with LiTFSI and SiO_2, amorphous behaviour was recorded in the range of -70 to 100 °C for PHU-N2N3

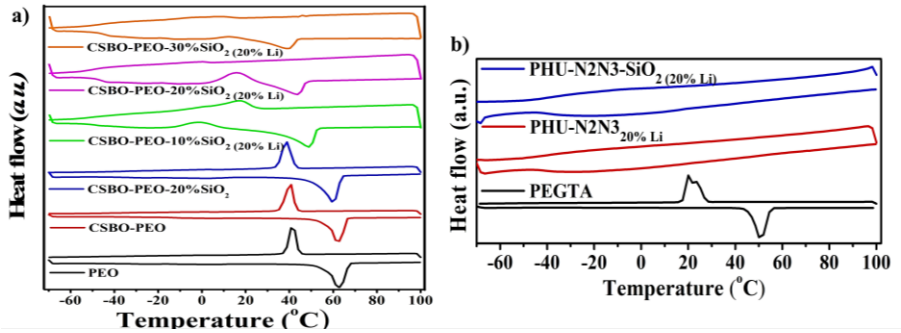

Figure 7.2: DSC thermograms a) CSBO-PEO-x%SiO_2 (with and without LiTFSI labelled as in subscript) with CBSO-PEO and PEO, respectively; and b) PHU-N2N3 (where, 75 mol% of N2 and 25 mol% of N3)) loaded with LiTFSI with and without 20% SiO_2 in comparison to PEGTA.

and PHU-N2N3-SiO_2. Moving on to the T_g, not much shift was measured on the addition of filler i.e. -40.7 °C and -40.2 °C for PHU-N2N3 CPEs with and without SiO_2, respectively. Further measurements and analysis can throw more light on the effect of fillers on T_g.

TGA analysis in the temperature range of 30 °C to 600 °C was performed to analyse the degradation of polymers and verify the experimental weight% of filler. The TGA spectra have been shown in Figure 7.3a for composites with and without LITFSI in relative to PEO and CSBO-PEO. The minor loss in weight around 100 °C can be credited to the absorbed moisture in respective samples. In the case of PEO and CSBO-PEO, one minor degradation occurs at ~246 °C. While the major degradation starts at appx. 310 °C and occurs maximum at ~ 420 °C for CSBO-PEO and CSBO-PEO-SiO_2, at ~426 °C for CSBO-PEO-$SiO_2$with LiTFSI. The LiTFSI-loaded CPEs demonstrated higher stability with degradation ranging in region 450 °C, while no other phase degradation was observed in CPEs without salt. Total weight loss up to 80% confirmed the ~20% of SiO_2 in the composite for CPE with and without LiTFSI. Globally, the thermal stability of the composites mimicked the PEO and CSBO-PEO samples and offered a high degree of operating temperature.

PHU networks in TGA undergo multiple-phase degradations due to their various functional groups, as shown in Figure 7.3b. Prior to major decomposition starting at 362 °C and maximum at ~395 °C, it witnessed phase degradation at ~340 °C, starting

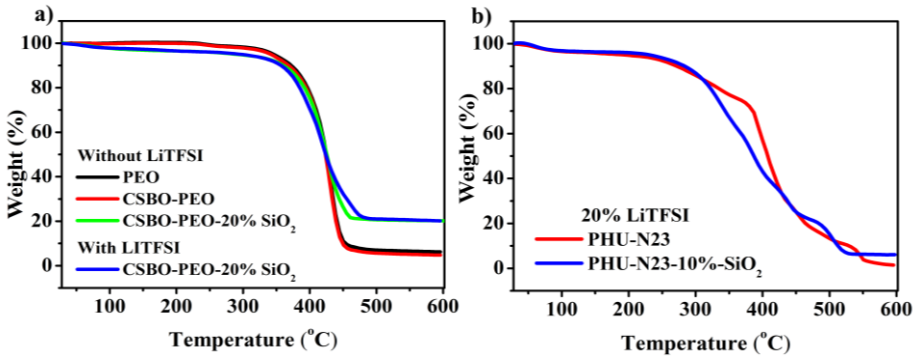

Figure 7.3: Thermogravimetric analysis of a) CSBO-PEO-SiO_2 compared to PEO and CSBO-PEO; and b) PHU-N2N3-SiO_2 (75 mol% of N2, 25 mol% of N3 and 10 wt% of SiO_2) with and without 20wt% LiTFSI throughout, respectively.

from ~220 °C for PHU-N2N3. While for PHU-N2N3-SiO_2, major phase degradation was observed below 400 °C, i.e. starting at ~246 °C with maximum at ~388 °C. The degradation of salt could be attributed to 450 °C onwards. However, at ~ 600 °C, measured weight (< 10%) could be assigned largely to SiO_2 from the CPEs. From this preliminary investigation, it can be deduced that the addition of SiO_2 fillers improved the thermal stability of certain functional groups.

7.4.3 Ionic conductivity

Cells assembled with CPE films in coin cells setup were subjected to potentiostatic electrical impedance spectroscopy (PEIS) for conductivity measurements at various temperatures in symmetric blocking cells with stainless steel electrodes. The conductivity (σ) was obtained by using bulk electrolyte resistance from the Nyquist plots by employing a conductivity equation involving the area and thickness of the films. Figure 7.4a shows the Arrhenius plot for temperature-dependent conductivity for the CSBO-PEO CPEs with 20wt% LiTFSI and variable SiO_2 loading. As depicted, the conductivity ranged in the order of ~10^{-6} to ~10^{-4} S cm^{-1} within 20-80 °C. The highest conductivity was recorded for the CPE with 10wt% SiO_2 i.e. 7.68 x 10^{-6} S cm^{-1} and 3.98 x 10^{-4} S cm^{-1} in comparison to 3.29 x 10^{-6} S cm^{-1} and 2.59 x 10^{-4} S cm^{-1} for pristine CSBO-PEO at 20 °C and 80 °C, respectively. The macroscopic appearance of both electrolyte films with 10wt% and 0% SiO_2 appeared the same, favouring higher wettability and softness compared to CPEs with > 10wt% SiO_2. For 20wt% filler, the

film demonstrated non-sticky and better handling while at 30wt%, the CPE appeared to possess cracks at RT. Therefore, the correlation between the conductivity with 30wt% SiO_2 is a little questionable and unreliable. However, a general trend in increasing conductivity was observed with decreasing SiO_2 loading and softness. The VFT behaviour within CPE has been investigated by considering glass transition temperature as depicted in supporting information, Figure S7.1.

The conductivities of pristine PHU-N2N3 and the related composite both loaded with 20 wt% LiTFSI were investigated at various temperatures. On employing the Arrhenius model for variable conductivity, it depicted higher conductivity of 7.01 x 10^{-7} S cm^{-1} for 20wt% SiO_2 against 4.5 x 10^{-7} S cm^{-1} for PHU-N2N3 at 20 ^oC (Figure 7.4b). However, a linear increase in conductivity could be recorded for both electrolytes with a similar slope. At 60 ^oC, the CPE with 20wt% SiO_2 delivered the conductivity of 2.13 x 10^{-5} S cm^{-1} while only 9.54 x 10^{-6} (~ 10^{-5}) S cm^{-1} were measured for the corresponding PHU-N2N3. The reason for superior conductivity in the presence of SiO_2 filler can be credited to decreased crystallinity and increased amorphous phase in the network. It can also be recalled that the PHU composite comprises unreacted CC rings, boasting Lewis acid-base interactions within the polymer network and filler particles. That can also explain the slight improvement in the conductivity due filler addition to the network.

7.4.4 Electrochemical stability window

The oxidation potential limit was investigated by LSV analysis at a slow scan rate of 0.5 mV/s. We calculated a wide electrochemical stability window > 4.8 V versus Li/Li^+ for the CSBO-PEO-SiO_2 CPE with an aluminium cathode and lithium anode as shown in Figure 7.4c. The lower decomposition of the electrolyte is credited to the addition of CSBO and SiO_2. Similar findings have been reported when CSBO was introduced alone in PEO and with terminal end group modification as discussed in Chapter 5.2.

Similarly, a broad oxidation potential limit is achieved for the filler incorporated PHU network i.e. ESW of > 4.41 V versus Li/Li^+ (Figure 7.4d) contrary to > 4.01 V for PHU without filler at 60 ^oC (as demonstrated in Chapter 6.2). Despite the structural differences, the presence of filler reduced the electrolyte reactivity possibly due to the

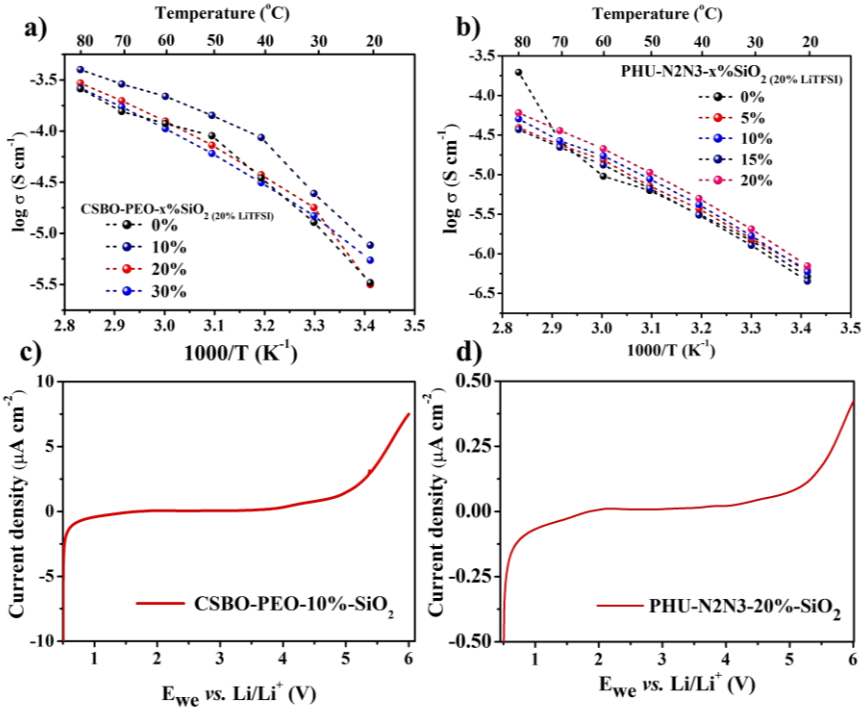

Figure 7.4: a) Temperature dependent ionic conductivity for CPEs, a) 0-30 wt% of SiO_2 (labelled as x) in CSBO-PEO-SiO_2; and b) 0-20 wt% of SiO_2 in PHU-N2N3-SiO_2; Linear sweep voltammetry, c) CSBO-PEO with 10 wt%-SiO_2; and d) PHU-N2N3 (where, 75 mol% of N2 and 25 mol% of N3) with 10 wt%-SiO_2 at 60 °C loaded with 20 wt% LiTFSI, respectively for all measurements above.

acid-base interactions between the filler and functional groups of the polymer chains which are normally reactive to lithium metal. As a result, the SiO_2 loaded PHU electrolytes can proffer good compatibility with high-voltage cathode operation, given good conductivity and other parameters involving a stable interface.

7.4.5 Stripping and plating

The exhaustive time-dependent charge-discharge with a symmetric lithium cell was performed for more than 600+ cycles (1200 h+) with the PHU-N2N3-SiO_2 CPE. The voltage profile with time has been depicted in Figure 7.5 to highlight the kinetic hindrances, polarization, and resistance of the CPE during lithium transport. With cut-off potential of ± 2 V for the first 45 cycles, the cell was run at the current density of 0.84 μA cm^{-2}. It recorded the overpotential of ~85 mV and ~124 mV at the 1st cycle

and 45th cycle, respectively. Subsequently, a drastic increment from ~376 mV was witnessed from the 46th cycle onwards, reaching to a cut-off voltage of +2 V at the 75th cycle. Thereafter, stabilization in output voltage was observed which decreased from ~410 mV (at ~76th) to ~200 mV (at ~500th cycle). This improvement in the mobility of lithium ions could be credited to the favourable morphology change and beneficial decomposition of the electrolyte over long cycling. The inset in the plot indicates the corresponding evolution in the potential for the first 5 cycles, the 95th to100th and 500th to 505th cycles, respectively, without much change in the plateau of stripping and plating. To understand the decomposition at the surface, XPS analysis has been performed on the electrode and electrolyte surface post-cycling as highlighted in a further section. It can be speculated that, with higher conductivity, the PHU-N2N3-SiO_2 can prove to be an interesting candidate for full lithium-metal batteries. Similar analysis for CSBO-PEO-SiO_2 based CPE has been undergoing.

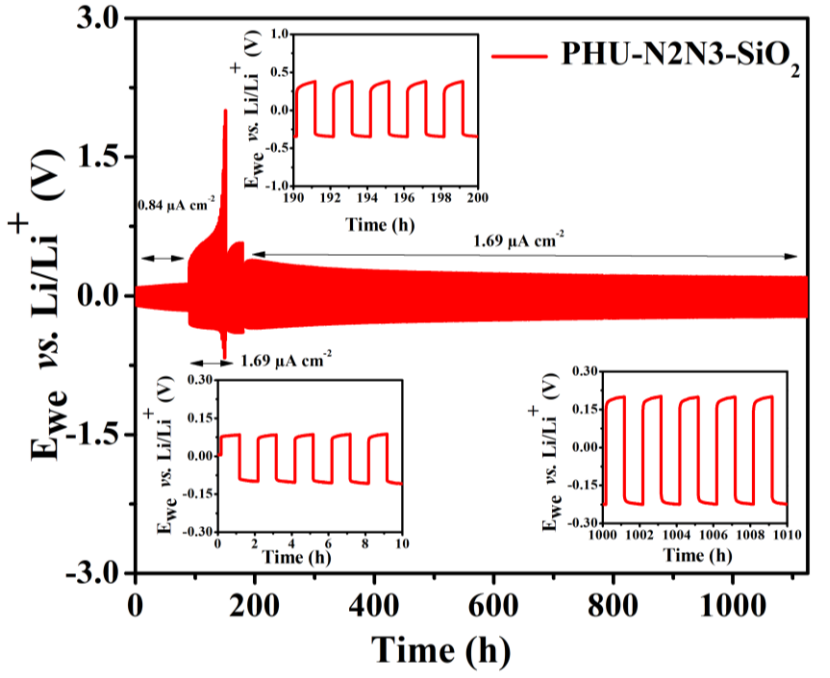

Figure 7.5: Galvanostatic charge-discharge voltage profile for stripping-plating at various current densities at 60 ºC with Li|PHU-N2N3-SiO_2-CPE|Li symmetric cells with magnified plots at respective time demonstrating the constant over potential in the inset.

However, due to higher conductivity of later, cycling measurements have been performed with LFP-Li cells as described in subsequent section.

7.4.6 Li-metal battery prototypes

The battery prototypes based on Li-$LiFePO_4$ electrodes and CSBO-PEO-SiO_2-CPE were subjected to constant current cycling using the GCPL technique in the range of 2-4 V at 60 ºC. At 0.1C, the cell delivered the discharge capacity of ~140 mAh g^{-1} with ~56 mV of polarization recorded in the 5th cycle, as shown in Figure 7.6a. On further cycling, the capacity fading was observed to approximately, 104 mAh g^{-1}, 68 mAh g^{-1} and 52 mAh g^{-1} with polarization of 77 mV, 105 mV, 126 mV in respective 55th, 200th and 300th cycles. The same cell was cycled with a variable current rate (C-rate) before to long-term cycling at 0.1C. As a result, huge polarization was observed, i.e. from ~47 mV to ~358 mV (along 0.1C to 2C) in subsequent charge-discharge with recorded discharge capacity of around 146 mAh g^{-1}, 120 mAh g^{-1}, 65 mAh g^{-1},

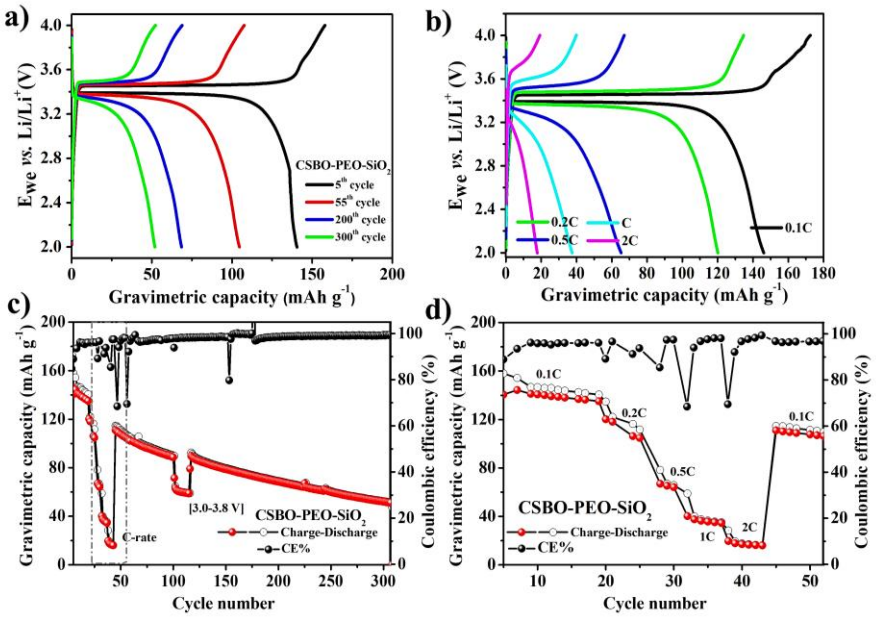

Figure 7.6: Galvanostatic charge-discharge voltage profiles, a) Gravimetric capacity at 0.1C for respective cycles; b) Gravimetric capacity at variable current densities; c) Global capacity retention plot with cycle number; and d) rate capability plot for Li|CSBO-PEO-10 wt% SiO_2-CPE|LFP at 60 ºC, respectively.

37 mAh g^{-1}, and 18 mAh g^{-1} at 0.1C, 0.2C, 0.5C, 1C and 2C, respectively as highlighted in Figure 7.6b. Upon further cycling at 0.1C, the cell undergoes huge capacity loss as observed in Figure 7.6c. This could be due to sluggish kinetics of Li-ion mobility at higher current density-led decomposition. Focusing on the rate capability, there was a clear loss in capacity and regain at 0.1C with not-so-promising Coulombic efficiency as observed in Figure 7.6d. However, the electrochemical performance can be improved with further optimizations, an understanding of the interface, and electrolyte-electrode compatibility aligned with battery measurements. The post-mortem analysis on the Li-anode surface has been presented in the following sections to analyst the decomposed species as a result of long cycling.

7.4.7 Post-mortem XPS analysis

In an attempt to analyse the SEI and other interfacial decomposition, post-mortem analysis has been conducted on the cycled cell from Li-CPE-LFP and Li-CPE-Li for CSBO-PEO-SiO_2 and PHU-SiO_2 CPEs with 10 wt% and 20 wt% of SiO_2, respectively. The surface element characterisation via XPS on the Li-anode from Li-LFP cell cycled for more than 300+ cycles at 60 ^oC was made with survey spectra provided in supporting information, Figure S7.2a and HR-XPS spectra depicted in Figure 7.7. The C 1s peak at 284.8 eV was used as a reference to calibrate the binding energy. In respective HR-XPS of C1s represented in Figure 7.7a, we found only three distinct contributions, C-C/C-H, a broad signal from O-C-O/C=O and lithium carbonate and M-C_x corresponding to ~284.8 eV, ~287.8 eV and ~283 eV, respectively. The exhaustive cycling for more than 300+ cycles at variable current density might led to the formation of lithium carbide in traces at anode interface.

While, SEI containing lithium species has been confirmed by the decomposition of Li 1s spectra, highlighting the formation of Li_2CO_3, LiOH, Li_2O and Li at the binding energies (B.E.) of 55.1 eV, 54.4 eV, 53.7 eV and 52.9 eV, respectively (Figure 7.7b). As a result of the decomposition of LiTFSI (Figure 7.7c), the LIF signal has been obtained at 685.1 eV while the -CF_3 signal is recorded at 688.5 eV. This has been further evidenced from HR-XPS of S2p with LITFSI species featuring -CF_3-SO_4, SO_3^{-2}, SO_x and Li_xS_y at 168.5 eV, 166.4 eV, 162.8 eV, and 160.3 eV, respectively, as recorded in Figure 7.7d. The Li_xS_y signal indicates relatively higher degree of salt

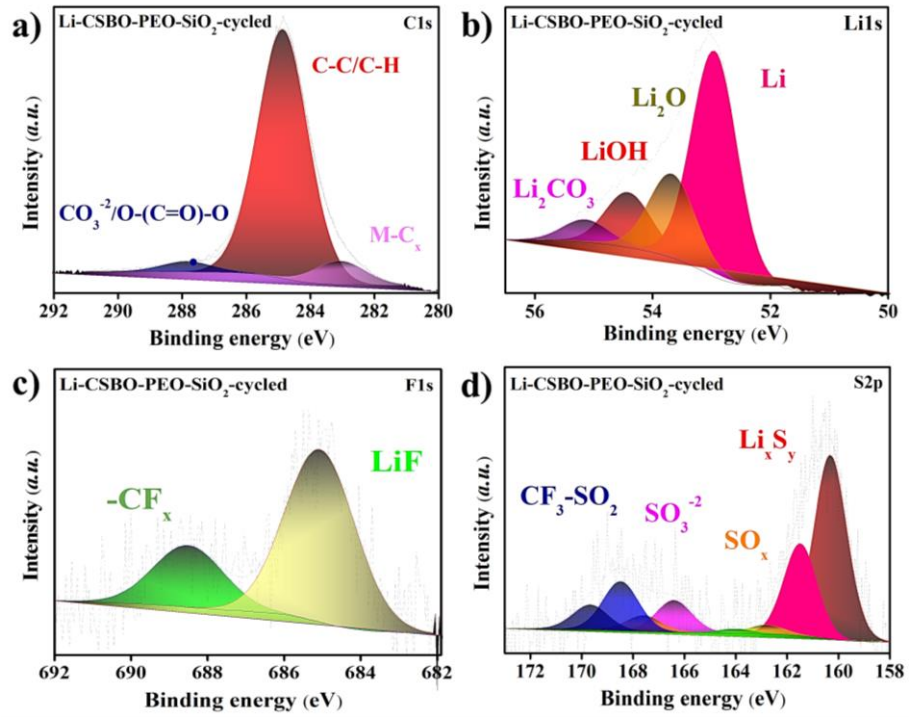

Figure 7.7: HR-XPS of a) Carbon, b) Lithium, c) Fluorine and d) Sulphur at the surface of lithium anode after cycling with LFP in Li|CSBO-PEO-SiO_2 CPE|LFP cell.

decomposition.HR-XPS for oxygen and nitrogen can be referred from Figure S7.2b and S7.2c.This preliminary analysis suggests that there is an active formation of interfacial stabilisation species. However, other factors contributing to detrimental cycling performance need to be investigated in line with modification CPE formulations.

As far as the post-mortem analysis of the PHU-based CPE is concerned, we experimented on Li-Li cells undergoing stripping and plating of Li for more than 600 cycles (> 1200 h). Both the Li-anode and the CPE surface have been depicted in the survey spectrum, showing conventional elements (refer to Figure S7.3a and S7.4). In the case of C1s spectra, C-C/C-H, C-O/N and O-C-O/C=O observed in both sample surfaces at the B.E. of 284.8 eV, 286.5 eV, 287.8 eV for Li and at 284.8 eV 286.3 eV, 287.8 eV for CPE, respectively. Lithium carbonate can be attributed to B.E. of 289.3 eV in combination with ester for li-anode and at 288.6 eV in the case of CPE. Moving on to Fluorine, F1s spectrum, a weak signal was recorded for LiF at 684.6 eV while,

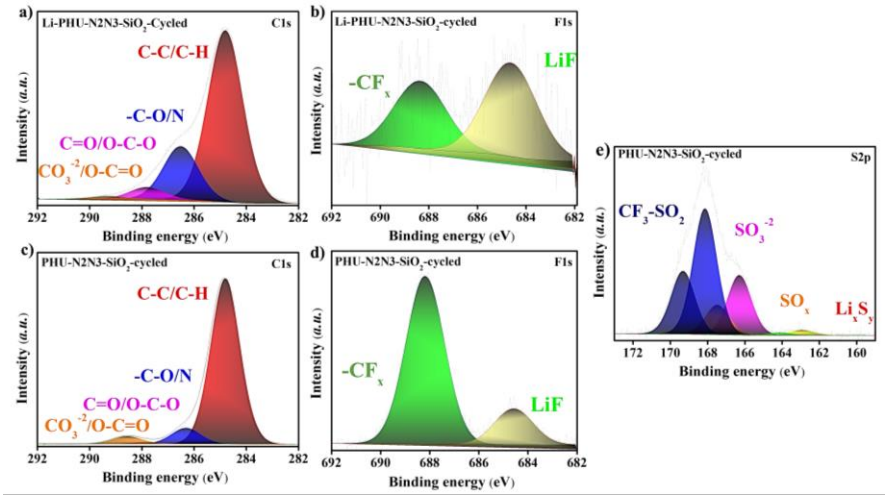

Figure 7.8: HR-XPS of a) and c) Carbon, b) and d) Fluorine and e) Sulphur at lithium anode and PHU-N2N3-SiO_2-CPE surface from the disassembled symmetric Li|PHU-N2N3-SiO_2 CPE|Li cell after stripping and plating

with stronger signal, major contribution is recorded from $–CF_3$ at 688.2 eV. However, there was no sulphur signal detected on the surface of the Li anode while at the CPE surface, S2p could be attributed largely to $-CF_3SO_3$ at 168.1 eV, minor composition of SO_3, SO_x at 166.3 eV and 162.8 eV, and negligible Li_xS_y at 160.58 eV. To our surprise, we could not detect the Si2p signal either due to its lower composition on the surface or sample mishandling. To further confirm that, XPS was also performed on the pristine SiO_2-based CPE on the top and bottom surface (see supporting information, Figure S7.3b, S7.5 and S7.6). Overall, the composition of silicon was lower than the actual loading, whereas relatively higher on the top surface as compared to the bottom. This could be due to SiO_2 entrapping in the bulk network rather than on the surface.

7.5 Conclusion

Hybrid electrolytes are foreseen as potential alternatives to deal with trade-offs and improve the key properties of organic and inorganic electrolytes. In our effort, we attempted to investigate the combined effect of SiO_2 and polymer electrolytes from our previous reports and presented a comparative study. Topologically different polymers, linear chains and networks have been used with in situ facile blending of

nanoparticles. In both cases, the addition of filler demonstrated lower flexibility and adhesive nature to the membrane with moreover no drastic change in the thermal behavior such as T_g and T_d. However, lower crystallinity in PEO was confirmed with addition of SiO_2. As far as ionic conductivity is concerned, CSBO-PEO-SiO_2-based CPE demonstrated slight improvement in the conductivity, i.e. 3.98 x 10^{-4} S cm^{-1} while ~6.1 x 10^{-5} S cm^{-1} were measured for PHU-based CPEs at 80 ^oC. To our expectations, we witnessed a broad widening in the ESW, higher for CSBO-PEO-based CPEs (> 4.8 V vs Li/Li^+) than PHU-CPEs (> 4.4 vs Li/Li^+). Furthermore, long-term charge-discharge validated CSBO-PEO-based CPEs as a result of symmetric cell and full-metal battery prototype testing. Subsequently, surface characterizations via XPS revealed the decomposed species at the electrode and electrolyte interface. Additional experiments can be performed with the potential scope for improvement, as this report paved the way for bio-sourced monomer-derived hybrid CPEs.

Bibliography

1. Boaretto, N.; Garbayo, I.; Valiyaveettil-SobhanRaj, S.; Quintela, A.; Li, C.; Casas-Cabanas, M.; Aguesse, F., Lithium solid-state batteries: State-of-the-art and challenges for materials, interfaces and processing. *Journal of Power Sources* **2021,** *502*, 229919.
2. Mauger, A.; Julien, C. M.; Paolella, A.; Armand, M.; Zaghib, K. Building Better Batteries in the Solid State: A Review *Materials* [Online], 2019.
3. Kalhoff, J.; Eshetu, G. G.; Bresser, D.; Passerini, S., Safer Electrolytes for Lithium-Ion Batteries: State of the Art and Perspectives. *ChemSusChem* **2015,** *8* (13), 2154-2175.
4. Manthiram, A.; Yu, X.; Wang, S., Lithium battery chemistries enabled by solid-state electrolytes. *Nature Reviews Materials* **2017,** *2* (4), 16103.
5. Chen, R.; Li, Q.; Yu, X.; Chen, L.; Li, H., Approaching Practically Accessible Solid-State Batteries: Stability Issues Related to Solid Electrolytes and Interfaces. *Chemical Reviews* **2020,** *120* (14), 6820-6877.
6. Liang, J.; Luo, J.; Sun, Q.; Yang, X.; Li, R.; Sun, X., Recent progress on solid-state hybrid electrolytes for solid-state lithium batteries. *Energy Storage Materials* **2019,** *21*, 308-334.
7. Fu, X.; Yu, D.; Zhou, J.; Li, S.; Gao, X.; Han, Y.; Qi, P.; Feng, X.; Wang, B., Inorganic and organic hybrid solid electrolytes for lithium-ion batteries. *CrystEngComm* **2016,** *18* (23), 4236-4258.
8. Armand, M., Polymers with Ionic Conductivity. *Advanced Materials* **1990,** *2* (6-7), 278-286.
9. Yang, H.; Wu, N., Ionic conductivity and ion transport mechanisms of solid-state lithium-ion battery electrolytes: A review. *Energy Science & Engineering* **2022,** *10* (5), 1643-1671.
10. Fu, J.; Li, Z.; Zhou, X.; Guo, X., Ion transport in composite polymer electrolytes. *Materials Advances* **2022,** *3* (9), 3809-3819.
11. Zhang, B.; Tan, R.; Yang, L.; Zheng, J.; Zhang, K.; Mo, S.; Lin, Z.; Pan, F., Mechanisms and properties of ion-transport in inorganic solid electrolytes. *Energy Storage Materials* **2018,** *10*, 139-159.
12. Lakshman Dissanayake, M. A. K., Nano-composite solid polymer electrolytes for solid state ionic devices. *Ionics* **2004,** *10* (3), 221-225.
13. Nan, C.-W.; Fan, L.; Lin, Y.; Cai, Q., Enhanced Ionic Conductivity of Polymer Electrolytes Containing Nanocomposite SiO2 Particles. *Physical Review Letters* **2003,** *91* (26), 266104.
14. Lin, D.; Liu, W.; Liu, Y.; Lee, H. R.; Hsu, P.-C.; Liu, K.; Cui, Y., High Ionic Conductivity of Composite Solid Polymer Electrolyte via In Situ Synthesis of Monodispersed SiO2 Nanospheres in Poly(ethylene oxide). *Nano Letters* **2016,** *16* (1), 459-465.
15. Lin, D.; Yuen, P. Y.; Liu, Y.; Liu, W.; Liu, N.; Dauskardt, R. H.; Cui, Y., A Silica-Aerogel-Reinforced Composite Polymer Electrolyte with High Ionic Conductivity and High Modulus. *Advanced Materials* **2018,** *30* (32), 1802661.
16. Liu, S.; Shan, H.; Xia, S.; Yan, J.; Yu, J.; Ding, B., Polymer Template Synthesis of Flexible SiO2 Nanofibers to Upgrade Composite Electrolytes. *ACS Applied Materials & Interfaces* **2020,** *12* (28), 31439-31447.
17. Shin, W.-K.; Cho, J.; Kannan, A. G.; Lee, Y.-S.; Kim, D.-W., Cross-linked Composite Gel Polymer Electrolyte using Mesoporous Methacrylate-Functionalized SiO2 Nanoparticles for Lithium-Ion Polymer Batteries. *Scientific Reports* **2016,** *6* (1), 26332.
18. Tu, J.; Wu, K.; Jiang, J.; Wu, M.; Hu, Q.; Xu, G.; Lou, P.; Zhang, W., A novel ceramic/polyurethane composite solid polymer electrolyte for high lithium batteries. *Ionics* **2021,** *27*, 1-7.
19. Panchireddy, S.; Thomassin, J. M.; Grignard, B.; Damblon, C.; Tatton, A.; Jerome, C.; Detrembleur, C., Reinforced poly(hydroxyurethane) thermosets as high performance adhesives for aluminum substrates. *Polymer Chemistry* **2017,** *8* (38), 5897-5909.
20. Rey, I.; Lassègues, J. C.; Grondin, J.; Servant, L., Infrared and Raman study of the PEO-LiTFSI polymer electrolyte. *Electrochimica Acta* **1998,** *43* (10), 1505-1510.
21. Wong, D. H. C.; Vitale, A.; Devaux, D.; Taylor, A.; Pandya, A. A.; Hallinan, D. T.; Thelen, J. L.; Mecham, S. J.; Lux, S. F.; Lapides, A. M.; Resnick, P. R.; Meyer, T. J.; Kostecki, R. M.; Balsara, N. P.; DeSimone, J. M., Phase Behavior and Electrochemical Characterization of Blends of Perfluoropolyether, Poly(ethylene glycol), and a Lithium Salt. *Chemistry of Materials* **2015,** *27* (2), 597-603.

c

Supporting Information

Composite polymer electrolytes based on silicon dioxide nanoparticles

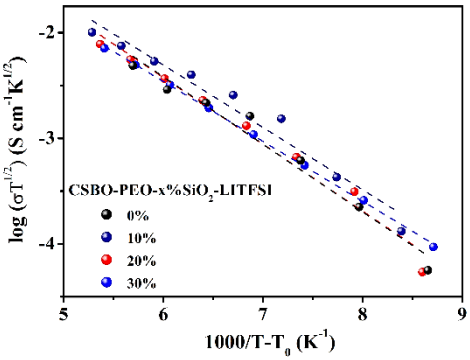

Figure S7.1: Temperature dependent ionic conductivity for investigated CPEs with VFT Model.

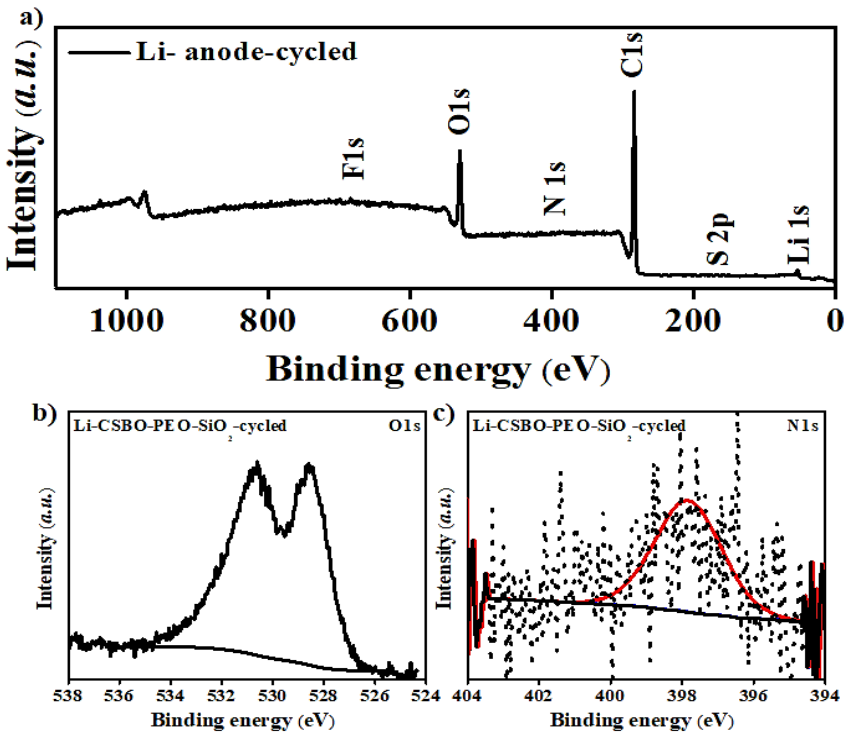

Figure S7.2: a) Survey spectrum, HR-XPS of b) Oxygen (O1s), and c) Nitrogen (N1s), at the surface lithium anode after cycling with LFP in Li|CSBO-PEO-SiO_2 CPE|LFP cell, respectively.

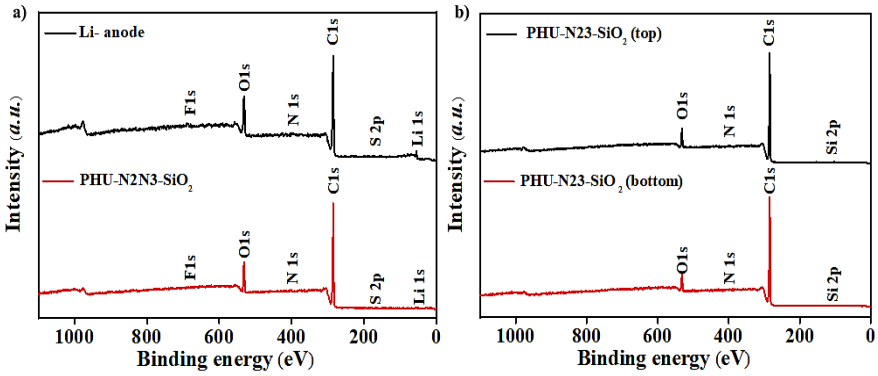

Figure S7.3: Survey spectrum of a) lithium anode and PHU-N2N3-SiO_2-CPE surface after stripping and plating with Li|PHU-N2N3-SiO_2-Li| cell and b) pristine PHU-N2N3-SiO_2-CPE films, respectively.

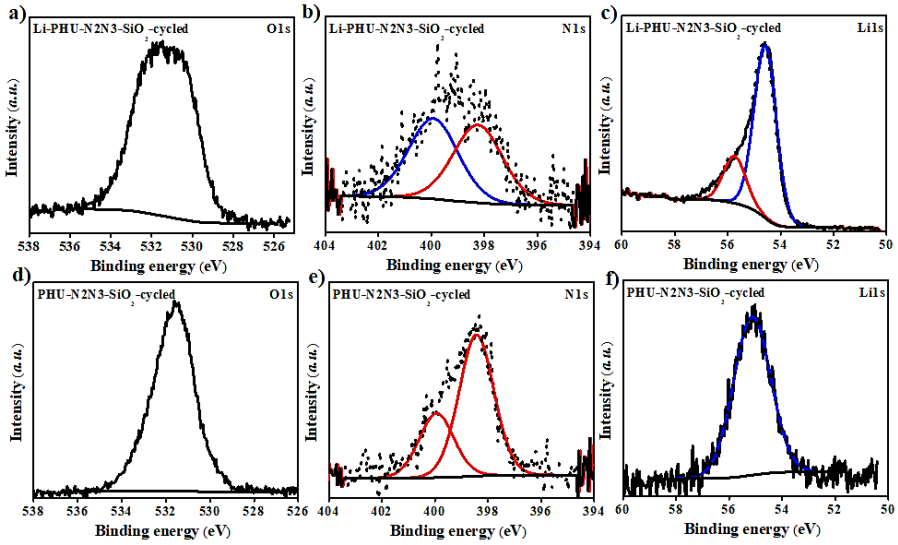

Figure S7.4: HR-XPS of a) and d) Oxygen (O1s), b) and e) Nitrogen (N1s), c) and f) Lithium at lithium anode and PHU-N2N3-SiO2-CPE surface after stripping and plating with Li|PHU-N2N3-SiO_2-Li| cell, respectively.

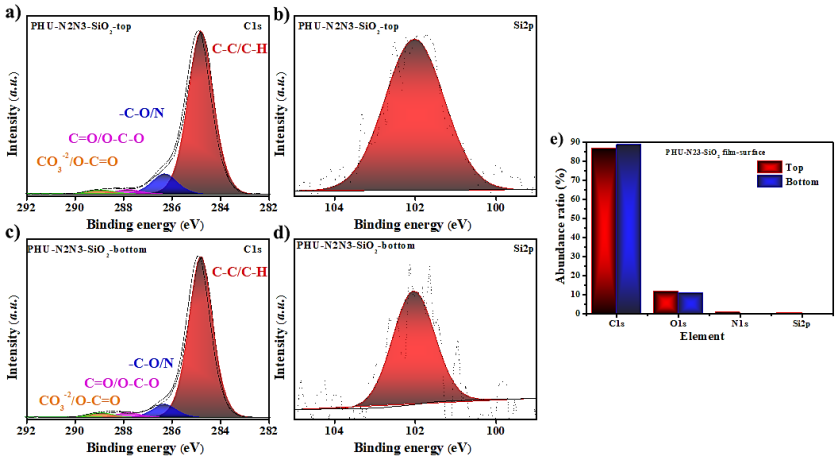

Figure S7.5: HR-XPS of a) and c) Carbon (C1s), b) and d) Silicon (Si2p), and e) abundance ratio% of top and bottom surface of pristine PHU-N2N3-SiO_2-CPE films, respectively.

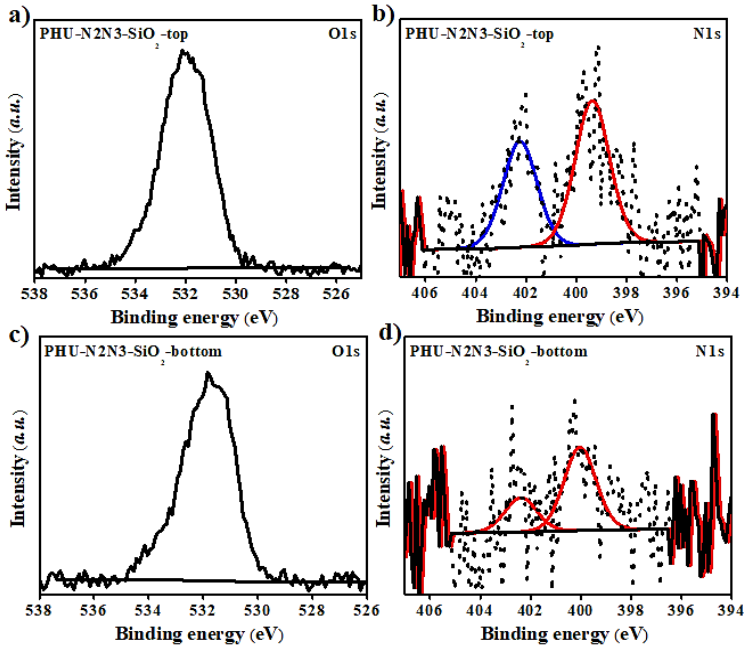

Figure S7.6: HR-XPS of a) and c) Oxygen (O1s), b) and d) Nitrogen (N1s), and e) abundance ratio% of top and bottom surface of pristine PHU-N2N3-SiO_2-CPE films, respectively.

Chapter 8 Conclusion and Perspective

Conclusion

Clean energy transition is an urgent need for coming decades more than ever, due to the accelerated climate change resulting in global warming and associated natural disasters. Renewables have already been adopted globally for cutting carbon dioxide emissions such as solar, wind, hydro, tidal, *etc*. But they pose a subtle drawback, coming out of their dependence on weather conditions and geolocation. This reflects the need for large-scale, robust energy storage technology for both stationary and mobile applications for vehicles. The revolutionary discovery of lithium batteries as a result of research over several decades brought a breakthrough in the innovation of electronics such as mobile phones, computers, watches and other devices. It did not take longer to overtake the other primary and secondary battery technologies and cover the huge market share, expanding their application to e-mobility and stationary grids as well. The reason lies behind their higher energy density than conventional batteries. The detailed history of LIBs over a century, right from the discovery of lithium, was briefed in the first few sections of Chapter 1.

Unlike any other batteries, LIBs consist of anodes, cathodes and electrolytes. However, they presented with huge complications and efforts before the commercialization of the first LIB battery in 1990. Goodenough and coworkers were credited with their remarkable discovery of cathode layered materials. On a similar line, various layered materials such as $LiCoO_2$, LiN_2O_3, $LiM_xM_yM_zO_2$, $LiFePO_4$ *etc*. have been discovered until now in the hope of overcoming the adhered challenges such as cost, sustainability, production and performance decay. Besides intercalation, other classes of materials involving conversion reactions (such as sulphur-based polyanionic cathode, orthosilicates *etc.*) also gained momentum but lacked in the race to reach the market due to structural instability and scalability. Simultaneously, significant research has been continued to enhance sustainability as well as cost via the development of toxic metal-free organic cathodes (such as polypyrrole, PTCDA, *etc.*). On the anode side, very few anode materials made their way to the market, including graphite, $LiTi_xO$ and silicon-based ones. Away from that, a variety of potential materials have continued to be under investigation so far following intercalation to conversion mechanism (such as nitrides, fluorides, phosphides,

sulphides *etc.*) including alloying (like silicon, tin, antimony *etc.*) and their combination as well.

As far as electrolytes are concerned, their development was less challenging due to the available studies on the reaction and stability of lithium with commonly used organic solvents. A brief yet crucial discussion has been provided on the type and characteristics of components of liquid electrolytes focused on organic solvents, salts and additives. Carbonate-based solvents gained much interest due to their higher donor number and dielectric constant with most of the lithium salts compared to ethers. They are chosen based on their electrochemical and thermodynamic stability with electrodes. Some of the commercial electrolytes comprise a binary mixture of carbonates, such as EC and DEC or EC-DMC with fluoride-based $LiPF_6$,LiTFSI and other salts. $LiPF_6$ and LiTFSI are the most utilised salts for liquid electrolytes due to good dissolution and passivation layer formation abilities.

An electrolyte not only provides the channel for ion transport but also makes interfaces with electrodes, such as SEI and CEI, whose stability cannot be ignored. For the past two decades, the research on electrolytes has escalated to interfacial engineering due to growing concern about durable and long-performing batteries. Besides solvents and salts, there are key supporting materials, such as co-solvents and additives, which stabilise and provide the electrolytes with additional properties. Additives such as FEC, VC, VEC *etc* are extensively used because of their SEI-stabilising species. However, researchers have also come up with additives which add up interesting characteristics such as fire retardant, overcharge prevention, self-healing behaviour, *etc*. As a safe alternative to LE, ionic liquids are trying to find their place in batteries. Nevertheless, it has some challenges in terms of ionic conductivity and wettability in addition to advantages like volatility and non-flammability. Some commonly known ionic liquid consists of cations such as imidazolium, pyridinium, pyrrolidinium (PYR) and anions like $TFSI^-$ and BF_4^-.

In the subsequent section of Chapter 1, a brief discussion has also been targeted on the adverse effects of clean energy, which are not so clean yet and sustainable. Though lithium batteries while storing and supplying energy do not cause any environmental hazard/pollution, their raw materials, processing and manufacturing involve huge

toxic and hazardous processes which question the impact of the technology over the long term. Starting with popular cathode materials, nickel and cobalt are toxic elements, and are extracted from mines via unfavorable conditions in African countries. Lithium metal extraction has drawn a huge backlash because of its large water consumption causing an imbalance in the local underground water level and ecosystem. The impact of other components of the existing lithium battery is also alarming due to their flammability and toxicity issues. On top of that, another futuristic problem which is gonna come across is battery waste and its disposal.

Gladly, many researchers are working on these issues, either with environmentally friendly materials or sustainable manufacturing processes. Another crucial industry which is finding its place in the market is recycling to reuse the materials after processing supported via carbon neutral steps and promote second life batteries. Life cycle assessment has been stressed for the same in the evaluation of each of these processes and reporting the mismatch.

In an extended introduction, Chapter 2 provides a detailed background on state-of-the-art polymer-based electrolytes, their design, operation mechanism and performance with batteries. Solid state electrolyte has been speculated to change the fate of the lithium battery technology not only from the safety aspect but also the performance. Organic polymer electrolytes together with inorganic solid electrolytes so far are entrusted to match with liquid electrolytes properties. However, it's not as easy as it seems due to various issues like interfacial resistance, diffusion length *etc*. PEO-based electrolytes were the first ones in the race of polymer electrolytes whose broad investigation built a strong foundation on the characteristic properties of polymer electrolytes. Sooner and later, gel polymer and composite polymer electrolytes found their way with certain advantages over existing dry polymer electrolytes.

The material of interest in this thesis is initiated with carbonates, which are widely used in commercial liquid electrolytes due to the various reasons highlighted in Chapter 1. In the last part of Chapter 2, cyclic carbonates, their synthesis and properties before polymerisation have been discussed. CCs, due to their superior coordination properties, have been well explored as polycarbonates and as a side

chains in polymer chains. Moreover, they are used as monomers for the synthesis of poly(hydroxyurethane)s, which is a noble alternative to polyurethanes. They offer a great degree of structural control and tunability. Interesting properties have been achieved with PUs with their blends and composites, either ionic conductivity or flexibility. However, toxic monomers and catalysts direction at PHUs and their derivatives.

Given the ambition of sustainable materials, bio-based polymers are equally exploited as battery materials with and without functional modifications. The three categories of these polymers involve: a) directly extracted from biomass, b) produced by microorganisms and c) chemically synthesised using bio-based monomers. The functionality and polar groups mark these materials as interesting for electrochemical applications. For instance, various groups are working on the functionalization of gums, cellulose, lactides, oil *etc* as binders, electrodes and electrolytes. Our interest lies in polymers derived from oil, which have not been explored much.

Chapter 3 is dedicated to the methodology and discussion of electrochemical techniques used for electrolytes and battery testing. The first step for material screening or its mechanism analysis is the correct choice of cell setup, type, and number of electrodes. Impedance spectroscopy driven by sinusoidal signals provides powerful information on the conductivity of materials, from electrodes to electrolytes. The conductivity of electrolytes is often calculated using PEIS with symmetric cells via Nyquist plots. Other key techniques are the voltammetry and charge-discharge experiments. Voltammetry is a universal technique for the evaluation of redox behaviour materials at the targeted voltage window. While constant current is applied for the evaluation of cell prototypes, either with potential or time limitations. These methods are important to discover the material response at various parameters over time before the green signal for commercial purposes.

While, Chapter 4 talks about the roadmap of objectives and engagement tools from synthesis to application. The goal of the thesis revolves around the synthesis and demonstration of the carbonate-based polymer electrolyte for lithium metal batteries in the first section. Within the same section, a polymer blend has been planned to be synthesized with PEO with cyclic carbonate rings. The following section focuses on

the polymer design via targeted CC ring opening. In addition to understanding the structural property relationships, interfacial analysis has also been aimed at stability and SEI investigations. Taking it further, the last work package combines the organic polymers and inorganic particles to demonstrate their mutual compatibilities and potential performance with further studies.

The work carried out in the thesis is split into three main chapters from 5 to 7. Sub-Chapter 5.1 discusses on salt-loaded soybean oil-derived cyclic carbonates for lithium metal battery electrolytes. With a higher salt concentration of 50wt%, the electrolyte recorded high ionic conductivity and transference number, which translated to room temperature cycling of LFP-Li cells. Extending that, a blend was prepared consisting of bio-derived CSBO and PEO for ion-conducting polymer segments and separator free-standing ability, as reported in Sub-Chapter 5.2. Almost ten times improvement in the ionic conductivity with 20wt% of LiTFSI to ~10^{-5} S cm^{-1} at RT was witnessed with higher ESW compared to PEO alone. Reduced decomposition of LiTFSI witht the CSBO-PEO composite as evident from comparative HR-XPS of F1s and S2p assured the stable cycling performance in Li-LFP cells.

In Chapter 6, our interest aligned with the synthesis of novel and yet sustainable polymer electrolytes with CC as utilised in Chapter 5. CC rings were opened via a reaction of CBSO and PEGTA under moderate reaction conditions. A novel idea of isocyanate and catalyst-free poly(hydroxyurethane)-based electrolytes is scripted in Sub-Chapter 6.1. The PHU polymer network was supported on cellulose fibre separator, exhibiting higher conductivity (> 10^{-5} S cm^{-1} at 60 °C) than CBSO as a result of the presence of polyether segments in PHU. With lower T_g and T_d, the

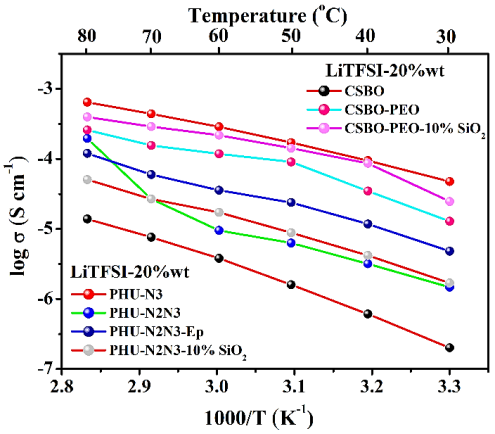

Figure 8.1: Comparative ionic conductivity plot of polymer investigated with 20 wt% LiTFSI using Arrhenius model.

PHU networks demonstrated good electrochemical properties with higher oxidation potential and cycling efficiency with electrodes of interest. Nevertheless, enduring effort was staged to obtain free standing membranes of PHU via variable crosslinking/blending/plasticization. Within the same section, we report various analogues of PHU developed via variable chain length cross-linkers. Most of these membranes in our investigations recorded optimum compatibility with lithium metal anode in both short to long-term experiments.

Chapter 7 highlighted the potential of composite polymer electrolytes. Usually, inorganic fillers are proven to enhance electrolyte performance with conductivity, lower crystallinity, and mechanical and thermal stability depending upon the type of filler. Given the environment's benignity, we investigated the effect of silicon dioxide nanoparticles incorporation within the linear chain of CSBO-PEO composite and into the crosslinked PHU networks during its formation. In both cases, up to 20% wt of SiO_2 was found to confer superior mechanical properties. However, more or less, no conductivity enhancement was observed for the hybrid composites credited to the passive nature of the fillers. While higher ESW was found to be an additional interesting parameter towards composite/hybrid electrolyte formulations. To sum up, we investigate various analogues in this thesis across different phase which trivially reflected on the ionic conductivity as depicted in the Figure 8.1. As observed, the conduvity increased from when the CC ring was opened and based on the functional group and mobility of chains. PHU-N3 recorded highest conduvity following the order, PHU-N3 > CSBO-PEO-SiO_2 > CSBO-PEO > PHU-N2N3-Ep > PHU-N2N3-SiO_2 > PHU-N2N3 > CSBO, respectively with LiTFSI (20 wt% of the polymer).

Perspective

Solid-state electrolytes, either organic or inorganic, could not match up to conventional liquid electrolytes so far, which limit their commercialisation. Associated drawbacks with the latter gave the momentum to the lithium-polymer batteries based on gel polymer electrolytes. Despite the hurdle in all-solid-state batteries, the efforts have never been decelerated. Right from the materials design and innovation, concentrated research has been carried out with compatible electrodes,

binders, and interfacial engineering supported by modelling and simulations. Some of the interesting results have been obtained in combination with organic and inorganic, which is seen as a potential approach. With more and more studies on electrolytes, salts, co-solvents, and additives, the performance of batteries is improving. In addition, advancements in cell design and packaging are also leading towards safety and robustness within existing technology.

There has been interesting studies on bio-based electrodes while very few interest lies in the bio-based electrolytes. With consolidated effort, there is need of bio-sourced sustainable battery materials which can be scaled and commercialized. Our effort was directed at the demonstration of vegetable oil sourced electrolyte which sparks the debate of inbalancing the ecosystem of food resources. However, drawing motivation from these non-edible oil/oil waste could be formalized in the similar direction which could fill the gap without disturbing the food supply chain.These polymers facilitate with ether, cyclic carbonate and urethane functionalities beneficial for an electrolyte.

Diving into polyurethane networks, we observe that it has vast potential in tunability in mechanical and structural properties. With a right balance in ion conduction and tensile strength, it can be thinned down to a few micrometre which is one of ambitious parameter of solid electrolyte. In addition to the network properties, we speculate that they could also buffer the trade off between conductivity and transference number by lowering the concentration gradient. They offer intresting potential to collaborate with other polymers and inorganic materials for exploiting the synergic effects. There are various aspects which of which have not been addressed in this thesis from the polymer design to its processing for the cell assembly. The ambitious and prospective steps could be investigating ring opening with Si-based crosslinker to get hybrid co-polymers, design of single lithium ion conducting PHU and end chain modification.

By incorporating higher number of ether units in the polymer and inclusion of active fillers, we can strategically enhance the ionic conductivity and other related electrochemical properties. One of the key issues faced in lower performance of electrolyte is high interfacial resistance at the electrode-electrolyte. For that, interfacial engeineering could be adoped, particularly catholyte preparation and optimization, polymer end chain modification and artificial coatings. Some of these

approaches have been attempted in this thesis as well. However, processing techniques such as thinning down the electrolyte films and optimum cell pressure could decrease the interfacial resistance. For instance, the blends and hybrid electrolytes in our thesis could be thinned down and impart potential performance with further optimized investigations.

Beyond Li-ion batteries is an open debate which motivates researchers across the globe to look for superior alternatives as discussed in brief in Chapter 1. Sodium-ion batteries are far ahead in that race due to the abundance of sodium metal in the earth's crust. It shares similar chemistry with lithium metal with challenges in size, lower capacity and performance. However, few companies in Asia and Europe have already moved towards the commercialisation of sodium ion batteries. However, it will take time for this technology to reach the maturity of lithium batteries. In parallel, other metal-ion battery technologies which seem promising are potassium, calcium, magnesium and aluminium ions. Each of these has its challenges and limitations, which block its progress. Away from that, redox flow batteries are quite seen as potential candidates due to their low cost, environmentally friendly and safety when it comes to energy storage at grid scale. Looking at the pace of material innovation and technical infrastructure, multiple battery technologies could be interesting to target regional sustainability and environmental balance.

Curriculum Vitae

Ashish Raj comes from Chapra, Bihar, India, where he did his primary and secondary education. He did 5-years (2013-18) Integrated MS (BS-MS dual degree) with major in Physics and minor in Chemistry, at IISER-Thiruvananthapuram, Kerala, India. Later in 2019, he moved to Belgium to start his PhD thesis on bio-based polymer electrolytes under supervision of Prof. Jean-François Gohy at UCLouvain as a part of BRIDGE-FUSE project funded by Innoviris (Brussels region) and in collaboration with CERM, University of Liège, Belgium.

Peer-reviewed journal publications:

- Lieven Bekaert, Ashish Raj, Jean-François Gohy, Annick Hubin, Frank De Proft, and Mesfin H. Mamme, Assessing the Long-Term Reactivity to Achieve Compatible Electrolyte–Electrode Interfaces for Solid-State Rechargeable Lithium Batteries Using First-Principles Calculations, J. Phys. Chem. C 2022, 126, 19, 8227–8237.
- Ashish Raj, Satyannarayana Panchireddy, Bruno Grignard, Christophe Detrembleur, Jean-François Gohy, Bio-Based Solid Electrolytes Bearing Cyclic Carbonates for Solid-State Lithium Metal Batteries, *ChemSusChem* 2022, 15, e202200913.

To be submitted:

- Ashish Raj, Bruno Grignard, Christophe Detrembleur, Jean-François Gohy, Carbonated Soybean oil blends with poly(ethylene oxide) as solid polymer electrolytes for lithium metal batteries.
- Ashish Raj, Bruno Grignard, Christophe Detrembleur, Jean-François Gohy, Bio-derived cyclic carbonates bearing poly(hydroxyurethane)-based networks as polymer electrolytes for solid-state lithium batteries.
- Ashish Raj, Bruno Grignard, Christophe Detrembleur, Jean-François Gohy, Non-isocyanate poly(hydroxyurethane)-based networks as solid polymer electrolytes for lithium metal batteries.

- Ashish Raj, Bruno Grignard, Christophe Detrembleur, Jean-François Gohy, Composite polymer electrolytes based on silicon dioxide nanoparticles mixed with carbonated soybean oil/poly(ethylene oxide blends or poly(hydroxyurethane) networks.

Other related manuscripts to be submitted/under preparation:

- Ashish Raj, Bruno Grignard, Christophe Detrembleur, Jean-François Gohy, Solid polymer electrolytes with sacrificial end groups for wide oxidative potential and stable interfaces in lithium metal batteries.
- Ashish Raj, Bruno Grignard, Christophe Detrembleur, Jean-François Gohy, Polyether based Poly(hydroxyurethane) network as solid polymer electrolyte.
- Ashish Raj, Satyannarayana Panchireddy, Jean-François Gohy, Thermal cured thiol-ene polymer network as lithium ion conducting solid polymer electrolyte.

Scientific conferences/seminar participations:

Oral presentations:

- Bio-based solid electrolytes bearing multi-functional cyclic carbonates for solid-state lithium batteries,
  - 240th ECS Meeting-2021(digital).
  - ACS-Fall Hybrid Meeting-2021(digital).
  - E-MRS Fall Meeting-2021(digital).
  - Brightlands Polymer Days 2021-Eindhoven, Netherlands.
- Bio-based solid electrolytes based on poly(hydroxyurethane) bearing cyclic carbonates for solid-state lithium batteries- Where polymers meet coatings-ATIPIC-BPG, 7 October 2021. Brabanthal, Leuven, Belgium.
- Exploring carbonates and polyhydroxy urethanes network as potential polymer electrolyte for lithium batteries, Virtual Seminar Solvay, 19 November, 2021, Brussels, Belgium (digital).

- Polyhydroxy urethanes and carbonates bearing bio-based electrolyte for solid-state lithium batteries, IMCN PhD day, 2022 and BSMA, IMCN Seminar, 2022, UCLouvain, Belgium.
- Cyclic carbonate bearing Carbonated Soybean oil composite with Polyethylene oxide as solid polymer electrolyte for lithium metal batteries, E-MRS Fall meeting-2022, Warsaw, Poland.
- Synthesis of Polyhydroxy Urethane Network Based Solid Polymer Electrolytes from Bio-Sourced Carbonates and Amines, 244th ECS Meeting-2023, Gothenburg, Sweden.

Poster/Video capsule presentation:

- Bio-based solid electrolytes bearing multi-functional cyclic carbonates for solid-state lithium Batteries, Belgian Polymer group meeting 2021(digital).
- Soybean Oil Derived Solid-State Electrolytes for Lithium Batteries, MRS Fall Meeting and Exhibit-2021 (digital).
- Extending Electrochemical Stability Window as a Result of Carbonate-Ketone Side Chain Modified Polyethylene Glycol Electrolytes for Lithium Batteries, 241st ECS Meeting-2022(digital).
- Polyhydroxy Urethanes and Carbonates Bearing Bio-Based Solid Electrolyte for Solid-State Lithium Batteries, 242nd ECS Meeting-2022(digital).
- Polyether based Polyhydroxy urethane Network as Polymer Electrolyte solid-state Lithium metal Batteries, IMCN-PhD day, 2023, UCLouvain, Belgium and at E-MRS Spring meeting-2023, Strasbourg, France.
- Investigating Bio-derived Polyhydroxy urethanes network bearing carbonates as solid polymer electrolyte, Organic battery days 2023, San Sebastien, Spain (Flash and poster presentation).

Workshops attended:

- 1st Sustainable Energy Storage days in Madrid - SESDIM 2019, Polymer Composite Group and Spanish National Research Council (CSIC), Spain.

- Polymers & Batteries workshop, UPV/EHU-POLYMAT, 1st October 2020 as part of the MSCA-ETN-POLYSTORAGE training activities (digital).
- 1st SUPERBAT international course (Batteries and Supercaps: Principles and Applications) 14-15 October of 2021 in Madrid, Spain (digital).